

Electronically Reconfigurable Wideband Microwave Filters

Alexander Miller

A Dissertation Submitted for the degree of Doctor of
Philosophy

Heriot – Watt University
School of Engineering and Physical Sciences
August 2012

This copy of the thesis has been supplied on the condition that anyone who consults it is understood to recognise that the copyright rests with its author and that no quotation from the thesis and no information derived from it may be published without the prior written consent of the author or of the University (as may be appropriate).

Abstract

Many systems require multi function capability in the filter aspects of systems; the method currently used is filter banks which take up a lot of board space. It is thought that reconfigurable filters hold the key to replacing filter banks in order to save board space and thus potentially increasing functionality of the systems. The aim of this research is to develop electronically reconfigurable microwave filters for future communication systems. The project investigates some key design issues of reconfigurable filters. Circuits were modelled and full-wave electromagnetic simulations were performed for the investigation. Experimental work was carried out to demonstrate advanced reconfigurable microwave devices. The components used in each concept investigated were pin diodes due to their superior performance in wideband and high frequency applications. Firstly a single coupled line concept was looked at for bandwidth reconfigurability. This concept was then further developed for industrial applications by simply cascading these sections to obtain a high selective filter. A design method was developed for any number of cascades both with and without an impedance transformer; the use of LCP was used to increase flexibility due to its desirable characteristics. The most desirable outcome would be filter to simultaneously control bandwidth and frequency. In order to tackle this issue the coupled line concept was adapted to incorporate frequency tunability, along with a design method being presented. Furthermore, a cascaded highpass/ lowpass filter was also explored for this concept for added flexibility in the design of a filter capable of control of both bandwidth and center frequency.

Dedication

To all my family and friends (you know who you are!), who have helped and supported me over the years; through all my decisions and aspirations.

Acknowledgements

I would like to acknowledge the help and assistance of Jia-Sheng Hong for his continuous support throughout this work. Especially for keeping me motivated and giving me guidance when I hit dead ends throughout the project.

I would also like to thank Colin Bird and Alan Burdis from Selex Galileo for their guidance and casting a critical eye over my reports and presentations.

Special thanks to my many friends who have given me their support and help throughout my PhD: Dr. Wenxing Tang, Dr. Zhang-Chen Hao, Shilong Qian, Elizabeth McKeever, Jia Ni, Francisco Cervera, Ross Aitken, Armando Fernandez Prieto, Miguel Angel Sanchez Soriano, Martin Aitken and anyone part of the office 3.32 who came and went or are still there (you know who you are!).

I would like to thank my parents and the rest of my family. To my Mum and Dad for always being there through the good and the bad times and their ever lasting love and support. Also to my brothers, also for their everlasting love and support, making me feel I could do anything. Also to my nieces and nephews who always cheer me up and put a smile on my face. To the rest of my family (ranging from my in laws, uncles, aunties and cousins) and close friends, you know who you are! Who have been there to support me and take my mind off things.

Without all the people mentioned above I would not be the person I am today, all giving me the strength and drive to succeed and complete this project.

Table of Contents

Chapter 1: Introduction	1
Chapter 2: Background	8
2.1) Introduction	8
2.2) Reconfigurable Bandwidth at a fixed Center Frequency	10
2.2.1) Reconfigurability Achieved Through Switch Circuitry	10
2.2.2) Reconfigurability Achieved Through Altering the Geometries of Circuitry.....	13
2.2.3) Tunable Filter Using Piezoelectric Structure	15
2.3) Reconfigurable center frequency and Bandwidth	17
2.3.1) Use of Varactor Elements for Simultaneous Tunability of Center Frequency and Bandwidth	17
2.3.2) Use of PIN diodes for Simultaneous Reconfigurability of Center Frequency and Bandwidth	21
2.3.3) Use of MEMS Devices for Simultaneous Reconfigurability of Center Frequency and Bandwidth.....	23
2.4) Liquid Crystal Polymer (LCP)	36
2.4.1) Alignment and Laser Processing.....	37
2.4.2) Lamination Technique	39
2.4.3) Lamination Pressure	40
2.5) Summary.....	41
2.6) References	41
Chapter 3: Microstrip Equations and Filter Theory	49
3.1) Introduction	49
3.2) Lowpass to Bandpass Transformation.....	49
3.2.1) Lowpass Prototype	49
3.2.2) Frequency and Element Transformations	52
3.2.3) Lowpass Transformation	53
3.2.4) Highpass Transformation.....	54
3.2.5) Bandpass Transformation.....	55
3.2.6) Bandstop Transformation.....	57
3.3) Butterworth Lowpass Prototype	57
3.4) Chebyshev Lowpass Prototype	58

3.5) Immittance Inverters	59
3.5.1) Transformations with Immittance Inverters	60
3.5.2) Filter Design With Immittance Inverters	61
3.5.3) Practical Realization of Immittance Inverters	64
3.6) Coupled Lines.....	65
3.6.1) Design Equations	66
3.6.2) Even and Odd Mode Extraction Technique	68
3.7) Stepped Impedance Resonators.....	69
3.8) References	69
Chapter 4: Filter Topologies	72
4.1) Introduction.....	72
4.2) Short Circuit Coupled Line Filters	72
4.2.1) Single Section Formulation	72
4.2.2) Multi – Section Coupled Line Filter Design Equations.....	76
4.3) Optimum Highpass Filter	80
4.4) Optimum Quasi Lowpass/Bandstop Filter	83
4.5) References	87
Chapter 5: System Integration Considerations	88
5.1) Introduction	88
5.2) Gain Compression.....	89
5.2.1) 1 dB Compression Point Set Up.....	91
5.3) Intermodulation Distortion.....	91
5.4) Third-Order Intercept Point.....	93
5.4.1) Third-Intercept Point Set Up.....	97
5.5) Passive Intermodulation	97
5.6) Intercept Point of Cascaded Components	98
5.7) Dynamic Range	101
5.8) Linear Dynamic Range (DR _l).....	102
5.9) Spurious Free Dynamic Range (DR _f).....	103
5.10) Summary.....	104
5.11) References	105

Chapter 6: Single Section Coupled Line Reconfigurable Filter	106
6.1) Introduction	106
6.2) Short Circuit Coupled Line Filters	106
6.2.1) Coupled Line Filters With Reconfigurability	106
6.2.2) Coupled Line Filter Design With Impedance Transformer	111
6.2.3) Experimental Demonstration	113
6.2.3.1) EM Simulation.....	113
6.2.3.2) Fabricated Filter	115
6.2.4) Isolation Scheme.....	117
6.3) Short Circuit Coupled Line Filters Combined	124
6.3.1) Experimental Demonstration	124
6.3.1.1) EM Simulation.....	124
6.3.1.2) Fabricated Filter	127
6.4) Non – Linearity Measurements	130
6.4.1) Third Intercept Point.....	130
6.4.2) 1 dB Compression Point.....	133
6.5) Summary.....	135
6.6) References	136
Chapter 7: Cascaded Coupled Line Reconfigurable Filters	137
7.1) Introduction	137
7.2) Reconfigurable Coupled Line Filter With Four Distinct Bandwidth States	137
7.2.1) Filter Design	137
7.2.2) EM Simulation.....	144
7.2.3) Experimental Results	147
7.3) Cascaded Coupled Line Filter Using LCP; Designed Using Matthaei Equations.....	149
7.3.1) Filter Design Theory	150
7.3.2) Filter Design	158
7.3.3) Physical Implementation	164
7.3.4) Experimental Filter	171
7.4) Non – Linearity Measurements	173
7.4.1) Third Intercept Point.....	173
7.4.2) 1 dB Compression Point.....	175
7.5) Summary.....	176

7.6) References	176
Chapter 8: Frequency and Bandwidth Tunability Using the Couple Line Concept	178
8.1) Introduction	178
8.2) Short Circuit Stub Filter Design	178
8.2.1) Filter Design	179
8.2.2) EM Simulation.....	181
8.2.3) Measured Filter Results	184
8.3) Summary.....	187
8.4) References	187
Chapter 9: Reconfigurable Bandwidth and Frequency Filter Using Cascaded Highpass/Lowpass Blocks	188
9.1) Introduction	188
9.2) Short Circuit Stub Filter Design	188
9.2.1) Theoretical Design	188
9.2.2) EM Simulation.....	191
9.3) Reconfigurable Optimum Lowpass Filter.....	198
9.3.1) Theoretical Design	198
9.3.2) EM Simulation.....	201
9.4) Reconfigurable Bandpass Filter	204
9.5) Non – Linearity Measurements	209
9.5.1) Third Intercept Point.....	209
9.5.2) 1 dB Compression Point.....	210
9.6) Highpass Filter Improved Design	210
9.7) Reconfigurable Filter With New Designed Highpass Filter	213
9.8) Summary.....	216
9.9) References	217
Chapter 10: Conclusion and Future Work	220
10.1) Introduction	220
10.2) Single Section Coupled Line Design	220
10.3) Cascaded Coupled Line Filter.....	221
10.4) Frequency and Bandwidth Tunable Filter Using Coupled Line Concept.....	221
10.5) Cascaded Highpass/Lowpass Filter Concept.....	222

10.6) Future Work.....	222
10.7) References	224
Appendix 1.....	225
Appendix 2.....	242
Appendix 3.....	253
Appendix 4.....	262
Appendix 5.....	273
Appendix 6.....	284
Appendix 7.....	293
Appendix 8.....	297

List of Figures

Figure 1.1: Electromagnetic Spectrum	2
Figure 1.2: Filter Bank Illustration.	4
Figure 1.3: Reconfigurable/Tunable Filter Linkage.	5
Figure 2.1: Circuit Layout for Bandpass Filter. [39]	10
Figure 2.2: Equivalent Circuit for the Bandpass Filter. [39]	11
Figure 2.3: Magnitude responses of filter transmission co-efficient for the wide-passband setting, the dotted line being the calculated and the solid line being the measured [39].	12
Figure 2.4: Magnitude responses of filter transmission co-efficient for the narrow-passband setting, the dotted line being the calculated and the solid line being the measured [39].	12
Figure 2.5: (a) layout of open end gap, (b) layout of proposed interdigital, (c) comparison of results. [40]	13
Figure 2.6: Structure of the filter, (a) Narrowband (b) Wideband [41].	14
Figure 2.7: Measured vs. simulated transmission and return loss of the filter in the narrowband state [41].	15
Figure 2.8: Measured vs. simulated transmission and return loss of the filter in the wideband state [41].	15
Figure 2.9: Schematic of Piezoelectric Resonator. [42]	16
Figure 2.10: (a) Circuit Diagram of Piezoelectric Resonant Filter, (b) Schematic View of lumped Model of the Piezoelectric Circuit Element. [42]	16
Figure 2.11: (a) Classic Second - Order Compline Filter. (b) Equivalent Circuit. [27]	18
Figure 2.12: Bandpass Filter Structure with Coupling Reducer. [27]	18
Figure 2.13: Topology With Coupling Reducer Inserted. [27]	19
Figure 2.14: Topology With Coupling Reducer Inserted. [28]	20
Figure 2.15: Topology Used in [30] and [31].	20
Figure 2.16: Proposed Filter Design with Pin diodes [32].	21

Figure 2.17: Wideband Results, measured (solid line), Simulated (dashed line). (a) Transmission loss, (b) Return Loss [32].	22
Figure 2.18: Narrowband Results, measured (solid line), Simulated (dashed line). (a) Transmission loss, (b) Return Loss [32].	23
Figure 2.19: Basic DBR Resonator. [33]	24
Figure 2.20: Ideal Second Order DBR Filter. [33]	24
Figure 2.21: Simulated S-parameters for central frequency tuning [33].	25
Figure 2.22: Simulated S-parameters for Bandwidth Tuning [33].	25
Figure 2.23: (a) Filter layout, (b) Photograph of Fabricated two Pole Filter, (c) Photograph of Resonator Sections, (d) Photograph of MEMS varactor [34].	26
Figure 2.24: (a) Filter Layout, (b) Photograph of 4 Pole Filter [34].	26
Figure 2.25: Measured Filter Bandwidth Tuning for a Fixed Center Frequency (two pole) [34].	27
Figure 2.26: Measured Filter Center Frequency Tuning with a Constant Bandwidth (two pole) [34].	27
Figure 2.27: Measured Filter Center Frequency Tuning with a Constant Bandwidth (four pole) [34].	28
Figure 2.28: Measured Filter Bandwidth Tuning with a Constant Center Frequency (four pole) [34].	28
Figure 2.29: Circuit Schematic Morphed to accommodate Fabrication onto a MEMS chip [35].	29
Figure 2.30: Insertion Loss and Return Loss of the Filter, demonstrating center frequency tunability [35].	30
Figure 2.31: Insertion loss and Return loss of filter, demonstrating bandwidth tunability [35].	30
Figure 2.32: Structure of Slow Wave DMTL Filter [36].	31
Figure 2.33: Insertion Loss of filter with bandwidth tuning Without Compensation of shift in Center Frequency [36].	31
Figure 2.34: Return Loss and Insertion Loss of The filter, demonstrating center frequency tunability and keeping a constant bandwidth [36].	31
Figure 2.35: Lumped Distributed Coupled Resonators [37].	32
Figure 2.36: Results for five of the Filters Capable states [37].	33

Figure 2.37: Measured Insertion Losses for five of the states [37].	33
Figure 2.38: Measured Insertion Loss of five states of the filter [37].	34
Figure 2.39: Measured Insertion Loss of five states of the filter [37].	34
Figure 2.40: Lowpass Filter Schematic and Microstrip Implementation [38].	35
Figure 2.41: Highpass Filter Schematic and Microstrip Implementation [38].	35
Figure 2.42: Showing Tunable Bandwidth [38].	35
Figure 2.43: Showing Tunable Center Frequency [38].	36
Figure 2.44: Circuit Etching.	37
Figure 2.45: Laser Drilling Setup.	38
Figure 2.46: Typical LCP Lamination Setup.	39
Figure 2.47: Temperature Settings for Lamination Process.	40
Figure 2.48: Pressure used in lamination process.	40
Figure 3.1: Ideal Lowpass Prototype Filter Response.	50
Figure 3.2: Lowpass Filter Form with Degree of n.	50
Figure 3.3: Lowpass to Lowpass Transformation.	53
Figure 3.4: Lowpass Prototype Transformation.	54
Figure 3.5: Highpass Response Transformation.	54
Figure 3.6: Highpass Transformation.	55
Figure 3.7: Bandpass Frequency Transformation.	55
Figure 3.8: Bandpass Transformation.	56
Figure 3.9: Bandstop Transformation.	57
Figure 3.10: Butterworth Lowpass Response.	58

Figure 3.11: Chebyshev Lowpass Response.	59
Figure 3.12: (a) Series Impedance Equivalence, (b) Parallel admittance Equivalence.	60
Figure 3.13: Bandpass Filter Equivalence.	61
Figure 3.14: Bandpass Filter Using Immittance Inverters.	63
Figure 3.15: Lumped Element Immittance Inverters.	64
Figure 3.16: Coupled Line Cross Section.	65
Figure 3.17: (a) Even Mode Excitation, (b) Odd Mode Excitation	65
Figure 3.18: (a) even mode excitation, (b) odd mode excitation.	68
Figure 4.1: Single Section Coupled Line Filter (a) Equivalent Circuit, (b) Coupled Line Structure.	72
Figure 4.2: J-inverter Cascaded Coupled Line Circuit.	76
Figure 4.3: Multi-Section Coupled Line Filter.	77
Figure 4.4: Equivalent Stub Filter J-inverter Circuit.	78
Figure 4.5: Short Circuit Stub Bandpass.	79
Figure 4.6: Optimum Distributed Highpass Filter.	80
Figure 4.7: Typical Filter Characteristic of Optimum Highpass Filter.	81
Figure 4.8: Transmission Line Network Representation of the Bandstop Filter.	83
Figure 4.9: Filtering Characteristic of the Bandstop Filter.	83
Figure 5.1: Nonlinear Device.	88
Figure 5.2: Typical Nonlinear Device Response.	90
Figure 5.3: 1 dB Compression Measurement Set Up.	91
Figure 5.4: Illustration of Second order Products.	92
Figure 5.5: Graphical Representation of IP 3 point.	94

Figure 5.6: IP3 Measurement Set Up.	97
Figure 5.7: Illustration of Cascade of Components.	98
Figure 5.8: Linear Dynamic Range on log-log Scales.	102
Figure 5.9: Spurious Free Dynamic Range Illustration.	103
Figure 6.1: Single Section Coupled Line Filter With Short Circuit Stubs for Reconfigurability (a) Equivalent Circuit, (b) Coupled Line Structure.	107
Figure 6.2: Reconfigurable Filter With Impedance Transformer Added.	111
Figure 6.3: Filter Designs (a) Narrowband, (b) Wideband.	112
Figure 6.4: Design of Implemented Filter with Narrowband Stubs.	113
Figure 6.5: Simulated results of the Coupled line Structure with Narrowband Stubs.	114
Figure 6.6: Simulated results of the Coupled line Structure with Wideband Stubs.	114
Figure 6.7: Fabricated reconfigurable filters: (a) Narrowband stubs, (b) Wideband Stubs.	116
Figure 6.8: Measured Filter Response of Filter with Narrowband stubs.	116
Figure 6.9: Measured Filter Response of Filter with Wideband stubs.	116
Figure 6.10: Case 1 (a) Layout, (b) State 1: $w = 5.6$ mm, (c) State 2: $w = 5.6$ mm, (d) State 1: $w = 0.2$ mm, (e) State 2: $w = 0.2$ mm	119
Figure 6.11: Case 2 (a) Layout, (b) State 1: $w = 5.6$ mm, (c) State 2: $w = 5.6$ mm, (d) State 1: $w = 0.2$ mm, (e) State 2: $w = 0.2$ mm	120
Figure 6.12: Case 3 (a) Layout, (b) State 1: $w = 5.6$ mm, (c) State 2: $w = 5.6$ mm, (d) State 1: $w = 0.2$ mm, (e) State 2: $w = 0.2$ mm	121
Figure 6.13: Case 4 (a) Layout, (b) State 1: $w = 5.6$ mm, (c) State 2: $w = 5.6$ mm, (d) State 1: $w = 0.2$ mm, (e) State 2: $w = 0.2$ mm	122
Figure 6.14: Case 5 (a) Layout, (b) State 1: $w = 5.6$ mm, (c) State 2: $w = 5.6$ mm, (d) State 1: $w = 0.2$ mm, (e) State 2: $w = 0.2$ mm	123
Figure 6.15: Filter Building Block with Four Bandwidth States.	124
Figure 6.16: Filter Obtained by Combining Both Filters from [2].	125

Figure 6.17: Simulated Insertion Losses (S21) of the Filter Circuit.	125
Figure 6.18: Simulated Return Losses (S11) of the Filter Circuit.	126
Figure 6.19: Fabricated reconfigurable filter block.	128
Figure 6.20: Simulated Insertion Losses (S21) of the Filter Circuit.	128
Figure 6.21: Measured Return Losses (S11) of the Filter Circuit.	129
Figure 6.22: IP3 of Coupled line filter With Wideband Stubs, when biasing current = 20 mA.	130
Figure 6.23: IP3 of Coupled line filter With Narrowband Stubs, when biasing current = 20 mA.	131
Figure 6.24: IP3 of Coupled line filter With Wideband Stubs, when biasing current = 50 mA.	131
Figure 6.25: IP3 of Coupled line filter With Narrowband Stubs, when biasing current = 50 mA.	132
Figure 6.26: Coupled Line Filter Combined.	132
Figure 6.27: 1 dB Compression measurement of coupled line filter with wideband stubs.	134
Figure 6.28: 1 dB Compression measurement of coupled line filter with narrowband stubs.	134
Figure 6.29: 1 dB Compression measurement of combined coupled line filter.	135
Figure 7.1: Single Section Coupled line Section with Impedance Transformer.	138
Figure 7.2: Single Section Coupled line Section with Impedance Transformer and stubs for	138
Figure 7.3: Graph in Order to Select the Stub Impedances.	139
Figure 7.4: Bandpass Filter Structure Once the Single is cascaded.	139
Figure 7.5: State 2 Impedances.	140
Figure 7.6: State 3 Impedances.	140
Figure 7.7: Filter Combined to Obtain State 2 and State 3.	140
Figure 7.8: S11 of Initially Designed Filter.	141
Figure 7.9: S21 of Initially Designed Filter.	141

Figure 7.10: S11 of Final Designed Filter.	142
Figure 7.11: S21 of Final Designed Filter.	142
Figure 7.12: Final Theoretical Design.	143
Figure 7.13: Microstrip Design with Bias Circuitry Included.	145
Figure 7.14: S11 Simulated Response.	146
Figure 7.15: S21 Simulated Response.	146
Figure 7.16: S11 Measured Response.	148
Figure 7.17: S21 Measured Response.	148
Figure 7.18: Filter With Maximum FBW = 50% Designed using Matthaei coupled line theory.	150
Figure 7.19: Reconfigurable Cascaded Coupled Line Filter.	150
Figure 7.20: Equivalent Stub Filter Circuit.	151
Figure 7.21: Simplified Reconfigurable Cascaded Coupled Line Filter.	154
Figure 7.22: Comparison between Simplified and Non - Simplified values; FBW = 60% and n = 7.	154
Figure 7.23: (a) Short circuit stub filter block with stubs switched on for reconfigurability. (b) Equivalent circuit.	155
Figure 7.24: Typical reconfigurable bandwidth responses of Figure 21 for n = 6, max FBW = 80 % filter designed using (7.1) – (7.16), $Z_{oe} = 85.437$, $Z_{oo} = 16.84$ (a) S11 (b) S21.	157
Figure 7.25: (a) Circuit schematic if the assumptions are met. (b) Decomposed circuit for cascade of the identical sections.	159
Figure 7.26: Comparison with and without assumptions implemented.	160
Figure 7.27: Coupled line structure derived from equivalent short circuit stub filter.	160
Figure 7.28: Variation of ripple fractional bandwidth against loaded short circuit stub impedance, Z_s.	161
Figure 7.29: Final circuit design for the reconfigurable filter having three reconfigurable bandwidth states (50%, 40% and 30%).	162
Figure 7.30: Theoretical S11.	162

Figure 7.31: Theoretical S21.	163
Figure 7.32: (a) Microstrip Re-entrant Mode Coupler Cross Section. (b) Even and Odd Mode Excitations.	164
Figure 7.33: (a) Variation of width of coupled lines on even and odd mode impedances, (b) Variation of gap on even and odd mode impedances.	166
Figure 7.34: 3D view of cascaded coupled line filter.	167
Figure 7.35: LCP Stack up.	168
Figure 7.36: (a) Top layer and (b) second layer of the designed multilayer reconfigurable filter.	169
Figure 7.37: Simulated S11 of the three distinct bandwidth states.	170
Figure 7.38: Simulated S21 of the three distinct bandwidth states.	170
Figure 7.39: Fabricated reconfigurable filter.	171
Figure 7.40: Measured S11 of the three distinct bandwidth states.	172
Figure 7.41: Measured S21 of the three distinct bandwidth states.	172
Figure 7.42: Cascaded Coupled Line Filter with Impedance Transformer.	174
Figure 7.43: Cascaded Coupled Line Filter without Impedance Transformer.	174
Figure 7.44: 1 dB Compression measurement of Cascaded Couple Line with Impedance Transformer.	175
Figure 7.45: 1 dB Compression measurement of Cascaded Coupled Line Filter Without Impedance Transformer.	175
Figure 8.1: Reconfigurable Filter Schematic.	179
Figure 8.2: Theoretical Responses of three designed states. (a) S21. (b) S11	181
Figure 8.3: Electronically reconfigurable wideband filter with all four states implemented.	182
Figure 8.4: EM-simulated responses of four states. (a) S21. (b) S11.	183
Figure 8.5: Fabricated electronically reconfigurable wideband filter.	185
Figure 8.6: Measured responses of the electronically reconfigurable wideband filter. (a) S21. (b) S11.	185

Figure 8.7: Measured wideband responses (S21) of the electronically reconfigurable wideband filter.	186
Figure 9.1: Highpass Filter Design with Calculated Values.	189
Figure 9.2: Theoretical Response Using [17].	189
Figure 9.3: New Circuit Parameters.	190
Figure 9.4: Theoretical Response with New Impedance Values and $\theta_0 = 90^\circ$.	190
Figure 9.5: Theoretical Response With $\theta_0 = 45^\circ$.	191
Figure 9.6: Highpass Filter Design.	192
Figure 9.7: Highpass Filter State 1.	192
Figure 9.8: Highpass Filter State 2.	193
Figure 9.9: State 1 with a second diode placed at the top of the stub, near the short circuit.	194
Figure 9.10: State 2 with the 2.3 GHz Stubs isolated from the circuit.	194
Figure 9.11: Highpass Filter design With Switchable Stepped Impedance Resonators.	195
Figure 9.12: State 1 of the final design of the highpass filter.	196
Figure 9.13: State 2 of the final design of the highpass filter.	196
Figure 9.14: Comparison of S11 to ascertain the resonance at 1.6 GHz.	197
Figure 9.15: SIR's connected ideally with no stubs.	197
Figure 9.16: SIR's ideally connected with switchable stubs.	198
Figure 9.17: Bandstop Filter Design.	199
Figure 9.18: Bandstop Response.	199
Figure 9.19: Lowpass Filter Design.	199
Figure 9.20: Lowpass Filter Response – State 1.	200
Figure 9.21: Lowpass filter parameters for state 2.	200

Figure 9.22: Lowpass Filter - State 2 Design.	201
Figure 9.23: Lowpass Filter Design with Bias Circuitry.	202
Figure 9.24: State 1 of the Lowpass Filter.	203
Figure 9.25: State 2 of the Lowpass Filter.	203
Figure 9.26: State 2 of the Lowpass Filter with a 1000 Ω Resistor in Series with the Inductors in the Bias Circuit.	204
Figure 9.27: Reconfigurable Microstrip Bandpass Filter.	205
Figure 9.28: Fabricated reconfigurable microstrip bandpass filter	206
Figure 9.29: Electronically Reconfigurable Bandpass Filter Response: (a) State 1, (b) State 2, (c) State 3, (d) State 4.	208
Figure 9.30: IP3 Measurements.	209
Figure 9.31: 1 dB Compression Measurement.	210
Figure 9.32: Improved Highpass Filter Design.	211
Figure 9.33: Improved Design Simulated State 1.	212
Figure 9.34: Improved Design Simulated State 2.	212
Figure 9.35: Improved Reconfigurable Filter Design.	213
Figure 9.36: Fabrication of New Designed Filter.	214
Figure 9.37: Response of Bandpass filter with newly designed Highpass Filter: (a) State 1, (b) State 2, (c) State 3 and (d) State 4	216

List of Tables

Table 2.1: Filter Response due to Diode biasing [32].	22
Table 4.1: Element values for the Optimum Distributed Highpass Filter with 0.1 dB ripple [3].	82
Table 4.2: Element values of optimum Bandstop Filter for $n = 2$ and $\epsilon = 1.005$	85
Table 4.3: Element values of optimum Bandstop Filter for $n = 3$ and $\epsilon = 1.005$	85
Table 4.4: Element values of optimum Bandstop Filter for $n = 4$ and $\epsilon = 1.005$	85
Table 4.5: Element values of optimum Bandstop Filter for $n = 5$ and $\epsilon = 1.005$	86
Table 4.6: Element values of optimum Bandstop Filter for $n = 6$ and $\epsilon = 1.005$	86
Table 6.1: Simulated Performance of the Filters Designed.	115
Table 6.2: Simulated Performance of the Filters Designed.	117
Table 6.3: Simulated Performance of Combined Filter.	126
Table 6.4: Measured Performance of Combined Filter.	129
Table 7.1: Simulated Performance.	147
Table 7.2: Measured Performance.	148
Table 7.3: Cascaded Coupled Line Filter Comparison.	164
Table 7.4: Simulated Performance.	171
Table 7.5: Measured Performance.	173
Table 8.1: Circuit Dimensions.	183
Table 8.2: Simulated Performance.	184
Table 8.3: Summary of Measured Performance.	186
Table 9.1: Simulated Performance.	205
Table 9.2: Measured Performance.	206
Table 9.3: Summary of Improved Design Performance (a) Simulated, (b) Measured	216

List of Publications by Candidate

A. Miller, J. Hong, “Wideband Bandpass Filter with Reconfigurable Bandwidth,” *IEEE Microwave and wireless components letters*, Vol. 20, No. 1, Jan 2010, pp 28 – 30.

A. Miller, J. Hong “Wideband Bandpass Filter with Multiple Reconfigurable Bandwidth States,” European Microwave Conference, Sep 2010, pp 1273 – 1276.

A. Miller, J. Hong, “Reconfigurable Cascaded Coupled Line Filter with Four Distinct Bandwidth States,” *IET Microwave Antennas and Propagation*, vol. 5 issue 4, Nov 18 2011, pp 1730 – 1737

A. Miller, J. Hong “Cascaded Coupled Line Filter with Reconfigurable Bandwidths Using LCP Multilayer Circuit Technology,” *IEEE Transactions on Microwave Theory and Technology*, Vol. 60, No. 6, June 2012, pp 1577 – 1586.

A. Miller, J. Hong, “Electronically Reconfigurable Multi-Channel Wideband Bandpass Filter With Bandwidth and Center Frequency Control,” *IET Antennas and propagation (in press)*

A. Miller, W. Tang, J. Hong, “Reconfigurable Filter with Frequency and Bandwidth Control Using a Cascaded Highpass/Lowpass Architecture,” *IEEE Microwave and wireless components letters* (being reviewed)

Chapter 1: Introduction

The electromagnetic spectrum is the range of all possible frequencies of electromagnetic radiation and can be divided into a number of frequency bands. Initially, the only known part of the spectrum was light. The ancient Greeks studied some of light's properties such as refraction and reflection, as they realized that light travels in straight lines. This study continued during the 16th and 17th century with many conflicting theories emerging as to whether light was a wave or particle. Michael Faraday in 1845 first linked it to electromagnetism when he noticed that it responded to a magnetic field. The first electromagnetic waves other than light were discovered by William Herschel in 1800, which he observed infrared. He noticed that the hottest temperature was beyond red which led him to believe that there was light which could not be observed. In 1801, Johann Ritter worked on the other end of the spectrum and observed rays beyond visible violet rays, which were later renamed ultraviolet. In the 1860s it was realised by James Maxwell that electromagnetic waves travelled at the speed of light. He then developed four partial differential equations to explain this correlation. Heinrich Hertz in 1886 attempted to prove Maxwell's equation by setting up an experiment to generate and detect radio waves. In doing so he observed that they travel at the speed of light and could be reflected and refracted. Later he eventually produced and measured microwaves, which paved the way for wireless telegraph and the radio. A new type of emission was discovered in 1895 during an experiment by Wilhelm Röntgen which he called x-rays. It was found that they were able to travel through parts of the human body but were reflected by denser matter such as bones, leading to many uses in medicine. The last portion of the electromagnetic spectrum was filled in with the discovery of gamma rays in 1900 when Paul Villard was studying radioactivity. His first theory was that they were similar to alpha and gamma particles. However, Ernest Rutherford measured their wavelengths in 1910 and found they were electromagnetic waves. **Figure 1.1** illustrates the Electromagnetic Spectrum.

The part of the spectrum which this thesis is concerned with is that of the RF/Microwave spectrum. The frequency ranges of microwaves are from 300 MHz to 300 GHz, which correspond to wavelengths ranging from 1 m to 1 mm. Between RF and Microwave spectrums the boundary is arbitrary, which obviously depends on the specific technology

being used. This meaning that the RF/Microwave applications can be extended to a number of different systems, which may include but not restricted to:

- communications
- radar
- navigation
- space
- sensing
- medical instrumentation

The applications mentioned all operate within the region of around 300 KHz to 300 GHz of the electromagnetic spectrum, with these being further divided into other frequency bands (please see **Figure 1.1**)

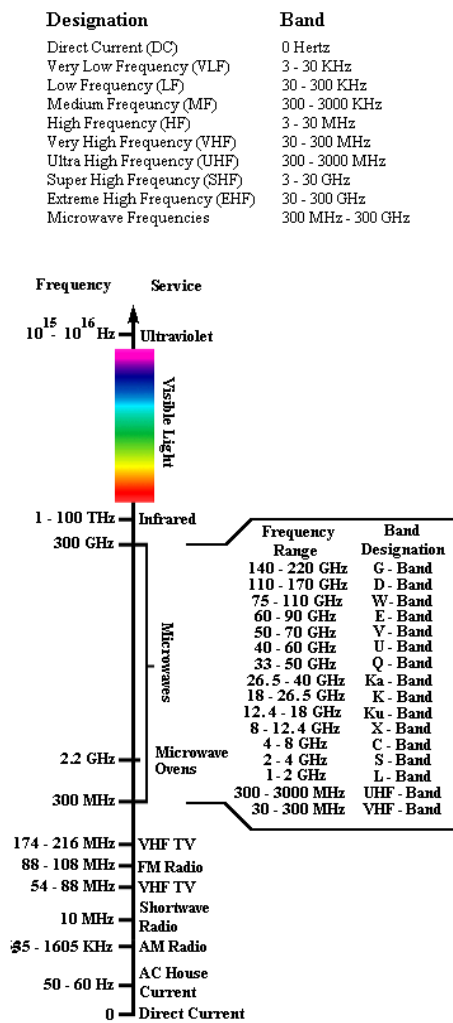


Figure 1.1: Electromagnetic Spectrum

In addition, it is apparent that the electromagnetic spectrum is limited and has to be shared, making filtering an important concept in RF/Microwave applications. The main function of a filter is to either separate or combine different frequencies and discriminate between wanted and unwanted frequencies. This makes them useful in order to confine the RF/Microwave signals within the assigned spectral limits discussed. They can be realised in a variety of ways which include waveguide, coaxial line or microstrip for instance; either as a lumped element or distributed circuits. More stringent requirements are being placed on filters as the emerging applications require more functionality. These requirements may include:

- Higher Performance
- Smaller Size
- Lighter weight
- Lower cost

As these multifunctional capability requirements increase, further development of new technologies is required, namely reconfigurable/tunable filters. With this increasing demand of this technology, it is thought that these will be an essential part of wireless communication systems in the future. Many systems require a filtering system with switchable/tunable frequency and/or bandwidth states. The method which this is carried out at the moment is using filter banks. A typical filter bank is illustrated in **Figure 1.2** which on inspection takes up a lot of space and requires high loss multi-throw switches. As mentioned, there is an ever increasing demand for more functionality meaning an increasing demand to develop reconfigurable/tunable filters. This forms the main focus of this thesis with preferred outcome a filter with simultaneous frequency and bandwidth control. By doing so this will save board space and hopefully allow more functionality to be added to systems such as but not limited to:

- Broadband receiver
- Wideband sampler
- Military Radar Systems
- Satellite Communication system

It is hoped that the filter banks in these systems will be replaced by reconfigurable/tunable filters at some stage in the future (see **Figure 1.2**).

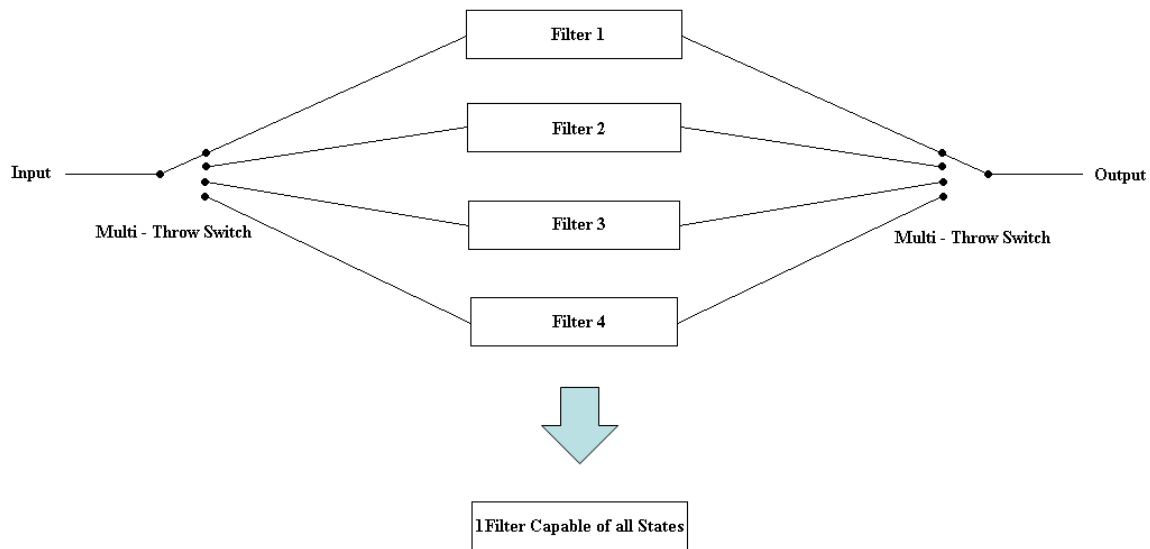


Figure 1.2: Filter Bank Illustration.

Obviously, there have been a number reconfigurable/tunable filters developed before but this thesis aims to enhance this. As there are gaps in the research with regard to wideband applications which require wideband filtering techniques. This has been made possible with the enhancement of a number of novel materials and fabrication techniques, for instance:

- Monolithic Microwave Integrated Circuits (MMIC)
- Microelectromechanical systems (MEMS)
- High Temperature Superconductor (HTS)
- Low Temperature Cofired Ceramics (LTCC)
- Liquid Crystal Polymer (LCP)

These have all contributed to the development of different types of filters and not just reconfigurable. In addition, there has also been a development in components used such as pin diodes and MEMS switches (used for discrete Reconfigurability) and varactors (used for continuous Tuning). (See **Figure 1.3**)

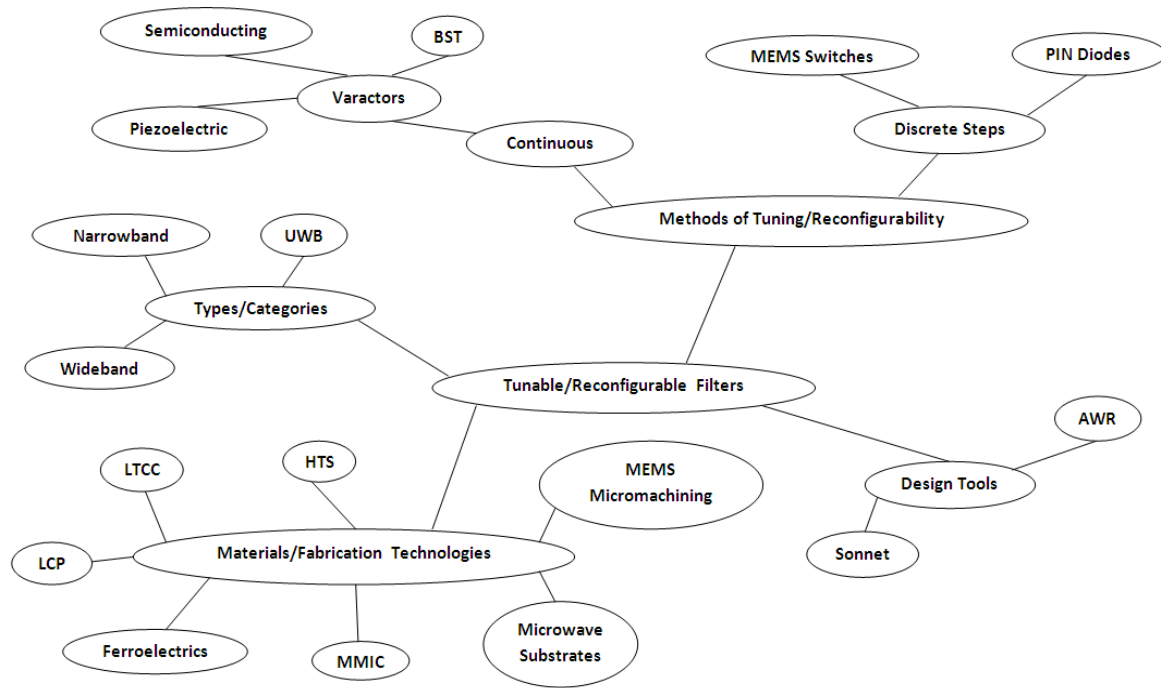


Figure 1.3: Reconfigurable/Tunable Filter Linkage.

The content of this thesis is organised as follows:

Chapter 2 gives an overview of what type of filters have been developed in the past and a description on what kind of filters this thesis intends to deal with. It also gives a description of LCP, why it is attractive and the fabrication technique used for filters designed in this thesis using LCP.

Chapter 3 introduces basic concepts and theories for the design of general filters. The topics covered include Transfer functions, lowpass prototype filters, frequency element transformations, Immittance inverters, introduction of coupled lines and stepped impedance resonators.

Chapter 4 outlines the filter topologies used in this thesis to develop the reconfigurable filters illustrated. It outlines the design theory of each and is referred to in a number of subsequent chapters.

In Chapter 5, the system integration problems are considered as to make the filters tunable/reconfigurable active components are introduced. This gives rise to a number of potential problems, namely 1 dB compression point and the third intercept point.

In Chapter 6, a single section coupled line structure is introduced and shows how the theory shown in chapter 4 can be used to design a reconfigurable bandpass filter. It also explains why such a topology was investigated. Two filters were designed and tested with two states; these were then combined in order to obtain a filter with four bandwidth states. This work culminated into two papers:

A. Miller, J. Hong, “Wideband Bandpass Filter with Reconfigurable Bandwidth,” *IEEE Microwave and wireless components letters*, Vol. 20, No. 1, Jan 2010

A. Miller, J. Hong “Wideband Bandpass Filter with Multiple Reconfigurable Bandwidth States,” European Microwave Conference, Sep 2010

Chapter 7 takes the single section filter and then shows how a higher order filter of the same type can be designed and tested. The filters designed are bandwidth reconfigurable with the fractional bandwidths ranging from around 20% to 50%. Again this led to two journal papers being published:

A. Miller, J. Hong, “Reconfigurable Cascaded Coupled Line Filter with Four Distinct Bandwidth States,” *IET Microwave Antennas and Propagation*, vol. 5 issue 4, Nov 18 2011, pp 1730 – 1737

A. Miller, J. Hong “Cascaded Coupled Line Filter with Reconfigurable Bandwidths Using LCP Multilayer Circuit Technology,” *IEEE Transactions on Microwave Theory and Technology*, (in Press)

Chapter 8, enhances the coupled line concept, by introducing frequency tunability as it is very desirable for communication systems to have multichannel capabilities. This also produced an IET journal paper:

A. Miller, J. Hong, “Electronically Reconfigurable Multi-Channel Wideband Bandpass Filter With Bandwidth and Center Frequency Control,” *IET Antennas and propagation* (in press)

Chapter 9 illustrates a cascaded highpass/lowpass filter configuration; where a reconfigurable highpass and reconfigurable lowpass are used in order to obtain a reconfigurable bandpass filter. This filter concept seems to be the most flexible when designing such a filter due to the simplicity of the concepts. The main points of these concepts are contained in the components letter paper:

A. Miller, W. Tang, J. Hong, “Reconfigurable Filter with Frequency and Bandwidth Control Using a Cascaded Highpass/Lowpass Architecture,” *IEEE Microwave and wireless components letters* (being reviewed)

Finally, chapter 10 is a summary of the work carried out in this thesis and also gives future work which could culminate into further PhD research project.

Chapter 2: Background

2.1) Introduction

Advances in many microwave systems and applications with multifunction capabilities means that there is an increasing demand to develop reconfigurable filters. Tunable/reconfigurable filters are essential for future wireless communication systems across commercial, defence and civil sectors. Microwave filter technologies hold the key to controlling the spectrum of RF signals and eliminating interference and preserving their dynamic range under any signal receiving conditions. Tunable/reconfigurable filters can be realised in a variety of ways, but no matter what method of tuning used they must conserve their transmission and reflection co-efficient over the tuning range specified. They offer many advantages over traditional filter banks, with the main two being size and flexibility.

Many tunable filters have been investigated in the past which control the center frequency [1] – [26]. The tunability of the center frequency is easily achieved by using reactive elements whose reactance values can be modified either continuously or by discrete amounts. There have been many filter structures proposed with varactors being the most popular choice to control the center frequency continuously, with there being different types, namely semiconducting [4] – [10], BST [11], [12] and piezoelectric [13], [14]. The reason for this is that they require the least amount of circuitry required for biasing. Conversely, tuning the center frequency in discrete steps has been gaining more and more popularity [15], [16] with the enhancements of PIN diode technology due to their lower RF losses and signal distortion compared to varactors, especially relating to wideband and ultra wideband applications where broad tuning ranges are desirable. However, when a large number of tuning steps are required, a proportionate number of switching elements and bias circuits are needed. This increases the circuit complexity and deleterious parasitic effects can become an issue. Moreover, the introduction of microelectromechanical switches has also contributed to this shift of method due to their low dc consumption and RF losses and their power handling capabilities [17] – [26]. These have high isolation without the need of bias circuits; however they have lower switching speeds than PIN diodes and have limited switching life.

On the contrary to tunability of center frequency, less effort has been made in tunability of bandwidth. A reason for this is the lack of methods to vary the inter-resonator couplings [27]. There have been a number of papers which have tackled this problem using a variety of methods; with some dealing with simultaneous control of center frequency and bandwidth [27] – [38] and others concentrating solely on bandwidth tunability at a fixed center frequency [39] – [43].

On inspection of the literature, it is clear that most of the reported methods of bandwidth and center frequency tunability are for narrowband applications. For this reason there is an ever increasing demand for reconfigurable wideband filter capable of simultaneous control of center frequency and bandwidth. This forms the main focus of this research project.

Due to the demands and complexity required for simultaneous control of frequency and bandwidth, multilayer circuitry can be used to give an extra dimension and give a bit of extra flexibility in filter design. After carefully consideration of the literature, Liquid Crystal Polymer (LCP) shows good promise in fabricating microwave filter circuits. LCP film has good electrical characteristics; which include static dielectric constant across a very wide frequency range, low water absorption and thermal expansion coefficients [44]. Multilayer fabrication using LCP is possible due to there being two types of LCP materials with different melting points. Core layers of a multilayer arrangement can be obtained by using the high temperature LCP (315°C), while the low temperature LCP (290°C) can be used as bonding ply. This means that multilayer designs can be realised similar to those in LTCC. Another advantage is the lower fabrication cost compared to LTCC, which makes it an attractive material for system-in-package based microwave and millimetre-wave applications, with this circuitry being utilised in ultra wideband filter design [45] – [47]. LCP is not a new idea for microwave circuits and has been around from the 1990s [48] – [50]. However, LCP has many fabrication difficulties, which have been overcome with this forming the main research focus over a number of years [51] – [59]. For example, one method was developed to solve tearing problems was a biaxial extrusion process, which gives the material uniform strength and it also creates additional processing benefits. Many of the limitations were overcome by 2002, and have been available commercially in thin films with single and double copper cladding since December 2001 and June 2003, respectively. This prompting new application of LCP, for example, the use in ultra wideband filters design [45] – [47].

This chapter highlights the work that has been already carried out and achieved in obtaining reconfigurable filters so far. It also shows the LCP fabrication process which was used on some of the circuitry designed in this thesis, in accordance with Rogers’s guidance notes. The reviews of different techniques were carefully considered in order to generate new ideas and develop reconfigurable filters with simultaneous control of frequency and bandwidth; some using LCP Fabrication.

2.2) Reconfigurable Bandwidth at a Fixed Center Frequency

2.2.1) Reconfigurability Achieved Through Switched Circuitry

One of the earliest papers to tackle the issue of bandwidth tunability was “Reconfigurable Bandpass Filter with a Three-to-One Switchable Pass band Width,” by Christen Rauscher [39]. The filter presented in the paper uses a mix of quasi – lumped elements and distributed circuit elements. Pin diodes were used in order to switch the reactance of the circuit seen by the ports. The filter can be switched between two discrete states with widely differing bandwidths of 500 and 1500 MHz, while keeping the center frequency at 10 GHz. The circuit layout and equivalent circuit are shown below:

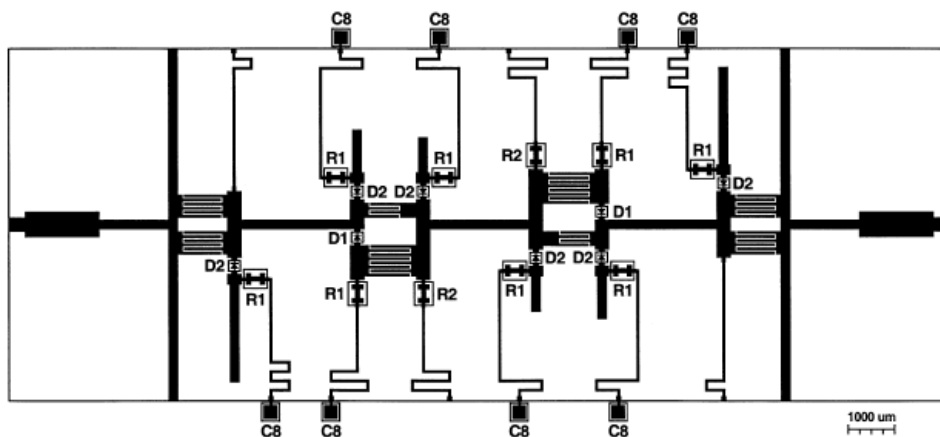


Figure 2.1: Circuit Layout for Bandpass Filter. [39]

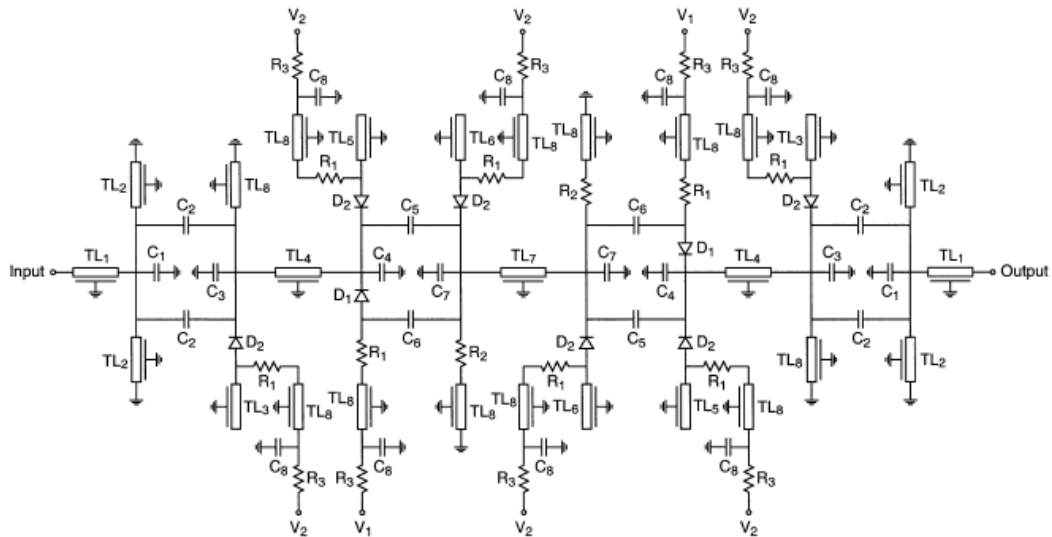


Figure 2.2: Equivalent Circuit for the Bandpass Filter. [39]

It can be clearly seen from the above layouts that by simply switching the diodes D1 and D2 the circuit geometry changes meaning that inter-resonator coupling is subsequently altered. This results with a filter that can be switched between a narrow band state and a wideband state. If the diodes D1 are forward biased the inter-resonator coupling is maximised because of the parallel connection of the interdigital capacitors represented by C5 and C6; if the diodes D2 are reversed biased simultaneously the open - circuited transmission - line stubs TL₃, TL₅ and TL₆ are isolated from the circuit thus switching to the filters wide - band state. For the narrow - band state opposite conditions are applied to diode sets D1 and D2. The paper showed that the measured results were of the same nature to the simulated with some discrepancies, which were accounted for due to manufacturing tolerances. The following shows the measured and simulated results:

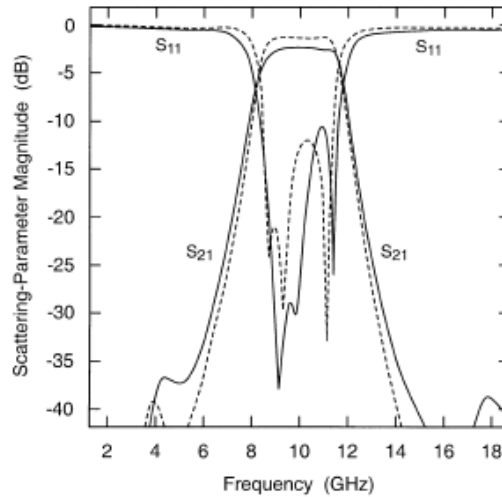


Figure 2.3: Magnitude responses of filter transmission co-efficient for the wide-passband setting, the dotted line being the calculated and the solid line being the measured [39].

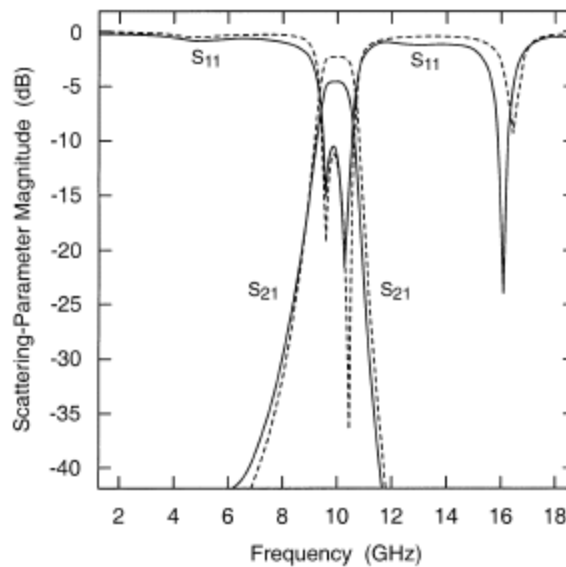


Figure 2.4: Magnitude responses of filter transmission co-efficient for the narrow-passband setting, the dotted line being the calculated and the solid line being the measured [39].

When comparing the narrow-band and wide-band states, it can be clearly seen that the insertion loss differs roughly by a factor of two. It can also be seen that there is a change in bandwidth of three-to-one.

2.2.2) Reconfigurability Achieved Through Altering Geometries of Circuitry

As mentioned in many papers regarding bandwidth tunability, the inter resonator coupling has to be altered to achieve this. This was investigated in the components letter “Adjustable bandwidth Filter Design Based on Interdigital Capacitors,” by Li Zhu, Vijay Devabhaktuni, Chunyan Wang, Ming Yu [40] which compares an open end gap, an interdigital capacitor with a rectangular ground plane below the interdigital capacitor or etched slots. The following layouts were compared:

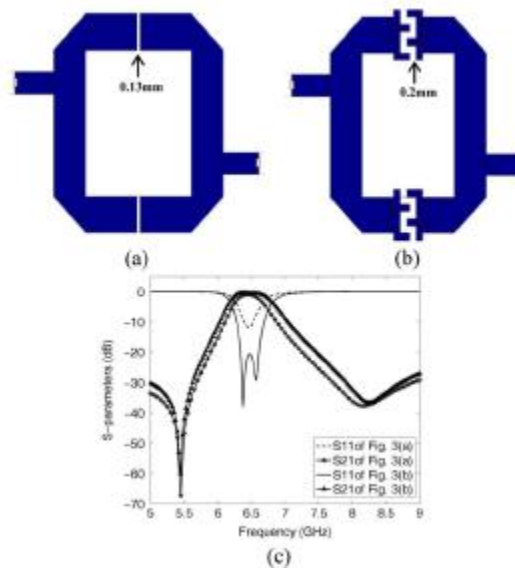


Figure 2.5: (a) layout of open end gap, (b) layout of proposed interdigital, (c) comparison of results. [40]

It can be clearly seen from the simulations that the interdigital capacitor shows a wider bandwidth because of the stronger coupling effect. The paper also shows the effect of increasing the number of fingers of the interdigital capacitor which increases the bandwidth while keeping the center frequency constant by adjusting the lengths of the harpin resonators. The etched slots layout was then compared and it was found that the bandwidth increased even further but with a change in quality factor meaning higher losses. There was a slight increase in f_0 which was countered by increasing N , the number of fingers.

Another paper, “Reconfigurable Bandpass filter with Variable Bandwidth at 5.8 GHz using a Capacitive Gap Variation Technique,” [41] also shows that changing the geometry of the circuit, the bandwidth can be reconfigured. The bandwidth is tuned at center frequency 5.8 GHz from a narrowband with a 4% bandwidth and wideband state with a 10% bandwidth, the following filter structure was employed:

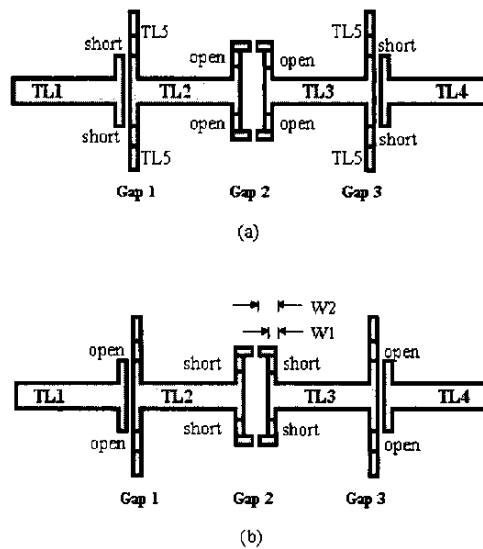


Figure 2.6: Structure of the filter, (a) Narrowband (b) Wideband [41].

The inner gap 2 is responsible for the bandwidth (i.e. the frequency separation between the resonant poles), as this is the inter-resonator coupling of the resonators. It can be clearly seen from **Figure 2.6 (b)** that the capacitance in the gap is increased when the short connections are placed, hence a change in bandwidth, namely a wideband configuration. Likewise, from **Figure 2.6 (a)** the open connections cause a much narrower gap, thus a narrowband configuration. However as the gap is changing there is also a shift in center frequency due to the change in resonator lengths. In order to avoid this Cesar Lugo Jr. et al introduced lateral extensions TL5 as seen from **Figure 2.6**. For instance when the inner gap 2 connections are open (narrowband configuration) the outer gaps 1 and 3 are shorted in order to keep a constant resonator length and vice versa for the wideband configuration. The following responses were obtained:

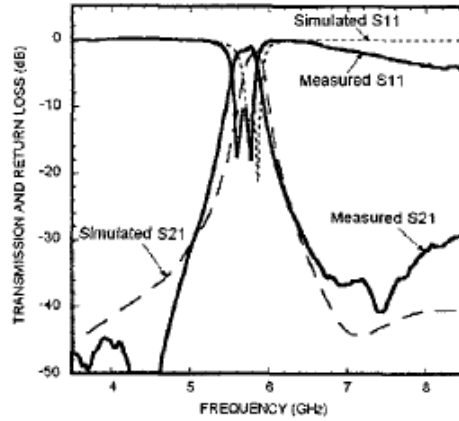


Figure 2.7: Measured vs. simulated transmission and return loss of the filter in the narrowband state [41].

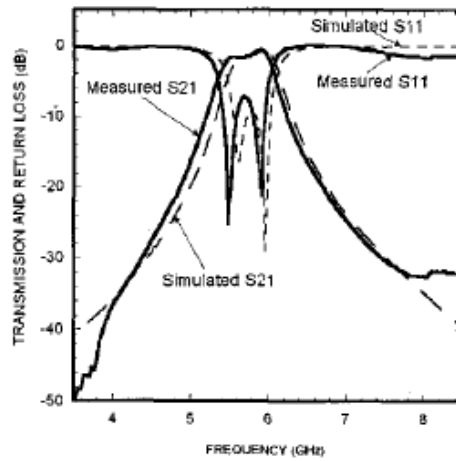


Figure 2.8: Measured vs. simulated transmission and return loss of the filter in the wideband state [41].

In the narrowband state the filter had an insertion loss of 1.821 dB at the center frequency, whereas in the wideband state the filter exhibits a 1.564 dB insertion loss.

2.2.3) Tunable Filter Using Piezoelectric Structure

In [42], the authors propose the design of a tunable filter using a lumped element model of a piezoelectric resonator. The paper shows the design through a lump element model of the piezoelectric resonator filter. A typical schematic of a piezoelectric resonator is shown below:

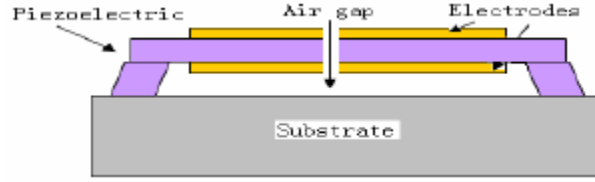


Figure 2.9: Schematic of Piezoelectric Resonator. [42]

If an ac signal is applied to the device with a frequency the same as the resonant frequency of the piezoelectric device the impedance is at a minimum. Conversely, the impedance is a maximum when the frequency of the ac signal is the same as the ant-resonant frequency. From ANSYS analysis and simulation a lumped model of the piezoelectric resonator is derived:

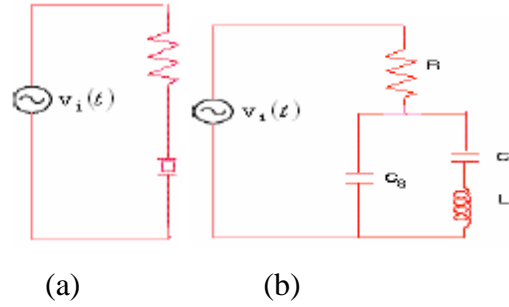


Figure 2.10: (a) Circuit Diagram of Piezoelectric Resonant Filter, (b) Schematic View of lumped Model of the Piezoelectric Circuit Element. [42]

From the analysis, the authors show that the resonant and anti resonant frequencies f_r and f_a can be represented:

$$f_r = \frac{1}{2\pi} \frac{1}{\sqrt{L_1 C_1}} \quad \text{And} \quad f_a = \frac{1}{2\pi} \sqrt{\frac{1}{L_1} \left(\frac{1}{C_s} + \frac{1}{C_1} \right)} \quad (2.1)$$

The net difference between the two is reported by the paper to be the intrinsic character of the piezoelectric device and has a direct effect on the bandwidth of the filter. The paper develops this further by applying a micro machined tunable capacitor, C_t , in parallel with the filter. This meaning that the expression for the anti-resonant frequency becomes:

$$f_a = \frac{1}{2\pi} \sqrt{\frac{1}{L_1} \left(\frac{1}{C_s + C_t} + \frac{1}{C_1} \right)} \quad (2.2)$$

It is shown that this capacitor will lower the anti-resonant frequency and hence lower the bandwidth. This implies that by adjusting the value of C_t , the bandwidth of the filter can be directly controlled. Similarly, a tunable inductor L_t can be placed in parallel with the filter, this making the equivalent impedance:

$$Z_e = \frac{1}{j\omega C_s + \frac{j\omega C_1}{1 - \omega^2 L_1 C_1} + \frac{1}{j\omega L_t}} \quad (2.3)$$

From manipulation of the expression it can be shown that, two anti – resonant frequencies exist when:

$$\omega^4 C_s L_t C_1 L_1 - \omega^2 (C_s L_t + C_1 L_t + C_1 L_1) + 1 = 0 \quad (2.4)$$

This implies that a resonant frequency is between two anti - resonant frequencies. This meaning that only one piezoelectric resonant filter with a tunable inductor rather than a ladder structure can behave like a bandpass filter. In summary, the paper illustrates the capacitor can easily control the bandwidth; while the use of an inductor can control the bandwidth.

2.3) Reconfigurable Center Frequency and Bandwidth

2.3.1) Use of Varactor Elements for Simultaneous Tunability of Center Frequency and Bandwidth

In order to tackle the issue of control of bandwidth and center frequency the paper “Tunable Comblin Filter with Continuous Control of Center Frequency and Bandwidth,” use coupling reducers in order to vary the inter-resonant coupling in a comblin filter structure. The coupling reducers are made up of line segments ending in a variable capacitor. A classic second-order comblin filter and equivalent circuit looks like:

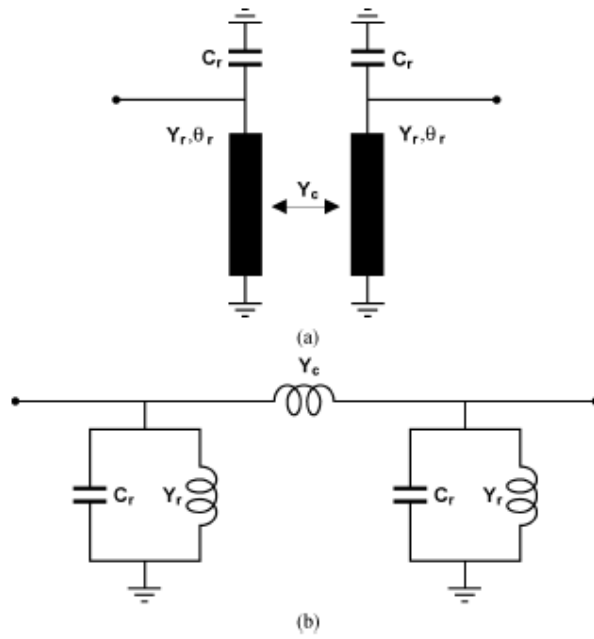


Figure 2.11: (a) Classic Second - Order Comblne Filter. (b) Equivalent Circuit. [27]

The paper then shows the structure of the equivalent circuit with the coupling reducer inserted:

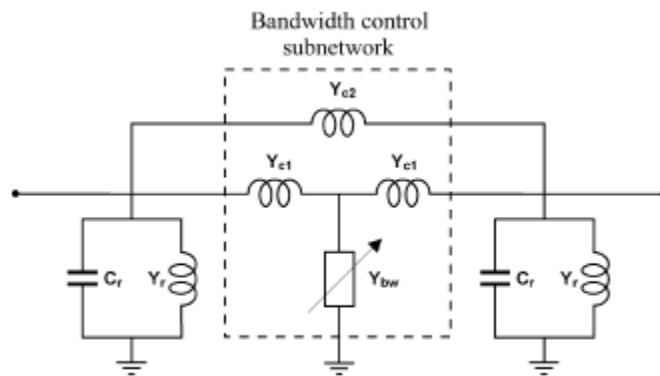


Figure 2.12: Bandpass Filter Structure with Coupling Reducer. [27]

With the topology being shown as follows:

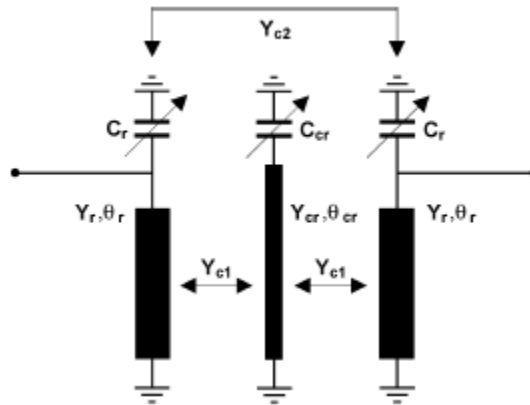


Figure 2.13: Topology With Coupling Reducer Inserted. [27]

With reference to **Figure 2.12** the paper investigates two extreme cases in which the admittance, Y_{bw} is varied, these being $Y_{bw} \rightarrow 0$ and $Y_{bw} \rightarrow \infty$. In the first case Y_{bw} is an open circuit resulting in the sub network having an admittance of $Y_{C1}/2 + Y_{C2}$. With reference to the latter case Y_{bw} acts as a short circuit meaning that the sub network has an equivalent admittance equal to Y_{C2} . On inspection of the equivalent admittances it can be clearly seen that the pass band width is varied as Y_{bw} is varied between $0 \rightarrow \infty$. This however, will modify the center frequency as the equivalent conductor length will change with the equivalent admittance changing as:

$$\theta_0 = \arctan\left(\frac{Y_r + Y_c}{2\pi C_r f_0}\right) \quad (2.5)$$

With this in mind variable capacitors are added to the combine resonators in order to tune the deviation in center frequency caused by the change of resonator length, as shown in **Figure 2.13**.

In addition, further work was carried out in two papers, namely, “A Reconfigurable Filter Based on Doublet Configuration” and “Varactor-Tuned Hairpin Bandpass Filter with an Attenuation Pole.”[28] and [29] both papers present an E shaped resonant topology with varactors on the ends of the resonators:

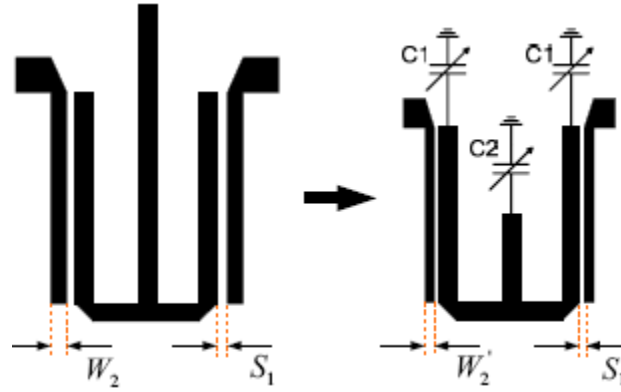


Figure 2.14: Topology With Coupling Reducer Inserted. [28]

These papers both use a hairpin structures and it can be clearly seen that the open stub with variable capacitor C2 can be used in order to control the bandwidth. Similarly all three capacitors are used to tune the centre frequency. The Hairpin filter designed in the in [28] had the following specification:

Bandwidth Tuning Range: 300 MHz

Centre Frequency Tuning Range: 300 MHz

Number Of Filter Orders: two

Type: 0.01-dB Chebyshev

The open stub enables the reduction in filter size as well as improved characteristics at the skirt frequencies. The filter is of compact size and has a wide-tuning range applicable to ultra-wideband systems.

Another compact structure was utilised in [30] and [31], where Emmanuel Pistono et al present a compact hybrid tune-all bandpass filter based on coupled slow wave resonators. The filter topology proposed is as follows:

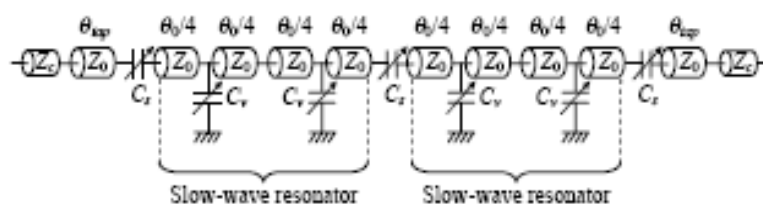


Figure 2.15: Topology Used in [30] and [31].

The shunt capacitors C_v are used in order to tune the electrical lengths of the slow wave resonators. The resonators are loaded at the far ends by series varactors C_s in order to tune the couplings between the resonators. The -3 dB bandwidth of the filter can be tuned between 50 and 78MHz and has a $\pm 18\%$ center frequency tuning around 0.7 GHz.

2.3.2) Use of PIN Diodes for Simultaneous Reconfigurability of Center Frequency and Bandwidth

PIN diodes can allow the manipulation of a filter topology in order to tune the bandwidth and center frequency. Cesar Lugo Jr. and John Papapolymerou [32] use these devices to do just that with the following configuration:

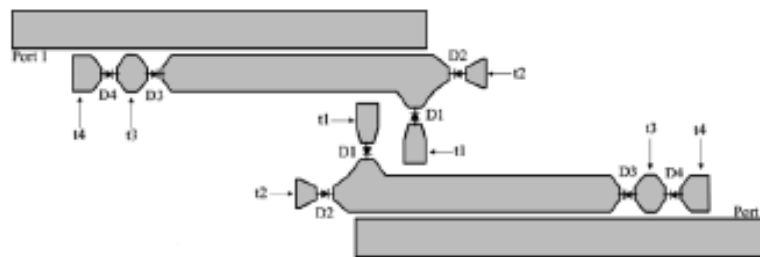


Figure 2.16: Proposed Filter Design with Pin diodes [32].

The topology produces filter responses with center frequencies $f_0 = 9, 10$ and 11 GHz with independent bandwidth control with an average tunable passband ratio of 1.73:1. Within the wideband configuration the bandwidth ranges from 13.4% to 14.7% and the narrowband configuration ranges from 7.7% to 8.5%. The fractional bandwidth is controlled by the set of diodes D1 and D2, wideband response is produced when D1 is forward biased and D2 is reversed biased. By doing this stubs t1 are connected to the circuit reducing the relative distance and increasing the coupling factor k . On the other hand, a narrowband response is created by forward biasing D1 and reverse biasing D2 thus reducing the coupling co-efficient, while compensating for the loss of resonator lengths with the connection of stub t2. Conversely, tuning of centre frequency is achieved through biasing diodes D3 and D4 thus isolating and connecting line sections t3 and t4 depending on how the diodes are biased. With regard to t3 and t4 stubs, these are designed in such a way to avoid excessive input/output coupling with the narrower side located closer to the coupling sections. A

reason for this is to eradicate as much as possible any undesired large ripples in the passband. The following table gives an overview of the filter configuration with switching diodes on and off:

Response Type	Center Frequency	D1	D2	D3	D4
Wideband	11 GHz	ON	OFF	OFF	OFF
Wideband	10 GHz	ON	OFF	ON	OFF
Wideband	9 GHz	ON	OFF	ON	ON
Narrowband	11 GHz	OFF	ON	OFF	OFF
Narrowband	10 GHz	OFF	ON	ON	OFF
Narrowband	9 GHz	OFF	ON	ON	ON

Table 2.1: Filter Response due to Diode biasing [32].

The following responses were achieved in the wideband and narrowband state:

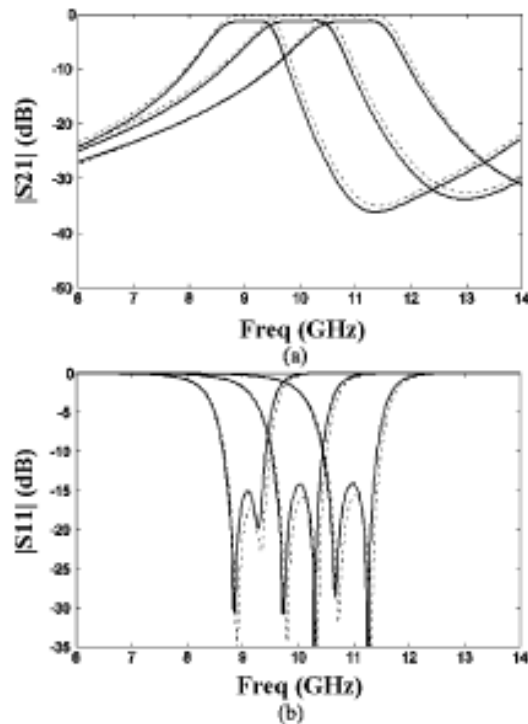


Figure 2.17: Wideband Results, measured (solid line), Simulated (dashed line). (a) Transmission loss, (b) Return Loss [32].

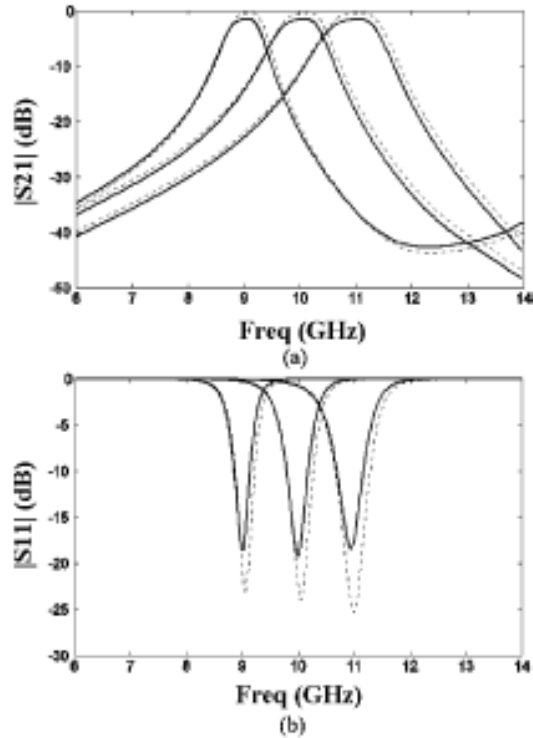


Figure 2.18: Narrowband Results, measured (solid line), Simulated (dashed line). (a) Transmission loss, (b) Return Loss [32].

The passband ratio between the narrow-band and wide-band states were 1.75:1, 1.73:1, 1.70:1 for f_0 being 9, 10 and 11 GHz respectively. The narrow band filter configuration had slightly higher insertion losses than the wide band ranging from 1.84 to 1.92 dB; while the wideband had insertion losses ranging from 1.74 to 1.79 dB.

2.3.3) Use of MEMS Devices for Simultaneous Reconfigurability of Center Frequency and Bandwidth

With development of MEMS devices, it has been increasingly beneficially to implement them in filter topologies (RF MEMS). This is due to their unique characteristics, which include – low loss, low power consumption and high linearity; making them suitable to build a low loss tunable filter. However, the drawbacks are the switching speed (compared with pin diodes) and limited switching life. To the best of one’s knowledge the earliest filter topology is that in [33] which use MEMS cantilevers as variable capacities attached to dual behaviour resonators (DBR) which are based on the parallel association of two different open – ended stubs. A pass band is created between the two transmission zeroes on each stub. The central

frequency and bandwidth tuning is obtained by adding MEMS cantilevers at the end of the open – ended stubs. A basic DBR resonator is illustrated within the paper:

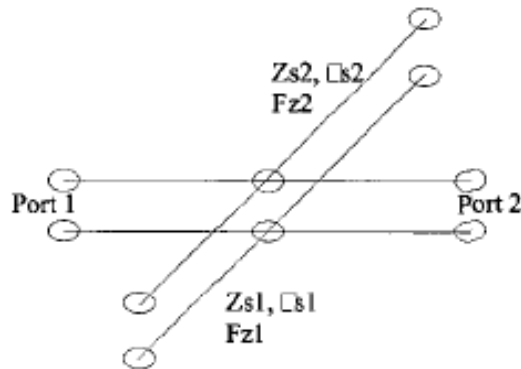


Figure 2.19: Basic DBR Resonator. [33]

It was proposed within the paper that by modifying the stub electrical characteristics the central frequency and bandwidth can be modified. An ideal second order DBR filter with variable capacitors C1 and C2 is shown:

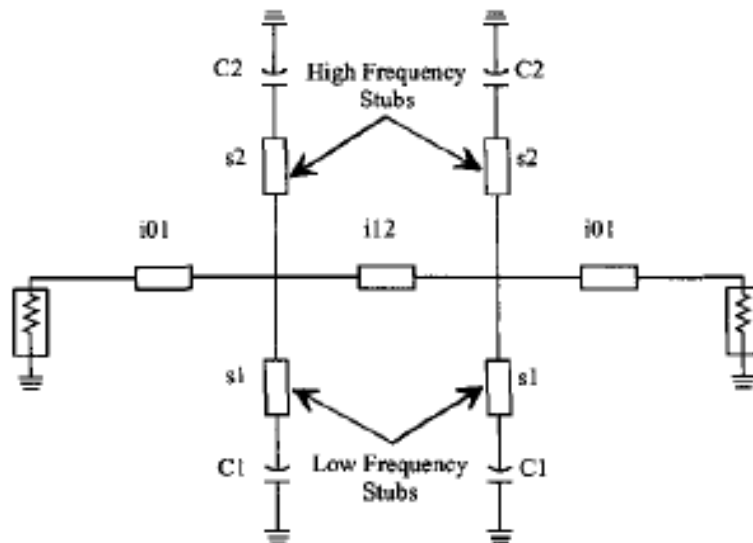


Figure 2.20: Ideal Second Order DBR Filter. [33]

The tunability of both the bandwidth and center frequency can be both controlled independently and simultaneously through varying the capacitances. The MEMS cantilevers are used in their stable region as their capacitance region is low. The following simulated responses were obtained for the second order topology used:

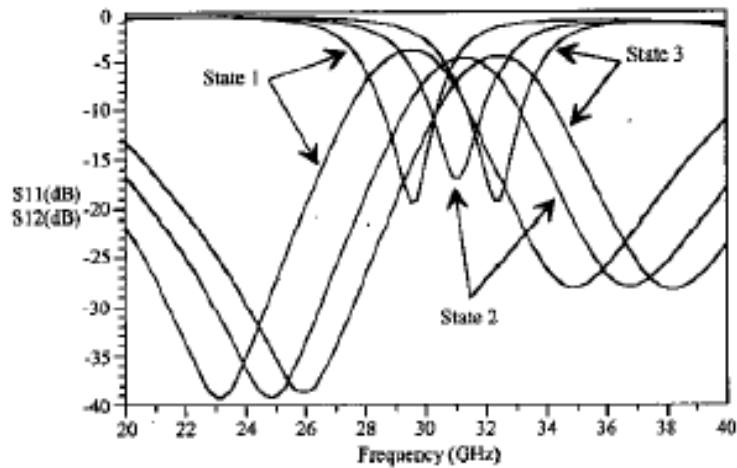


Figure 2.21: Simulated S-parameters for central frequency tuning [33].

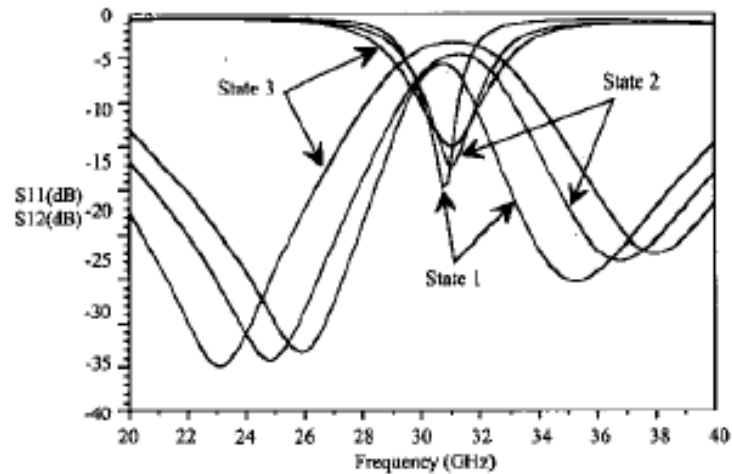


Figure 2.22: Simulated S-parameters for Bandwidth Tuning [33].

From the above **Figures** it can be clearly seen that the center frequency can be tuned from 29.5 GHz to 32.4 GHz. Likewise, the bandwidth is tuned from 6.3% to 12.7%, meaning that the bandwidth variation is 76.2%. The center frequency or bandwidth is not constant in both cases, but control remains possible through precise adjustments of MEMS heights.

Additionally, another reference in which the use of MEMS varactor is employed is “Millimetre-Wave Tune-All Bandpass Filters.” [34] The paper presents a two pole and a four pole filter; these can be seen in **Figure 2.23** and **Figure 2.24** respectively:

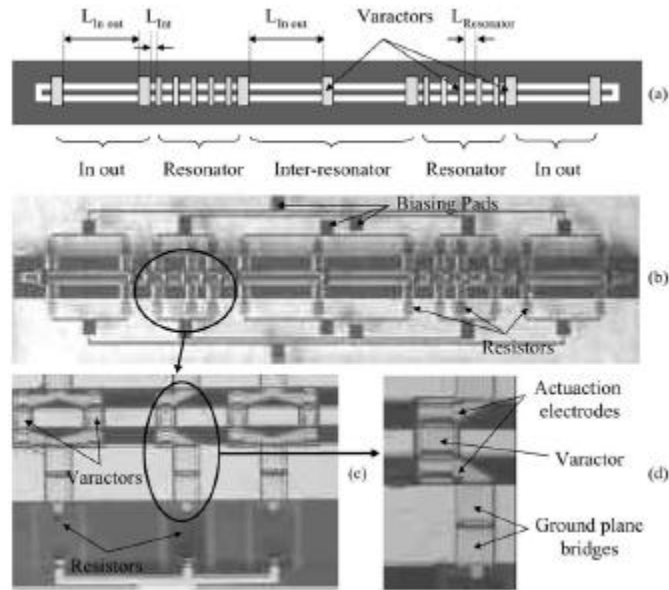


Figure 2.23: (a) Filter layout, (b) Photograph of Fabricated two Pole Filter, (c) Photograph of Resonator Sections, (d) Photograph of MEMS varactor [34].

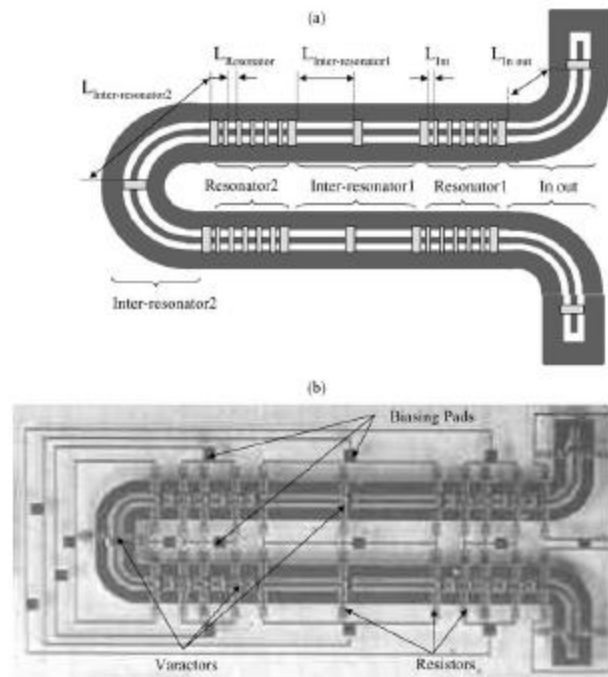


Figure 2.24: (a) Filter Layout, (b) Photograph of 4 Pole Filter [34].

In both cases the bandwidth and center frequency is controlled in the same manner. The bandwidth is changed when the inter-resonator varactors are biased; however there is a change in center frequency, which in order to maintain this parameter, f_0 is re-adjusted by biasing the resonator varactors. Likewise, it easily seen the center frequency tuning is

achieved varying the resonator varactors. However a bias voltage needs to be applied to the Input/Output varactors in order to maintain a low return loss and a bias voltage to the inter-resonant sections in order to maintain a constant bandwidth. The frequency and bandwidth responses are shown below:

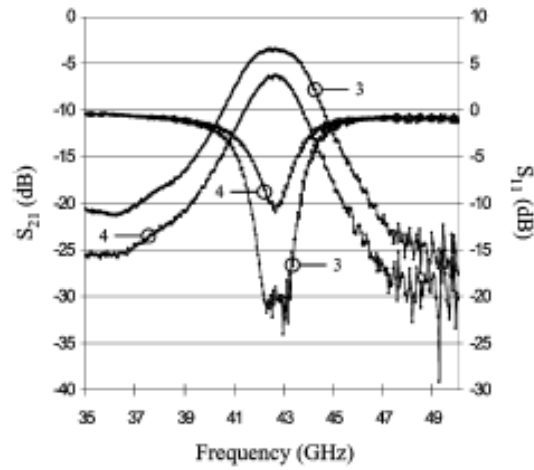


Figure 2.25: Measured Filter Bandwidth Tuning for a Fixed Center Frequency (two pole) [34].

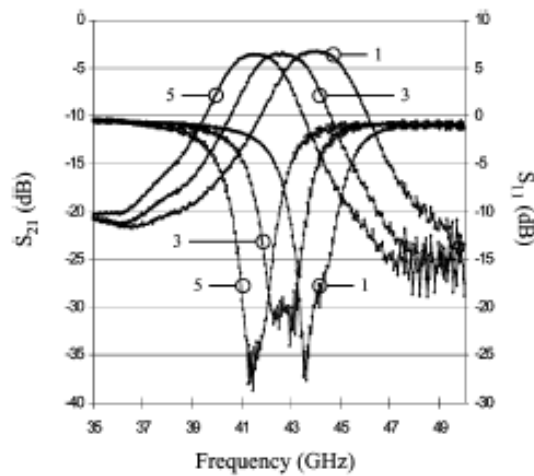


Figure 2.26: Measured Filter Center Frequency Tuning with a Constant Bandwidth (two pole) [34].

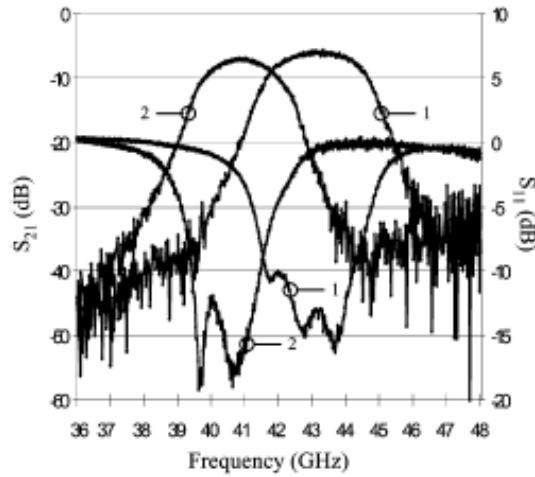


Figure 2.27: Measured Filter Center Frequency Tuning with a Constant Bandwidth (four pole) [34].

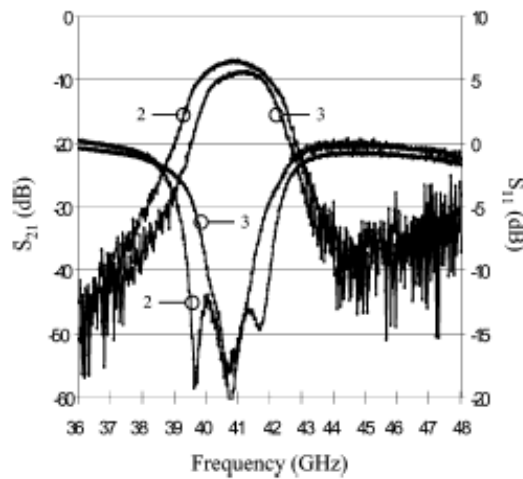


Figure 2.28: Measured Filter Bandwidth Tuning with a Constant Center Frequency (four pole) [34].

From the two pole filter it can be clearly seen that the bandwidth can be changed from 2.8 to 2.05 GHz when the inter-resonator varactors are biased. It is also deduced that when the inter-resonator varactors are actuated the center frequency shifts, in order to compensate for this, f_0 is re-adjusted by biasing the resonator varactors. Likewise, when the center frequency is tuned the bandwidth changes also. A biasing voltage is applied on the in/out sections at the maximum frequency shift to maintain low return loss. With reference to the four pole arrangement the concepts hold the same as the two pole filter topology. The center frequency can be tuned from 40.95 to 43.25 GHz and the bandwidth can be changed from 1.9 to 2.1 GHz.

A different type of MEMS varactor type is used such as MEMS capacitor switches in “Low-loss Bandpass RF Filter Using MEMS Capacitance Switches to Achieve a One-Octave Tuning Range and Independently Variable Bandwidth” [35]. The paper utilises capacitive switches with a total of 34 MEMS bridges where each array is independently addressable. The morphed circuit to fit onto a MEMS chip is shown as follows:

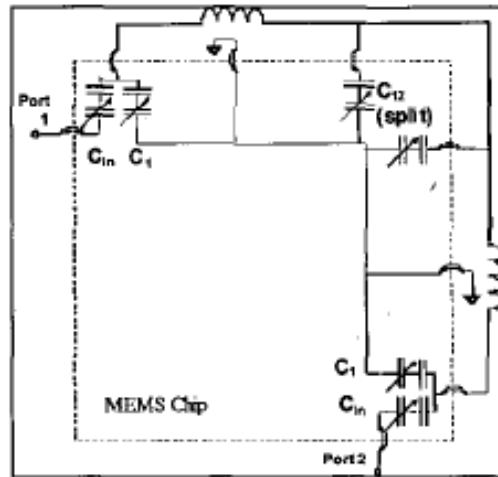


Figure 2.29: Circuit Schematic Morphed to accommodate Fabrication onto a MEMS chip [35].

With the two inductors at right angles the cross coupling of the resonators is reduced, however by doing this allows for a more compact design. The center capacitor C_{21} allows for control of bandwidth with sixteen different positions on the MEMS capacitor switches. The center frequency is controlled by capacitors C_1 , thus independent control of both bandwidth and center frequency. The filter is capable of one octave tuning from 860 to 1750 MHz, with an insertion loss of 1 dB and a return loss of 13 dB:

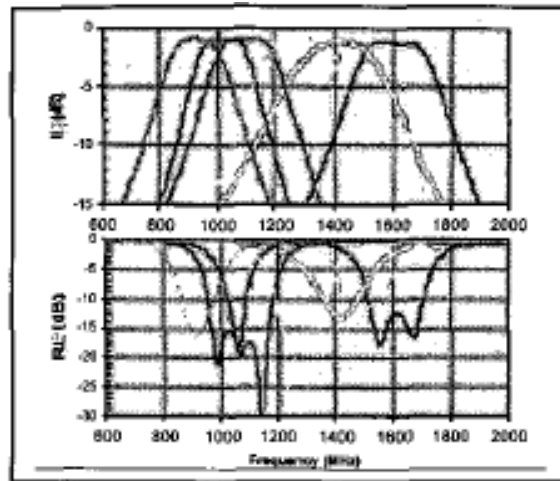


Figure 2.30: Insertion Loss and Return Loss of the Filter, demonstrating center frequency tunability [35].

The filter also exhibits bandwidth Reconfigurability, with a center frequency 1300 MHz and 3 dB bandwidth varying from 9% to 40%:

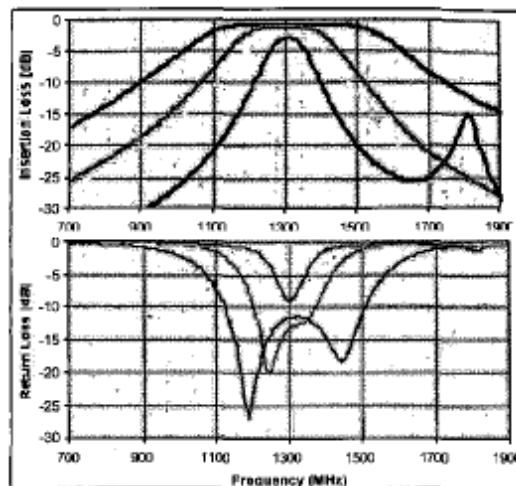


Figure 2.31: Insertion loss and Return loss of filter, demonstrating bandwidth tunability [35].

A Widely Tunable RF MEMS Filter was developed also using this form of MEMS varactor, which is presented in [36]. The paper uses distributed MEMS transmission lines (DMTL) in order to implement this filter topology:

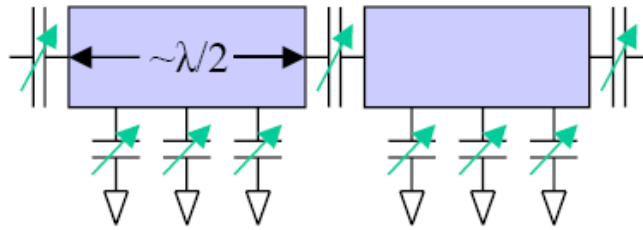


Figure 2.32: Structure of Slow Wave DMTL Filter [36].

The center frequency is reconfigured by loading the transmission lines with capacitive RF MEMS varactors in order to alter the resonator characteristics. The bandwidth tuning is achieved by tuning the inter-coupling capacitor. Both sets of capacitors need to be tuned simultaneously as changing the bandwidth results in a shift in center frequency and vice versa. The paper demonstrates the center frequency capabilities as shown:

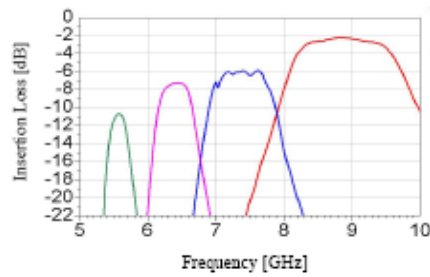


Figure 2.33: Insertion Loss of filter with bandwidth tuning Without Compensation of shift in Center Frequency [36].

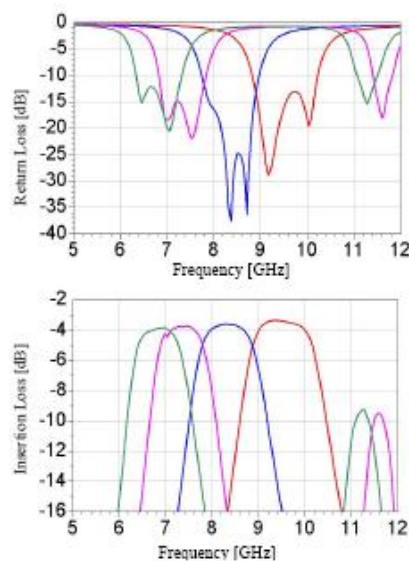


Figure 2.34: Return Loss and Insertion Loss of The filter, demonstrating center frequency tunability and keeping a constant bandwidth [36].

The filter is demonstrated to have a 35% tuning range centered around 8.2 GHz, with an insertion loss of 3.5 ± 0.25 dB and a return loss of greater than 12 dB. The tunable coupling capacitor was used in order to maintain a constant bandwidth across all tuning ranges. It is then clearly deduced that the filter can exhibit independent control of center frequency and bandwidth.

As aforementioned RF MEMS are becoming more and more common in filter applications and Bruce E. Carey-Smith et al [37] use a very simple topology which employs MEMS capacitor switches to control the center frequency and bandwidth. The arrangement used is as follows:

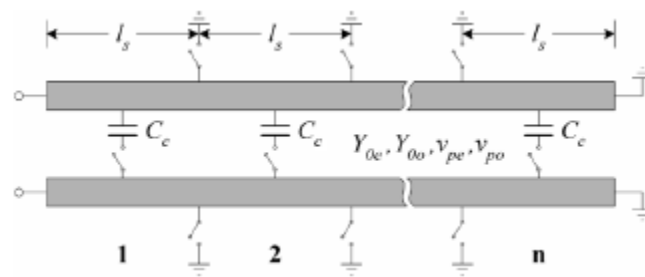


Figure 2.35: Lumped Distributed Coupled Resonators [37].

Tuning of center frequency is obviously obtained from varying the resonator lengths discretely, with a constant fractional bandwidth being achieved by switching all the coupling capacitors in the circuit. Likewise, for bandwidth tuning the coupling capacitors are switched such that the coupling co-efficient between the resonators is varied hence the bandwidth is changed. This topology has a number of advantages, which include:

- Only a single grounding switch is in-circuit regardless of selected length, therefore, the impact of the resistive switch losses on the resonator Q remains constant.
- It retains a constant overlap region and coupling factor regardless of the coupled line length.
- The coupling between the transmission lines is anti-phase to the lumped capacitive coupling; very low coupling coefficients can be obtained regardless of coupled line spacing.

However, the circuit possesses some disadvantages, namely:

- Tuning ranges are not uniform; at lower frequencies, there is a greater choice of both center frequency and bandwidth.

The following responses were obtained while demonstrating center frequency and bandwidth control:

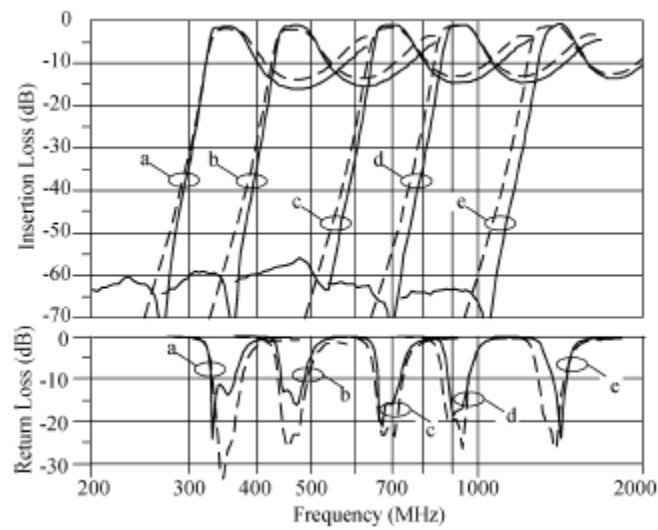


Figure 2.36: Results for five of the Filters Capable states [37].

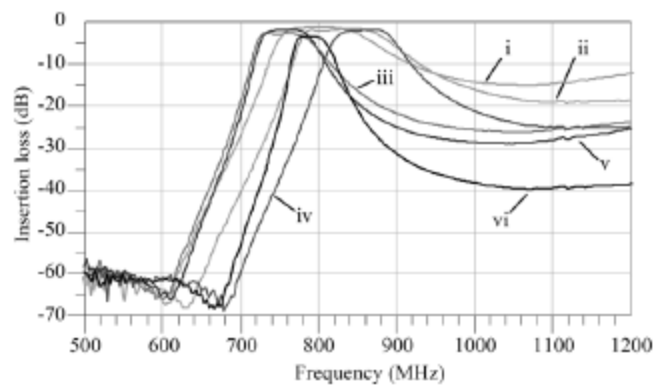


Figure 2.37: Measured Insertion Losses for five of the states [37].

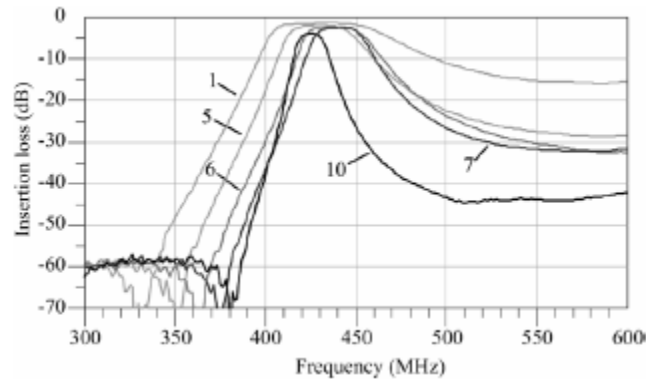


Figure 2.38: Measured Insertion Loss of five states of the filter [37].

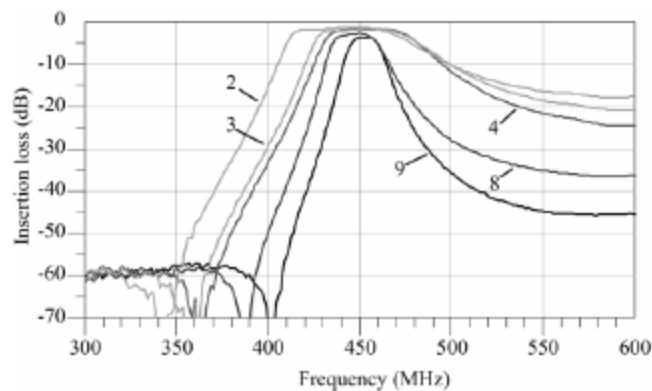


Figure 2.39: Measured Insertion Loss of five states of the filter [37].

The filter could be tuned in discrete steps over two octaves of center frequency (350 MHz to 1.4 GHz). Moreover, there were a number of different bandwidth settings that could be selected ranging from 3.8% to 14.5%; however the tuning ranges are not uniform.

Moreover, another filter which employed RF MEMS switches in order to implement center frequency and bandwidth tuning is that of [38]. The MEMS switches are used in order to adaptively tune microwave filter elements. Three banks of tunable high pass and low pass filters were designed and tested covering 6-15 GHz. These filters were then cascading in order to form a bandpass filter. The initial designs of the filter were synthesized as lumped elements and then converted to microstrip configurations.

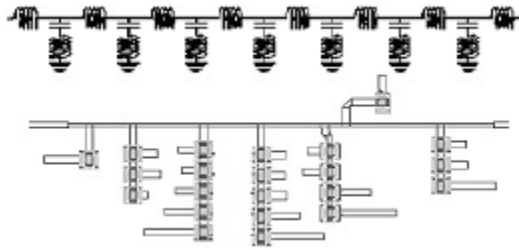


Figure 2.40: Lowpass Filter Schematic and Microstrip Implementation [38].

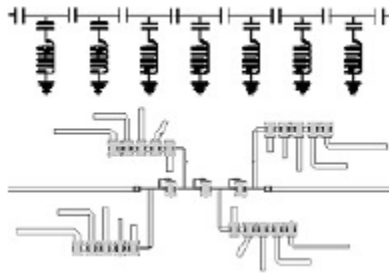


Figure 2.41: Highpass Filter Schematic and Microstrip Implementation [38].

In the low pass schematic, MEMS switches that attach to capacitive stubs are used to realise the shunt resonators. When the switches are actuated, a capacitance is added to the circuit and the filter tunes towards lower frequencies. Similarly, in the high pass filter design the MEMS switches are added to the series lines. The switches are in parallel with the fixed capacitors meaning that, the series capacitor values increase when the switches are actuated. It can be seen that by cascading these filters allows a bandpass filter to be implemented with tunable bandwidth and center frequency. The following shows the tunable bandwidth and center frequency:

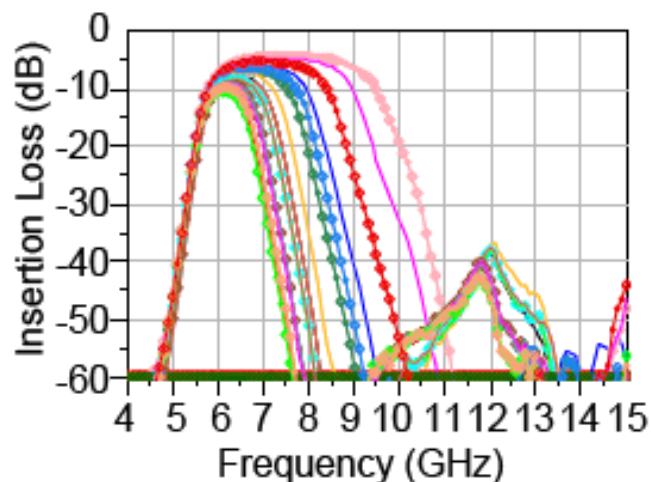


Figure 2.42: Showing Tunable Bandwidth [38].

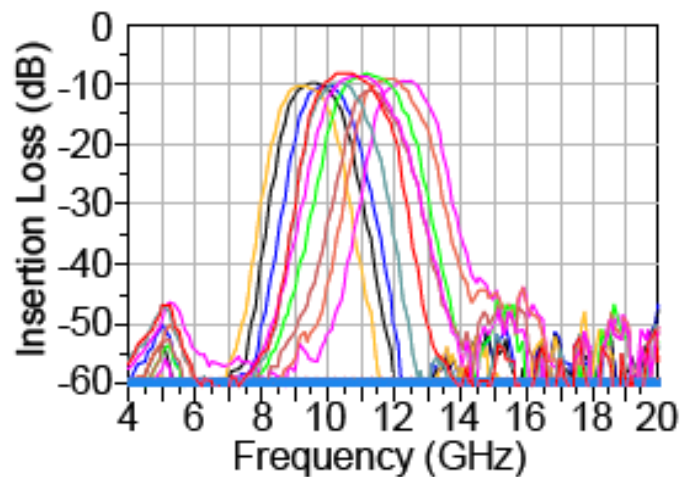


Figure 2.43: Showing Tunable Center Frequency [38].

From the above figures it is seen that the bandwidth and center frequency are controlled by varying the high pass and low pass filter responses. **Figure 2.42** shows the high pass filter is held at the lowest frequency while the low pass filter is tuned. From **Figure 2.43** the high pass and low pass are set to achieve roughly a 1GHz bandwidth across the frequency tuning range.

2.4) Liquid Crystal Polymer (LCP) Fabrication

Much of the promise of LCP is due to the potential to use it for multilayer RF circuits and systems. Multilayer circuits are possible as a result of two types of LCP material with different melting temperatures, but identical electrical characteristics. High melting temperature LCP (315 °C) can be used as core layers; while low melting temperature LCP (285 °C) is used as a bond ply. Thus, vertically integrated designs may be realized similar to those in LTCC.

Multilayer LCP circuits can be fabricated using the following steps:

- Plotting Masks - same as normal print-circuited-board (PCB) circuits and can be realized using normal PCB technique.

- Etching Circuits - same as normal print-circuited-board (PCB) circuits and can be realized using normal PCB technique.
- Alignment - The alignment process includes laser drilling and design of Lamination Fixture.
- Lamination – The Lamination process includes setting of the pressure, lamination time and lamination temperature.
- Drilling – further drilling may be required for vias and windows for components on embedded layers.



Figure 2.44: Circuit Etching.

2.4.1) Alignment and Laser Processing

Before fabrication all the LCP films need to be fixed on the fixture plates with good alignment accuracy. In order to do this each layer has laser drilled alignment holes in order to ensure precise alignment. Alignment holes are made on the mask which matches the alignment pins on the press plates in order to line them concentrically during the duration of the lamination process. As LCP is very thin mechanical drill is not suitable as smooth clean cut edges are required. The laser available for drilling is the Spectra physics Inazuma ns-pulse duration laser system delivering approximately 1.8 W (average power) of light at 355 nm. The pulse repetition rate is 15 kHz and cutting is done with many (approximately 30) passes at a relatively high scan speed of 250 mm/s to minimize thermal damage to the polymer. A Nutfield XLR8 two axis optical scan head was used, which enables precise and repeatable location of the beam across a work piece.

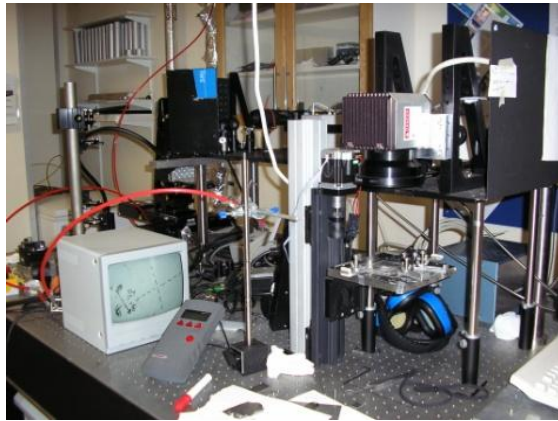


Figure 2.45: Laser Drilling Setup.

To fix and align the multiple LCP films in they are fixed on a lamination fixture with alignment pins. However, special considerations need to be made to accommodate the bonding, these include:

- The size of the plates is limited to less than 12 cm by 10 cm.
- The total vertical dimension of the stacked plates plus the inserted samples cannot be more than 2.8 cm, which indicates that the thickness of fabricated circuits is smaller than 8.0 mm.
- Finally, due to the mechanical fabrication errors, shrinking of printed mask and errors of etching, adjustable pins is designed to hold all of the LCP films.

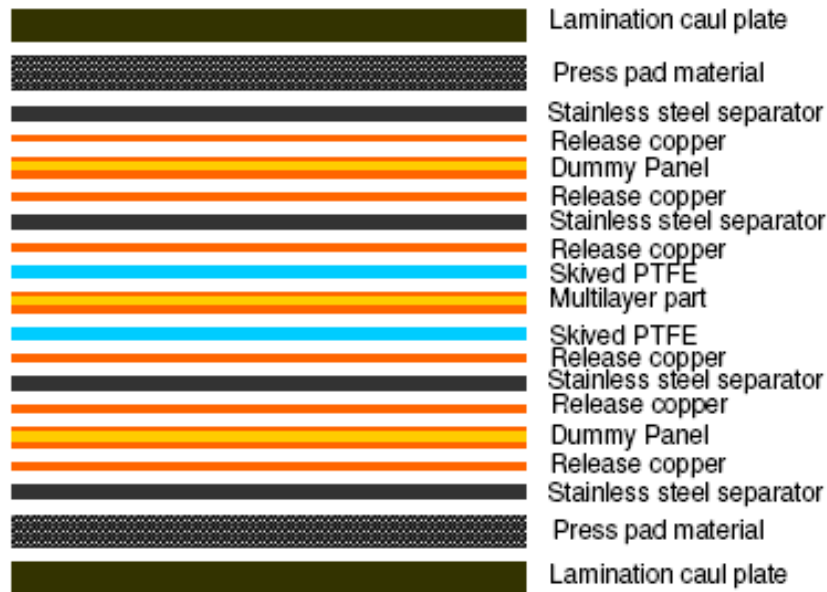


Figure 2.46: Typical LCP Lamination Setup.

2.4.2) Lamination Temperature

The lamination process of multilayer LCP circuits requires carefully controlled lamination temperature. LCP has a steep change in modulus of elasticity meaning that the bonding/lamination process requires tight temperature control. LCP keeps its full mechanical properties when below its melting point; however beyond melting point, a small increase in temperature may drastically increase its flow characteristics. The desired temperature conditions is 285°C across the plates, however this uniformity and accuracy is not possible with electrically heated presses. In our bonding process, we used a temperature of 285 °C with a variation of ± 5 °C for keeping LCP bonding films in a melting state. The temperature should be changed for the duration of the lamination process; the temperature settings are based on Rogers Duroid guidelines and are depicted below:

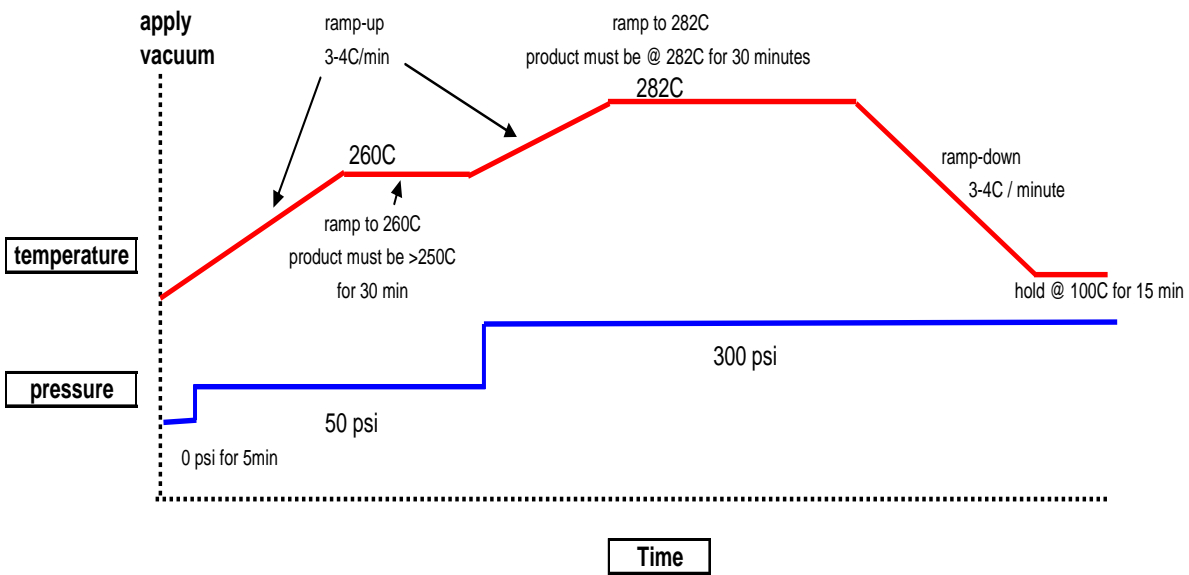


Figure 2.47: Temperature Settings for Lamination Process.

2.4.3) Lamination Pressure

During the bonding process the pressure has to be controlled manually by adjusting the screw release and lever accordingly to pressure gauge readout. The pressure could not be controlled tightly enough in temperature and often over-melted the LCP layers forcing them to flow and bubble. If the pressure is too high, the layers would visually flow too much and if it is too low, the layers would be easily pulled apart. In our fabrication set up, a suitable pressure is adopted as illustrated:

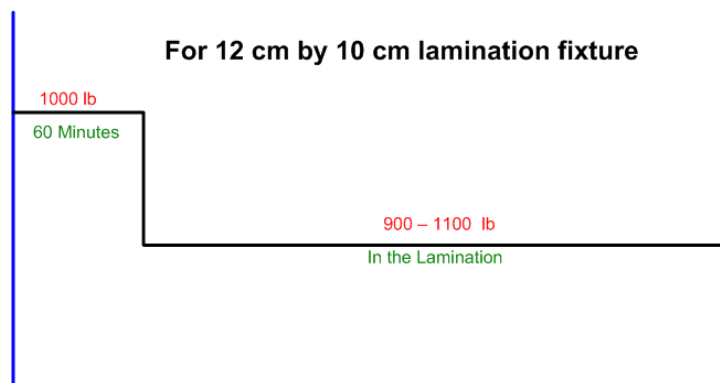


Figure 2.48: Pressure used in lamination process.

(See Appendix 1 for Rogers Guidelines – paper titled: “Various LCP Based Circuit Constructions and Fabrication Techniques”)

2.5) Summary

A lot of research and effort has been made in tunability of the center frequency; very little effort has been made in the past with tunability of bandwidth, however more and more effort has been made in recent years. This is mostly because there are an inadequate number of methods to vary the inter-resonator coupling of the resonators. Most of the effort was made initially in tuning the bandwidth with a fixed center frequency. In contrast, there have been many papers in recent times which present methods in order to control both the center frequency and bandwidth, namely [27] - [38]. The most desirable outcome is a filter that can simultaneously control both bandwidth and center frequency. A summary of the investigation shown in previous sections of this chapter is shown in Appendix 2.

Due to the complexity of the task in hand multilayer circuitry was used in some cases. Liquid crystal polymer offers an attractive option due to its electrical characteristics. These include static dielectric constant across a very wide frequency range, low water absorption and thermal expansion coefficients [44]. In the early years LCP had many fabrication issues which had to be overcome over a number of years [51] – [59]. By 2002 these issues had been overcome, prompting many applications being designed using this material, in ultra wideband filter design for instance [45] – [47].

2.6) References

[1] I. C. Hunter and J. D. Rhodes, “Electronically tunable microwave bandpass filters,” *IEEE Trans. Microw. Theory Tech.*, vol. *MTT-30*, no. 9, pp.1353–1360, Sep. 1980.

[2] J. Uher and W. J. R. Hoefer, “Tunable microwave and millimeter-wave band-pass filters,” *IEEE Trans. Microwave Theory Tech.*, vol. 39, pp. 643–653, Apr. 1991.

[3] G. Torregrosa *et al.*, “A simple method to design wide-band electronically tunable combline filters,” *IEEE Trans. Microw. Theory Tech.*, vol. 50, no. 1, pp. 172–177, Jan. 2002.

- [4] S. R. Chandler *et al.*, “Active varactor tunable bandpass filter,” *IEEE Microw. Guided Wave Lett.*, vol. 3, no. 3, pp. 70–71, Mar. 1993.
- [5] A. R. Brown and G. M. Rebeiz, “A varactor-tuned RF filter,” *IEEE Trans. Microw. Theory Tech.*, vol. 48, no. 7, pp. 1157–1160, Jul. 2000.
- [6] B. Kapilevich, A. Shulzinger, R. Lukjanets, “Bandpass Varactor Tunable Filters Using Step impedance Resonators,” *Electrical and Electronic Engineers in Israel 2004*.
- [7] B. W. Kim and S. W. Yun, “Varactor-tuned combline bandpass filter using step-impedance microstrip lines,” *IEEE Trans. Microw. Theory Tech.*, vol. 52, no. 4, pp. 1279–1283, Apr. 2004.
- [8] A. Presser, “Design, Simulation and Fabrication of a Varactor Tunable Combline Microwave Filter,” *APMC Proceedings 2005*
- [9] Wael M. Fathelbab, “A New Class of Reconfigurable Microwave Bandpass Filter,” *IEEE Transactions on Circuits and Systems – II: Express Briefs*, Vol. 55, No.3, pp. 264 – 268, March 2008
- [10] Young-Hoon Chun and Jia-sheng Hong, “Electronically Reconfigurable Dual-Mode Microstrip Open-Loop Resonator Filter,” *IEEE Microwave and Wireless Components Letters*, Vol. 18, No.7, pp. 449–451, July 2008
- [11] Jayesh Nath, Dipankar Ghosh, Jon-Paul Maria, Angus I. Kingon, Wael Fathelbab, Paul D. Franzon and Michael B. Steer, “An Electronically Tunable Microstrip Bandpass Using Thin-Film Barium-Strontium-Titanate (BST) Varactors,” *IEEE Transactions On Microwave Theory and Techniques*, Vol. 53, No. 9, pp. 2707 – 2712, September 2005
- [12] Young-Hoon Chun, Jia-Sheng Hong, Peng Bao, Timothy J. Jackson, Michael J. Lancaster, “Tunable Bandstop filter Using BST Varactor Chips,” *Proceedings of the 37th European Microwave Conference*, October 2007

- [13] Mahmoud Al-Ahmad, Richard Matz, and Peter Russer, "Wide Piezoelectric Tuning of LTCC Bandpass Filters," *Proceedings of the IEEE Microwave Symposium*, vol. x, Long Beach, USA, June 2005, pp. 1275 - 1278.
- [14] Mahmoud Al-Ahmad, Richard Matz, and Peter Russer, "0.8 GHz to 2.4 GHz Tunable Ceramic Microwave Bandpass Filters," *Microwave Symposium, IEEE/MTT-S International*, pp. 1615 – 1618, July 2007
- [15] Y.-H. Shu, J. A. Navarro, and K. Chang, "Electronically switchable and tunable coplanar waveguide-slotline band-pass filters," *IEEE Trans. Microwave Theory Tech.*, vol. 39, pp. 548–554, Mar. 1991.
- [16] Cesar Lugo and John Papapolymerou, "Dual Mode Reconfigurable Filter with Asymmetrical Transmission Zeros and Center Frequency Control," *IEEE Microwave and Wireless Components Letters*, Vol. 16, No. 9, pp. 499 – 501, September 2006
- [17] D. Peroulis, S. Pacheco, K. Sarabandi, and L. P. B. Katehi, "Tunable lumped components with applications to reconfigurable MEMS filters," in *IEEE MTT-S Int. Microwave Symp. Dig.*, vol. 1, 2001, pp. 341–344.
- [18] Abbas Abaspour – Tamijani, Laurent Dussopt and Gabriel M. Rebeiz, "A Millimetre-wave Tunable Filter Using MEMS Varactors," *European Microwave Conference 2002*
- [19] Erwan Fourn, Arnaud Pothier, Corinne Champeaux, Pascal Tristant, Alain Catherinot, Pierre Blondy, Gerard Tanne, Eric Ruis, Christian Peron and Fabrice Huret, "MEMS Switchable Interdigital Coplanar Filter," *IEEE Transactions on Microwave Theory and Techniques*, Vol. 51, No. 1, pp. 320 – 324, January 2003
- [20] C. A. Hall *et al.*, "A 25 watt RF MEMS-tuned VHF bandpass filter," in *IEEE MTT-S Int. Microwave Symp. Dig.*, vol. 1, Jun. 2003, pp. 503–506.

- [21] A. Abbaspour-Tamijani *et al.*, “Miniature and tunable filters using MEMS capacitors,” *IEEE Trans. Microw. Theory Tech.*, vol. 51, no. 7, pp. 1878–1885, Jul. 2003
- [22] Arnaud Pothier, Jean-Christophe Orlianges, Guizhen Zheng, Corrine Champeaux, Alain Catherinot, Dominique Cros, Pierre Blondy and John Papapolymerou, “Low-Loss 2-Bit Tunable Bandpass Filters Using MEMS DC Contact Switches,” *IEEE Transactions and Microwave Theory And Techniques*, Vol. 53, No. 1, pp. 354 – 360 January 2005
- [23] Isak C. Reines, Charles L. Goldsmith, Christopher D. Nordquist, Christopher W. Dyck, Garth M. Kraus, Thomas A. Plut, Patrick S. Finnegan, Franklin Austin IV and Charles T. Sullivan, “A Low Loss RF MEMS Ku-band Integrated Switched Filter Bank,” *IEEE Microwave And Wireless Components Letters*, Vol. 15, No. 2, pp. 74 – 76, February 2005
- [24] Eric M. Prophet, Jurgen Musolf, Betty F. Zuck, Silverio Jimenez, Kenneth E. Kihlstrom and Balam A. Willemsen, “Highly-Selective Electronically-Tunable Cryogenic Filters Using Monolithic, Discretely-Switchable MEMS Capacitor Arrays,” *IEEE Transactions on Applied Superconductivity*, Vol. 15, No. 2, pp. 956 – 959, June 2005
- [25] Kamran Entesari and Gabriel M. Rebeiz, “A 12-18 GHz Three-Pole RF MEMS Tunable Filter,” *IEEE Transactions On Microwave Theory and Techniques*, Vol. 53, No. 8, pp. 2566-2571, August 2005
- [26] Md. Fokhrul Islam, M.A. Mohd. Ali and Burhanuddin Yeop Majlis, “RF MEMS-Based Filter for X-Band Applications,” *Journal of Applied Sciences* 8 (1): 189-191, 2008
- [27] Manuel Sánchez-Renedo, Roberto Gómez-García, José I. Alonso, and César Briso-Rodríguez, “Tunable Compline Filter With Continuous Control of Center Frequency and Bandwidth,” *IEEE Trans. Microw. Theory Tech.*, vol. 53, no. 1, Jan. 2003, pp. 191–199.
- [28] Moon-Soek Chung, Il-Soo Kim and Sang-Won Yun, “Varactor-Tuned Hairpin Bandpass Filter With An Attenuation Pole,” *APM 2005 Proceedings*

- [29] Ching-Ku Liao, Chi-Yang Chang and Jenshan Lin, "A Reconfigurable Filter Based on Doublet Configuration," *Microwave Symposium, IEEE/MTT-S International*, pp. 1607 – 1610, July 2007
- [30] Emmanuel Pistono, Philippe Ferrari, Lionel Duvillaret, Jean-Marc Duchamp and Ann Vilcot, "A Compact Tune-All Bandpass Filter Based on Coupled Slow-Wave resonators," 35th *European Conference, October 2005*, pp. 1243 – 1246
- [31] Emmanuel Pistono, Mathieu Robert, Lionel Duvillaret, Jean-Marc Duchamp, Ann Vilcot and Philippe Ferrari, "A Compact Tune-All Bandpass Filter Based on Coupled Slow-Wave resonators," *IEEE Transactions On Microwave Theory and Techniques*, Vol. 54, No. 6, June 2006 , pp. 2790 – 2799
- [32] Cesar Lugo Jr. and John Papapolymerou, "Six State Reconfigurable Filter Structure for Antenna Based Systems," *IEEE Transactions on Antennas and propagation*, Vol. 54, No. 2, February 2006, pp. 479 – 483
- [33] E. Fourn, C. Quendo, E. Ruis, A. Pothier, P. Blondy, C. Champeaux, J.C. Orlianges, A. Catherinot, G. Tanne, C. Person, F. Huret, "Bandwidth and Central Frequency Control On Tunable Bandpass Filter By Using MEMS Cantilevers," *IEEE MTT-S Digest, 2003*, pp. 523–526.
- [34] Denis Mercier, Jean-Christophe Orlianges, Thierry Delage, Corinne Champeaux, Alain Catherinot, Dominique Cros and Pierre Blondy, "Millimetre-Wave Tune-All Bandpass Filters," *IEEE Transactions On Microwave Theory and Techniques*, Vol. 52, No. 4, April 2004, pp. 1175 – 1181
- [35] Robert M. Young et al, "Low-loss Bandpass RF Filter Using MEMS Capacitance Switches to Achieve a One-Octave Tuning Range And Independently Variable Bandwidth," *Microwave Symposium Digest, 2003 IEEE MTT-S International, June 2003*, pp. 1781 – 1784
- [36] Garth M.Kraus, Charles L. Goldsmith, Christopher D. Nordquist, Christopher W. Dyuck, Patrick S. Finnegan, Franklin Austin IV, Arnoldo Muyschondt and Charles T.

Sullivan, "A Widely Tunable RF MEMS End-coupled Filter," *Microwave Symposium Digest, 2004 IEEE MTT-S International, June 2004*, pp. 429 – 432

[37] Bruce E. Carey Smith, Paul A. Warr, Mark A. Beach and Tayfun Nesimoglu, "Wide Tuning-Range Planar Filters Using Lumped-Distributed Coupled Resonators," *IEEE Transactions on Microwave Theory And Techniques, Vol. 53, No. 2, February 2005*. pp. 777 – 785

[38] Brandon Pillans, Andrew Malczewski, Ron Allison and Jim Brank, "6-15 GHz RF MEMS Tunable Filters," *Microwave Symposium Digest, 2005 IEEE MTT-S International, June 2005*, pp. 919 – 922

[39] C. Rauscher, "Reconfigurable bandpass filter with a three-to-one switchable passband width," *IEEE Trans. Microw. Theory Tech.*, vol. 51, pp. 573–577, Feb. 2003

[40] Li Zhu, Vijay Devabhaktuni, Chunyan Wang, Ming Yu, "Adjustable Bandwidth Filter Design Based on Interdigital Capacitors," *IEEE Microwave and Wireless Coponents Letters*, vol. 18, pp. 16–18, Jan. 2008

[41] Cesar Lugo Jr., Dane Thompson, John Papapolymerou, "Reconfigurable filter with Variable Bandwidth at 5.8 GHz Using a Capacitive Gap Variation Technique," *33rd European Microwave Conference – Munich 2003*

[42] Jian Chen, Deyong Chen, "Design of Piezoelectric Resonant Filter with Tunable Bandwidth," *Solid-State and Integrated Circuit Technology, 2006. ICSICT '06. 8th International Conference*, pp. 566–568, Oct. 2006

[43] A. Miller, J. Hong "Wideband Bandpass Filter with Reconfigurable Bandwidth," *IEEE Microwave and Wireless Components Letters, Vol. 20, No. 1, Jan 2010*, pp 28 – 30.

[44] D. C. Thompson, O. Tantot, H. Jallageas, G. E. Ponchak, M. Tentzeris, and J. Papapolymerou, "Characterization of liquid crystal polymer (LCP) material and transmission

lines on LCP substrate from 30 to 110 GHz,” *IEEE Trans. Microw. Theory Tech.*, vol. 52, no. 4, pp. 1343–1352, Apr. 2004.

[45] Z.C. Hao, J. Hong, “Compact Wide Stopband Ultra Wideband Bandpass Filter Using Multilayer Liquid Crystal Polymer Technology”, *IEEE Microwave and Wireless Components Letters*, vol. 19, no. 5, May 2009.

[46] Z.C. Hao, J. Hong, “UWB Bandpass Filter using Cascaded Miniature Highpass and Lowpass Filters with Multilayer Liquid Crystal Polymer Technology”, *IEEE Trans. Microw. Theory Tech*, Vol. 58, No. 4, April 2010, pp 941 – 948.

[47] Z.C. Hao, J. Hong, S. K. Alotaibi, “A novel Ultra Wideband Bandpass Filter using Broadside Coupled Structures on Multilayer Organic Liquid Crystal Polymer Substrate”, *Proceedings of the 38th European Microwave Conference, October 2008 Amsterdam, The Netherlands*, pp 998 – 1001.

[48] K. Jayaraj, T. E. Noll, and D. R. Singh, “RF characterization of a low cost multichip packaging technology for monolithic microwave and millimeter wave integrated circuits,” in *URSI Int. Signals, Systems, and Electronics Symp.*, Oct. 1995, pp. 443–446.

[49] E. C. Culbertson, “A new laminate material for high performance PCBs: Liquid crystal polymer copper clad films,” in *IEEE Electronic Components and Technology Conf.*, May 1995, pp. 520–523.

[50] K. Jayaraj, T. E. Noll, and D. R. Singh, “A low cost multichip packaging technology for monolithic microwave integrated circuits,” *IEEE Trans. Antennas Propagat.*, vol. 43, pp. 992–997, Sept. 1995.

[51] C. Khoo, B. Brox, R. Norrhede, and F. Maurer, “Effect of copper lamination on the rheological and copper adhesion properties of a thermotropic liquid crystalline polymer used in PCB applications,” *IEEE Trans. Comp., Packag, Manufact., Technol.*, vol. 20, pp. 219–226, July 1997.

- [52] T. Suga, A. Takahashi, K. Saijo, and S. Oosawa, "New fabrication technology of polymer/metal lamination and its application in electronic packaging," in *IEEE 1st Int. Polymers and Adhesives in Microelectronics and Photonics Conf.*, Oct. 2001, pp. 29–34.
- [53] X. Wang, L. Lu, and C. Liu, "Micromachining techniques for liquid crystal polymer," in *14th IEEE Int. MEMS Conf.*, Jan. 2001, pp. 21–25.
- [54] K. Brownlee, S. Bhattacharya, K. Shinotani, C. P. Wong, and R. Tummala, "Liquid crystal polymers (LCP) for high performance SOP applications," in *8th Int. Adv. Packag. Materials Symp.*, Mar. 2002, pp. 249–253.
- [56] J. Kivilahti, J. Liu, J. E. Morris, T. Suga, and C. P. Wong, "Panel-size component integration (PCI) with molded liquid crystal polymer (LCP) substrates," in *IEEE Electronic Components and Technology Conf.*, May 2002, pp. 955–961.
- [57] T. Suga, A. Takahashi, M. Howlander, K. Saijo, and S. Oosawa, "A lamination technique of LCP/Cu for electronic packaging," in *2nd Int. IEEE Polymers and Adhesives in Microelectronics and Photonics Conf.*, June 2002, pp. 177–182.
- [58] T. Zhang, W. Johnson, B. Farrell, and M. St. Lawrence, "The processing and assembly of liquid crystalline polymer printed circuits," presented at the *Int. Microelectronics Symp.*, 2002.
- [59] L. Chen, M. Crnic, L. Zonghe, and J. Liu, "Process development and adhesion behavior of electroless copper on liquid crystal polymer (LCP) for electronic packaging application," *IEEE Trans. Electron. Packag. Manufact.*, vol. 25, pp. 273–278, Oct. 2002.

Chapter 3: Microstrip Equations and Filter Theory

3.1) Introduction

In this chapter the basic theory behind the work undertaken in this PhD is presented. Firstly, the use of lowpass to other topology transformations with the Chebyshev and Butterworth approaches are explained; Chebyshev is utilized in most filter designs. J- and K-inverters are explained and it is shown how these can be used in order to design filter circuits. Principles behind coupled lines and equations used in the design of such filters are explained and presented. An extraction method using an EM simulator, which allows the even and odd mode impedance of coupled lines to be obtained, is also shown. Finally, the principles behind stepped impedance resonators (SIR) are outlined briefly.

3.2) Lowpass Transformations

3.2.1) Lowpass Prototype

A lowpass prototype filter is in general defined as a lowpass filter whose element values are normalised to make the source resistance or conductance equal to one, denoted by $g_0 = 1$. The cut off angular frequency is unity, and is denoted by $\Omega_c = 1$ (rad/s). Filter design usually begins with the lowpass prototype filter, which can then be transformed into any other form of practical filter, namely highpass, bandpass and Bandstop filters. The element values for the lowpass prototype were initially obtained by network synthesis methods of Darlington et al [1] – [3]. However, over the years more concise equations were derived for ease of computer programming, with the element values of the prototype filters being obtained [4] – [11]. Having these prototype values, it is shown in a number of books that these elements values can be used to design filters of different forms [12] – [14].

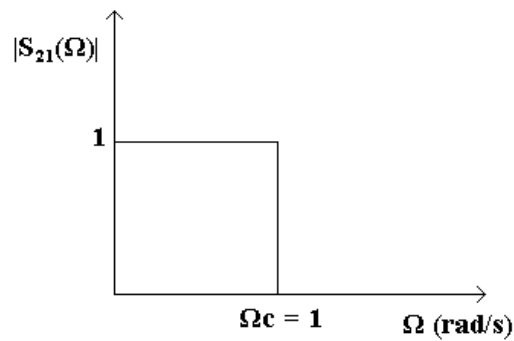


Figure 3.1: Ideal Lowpass Prototype Filter Response.

The Lowpass prototype can have different forms of representation, depending on filter structures and characteristics. In general the form shown below is used:

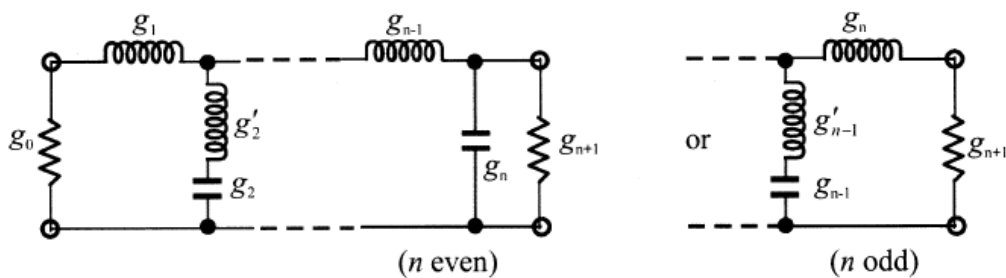


Figure 3.2: Lowpass Filter Form with Degree of n.

Where:

- g_0 is defined as the source resistance/conductance.
- g_i for $i = 1$ to n represent either the inductance of a series inductor or the capacitance of a shunt capacitor, therefore n is also the number of reactive elements.
- g_{n+1} is the load resistance/conductance.
- The g – values are the inductance in henries (H), capacitance in farads (F), resistance in ohms (Ω) and conductance in siemens (S) or mhos.

The above n -pole prototype demonstrates two forms of filter with the same response, namely Butterworth and Chebyshev. In an ideal case the filter would require an infinite number of

reactance elements ($n \rightarrow \infty$), however this not practical and the ideal response can only be approximated.

The transfer function of a two port network is a mathematical description of the network response characteristics, i.e. a mathematical expression for S_{21} . An amplitude squared transfer function for a lossless passive filter network is defined as:

$$|S_{21}(j\Omega)|^2 = \frac{1}{1 + \varepsilon^2 F_n^2(\Omega)} \quad (3.1)$$

Where ε is the ripple constant, $F_n(\Omega)$ represents a filtering or characteristic function and Ω is the frequency variable. It is convenient to allow Ω to be equal to the angular frequency variable of the lowpass prototype filter which has a cut off frequency at $\Omega = \Omega_c$ for $\Omega_c = 1$ (rad/s).

The insertion loss of the filter can be then computed from:

$$L_A(\Omega) = 10 \log \frac{1}{|S_{21}(\Omega)|^2} \text{ dB} \quad (3.2)$$

The return loss is defined by:

$$L_R(\Omega) = 10 \log |S_{11}(\Omega)|^2 \text{ dB} \quad (3.3)$$

As $|S_{11}|^2 + |S_{21}|^2 = 1$ for a lossless passive two – port network, the return loss of the filter can be found using (3.4):

$$L_R(\Omega) = 10 \log [1 - |S_{21}(\Omega)|^2] \text{ dB} \quad (3.4)$$

3.2.2) Frequency and Element Transformations

To obtain a practical filter design with element values from the lowpass prototype filter we can apply frequency and element transformations.

Frequency transformations (frequency mapping) are required to map the response in the lowpass filter prototype frequency domain, Ω , to that in the frequency domain, ω . In which a practical response such as highpass, bandpass and Bandstop characteristics are obtained. The frequency transformation will have an effect on the reactive elements but no effect on the resistive elements.

Impedance scaling is also required to accomplish the transformation from the prototype to practical filters. The impedance scaling will remove the $g_0 = 1$ normalisation and adjusts the filter to work for any value of the source impedance denoted by Z_0 . In general the formulation used is as follows:

$$\gamma_0 = \begin{cases} Z_0/g_0 & \text{for } g_0 \text{ being the resistance} \\ g_0/Y_0 & \text{for } g_0 \text{ being the conductance} \end{cases} \quad (3.5)$$

In principle, applying the impedance scaling upon a filter network in such a way that:

$$\begin{aligned} L &\rightarrow \gamma_0 L \\ C &\rightarrow C/\gamma_0 \\ R &\rightarrow \gamma_0 R \\ G &\rightarrow G/\gamma_0 \end{aligned} \quad (3.6)$$

has no effect on the response shape.

3.2.3) Lowpass Transformation

The frequency transformation from a lowpass prototype to a practical lowpass filter having a cut off frequency ω_c in the angular frequency axis, ω is simply given by:

$$\Omega = \left(\frac{\Omega_c}{\omega_c} \right) \omega \quad (3.5)$$

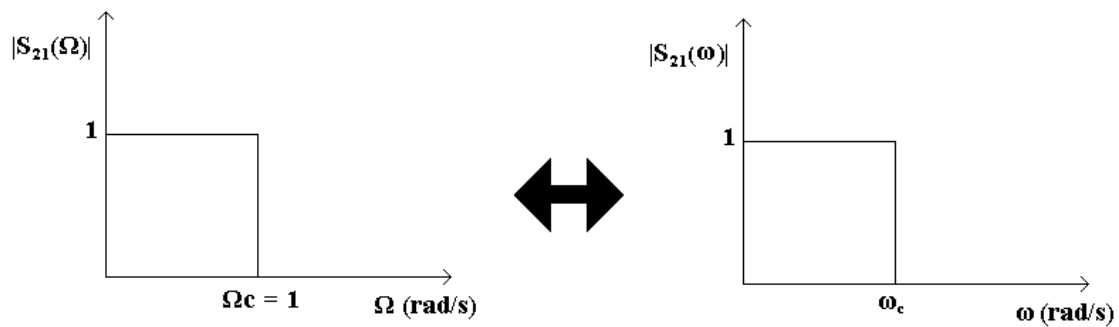


Figure 3.3: Lowpass to Lowpass Transformation.

Applying the frequency transformation and the impedance scaling factor, the following is obtained:

$$\begin{aligned} R &= \gamma_0 g \quad \text{for } g \text{ representing the resistance} \\ G &= \frac{g}{\gamma_0} \quad \text{for } g \text{ representing the conductance} \end{aligned} \quad (3.6)$$

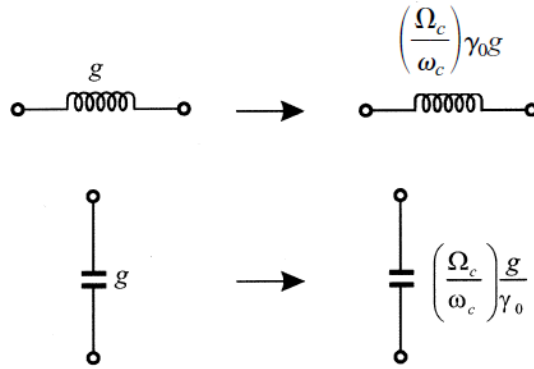


Figure 3.4: Lowpass Prototype Transformation.

3.2.4) Highpass Transformation

The lowpass prototype filter can be easily transformed into a highpass filter in the same way using the following frequency transformation:

$$\Omega = -\frac{\omega_c \Omega_c}{\omega} \tag{3.7}$$

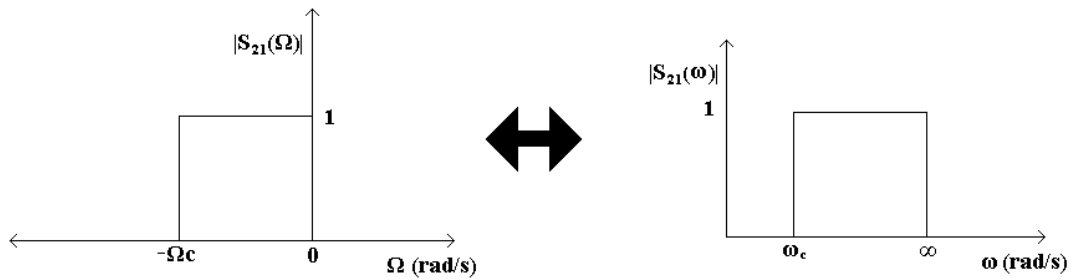


Figure 3.5: Highpass Response Transformation.

From the frequency transformation it can be clearly seen that the capacitive element values will be inversely transformed to an inductive element values in the highpass filter, and vice versa. Applying this frequency transformation to the reactive elements, g , the lowpass prototype leads to:

$$j\Omega g \rightarrow \frac{\omega_c \Omega_c g}{j\omega} \quad (3.8)$$

With the impedance scaling factor taken into account the element transformations are given by:

$$C = \left(\frac{1}{\omega_c \Omega_c} \right) \frac{1}{\gamma_0 g} \quad \text{for } g \text{ representing the inductance}$$

$$L = \left(\frac{1}{\omega_c \Omega_c} \right) \frac{\gamma_0}{g} \quad \text{for } g \text{ representing the capacitance} \quad (3.9)$$

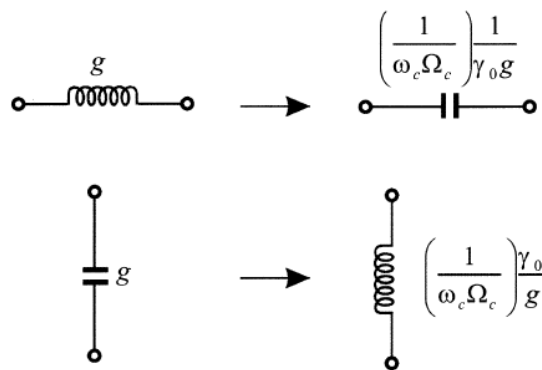


Figure 3.6: Highpass Transformation.

3.2.5) Bandpass Transformation

Assuming that the lowpass prototype is to be transformed into a bandpass response; having a passband $\omega_2 - \omega_1$, with ω_2 and ω_1 , being the passband edge angular frequencies.

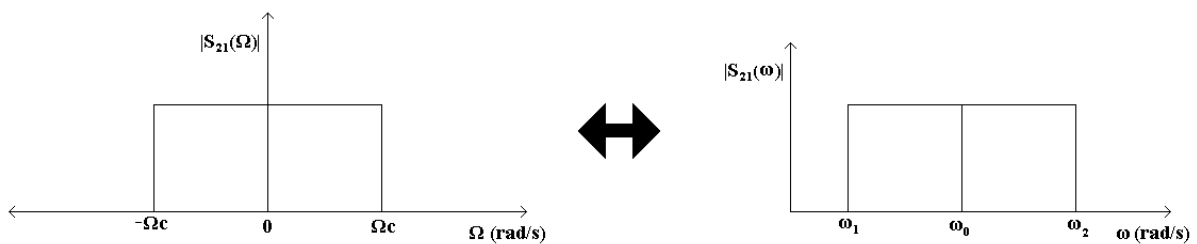


Figure 3.7: Bandpass Frequency Transformation.

The required frequency transformation is:

$$\Omega = \frac{\Omega_c}{FBW} \left(\frac{\omega}{\omega_0} - \frac{\omega_0}{\omega} \right) \quad (3.10)$$

Where:

$$FBW = \frac{\omega_2 - \omega_1}{\omega_0}$$

$$\omega_0 = \sqrt{\omega_1 \omega_2} \quad (3.11)$$

When this frequency transformation is applied to the inductive elements convert to a series combination of an inductor and capacitor. On the other hand, the capacitive elements will convert to a parallel LC resonant circuit.

$$j\Omega g \rightarrow j\omega \frac{\Omega_c g}{FBW \omega_0} + \frac{1}{j\omega} \frac{\Omega_c \omega_0 g}{FBW} \quad (3.12)$$

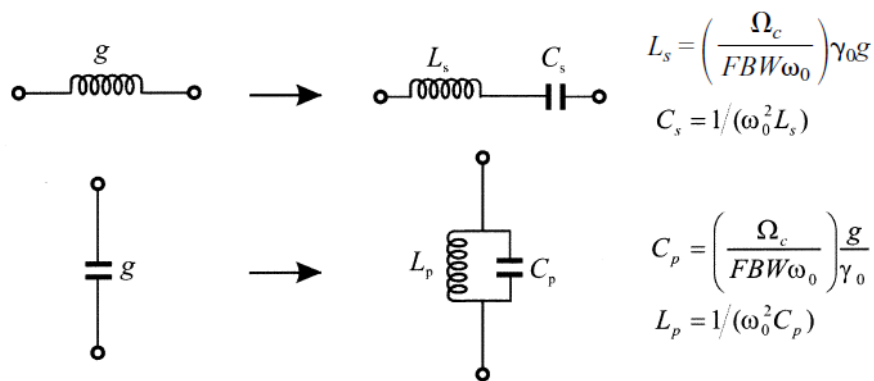


Figure 3.8: Bandpass Transformation.

3.2.6) Bandstop Transformation

The frequency transformation to the Bandstop filter is achieved by the frequency mapping:

$$\Omega = \frac{\Omega_c FBW}{(\omega_0/\omega - \omega/\omega_0)} \quad (3.13)$$

With:

$$\begin{aligned} \omega_0 &= \sqrt{\omega_1 \omega_2} \\ FBW &= \frac{\omega_2 - \omega_1}{\omega_0} \end{aligned} \quad (3.14)$$

This transformation is the opposite of the bandpass transformation with the inductive elements, g , transforming to a parallel LC circuit and the capacitive elements transforming to series circuit.

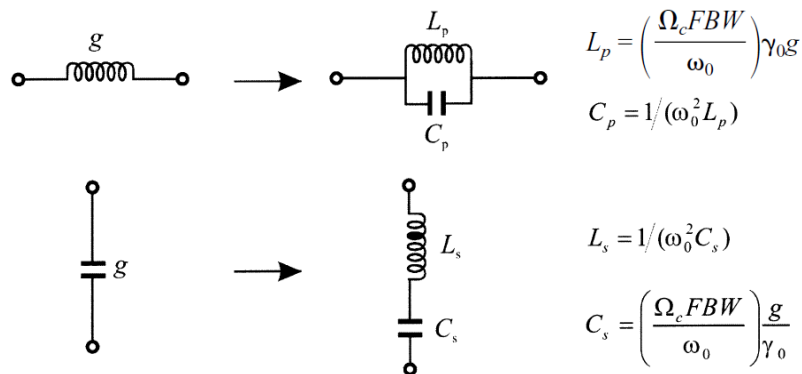


Figure 3.9: Bandstop Transformation.

3.3) Butterworth Lowpass Prototype

As mentioned filters can have different characteristics depending on the function response chosen. The amplitude squared transfer function for Butterworth filters which have an insertion loss $L_{AR} = 3.01$ dB at the cut off frequency, $\Omega_c = 1$ is given by:

$$|S_{21}(\Omega)|^2 = \frac{1}{1+\Omega^{2n}} \quad (3.15)$$

Where n is the degree or the order of filter, or the number of reactive elements in the lowpass prototype filter.

This type of response is also referred to as a maximally flat response form the fact that its amplitude squared transfer function defined has a maximum number $(2n - 1)$ zero derivatives at $\Omega = 0$. This meaning that the Butterworth approximation to the ideal lowpass filter in the passband is best at $\Omega = 0$, but deteriorates as Ω approaches the cut off frequency Ω_c . A typical Butterworth response is as follows:

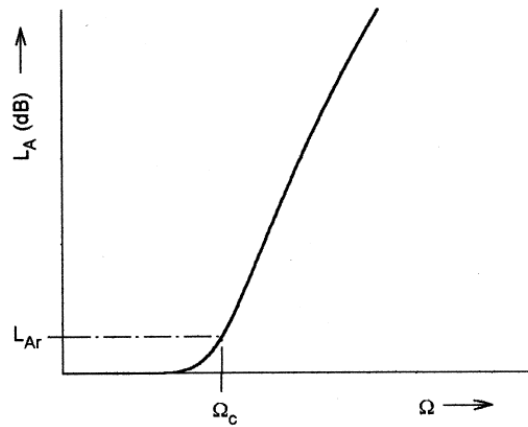


Figure 3.10: Butterworth Lowpass Response.

3.4) Chebyshev Lowpass Prototype

The Chebyshev prototype filter has an amplitude squared transfer function:

$$|S_{21}(j\Omega)|^2 = \frac{1}{1+\varepsilon^2 T_n^2(\Omega)} \quad (3.16)$$

Where the ripple constant, ε , is related to a given passband ripple L_{AR} in dB by:

$$\varepsilon = \sqrt{10^{\frac{L_{AR}}{10}} - 1} \quad (3.17)$$

$T_n(\Omega)$ is the Chebyshev function of the first kind of order n , which is defined as:

$$T_n(\Omega) = \begin{cases} \cos(n \cos^{-1} \Omega) & |\Omega| \leq 1 \\ \cosh(n \cosh^{-1} \Omega) & |\Omega| \geq 1 \end{cases} \quad (3.18)$$

Hence, the filters are commonly known as Chebyshev filters. The Chebyshev response exhibits the equal – ripple passband and maximally flat stopband.

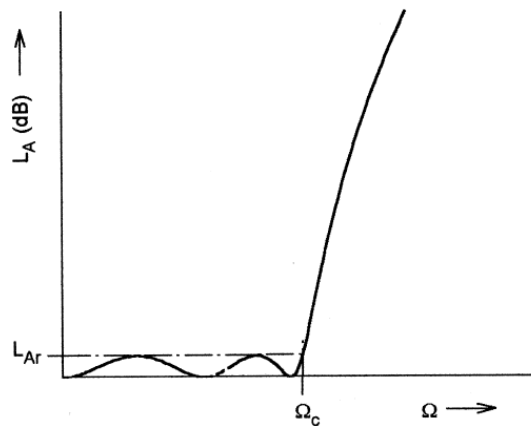


Figure 3.11: Chebyshev Lowpass Response.

The calculations for the element values of the Butterworth and Chebyshev responses can be found in many textbooks [12] – [14].

3.5) Immittance Inverters

Immittance inverters can be either impedance (K) or admittance (J) Inverters. An ideal impedance inverter as a two port network is represented by the following ABCD matrix:

$$\begin{bmatrix} A & B \\ C & D \end{bmatrix} = \begin{bmatrix} 0 & \mp jK \\ \pm \frac{1}{jK} & 0 \end{bmatrix} \quad (3.19)$$

Where K is real and defined as the characteristic impedance of the inverter; the characteristic admittance of an Immittance inverter can also be defined as:

$$j = \frac{1}{K} \tag{3.20}$$

This meaning that the ABCD matrix for an ideal admittance inverter is given by:

$$\begin{bmatrix} A & B \\ C & D \end{bmatrix} = \begin{bmatrix} 0 & \pm \frac{1}{jJ} \\ \mp jJ & 0 \end{bmatrix} \tag{3.21}$$

3.5.1) Transformations with Immittance Inverters

It can be easily shown that series impedance can be transformed to a parallel admittance with an inverter on each side. And likewise a parallel admittance branch can be transformed to a series impedance branch with an inverter on each side. As shown:

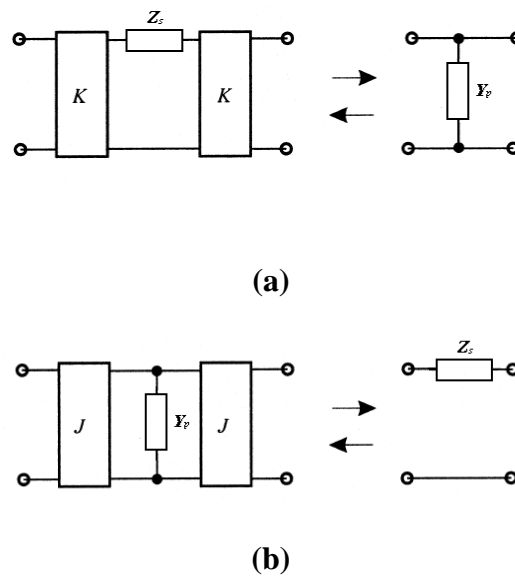


Figure 3.12: (a) Series Impedance Equivalence, (b) Parallel admittance Equivalence.

Considering Case (a):

The ABCD matrix for a parallel admittance circuit is:

$$\begin{bmatrix} 1 & 0 \\ Y_p & 1 \end{bmatrix} \tag{3.22}$$

The ABCD matrix for the two K inverters with a series impedance circuit placed in between them is:

$$\begin{bmatrix} 0 & jK \\ -\frac{1}{jK} & 0 \end{bmatrix} \cdot \begin{bmatrix} 1 & Z_s \\ 0 & 1 \end{bmatrix} \cdot \begin{bmatrix} 0 & jK \\ -\frac{1}{jK} & 0 \end{bmatrix} = -\begin{bmatrix} 1 & 0 \\ \frac{Z_s}{K^2} & 1 \end{bmatrix} \quad (3.23)$$

The negative sign has no effect on the amplitude of the response of the network, meaning that it can be ignored. On comparing the parallel admittance circuit ABCD matrices gives:

$$\frac{Z_s}{K^2} = Y_p \quad (3.24)$$

This means that as long as the above equation holds the two networks are equivalent. Case (b) can be analysed in the same way to yield the same result.

3.5.2) Filter Design with Immittance Inverters

If a bandpass filter designed from the lowpass filter prototype is considered, it can be shown that this can be converted to filters with Immittance inverters, as shown below:

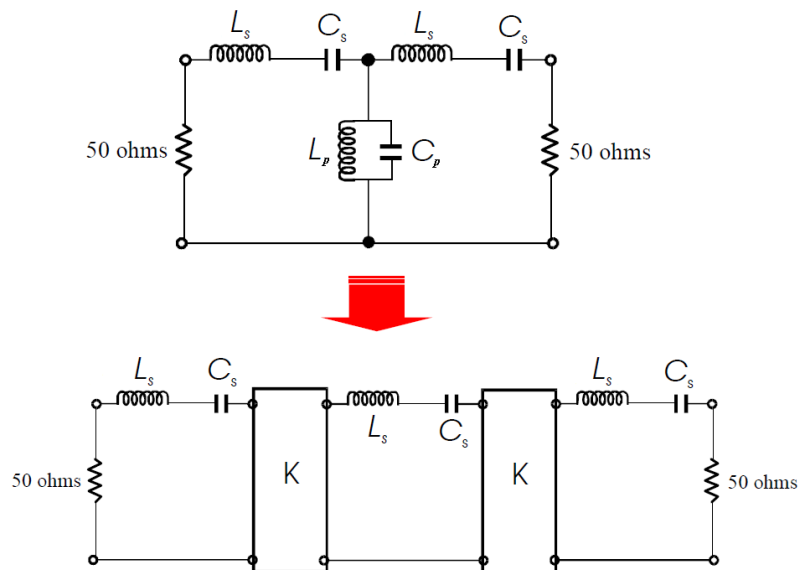


Figure 3.13: Bandpass Filter Equivalence.

The immittance for the shunt resonator in the original design is:

$$Y_p = j \left(\omega C_p - \frac{1}{\omega L_p} \right) \quad (3.24)$$

The shunt resonator is to be transformed to a series resonator of the impedance:

$$Z_s = j \left(\omega L_s - \frac{1}{\omega C_s} \right) \quad (3.25)$$

According to the equation:

$$\frac{Z_s}{K^2} = Y_p \quad \text{or} \quad Z_s = K^2 Y_p \quad (3.26)$$

and by inspection we obtain:

$$\omega L_s = K^2 \omega C_p \quad (3.27)$$

$$\omega C_s = \frac{K^2}{\omega L_p} \quad (3.28)$$

Where ω is in rad/s, K is in ohms (Ω), L is in henries (H) and C is in farads (F).

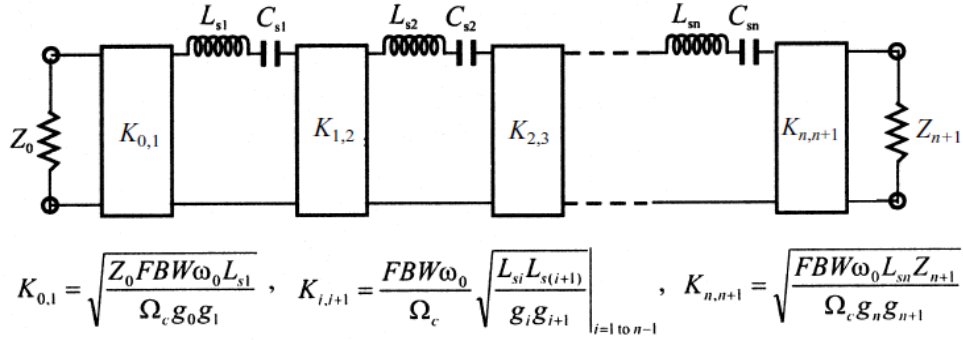
Hence, numerically:

$$L_s = K^2 C_p \quad (3.29)$$

$$C_s = \frac{L_p}{K^2} \quad (3.30)$$

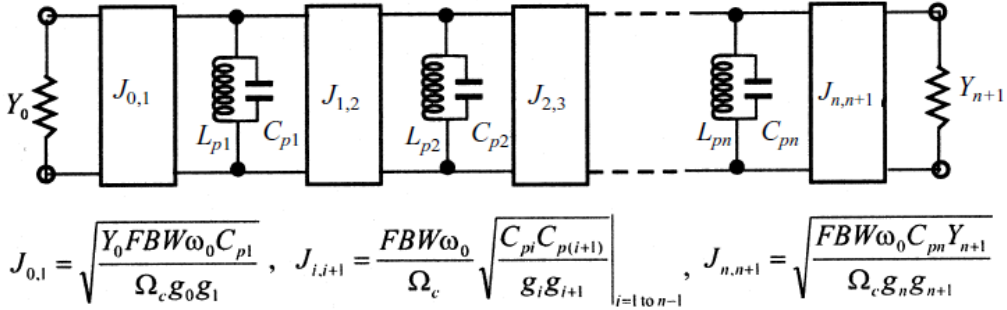
This meaning that K can be chosen such that desired values of L_s and C_s can be obtained.

Based on this transformation principle, a more general bandpass filter design with immittance inverters can be shown:



$$C_{s_i} = \frac{1}{\omega_0^2 L_{s_i}} \Big|_{i=1 \text{ to } n}$$

(a)



$$L_{p_i} = \frac{1}{\omega_0^2 C_{p_i}} \Big|_{i=1 \text{ to } n}$$

(b)

Figure 3.14: Bandpass Filter Using Immittance Inverters.

Where the g values are those of the lowpass filter prototype directly.

There is a great flexibility of designing this type of filter; for example we may choose a desired inductance or capacitance value that is more convenient for microwave implementation. We can also make all the resonators have the same inductance and capacitance. Furthermore, by using input/output inverters give extra flexibility of the choice of source/load impedances, i.e. Z_0 and Z_{n+1} .

3.5.3) Practical Realisation of Immittance Inverters

There are a number of circuits or a combination of circuits which operate as an Immittance inverter, however the simplest form of a distributed – element is a quarter – wavelength of transmission line with $k = Z_c$ ohms, where Z_c is the characteristic impedance of the line.

Moreover, there are numerous other circuits which operate as Immittance inverters, four typical circuits include:

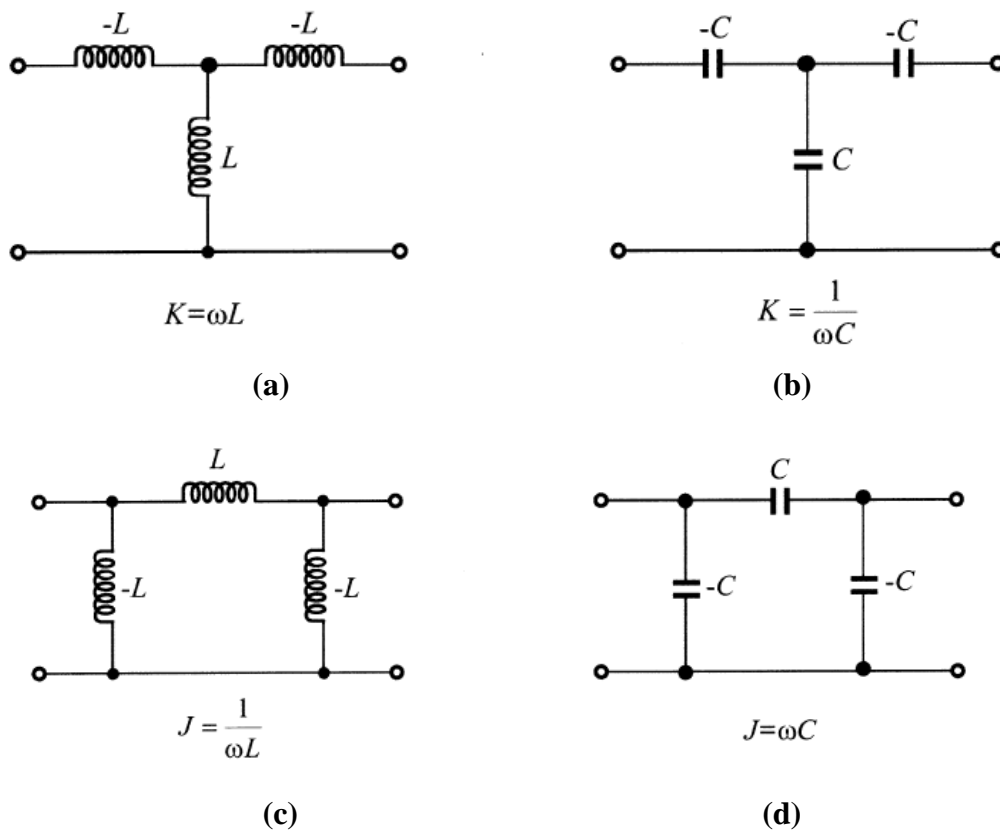


Figure 3.15: Lumped Element Immittance Inverters.

It is possible to implement some of the inverters by absorbing the negative components into adjacent elements.

In reality, J and K parameters of immittance inverters are frequency dependant, meaning they can only approximate an ideal immittance for a constant J and K. This meaning that, in general the inverter theories are best applied to narrowband filters.

3.6) Coupled Lines

Coupled lines are widely used in the implementation of couplers and microwave filters. A cross section of a typical edge coupled line set up is shown below, where the two microstrip lines with width W and separated by a gap s .

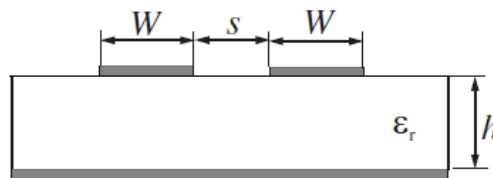


Figure 3.16: Coupled Line Cross Section.

As can be seen the structure consists of two transmission lines placed parallel to each other, meaning that coupling is achieved due to electromagnetic energy being transferred between the two lines. This structure supports two quasi-TEM modes, namely even and odd modes. In microstrip coupled lines the dielectric mediums are not homogeneous, with air above and the dielectric medium below. In these two modes the fields are distributed in different ways above and below the substrate. As microstrip is not pure TEM the two modes experience different permittivity's, meaning the phase velocities are unequal in the two modes. This means that the coupled microstrip lines are characterised by the characteristic impedances as well as the effective dielectric constants for the two modes.

For an even mode excitation, both microstrip lines have the same voltage potentials or carry the same sign charges, which results in a magnetic wall at the symmetry plane. In the odd mode case both microstrip lines have opposite voltages or carry opposite sign charges, therefore the symmetric plane acts as an electric wall.

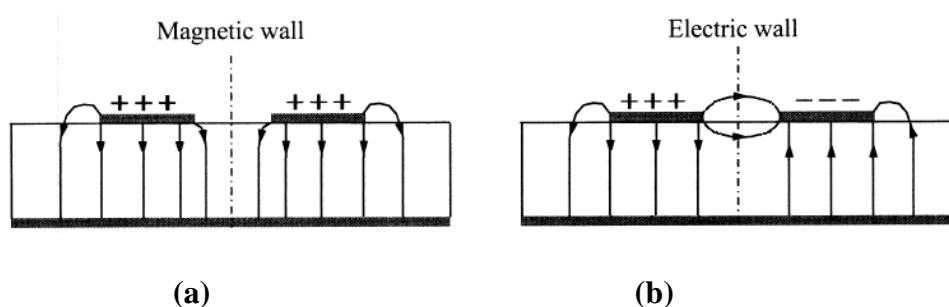


Figure 3.17: (a) Even Mode Excitation, (b) Odd Mode Excitation

3.6.1) Design Equations

In order to design such a coupled line structure, there are a number of equations presented, for instance in [15] accurate closed form expressions for the effective dielectric constant and the characteristic impedances are given as follows:

$$\epsilon_{re}^e = \frac{\epsilon_r + 1}{2} + \frac{\epsilon_r - 1}{2} \left(1 + \frac{10}{v}\right)^{-a_e b_e} \quad (3.32)$$

With

$$\begin{aligned} v &= \frac{u(20 + g^2)}{10 + g^2} + g \exp(-g) \\ a_e &= 1 + \frac{1}{49} \ln \left[\frac{v^4 + (v/52)^2}{v^4 + 0.432} \right] + \frac{1}{18.7} \ln \left[1 + \left(\frac{v}{18.1} \right)^3 \right] \\ b_e &= 0.564 \left(\frac{\epsilon_r - 0.9}{\epsilon_r + 3} \right)^{0.053} \end{aligned} \quad (3.33)$$

Where $u = W/h$ and $g = s/h$. The error in ϵ_{re}^e is within 0.7% over the ranges of $0.1 \leq u \leq 10$, $0.1 \leq g \leq 10$, and $1 \leq \epsilon_r \leq 18$.

$$\epsilon_{re}^o = \epsilon_{re} + [0.5(\epsilon_r + 1) - \epsilon_{re} + a_o] \exp(-c_o g^{d_o}) \quad (3.34)$$

With

$$\begin{aligned} a_o &= 0.7287[\epsilon_{re} - 0.5(\epsilon_r + 1)][1 - \exp(-0.179u)] \\ b_o &= \frac{0.747\epsilon_r}{0.15 + \epsilon_r} \\ c_o &= b_o - (b_o - 0.207)\exp(-0.414u) \\ d_o &= 0.593 + 0.694 \exp(-0.526u) \end{aligned} \quad (3.35)$$

Where ϵ_{re} is the static effective dielectric constant of a single microstrip of width W . The error in ϵ_{re}^o is stated to be in the order of 0.5%. The even and odd mode characteristic

impedances given by the following closed form expressions are accurate to within 0.6% over the ranges $0.1 \leq u \leq 10$, $0.1 \leq g \leq 10$, and $1 \leq \epsilon_r \leq 18$.

$$Z_{ce} = \frac{Z_c \sqrt{\epsilon_{re}'} \epsilon_{re}^e}{1 - Q_4 \sqrt{\epsilon_{re}'} \cdot Z_c / 377} \quad (3.36)$$

$$Z_{co} = \frac{Z_c \sqrt{\epsilon_{re}'} \epsilon_{re}^o}{1 - Q_{10} \sqrt{\epsilon_{re}'} \cdot Z_c / 377} \quad (3.37)$$

Where Z_c is the characteristic impedance of a single microstrip of width W , and

$$\begin{aligned} Q_1 &= 0.8685u^{0.194} \\ Q_2 &= 1 + 0.7519g + 0.189g^{2.31} \\ Q_3 &= 0.1975 + \left[16.6 + \left(\frac{8.4}{g} \right)^6 \right]^{-0.387} + \frac{1}{241} \ln \left[\frac{g^{10}}{1 + (g/3.4)^{10}} \right] \\ Q_4 &= \frac{2Q_1}{Q_2} \cdot \frac{1}{u^{Q_3} \exp(-g) + [2 - \exp(-g)]u^{-Q_3}} \\ Q_5 &= 1.794 + 1.14 \ln \left[1 + \frac{0.638}{g + 0.517g^{2.43}} \right] \\ Q_6 &= 0.2305 + \frac{1}{281.3} \ln \left[\frac{g^{10}}{1 + (g/5.8)^{10}} \right] + \frac{1}{5.1} \ln(1 + 0.598 g^{1.154}) \\ Q_7 &= \frac{10 + 190g^2}{1 + 82.3 g^3} \\ Q_8 &= \exp[-6.5 - 0.95 \ln(g) - (g/0.15)^5] \\ Q_9 &= \ln(Q_7) \cdot (Q_8 + 1/16.5) \\ Q_{10} &= Q_4 - \frac{Q_5}{Q_2} \exp \left[\frac{Q_6 \ln(u)}{u^{Q_9}} \right] \end{aligned} \quad (3.38)$$

3.6.2) Even and Odd Mode Extraction Technique

An extraction technique can be used in order to obtain the even and odd mode impedances using an EM simulator such as [16]. The following shows the microstrip layouts for the even and odd mode excitations:

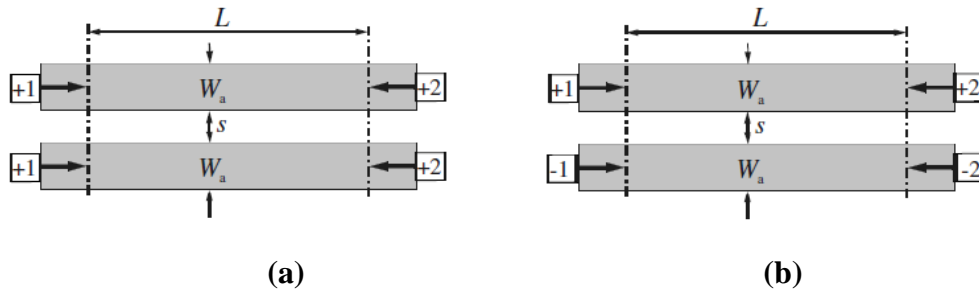


Figure 3.18: (a) even mode excitation, (b) odd mode excitation.

From the EM simulation, a set of two port S-parameters for each mode can be found in the form:

$$\begin{aligned} S_{11} &= S_{22} = |S_{11}|e^{j\phi_{11}} \\ S_{12} &= S_{21} = |S_{21}|e^{j\phi_{21}} \end{aligned} \quad (3.39)$$

From this the effective dielectric constant for the mode under consideration by:

$$\epsilon_{re} = \left(\frac{\phi_{21}}{2\pi} \frac{\lambda_0}{L} \right)^2 \quad (3.40)$$

Where ϕ_{21} is the phase in radians, λ_0 is the wavelength in free space at the frequency specified, and L is the line length between the two reference planes, where the S-parameters are de-embedded. Theoretically, the L can be set to any length, however practically it should be set to quarter wave-length for accurate data. The characteristic impedance can also be extracted:

$$Z_c = \text{Re} \left\{ \frac{Z_{in} - Z_0 + \sqrt{(Z_{in} - Z_0)^2 - 4Z_0 Z_{in} \tan^2 \phi_{21}}}{j2 \tan \phi_{21}} \right\} \quad (3.41)$$

With

$$Z_{in} = Z_0 \frac{1 + S_{11}}{1 - S_{11}} \quad (3.42)$$

Where Z_0 is the port terminal impedance; some EM simulators such as [16] can automatically extract ϵ_{re} and Z_c . In order to find the even and odd mode impedances the following can be used:

$$Z_{0e} = 2Z_c \quad (3.43)$$

$$Z_{0o} = Z_c/2 \quad (3.44)$$

3.7) Stepped Impedance Resonators

Stepped impedance resonators consist of two transmission lines with different characteristic impedances [17]. The resonance of a stepped impedance resonator is changed by adjusting the ratio of the low to high impedance step, which is defined as:

$$R = \frac{Z_2}{Z_1} \quad (3.45)$$

Where Z_2 is the low impedance element and Z_1 is the high impedance element.

Since $R < 1$ then the overall size of the resonator is reduced; using a low value of R will increase the frequency of the second resonance, increasing the out of band rejection.

3.8) References

[1] S. Darlington, "Synthesis of Reactance 4 poles which Produce Prescribed Insertion Loss Characteristics," *Journal of Mathematics and Physics*, Vol. 18, pp. 257 – 353, September 1939.

- [2] E. A. Guillemin, "Synthesis of Passive Networks," John Wiley and Sons, Inc., New York, 1957.
- [3] M. E. van Valkenberg, "Introduction to modern Network Synthesis," John Wiley and Sons, Inc., New York, 1960.
- [4] V. Belevitch, "Tchebyshev Filters and Amplifier Networks," *Wireless Engineer*, Vol. 29, pp. 106 – 110, April 1952.
- [5] H. J. Orchard, "Formula For Ladder Filters," *Wireless Engineer*, Vol. 30, pp. 3 – 5, January 1953.
- [6] E. Green, "Synthesis of Ladder Networks to Give Butterworth or Chebyshev Response in the Passband," *Proceeding IEE London, Part IV, Monograph No. 88*, 1954.
- [7] E. Green, "Amplitude – Frequency Characteristics of Ladder Networks," pp. 62–78, *Wireless Telegraph Co., Ltd., Chelmsford, Essex, England*, 1954.
- [8] L. Weinberg, "Network Design By use of Modern Synthesis Techniques and Tables," *Proceedings of National Electronic Conference*, Vol. 12, 1956.
- [9] L. Weinberg, "Additional Tables for Design of Optimum Ladder Networks," *Parts I and II, Journal of the Franklin Institute*, Vol. 264, pp. 7 – 23 and pp. 127 – 138, July and August 1957.
- [10] L. Storch, "Synthesis of Constant – Time – Delay Ladder Network Using Bessel Polynomials," *Proceedings IRE* 42, pp. 1666–1675, November 1954.
- [11] W. E. Thomson, "Networks with Maximally Flat Delay," *Wireless Engineer*, Vol. 29, pp. 255 – 263, October 1952.
- [12] J. S. Hong, M. J. Lancaster, "Microstrip Filters for RF/Microwave Applications," *Wiley*, New York, 2001.

- [13] George L. Matthaei, Leo Young, E. M. T. Jones, “Microwave Filters, Impedance – Matching Networks, and Coupling Structures,” *McGraw – Hill, Inc., New York 1964*.
- [14] D. M. Pozar, “Microwave Engineering,” John Wiley & Sons, Inc., New York 2005.
- [15] M. Kirschning, R. H. Jansen, “Accurate wide-range design equations for parallel coupled microstrip lines,” *IEEE Trans. Microwave Theory Tech.*, vol. 32, pp. 83–90, Jan. 1984.
- [16] Sonnet Software Inc., EM User’s Manual, Version 12, NY 2009.
- [17] M. Makimoto, S. Yamashita, “Compact Bandpass filters Using stepped impedance resonators,” *Proceedings of the IEEE. Dig.*, vol. 67, Jan 1979, pp. 16–19

Chapter 4: Filter Topologies

4.1) Introduction

The aim of this chapter is to introduce the filter topologies used in this research along with respective design equations and theory. The coupled line structure is shown with an equivalent circuit and how this can be utilised in order to obtain a filter with higher selectivity. Optimum Highpass and Bandstop/Lowpass filter design equations are also presented. Each topology described is heavily used in later chapters; therefore each topology is described in great detail with all theory, design equations and circuits clearly illustrated.

4.2) Short Circuit Coupled Line Filter

4.2.1) Single Section Formulation

Using [1] it can be shown that a short circuit coupled line section is equivalent to the circuit shown below:

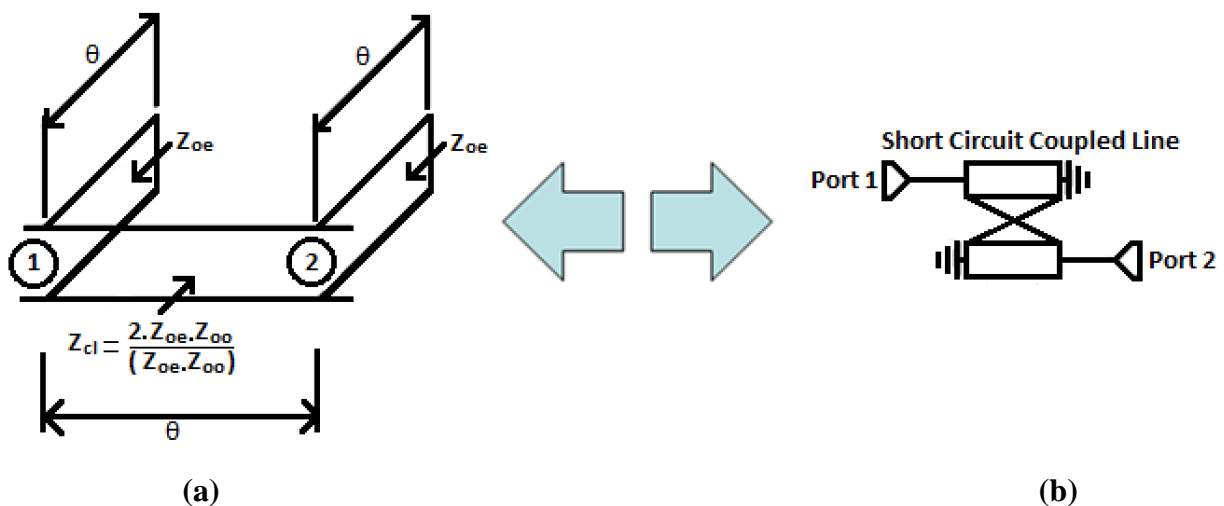


Figure 4.1: Single Section Coupled Line Filter (a) Equivalent Circuit, (b) Coupled Line Structure.

From this equivalent circuit it can be deduced using ABCD parameters that:

$$\begin{aligned}
 \begin{pmatrix} A & B \\ C & D \end{pmatrix} &= \begin{pmatrix} 1 & 0 \\ Y & 1 \end{pmatrix} \cdot \begin{pmatrix} \cos(\theta) & j \cdot Z_{cl} \cdot \sin(\theta) \\ \frac{j \cdot \sin(\theta)}{Z_{cl}} & \cos(\theta) \end{pmatrix} \cdot \begin{pmatrix} 1 & 0 \\ Y & 1 \end{pmatrix} \\
 &= \begin{pmatrix} \cos(\theta) & j \cdot Z_{cl} \cdot \sin(\theta) \\ Y \cdot \cos(\theta) + \frac{j \cdot \sin(\theta)}{Z_{cl}} & Y \cdot j \cdot Z_{cl} \cdot \sin(\theta) + \cos(\theta) \end{pmatrix} \cdot \begin{pmatrix} 1 & 0 \\ Y & 1 \end{pmatrix} \quad (4.1) \\
 &= \begin{pmatrix} \cos(\theta) + j \cdot Z_{cl} \cdot Y \cdot \sin(\theta) & j \cdot Z_{cl} \cdot \sin(\theta) \\ Y \cdot \cos(\theta) + \frac{j \cdot \sin(\theta)}{Z_{cl}} + Y \cdot (Y \cdot j \cdot Z_{cl} \cdot \sin(\theta) + \cos(\theta)) & Y \cdot j \cdot Z_{cl} \cdot \sin(\theta) + \cos(\theta) \end{pmatrix}
 \end{aligned}$$

Where:

$$Y = \frac{1}{j \cdot Z_{oe} \cdot \tan(\theta)} \quad (4.2)$$

And

$$Z_{cl} = \frac{2 \cdot Z_{oe} \cdot Z_{oo}}{Z_{oe} - Z_{oo}} \quad (4.3)$$

Substituting (4.2) and (4.3) into the ABCD matrix in (4.1) and simplifying gives the following values:

$$\begin{aligned}
 A &= \cos(\theta) + Y \cdot j \cdot Z_{cl} \cdot \sin(\theta) \\
 &= \cos(\theta) + \left(-\frac{1}{j \cdot Z_{oe} \cdot \tan(\theta)} \right) \cdot j \cdot \left(\frac{2 \cdot Z_{oe} \cdot Z_{oo}}{Z_{oe} - Z_{oo}} \right) \cdot \sin(\theta) \\
 &= \cos(\theta) + \left(\frac{2 \cdot Z_{oe} \cdot Z_{oo} \cdot \sin(\theta)}{Z_{oe} \cdot \tan(\theta) \cdot (Z_{oe} - Z_{oo})} \right) \quad (4.4) \\
 &= \cos(\theta) + \frac{2 \cdot Z_{oe} \cdot Z_{oo} \cdot \cos(\theta)}{Z_{oe} \cdot (Z_{oe} - Z_{oo})} \\
 &= \cos(\theta) \left(1 + \frac{2 \cdot Z_{oe} \cdot Z_{oo}}{Z_{oe} \cdot (Z_{oe} - Z_{oo})} \right)
 \end{aligned}$$

$$\begin{aligned}
B &= j \cdot Zcl \cdot \sin(\theta) \\
&= j \cdot \left(\frac{2 \cdot Zoe \cdot Zoo}{Zoe - Zoo} \right) \cdot \sin(\theta)
\end{aligned} \tag{4.5}$$

$$\begin{aligned}
C &= \left(Y \cdot \cos(\theta) + \frac{j \cdot \sin(\theta)}{Zcl} \right) + \left[\left(Y \cdot j \cdot Zcl \cdot \sin(\theta) + \cos(\theta) \right) \cdot Y \right] \\
&= \left(-\frac{j \cdot \cos(\theta)}{Zoe \cdot \tan(\theta)} \right) + \frac{j \cdot \sin(\theta)}{\left(\frac{2 \cdot Zoe \cdot Zoo}{Zoe - Zoo} \right)} + \left[\left(\cos(\theta) + \frac{2 \cdot j \cdot Zoe \cdot Zoo \cdot \sin(\theta)}{(Zoe - Zoo)} \cdot \frac{1}{j \cdot Zoe \cdot \tan(\theta)} \right) \cdot \left(\frac{1}{j \cdot Zoe \cdot \tan(\theta)} \right) \right] \\
&= \left(-\frac{j \cdot \cos(\theta)}{Zoe \cdot \tan(\theta)} \right) + \frac{j \cdot \sin(\theta) \cdot (Zoe - Zoo)}{2 \cdot Zoe \cdot Zoo} + \left(\frac{2 \cdot Zoe \cdot Zoo \cdot \cos(\theta)}{Zoe(Zoe - Zoo)} + \cos(\theta) \right) \cdot \frac{1}{j \cdot Zoe \cdot \tan(\theta)} \\
&= \left(-\frac{2 \cdot j \cdot \cos(\theta)}{Zoe \cdot \tan(\theta)} \right) + \frac{j \cdot \sin(\theta) \cdot (Zoe - Zoo)}{2 \cdot Zoe \cdot Zoo} + \left(\frac{-2 \cdot j \cdot Zoe \cdot Zoo \cdot \cos(\theta)}{Zoe^2(Zoe - Zoo) \cdot \tan(\theta)} \right) \\
&= -\frac{2 \cdot j \cdot \cos(\theta)}{Zoe \cdot \tan(\theta)} \left(1 + \frac{Zoe \cdot Zoo}{Zoe \cdot (Zoe - Zoo)} \right) + \frac{j \cdot \sin(\theta) \cdot (Zoe - Zoo)}{2 \cdot Zoe \cdot Zoo}
\end{aligned} \tag{4.6}$$

$$D = A \tag{4.7}$$

From these expressions, the S11 and S21 parameters can be obtained using the following well known terms [2], [3]:

$$S_{11} = \frac{A + \left(\frac{B}{Zo} \right) - (C \cdot Zo) - D}{A + \left(\frac{B}{Zo} \right) + (C \cdot Zo) + D} \tag{4.8}$$

$$S_{21} = \frac{2}{A + \left(\frac{B}{Zo} \right) + (C \cdot Zo) + D} \tag{4.9}$$

These in turn, give:

$$S_{11} = \frac{j \cdot \left(\frac{2 \cdot Z_{oe} \cdot Z_{oo}}{Z_{oe} - Z_{oo}} \right) \cdot \sin(\theta)}{Z_0} - \left(-\frac{2 \cdot j \cdot \cos(\theta)}{Z_{oe} \cdot \tan(\theta)} \left(1 + \frac{Z_{oe} \cdot Z_{oo}}{Z_{oe} \cdot (Z_{oe} - Z_{oo})} \right) + \frac{j \cdot \sin(\theta) \cdot (Z_{oe} - Z_{oo})}{2 \cdot Z_{oe} \cdot Z_{oo}} \right) \cdot Z_0}{2 \cdot \left(\cos(\theta) \cdot \left(1 + \frac{2 \cdot Z_{oe} \cdot Z_{oo}}{Z_{oe} \cdot (Z_{oe} - Z_{oo})} \right) \right) + \frac{j \cdot \left(\frac{2 \cdot Z_{oe} \cdot Z_{oo}}{Z_{oe} - Z_{oo}} \right) \cdot \sin(\theta)}{Z_0} + \left(-\frac{2 \cdot j \cdot \cos(\theta)}{Z_{oe} \cdot \tan(\theta)} \left(1 + \frac{Z_{oe} \cdot Z_{oo}}{Z_{oe} \cdot (Z_{oe} - Z_{oo})} \right) + \frac{j \cdot \sin(\theta) \cdot (Z_{oe} - Z_{oo})}{2 \cdot Z_{oe} \cdot Z_{oo}} \right) \cdot Z_0}$$

(4.10)

$$S_{21} = \frac{2}{2 \cdot \left(\cos(\theta) \cdot \left(1 + \frac{2 \cdot Z_{oe} \cdot Z_{oo}}{Z_{oe} \cdot (Z_{oe} - Z_{oo})} \right) \right) + \frac{j \cdot \left(\frac{2 \cdot Z_{oe} \cdot Z_{oo}}{Z_{oe} - Z_{oo}} \right) \cdot \sin(\theta)}{Z_0} + \left(-\frac{2 \cdot j \cdot \cos(\theta)}{Z_{oe} \cdot \tan(\theta)} \left(1 + \frac{Z_{oe} \cdot Z_{oo}}{Z_{oe} \cdot (Z_{oe} - Z_{oo})} \right) + \frac{j \cdot \sin(\theta) \cdot (Z_{oe} - Z_{oo})}{2 \cdot Z_{oe} \cdot Z_{oo}} \right) \cdot Z_0}$$

(4.11)

At Cut off frequency, i.e. $\theta = 90^\circ$, these expressions simplify to:

$$S_{11} = \frac{\frac{j \cdot \left(\frac{2 \cdot Z_{oe} \cdot Z_{oo}}{Z_{oe} - Z_{oo}} \right)}{Z_0} - j \cdot \left[\frac{Z_{oe} - Z_{oo}}{2 \cdot Z_{oe} \cdot Z_{oo}} \right] \cdot Z_0}{\frac{j \cdot \left(\frac{2 \cdot Z_{oe} \cdot Z_{oo}}{Z_{oe} - Z_{oo}} \right)}{Z_0} + j \cdot \left[\frac{Z_{oe} - Z_{oo}}{2 \cdot Z_{oe} \cdot Z_{oo}} \right] \cdot Z_0}$$

(4.12)

$$= \frac{(2 \cdot Z_{oe} \cdot Z_{oo})^2 - (Z_{oe} - Z_{oo})^2 \cdot Z_0^2}{(2 \cdot Z_{oe} \cdot Z_{oo})^2 + (Z_{oe} - Z_{oo})^2 \cdot Z_0^2}$$

$$S_{21} = \frac{2}{\frac{j \cdot \left(\frac{2 \cdot Z_{oe} \cdot Z_{oo}}{Z_{oe} - Z_{oo}} \right)}{Z_0} + j \cdot \left[\frac{Z_{oe} - Z_{oo}}{2 \cdot Z_{oe} \cdot Z_{oo}} \right] \cdot Z_0}$$

(4.13)

$$= \frac{-4 \cdot j \cdot (Z_{oe} - Z_{oo}) \cdot Z_0 \cdot Z_{oe} \cdot Z_{oo}}{(2 \cdot Z_{oe} \cdot Z_{oo})^2 + (Z_{oe} - Z_{oo})^2 \cdot Z_0^2}$$

4.2.2) Multi-Section Coupled Line Filter Design Equations

The above equations can be used in order to design a single section filter, however in [1], Matthaei presents design equations in order to design higher order filters. In order to derive these equations the equivalent J-inverter circuit is analysed:

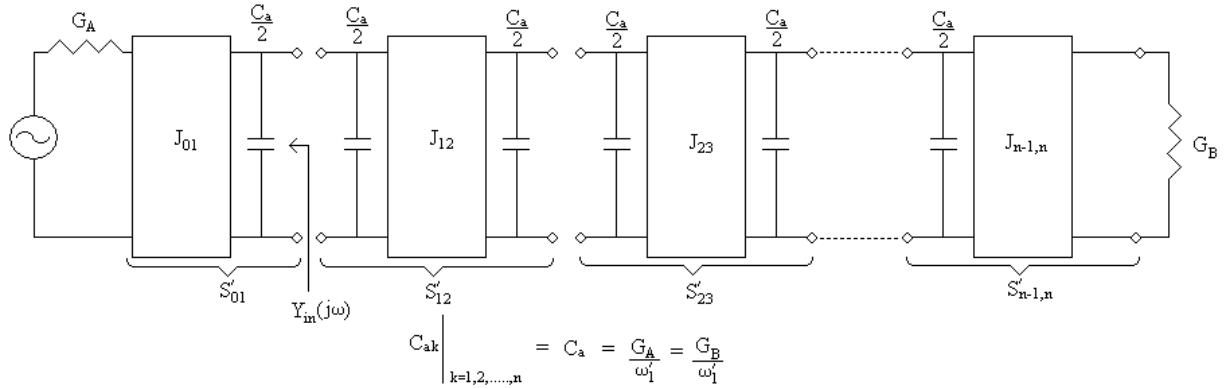


Figure 4.2: J-inverter Cascaded Coupled Line Circuit.

From the circuit diagram, there will be $n+1$ parallel coupled sections for an n -reactive element prototype filter. In order to compute the end sections, i.e. 0, 1 and n , $n+1$, the following expressions are used:

$$\begin{aligned}
 \frac{J_{k,k+1}}{Y_A} &= \frac{1}{\sqrt{g_k g_{k+1} \omega_1^2}} \quad , \quad (Y_{oo}^a)_{k,k+1} = Y_A \left(\frac{J_{k,k+1}}{Y_A} \sqrt{h} + 1 \right) \\
 (Y_{oe}^a)_{k,k+1} &= 2Y_A - (Y_{oo}^a)_{k,k+1} \quad , \quad \text{FBW} = \frac{f_2 - f_1}{f_0} \quad , \quad \theta_1 = \frac{\pi}{2} \left(1 - \frac{\text{FBW}}{2} \right) \\
 (Y_{oe}^b)_{k,k+1} &= (Y_{oe}^a)_{k,k+1} + h Y_A \left[\frac{\tan \theta_1}{2} + \left(\frac{J_{k,k+1}}{Y_A} \right)^2 \right] - Y_A \\
 (Y_{oo}^b)_{k,k+1} &= (Y_{oe}^b)_{k,k+1} + (Y_{oo}^a)_{k,k+1} + (Y_{oe}^a)_{k,k+1}
 \end{aligned} \tag{4.14}$$

The parameter h , is a dimensionless scale factor which can be chosen arbitrarily so as to give a convenient admittance level in the filter. A value for h which is usually satisfactory (and makes the parallel coupled section, S_{01} , of the filter have strips f_0 equal width) is:

$$h = \frac{1}{\frac{\tan\theta_1}{2} + \left(\frac{J_{01}}{Y_A}\right)^2} \quad (4.15)$$

Once the input and output sections have been computed, the interior sections 1, 2 to n-1, n for $k = 1$ to $k = n-1$ then have to be calculated using:

$$\begin{aligned} \frac{J_{k,k+1}}{Y_A} &= \frac{1}{\omega_1 \sqrt{g_k g_{k+1}}} \quad , \quad N_{k,k+1} = \sqrt{\left(\frac{J_{k,k+1}}{Y_A}\right)^2 + \left(\frac{\tan\theta_1}{2}\right)^2} \\ (Y_{oo})_{k,k+1} &= h Y_A \left[N_{k,k+1} + \left(\frac{J_{k,k+1}}{Y_A}\right)^2 \right] \\ (Y_{oe})_{k,k+1} &= h Y_A \left[N_{k,k+1} - \left(\frac{J_{k,k+1}}{Y_A}\right)^2 \right] \end{aligned} \quad (4.16)$$

The even and odd mode admittances are then known and the multi section filter can now be implemented:

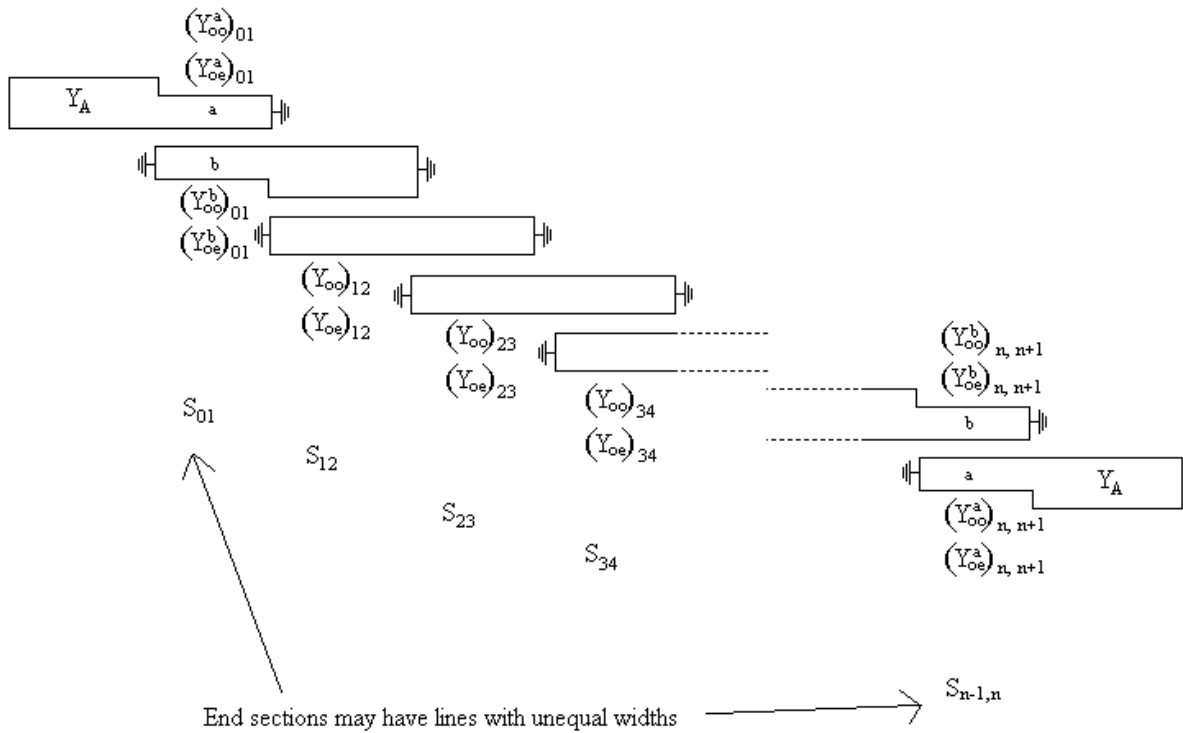


Figure 4.3: Multi-Section Coupled Line Filter.

On inspection of the filter, it can be clearly seen from the J-inverter circuit, the input and output sections do not contribute anything to the order of filter. These sections only contribute to the input and output impedance. If however, we examine the equivalent circuit J-inverter section [1]:

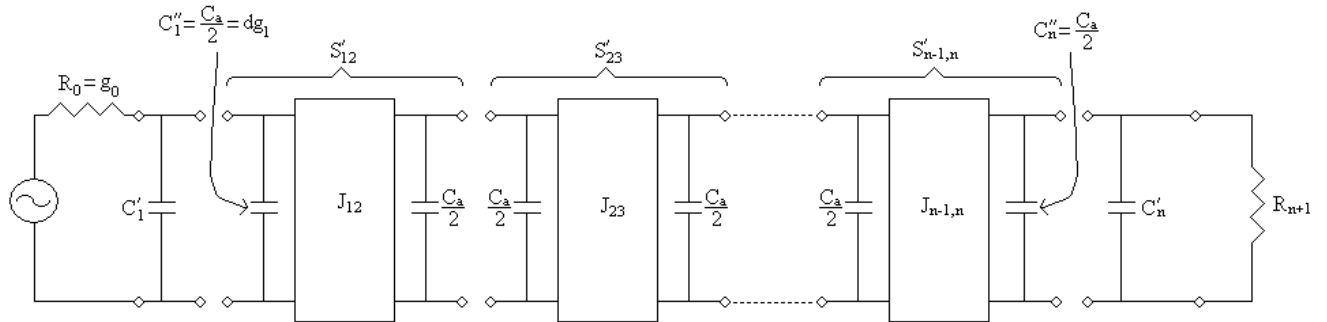


Figure 4.4: Equivalent Stub Filter J-inverter Circuit.

In order to calculate the circuit parameters:

$$\begin{aligned}
 C_1' &= g_1(1-d) & \text{FBW} &= \frac{f_2-f_1}{f_0} & , & \quad \theta_1 = \frac{\pi}{2} \left(\frac{1-\text{FBW}}{2} \right) & & C_n' = \frac{g_n g_{n+1} - dg_1 R_{n+1}}{R_{n+1}} \\
 C_1 &= g_1 = C_1' + C_1'' & C_a &= 2dg_1 & & & & C_n = g_n \frac{g_{n+1}}{R_{n+1}} \\
 J_{12} &= g_0 \sqrt{\frac{C_a}{g_2}} & , & \quad J_{k,k+1} \Big|_{k=2 \text{ to } n-2} &= \frac{g_0 C_a}{\sqrt{g_k g_{k+1}}} & , & & J_{n-1,n} = g_0 \sqrt{\frac{C_a g_{n+1}}{g_{n-1} g_n}}
 \end{aligned} \tag{4.17}$$

d is usually a dimensionless constant (typically chosen to be 1) which can be chosen in order to give a convenient admittance level in the interior of the filter.

$$N_{k,k+1} \Big|_{k=1 \text{ to } n-1} = \sqrt{\left(\frac{J_{k,k+1}}{Y_A} \right)^2 + \left(\frac{g_0 \omega' C_a \tan \theta_1}{2} \right)^2} \tag{4.18}$$

The characteristic admittances of the stubs are:

$$\begin{aligned}
Y_1 &= g_0 \omega_1' Y_A (1-d) g_1 \tan \theta_1 + Y_A \left(N_{12} - \frac{J_{12}}{Y_A} \right) \\
Y_k \Big|_{k=2 \text{ to } n-1} &= Y_A \left(N_{k-1,k} + N_{k,k+1} - \frac{J_{k-1,k}}{Y_A} - \frac{J_{k,k+1}}{Y_A} \right) \\
Y_n &= Y_A \omega_1' (g_n g_{n+1} - d g_0 g_1) \tan \theta_1 + Y_A \left(N_{n-1,n} - \frac{J_{n-1,n}}{Y_A} \right)
\end{aligned} \tag{4.19}$$

The characteristic admittances of the connecting lines are:

$$Y_{k,k+1} \Big|_{k=1 \text{ to } n-1} = Y_A \left(\frac{J_{n-1,n}}{Y_A} \right) \tag{4.20}$$

All Stubs and Connecting lines are $\lambda_0/4$ long, where λ_0 is the wavelength in the medium of propagation at the midband frequency f_0 .

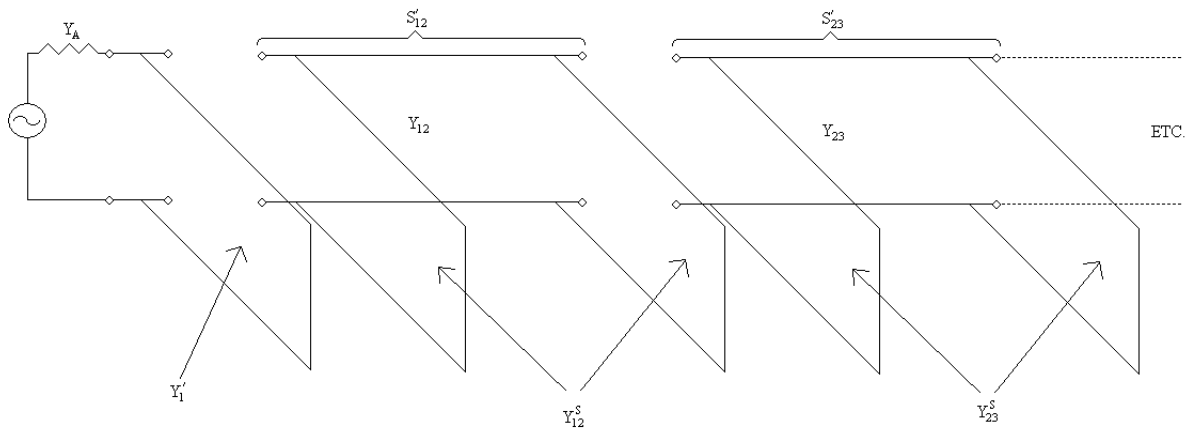


Figure 4.5: Short Circuit Stub Bandpass.

As shown before, this circuit has direct equivalence to the coupled line filter; meaning that it can be easily converted. A reason for this is that each section contributes to the order of the filter meaning that a higher order filter can be obtained for less number of sections. The reason for converting to the coupled line structure is that this structure is already de-coupled meaning that it is much easier to introduce bias circuits for bandwidth reconfigurability (as

will be shown in later chapters). In general, when this type of circuit is designed, the following can be observed:

- All connecting lines have equal impedance.
- Input and output stubs have equal impedance.
- All interior stubs are of equal impedance.
- The impedance of the interior stubs are half of the impedance of the input and output stubs.

These all allow for easy conversion, and re-iterate the fact that these structures are equivalent.

4.3) Optimum Highpass Filter

The optimum highpass filter has an equivalent circuit of **Figure 4.6**, where both the short circuit stubs and connecting lines contribute to the selectivity [3]. This type of filter consists of a cascade of short circuit stubs of electrical length θ_c separated by connecting lines $2\theta_c$ at some specified frequency f_c , which is usually the cut off frequency of the Highpass filter. The main reason for using this type of filter is that even although the filter consists of n number of stubs, it has an insertion function of degree $2n-1$ in frequency so that its Highpass response has $2n-1$ ripples. This means that the filter will not only have a high rate of cut off, it will also limit the number of PIN diodes needed to implement a high order reconfigurable filter.

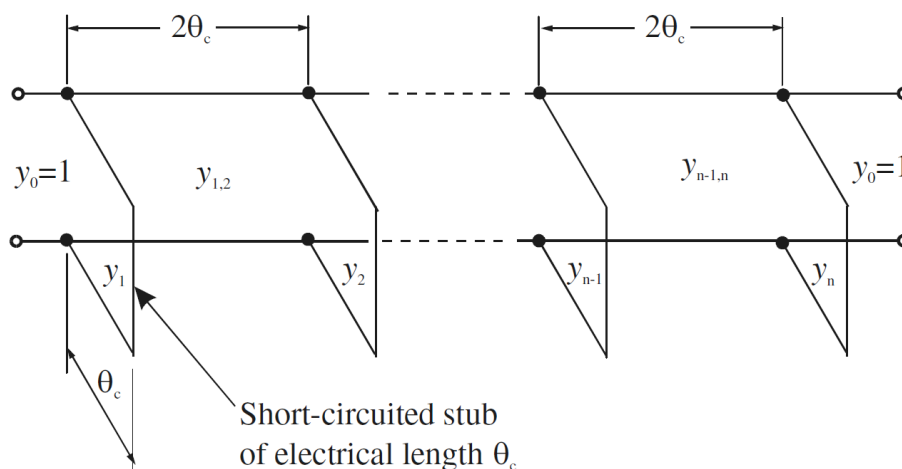


Figure 4.6: Optimum Distributed Highpass Filter.

The typical response of an optimum highpass filter is shown in **Figure 4.7**

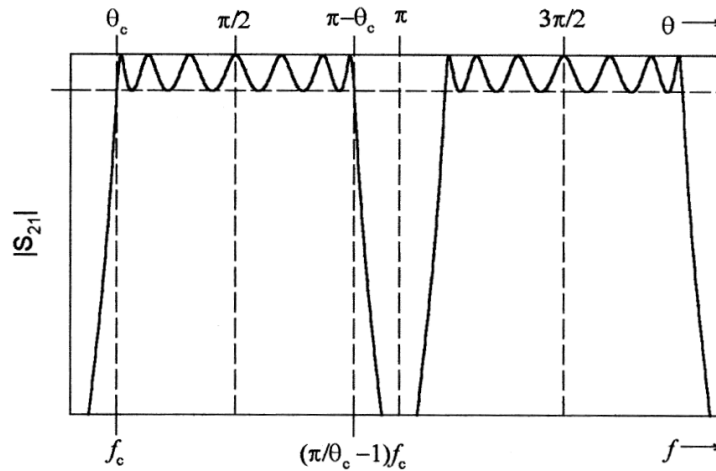


Figure 4.7: Typical Filter Characteristic of Optimum Highpass Filter.

where f is the frequency variable and θ is the electrical length, where f is proportional to θ :

$$\theta = \theta_c \frac{f}{f_c} \quad (4.21)$$

In using this filter for Highpass applications the primary passband is from θ_c to $\pi - \theta_c$ with a cut off at θ_c . The harmonic passbands occur periodically after this, each centered at $\theta = 3\pi/2$, $5\pi/2$, and so on. Each harmonic is separated by attenuation poles located at $\theta = \pi$, 2π , and so forth. The filtering characteristic of this filter can be described by the following transfer function:

$$|S_{21}(\theta)|^2 = \frac{1}{1 + \varepsilon^2 F_N^2(\theta)} \quad (4.22)$$

Where ε is the passband ripple constant, θ is the electrical length and F_N is the filtering function defined by:

$$F_N(\theta) = \frac{(1 + \sqrt{1 - x_c^2})T_{2n-1}\left(\frac{x}{x_c}\right) - (1 - \sqrt{1 - x_c^2})T_{2n-3}\left(\frac{x}{x_c}\right)}{2 \cos\left(\frac{\pi}{2} - \theta\right)} \quad (4.23)$$

where n is the number of short-circuit stubs,

$$x = \sin\left(\frac{\pi}{2} - \theta\right), \quad x_c = \sin\left(\frac{\pi}{2} - \theta_c\right) \quad (4.24)$$

and $T_n = \cos(n \cos^{-1} x)$ is the Chebyshev function of the first kind of degree n . This type of Highpass filter can theoretically provide an extremely wide passband as θ_c becomes very small, but this may require very high impedance short circuit stubs which may tend to unreasonable values for implementation. **Table 4.1** shows some typical element values of the filter with two to six stubs and a passband ripple of 0.1 dB for $\theta_c = 25^\circ, 30^\circ$ and 35° . These values are normalized characteristic admittances of transmission line elements and in order to calculate the associated characteristic line impedance, the following is used:

$$\begin{aligned} Z_i &= Z_0/y_i \\ Z_{i,i+1} &= Z_0/y_{i,i+1} \end{aligned} \quad (4.25)$$

where Z_0 is the terminal characteristic impedance.

n	θ_c	y_1 y_n	$y_{1,2}$ $y_{n-1,n}$	y_2 y_{n-1}	$y_{2,3}$ $y_{n-2,n-1}$	y_3 y_{n-2}	$y_{3,4}$
2	25°	0.15436	1.13482				
	30°	0.22070	1.11597				
	35°	0.30755	1.08967				
3	25°	0.19690	1.12075	0.18176			
	30°	0.28620	1.09220	0.30726			
	35°	0.40104	1.05378	0.48294			
4	25°	0.22441	1.11113	0.23732	1.10361		
	30°	0.32300	1.07842	0.39443	1.06488		
	35°	0.44670	1.03622	0.60527	1.01536		
5	25°	0.24068	1.10540	0.27110	1.09317	0.29659	
	30°	0.34252	1.07119	0.43985	1.05095	0.48284	
	35°	0.46895	1.02790	0.66089	0.99884	0.72424	
6	25°	0.25038	1.10199	0.29073	1.08725	0.33031	1.08302
	30°	0.35346	1.06720	0.46383	1.04395	0.52615	1.03794
	35°	0.48096	1.02354	0.68833	0.99126	0.77546	0.98381

Table 4.1: Element values for the Optimum Distributed Highpass Filter with 0.1 dB ripple [3].

4.4) Optimum Quasi Lowpass/Bandstop Filter

This type of filter is very similar to the Highpass filter except that it is a cascade of 90° open circuit stubs connecting with 90° transmission line [3]. A typical Bandstop arrangement is shown below:

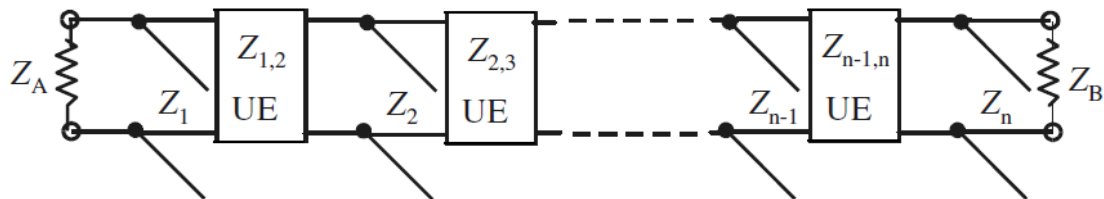


Figure 4.8: Transmission Line Network Representation of the Bandstop Filter.

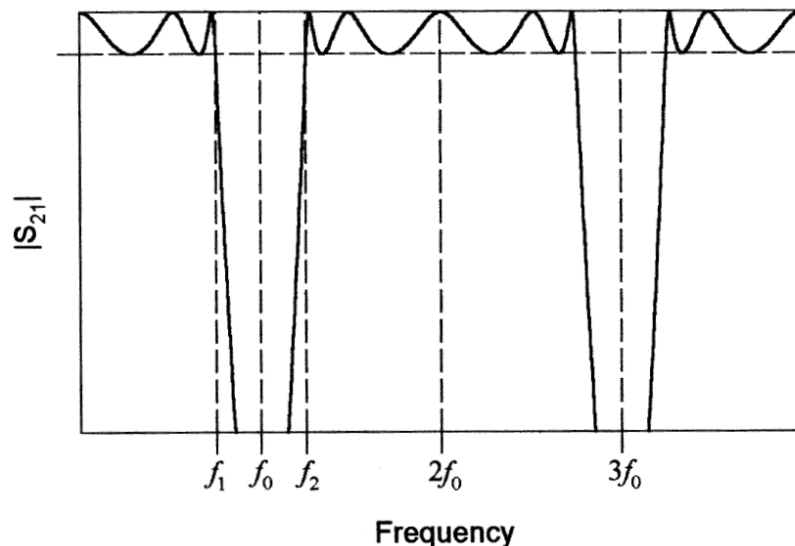


Figure 4.9: Filtering Characteristic of the Bandstop Filter.

The filtering characteristics of this entirely depend on the characteristic impedance of the open circuit stubs and the impedances of the connecting lines, in relation to the terminating impedances. Theoretically, this type of filter can be designed to have any stopband width; however as the stopband width becomes very narrow the impedance of the stubs becomes very high. With this design method [4] the unit elements of the filter become redundant meaning their filtering properties are not utilized. In [5] and [6] it was stated that these unit elements can be made just as effective as the open circuit stubs. By including these elements in the design, steeper attenuation characteristics can be obtained for the same number of stubs compared with filters with redundant unit elements. This means a more compact design can be made to meet the same filter characteristics. In order to design such a filter, the circuit is synthesized using the following transfer function:

$$|S_{21}(f)|^2 = \frac{1}{1 + \varepsilon^2 F_N^2(f)} \quad (4.26)$$

Where ε is the passband ripple constant and F_N is the filtering function given by:

$$F_N(f) = T_n\left(\frac{t}{t_c}\right) T_{n-1}\left(\frac{t\sqrt{1-t_c^2}}{t_c\sqrt{1-t^2}}\right) - U_n\left(\frac{t}{t_c}\right) U_{n-1}\left(\frac{t\sqrt{1-t_c^2}}{t_c\sqrt{1-t^2}}\right) \quad (4.27)$$

In which t is the Richardson transformation:

$$t = j \tan\left(\frac{\pi}{2} \frac{f}{f_0}\right) \quad (4.28)$$

And

$$t_c = j \tan\left(\frac{\pi}{4}(2 - FBW)\right) \quad (4.29)$$

Where f_0 is the midband frequency of the filter and FBW is the fractional bandwidth. The Chebyshev function of the first and second kinds of order n are:

$$\begin{aligned} T_n(x) &= \cos(n \cos^{-1} x) \\ U_n(x) &= \sin(n \cos^{-1} x) \end{aligned} \quad (4.30)$$

Referring to [6] the element values for this filter with two to six stubs and a passband return loss of -20 dB are tabulated below for bandwidths between 30% to 150%:

FBW	$g_1 = g_2$	$J_{1,2}$
0.3	0.16989	0.98190
0.4	0.23418	0.93880
0.5	0.30386	0.89442
0.6	0.38017	0.84857
0.7	0.46470	0.80106
0.8	0.55955	0.75173
0.9	0.66750	0.70042
1.0	0.79244	0.64700
1.1	0.93992	0.59137
1.2	1.11821	0.53346
1.3	1.34030	0.47324
1.4	1.62774	0.41077
1.5	2.01930	0.34615

Table 4.2: Element values of optimum Bandstop Filter for $n = 2$ and $\epsilon = 1.005$

FBW	$g_1 = g_3$	g_2	$J_{1,2} = J_{2,3}$
0.3	0.16318	0.26768	0.97734
0.4	0.23016	0.38061	0.92975
0.5	0.37754	0.63292	0.83956
0.6	0.46895	0.79494	0.78565
0.7	0.56896	0.97488	0.73139
0.8	0.67986	1.17702	0.67677
0.9	0.80477	1.40708	0.62180
1.0	0.94806	1.67311	0.56648
1.1	1.11601	1.98667	0.51082
1.2	1.15215	2.06604	0.49407
1.3	1.37952	2.49473	0.43430
1.4	1.67476	3.05136	0.37349
1.5	2.07059	3.79862	0.31262

Table 4.3: Element values of optimum Bandstop Filter for $n = 3$ and $\epsilon = 1.005$

FBW	$g_1 = g_4$	$g_2 = g_3$	$J_{1,2} = J_{3,4}$	$J_{2,3}$
0.3	0.23069	0.40393	0.93372	0.91337
0.4	0.31457	0.55651	0.87752	0.85157
0.5	0.40366	0.72118	0.82172	0.79093
0.6	0.49941	0.90054	0.76623	0.73145
0.7	0.60366	1.09802	0.71101	0.67313
0.8	0.71884	1.31815	0.65598	0.61597
0.9	0.79436	1.46655	0.62025	0.57951
1.0	0.99642	1.85355	0.54634	0.50503
1.1	1.10390	2.06672	0.50871	0.46793
1.2	1.37861	2.59505	0.43702	0.39831
1.3	1.55326	2.94111	0.39654	0.35972
1.4	1.97310	3.74861	0.32781	0.29526
1.5	2.43047	4.63442	0.27321	0.24488

Table 4.4: Element values of optimum Bandstop Filter for $n = 4$ and $\epsilon = 1.005$

<i>FBW</i>	$g_1 = g_5$	$g_2 = g_4$	g_3	$J_{1,2} = J_{4,5}$	$J_{2,3} = J_{3,4}$
0.3	0.23850	0.42437	0.45444	0.92798	0.90213
0.4	0.32455	0.58273	0.62307	0.87068	0.83818
0.5	0.41542	0.75293	0.80324	0.81413	0.77611
0.6	0.51385	0.93717	0.99711	0.75705	0.71472
0.7	0.62178	1.14215	1.21166	0.70221	0.65683
0.8	0.74624	1.38212	1.46326	0.64418	0.59700
0.9	0.87071	1.62166	1.71464	0.59299	0.54475
1.0	1.01167	1.89960	2.00417	0.54092	0.49299
1.1	1.20308	2.26455	2.38104	0.48338	0.43663
1.2	1.40157	2.66645	2.79799	0.42804	0.38305
1.3	1.68069	3.19873	3.36796	0.37569	0.33651
1.4	2.00690	3.84473	4.02293	0.32252	0.28580
1.5	2.47075	4.74882	4.96115	0.26871	0.23694

Table 4.5: Element values of optimum Bandstop Filter for $n = 5$ and $\epsilon = 1.005$

<i>FBW</i>	$g_1 = g_6$	$g_2 = g_5$	$g_3 = g_4$	$J_{1,2} = J_{5,6}$	$J_{2,3} = J_{4,5}$	$J_{3,4}$
0.3	0.24270	0.43420	0.47301	0.92496	0.89714	0.89192
0.4	0.32964	0.59521	0.64657	0.86715	0.83242	0.82616
0.5	0.42153	0.76772	0.83149	0.81025	0.76986	0.76287
0.6	0.51988	0.95454	1.03066	0.75411	0.70933	0.70191
0.7	0.62664	1.15929	1.24785	0.69860	0.65071	0.64311
0.8	0.74437	1.38676	1.48806	0.64361	0.59385	0.58629
0.9	0.87646	1.64341	1.75810	0.58904	0.53863	0.53128
1.0	1.02761	1.93826	2.06742	0.53481	0.48491	0.47793
1.1	1.20459	2.28427	2.42968	0.48084	0.43255	0.42606
1.2	1.41745	2.70085	2.86529	0.42707	0.38142	0.37550
1.3	1.68193	3.21846	3.40624	0.37346	0.33137	0.32610
1.4	2.02423	3.88780	4.10584	0.31997	0.28228	0.27769
1.5	2.49141	4.80007	5.05987	0.26655	0.23399	0.23014

Table 4.6: Element values of optimum Bandstop Filter for $n = 6$ and $\epsilon = 1.005$

These element values are normalized admittance values and in order to calculate the relevant impedance values, the following are used:

$$\begin{aligned}
Z_A &= Z_B = Z_0 \\
Z_i &= Z_0/g_i \\
Z_{i,i+1} &= Z_0/J_{i,i+1}
\end{aligned} \tag{4.31}$$

Where Z_0 is the input/output terminating impedance.

This type of filter can be further optimized using a method described in [7] to create a good performance filter, where the stub lengths and connecting lines are altered in order to change

the positions of the transmission zeroes which in turn increase the selectivity and stopband width and performance.

4.5) References

[1] George L. Matthaei, Leo Young, E. M. T. Jones, “Microwave Filters, Impedance – Matching Networks, and Coupling Structures,” *McGraw – Hill, Inc., New York 1964*.

[2] D. M. Pozar, “Microwave Engineering,” John Wiley & Sons, Inc., New York 2005.

[3] J. S. Hong, M. J. Lancaster, “Microstrip Filters for RF/Microwave Applications,” *Wiley, New York, 2001*.

[4] B. M. Schiffman and G. L. Mathei, “Exact Design of band-stop microwave filters,” *IEEE Trans., MTT-12, 1964, 6 – 15*.

[5] M. C. Horton and R. J. Menzel, “General Theory and Design of Optimum quarter wave TEM filters,” *IEEE Trans., MTT-13, 3 May 1965, 316 – 327*.

[6] O. P. Gupta, R. J. Menzel, “Design tables for a class of optimum microwave Bandstop Filters,” *IEEE Trans., MTT-18, July 1970, 402 – 404*.

[7] Z.-C. Hao and J.-S. Hong, “UWB Bandpass Filter using Cascaded Miniature Highpass and Lowpass Filters with Multilayer Liquid Crystal Polymer Technology,” *IEEE Trans. Microw. Theory Tech.*, vol. 58, no. 4, pp. 941 – 948, April 2010

Chapter 5: System Integration

Considerations

5.1) Introduction

Many communication systems require filtering; and as discussed in previous chapters with multifunctional capabilities. In systems such as a receiver, in order to detect a desirable signal a minimum input signal power is required (MDS). However, if the input signal is too high, a receiver can not function properly. This is because of a number of problems, namely gain compression and third intermodulation distortion. These problems need to be considered in the design of reconfigurable filters as the devices are essentially non linear devices, similar to amplifiers and mixers; which are also apparent in receivers. These problems are documented in [1] and [2] and occur as active non linear devices are introduced for reconfigurability. For the discussion in this chapter, a general nonlinear network, having an input voltage v_i and an output voltage v_o , is shown below:

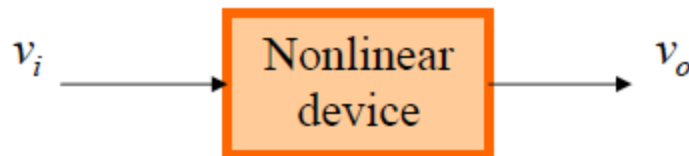


Figure 5.1: Nonlinear Device.

In the most general sense, the output response of a nonlinear device can be modelled as a Taylor series in terms of v_i :

$$v_o = a_0 + a_1v_i + a_2v_i^2 + a_3v_i^3 + \dots \quad (5.1)$$

Where a_0 , a_2 and a_3 are the Taylor coefficient of the first three terms; different non-linear devices will have different sets of the Taylor coefficients. This chapter describes the problems which could arise due to nonlinearity in reconfigurable filters.

5.2) Gain Compression

Consider the case where a sinusoidal voltage:

$$v_i = V_m \cos \omega t \quad (5.2)$$

is applied to the input of a nonlinear two-port network, such as nonlinear device. The output can be expressed in terms of this input using the Taylor series:

$$\begin{aligned} v_o &= a_0 + a_1 v_i + a_2 v_i^2 + a_3 v_i^3 + \dots \\ &= a_0 + a_1 V_m \cos \omega t + a_2 V_m^2 \cos^2 \omega t + a_3 V_m^3 \cos^3 \omega t + \dots \\ &= \left(a_0 + \frac{1}{2} a_2 V_m^2 + \dots \right) + \left(a_1 V_m + \frac{3}{4} a_3 V_m^3 + \dots \right) \cos \omega t \\ &\quad + \left(\frac{1}{2} a_2 V_m^2 + \dots \right) \cos 2\omega t + \dots \end{aligned} \quad (5.3)$$

As can be seen there have been trigonometric identities applied.

In general, the output will have a DC, a fundamental and a harmonic frequency component. Only the output at the fundamental frequency ω is of interest. Assuming that both input and output of the network are matched to terminal impedance Z_0 , we can express the input and output powers at ω as:

$$\begin{aligned} P_{in} &= \frac{1}{2} \frac{V_m^2}{Z_0} \\ P_{out} &= \frac{1}{2Z_0} \left(a_1 V_m + \frac{3}{4} a_3 V_m^3 + \dots \right)^2 \end{aligned} \quad (5.4)$$

If there were only $a_1 \neq 0$ in the expression, we have a linear power gain of a_1^2 and the output power would become:

$$P_{out} = \frac{a_1^2 V_m^2}{2Z_0}$$

or

$$\begin{aligned} P_{out}(\text{dBm}) &= 10 \log \left(\frac{1}{2} \frac{V_m^2}{Z_0} \right) + 10 \log a_1^2 \\ &= P_{in}(\text{dBm}) + G(\text{dB}) \end{aligned} \quad (5.5)$$

Where $G(\text{dB})$ is the power gain.

If we plot the input and output powers on log scales (or in dBm), we have a straight line with a slope of unity, since for a constant G ,

$$\frac{dP_{out}(\text{dBm})}{dP_{in}(\text{dBm})} = 1 \quad (5.6)$$

This result is only for an ideal case where only the linear response is considered. In most practical devices, with additional non-zero high order terms the response is not linear, and the gain of the device is a function of the input power, which tends to decrease for large input powers. This effect is called gain compression, or saturation.

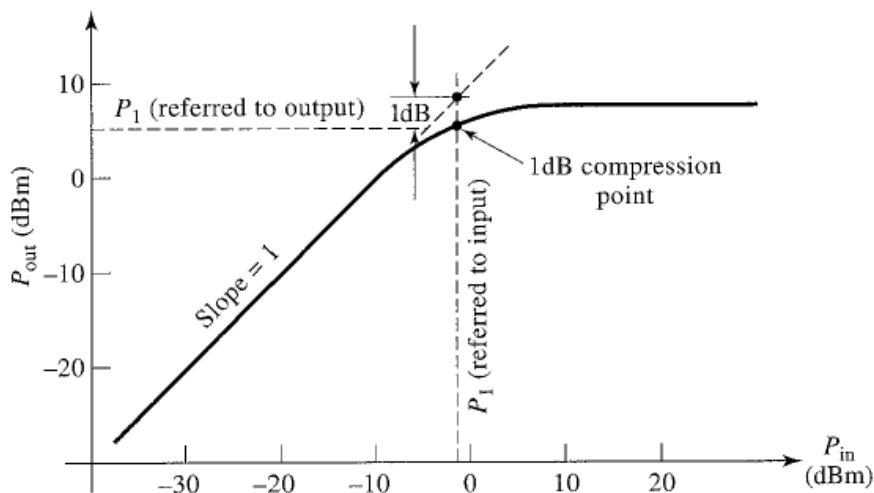


Figure 5.2: Typical Nonlinear Device Response.

5.2.1) 1 dB Compression Point Set up

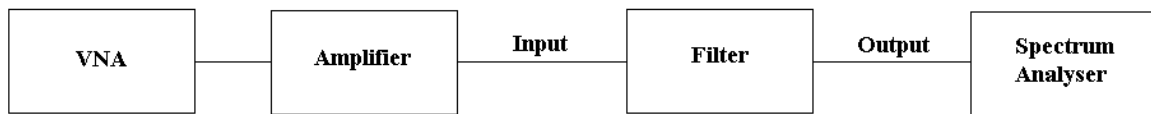


Figure 5.3: 1 dB Compression Measurement Set Up.

A set up for 1 dB compression measurement and the one that was used in this research project is shown above. A signal generator was used to generate the signal for testing. In the set up, an Agilent 8720 VNA was used as a signal generator. In order to get a high enough signal power, a broadband amplifier from mini-circuit was used to amplify the signal. The signal is then fed into the input of the reconfigurable bandpass filter being tested and the filter output is then fed the spectrum analyser.

The pin diodes used in each filter in subsequent chapters can only support a maximum of 23 dBm; the input signal never exceeded 20 dBm in order to protect the device under test.

5.3) Intermodulation Distortion

For a single input frequency, or tone, ω_0 , the output will in general consist of harmonics of the input frequency of the form $n\omega_0$, (for $n = 0, 1, 2, \dots$). Usually these harmonics lie outside the passband and so do not interfere with the desired signal at frequency ω_0 . However, the situation is different when the input signal consists of two closely spaced frequencies, or two tones.

If we consider a two-tone input voltage:

$$v_i = V_0(\cos \omega_1 t + \cos \omega_2 t) \quad (5.7)$$

Expressing the output in terms of this input in Taylor Series form:

$$\begin{aligned}
v_o &= a_0 + a_1 v_i + a_2 v_i^2 + a_3 v_i^3 + \dots \\
&= a_0 + \{a_1 V_0 \cos \omega_1 t + a_1 V_0 \cos \omega_2 t\} \\
&\quad + \frac{1}{2} \left\{ a_2 V_0^2 (1 + 2 \cos \omega_1 t) + a_2 V_0^2 (1 + 2 \cos \omega_2 t) + \right. \\
&\quad \left. 2a_2 V_0^2 \cos(\omega_1 - \omega_2)t + 2a_2 V_0^2 \cos(\omega_1 + \omega_2)t \right\} \\
&\quad + \frac{1}{4} \left\{ a_3 V_0^3 (3 \cos \omega_1 t + \cos 3\omega_1 t) + a_3 V_0^3 (3 \cos \omega_2 t + \cos 3\omega_2 t) + \right. \\
&\quad \left. a_3 V_0^3 [6 \cos \omega_2 t + 3 \cos(2\omega_1 - \omega_2)t + 3 \cos(2\omega_1 + \omega_2)t] + \right. \\
&\quad \left. a_3 V_0^3 [6 \cos \omega_1 t + 3 \cos(2\omega_2 - \omega_1)t + 3 \cos(2\omega_2 + \omega_1)t] \right\} \\
&\quad + \dots
\end{aligned} \tag{5.8}$$

It can be clearly seen that the output spectrum consists of harmonics of the form:

$$m\omega_1 + n\omega_2 \text{ for } m, n = 0, \pm 1, \pm 2, \pm 3, \dots \tag{5.9}$$

These combinations of the two input frequencies are called the Intermodulation products, and the order of a given product is defined as $|m| + |n|$.

For example, there are four second order Intermodulation products, which are $2\omega_1$, $2\omega_2$, $\omega_1 - \omega_2$, and $\omega_1 + \omega_2$, all of which are undesired in the passband. If the two tones are close, all the second order products will be far away from ω_1 or ω_2 as illustrated.

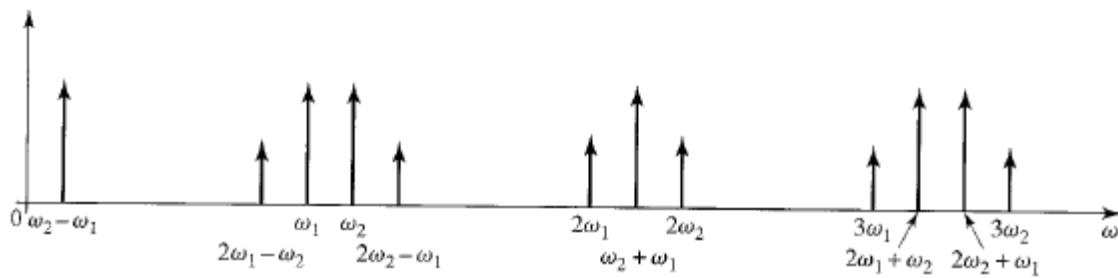


Figure 5.4: Illustration of Second order Products.

The cubed term of the above Taylor Series leads to six third order intermodulation products:

$$3\omega_1, 3\omega_2, 2\omega_1 + \omega_2, 2\omega_2 + \omega_1, 2\omega_1 - \omega_2, \text{ and } 2\omega_2 - \omega_1 \tag{5.10}$$

The first four of these will again be located far from the two signal tones, and will be typically outside of the passband of the component. However, the two difference terms, i.e. $2\omega_1 - \omega_2$, and $2\omega_2 + \omega_1$ are located near the desired signals at ω_1 and ω_2 and can be within the passband, hence these two third order intermodulation (IM3) products present a major interference. For an arbitrary input signal consisting of many frequencies, the resulting in-band intermodulation products will cause distortion of the output signal. This effect is called third order modulation distortion.

5.4) Third - Order Intercept point

From the expanded Taylor series; we can see that as the input voltage amplitude V_0 increases, the voltage associated with the third-order products increases as V_0^3 .

$$\begin{aligned}
 v_o &= a_0 + a_1 v_i + a_2 v_i^2 + a_3 v_i^3 + \dots \\
 &= a_0 + \dots \\
 &\quad + \frac{1}{4} \left\{ \begin{aligned} &a_3 V_0^3 (3 \cos \omega_1 t + \cos 3\omega_1 t) + a_3 V_0^3 (3 \cos \omega_2 t + \cos 3\omega_2 t) + \\ &a_3 V_0^3 [6 \cos \omega_2 t + 3 \cos(2\omega_1 - \omega_2)t + 3 \cos(2\omega_1 + \omega_2)t] + \\ &a_3 V_0^3 [6 \cos \omega_1 t + 3 \cos(2\omega_2 - \omega_1)t + 3 \cos(2\omega_2 + \omega_1)t] \end{aligned} \right\} \\
 &\quad + \dots
 \end{aligned} \tag{5.11}$$

This means that the output power of the third order products must increase as the cube of the input power. Thus, for small input powers the third – order intermodulation products must be very small, but will increase quickly as the input power increases. This effect can be viewed graphically by plotting the output power for the first and third – order products against input power on log scales as shown:

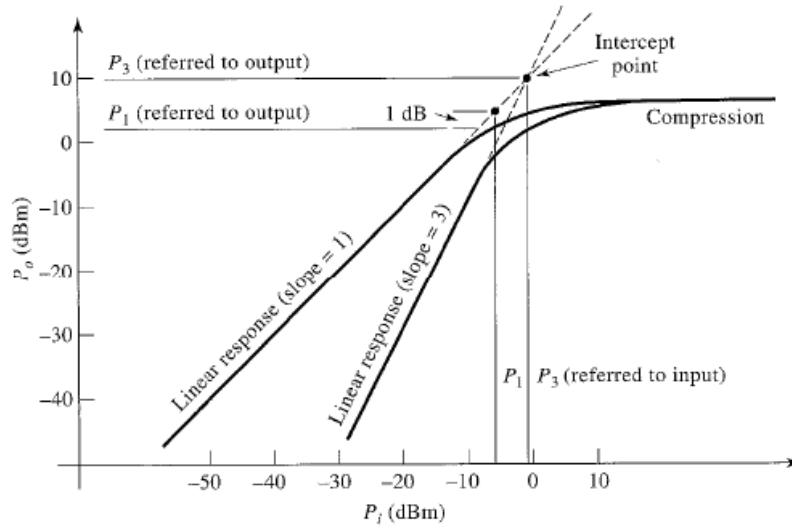


Figure 5.5: Graphical Representation of IP 3 point.

The output power of the first order, or linear, product is proportional to the input power, and so this response has a slope of unity before the onset of compression. The output power of third-order intermodulation (IM3) products has a slope of 3, and will exhibit compression at high power as well. If the non-compression responses of the first and third order products are extended with dotted lines as shown, we can see that these two lines will intersect, typically at a point above the onset of compression. This virtual intersection point is called the third – order intercept point, denoted P_3 in **Figure 5.5**. It is also referred to as IP3 or TOI. Higher IP3 indicates less third – order modulation distortion, which is desirable.

IP3 can be specified as the power level referred at either the input or output. $IP3_{in}$ is used to denote the input, and $IP3_{out}$ is the output. Assuming that a two-port non-linear network has a power gain G over the desired signal band between ω_1 and ω_2 ; when the input signal power reaches a level equal to $IP3_{in}$, the input power for the desired signal is $G \times IP3_{in}$. This output signal power at the third order intercept point, by definition, is equal to the $IP3_{out}$. Hence,

$$IP3_{out} = G \times IP3_{in} \quad (5.12)$$

$IP3_{out}$ can also be expressed in terms of Taylor coefficients of the expansion:

- Define P_{ω_1} as the output power of the desired signal at frequency ω_1 .

- Define $P_{2\omega_1 - \omega_2}$ as the output power of the intermodulation product of frequency $2\omega_1 - \omega_2$.
- Then from the expanded Taylor Series:

$$P_{\omega_1} = \frac{1}{2} (a_1 V_0)^2 \quad (5.22)$$

$$P_{2\omega_1 - \omega_2} = \frac{1}{2} \left(\frac{3}{4} a_3 V_0^3 \right)^2 \quad (5.23)$$

Both expressions are for a terminal impedance of $Z_0 = 1 \Omega$

- By definition, these two powers are equal at the IP3 when the input voltage amplitude is to as V_{IP} . Thus,

$$\frac{1}{2} (a_1 V_{IP})^2 = \frac{1}{2} \left(\frac{3}{4} a_3 V_{IP}^3 \right)^2 = IP3_{out} \quad (5.24)$$

- Solving for V_{IP} in terms of a_1 and a_3 yields:

$$V_{IP} = \sqrt{\frac{4a_1}{3a_3}} \quad (5.25)$$

- Therefore,

$$IP3_{out} = \frac{1}{2} (a_1 V_{IP})^2 = \frac{2a_1^3}{3a_3} \quad (5.26)$$

- If $a_3 \rightarrow 0$, $IP3_{out} \rightarrow \infty$, the device does not result in any third - order distortion.

From the above equations we have,

$$a_3 = \frac{2a_1^3}{3 \times \text{IP3}_{\text{out}}} \quad (5.27)$$

Thus,

$$\begin{aligned} P_{2\omega_1-\omega_2} &= \frac{1}{2} \left(\frac{3}{4} a_3 V_0^3 \right)^2 \\ &= \frac{1}{2} \left(\frac{3}{4} \times \frac{2a_1^3}{3 \times \text{IP3}_{\text{out}}} V_0^3 \right)^2 = \frac{1}{8} \times \frac{(a_1^2 V_0^2)^3}{\text{IP3}_{\text{out}}^2} \end{aligned} \quad (5.28)$$

But,

$$P_{\omega_1} = \frac{1}{2} (a_1 V_0)^2 \quad \text{or} \quad (a_1 V_0)^2 = 2P_{\omega_1} \quad (5.29)$$

By Substitution,

$$P_{2\omega_1-\omega_2} = \frac{1}{8} \times \frac{(2P_{\omega_1})^3}{\text{IP3}_{\text{out}}^2} = \frac{(P_{\omega_1})^3}{\text{IP3}_{\text{out}}^2} \quad (5.30)$$

$P_{2\omega_1 - \omega_2}$ is the output power of the unwanted third – order intermodulation (IM3) product which is smaller for a higher IP3_{out} . (5.30) can be expressed in dBm:

$$P_{2\omega_1-\omega_2} (\text{dBm}) = 3 \times P_{\omega_1} (\text{dBm}) - 2 \times \text{IP3}_{\text{out}} (\text{dBm}) \quad (5.31)$$

Thus,

$$\text{IP3}_{\text{out}} (\text{dBm}) = \frac{3 \times P_{\omega_1} (\text{dBm}) - P_{2\omega_1-\omega_2} (\text{dBm})}{2} \quad (5.32)$$

5.4.1) Third - Intercept Point Set up

Third intercept point was measured using the following typical set up:

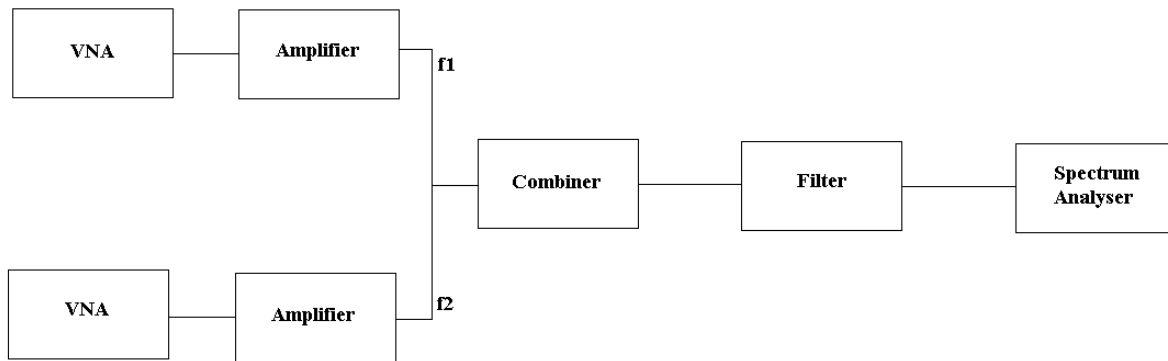


Figure 5.6: IP3 Measurement Set Up.

The set up for the IP3 test for each filter measurement had two VNA's in order to generate the two signal tones for testing. The VNA's used were Agilent Network Analysers, 8720 and 8510. In order to obtain a high enough power level, two broadband Amplifiers were used to amplify the power. An important consideration is that the isolation between the two input signal generators should be high enough. If this is not the case, they could produce unwanted intermodulation products. In the set up shown a power combiner was used with good isolation. The reconfigurable filters described in later sections were then connected to the power combiner at one port, with the other connected to the spectrum analyser.

5.5) Passive Intermodulation

The above sections of intermodulation distortion concerns circuits involving diodes and transistors, but it is also possible for intermodulation products to be generated by passive components. This effect is called Passive Intermodulation (PIM). Passive intermodulation can be caused by a number of factors, such as poor mechanical contact, oxidation of junctions between metals, contamination of conducting surfaces at RF junctions, or the use of nonlinear materials such as ferromagnetic materials. In addition, when high powers are involved, thermal effects may contribute to the overall nonlinearity of a junction. It is very difficult to predict PIM levels from first principles, so measurement techniques must usually be used. Because of the third-power dependence of the third-order intermodulation products with

input power, passive intermodulation is usually only significant when input signal powers are relatively large.

This is frequently the case in cellular telephone base station transceivers, which operate with powers of 30-40 dBm, with many closely spaced RF channels, it is often desired to maintain the PIM level below -125 dBm, with two 40 dBm transmit signals. This is a very wide dynamic range, and requires careful selection of components used in the high-power portions of the transceiver. Passive intermodulation is generally not a problem in receive parts, due to the much lower power levels.

5.6) Intercept point of Cascaded Components

The cascaded connection of components has the effect of degrading (lowering) the third-order intercept point (IP3). Unlike the case of a cascade of noisy components, however, the intermodulation products in a cascaded system are coherent in general. This means that the third order products produced by the two cascaded components are phase related, and they could be partially cancelled out if they are out of phases. Nevertheless, it can be assumed they are uncorrelated and estimate a worst case third-order distortion or IP3 for any two cascaded networks as follows. With reference to the following figure, let G_1 and P'_3 be the power gain and third order intercept point for the first stage, and G_2 and P''_3 be the corresponding values for the second stage.

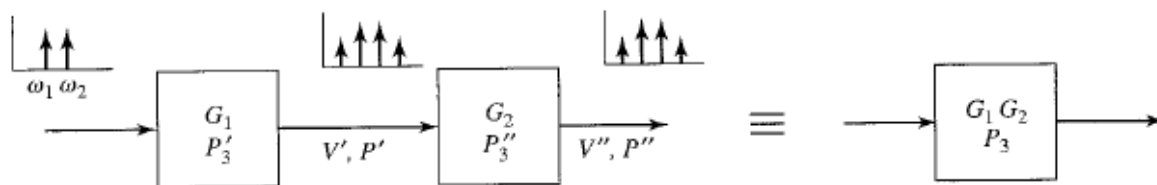


Figure 5.7: Illustration of Cascade of Components.

Since the intermodulation products in a cascade system are coherent, powers cannot be simply added. But voltages must be dealt with.

- At the output port of the first network:

$$V'_{2\omega_1-\omega_2} = \sqrt{P'_{2\omega_1-\omega_2} Z_0} \tag{5.33}$$

Where Z_0 is the system impedance.

But,

$$P'_{2\omega_1-\omega_2} = \frac{(P'_{\omega_1})^3}{IP_{out}^{\prime 2}} \quad (5.34)$$

Which leads to

$$V'_{2\omega_1-\omega_2} = \sqrt{P'_{2\omega_1-\omega_2} Z_0} = \frac{\sqrt{(P'_{\omega_1})^3 Z_0}}{IP_{out}^{\prime}} \quad (5.35)$$

- At the output of the second network being cascaded:

$$V''_{2\omega_1-\omega_2} = \sqrt{G_2} V'_{2\omega_1-\omega_2} + \frac{\sqrt{(P''_{\omega_1})^3 Z_0}}{IP_{out}''} \quad (5.36)$$

The second term is the third-order product generated by the second network alone; $\sqrt{G_2}$ corresponds to the voltage gain.

By substitution,

$$\begin{aligned} V''_{2\omega_1-\omega_2} &= \sqrt{G_2} \frac{\sqrt{(P'_{\omega_1})^3 Z_0}}{IP_{out}^{\prime}} + \frac{\sqrt{(P''_{\omega_1})^3 Z_0}}{IP_{out}''} \\ &= \frac{\sqrt{(G_2 P'_{\omega_1})^3 Z_0}}{G_2 IP_{out}^{\prime}} + \frac{\sqrt{(P''_{\omega_1})^3 Z_0}}{IP_{out}''} = \frac{\sqrt{(P''_{\omega_1})^3 Z_0}}{G_2 IP_{out}^{\prime}} + \frac{\sqrt{(P''_{\omega_1})^3 Z_0}}{IP_{out}''} \\ &= \left(\frac{1}{G_2 IP_{out}^{\prime}} + \frac{1}{IP_{out}''} \right) \sqrt{(P''_{\omega_1})^3 Z_0} \end{aligned} \quad (5.37)$$

Because,

$$P''_{\omega_1} = G_2 P'_{\omega_1} \quad (5.38)$$

- Then the output distortion power of the equivalent network after cascade connection is

$$\begin{aligned} P''_{2\omega_1-\omega_2} &= \frac{(V''_{2\omega_1-\omega_2})^2}{Z_0} = \left(\frac{1}{G_2 IP3'_{out}} + \frac{1}{IP3''_{out}} \right)^2 (P''_{\omega_1})^3 \\ &= \frac{(P''_{\omega_1})^3}{IP3_{out}^2} \end{aligned} \quad (5.39)$$

Where $IP3_{out}$ is the output third order intercept point of the cascaded system, and is given by:

$$IP3_{out} = \left(\frac{1}{G_2 IP3'_{out}} + \frac{1}{IP3''_{out}} \right)^{-1} \quad (5.40)$$

- Note that $IP3_{out} = G_2 IP3'_{out}$ for $IP3''_{out} \rightarrow \infty$, which is the limiting case when the second network has no third order distortion.
- Since $IP3_{out} = G \times IP3_{in}$, the above result can be expressed in terms of the input intercept points.
 - For $G = G_1 \times G_2$

$$IP3_{in} = \frac{IP3_{out}}{G_1 \times G_2} = \left(\frac{G_1 \times G_2}{G_2 IP3'_{out}} + \frac{G_1 \times G_2}{IP3''_{out}} \right)^{-1} \quad (5.41)$$

- But, $IP3'_{out} = G_1 \times IP3'_{in}$ and $IP3''_{out} = G_2 \times IP3''_{in}$ which leads to

$$IP3_{in} = \left(\frac{1}{IP3'_{in}} + \frac{G_1}{IP3''_{in}} \right)^{-1} \quad (5.42)$$

For evaluating the IP3 of a cascade of systems of more than two components, in principle the formulation for the two cascade networks can be used repeatedly. However, the formulation can be generalised for N cascade networks.

$$IP3_{in} = \left(\frac{1}{IP3_{in,1}} + \frac{G_1}{IP3_{in,2}} + \frac{G_1 G_2}{IP3_{in,3}} + \dots + \frac{G_1 G_2 \dots G_{N-1}}{IP3_{in,N}} \right)^{-1} \quad (5.43)$$

Where $IP3_{in,1}$ to $IP3_{in,N}$ are the input third order intercept points of individual networks, and G_i denotes the gain of each network.

5.7) Dynamic Range

Dynamic range is defined, in a general sense, as the operating range of input signal level for which a component or system has desirable characteristics. The low end of dynamic range is usually limited by noise or the minimum detectable signal (MDS) level. However, the high end of dynamic range may be limited by either the gain compression or the intermodulation distortion. If the allowable power level is limited at the high end by the 1-dB compression point, the associated dynamic range is called the linear dynamic range (DR_l). If the high end of dynamic range is limited by the maximum power level for which intermodulation distortion or spurious response becomes unacceptable, the resultant dynamic range is called the spurious-free dynamic range (DR_f).

5.8) Linear Dynamic Range (DR_l)

The linear dynamic range can be computed as the ratio of the 1-dB compression point to the minimum detectable signal (MDS) referenced either at the input or output.

$$DR_l = \frac{P_{in,1dB}}{MDS} = \frac{P_{out,1dB}}{MDS_{out}} \quad (5.44)$$

Express the DR_l in terms of dB

$$\begin{aligned} DR_l(\text{dB}) &= P_{in,1dB}(\text{dBm}) - MDS(\text{dBm}) \\ &= P_{out,1dB}(\text{dBm}) - MDS_{out}(\text{dBm}) \end{aligned} \quad (5.45)$$

On a log-log scale, it is simply the difference (dB) between the two powers in dBm.

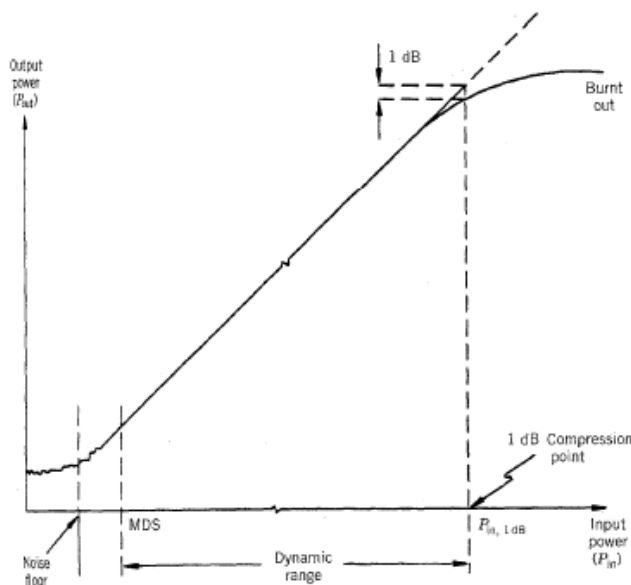


Figure 5.8: Linear Dynamic Range on log-log Scales.

If the input power is below the minimum detectable signal (MDS), the noise dominates. If the input power is above the 1-dB compression point, or $P_{in,1dB}$, the output starts to saturate. For

an application such as a receiver system, a high dynamic range is desirable so that the system can operate over a wide range of input power levels.

5.9) Spurious Free Dynamic Range (DR_f)

Since the unwanted third-order intermodulation product is the most harmful in communications systems, the spurious-free dynamic range is defined as the maximum output power for which the power of the third-order intermodulation product is equal to the noise or the MDS of the network/system. This situation is shown in the figure below.

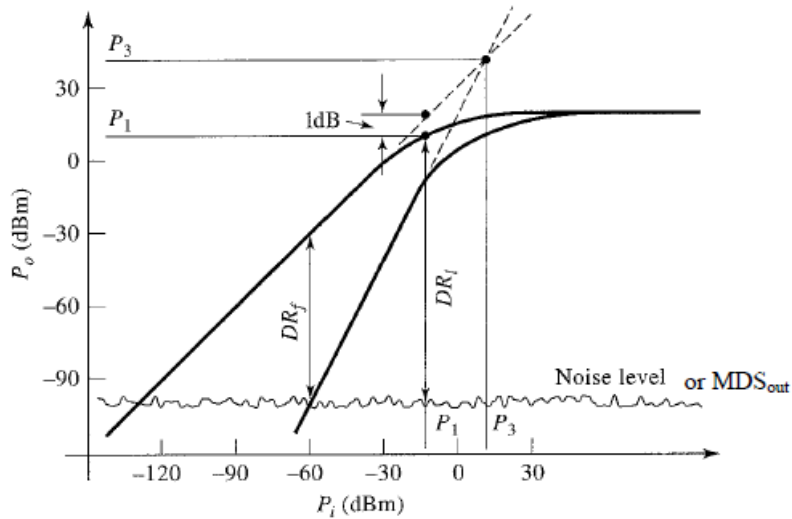


Figure 5.9: Spurious Free Dynamic Range Illustration.

If P_{ω_1} is the output power of the desired signal, and $P_{2\omega_1 - \omega_2}$ is the output power of the unwanted IM3 product, then the spurious free dynamic range can be expressed as

$$DR_f = \frac{P_{\omega_1}}{P_{2\omega_1 - \omega_2}} \Big|_{P_{2\omega_1 - \omega_2} = MDS_{out}} \quad (5.46)$$

With $P_{2\omega_1 - \omega_2}$ taken equal to the network noise or MDS_{out} level (as to be spurious free).

On the other hand

$$P_{2\omega_1-\omega_2} = \frac{(P_{\omega_1})^3}{IP3_{out}^2} \quad \text{or} \quad P_{\omega_1} = \left(P_{2\omega_1-\omega_2} \times IP3_{out}^2 \right)^{1/3} \quad (5.47)$$

By Substitution

$$DR_f = \frac{P_{\omega_1}}{P_{2\omega_1-\omega_2}} \Big|_{P_{2\omega_1-\omega_2}=MDS_{out}} = \left(\frac{IP3_{out}}{MDS_{out}} \right)^{2/3} \quad (5.48)$$

This result in terms of dB is:

$$DR_f(\text{dB}) = \frac{2}{3} [IP3_{out}(\text{dBm}) - MDS_{out}(\text{dBm})] \quad (5.49)$$

With $IP3_{out} = G \times IP3_{in}$ and $MDS_{out} = G \times MDS$. The spurious free dynamic range can also be given by:

$$DR_f(\text{dB}) = \frac{2}{3} [IP3_{in}(\text{dBm}) - MDS(\text{dBm})] \quad (5.50)$$

Where MDS denotes the input minimum detectable signal; this same result applies for the $2\omega_2 - \omega_1$ product.

5.10) Summary

As active devices are being added in order to make the filters reconfigurable, consideration needs to be taken in terms of non – linearity when integrating them into a system chain. The above shows the theory of the non – linearity considerations which need to be ascertained in order to check whether the reconfigurable filters designed have any issues when integrated into a system chain. Where possible some of these measurements will be taken on the reconfigurable filters designed and illustrated in the subsequent chapters.

5.11) References

[1] George L. Matthaei, Leo Young, E. M. T. Jones, “Microwave Filters, Impedance – Matching Networks, and Coupling Structures,” *McGraw – Hill, Inc., New York 1964.*

[2] D. M. Pozar, *Microwave and RF Design of wireless Systems*, John Wiley & Sons. Inc., 2001

Chapter 6: Single Section Coupled Line Reconfigurable Filter

6.1) Introduction

In Chapter 4 the single coupled line structure was highlighted and analysed; this chapter will show how the couple line section has many advantages which make it appealing for reconfigurable filters by adding and switching short circuit stubs into the topology. The main two advantages for this are that for a given set of even and odd mode impedances the filter maintains the return and insertion loss at center frequency regardless of the impedance of the stubs added (which makes bandwidth tuning easy and will be shown in this section); and by cascading more than one section increases the selectivity but maintains the filter characteristics at center frequency (filter of this type will be designed in later chapters). This chapter will deal with the design of a one section filter and how the bandwidth is made tunable. It will then show how the number of filter states can be increased by combining two filters into one. In each case the designs shown are documented in [1] and [2].

6.2) Short Circuit Coupled Line Filters

6.2.1) Coupled Line Filters with Reconfigurability

It was found that by adding short circuit stubs to the single section described in chapter 4 a reconfigurable filter can be achieved. Even with these stubs added the filter still maintains its return and insertion loss at centre frequency for a given set of even and odd mode impedances. If the single section equivalent circuit is analysed in the same way as before we obtain the same expressions for the losses at cut off, i.e. shown that the return loss in the passband only depends on the pair of even- and odd- mode impedances and is independent of the characteristic impedance of the other stubs:

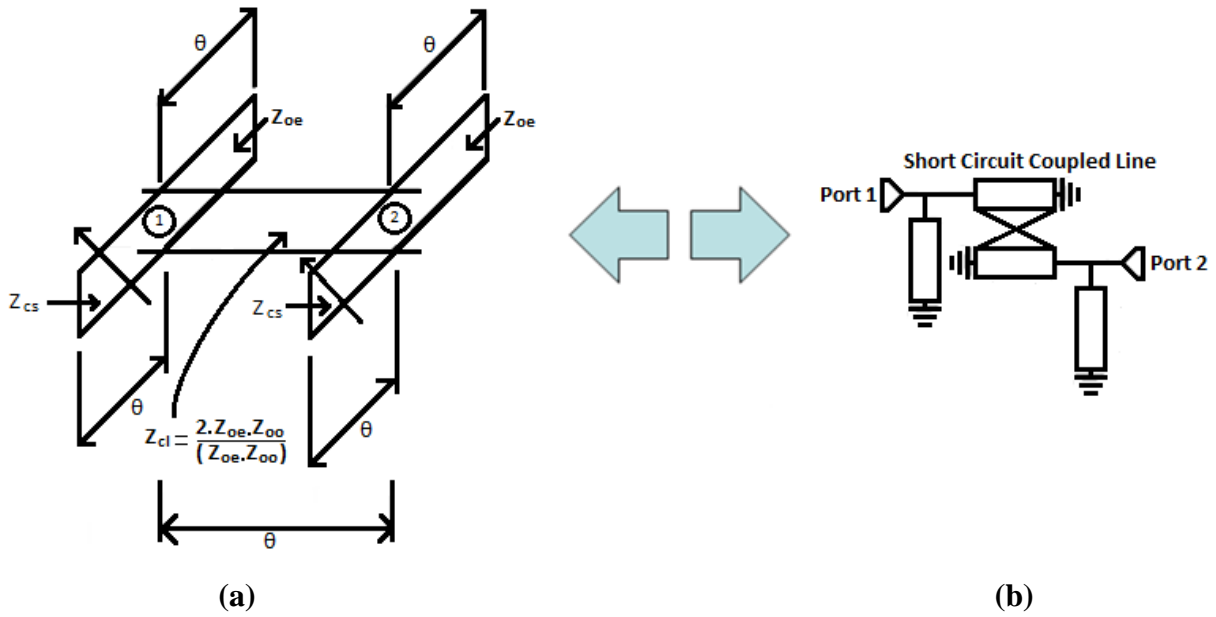


Figure 6.1: Single Section Coupled Line Filter With Short Circuit Stubs for Reconfigurability (a) Equivalent Circuit, (b) Coupled Line Structure.

Again from the deduced circuit we can simply cascade the ABCD parameters for each circuit element as before as in (4.1) but substituting (6.1) and (6.2)

$$\begin{aligned}
 Y &= \frac{1}{j \cdot Z_{oe} \cdot \tan(\theta)} + \frac{1}{j \cdot Z_{cs} \cdot \tan(\theta)} \\
 &= \frac{(j \cdot Z_{oe} \cdot \tan(\theta)) + (j \cdot Z_{cs} \cdot \tan(\theta))}{(j \cdot Z_{oe} \cdot \tan(\theta)) \cdot (j \cdot Z_{cs} \cdot \tan(\theta))} \\
 &= \frac{j \cdot Z_{oe} + j \cdot Z_{cs}}{j^2 \cdot Z_{oe} \cdot Z_{cs} \cdot \tan(\theta)} \\
 &= \frac{j \cdot Z_{oe} + j \cdot Z_{cs}}{-Z_{oe} \cdot Z_{cs} \cdot \tan(\theta)} \\
 &= -\frac{j \cdot (Z_{oe} + Z_{cs})}{Z_{oe} \cdot Z_{cs} \cdot \tan(\theta)} \tag{6.1}
 \end{aligned}$$

$$Z_{cl} = \frac{2 \cdot Z_{oe} \cdot Z_{oo}}{Z_{oe} - Z_{oo}} \quad (6.2)$$

We obtain the following:

$$\begin{aligned} A &= \cos(\theta) + Y \cdot j \cdot Z_{cl} \cdot \sin(\theta) \\ &= \cos(\theta) + \left(-\frac{j \cdot (Z_{oe} + Z_{cs})}{Z_{oe} \cdot Z_{cs} \cdot \tan(\theta)} \right) \cdot j \cdot \left(\frac{2 \cdot Z_{oe} \cdot Z_{oo}}{Z_{oe} - Z_{oo}} \right) \cdot \sin(\theta) \\ &= \cos(\theta) + \left(\frac{-j^2 \cdot 2 \cdot (Z_{oe} + Z_{cs}) \cdot Z_{oe} \cdot Z_{oo} \cdot \sin(\theta)}{Z_{oe} \cdot Z_{cs} \cdot \tan(\theta) \cdot (Z_{oe} - Z_{oo})} \right) \\ &= \cos(\theta) + \frac{2 \cdot (Z_{oe} + Z_{cs}) \cdot Z_{oe} \cdot Z_{oo} \cdot \sin(\theta)}{Z_{oe} \cdot Z_{cs} \cdot \tan(\theta) \cdot (Z_{oe} - Z_{oo})} \\ &= \cos(\theta) + \frac{2 \cdot (Z_{oe} + Z_{cs}) \cdot Z_{oe} \cdot Z_{oo} \cdot \cos(\theta)}{Z_{oe} \cdot Z_{cs} \cdot (Z_{oe} - Z_{oo})} \end{aligned} \quad (6.3)$$

$$\begin{aligned} B &= j \cdot Z_{cl} \cdot \sin(\theta) \\ &= j \cdot \left(\frac{2 \cdot Z_{oe} \cdot Z_{oo}}{Z_{oe} - Z_{oo}} \right) \cdot \sin(\theta) \end{aligned} \quad (6.4)$$

$$\begin{aligned} C &= \left(Y \cdot \cos(\theta) + \frac{j \cdot \sin(\theta)}{Z_{cl}} \right) + \left[(Y \cdot j \cdot Z_{cl} \cdot \sin(\theta) + \cos(\theta)) \cdot Y \right] \\ &= \left(-\frac{j \cdot (Z_{oe} + Z_{cs}) \cdot \cos(\theta)}{Z_{oe} \cdot Z_{cs} \cdot \tan(\theta)} \right) + \frac{j \cdot \sin(\theta)}{\left(\frac{2 \cdot Z_{oe} \cdot Z_{oo}}{Z_{oe} - Z_{oo}} \right)} + \left[\left(\cos(\theta) + \frac{2 \cdot (Z_{oe} + Z_{cs}) \cdot Z_{oe} \cdot Z_{oo} \cdot \cos(\theta)}{Z_{oe} \cdot Z_{cs} \cdot (Z_{oe} - Z_{oo})} \right) \cdot \left(-\frac{j \cdot (Z_{oe} + Z_{cs})}{Z_{oe} \cdot Z_{cs} \cdot \tan(\theta)} \right) \right] \\ &= \left(-\frac{j \cdot (Z_{oe} + Z_{cs}) \cdot \cos(\theta)}{Z_{oe} \cdot Z_{cs} \cdot \tan(\theta)} \right) + \frac{j \cdot \sin(\theta) \cdot (Z_{oe} - Z_{oo})}{2 \cdot Z_{oe} \cdot Z_{oo}} + \left(-\frac{j \cdot (Z_{oe} + Z_{cs})}{Z_{oe} \cdot Z_{cs} \cdot \tan(\theta)} \right) \cdot \cos(\theta) + \left(\frac{-2 \cdot j \cdot (Z_{oe} + Z_{cs})^2 \cdot Z_{oe} \cdot Z_{oo} \cdot \cos(\theta)}{(Z_{oe} \cdot Z_{cs})^2 \cdot (Z_{oe} - Z_{oo}) \cdot \tan(\theta)} \right) \\ &= \left(-\frac{2 \cdot j \cdot (Z_{oe} + Z_{cs}) \cdot \cos(\theta)}{Z_{oe} \cdot Z_{cs} \cdot \tan(\theta)} \right) + \frac{j \cdot \sin(\theta) \cdot (Z_{oe} - Z_{oo})}{2 \cdot Z_{oe} \cdot Z_{oo}} + \left(\frac{-2 \cdot j \cdot (Z_{oe} + Z_{cs})^2 \cdot Z_{oe} \cdot Z_{oo} \cdot \cos(\theta)}{(Z_{oe} \cdot Z_{cs})^2 \cdot (Z_{oe} - Z_{oo}) \cdot \tan(\theta)} \right) \\ &= -\frac{2 \cdot j \cdot (Z_{oe} + Z_{cs}) \cdot \cos(\theta)}{Z_{oe} \cdot Z_{cs} \cdot \tan(\theta)} \left(1 + \frac{(Z_{oe} + Z_{cs}) \cdot Z_{oe} \cdot Z_{oo}}{Z_{oe} \cdot Z_{cs} \cdot (Z_{oe} - Z_{oo})} \right) + \frac{j \cdot \sin(\theta) \cdot (Z_{oe} - Z_{oo})}{2 \cdot Z_{oe} \cdot Z_{oo}} \end{aligned} \quad (6.5)$$

$$D = A \tag{6.6}$$

The S – parameters can then again be deduced from (4.8) and (4.9) which obtain expressions (6.7) and (6.8).

These give:

$$S_{11} = \frac{j \cdot \left(\frac{2 \cdot Z_{oe} \cdot Z_{oo}}{Z_{oe} - Z_{oo}} \right) \cdot \sin(\theta)}{Z_o} - \left(-\frac{2 \cdot j \cdot (Z_{oe} + Z_{cs}) \cdot \cos(\theta)}{Z_{oe} \cdot Z_{cs} \cdot \tan(\theta)} \left(1 + \frac{(Z_{oe} + Z_{cs}) \cdot Z_{oe} \cdot Z_{oo}}{Z_{oe} \cdot Z_{cs} \cdot (Z_{oe} - Z_{oo})} \right) + \frac{j \cdot \sin(\theta) \cdot (Z_{oe} - Z_{oo})}{2 \cdot Z_{oe} \cdot Z_{oo}} \right) \cdot Z_o}{2 \cdot \left(\cos(\theta) + \frac{(Z_{oe} + Z_{cs}) \cdot (Z_{oe} - Z_{oo}) \cdot \cos(\theta)}{Z_{oe} \cdot Z_{cs} \cdot (Z_{oe} - Z_{oo})} \right) + \left(\left(\frac{j \cdot \left(\frac{2 \cdot Z_{oe} \cdot Z_{oo}}{Z_{oe} - Z_{oo}} \right) \cdot \sin(\theta)}{Z_o} \right) + \left(-\frac{2 \cdot j \cdot (Z_{oe} + Z_{cs}) \cdot \cos(\theta)}{Z_{oe} \cdot Z_{cs} \cdot \tan(\theta)} \left(1 + \frac{(Z_{oe} + Z_{cs}) \cdot Z_{oe} \cdot Z_{oo}}{Z_{oe} \cdot Z_{cs} \cdot (Z_{oe} - Z_{oo})} \right) + \frac{j \cdot \sin(\theta) \cdot (Z_{oe} - Z_{oo})}{2 \cdot Z_{oe} \cdot Z_{oo}} \right) \cdot Z_o \right)}$$

(6.7)

$$S_{21} = \frac{2}{2 \cdot \left(\cos(\theta) + \frac{(Z_{oe} + Z_{cs}) \cdot (Z_{oe} - Z_{oo}) \cdot \cos(\theta)}{Z_{oe} \cdot Z_{cs} \cdot (Z_{oe} - Z_{oo})} \right) + \left(\left(\frac{j \cdot \left(\frac{2 \cdot Z_{oe} \cdot Z_{oo}}{Z_{oe} - Z_{oo}} \right) \cdot \sin(\theta)}{Z_o} \right) + \left(-\frac{2 \cdot j \cdot (Z_{oe} + Z_{cs}) \cdot \cos(\theta)}{Z_{oe} \cdot Z_{cs} \cdot \tan(\theta)} \left(1 + \frac{(Z_{oe} + Z_{cs}) \cdot Z_{oe} \cdot Z_{oo}}{Z_{oe} \cdot Z_{cs} \cdot (Z_{oe} - Z_{oo})} \right) + \frac{j \cdot \sin(\theta) \cdot (Z_{oe} - Z_{oo})}{2 \cdot Z_{oe} \cdot Z_{oo}} \right) \cdot Z_o \right)}$$

(6.8)

At Cut off frequency, i.e. $\theta = 90^\circ$, these expressions simplify to:

$$S_{11} = \frac{\frac{j \cdot \left(\frac{2 \cdot Z_{oe} \cdot Z_{oo}}{Z_{oe} - Z_{oo}} \right)}{Z_0} - j \cdot \left[\frac{Z_{oe} - Z_{oo}}{2 \cdot Z_{oe} \cdot Z_{oo}} \right] \cdot Z_0}{\frac{j \cdot \left(\frac{2 \cdot Z_{oe} \cdot Z_{oo}}{Z_{oe} - Z_{oo}} \right)}{Z_0} + j \cdot \left[\frac{Z_{oe} - Z_{oo}}{2 \cdot Z_{oe} \cdot Z_{oo}} \right] \cdot Z_0} \quad (6.9)$$

$$= \frac{(2 \cdot Z_{oe} \cdot Z_{oo})^2 - (Z_{oe} - Z_{oo})^2 \cdot Z_0^2}{(2 \cdot Z_{oe} \cdot Z_{oo})^2 + (Z_{oe} - Z_{oo})^2 \cdot Z_0^2}$$

$$S_{21} = \frac{2}{\frac{j \cdot \left(\frac{2 \cdot Z_{oe} \cdot Z_{oo}}{Z_{oe} - Z_{oo}} \right)}{Z_0} + j \cdot \left[\frac{Z_{oe} - Z_{oo}}{2 \cdot Z_{oe} \cdot Z_{oo}} \right] \cdot Z_0} \quad (6.10)$$

$$= \frac{-4 \cdot j \cdot (Z_{oe} - Z_{oo}) \cdot Z_0 \cdot Z_{oe} \cdot Z_{oo}}{(2 \cdot Z_{oe} \cdot Z_{oo})^2 + (Z_{oe} - Z_{oo})^2 \cdot Z_0^2}$$

When (6.9) and (6.10) are compared with (4.12) and (4.13) it is apparent that as stated, the insertion loss and return is the same level at center frequency regardless of the impedance of the short circuit stub.

6.2.2) Coupled Line Filter Design with Impedance Transformer

For matching purposes impedance transformers may be needed; as the even and odd mode impedances may be difficult to obtain on single layer circuits.

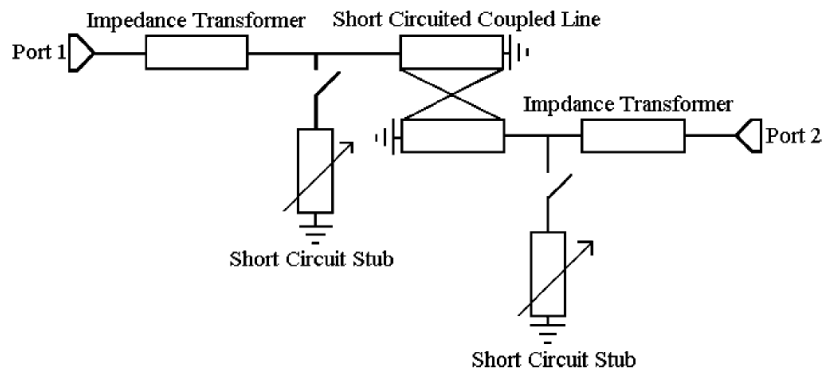


Figure 6.2: Reconfigurable Filter With Impedance Transformer Added.

From the theory presented before the impedance transformer can be added and cascaded with the ABCD parameters obtained in the previous section.

$$\begin{pmatrix} A & B \\ C & D \end{pmatrix} = \begin{pmatrix} A1 & B1 \\ C1 & D1 \end{pmatrix} \cdot \begin{pmatrix} A2 & B2 \\ C2 & D2 \end{pmatrix} \cdot \begin{pmatrix} A3 & B3 \\ C3 & D3 \end{pmatrix} \quad (6.11)$$

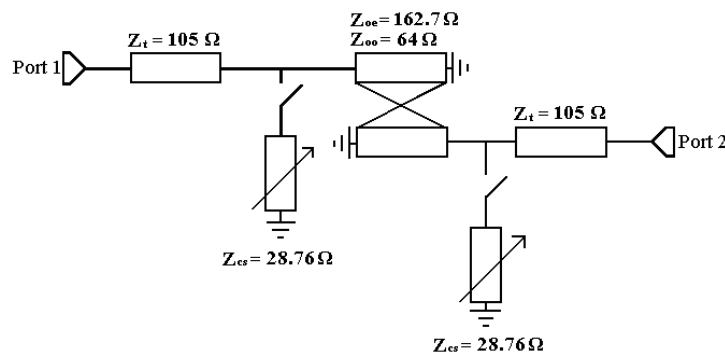
Where:

$\begin{pmatrix} A2 & B2 \\ C2 & D2 \end{pmatrix}$ Is the ABCD matrix obtained from (6.1) to (6.6)

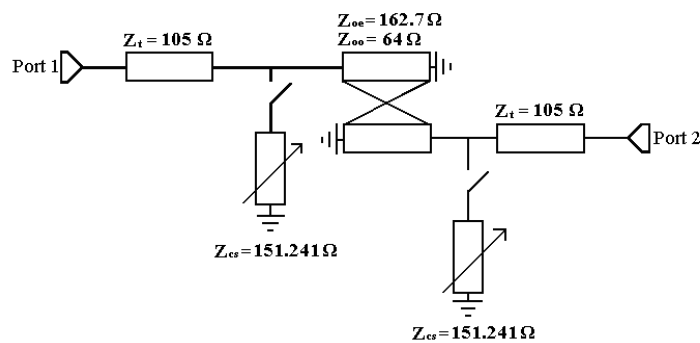
And

$$\begin{pmatrix} A1 & B1 \\ C1 & D1 \end{pmatrix} = \begin{pmatrix} A3 & B3 \\ C3 & D3 \end{pmatrix} = \begin{pmatrix} \cos(\theta) & j \cdot Z_t \cdot \sin(\theta) \\ j \cdot Y_t \cdot \sin(\theta) & \cos(\theta) \end{pmatrix} \quad (6.12)$$

Z_t is the characteristic impedance of the transformer. These matrices can then be used to design a filter structure for implementation. (See Appendix 3).



(a)



(b)

Figure 6.3: Filter Designs (a) Narrowband, (b) Wideband.

In each of the designs shown above the tunability of the proposed filter is based on the concept that, for a given pair of coupled lines with fixed even- and odd-mode impedance, altering the impedance of the stubs alters the coupling and in turn alters the bandwidth, hence by switching the stubs on and off alters the passband width. This makes bandwidth tuning easy.

6.2.3) Experimental Demonstration

6.2.3.1) EM Simulation

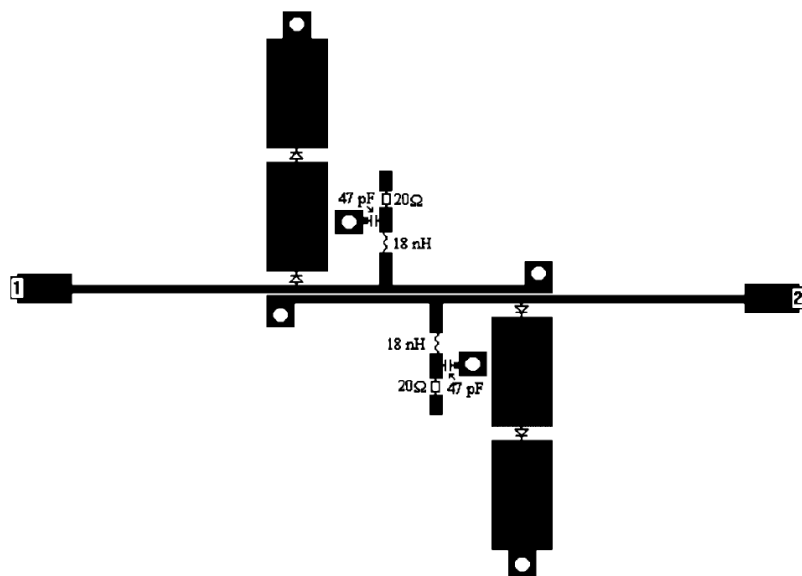


Figure 6.4: Design of Implemented Filter with Narrowband Stubs.

Figure 6.4 shows an implemented reconfigurable microstrip filter on a substrate with $\epsilon_r = 3$ and thickness = 1.02mm. The pin diodes were modelled by using a capacitor of value 0.025 pF for isolation and a resistor of value of 4 Ω for connection. The initial dimensions of the circuits were obtained using [3] and finalized using EM software [4]. The dimensions of the stubs are $w = 5.6$ mm and $l = 24.8$ mm (narrowband stubs) while the coupled lines have a gap $s = 0.2$ mm, $l = 25.9$ mm and $w = 0.5$ mm. In this case, the impedance transformer has a width and length of 0.6 mm and 24.8 mm, respectively. **Figure 6.5** plots the simulated results, showing the filter can be switched between two distinct bandwidth states.

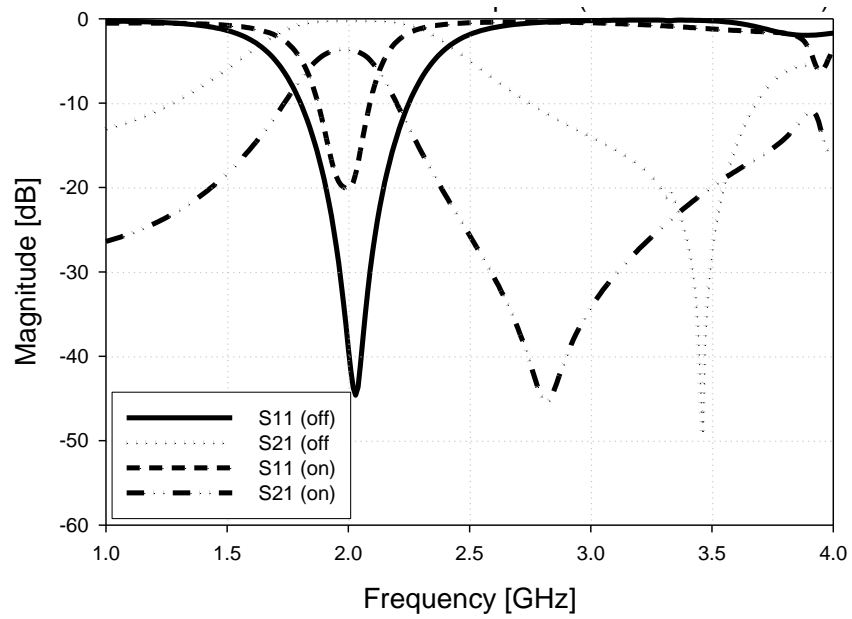


Figure 6.5: Simulated results of the Coupled line Structure with Narrowband Stubs.

In **Figure 6.4**, just replacing the narrowband stubs with two wideband stubs ($w = 0.2$ mm and $l = 28.2$ mm), we obtain the second reconfigurable filter block, whose simulated response is shown in **Figure 6.6**. The simulated performances of these two filters are summarized in **Table 6.1**.

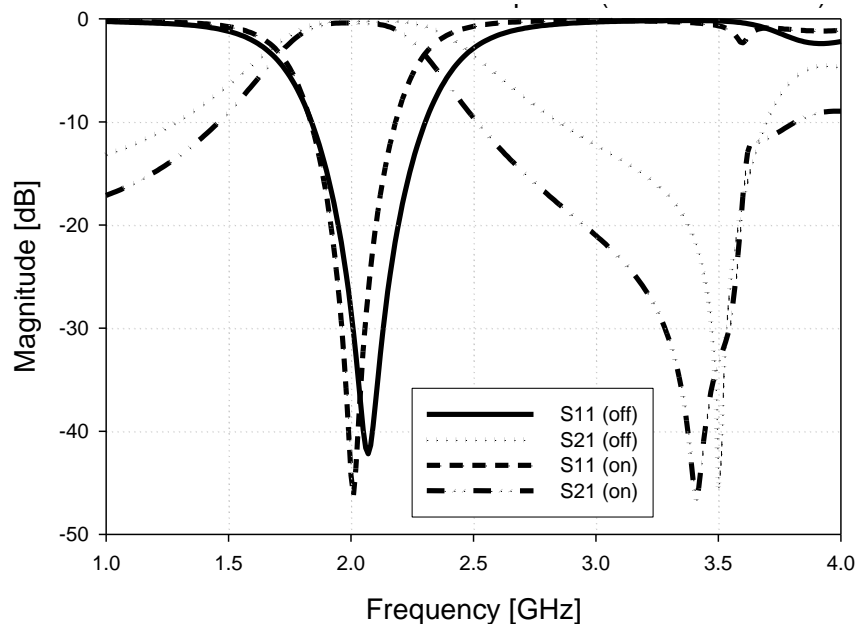


Figure 6.6: Simulated results of the Coupled line Structure with Wideband Stubs.

	Narrowband stub “off”	Narrowband stub “on”	Wideband stub “off”	Wideband stub “on”
<i>FBW</i> (3 dB)	37.9%	14%	39.6%	30%
<i>f</i> ₀	2.03 GHz	2 GHz	2.07GHz	2 GHz
Insertion Loss	0.2 dB	3.86 dB	0.19 dB	0.41 dB

Table 6.1: Simulated Performance of the Filters Designed.

There are some shifts in the center frequencies, which are accounted for by unequal even and odd mode electrical lengths and some effect from the bias circuit. Furthermore, these unequal even and odd mode phase velocities also cause the spurious response at 4 GHz; the next spurious response should be at 6 GHz i.e. $3f_0$. This is due to the fact that microstrip are not pure TEM transmission lines. In the “on” state of the narrowband stub configuration there is more losses associated with the response; this is due to the isolation scheme used in order to suppress any unwanted spikes in the passband (See **6.2.4) Isolation Scheme**).

6.2.3.2) Fabricated Filter

The filters were fabricated using a Rogers Duroid 3003 substrate in compliance with the design; **Figure 6.7** illustrates the fabricated filters with bias lines to apply bias voltages to the circuit having MACOM PIN diodes (MA4AGSBP907) implemented. The circuits were measured using a Hewlett Packard 8510B network analyzer. **Figures 6.8** and **6.9** show the measured responses. The components used for the bias circuitry were chosen solely on the premise of their self resonances. The bias circuit was made up of an inductor, capacitor and a resistor. The inductors used were Murata’s LQW18A_00 series inductors, Johanson’s Multi-Layer High-Q Capacitors and Tyco Electronics RN73 series resistors. The resistors were used in order to protect the pin diodes when biasing. All data sheets for the components used can be found in Appendix 8.

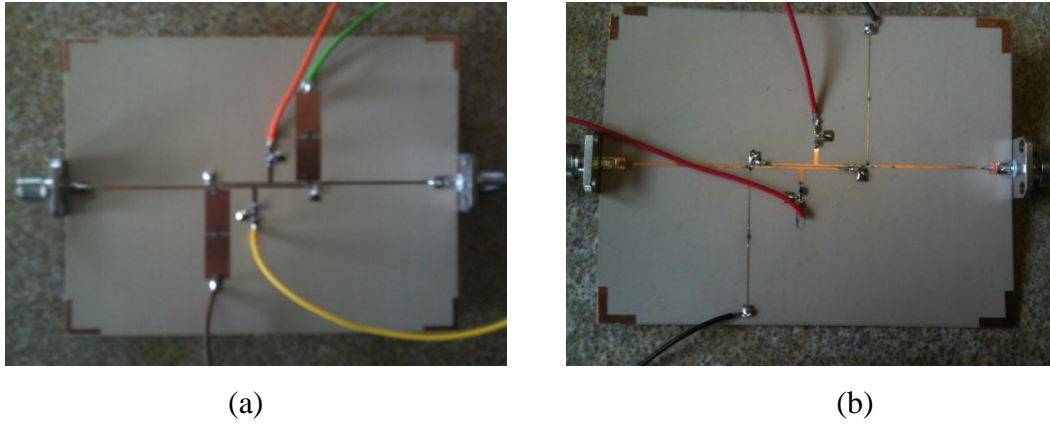


Figure 6.7: Fabricated reconfigurable filters: (a) Narrowband stubs, (b) Wideband Stubs.

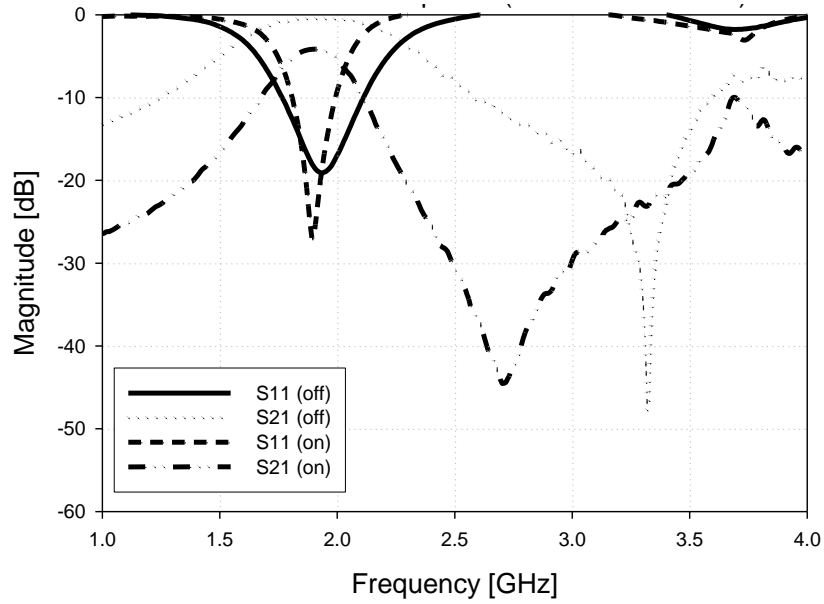


Figure 6.8: Measured Filter Response of Filter with Narrowband stubs.

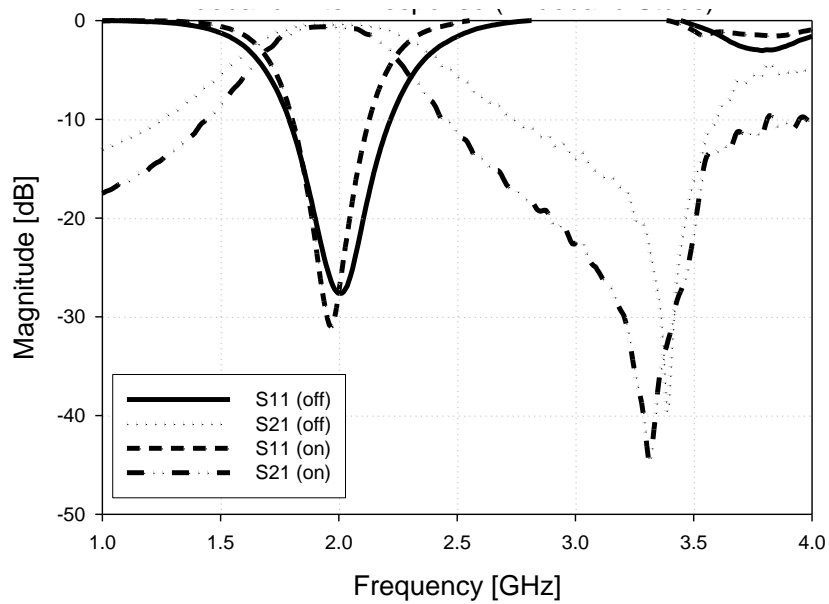


Figure 6.9: Measured Filter Response of Filter with Wideband stubs.

Table 6.2 summarizes the measured performance. The fabricated filters show good agreement with the simulations. The small discrepancies in the insertion losses, the center frequency f_0 and 3-dB fractional bandwidth FBW are attributed to the tolerances of components and fabrication process. It should also be noted that the Chebyshev response is contributed to by the bias lines being placed in the middle of the coupled lines.

	Narrowband stub “off”	Narrowband stub “on”	Wideband stub “off”	Wideband stub “on”
FBW (3 dB)	35%	16.3%	37.4%	27.8%
f_0	1.93 GHz	1.9 GHz	2 GHz	1.98 GHz
Insertion Loss	0.4 dB	4.17 dB	0.43 dB	0.73 dB

Table 6.2: Simulated Performance of the Filters Designed.

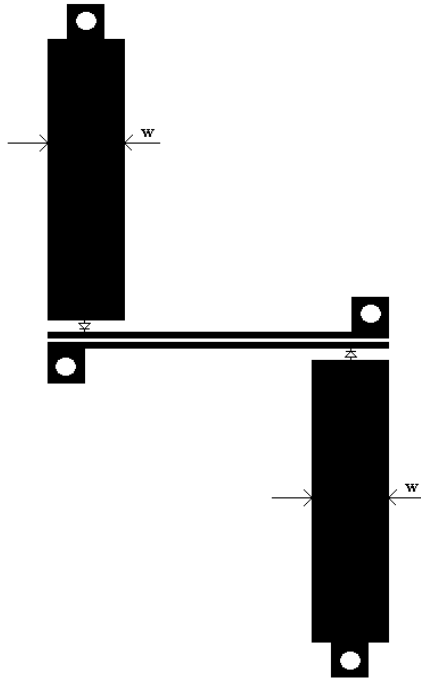
6.2.4) Isolation Scheme

When implementing the losses due to the diode for switching, a 4Ω resistor was inserted for modelling switching “on” and a 0.025 pF capacitor for modelling switching “off.” Initially, a single diode was used at the bottom of the stub for isolation; however there were unwanted spikes developed in the passband. Different isolation layouts were investigated, a total of 5 cases being analysed (See **Figures 6.10 – 6.14**).

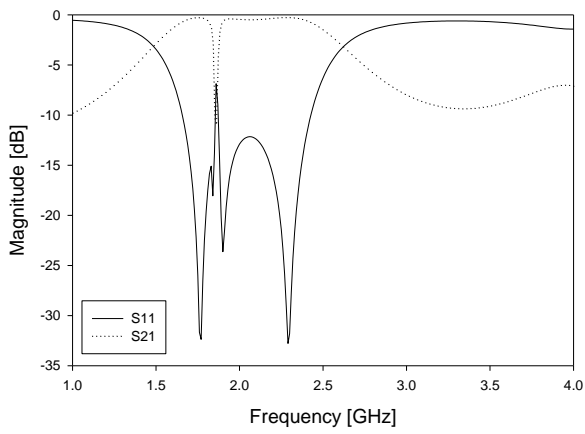
Firstly, the responses regarding the stubs with $w = 5.6 \text{ mm}$ will be considered. With reference to the first two cases (i.e. cases 1 and 2) there are spikes which have developed in the passband in the “off” state. However, in the “on” state the responses are relatively unchanged; there is a slight change in bandwidth and center frequency with the response becoming slightly asymmetric. Furthermore, in case 3 the “off” state looks promising as no spikes occur in the passband. Nevertheless, offers too much loss in the “on” state which contributes to adverse effects on the passband. The latter two cases, namely case 4 and case 5, show similar characteristics. Case 4 also shows losses but to a lesser extent than case 3 in the “on” state; meaning it gives a much more reasonable response. In the “off” state there are no spikes or adverse effects in the passband. With reference to case 5; the “on” state shows good promise but as can be seen from the response in the “off” state there is a spike in the passband. On weighing up the different cases, the most suitable would be case 4, as even

although there are some losses in the “on” state, the adverse effects are a reasonable trade off in order to eradicate the spikes in the “off” state responses.

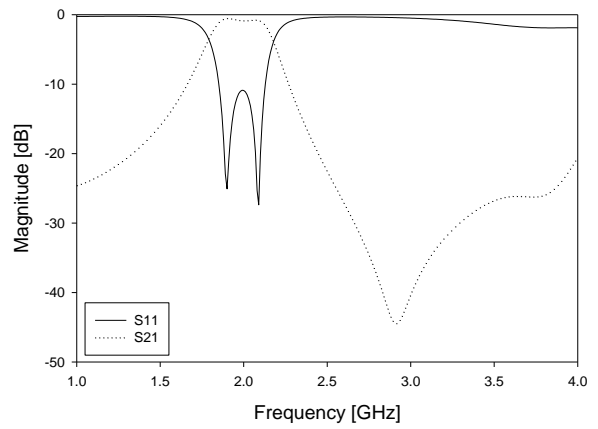
Secondly, the filter responses with the short circuit stubs of width, $w = 0.2$ mm are considered. On inspection it can be clearly seen that in all the “on” state cases there were negligible adverse effects, with the responses remaining relatively unchanged. However in the “off” state there are some adverse effects in the passband in some of the cases. Again with regard to Case 1 and 2, there are spikes present in the passband, which makes them unsuitable for implementation in the filter design. Case 3 has a very strong case, except for the spurious spike response around 3.5 GHz. The remaining two cases have unchanged shapes and show good agreement with the responses expected. In making a decision on the schematic to use for isolation, these points re – iterate the best case to use is Case 4, with the only significant trade off being made is the losses in the narrowband “on” state.



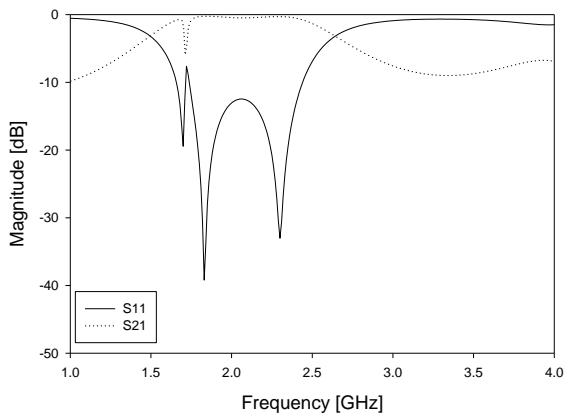
(a)



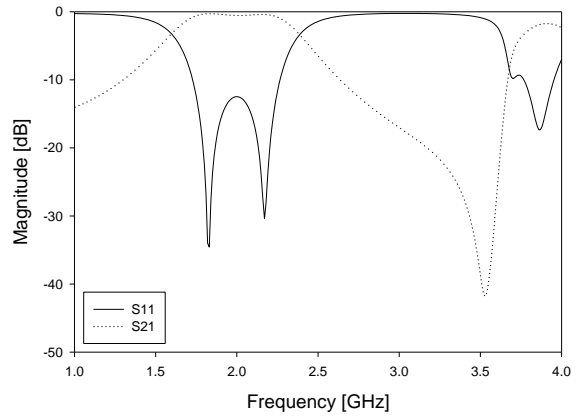
(b)



(c)

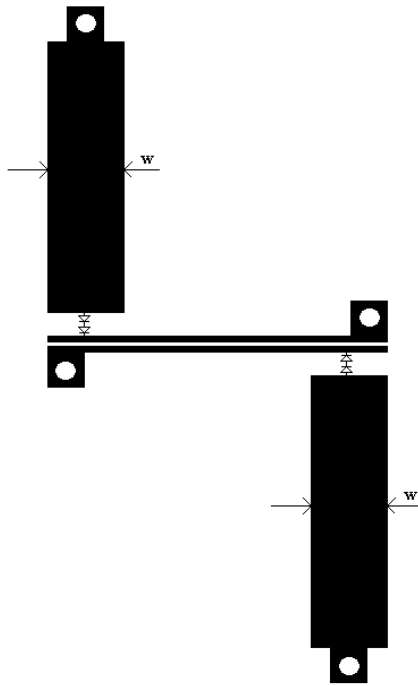


(d)

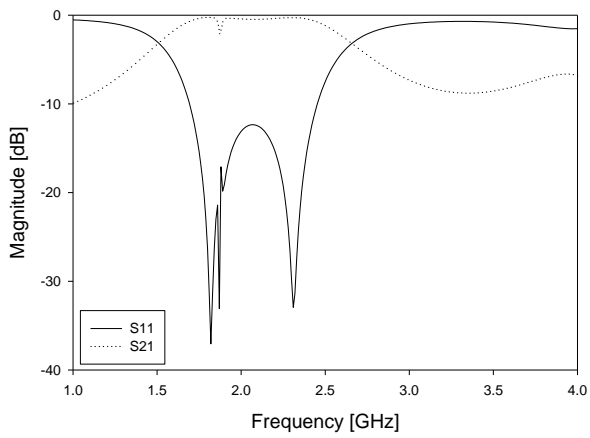


(e)

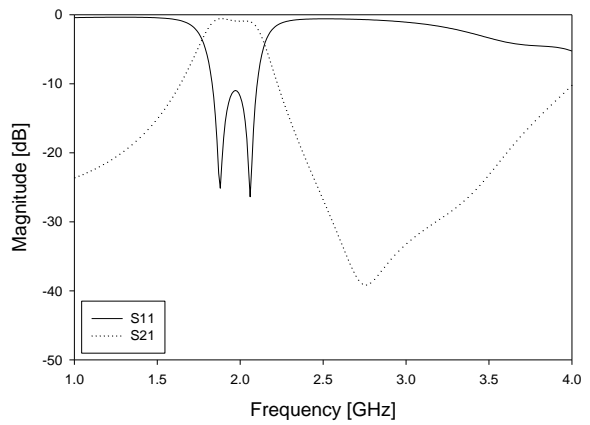
Figure 6.10: Case 1 (a) Layout, (b) State 1: $w = 5.6$ mm, (c) State 2: $w = 5.6$ mm, (d) State 1: $w = 0.2$ mm, (e) State 2: $w = 0.2$ mm



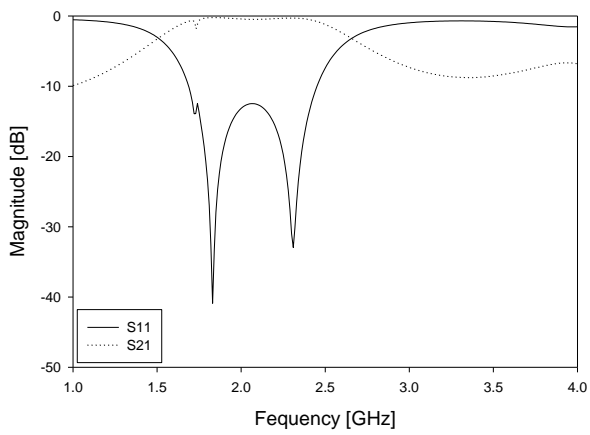
(a)



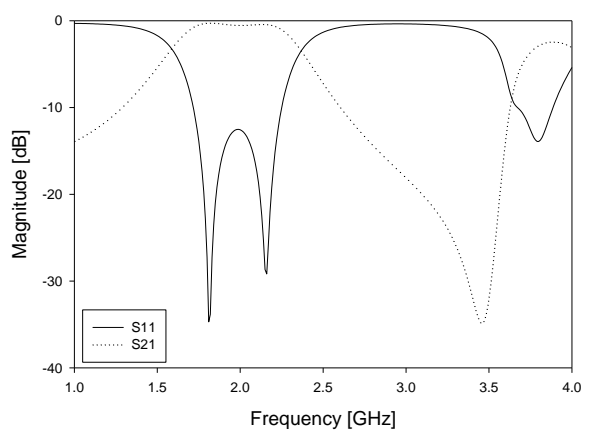
(b)



(c)

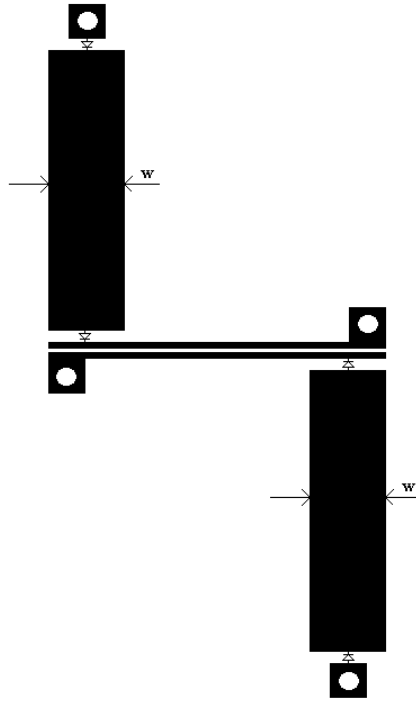


(d)

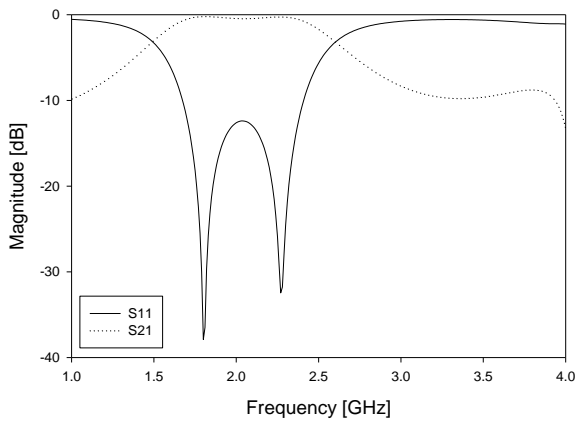


(e)

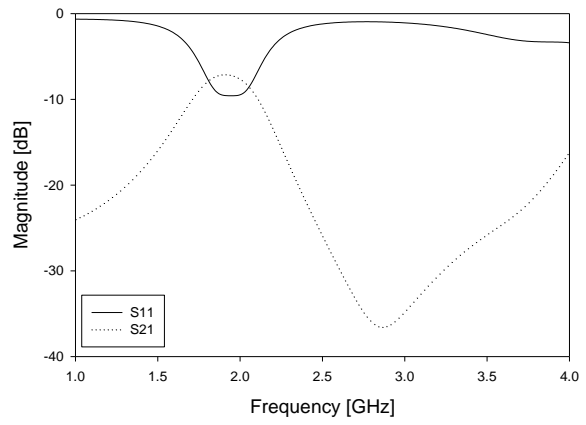
Figure 6.11: Case 2 (a) Layout, (b) State 1: $w = 5.6$ mm, (c) State 2: $w = 5.6$ mm, (d) State 1: $w = 0.2$ mm, (e) State 2: $w = 0.2$ mm



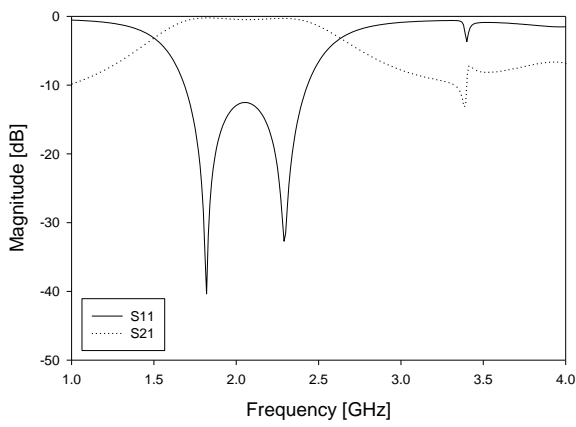
(a)



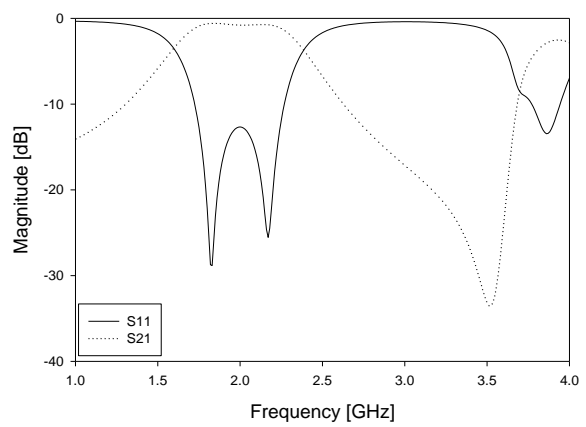
(b)



(c)

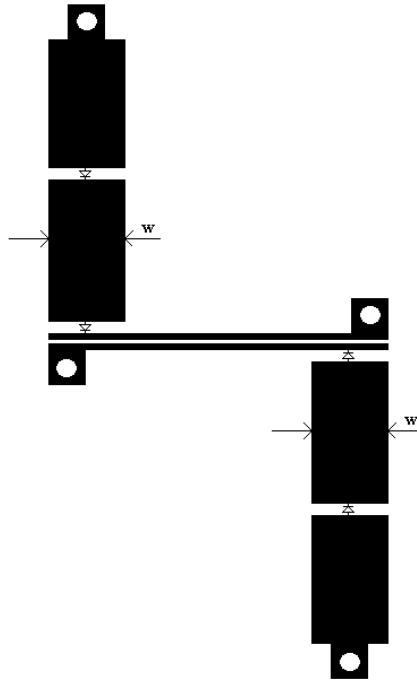


(d)

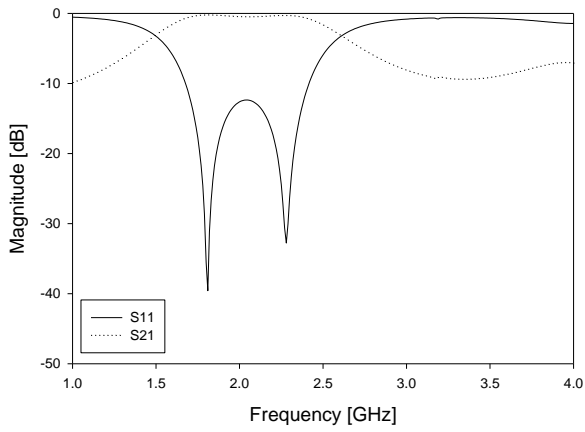


(e)

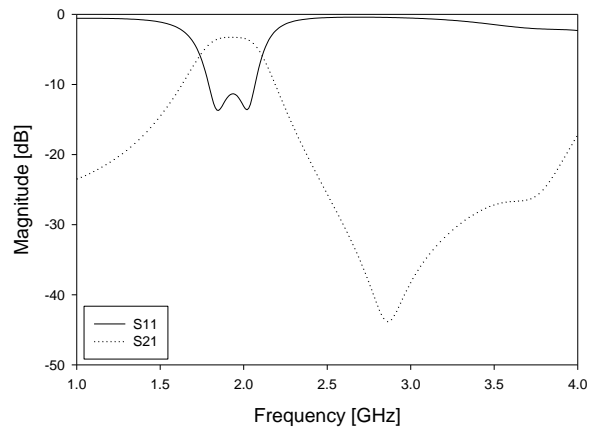
Figure 6.12: Case 3 (a) Layout, (b) State 1: $w = 5.6$ mm, (c) State 2: $w = 5.6$ mm, (d) State 1: $w = 0.2$ mm, (e) State 2: $w = 0.2$ mm



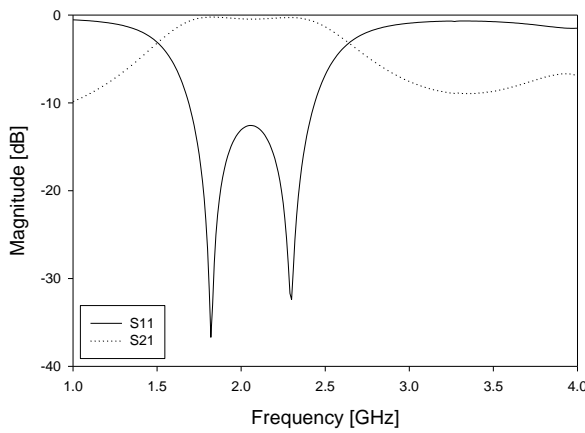
(a)



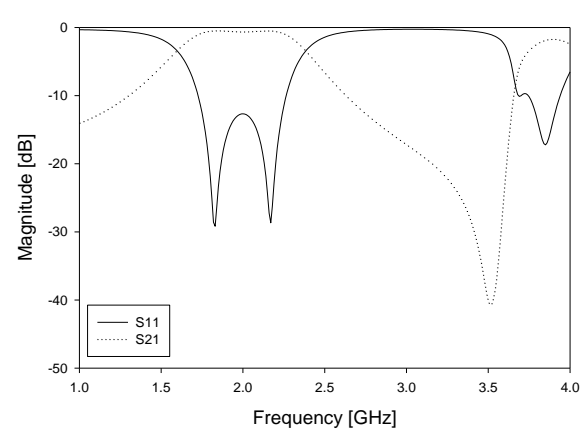
(c)



(c)

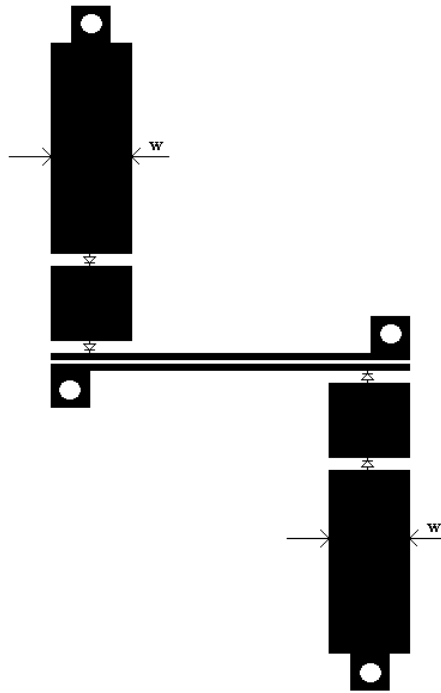


(d)

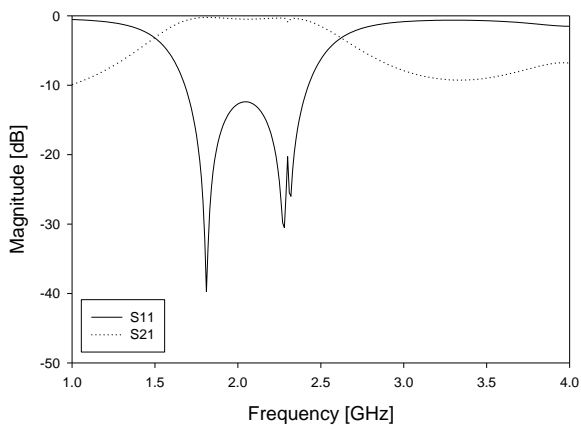


(e)

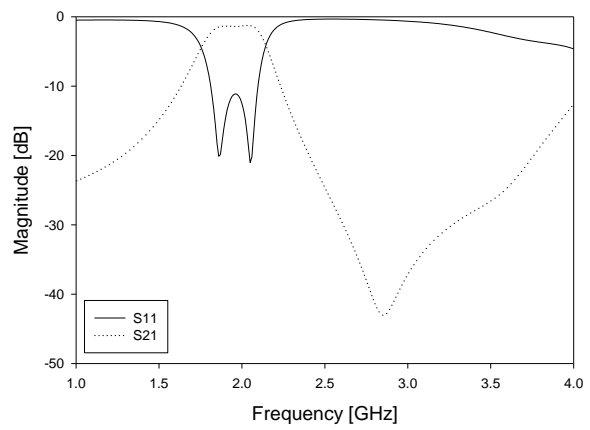
Figure 6.13: Case 4 (a) Layout, (b) State 1: $w = 5.6$ mm, (c) State 2: $w = 5.6$ mm, (d) State 1: $w = 0.2$ mm, (e) State 2: $w = 0.2$ mm



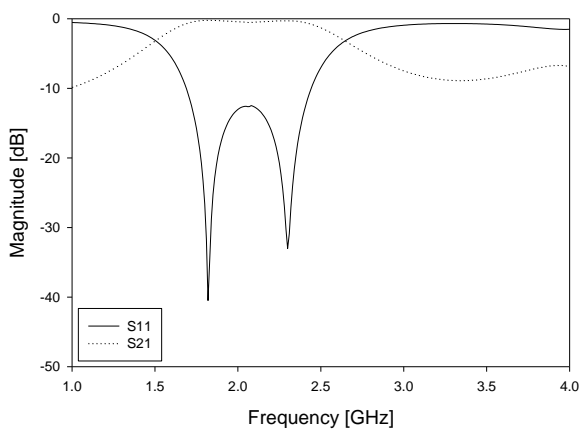
(a)



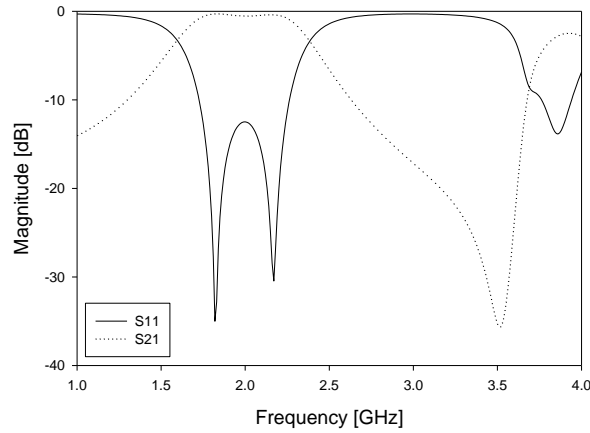
(b)



(c)



(d)



(e)

Figure 6.14: Case 5 (a) Layout, (b) State 1: $w = 5.6$ mm, (c) State 2: $w = 5.6$ mm, (d) State 1: $w = 0.2$ mm, (e) State 2: $w = 0.2$ mm

6.3) Short Circuit Coupled Line Filters Combined

In the previous filter blocks it was possible to obtain two bandwidth states. The number of bandwidth states can be increased by a simple combination of the previous filter configuration. As aforementioned this can be easily done as the return loss in the passband only depends on the pair of even- and odd- mode impedances and is independent of the characteristic impedance of the other stubs. The proposed circuit design can be seen below:

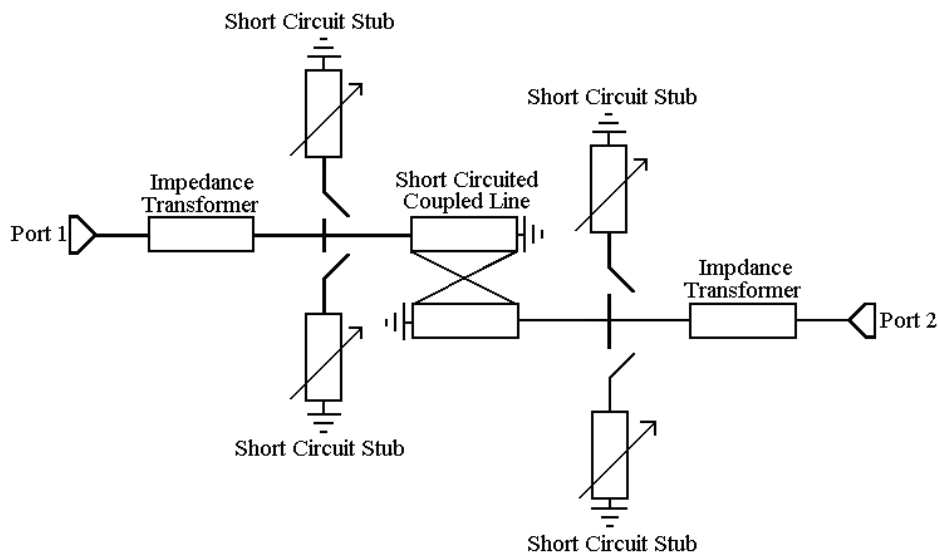


Figure 6.15: Filter Building Block with Four Bandwidth States.

6.3.3) Experimental Demonstration

6.3.3.1) EM Simulation

Figure 6.16 shows the reconfigurable microstrip filter developed by combining the two filters from [1]. The filter is implemented on a substrate with $\epsilon_r = 3$ and thickness = 1.02mm. The pin diodes were modeled by using a capacitor of value 0.025 pF for isolation and a resistor of value of 4Ω for connection (these values being obtained from the data sheet for the diode used). The initial dimensions of the circuits were obtained using Microwave Office [3] and finalized using EM software Sonnet [4]. The dimensions of the circuit needed to be slightly altered from the previously designed filters in order to compensate for the shifts in center frequency, and are as follows: $w(\text{width}) = 5.6 \text{ mm}$ and $l(\text{length}) = 20.1 \text{ mm}$ (narrowband

stubs); $w(\text{width}) = 0.2 \text{ mm}$ and $l(\text{length}) = 25.8 \text{ mm}$ (Wideband Stubs). The coupled lines have a gap $s = 0.2 \text{ mm}$, $l(\text{length}) = 26.85 \text{ mm}$ and $w(\text{width}) = 0.5 \text{ mm}$. In this case, the impedance transformer has a width and length of 0.6 mm and 25 mm , respectively. **Figures 6.17 & 6.18** show the simulated results, showing the filter can be switched between four distinct bandwidth states.

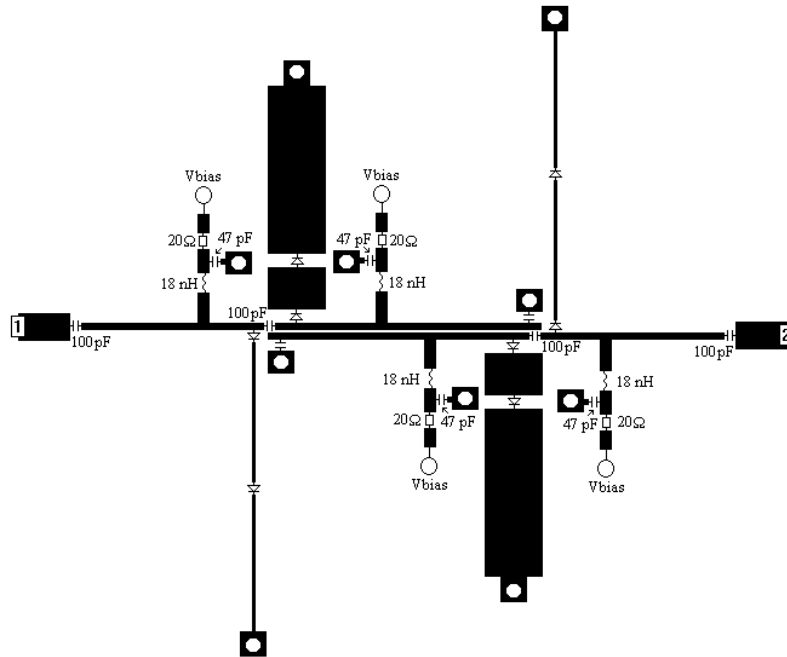


Figure 6.16: Filter Obtained by Combining Both Filters from [2].

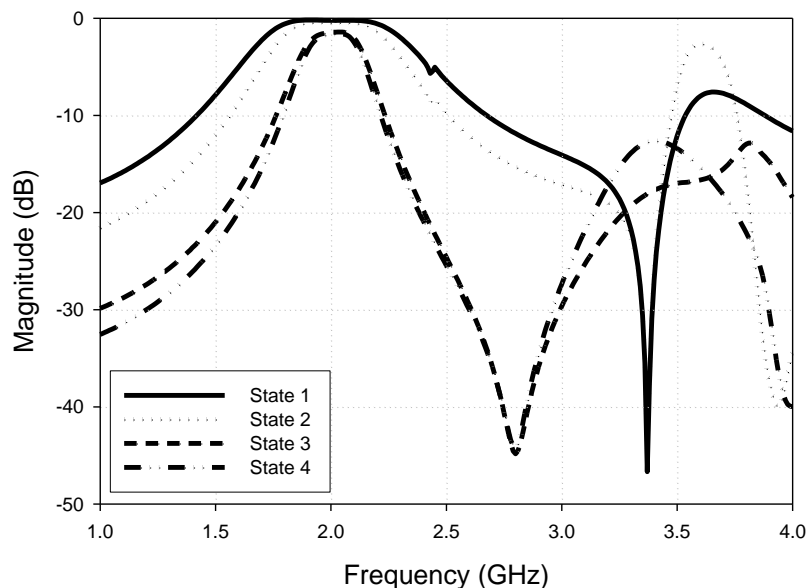


Figure 6.17: Simulated Insertion Losses (S21) of the Filter Circuit.

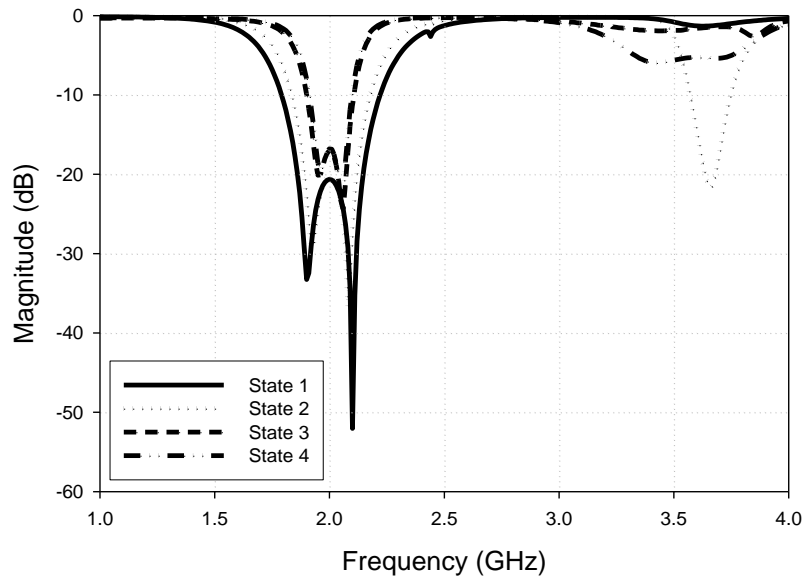


Figure 6.18: Simulated Return Losses (S11) of the Filter Circuit.

State 1: All Diodes “Off.”

State 2: Wideband Stubs “On” and Narrowband Stubs “Off.”

State 3: Narrowband Stubs “On” and Wideband Stubs “Off.”

State 4: All Diodes “On”

The simulated performance of the filter is summarized in **Table 6.3**. The noise figure of the filter may be considered equal to its insertion loss since the Pin diodes are basically a resistive element.

	State 1	State 2	State 3	State 4
<i>FBW</i> (3 dB)	34%	27%	15%	13.5%
f_0	2 GHz	2 GHz	2 GHz	2 GHz
Insertion Loss	0.22 dB	0.45 dB	1.45 dB	1.66 dB

Table 6.3: Simulated Performance of Combined Filter.

There are no shifts in the center frequency, as the electrical lengths of the coupled line and short circuit stubs were altered in order to compensate for shifts in center frequency. As mentioned before, because of unequal even and odd mode phase velocities a second harmonic is caused around 4 GHz ($2f_0$). This is due to the fact that microstrip lines are not pure TEM

transmission lines. However, in this case the harmonic has been shifted down due to the electrical lengths of the coupled line and short circuit stubs being altered. Also the inclusion of the extra bias circuit components and diodes affects the losses of the circuit thus affecting the return loss; this can be especially seen in the states where the wideband stubs are turned on. As with the previous filters designed the insertion losses associated with the narrowband state are much higher as expected, however the isolation scheme used for the narrowband stubs is slightly different than used before. It was found from Section 6.2.4) that moving the diode down the stub decreases the insertion losses however a spike begins to appear closer to the passband. This is because any spike produced will be shifted up the band dependant on the position of the second diode. This meaning a trade off was made in order to limit the losses but at the same time keep the spike negligible and in a position out of the passband, as can be seen from **Figures 6.17 and 6.18**. The reason for more losses in the narrowband state is due to the current density being higher at the position of the second diode as it is nearer the short circuit. Thus by comparing **Figures 6.17 & 6.18** with **Figure 6.5 and 6.6** it can be clearly seen the insertion losses in the narrowband states are much more desirable for wideband applications in the combined circuit. Furthermore, the wideband state insertion losses are slightly higher than before, as expected due to the increased number of components and bias circuits used. Moreover, the bias circuits added to the coupled lines affect the coupling of the coupled line, thus a slight degradation of bandwidth is observed.

6.3.3.2) Fabricated Results

The filter was fabricated using a Rogers Duroid 3003 substrate in compliance with the design; **Figure 6.19** illustrates the fabricated filter with bias lines to apply bias voltages to the circuit having MACOM PIN diodes (MA4AGSBP907) implemented. The circuit was measured using a Hewlett Packard 8510B network analyzer. The bias circuitry used was the same as the previous deigned filter. **Figures 6.20 and 6.21** show the measured responses.

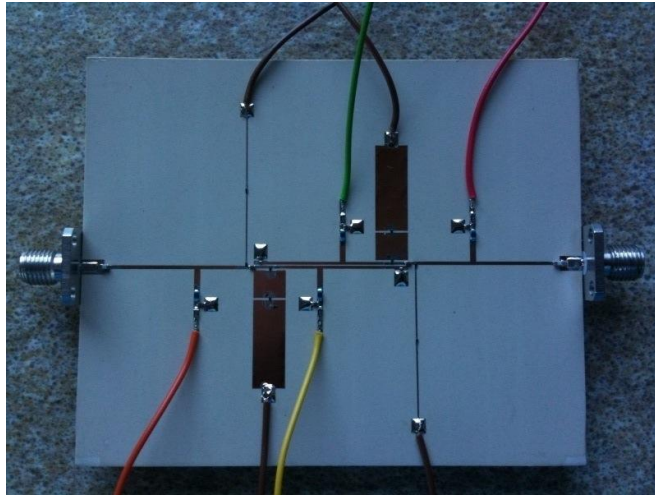


Figure 6.19: Fabricated reconfigurable filter block.

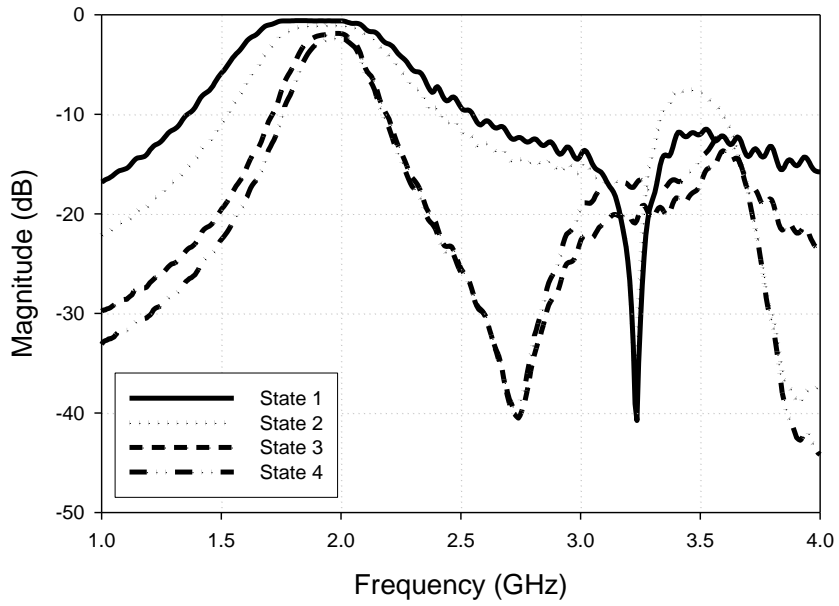


Figure 6.20: Simulated Insertion Losses (S21) of the Filter Circuit.

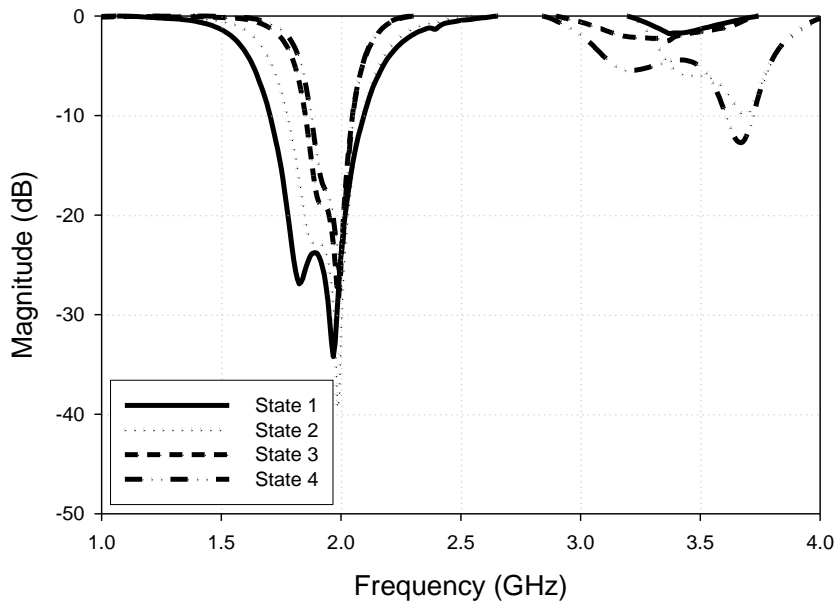


Figure 6.21: Measured Return Losses (S11) of the Filter Circuit.

State 1: All Diodes “Off.”

State 2: Wideband Stubs “On” and Narrowband Stubs “Off.”

State 3: Narrowband Stubs “On” and Wideband Stubs “Off.”

State 4: All Diodes “On”

Table 6.4 summarizes the measured performance. The fabricated filter shows good agreement with the simulations. The small discrepancies in the insertion losses, the center frequency f_0 and 3-dB fractional bandwidth FBW are attributed to the tolerances of components and fabrication process. The increased losses are also attributed to the increased number of components used. Again comparing **Figures 6.20 & 6.21** and **Figures 6.8 & 6.9** the same traits are seen as the comparison between simulated results. The most notable is the improved insertion loss in the narrowband state as aforementioned in earlier sections is it is desirable to limit the losses whilst designing wideband filters of a higher order.

	State 1	State 2	State 3	State 4
FBW (3 dB)	33.5%	23.23%	14.65%	13.06%
f_0	1.9 GHz	1.9375 GHz	1.945 GHz	1.9525 GHz
Insertion Loss	0.62 dB	1.07 dB	1.91 dB	2.5 dB

Table 6.4: Measured Performance of Combined Filter.

6.4) Non – Linearity Measurements

6.4.1) Third Intercept Point

As mentioned in previous chapters, there are some physical implementation issues that arise when considering non – linearity of the filters. The third intercept point was measured using the same set up as section 5.4.1) and Figure 5.6. Each circuit was measured with the following IP3 being obtained; for the separate narrowband and wideband filters two different current values were used for biasing for comparison of results.

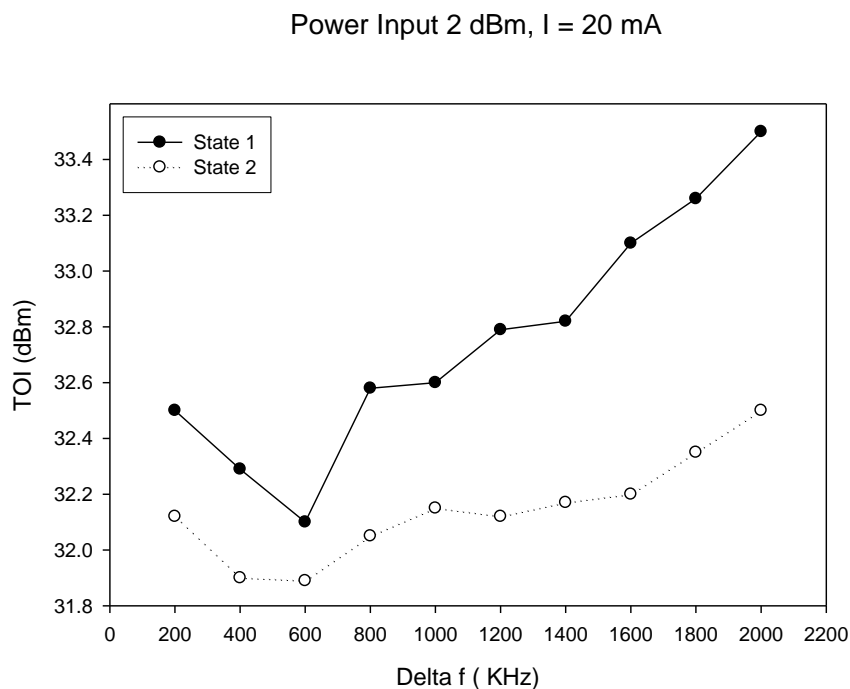


Figure 6.22: IP3 of Coupled line filter With Wideband Stubs, when biasing current = 20 mA.

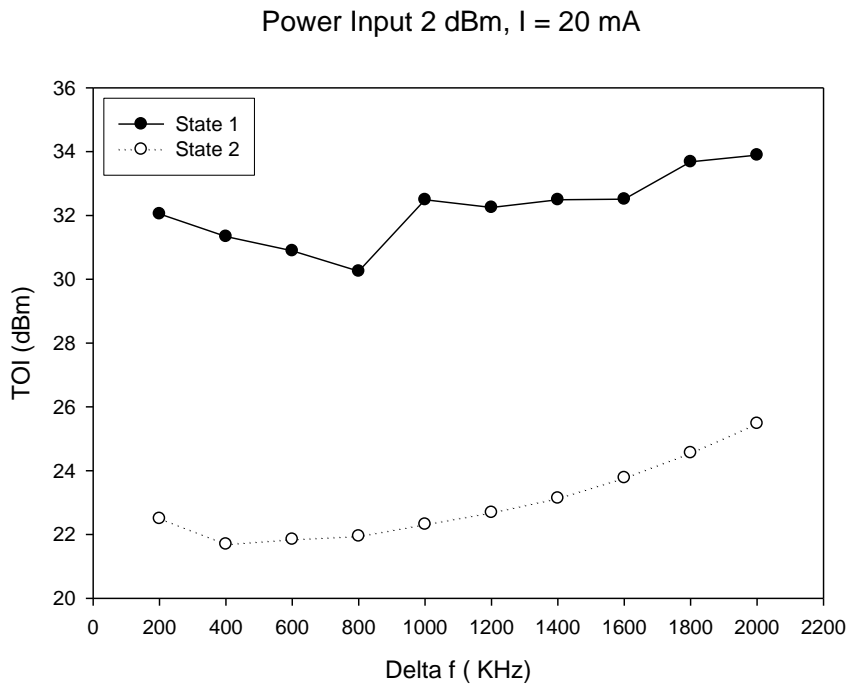


Figure 6.23: IP3 of Coupled line filter With Narrowband Stubs, when biasing current = 20 mA.

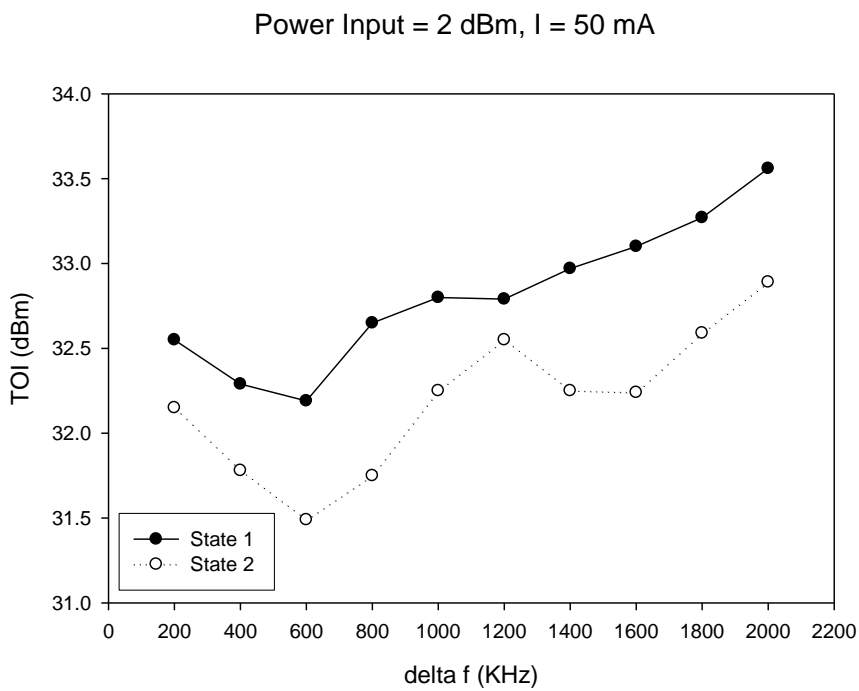


Figure 6.24: IP3 of Coupled line filter With Wideband Stubs, when biasing current = 50 mA.

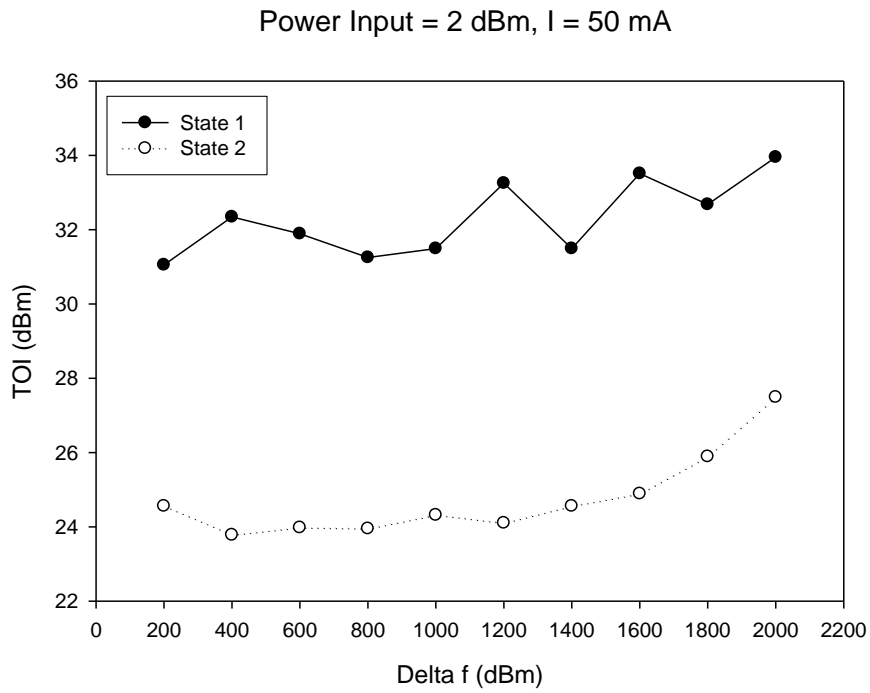


Figure 6.25: IP3 of Coupled line filter With Narrowband Stubs, when biasing current = 50 mA.

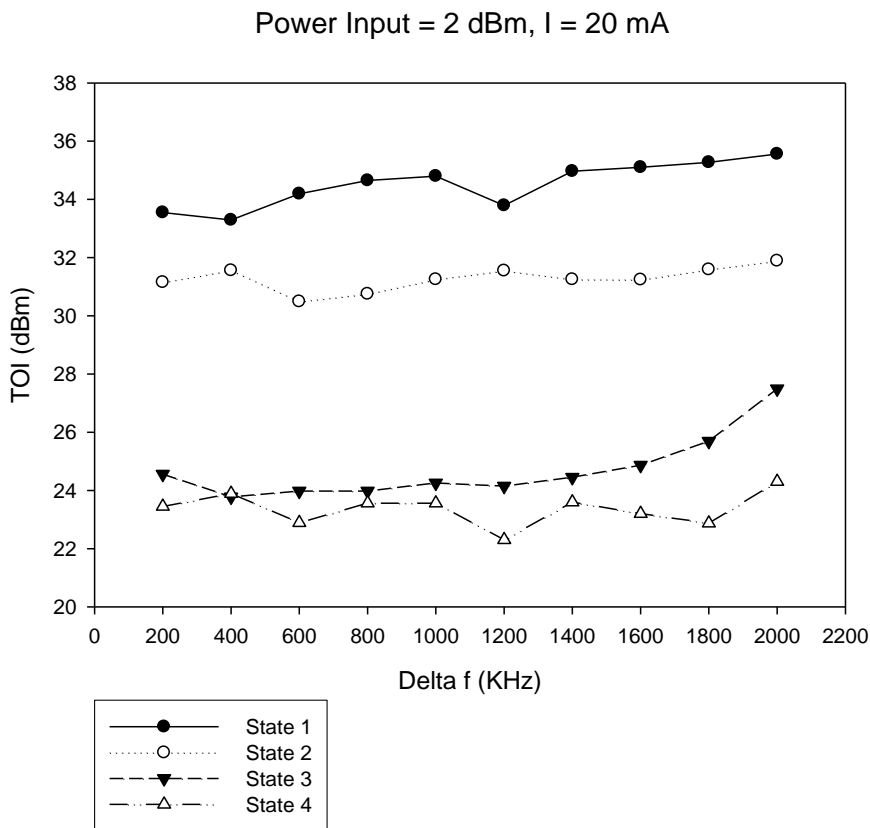


Figure 6.26: Coupled Line Filter Combined.

In the taking of the measurements, several two tone separations were used, which were symmetrical with respect to the center frequency. In principal the lower the bandwidth the lower the IP3 is. In addition, the number and location of the pin diodes being switched on in the circuit can have an effect on the non linear performance. Also the current being applied to the pin diodes also affects the IP3 (compare **Figure 6.23** to **Figure 6.26**) as the insertion loss due to the pin diodes is reduced slightly. It is worth noting that as the tone separation increases; the intermodulation becomes weaker, meaning that larger errors may occur due to the dynamic range of the spectrum analyser. In order to calculate the third intercept point, the spectrum analyser uses the power level of f_1 i.e. $P(f_1)$ and the power level of the third harmonic $P(2f_2 - f_1)$. From these the intermodulation ratio can be calculated, which then gives rise to the third intercept point:

$$\text{Intermodulation Ratio} = P(f_1) - P(2f_2 - f_1) \text{ (units : dBm)} \quad (6.13)$$

$$TOI = P(f_1) + 1/2 \times \text{Intermodulation Ratio (units : dBm)} \quad (6.14)$$

(6.14) directly relates to expression (5.32) as,

$$TOI = P(f_1) + \frac{1}{2} [P(f_1) - P(2f_2 - f_1)] \quad (6.15)$$

$$TOI = 2 \times \frac{P(f_1)}{2} + \frac{P(f_1) - P(2f_2 - f_1)}{2} = \frac{3 \times P(f_1) - P(2f_2 - f_1)}{2} \quad (6.16)$$

6.4.2) 1 dB Compression Point

The pin diodes can only support a maximum of 23 dBm; the input signal never exceeded 20 dBm in order to protect the device under test. The coupled line filters in this chapter were measured for each state with the difference between the input and output mainly being the result of insertion loss. In each case provided below, it can be clearly seen that they all have good linearity and their 1 dB compression points above 20 dBm. The set up used was that of Section 5.2.1) and **Figure 5.3**.

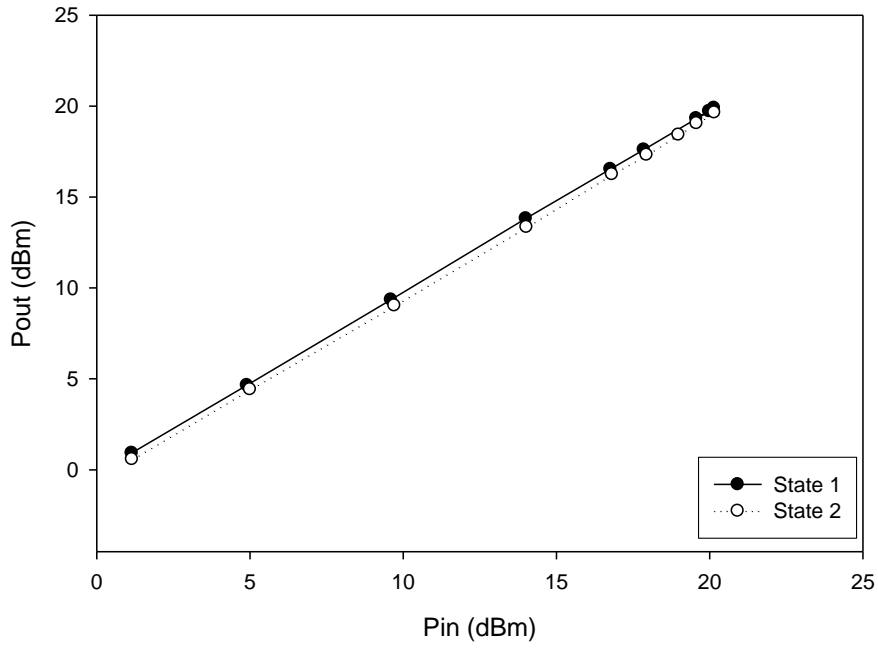


Figure 6.27: 1 dB Compression measurement of coupled line filter with wideband stubs.

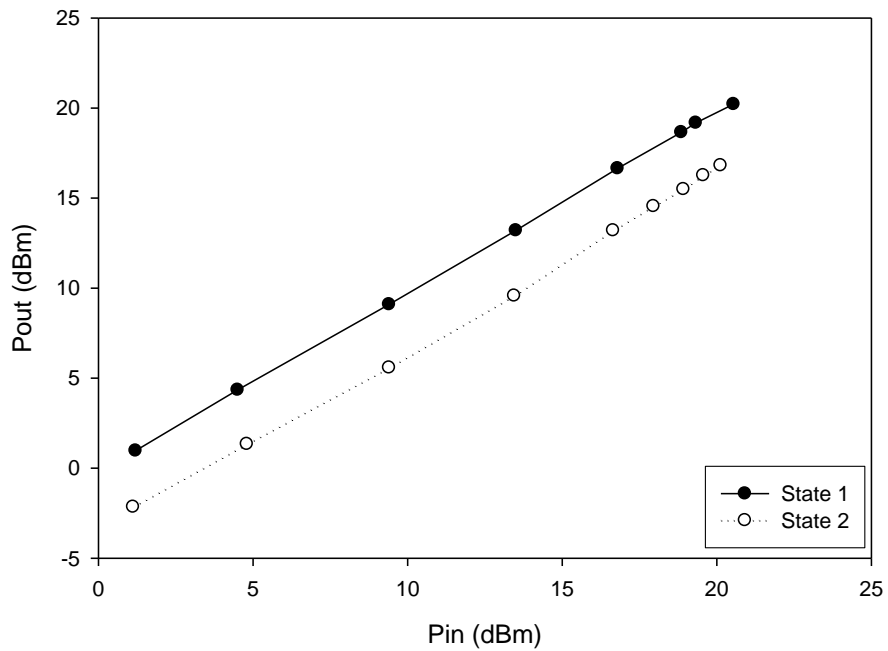


Figure 6.28: 1 dB Compression measurement of coupled line filter with narrowband stubs.

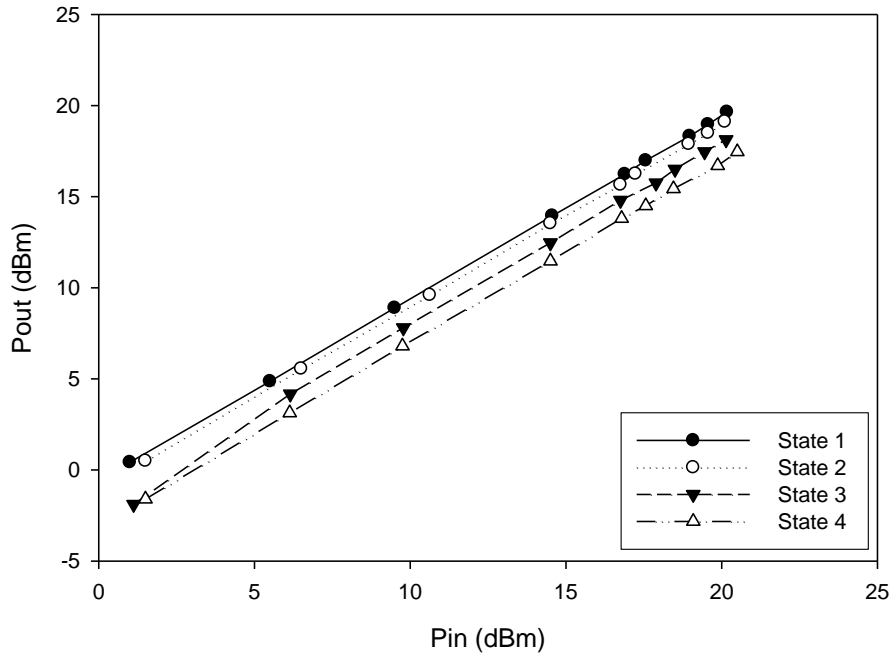


Figure 6.29: 1 dB Compression measurement of combined coupled line filter.

6.5) Summary

The novel structures presented used a pair of short-circuited coupled lines and the coupling between the two lines is controlled by switching short circuit stubs in and out of the circuit. Firstly two filters were designed, each with two states; one with narrowband stubs and the other wideband stubs. Some issues arose from the design of the filters, the main being isolation of the stubs. An investigation of different cases was carried out and based on tradeoffs the best isolation scheme was chosen. The demonstrated filters show good agreement between measured and simulated results with reconfigurable bandwidths ranging from 16% to 37%. Both filters also showed good linearity performance, with a 1 dB compression point above 20 dBm. This concept was then further enhanced by combining these two filters to then obtain a filter with four bandwidth states. This new combined filter circuit shows an improved insertion loss, which is more desirable in the design of wideband reconfigurable filters. There is some degradation of losses in the wideband states which is expected as there is an increase in the number of circuit components and bias circuits. The bias circuits also affect the coupling of the coupled lines which explains the slight change in bandwidth from the separate filters. The demonstrated filter shows good agreement between measured and simulated results with reconfigurable bandwidths ranging from 13% to 33%.

Furthermore, this filter also shows good linearity performance with a 1 dB compression point also above 20 dBm.

6.6) References

[1] A. Miller, J. Hong, “Wideband Bandpass Filter with Reconfigurable Bandwidth,” *IEEE Microwave and wireless components letters*, Vol. 20, No. 1, Jan 2010, pp 28 – 30.

[2] A. Miller, J. Hong “Wideband Bandpass Filter with Multiple Reconfigurable Bandwidth States,” European Microwave Conference, Sep 2010, pp 1237 – 1276.

[3] Applied Wave Research Inc, User’s Manual, Version 7.5, June 2007

[4] Sonnet Software Inc, EM User’s Manual, Version 12 NY, 2009

Chapter 7: Cascaded Coupled Line Reconfigurable Filters

7.1) Introduction

The next progressive stage of the coupled line concept is to cascade this coupled line section to create high order filters, which is discussed in this chapter. A reconfigurable bandpass filter of this type which is capable of switching between four distinct bandwidth states ranging from around 20% to 50% 3 dB fractional bandwidth (FBW) centered at 2 GHz, is designed using the theory in section 4.2.1) and 6.2.1). The filter designed exhibits insertion losses ranging from 0.47 dB to 5.5 dB. The fabrication and designed filter is tested in order to make comparisons of the conformity of the design. On inspection of the design it is clear that the impedance transformer for matching degrades the passband performance. For this reason an improved design procedure is used from Matthaei design equations presented in section 4.2.2). A reconfigurable bandpass filter of this type is shown which can switch between three distinct bandwidth states ranging from around 30% to 50% ripple fractional bandwidth (FBW) centered at 2 GHz. Furthermore, due to the flexibility needed for the even and odd mode impedances LCP technology is used for the fabrication. The reconfigurable filter exhibits insertion losses ranging from 0.57 dB for the widest passband state to 1.95 dB for the narrowest passband state. Both filters discussed are documented in [1] and [2].

7.2) Reconfigurable Coupled Line Filter with Four Distinct Bandwidth States

7.2.1) Filter Design

The first step of the design is to design a single section with the impedance transformer included. In order to design this, expressions from Section 4.2.1) are used. The specification which was followed was:

State 1: 3 dB FBW = 50%

State 2: 3 dB FBW = 40%

State 3: 3 dB FBW = 30%

State 4: 3 dB FBW = 20%

All at center frequency 2 GHz

Return loss across any passband better than 10 dB

Rejection level better than 20 dB at 1 GHz and 3GHz.

Firstly, the even and odd mode impedances for the couple line section without any connecting stubs for reconfigurability are found for the widest state, i.e. 50% FBW, (see appendix 4). For realizable even and odd mode impedances on a single layer circuit the values for a given substrate must be considered. Furthermore, an impedance transformer is usually required. In general impedance transformers are narrowband, and can have noticeable effects on the return loss response.

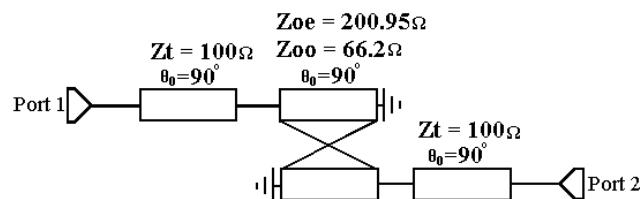


Figure 7.1: Single Section Coupled line Section with Impedance Transformer.

From this the stubs can then be added for reconfigurability, in order to choose the required stub impedances for the bandwidths in the specification, the stub impedances are varied with the given parameters in the above **Figure 7.1** in order to plot the 3 dB bandwidths as a function of stub impedance (again see Appendix 4).

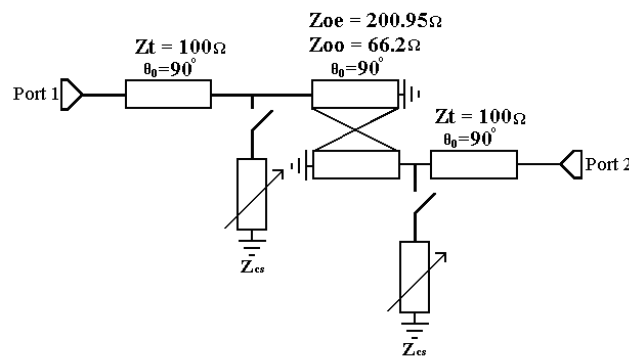


Figure 7.2: Single Section Coupled line Section with Impedance Transformer and stubs for Reconfigurability.

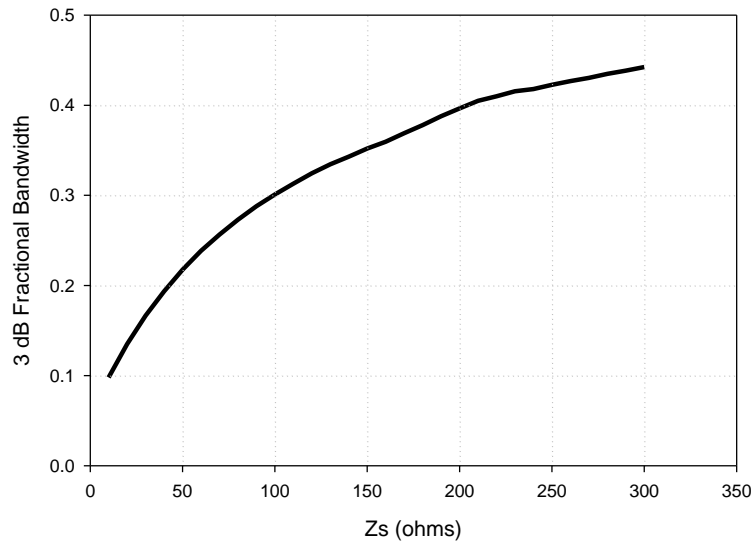


Figure 7.3: Graph in Order to Select the Stub Impedances.

From the graph the impedance of the stubs required for each bandwidth state can be chosen. Referring back to the specification, the bandwidths required are 40%, 30% and 20%. For the first two bandwidth states the impedances of the stubs chosen are 200 Ω and 100 Ω respectively. Therefore once cascaded the two passive filters with these bandwidths are of the form, which is simply a cascade of the coupled line section shown in **Figure 6.1**:

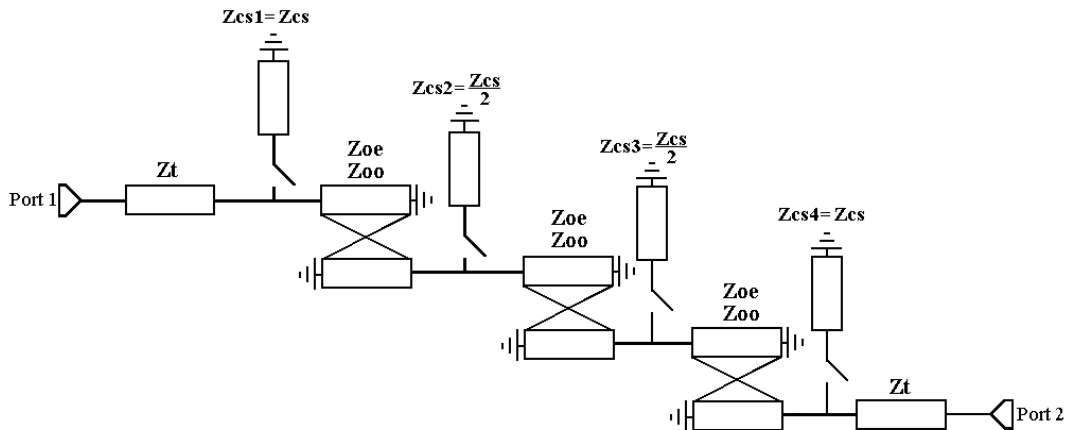


Figure 7.4: Bandpass Filter Structure Once the Single is cascaded.

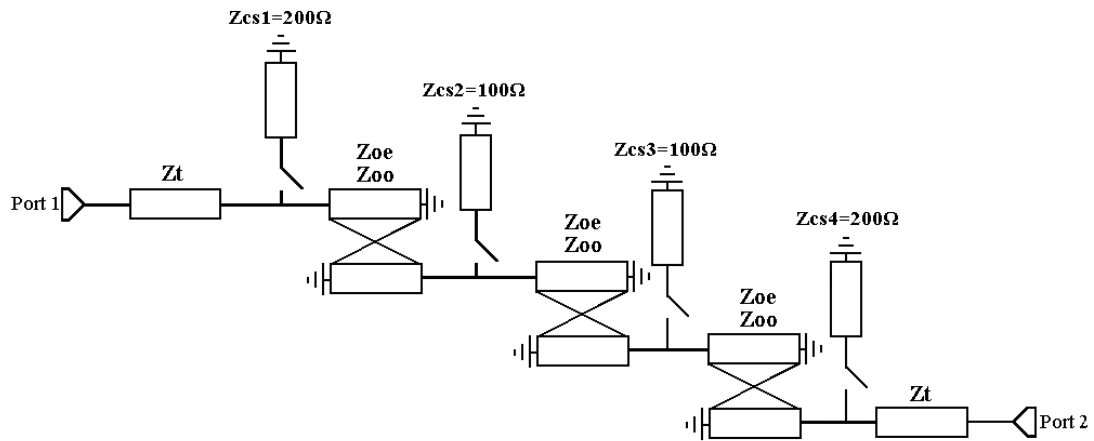


Figure 7.5: State 2 Impedances.

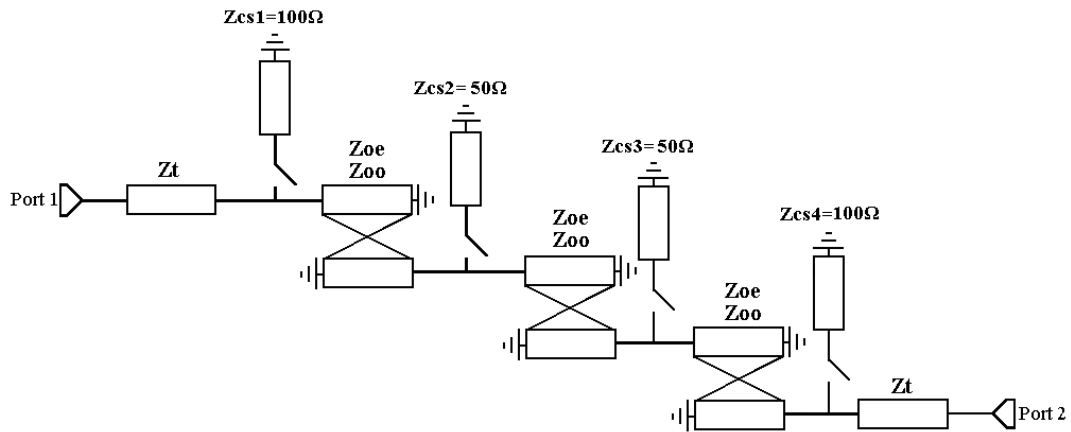


Figure 7.6: State 3 Impedances.

In order to obtain a filter with four states the two filters from **Figure 7.5** and **Figure 7.6** are combined using the similar method documented in [3] and section 6.3). Once combined it was found that by omitting the input and output stubs had very little effect on the matching or the FBW, this meaning that the number of diodes needed for reconfigurability is limited.

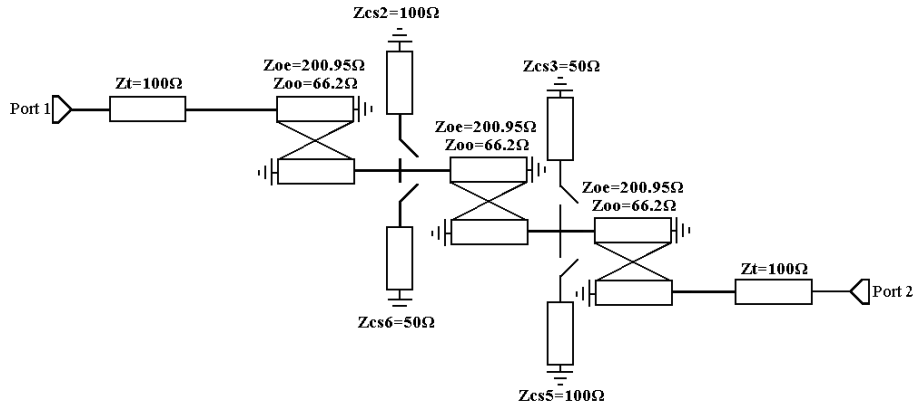


Figure 7.7: Filter Combined to Obtain State 2 and State 3.

This filter shown can switch between four states by switching the short circuit stubs in different combinations, namely:

- State 1: All off
- State 2: Z_{cs2} and Z_{cs5} on
- State 3: Z_{cs3} and Z_{cs6} on
- State 4: All on

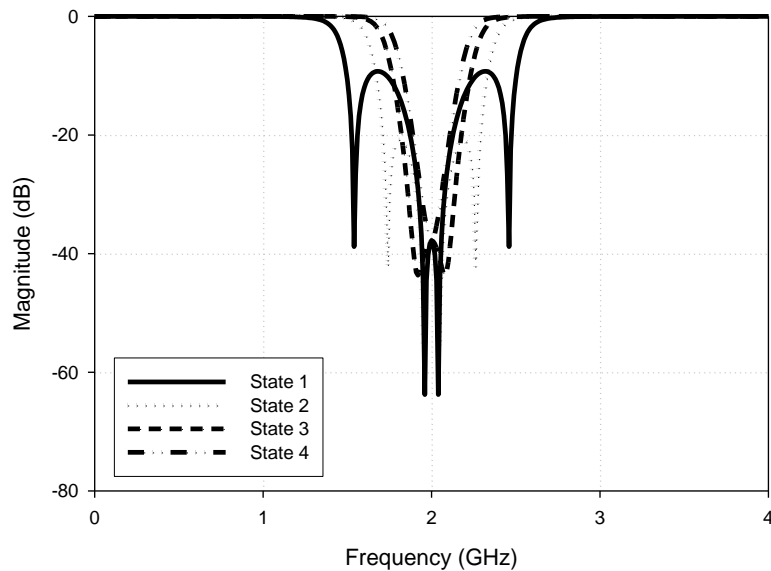


Figure 7.8: S11 of Initially Designed Filter.

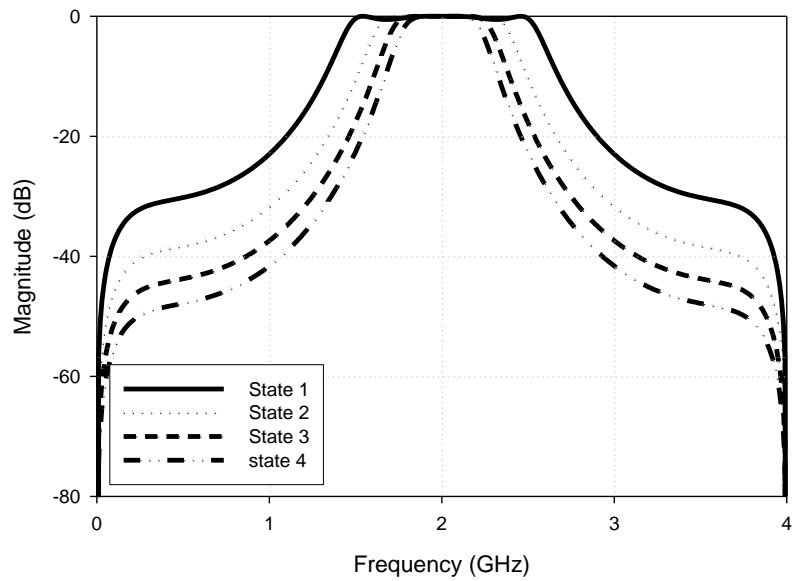


Figure 7.9: S21 of Initially Designed Filter.

On inspection of the narrowest state the FBW bandwidth is higher than that specified. In order to meet the specification two switchable short circuit stubs of impedance 80Ω were added at the output and input for compliance.

- State 1: All off
- State 2: Zcs2 and Zcs5 on
- State 3: Zcs3 and Zcs6 on
- State 4: All on

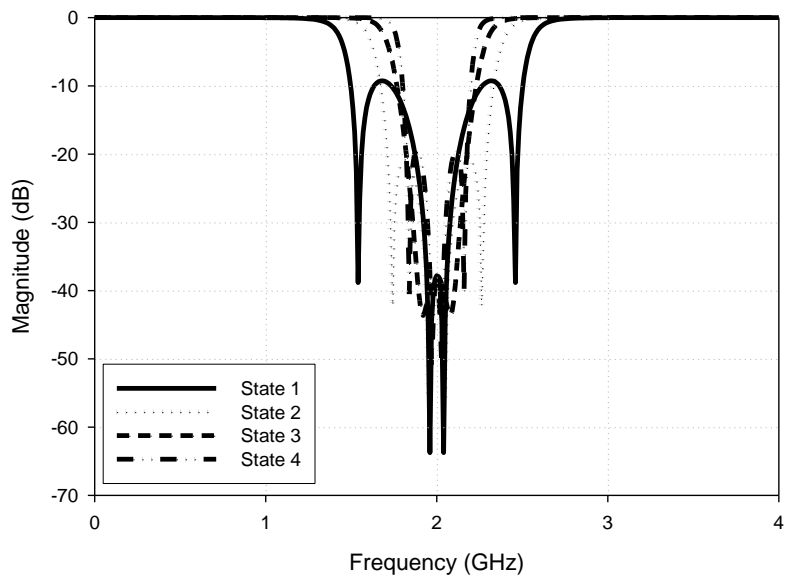


Figure 7.10: S11 of Final Designed Filter.

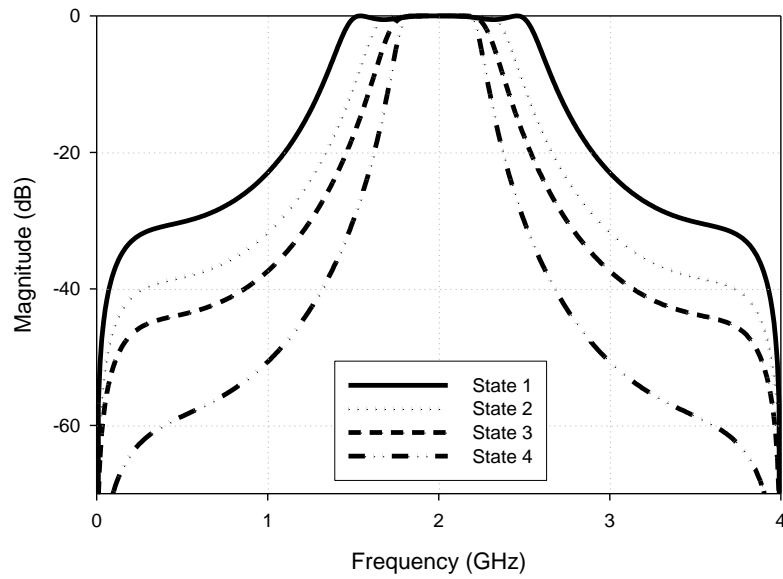


Figure 7.11: S21 of Final Designed Filter.

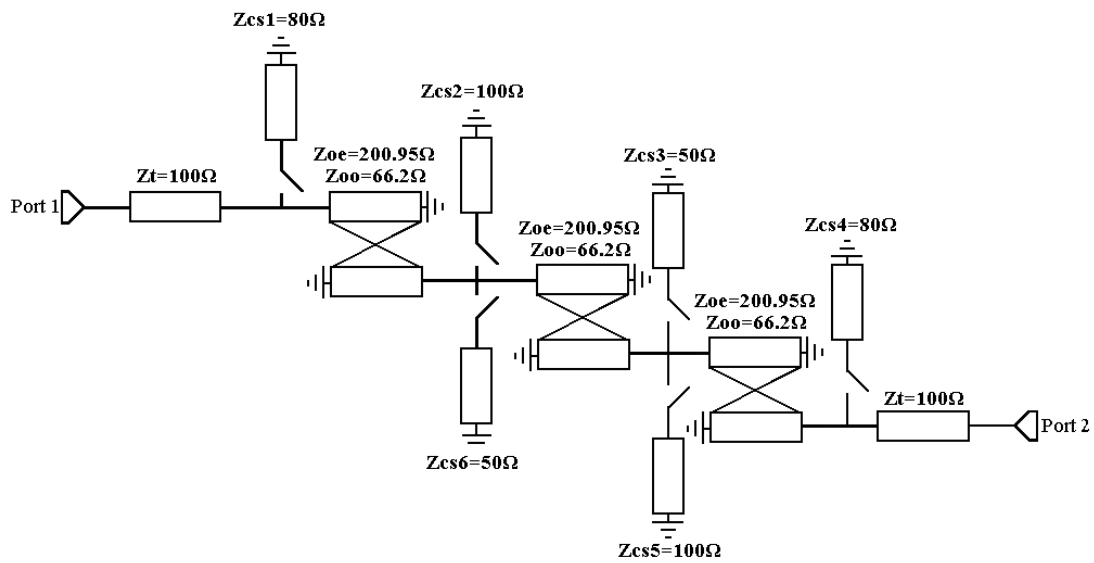


Figure 7.12: Final Theoretical Design.

The final Circuit impedances are as follows:

$$Z_t = 100 \Omega$$

$$Z_{oe} = 200.95 \Omega$$

$$Z_{oo} = 66.2 \Omega$$

$$Z_{cs1} = Z_{cs4} = 80 \Omega$$

$$Z_{cs2} = Z_{cs5} = 100 \Omega$$

$$Z_{cs3} = Z_{cs6} = 50 \Omega$$

All electrical lengths are set to $\theta = 90^\circ$ at center frequency (2 GHz).

7.2.2) EM Simulation

The microstrip circuit as shown in **Figure 7.13** was designed for a substrate with a thickness of 1.52 mm and dielectric constant of 3. The dimensions were found using AWR's microwave office [4], then finalized using sonnet [5]. **Figure 7.13** also shows the bias circuitry included in the designed reconfigurable filter. The dimensions of the filter are as follows:

- Impedance Transformer
 $w = 0.95 \text{ mm}, l = 25 \text{ mm}$

- Coupled Lines
 $w = 0.5 \text{ mm}, l = 24.9 \text{ mm}, s = 0.2 \text{ mm}$

- Stub 1 and Stub 4
 $w = 1.6 \text{ mm}, l = 24.9 \text{ mm}$

- Stub 2 and Stub 5
 $w = 1 \text{ mm}, l = 24.9 \text{ mm}$

- Stub 3 and Stub 6
 $w = 3.8 \text{ mm}, l = 21.9 \text{ mm}$

As designed the filter can be switched between four distinct bandwidth states; ranging from around 50% to 20% 3 dB FBW. The switching is done using PIN diodes. There are two for every stub for isolation purposes as stated in [6] and section 6.2) one diode is not enough for isolation thus a second is used to shift up any unwanted spikes in the passband. If one diode is used spikes appear in the passband and in order to shift these up a second diode was placed

at first near the via hole. It was found that by placing a diode here increases the losses of the circuit as there is a bigger density of current at this point. By moving the diode down the stub incurs fewer losses but brings the spikes nearer the passband. For this reason a trade off is once again made for the position of the second diode between the losses and the shifting up of the unwanted spikes obtained. This in itself caused another minor issue when finalizing the final circuit dimensions; which was the discontinuities and gaps caused some phase shifts which were compensated for by altering the lengths of resonators slightly. The four states as discussed before can be obtained by having the following stubs switched on and off:

- State 1: All stubs “off”
- State 2: Stubs 2 and 5 “on”
- State 3: Stubs 3 and 6 “on”
- State 4: All Stubs “on”

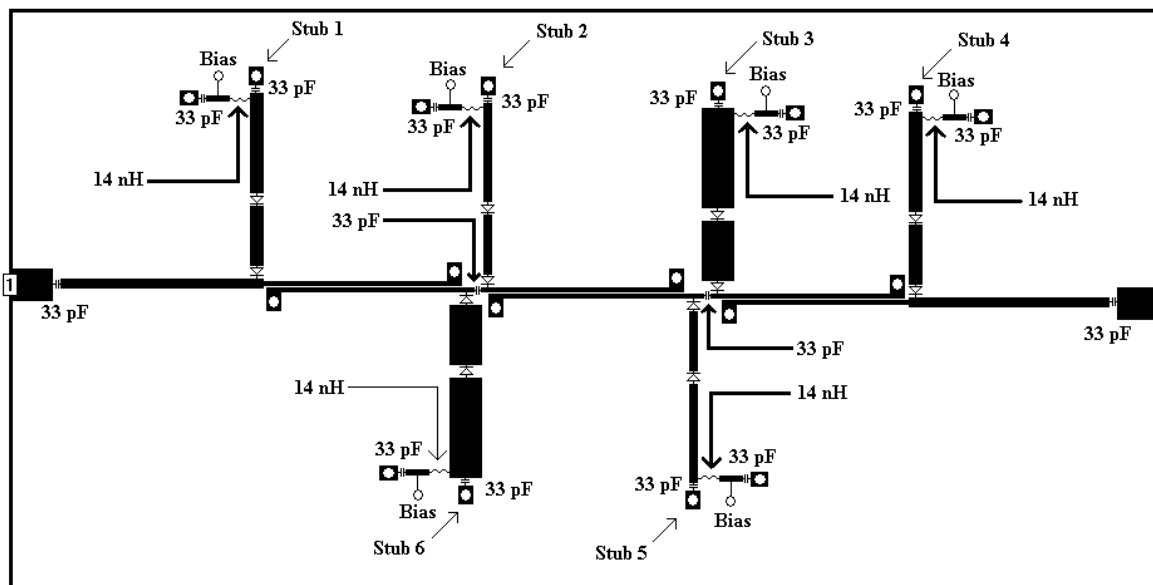


Figure 7.13: Microstrip Design with Bias Circuitry Included.

The PIN diodes were modelled in simulation using the values of 4Ω resistances for switch “on” and 0.025 pF capacitance for switch “off,” which were extracted from the data sheet of the PIN diode used. The circuit was simulated, and the responses obtained were plotted in **Figures 7.14 and 7.15:**

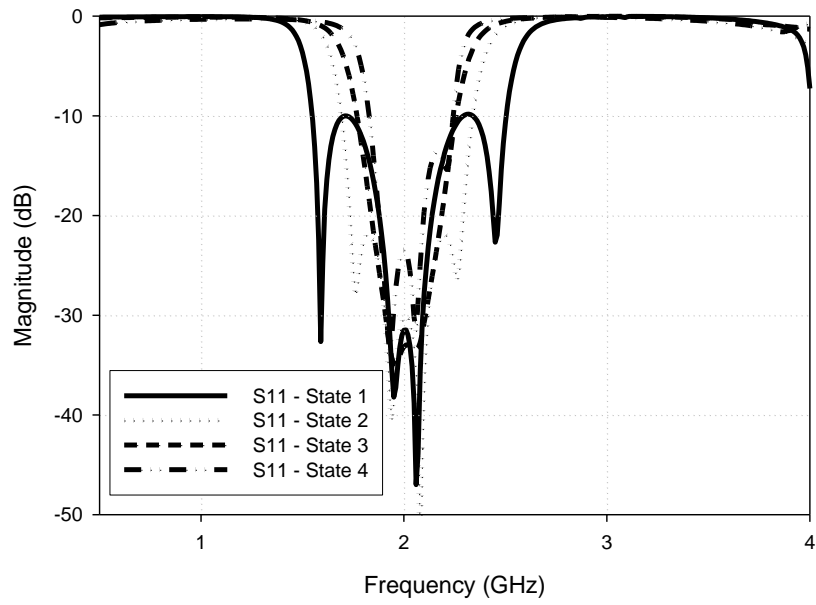


Figure 7.14: S11 Simulated Response.

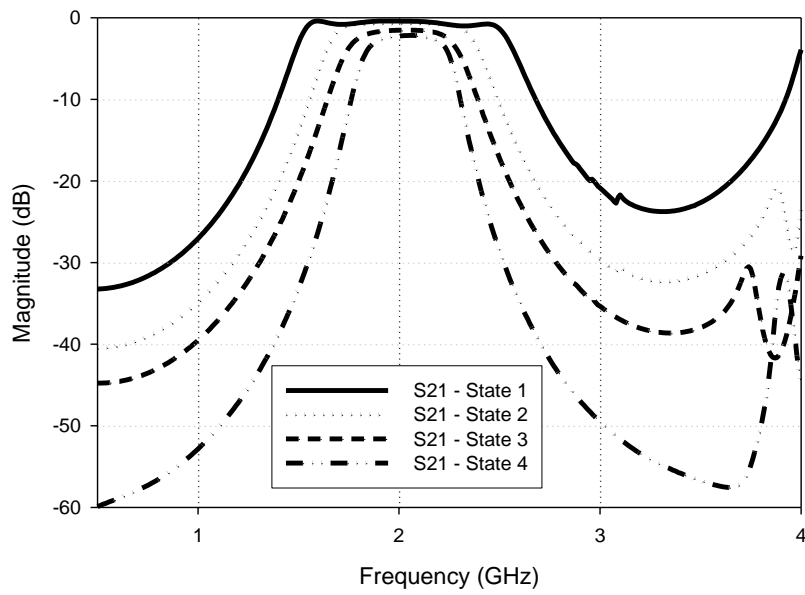


Figure 7.15: S21 Simulated Response.

Table 7.1 summarises the simulated performance of the filter:

	State 1	State 2	State 3	State 4
<i>FBW</i> (3 dB)	53.5%	37.5%	28.5%	21.7%
<i>f</i> ₀	2 GHz	2 GHz	2 GHz	2.03 GHz
Insertion Loss	0.4 dB	0.7 dB	1.53 dB	2.2 dB

Table 7.1: Simulated Performance.

As expected there are much more insertion losses associated with the narrowband states [7]. It is also clear that like the single section filters seen in earlier sections that there is a spurious response at $2f_0$, which is due to the unequal even and odd mode phase velocities, as microstrip is not pure TEM. However this can be easily suppressed using a variety of methods [8].

7.2.3) Experimental Results

The filter was fabricated on a Rogers substrate as per the design (RO 3003 Rogers Duroid), i.e. the thickness = 1.53 mm and $\epsilon_r = 3$. The pin diodes used were MACOMM's MA4AGSBP907 series diodes. In order to bias the pin diodes the bias circuits consist of Johanson's Multi-layer High-Q Capacitors and Coil Craft's 0201 DS Series Inductors. The data sheets of the components can be found in appendix 8. Furthermore, as a final check the bias circuit was measured when connected to a 50Ω to ascertain its wideband performance (see appendix 7). The circuit was measured and the results obtained are shown, with the performance being summarised in **Table 7.2**:

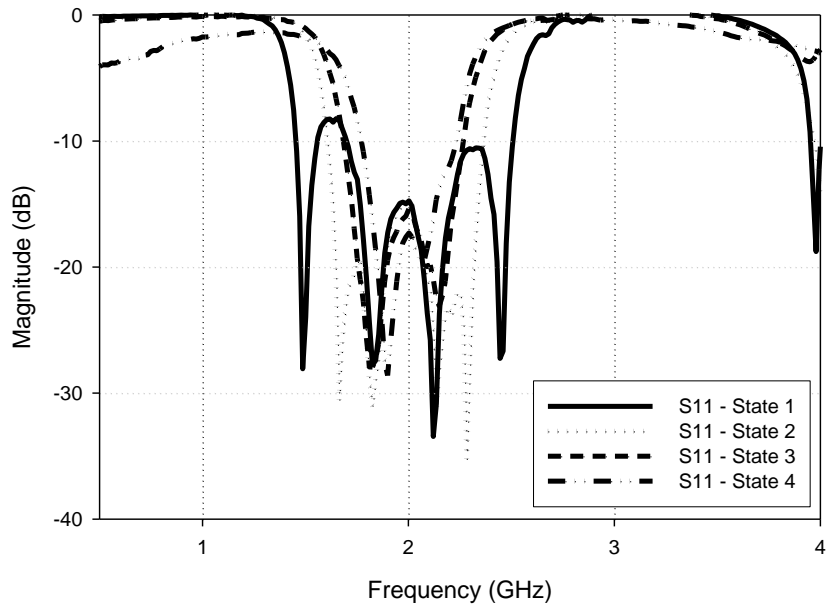


Figure 7.16: S11 Measured Response.

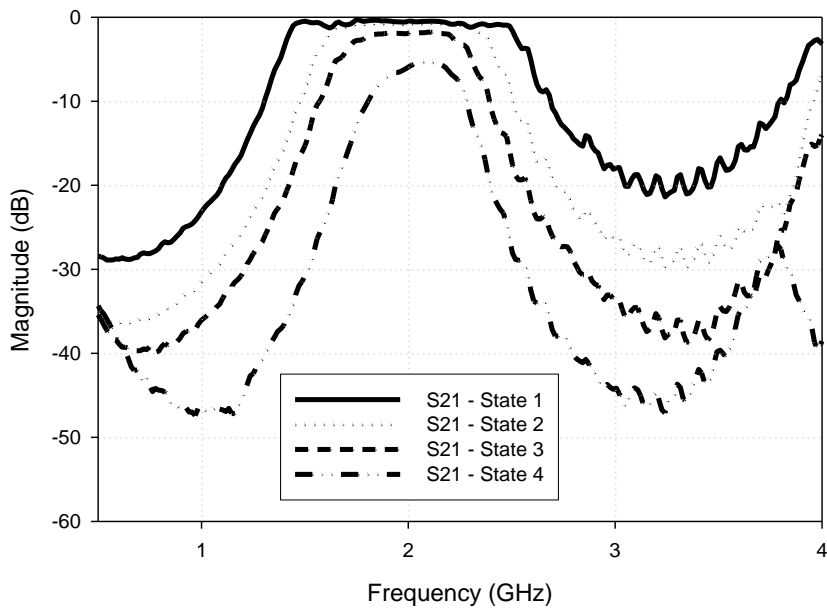


Figure 7.17: S21 Measured Response.

	State 1	State 2	State 3	State 4
<i>FBW</i> (3 dB)	58%	41%	33%	19.5%
<i>f</i> _o	1.98 GHz	1.98 GHz	1.98 GHz	2.05 GHz
Insertion Loss	0.47 dB	0.9 dB	1.97 dB	5.5 dB

Table 7.2: Measured Performance.

In general, the fabricated filter shows good agreement with EM Simulation. **Table 7.2** summarizes the measured performance of the filter. As compared to **Table 7.1**, there are some discrepancies in centre frequency, bandwidth and insertion loss; these are all attributed to fabrication tolerances. One thing to note is the improved bandwidth performance in the wider bandwidth states; i.e. a wider tunable bandwidth. On a negative note the losses in the narrowest band state are much higher than in simulation. The reason for this may be twofold. Firstly, the measured 3 dB FBW is smaller than the simulated one, which normally leads to a higher insertion loss. Secondly, at this state, all the dc bias circuits are active and it would seem that additional losses due to dc bias components, in particular the inductors, are more significant.

7.3) Cascaded Coupled Line Filter Using LCP; Designed using Matthaei Equations

On inspection of the above filter it is clear that the impedance transformer causes degradation in the passband as it is only applicable to the center frequency. For this reason a design method needs to be adopted in order to eliminate the use of the transformer in order to improve filter performance. In [9] there are equations which allow for cascaded coupled line sections to be designed with no impedance transformer. However, as can be seen in Section **4.2.2**) not all coupled line sections contribute to the selectivity of the filter. This can be shown in the design of say a five pole filter with a ripple constant of 0.04321 dB, Maximum FBW = 50% and $f_0 = 2$ GHz; the design calculation is shown in Appendix 5. From the following figure it is clear that there is $n+1$ number of sections, in the subsequent sections a design procedure is presented in order to reduce the number of sections needed in reconfigurable filter design. A reason for this is to not only to make the filter more compact but also to reduce the number of stubs to be loaded for reconfigurability, hence reduce the number of tuning elements.

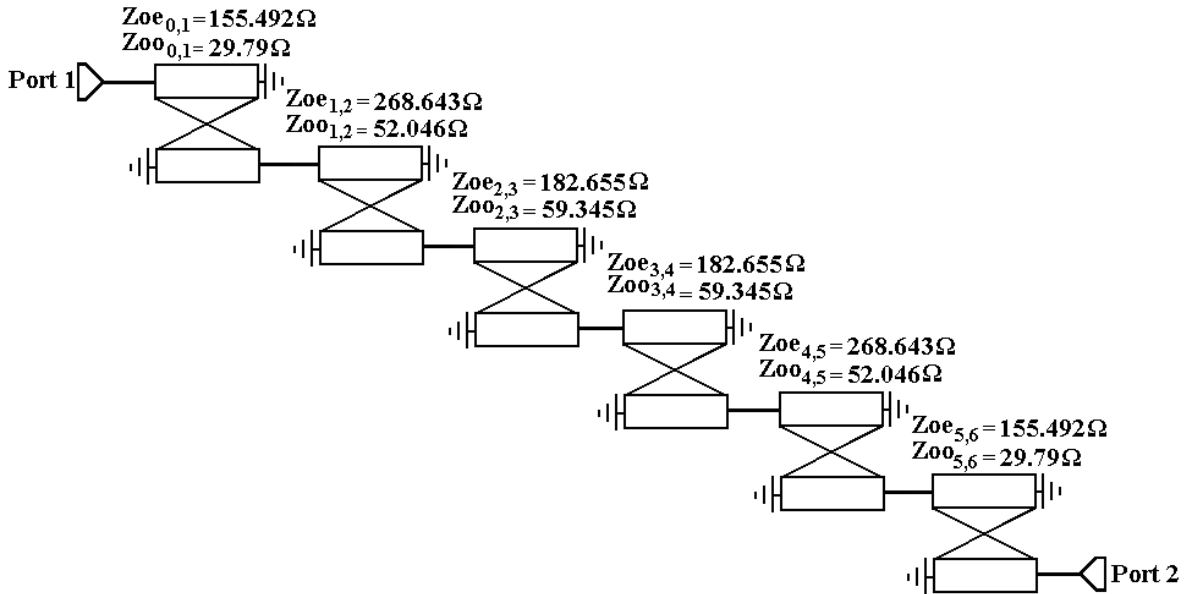


Figure 7.18: Filter With Maximum FBW = 50% Designed using Matthaei coupled line theory.

7.3.1) Filter Design Theory

A general circuit schematic for the design of the reconfigurable filter is shown in **Figure 7.19**, which consists of $n-1$ coupled line sections in cascade and n switchable short circuit stubs; hence n is the equivalent number of poles.

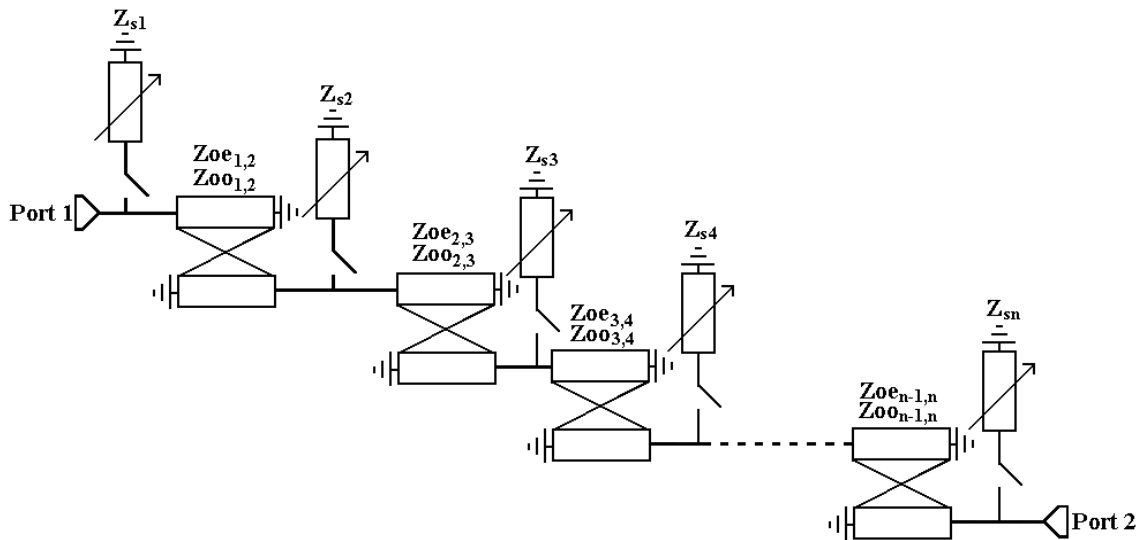


Figure 7.19: Reconfigurable Cascaded Coupled Line Filter.

Without the stubs for reconfigurability, the filter is operated at a state of desired largest bandwidth. This state can be initially designed using the equivalent circuit in **Figure 7.20**, using the theory in [9] and documented in section **4.2.2**).

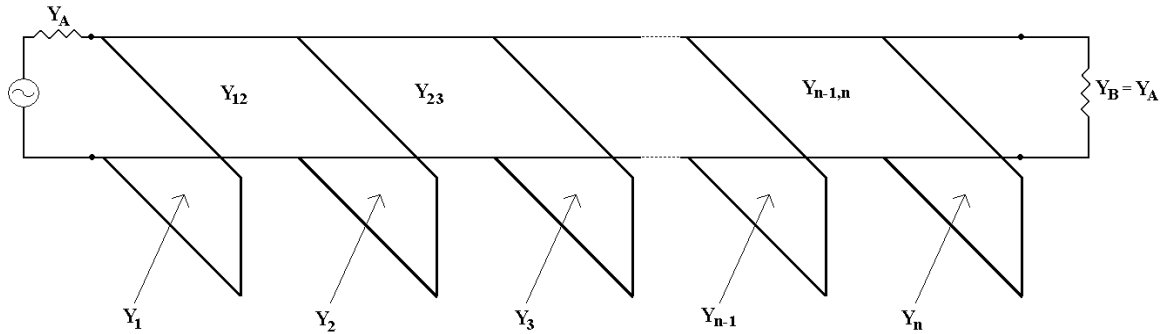


Figure 7.20: Equivalent Stub Filter Circuit.

The design equations for this type of filter seen in section **4.2.2**) can be further simplified in order to make the design procedure simpler. So for a given fractional bandwidth (FBW) of a desired largest bandwidth and the g values of a chosen lowpass prototype of order n , the circuit parameters in **Figure 7.20** are calculated as follows:

$$Y_{1,2} = g_0 \sqrt{\frac{C_a}{g_2}} Y_A \quad (7.1)$$

$$Y_{n-1,n} = g_0 \sqrt{\frac{C_a g_{n+1}}{g_{n-1} g_0}} Y_A \quad (7.2)$$

$$Y_{k,k+1} \Big|_{k=2 \text{ to } n-2} = \frac{g_0 C_a}{\sqrt{g_k g_{k+1}}} Y_A \quad (7.3)$$

Where $C_a = 2dg_1$

Note d is a dimensionless constant (typically chosen to be 1) which can be chosen to give a convenient admittance level of the interior of the filter. Assuming the cut off of the filter is normalised to 1. The following is then obtained in order to calculate the stub admittances:

$$N_{k,k+1} \Big|_{k=1 \text{ to } n-1} = \sqrt{\left(\frac{Y_{k,k+1}}{Y_A}\right)^2 + \left(\frac{g_0 C_a \tan \theta_1}{2}\right)^2} \quad (7.4)$$

where

$$\theta_1 = \frac{\pi}{2} \left(1 - \frac{\text{FBW}}{2} \right) \quad (7.5)$$

The characteristic admittance of the input stub is:

$$Y_1 = g_0 Y_A (1 - d) g_1 \tan \theta_1 + Y_A \left(N_{12} - \frac{Y_{12}}{Y_A} \right) \quad (7.6)$$

Interior stubs are calculated with:

$$Y_k |_{k=2 \text{ to } n-1} = Y_A \left(N_{k-1,k} + N_{k,k+1} - \frac{Y_{k-1,k}}{Y_A} - \frac{Y_{k,k+1}}{Y_A} \right) \quad (7.7)$$

Output stub is calculated as follows:

$$Y_n = Y_A (g_n g_{n+1} - d g_0 g_1) \tan \theta_1 + Y_A \left(N_{n-1,n} - \frac{Y_{n-1,n}}{Y_A} \right) \quad (7.8)$$

All the stubs and connecting lines are 90° at the center or mid-band frequency. The impedances values, being the inverse of the admittances values, are calculated as

$$Z_{k,k+1} |_{k=1 \text{ to } n-1} = \frac{1}{Y_{k,k+1} |_{k=1 \text{ to } n-1}} \quad (7.9)$$

$$Z_k = \frac{1}{Y_k} \quad (7.10)$$

To make sure the design and implementation easy for the reconfigurable parallel coupled line structure of **Figure 7.19**, the following assumptions are made:

- Connecting lines have equal impedance.
- Input and output stubs have equal impedance.
- Interior stubs have equal impedance.
- The input and output stubs are double the impedance of the interior short circuit stubs.

The reasons are for this is that, firstly, each coupled line section once converted from its equivalent circuit obtained will have equal even and odd mode impedances; and secondly, stubs needed for reconfigurability only depend on a single variable, i.e., the characteristic impedance Z_s , as shown in **Figure 7.21** for the simplified reconfigurable cascaded coupled line filter. There is also no need for the impedance transformer as the filter is already matched from the design equations.

In order to meet these assumptions the following design equations were used:

$$Z'_2 = Z'_3 = \dots Z'_{n-1} = \frac{Z_2 + Z_3 + \dots + Z_{n-1}}{n-2} \quad (7.11)$$

$$Z'_1 = 2Z'_2 \quad (7.12)$$

$$Z'_{12} = Z'_{23} = \dots Z'_{n-1,n} = \frac{Z_{12} + Z_{23} + \dots + Z_{n-1,n}}{n-1} \quad (7.13)$$

All the coupled line sections in **Figure 7.21** are identical having the even- and odd-modal impedances given by:

$$Z_{oe} = Z'_1 \quad (7.14)$$

And:

$$Z_{oo} = \frac{Z'_1 Z'_{n,n-1}}{2Z'_1 + Z'_{n,n-1}} \quad (7.15)$$

These expressions directly relate to **Figure 7.20** and are used in order to convert the circuit into the equivalent coupled line form.

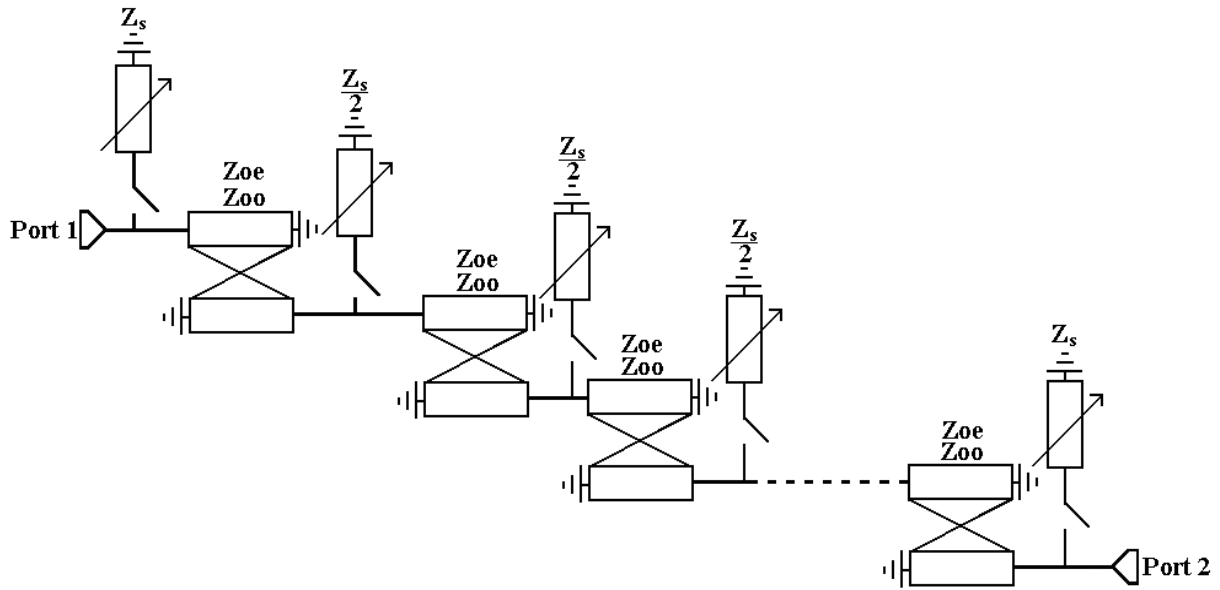


Figure 7.21: Simplified Reconfigurable Cascaded Coupled Line Filter.

In order to validate these assumptions, a comparison is made between a filter with and without the simplification. The designed filter compared was a seven pole filter with a max FBW = 60 %.

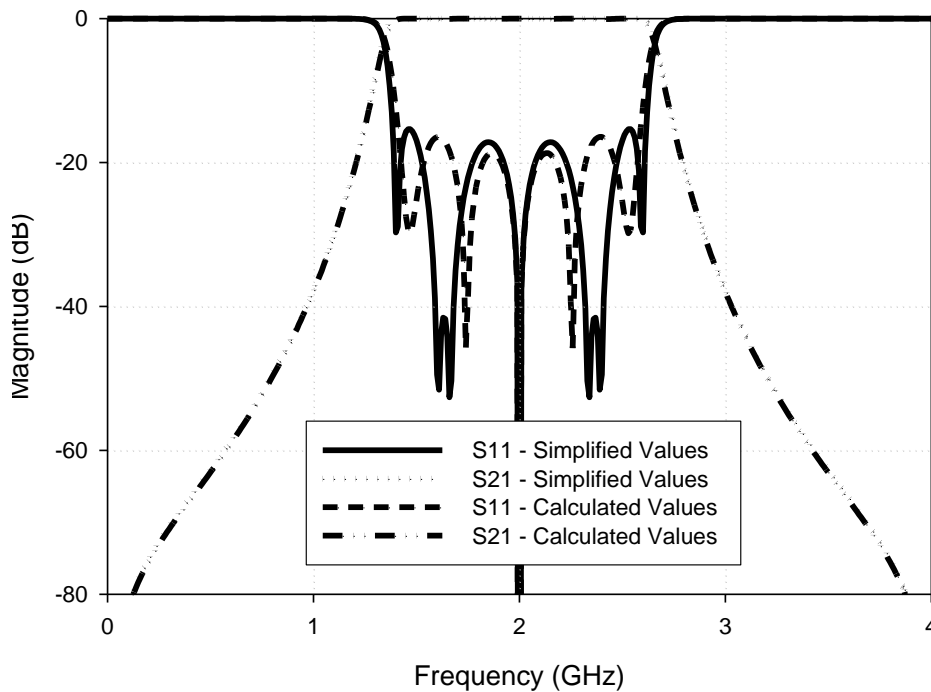


Figure 7.22: Comparison between Simplified and Non - Simplified values; FBW = 60% and $n = 7$.

Figure 7.21 can be decomposed into several identical sections in cascade, this meaning that the design and implementation of this reconfigurable filter becomes easier. The single identical section with loaded short circuit stubs and its equivalent circuit from section 6.2.1) are illustrated in **Figure 7.23** for further design analysis.

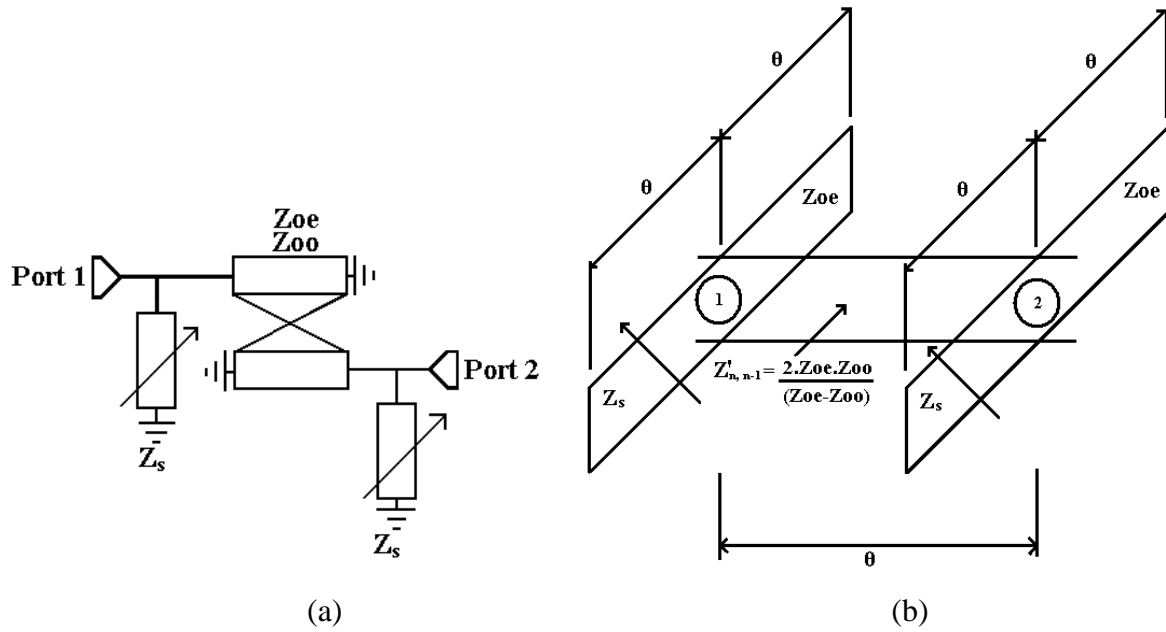


Figure 7.23: (a) Short circuit stub filter block with stubs switched on for reconfigurability. (b) Equivalent circuit.

the connecting line has the impedance equivalent to:

$$Z'_{n,n-1} = \frac{2Z_{oe}Z_{oo}}{(Z_{oe}-Z_{oo})} \quad (7.16)$$

The ABCD parameters for this single section can be found to be:

$$A_s = \cos \theta + \frac{2Z_{oe}Z_{oo}(Z_{oe} + Z_{oo}) \cos \theta}{(Z_{oe} - Z_{oo})Z_s}$$

$$B_s = \frac{2jZ_{oe}Z_{oo} \sin \theta}{(Z_{oe} - Z_{oo})}$$

$$C_s = \frac{-2j(Z_{oe} - Z_s) \cos \theta}{Z_s Z_{oe} \tan \theta} \left(1 + \frac{(Z_{oe} + Z_s)Z_{oo}Z_{oe}}{Z_s Z_{oe} (Z_{oe} - Z_{oo})} \right) + \frac{j \sin \theta (Z_{oe} - Z_{oo})}{2Z_{oo}Z_{oe}}$$

$$D_s = A_s \quad (7.17)$$

where

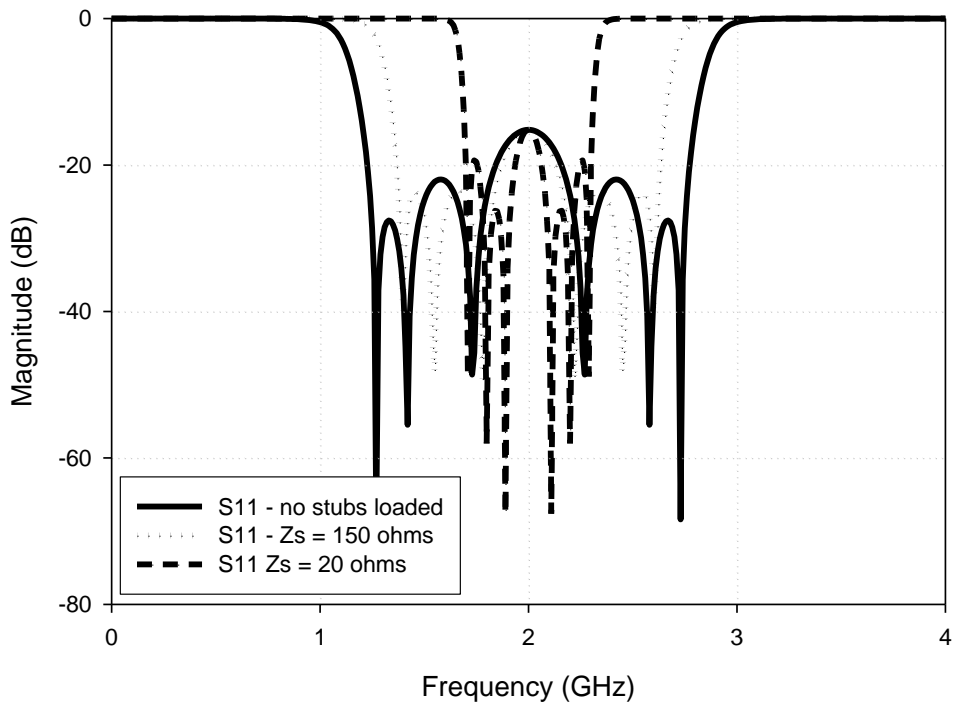
$$\theta = \frac{f}{f_0} \theta_0 \quad (7.18)$$

When $(n - 1)$ identical sections of this type circuit being cascaded, the resultant ABCD matrix is given by

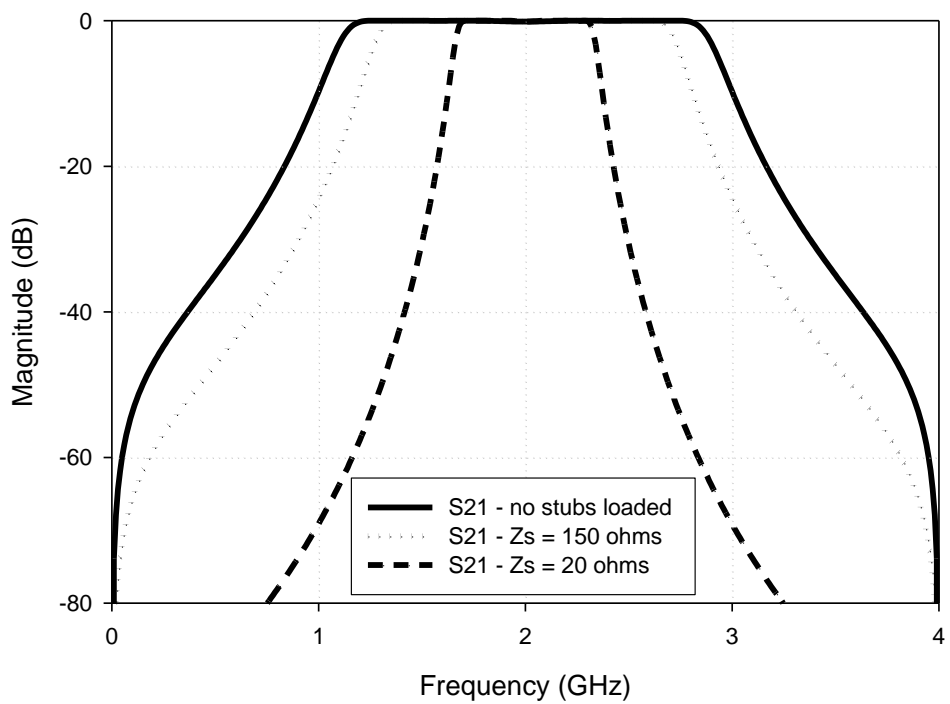
$$\begin{bmatrix} A & B \\ C & D \end{bmatrix} = \prod_{i=1}^{n-1} \begin{bmatrix} A_{si} & B_{si} \\ C_{si} & D_{si} \end{bmatrix} = \begin{bmatrix} A_s & B_s \\ C_s & D_s \end{bmatrix}^{n-1} \quad (7.19)$$

This can be converted to the S parameters [7] using (4.8) and (4.9).

For a given set of Z_{oe} and Z_{oo} , determined by the desired largest bandwidth using (7.1) to (7.15), the reconfigurable frequency response in each state is obtained when the characteristic impedance (Z_s) of the loaded stubs are varied. **Figure 7.24** plots typical reconfigurable bandwidth responses for the proposed reconfigurable filter of **Figure 7.21**. As can be seen, the bandwidth of the filter can be tuned effectively by a single parameter, i.e. the characteristic impedance Z_s of the loaded stubs. Furthermore, the passband characteristics such as the return loss or insertion loss do not change when the bandwidth varies over a wide range. As mentioned before, these features are all desired for the development of reconfigurable filters.



(a)



(b)

Figure 7.24: Typical reconfigurable bandwidth responses of Figure 21 for $n = 6$, max FBW = 80 % filter designed using (7.1) – (7.16), $Z_{oe} = 85.437$, $Z_{oo} = 16.84$ (a) S11 (b) S21.

7.3.2) Filter Design

In order to make a direct comparison between the filter in section 7.3) the same filter characteristics were used; i.e. $n = 5$ ($n-1$ coupled line sections) ripple fractional bandwidth of 50%, $f_0 = 2$ GHz and a ripple constant of 0.04321 dB. With this specification in mind the prototype element values are: $g_0=g_6=1$, $g_1=g_5=0.9714$, $g_2=g_4=1.3721$, $g_3=1.8014$. Using 7.1 – 7.10, the following impedance values for the equivalent circuit are calculated (see Appendix 5):

$$\begin{aligned}Z_{1,2} &= Z_{4,5} = 42.019 \Omega \\Z_{2,3} &= Z_{3,4} = 40.461 \Omega \\Z_1 &= Z_5 = 34.726 \Omega \\Z_2 &= Z_4 = 19.093 \Omega \\Z_3 &= 17.667 \Omega\end{aligned}\tag{7.20}$$

To meet the assumptions discussed, then, applying (7.11) – (7.13) gives:

$$\begin{aligned}Z'_2 &= Z'_3 = Z'_4 = 18.62 \Omega \\Z'_1 &= Z'_5 = 37.24 \Omega \\Z'_{1,2} &= Z'_{2,3} = Z'_{3,4} = Z'_{4,5} = 41.276 \Omega\end{aligned}\tag{7.21}$$

The resultant circuit can be decomposed into four identical sections in cascade, as depicted in below:

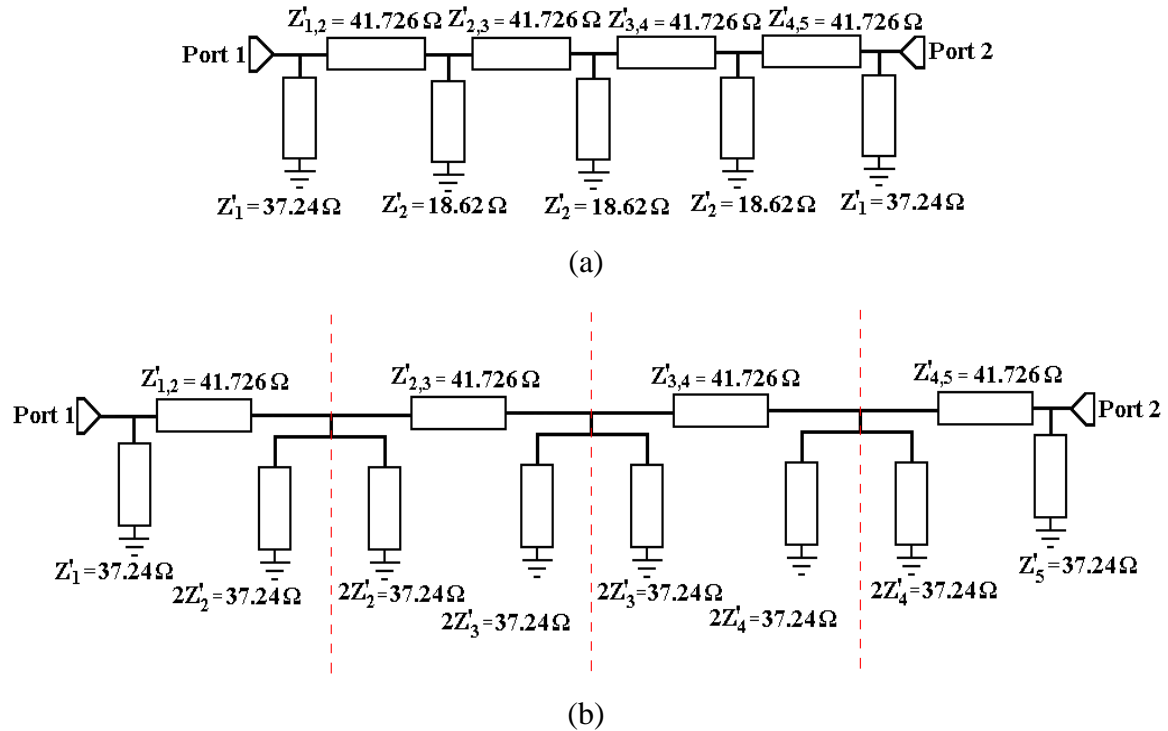


Figure 7.25: (a) Circuit schematic if the assumptions are met. (b) Decomposed circuit for cascade of the identical sections.

In order to show that there is very little difference between the circuit with and without the assumptions, a comparison is made between the responses. On close inspection of (7.20) it can be clearly seen that if the assumptions are not met the impedances for each section are not equal. This makes it a lot more difficult when converting to the coupled line structure for the implementation of the reconfigurable filter. It also makes the choice of impedance of the stubs for reconfigurability more complex. If the calculated values of (7.20) are used, the interior stub impedances for reconfigurability will all be different (i.e. $Z_2 = Z_4 \neq Z_3$). The input and output stubs are also not exactly double of the interior stubs. Thus by using the assumed values, such as those given in (7.21), the reconfigurable stubs can be calculated much easier when added in parallel to the stubs from **Figure 7.25 (a)**.

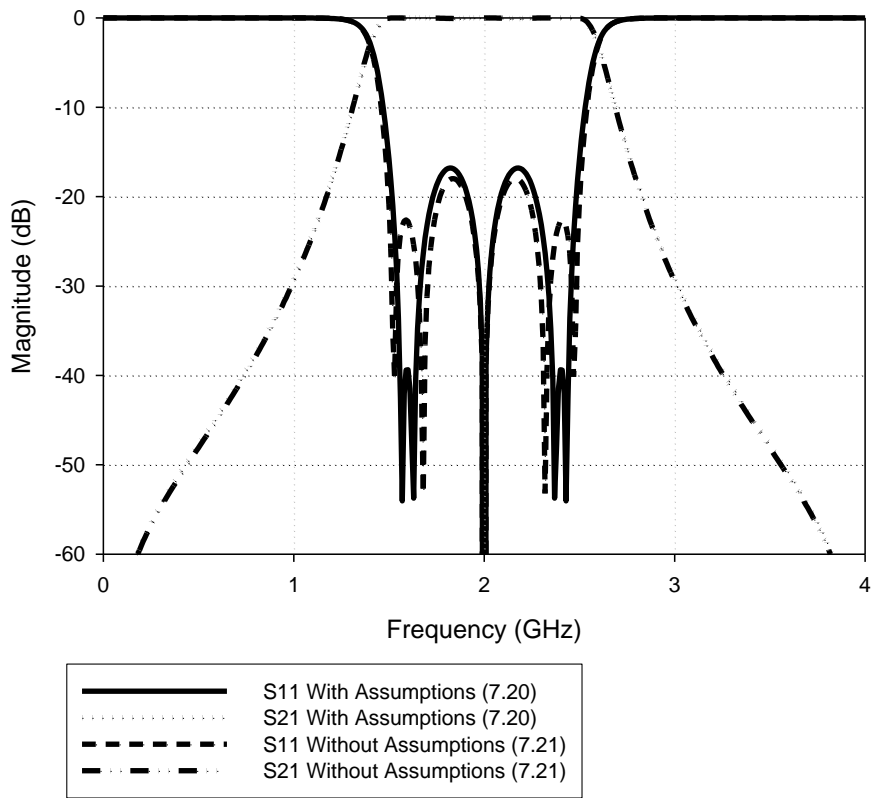


Figure 7.26: Comparison with and without assumptions implemented.

The coupled line filter even and odd mode impedances for maximum FBW (i.e. State 1) can then be found using (7.14) and (7.15). **Figure 7.25** can then be converted to the equivalent coupled line structure.

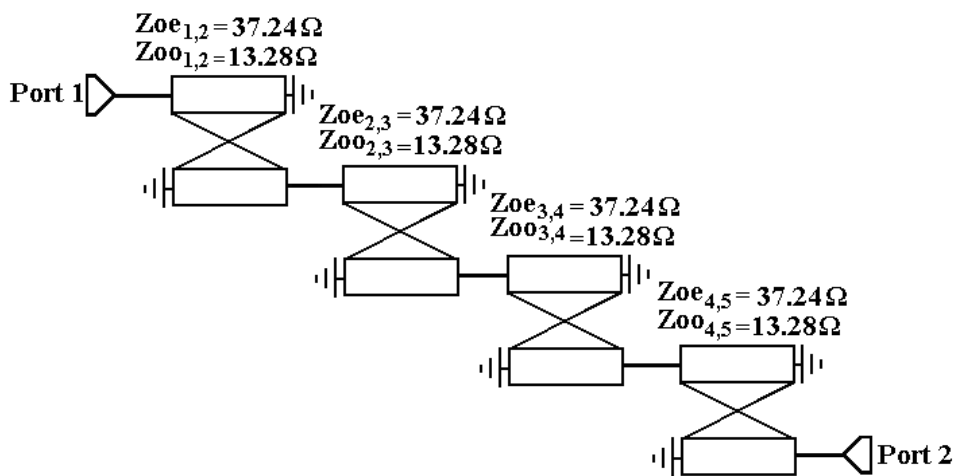


Figure 7.27: Coupled line structure derived from equivalent short circuit stub filter.

Short circuit stubs were then added in order to have other desired bandwidths. Using (7.17) – (7.19), the rippled fractional bandwidth can be extracted against the loaded short circuit stubs impedance (using program from Appendix 5).

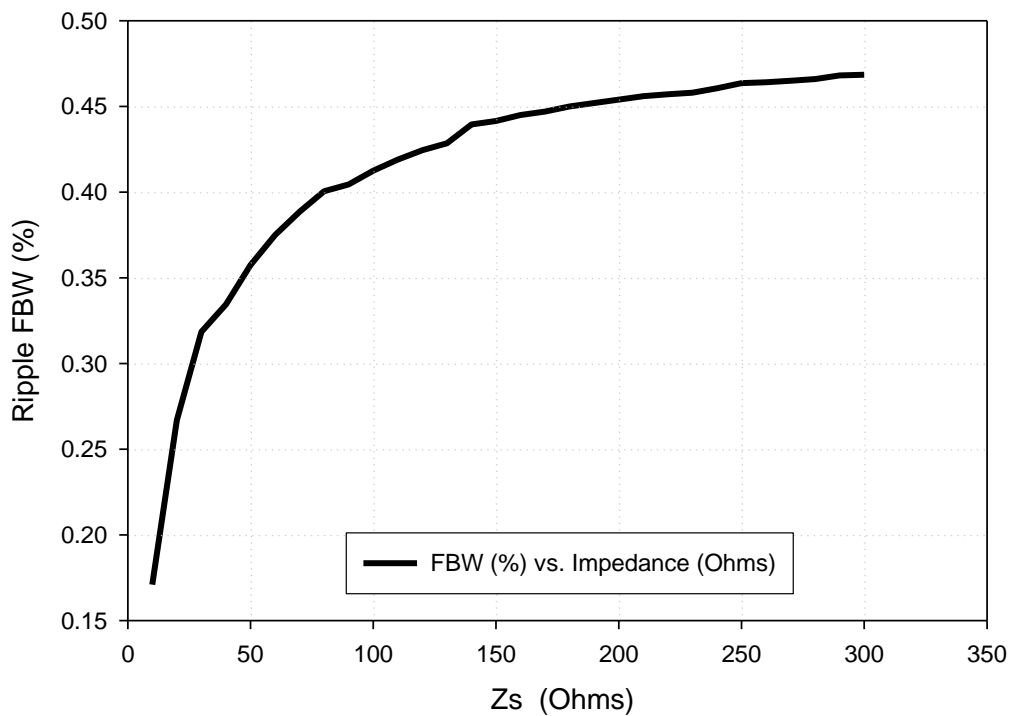


Figure 7.28: Variation of ripple fractional bandwidth against loaded short circuit stub impedance, Z_s .

For each bandwidth state required in the design the short circuit stub impedance can be chosen from this graph. For a 40% fractional bandwidth a stub impedance of 83 Ω is required, and for a 30% fractional bandwidth an impedance of 28 Ω is required. The final state can potentially be the parallel combination of the two stubs. However, the impedance level is not high enough such that a big enough bandwidth change would occur. The final circuit design with switchable short circuit stubs for the reconfigurable filter can be seen below. All line lengths are $\theta = 90^\circ$ at the center frequency of 2 GHz. **Figure 7.30** and **7.31** show the theoretical S_{11} and S_{21} using (7.20) and (7.21).

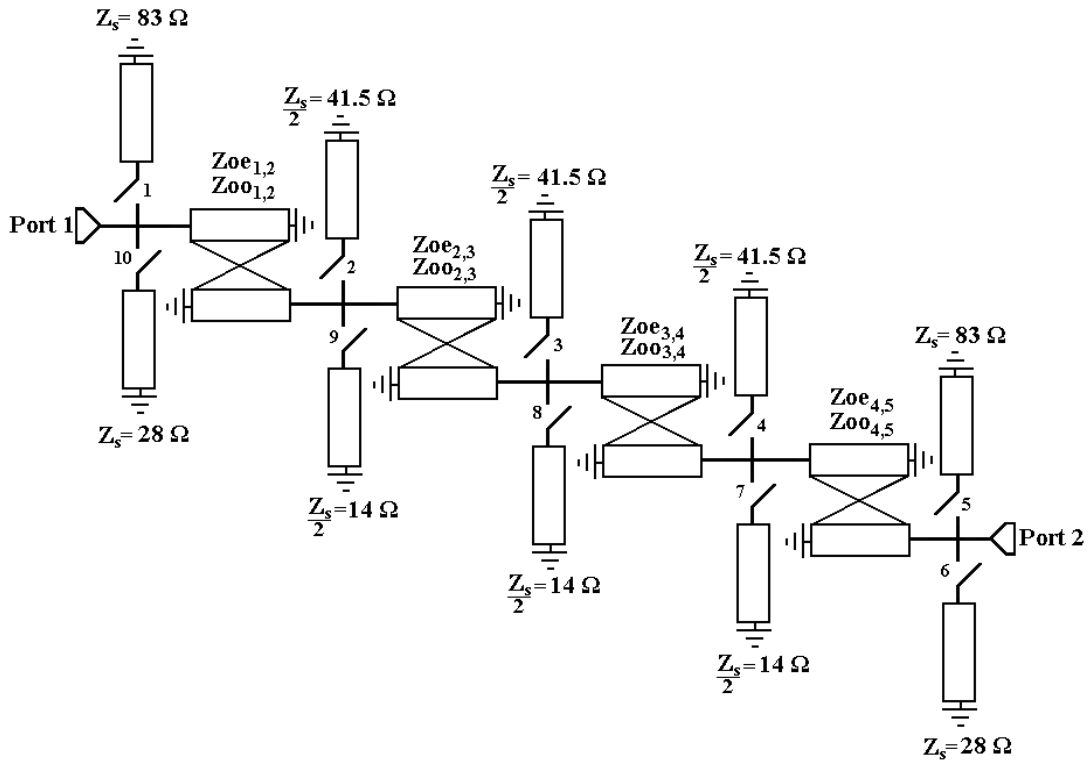


Figure 7.29: Final circuit design for the reconfigurable filter having three reconfigurable bandwidth states (50%, 40% and 30%).

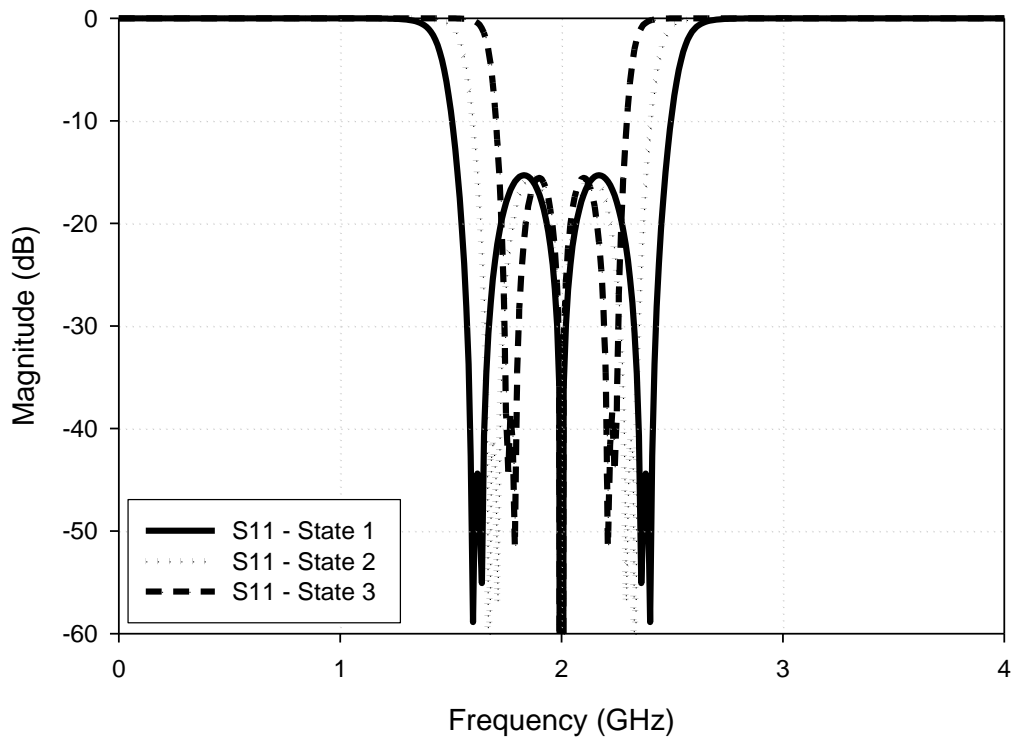


Figure 7.30: Theoretical S11.

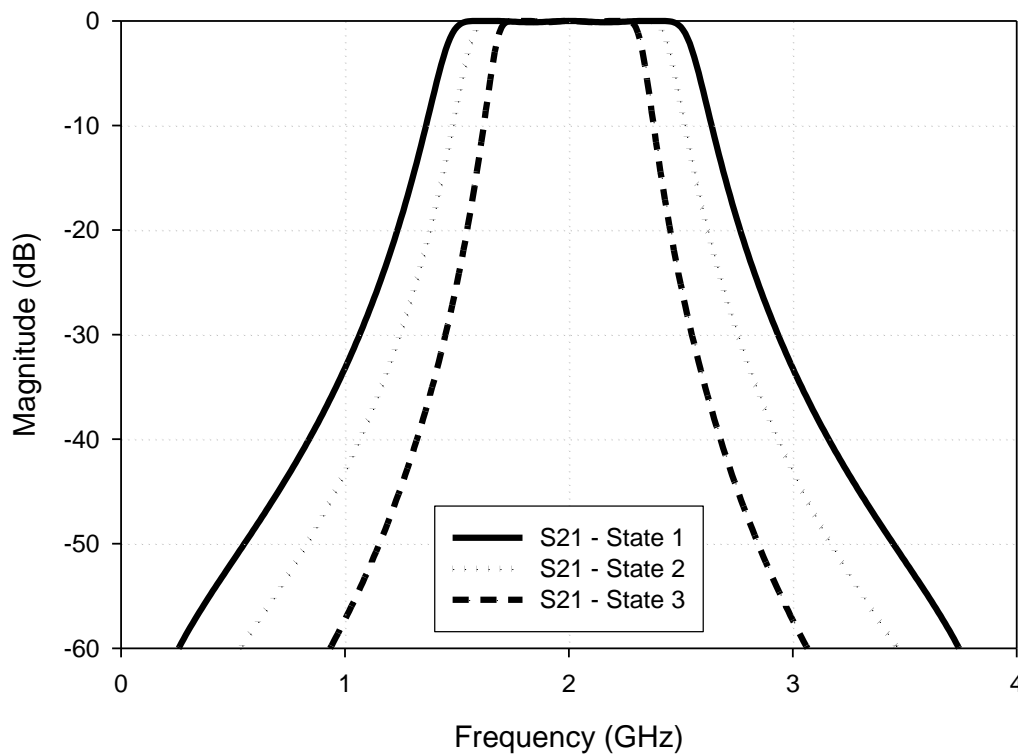


Figure 7.31: Theoretical S21.

The three states are achievable by the following switching arrangement for each state:

- 50% - all switches turned off.
- 40% - switches 1, 2, 3, 4, and 5.
- 30% - switches 6, 7, 8, 9, and 10.

Referring to **Figure 7.29** it is justifiable using this design method as opposed to the design shown in **Figure 7.18**. It is apparent that the circuit designed before using the Matthaei coupled line design equations uses more section for the same order of filter. This is due to the input and output sections not contributing to the order of the filter. Thus using this design method reduces the number of sections needed for the same order of filter and also the number of short circuit stubs for reconfigurability. This is very desirable in the design of reconfigurable filters as this limits the number of pin diodes need, meaning the losses are limited. Furthermore, the impedance values are much lower than the first which can create an issue with the implementation of the four section filter; this meaning that a degree of

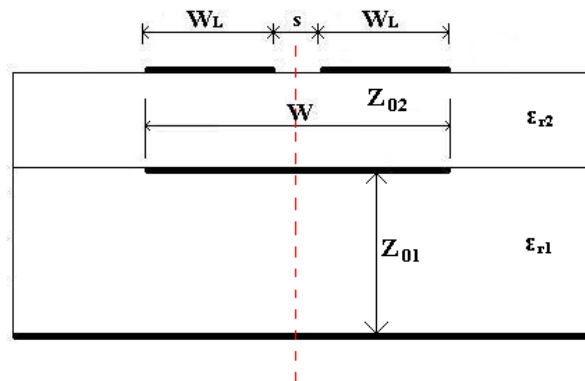
flexibility needs to be introduced. LCP was used to introduce this flexibility; which is discussed in subsequent sections of this chapter.

Filter	Number of Sections	Ripple Constant	Even Mode Impedance Range	Odd Mode Impedance Range
Figure 7.18	6	0.04321 dB	268.643 Ω – 155.492 Ω	59.345 Ω – 29.79 Ω
Figure 7.27	4	0.04321 dB	37.2 Ω	13.28 Ω

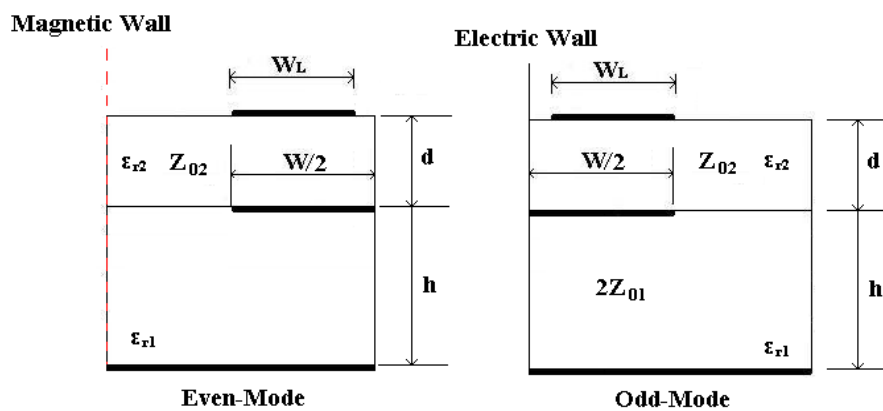
Table 7.3: Cascaded Coupled Line Filter Comparison.

7.3.3) Physical Implementation and EM Simulation

In order to obtain the required level of coupling a high degree of freedom was needed in the implementation of this filter. The designed filter was implemented using LCP multilayer circuit technology. In this circumstance a broadside re-entrant structure with floating conductor [8] and [10] was used:



(a)



(b)

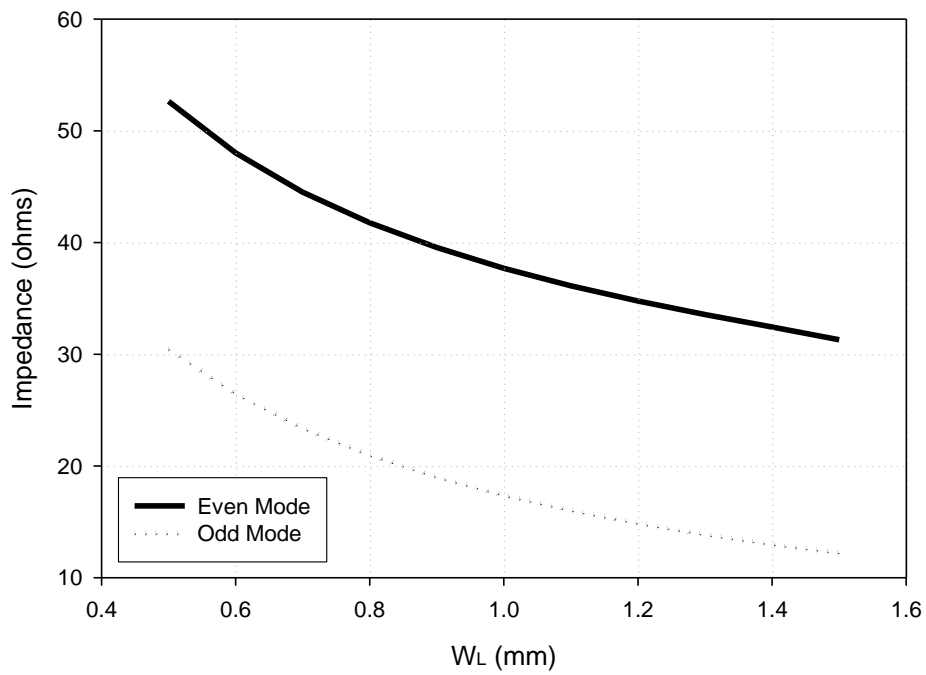
Figure 7.32: (a) Microstrip Re-entrant Mode Coupler Cross Section. (b) Even and Odd Mode Excitations.

W_L is the coupled line conductor widths, s is the gap and W is the width of the floating conductor. In order to obtain the required even and odd mode impedances the following expressions are used:

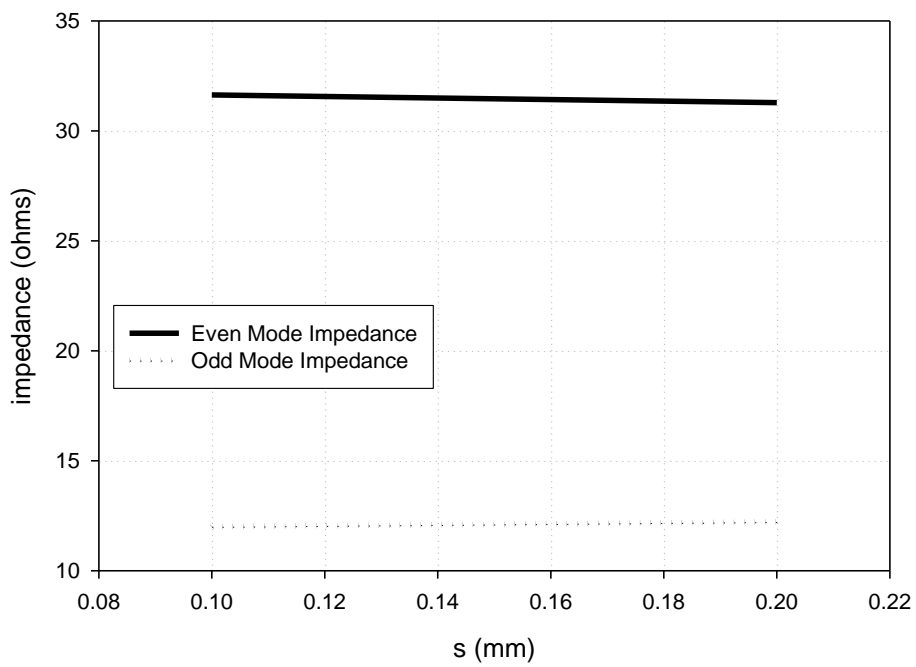
$$Z_{oe} = Z_{o2} + 2Z_{o1} \quad (7.22)$$

$$Z_{oo} = Z_{o2} \quad (7.23)$$

These only hold if the floating conductor is larger than the sum of the coupled line widths and the gap. In (7.22) and (7.23), Z_{o2} is the impedance of one of the lines in the first layer and Z_{o1} is the impedance of the floating conductor in the second layer. It is stated in [8] that the coupling co-efficient mostly depends on the dielectric constant and thickness, meaning the gap, s , can be fixed to say 0.2 mm. From (7.22) and (7.23) $Z_{o1} = 11.1 \Omega$ $Z_{o2} = 13.3 \Omega$. By using a transmission line calculator in [4] the dimensions of the coupled line structure can then be obtained as previously. As a final check the full-wave EM simulator [5] can be used in order to extract the even and odd mode impedances which match the dimension values calculated using (7.22) and (7.23). For instance, **Figure 7.32 (a)** shows the change of modal impedances against W_L , when W and s are kept constant as 3 and 0.2 mm respectively. If $W=3$ mm and $W_L=1.4$ mm are kept unchanged while varying s ; the behaviour of the even and odd mode impedances are shown in **Figure 7.32 (b)**. It can be seen that the modal impedances is less dependent on the gap s , which is desired as a tiny gap can be avoided to relax the fabrication tolerance.



(a)



(b)

Figure 7.33: (a) Variation of width of coupled lines on even and odd mode impedances, (b) Variation of gap on even and odd mode impedances.

From this theory the thicknesses of each layer can be calculated, and are as follows: $h_1 = 0.1$ mm and $h_2 = 0.175$ mm. Each coupled line section has a gap of $s = 0.2$ mm, a line length and width of, 22.5 mm and 1.4 mm respectively. The floating conductor on the second layer has a length of 21.15 mm and width of 3 mm. For each of the short circuit stub line impedances shown in **Figure 7.36**, the dimensions are as follows:

- 83Ω : $l = 25.3$ mm, $w = 0.15$ mm
- 41.5Ω : $l = 24.35$ mm, $w = 0.55$ mm
- 28Ω : $l = 23.35$ mm, $w = 0.8$ mm
- 14Ω : $l = 22.65$, $w = 1.95$ mm

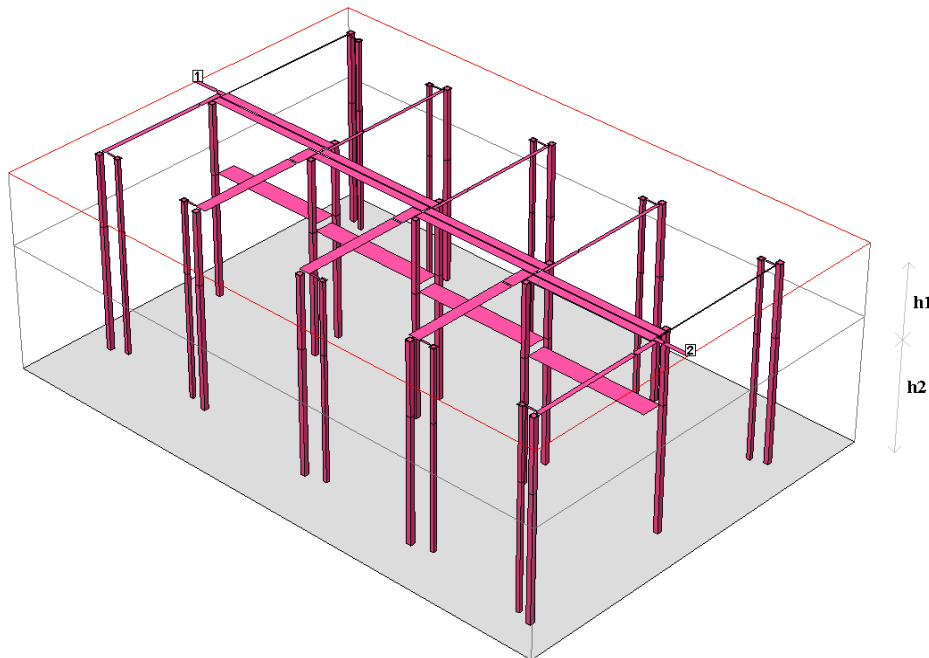


Figure 7.34: 3D view of cascaded coupled line filter.

In order to obtain the thicknesses of each layer, it was planned to use a succession of core layers and bonding layers of LCP ($\epsilon_r = 3$) are used. The stack up of the structure is illustrated:

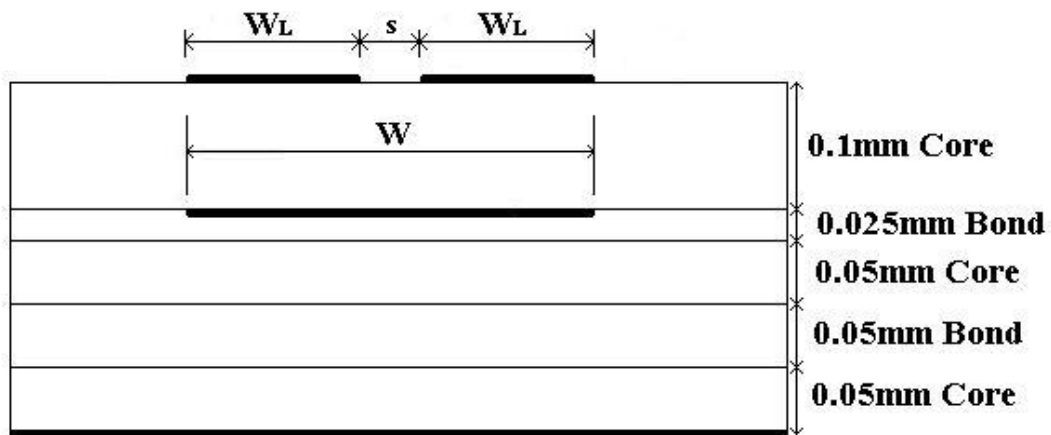
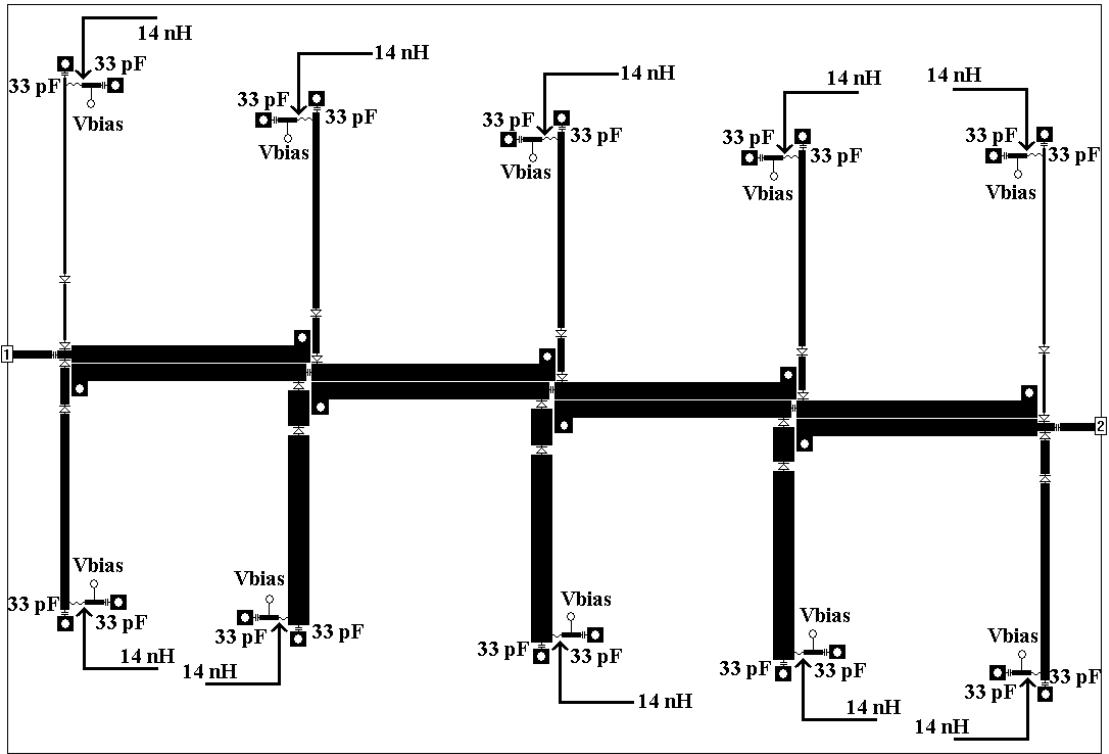
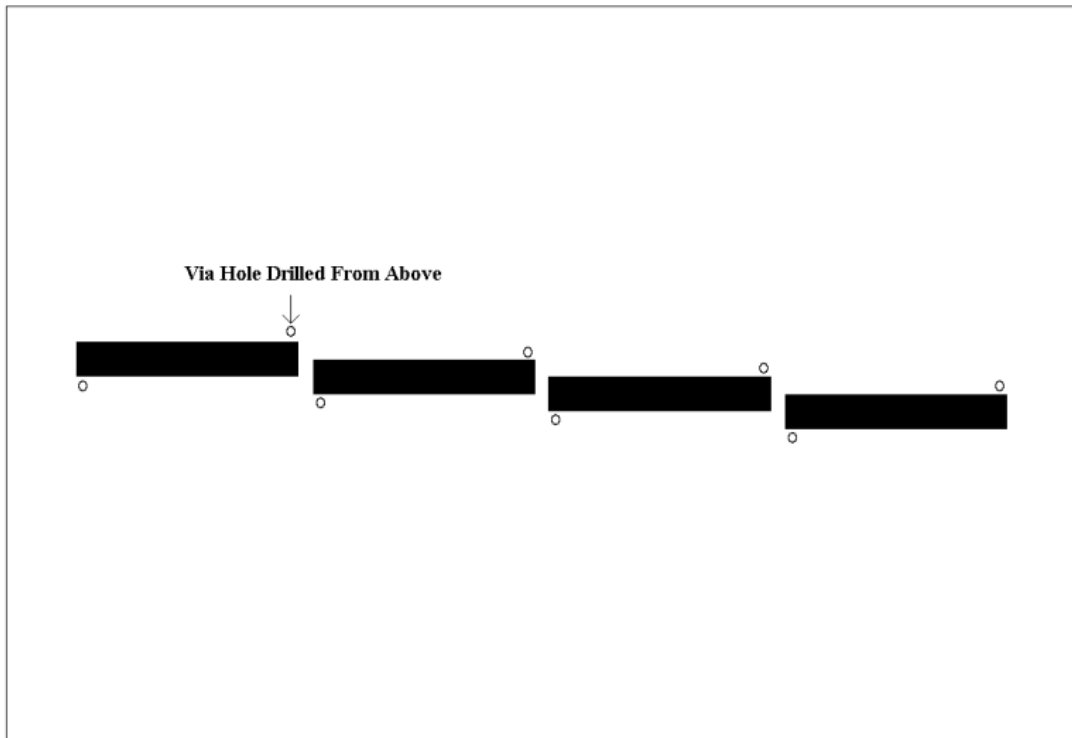


Figure 7.35: LCP Stack up.

PIN diodes are deployed for switching on/off the short circuit stubs and the designed layout including dc bias elements on the top layer is shown in **Figure 7.36 (a)**; while the floating circuit on the second layer is shown in **Figure 7.37 (b)**. The filter was simulated using [5], with ideal components being used to mimic the behaviour of the diode. A resistor value of $4\ \Omega$ was used for switch on and a capacitor value of $0.025\ \text{pF}$ was used for switch off; these values were extracted from the data sheet (diode used: MA/COM's MA4AGBLP912). **Figures 7.37 –7.38** show the simulated filter responses.



(a)



(b)

Figure 7.36: (a) Top layer and (b) second layer of the designed multilayer reconfigurable filter.

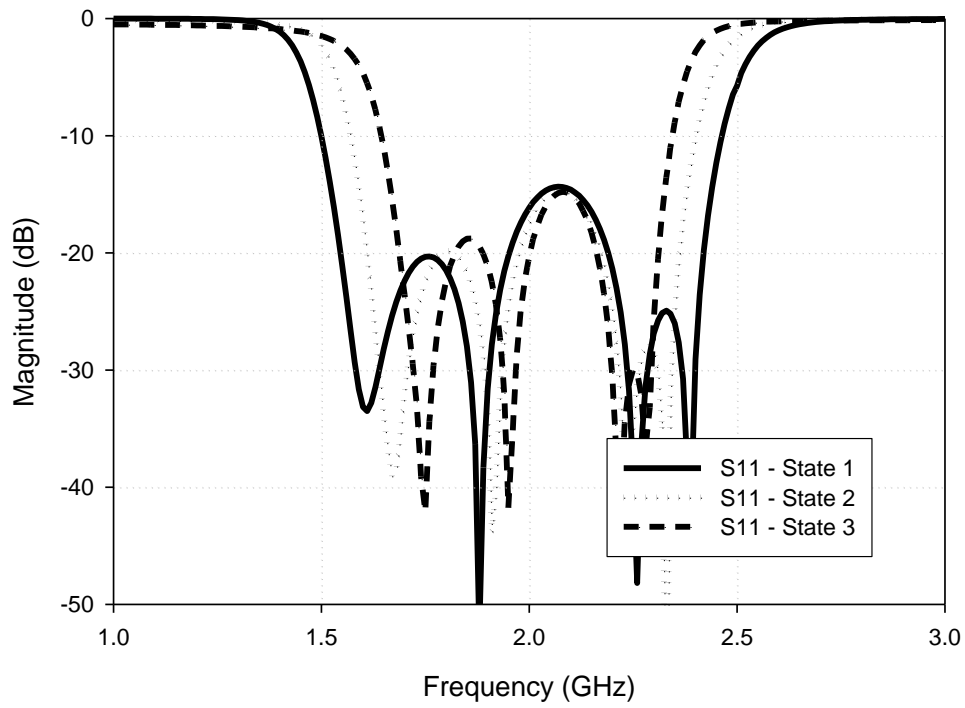


Figure 7.37: Simulated S11 of the three distinct bandwidth states.

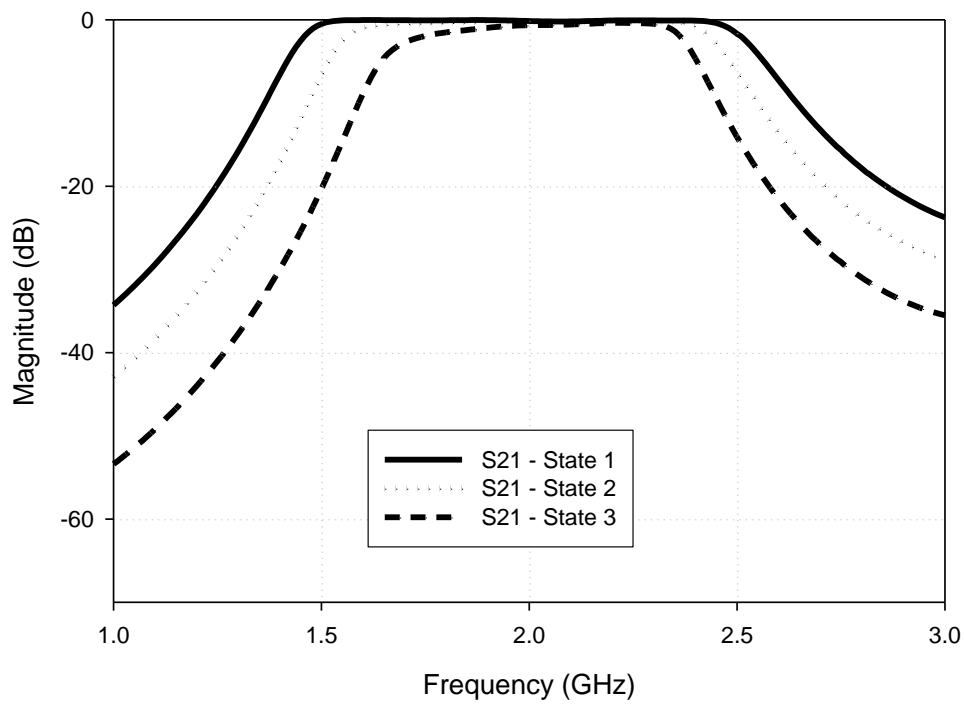


Figure 7.38: Simulated S21 of the three distinct bandwidth states.

Table 7.4 Summarises the performance of the simulated Filter:

	State 1	State 2	State 3
<i>Ripple FBW</i> (0.04321 dB)	50%	40%	30%
f_0	2 GHz	2 GHz	2 GHz
Insertion Loss	0.15 dB	0.3 dB	0.65 dB

Table 7.4: Simulated Performance.

7.3.4) Experimental Filter

The filter was fabricated using an LCP lamination technique as per the stack up from **Figure 7.35**. A photograph of the fabricated filter is illustrated in **Figure 7.39**. The same bias circuit was used as before in the other cascaded coupled line filter. The measured filter responses are plotted in **Figures 7.40 – 7.41**. The measured performance of the fabricated filter is summarized in **Table 7.5**.

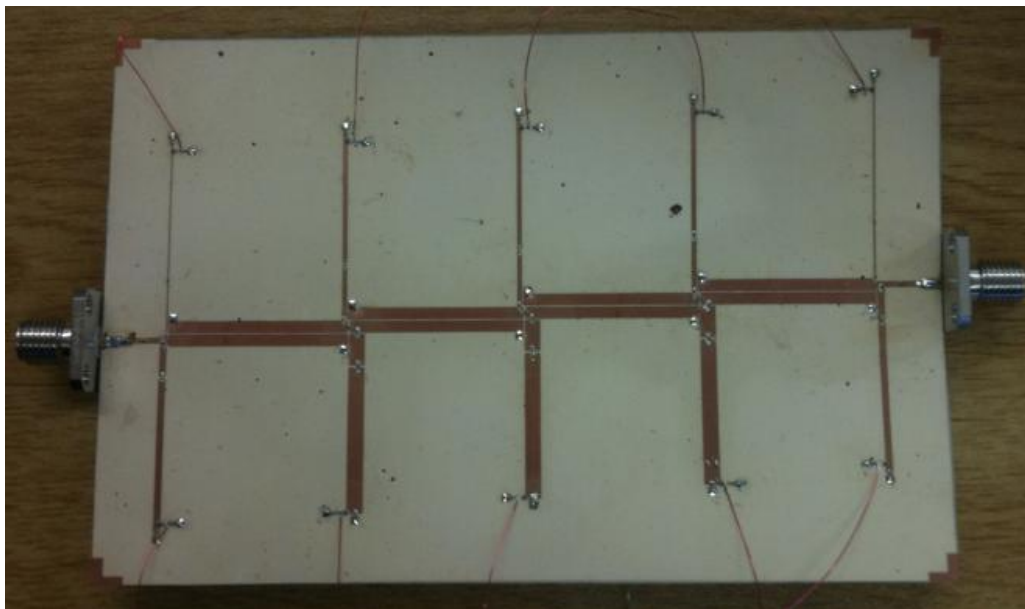


Figure 7.39: Fabricated reconfigurable filter.

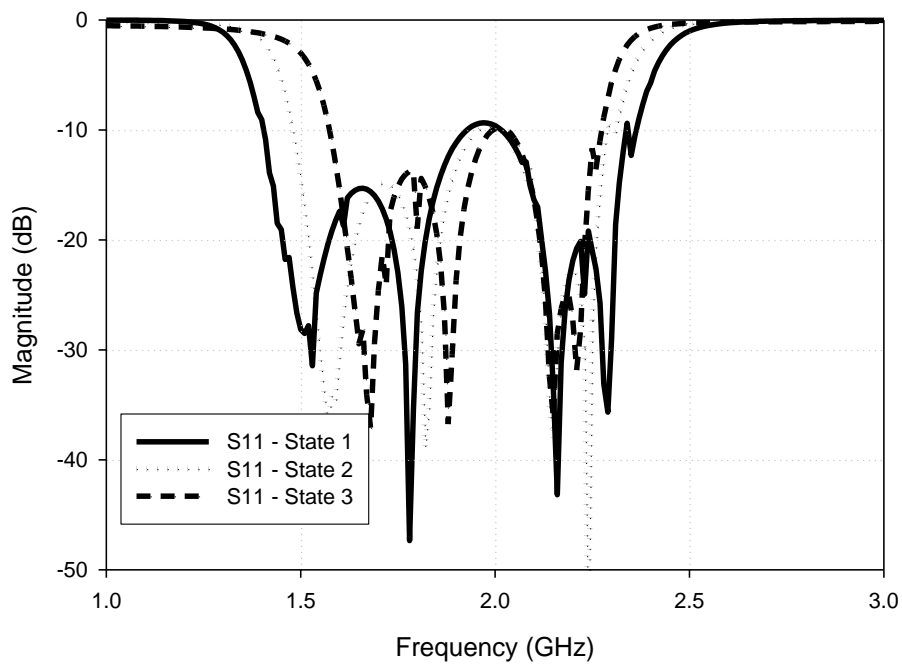


Figure 7.40: Measured S11 of the three distinct bandwidth states.

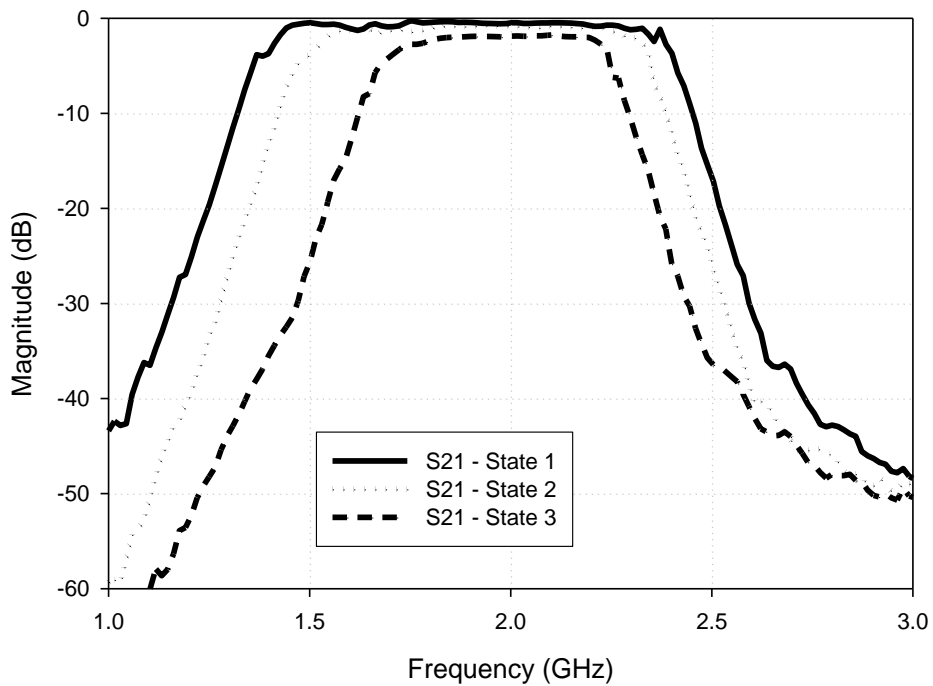


Figure 7.41: Measured S21 of the three distinct bandwidth states.

	State 1	State 2	State 3
<i>Ripple FBW</i> (0.04321 dB)	49.8%	42%	26%
f_0	1.9 GHz	1.9 GHz	1.95 GHz
Insertion Loss	0.57 dB	0.82 dB	1.95 dB

Table 7.5: Measured Performance.

In general, the fabricated filter shows good agreement with the simulated results. However, there are some differences with the center frequencies and fractional bandwidths, which may attribute to the fabrication tolerance as well as the ideal components assumed in the simulation.

7.4) Non – Linearity Measurements

7.4.1) Third Intercept Point

The third intercept point was measured in the same way as the single section coupled line filters from the previous chapter; with the tone separation being symmetrical with respect to the center frequency. The tone separation is plotted against the intermodulation for both the cascaded coupled line filter with the impedance transformer and the cascaded coupled line filter without the impedance transformer. From the measurements the same observations were made as the single section coupled line filters.

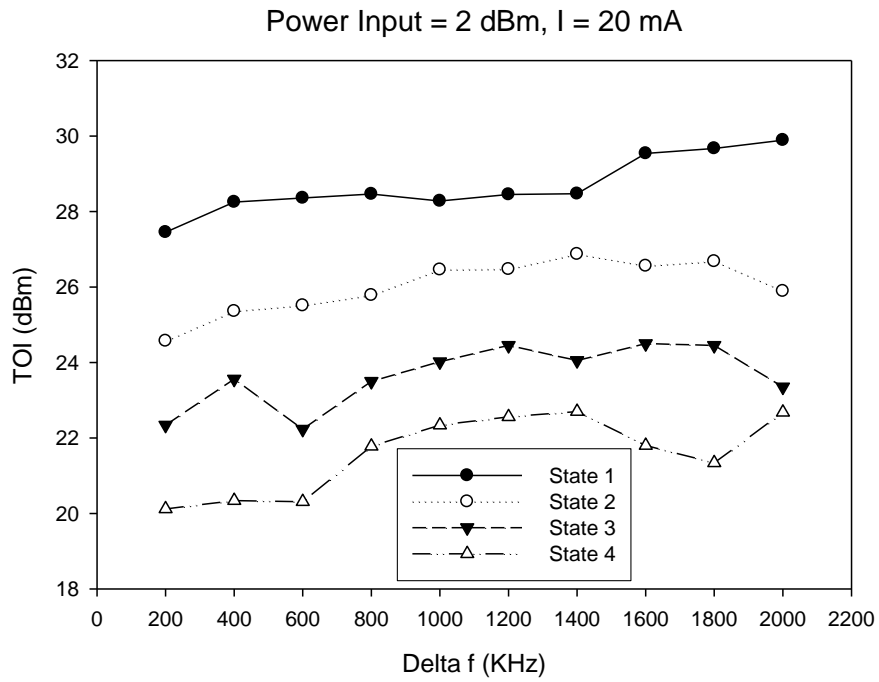


Figure 7.42: Cascaded Coupled Line Filter with Impedance Transformer.

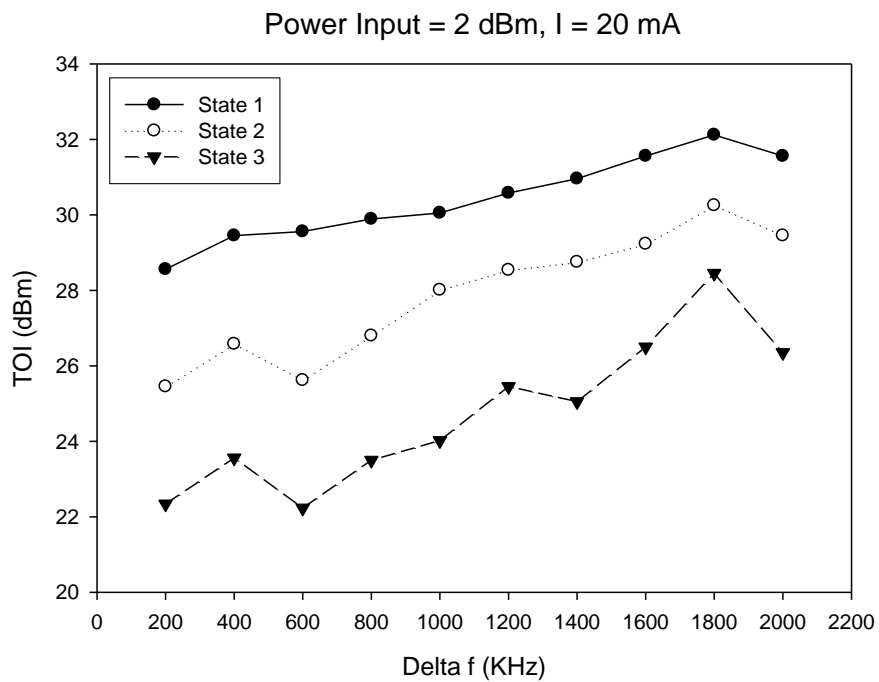


Figure 7.43: Cascaded Coupled Line Filter without Impedance Transformer.

7.4.2) 1 dB Compression Point

Again the 1 dB compression point was measured in the same way as detailed in section 5.4.2). The power difference is due to the insertion loss which is much higher than the single section filters due to the increased number of pin diodes.

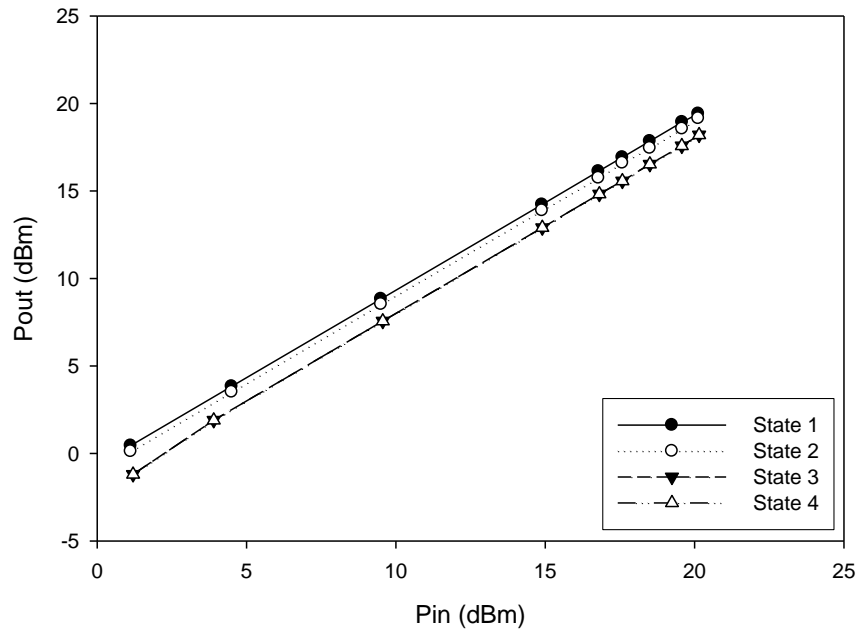


Figure 7.44: 1 dB Compression measurement of Cascaded Couple Line with Impedance Transformer.

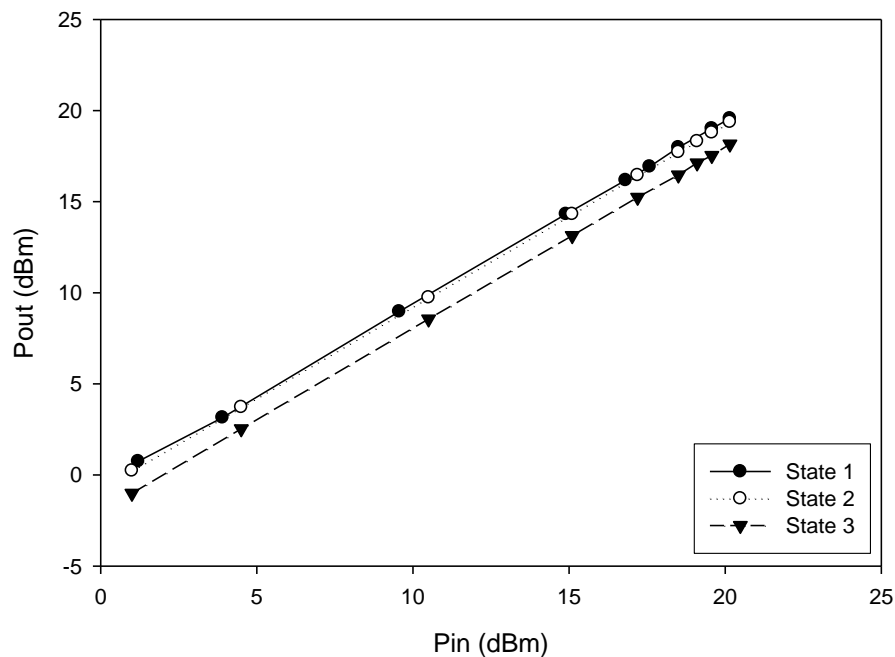


Figure 7.45: 1 dB Compression measurement of Cascaded Coupled Line Filter Without Impedance Transformer.

7.5) Summary

The coupled line structure investigated before was further developed to have more sections cascaded to increase selectivity for industrial applications. A design method was introduced to design any degree of filter. Firstly, a multi-section coupled line filter was designed using the single section formulas obtained in previous chapters. The filter could be tuned from a 3 dB FBW = 20% to a FBW = 50% centered at 2 GHz. It was apparent that the performance of the filter was hindered through the use of the impedance transformers. In order to improve this design a method was used which was adapted from Matthaei theory. There was a comparison made between the direct design equations for a coupled line filter and the new design procedure presented in this chapter. It was found that the modified design approach allows for a coupled line filter to be designed with fewer sections; this being very desirable to in the design of reconfigurable filters. The reason for this is that with fewer sections less tunable elements are needed, meaning that losses are reduced and a much higher performance filter is obtained. The new filter had an improved performance and a reduced size again another desirable trait. The filter had a tuning range between 26% and 50% ripple fractional bandwidth (FBW) centered at 2 GHz. The reconfigurable filter exhibits insertion losses ranging from 0.57 dB for the widest passband state to 1.95 dB for the narrowest passband state. In order to obtain the even and odd mode impedances a novel manufacturing technique was needed, namely LCP technology. In doing so this allowed the flexibility to obtain the impedances needed. Both cascaded filters have similar behaviour with regard to non – linearity. The behaviour is very similar to the single section filters, with the difference in power level due to the increased insertion loss due to the number of pin diodes and components. This is a good pre-cursor to filter which can control both bandwidth and frequency simultaneously; in which the subsequent chapters deal with and present.

7.6) References

[1] A. Miller, J. Hong, “Reconfigurable Cascaded Coupled Line Filter with Four Distinct Bandwidth States,” *IET Microwave Antennas and Propagation*, vol. 5 issue 4, Nov 18 2011, pp 1730 – 1737

- [2] A. Miller, J. Hong “Cascaded Coupled Line Filter with Reconfigurable Bandwidths Using LCP Multilayer Circuit Technology,” *IEEE Trans. Microw. Theory Tech*, Vol. 60, No. 6, June 2012, pp 1577 - 1586
- [3] A. Miller, J. Hong “Wideband Bandpass Filter with Multiple Reconfigurable Bandwidth States,” European Microwave Conference, Sep 2010, pp 1273 – 1276.
- [4] Applied Wave Research Inc, User’s Manual, Version 7.5, June 2007
- [5] Sonnet Software Inc, EM User’s Manual, Version 12 NY, 2009.
- [6] A. Miller, J. Hong, “Wideband Bandpass Filter with Reconfigurable Bandwidth,” *IEEE Microwave and wireless components letters*, Vol. 20, No. 1, Jan 2010, pp 28 – 30.
- [7] J.-S. Hong, M.J. Lancaster, “Microstrip Filters for RF/Microwave Applications,” John Wiley & Sons, Inc. 2001.
- [8] R. K. Mongia, I. J. Bahl, P. Bhartia, J. Hong, “RF and Microwave Coupled – Line Circuits,” Artech House, Inc. 2007.
- [9] George L. Matthaei, Leo Young, E. M. T. Jones, “Microwave Filters, Impedance – Matching Networks, and Coupling Structures,” *McGraw – Hill, Inc., New York 1964*.
- [10] A. M. Pavio, S. K. Sutton, “A Microstrip Re-entrant Structure Mode Quadrature Coupler for Hybrid and Monolithic Circuit Applications,” *Microwave symposium digest, 1990*, IEEE MTT-S International, No. 1, pp. 573 – 576, May 2004

Chapter 8: Frequency and Bandwidth Tunability Using the Coupled Line Concept

8.1) Introduction

In order to enhance the coupled line concept, it is thought to be essential to introduce frequency tunability. Furthermore, a filter which can simultaneously control frequency and bandwidth with multichannel capabilities is very desirable for many communication systems. This is what is illustrated in this chapter, with the design of the filter illustrated using the aforementioned theory in previous chapters. However, instead of converting to the coupled line schematic, the short circuit stub equivalent is used. A reason for this is that the value d can be chosen such that the connecting lines are all 50Ω . This makes the frequency tuning easier due to the increased flexibility. This chapter outlines the steps to design the filter and verifies the design through fabrication and testing. The simulated filter exhibits an insertion loss ranging from 0.5 dB to 1.36 dB, a center frequency tuning range between 3.1 GHz to 4.9 GHz and a FBW Tuning range of 36.7 % to 90 %. In the fabricated filter the tuning ranges are very similar to the simulated; however the insertion losses range from 0.68 dB to 2.6 dB. This filter is documented in [1].

8.2) Short Circuit Stub filter Design

The filter is designed, as mentioned using the theory in previous sections, however instead of converting to the coupled line structure as seen before, the circuit is kept in the stub filter equivalent circuit. The reason for this is that it makes it much easier to reconfigure the center frequency and bandwidth simultaneously. With coupled line arrangement it is much more difficult to change the electrical lengths of the coupled line sections, due to the short circuits at either end of the coupled lines. The circuit schematic for the reconfigurable wideband filter with simultaneous bandwidth and frequency control is shown in **Figure 8.1**. The circuit consists of n number of short circuit stubs and $n-1$ number of connecting lines. In order for

bandwidth control the impedances of the stubs need to be altered, whereas frequency control requires the electrical length of the stubs and connecting lines to be changed. In order to make this concept both frequency and bandwidth controllable, flexibility needs to be introduced especially with regard to the connecting lines.

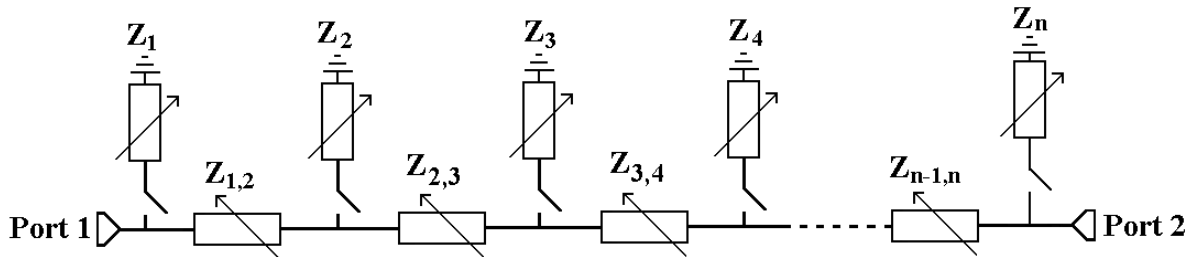


Figure 8.1: Reconfigurable Filter Schematic.

8.2.1) Filter Design

In order to design such a filter, the design equations (7.1) – (7.10) can be used to design a number of filters with specific bandwidth and frequency specifications, which then can be combined to obtain a reconfigurable filter. The connecting lines in all filters are designed to 50Ω , in order to do this the value of d is chosen such that this can be the case. Three third order filters could be considered for demonstration, for instance:

State 1: $f_0 = 3.1$ GHz, FBW = 58.06%

State 2: $f_0 = 4.9$ GHz, FBW = 36.7%

State 3: $f_0 = 4$ GHz, FBW = 90 %

All filter states have a ripple constant (L_{Ar}) of 0.04321 dB (Chebyshev Lowpass prototype element values: $g_0=g_6=1$, $g_1=g_5=0.9714$, $g_2=g_4=1.3721$, $g_3=1.8014$). There is also another advantage that each state in the final designed filter can have different L_{Ar} as each filter state is designed independently. However, for the purposes of this demonstration this characteristic is kept constant across all states designed. Moreover, this will create a fourth state as a through line can be introduced for an all pass state. Using (7.1) – (7.10) and setting $d = 0.647$ the following element impedance values are calculated for each filter state (see Appendix 6):

State 1:

$$Z_{1,2} = Z_{2,3} = 50 \Omega$$

$$Z_1 = Z_3 = 44.766\Omega \quad (8.1)$$

$$Z_2 = 54.195\Omega$$

State 2:

$$Z_{1,2} = Z_{2,3} = 50 \Omega$$

$$Z_1 = Z_3 = 23.565 \Omega \quad (8.2)$$

$$Z_2 = 24.038 \Omega$$

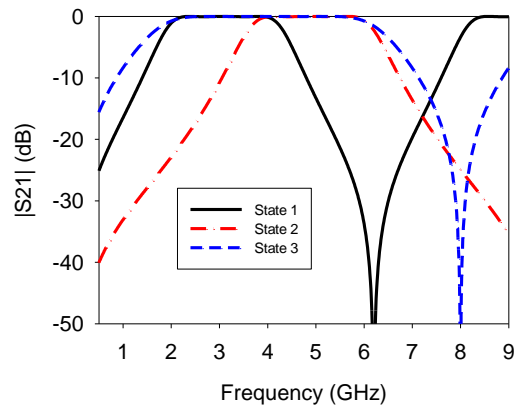
State 3:

$$Z_{1,2} = Z_{2,3} = 50 \Omega$$

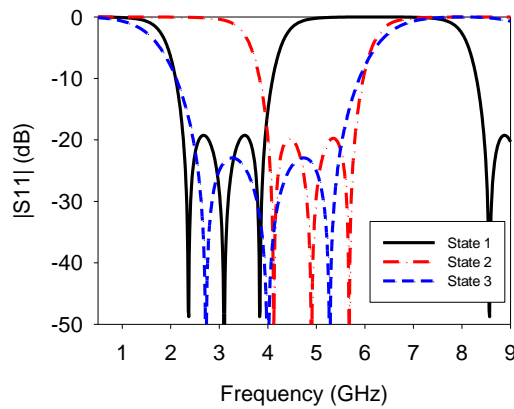
$$Z_1 = Z_3 = 92.234\Omega \quad (8.3)$$

$$Z_2 = 146.817\Omega$$

Theoretical responses of the three designed states are plotted in **Figure 8.2**.



(a)



(b)

Figure 8.2: Theoretical Responses of three designed states. (a) S21. (b) S11

8.2.2) EM Simulation

From the filter parameters calculated in (8.1) – (8.3) a reconfigurable filter capable of four distinct states can be obtained. Due to the connecting lines being 50Ω , the filter states designed above can be combined with each set of stubs switched on and off. A fourth state can also be obtained when all the stubs are turned off; this state acts as a through line. The four states obtainable with the designed reconfigurable filter illustrated in **Figure 8.3** are:

State 1: $f_0 = 3.1$ GHz, FBW = 58.06% (State 1 stubs on)

State 2: $f_0 = 4.9$ GHz, FBW = 36.7% (State 2 stubs on)

State 3: $f_0 = 4$ GHz, FBW = 90 % (State 3 stubs on)

State 4: Through Line or all-pass (all stubs off)

The circuit dimensions were calculated using [3] with them being finalized using [4]; the Pin diodes, which are used for the electronically switching, were mimicked using the s2p files provided by the manufacturer to take into account the component loss and frequency-dependent characteristics. As discussed in previous chapters there were some isolation issues with spikes in the passband. In order to eradicate this, a second diode was placed further up the stubs. The position of this second diode had an effect on the losses and the position of the spike seen in the passband. Thus a trade off was made in order to make the losses sufficient whilst shifting up any unwanted spikes out with the passband. In addition, the conductor (copper) and dielectric (substrate) losses were taken into account. The circuit of **Figure 8.3** as a whole including all dc bias components was simulated using [4], and the EM simulated responses of the four states are shown in **Figure 8.4**.

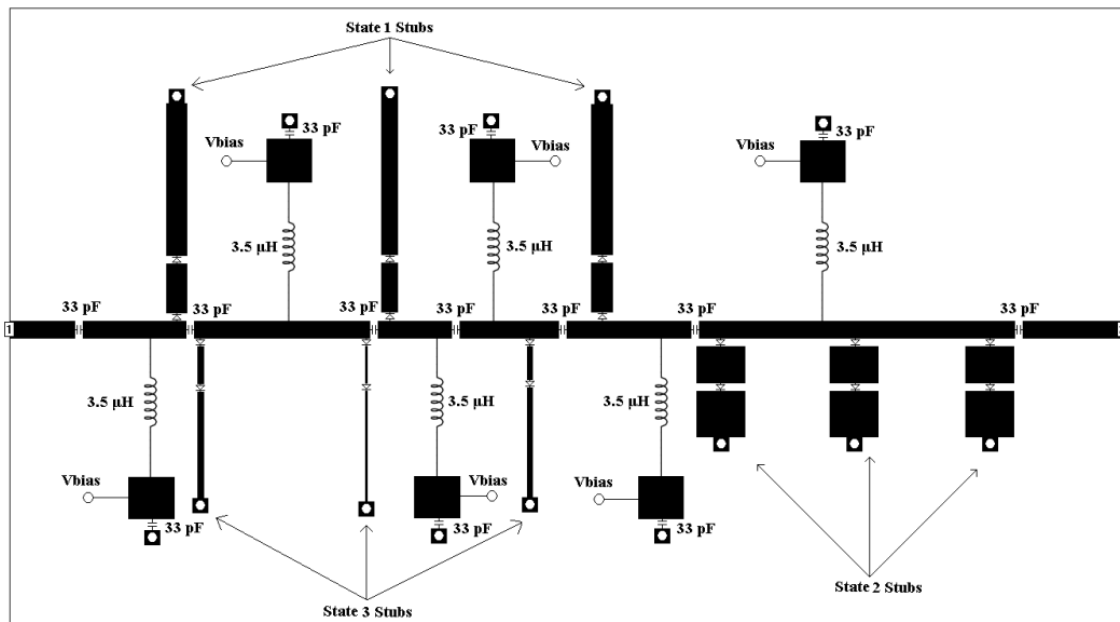
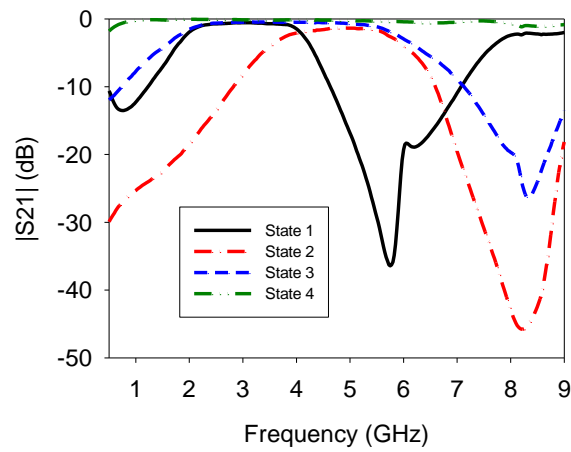


Figure 8.3: Electronically reconfigurable wideband filter with all four states implemented.

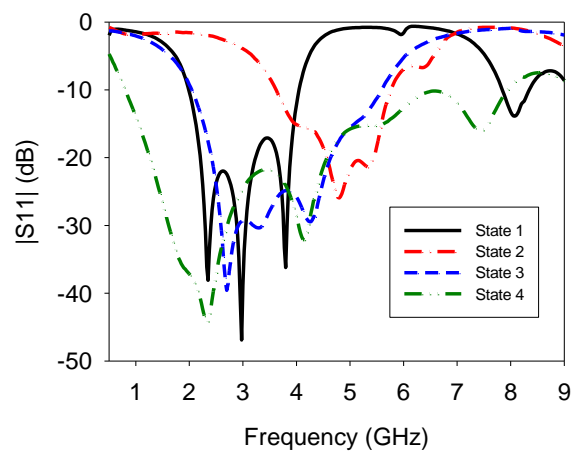
Circuit dimensions were calculated using [3] and finalised using [4]:

State Stubs	Z_1, Z_3 Stub Dimensions	Z_2 Stub Dimensions	Connecting Line Dimensions
1	$l = 15.6$ mm, $w = 1.5$ mm	$l = 15.6$ mm, $w = 1.1$ mm	$l = 15.6$ mm, $w = 1.25$ mm
2	$l = 7.2$ mm, $w = 3.5$ mm	$l = 7.2$ mm, $w = 3.45$ mm	$l = 7.2$ mm, $w = 1.25$ mm
3	$l = 11.65$ mm, $w = 0.4$ mm	$l = 11.65$ mm, $w = 0.1$ mm	$l = 11.65$, $w = 1.25$ mm
4	N/A	N/A	$l = 80$, $w = 1.25$ mm

Table 8.1: Circuit Dimensions.



(a)



(b)

Figure 8.4: EM-simulated responses of four states. (a) S_{21} . (b) S_{11} .

S2P files were used in the simulation meaning all the losses associated with the pin diodes were taken into account; therefore the degradation effects can be easily seen. It is apparent as the number of pin diodes turned on increases and the fractional bandwidth decreases, the insertion loss increases. The biggest effect is in state 2, which is due to it having the smallest fractional bandwidth, which means a higher insertion loss for the same value of Q factor [5]. The reason for the reduced fractional bandwidth is that some systems require the same absolute bandwidth as frequency is altered; this state was designed to have the same absolute bandwidth as State 1. A summary of the performance of the filter in each state is shown in **Table 8.2**.

	State 1	State 2	State 3	State 4
<i>FBW</i> (3 dB)	58.06%	36.7%	90%	N/A
<i>f_o</i>	3.1 GHz	4.9 GHz	4.1 GHz	N/A
Insertion Loss	0.85 dB	1.76 dB	0.82 dB	0.57 dB @ 5 GHz

Table 8.2: Simulated Performance.

8.2.3) Measured Filter Results

The filter was fabricated in accordance with the design specified in the previous section on a Rogers 3003 substrate with a thickness of 0.5 mm and $\epsilon_r = 3$. The capacitors used were Johanson's Multi-Layer High-Q Capacitors, due to their high self resonances, current handling capabilities and size. The inductance needed has to be high enough in order to isolate the circuit from the RF. In this filter the inductors chosen were Coilcraft's Wideband Bias Chokes – 4310LC this was due to their superior performance; with their very high inductance and very low self resonance (see appendices 7 and 8). However, a trade-off had to be made with regard to their size as the case size is much larger than the 0201 case size of the capacitor used. It was felt that this was a fair trade-off as the higher inductance used the better isolation from the RF is achieved, which allows for a superior performance filter to be obtained; especially in State 4 (through line) of the reconfigurable filter designed. The pin diodes used were MA/COM's MA4AGBLP912; the bias voltage for these can be easily extracted from the data sheet provided by the manufacture, and was chosen to be 2.8 V (as there are two pin diodes in series). The fabricated electronically reconfigurable wideband

filter, as seen in **Figure 8.5** with SMA connectors, was measured using a Hewlett Packard 8510B network analyzer.

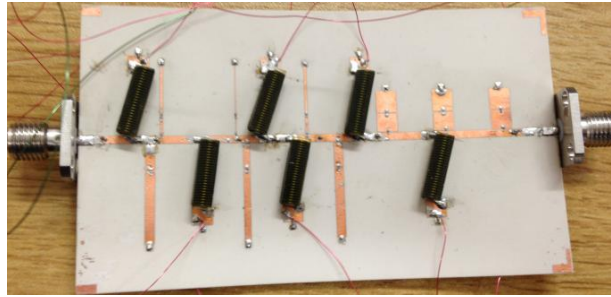
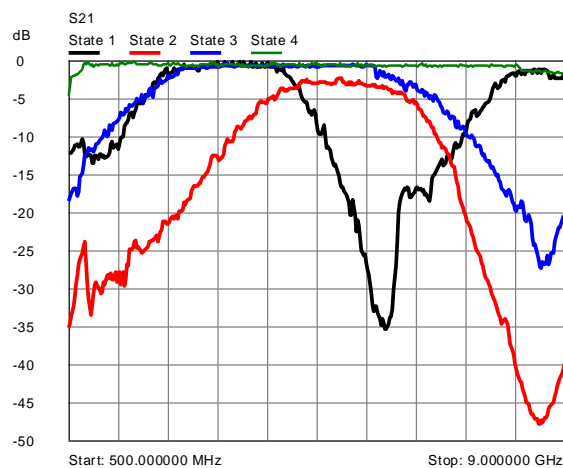
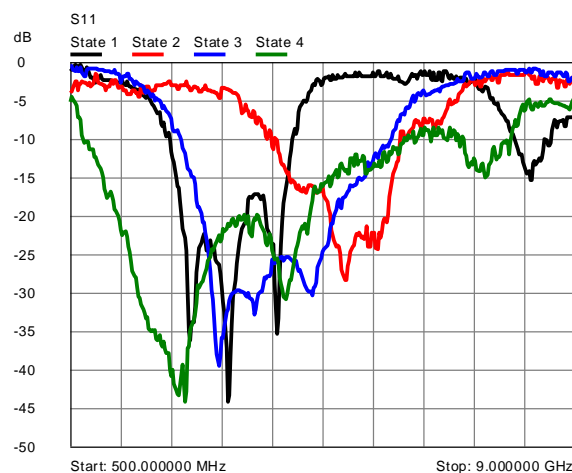


Figure 8.5: Fabricated electronically reconfigurable wideband filter.

The measured filter shows good agreement with the simulated one as is shown in **Figure 8.6**; there are however some shifts in center frequency and changes in fractional bandwidth which are attributed to fabrication tolerance. The measured performance of the fabricated filter is summarized in **Table 8.3**.



(a)



(b)

Figure 8.6: Measured responses of the electronically reconfigurable wideband filter. (a) S21. (b) S11.

	State 1	State 2	State 3	State 4
<i>FBW</i> (3 dB)	57.9%	35.9%	89.5%	N/A
f_0	3.15 GHz	4.96 GHz	4.14 GHz	N/A
Insertion Loss	0.96 dB	2.6 dB	0.87 dB	0.68 dB @5 GHz

Table 8.3: Summary of Measured Performance.

The measured wideband frequency responses (S_{21}) of all the four states are shown in **Figure 8.7**. In general, the band seen at $2f_0$ is suppressed as the structure used in this section is not converted to a cascaded coupled structure from previous chapters, where there are unequal even and odd mode phase velocities. In addition, from the measured wideband response of the state 4 (all pass), it is evident that the dc bias circuit designed can operate over a very wide frequency range, which is essential for the development of electronically reconfigurable wideband filters. However, its increased case size may cause problems when packaging the filter in a metallic enclosure for instance.

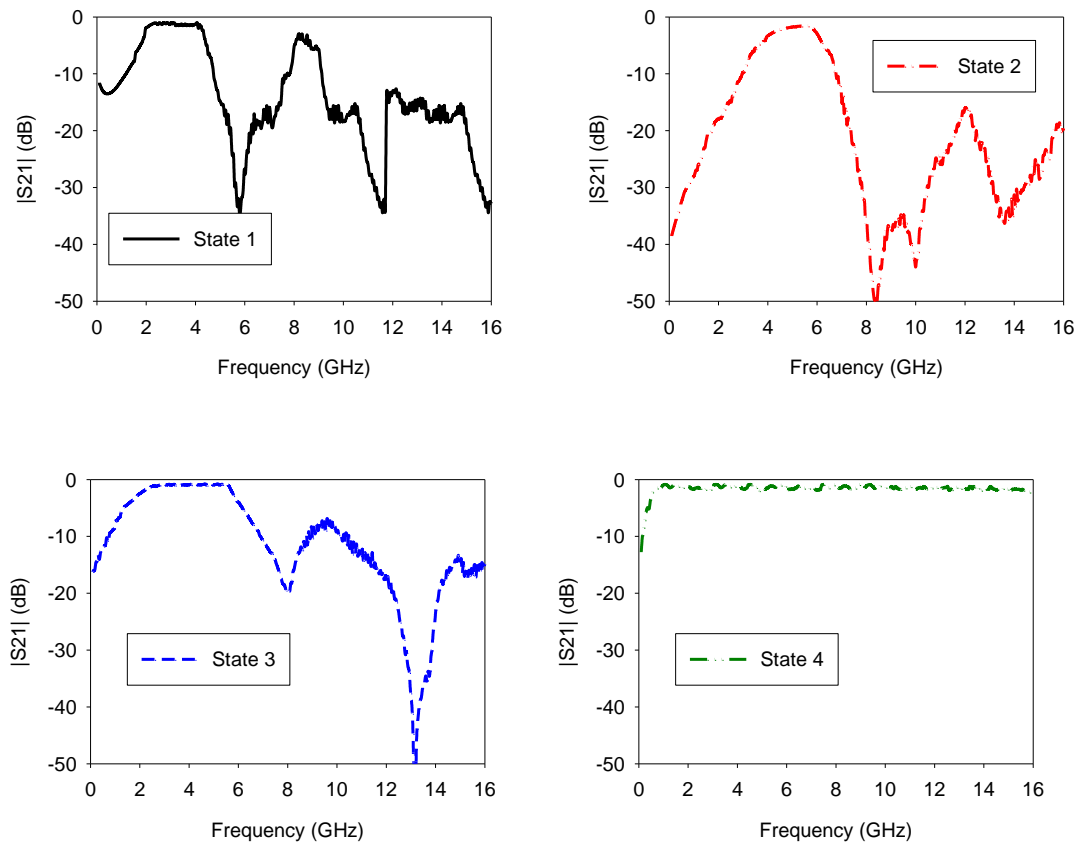


Figure 8.7: Measured wideband responses (S_{21}) of the electronically reconfigurable wideband filter.

8.3) Summary

In conclusion, an electronically reconfigurable microstrip wideband bandpass filter was designed by designing three short circuit stub filter states with connecting lines of 50Ω ; by doing so it allows these filter states to be combined to obtain a reconfigurable filter with four distinct states. The design was verified by EM simulation and measurement. In general, the simulated and measured results show good agreement. The measured reconfigurable bandpass filter shows a wide range of reconfigurability including fractional bandwidths from around 57.9% to 89.5% with center frequencies ranging from 3.15 GHz to 4.96 GHz. This filter shows a good approach in replacing a filter bank structure within communication and radar systems requiring multi channel capabilities.

8.4) References

- [1] A. Miller, J. Hong, "Electronically Reconfigurable Multi-Channel Wideband Bandpass Filter With Bandwidth and Center Frequency Control," *IET Antennas and propagation (in review)*
- [2] George L. Matthaei, Leo Young, E. M. T. Jones, "Microwave Filters, Impedance – Matching Networks, and Coupling Structures," *McGraw – Hill, Inc., New York 1964.*
- [3] Applied Wave Research Inc, User's Manual, Version 7.5, June 2007
- [4] Sonnet Software Inc, EM User's Manual, Version 12 NY, 2009
- [5] J. S. Hong, M. J. Lancaster, "Microstrip Filters for RF/Microwave Applications," *Wiley, New York, 2001*

Chapter 9: Reconfigurable Bandwidth and Frequency Filter Using Cascaded Highpass/Lowpass Blocks

9.1) Introduction

As mentioned previously there is an increasing demand for reconfigurable filters as systems need multifunctional capabilities. Filter topologies explored in earlier sections, involved coupled lines and short circuit stubs. This section describes another method, which involves cascading a reconfigurable Highpass filter with a reconfigurable Lowpass filter in order to create a reconfigurable wideband bandpass filter. As will be seen, this design is very flexible in the approach but obviously has some drawbacks, as with any filter. The idea of cascading a Highpass and Lowpass filter is not a new concept [1] – [7], however to the best of the authors knowledge there has been no cascaded filters as described above which have reconfigurability. Also to the best of the author’s knowledge, there have been little or no reconfigurable Highpass filters reported in literature. However, there have been some reconfigurable Lowpass filters demonstrated [8] – [13]. This chapter describes a reconfigurable wideband filter concept which uses a cascade of reconfigurable optimum Highpass and reconfigurable optimum Lowpass filters in order to create a reconfigurable wideband bandpass filter with four states. The reason for using the optimum designs is that less tuning elements are used resulting in less losses from the tuning elements. This work is documented in [14].

9.2) Reconfigurable Optimum Highpass Filter

9.2.1) Theoretical Design

The filter was designed using the method in section **4.3) Optimum Highpass Filter**; if it is considered to design a highpass filter having a cut off frequency of 2.3 GHz and a 0.1 dB

passband ripple up to 10.5 GHz, referring to **Figure 4.7**, the electrical length θ_c can be found using:

$$\left(\frac{\pi}{\theta_c} - 1\right) f_c = 10.5 \quad (9.1)$$

This gives $\theta_c = 0.564$ radians or $\theta_c = 32.34^\circ$, assuming that the filter is designed with three short circuit stubs, the element values for $\theta_c = 35^\circ$ can then be chosen. Which would mean the passband width would be 9.5 GHz instead. This meaning that the circuit parameters can be taken from **Table 4.1** and are as follows:

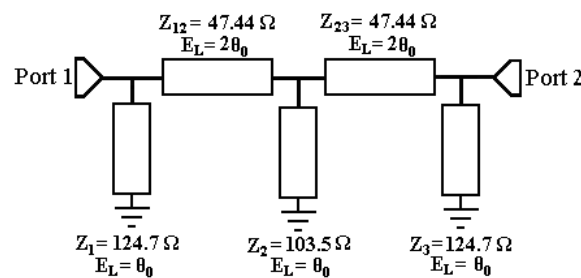


Figure 9.1: Highpass Filter Design with Calculated Values.

Where $\theta_0 = 90^\circ$ at center frequency $f_0 = 6.4$ GHz.

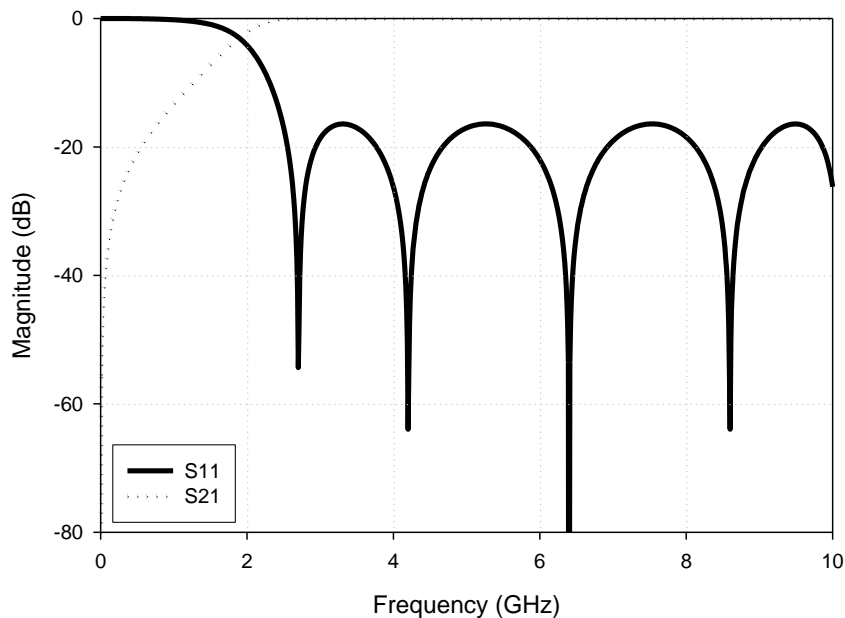


Figure 9.2: Theoretical Response Using [17].

In order to reconfigure the cut off, the electrical lengths of the stubs and connecting lines need to be altered simultaneously. The short circuit stubs can be easily varied by simply switching a short circuit in whatever position is necessary for the desired cut off. Conversely, the connecting lines create a problem; one solution would be to bend the line and connect a pin diode across the gap of the bend. However, this means they would act like hairpin resonators, due to the widths and lengths of the lines. After careful consideration it can be clearly seen that in this topology the connecting lines are almost 50Ω . If the lines were made equal to 50Ω , this would allow flexibility to move different sizes of stubs where needed to reduce the length of the connecting lines. If we also increase the impedance values of the stubs, this will slightly increase the selectivity of the filter. Using [16] to tune these values, the following is obtained:

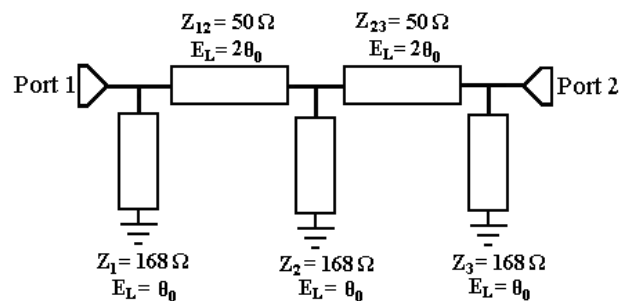


Figure 9.3: New Circuit Parameters.

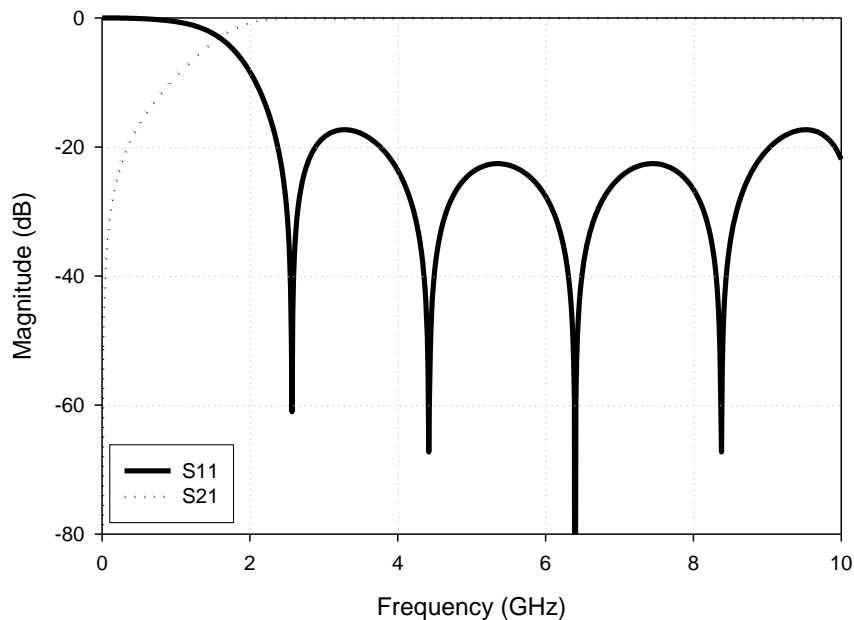


Figure 9.4: Theoretical Response with New Impedance Values and $\theta_0 = 90^\circ$.

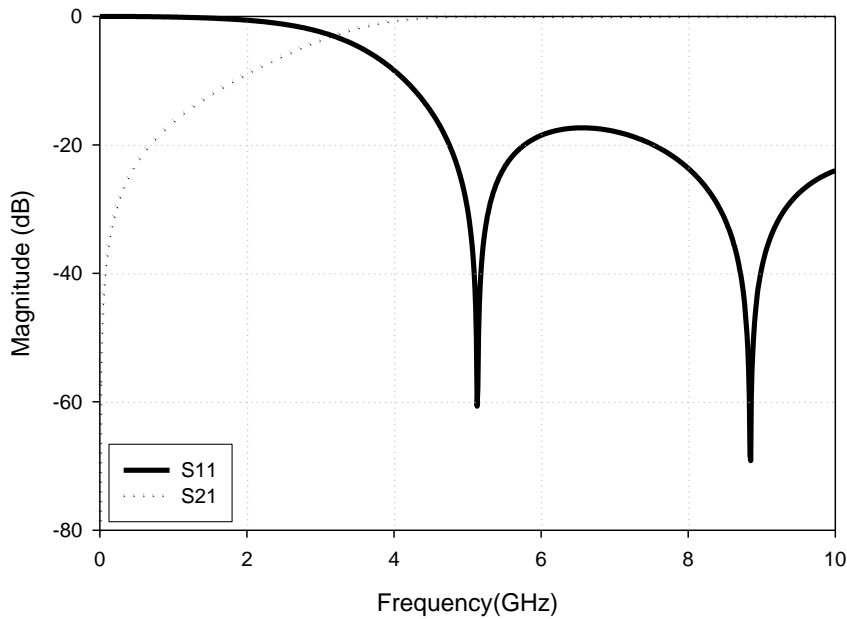


Figure 9.5: Theoretical Response With $\theta_0 = 45^\circ$.

9.2.2) EM Simulation

These calculated circuit parameters can be converted to microstrip lines using [16], once these have been obtained the circuit can be drawn and simulated in a full EM simulator [17]. In the simulations the bias circuits are modelled using ideal components and diodes are modelled with S2P files from the manufacturer. The filter was designed for a substrate with thickness of 0.76 mm and a dielectric constant of $\epsilon_r = 3$. The dimensions were calculated using [16] and then finalised in [17]. This means that the dimensions are as follows:

Connecting lines: $w = 1.9$ mm, $l = 10.5$ mm (state 1) and $l = 5.15$ mm (state 2)

Stubs: $w = 0.1$ mm, $l = 5.65$ mm (state 1) and $l = 3.1$ mm (state 2).

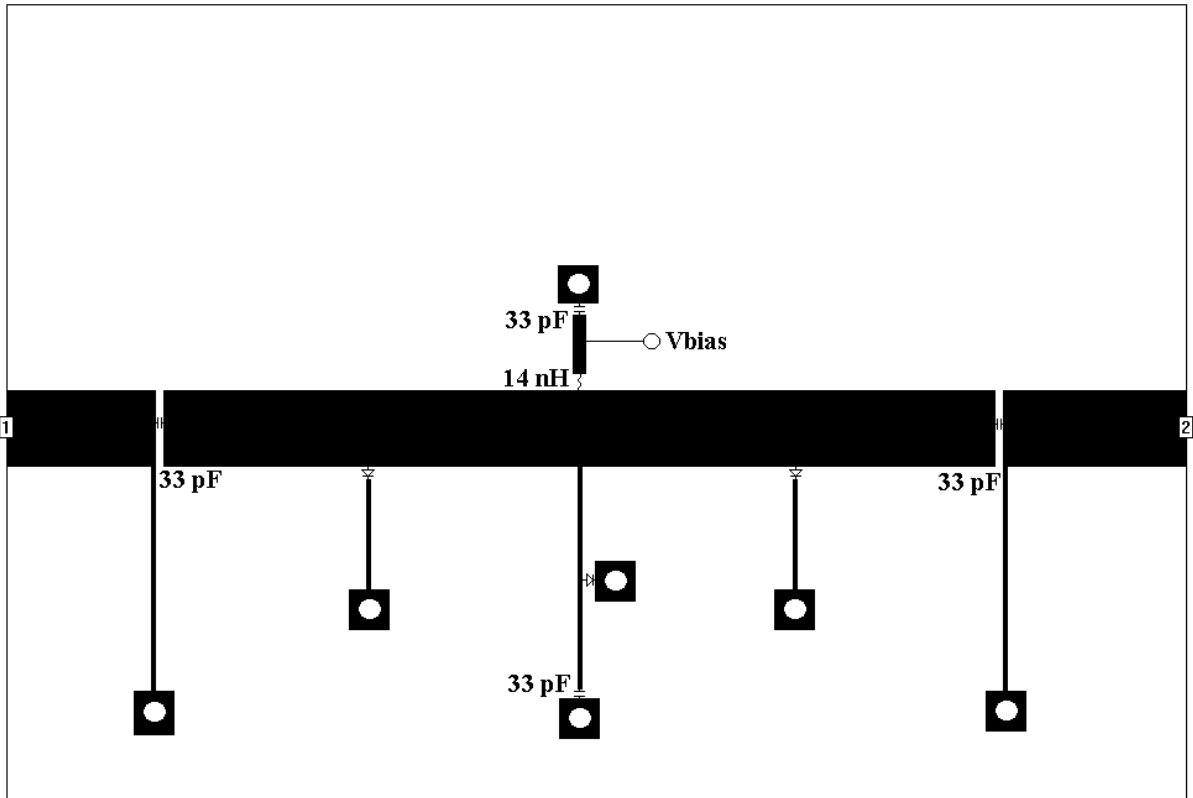


Figure 9.6: Highpass Filter Design.

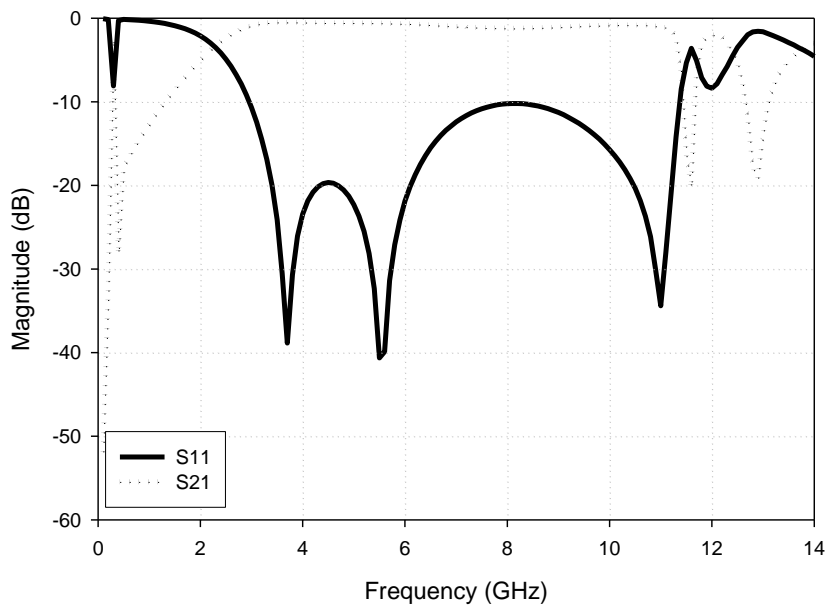


Figure 9.7: Highpass Filter State 1.

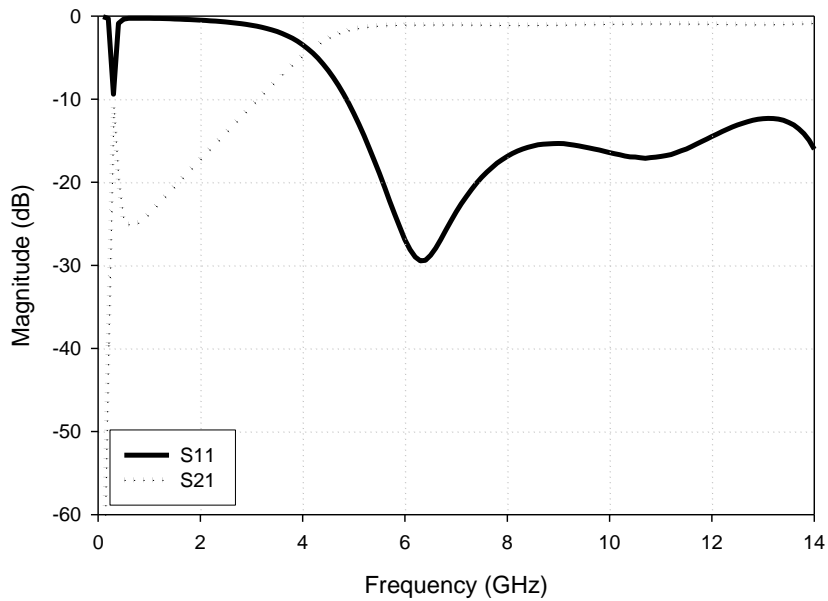


Figure 9.8: Highpass Filter State 2.

On inspection of the responses it can be clearly seen there are some discrepancies, one being the spike at low frequencies and the other being: a resonance between around 11.3 GHz in state 1. The first issue is attributed to the bias circuit and blocking capacitors, while the second issue is because of the isolation of the 4.6 GHz stubs. This can be eradicated by adding a second diode at the short circuit near the short circuit (see **Figure 9.9**). However, these issues should not cause a problem as there are out with the passband and the lowpass filter is designed between 5 GHz and 10 GHz. This meaning a trade-off can be made to use only one pin diode for switching each stub in order to limit the losses. Furthermore, the lines for the lower cut off of 2.3 GHz are always connected and have no adverse effects on the frequency range; these actually increase the selectivity of the filter in the second state (see **Figure 9.10**).

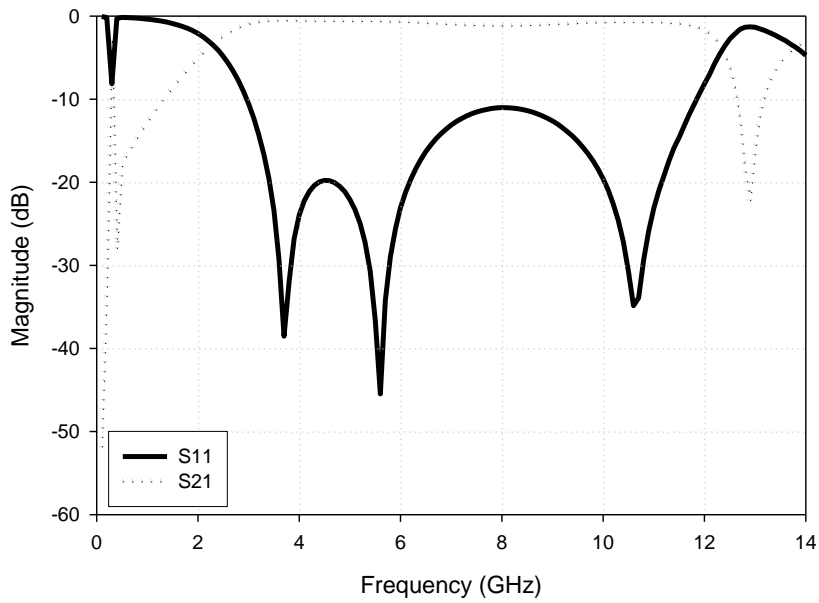


Figure 9.9: State 1 with a second diode placed at the top of the stub, near the short circuit.

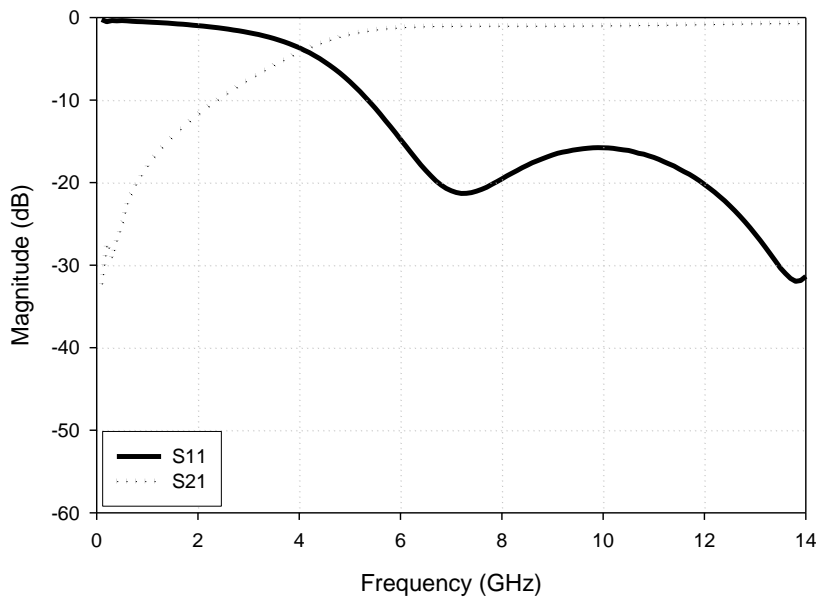


Figure 9.10: State 2 with the 2.3 GHz Stubs isolated from the circuit.

Referring to **Figure 9.8**, it is clear that there will be problems at narrow bandwidths when cascaded with a lowpass filter due to the selectivity. For this reason two stepped impedance resonators were added at the input and output with different impedance ratios. In doing so there were two transmission zeroes created at 2.2 GHz and 3.3 GHz, with the second harmonic being above 14 GHz. The impedance ratios and dimensions are:

Input Stub: $Z_1 = 164.5 \Omega$ ($w = 0.1\text{mm}$, $l = 6.3 \text{ mm}$), $Z_2 = 21 \Omega$ ($w = 6.2 \text{ mm}$, $l = 2.2 \text{ mm}$)

Output Stub: $Z_1 = 164.5 \Omega$ ($w = 0.1\text{mm}$, $l = 3.85 \text{ mm}$), $Z_2 = 21.3 \Omega$ ($w = 6.1 \text{ mm}$, $l = 1.6 \text{ mm}$)

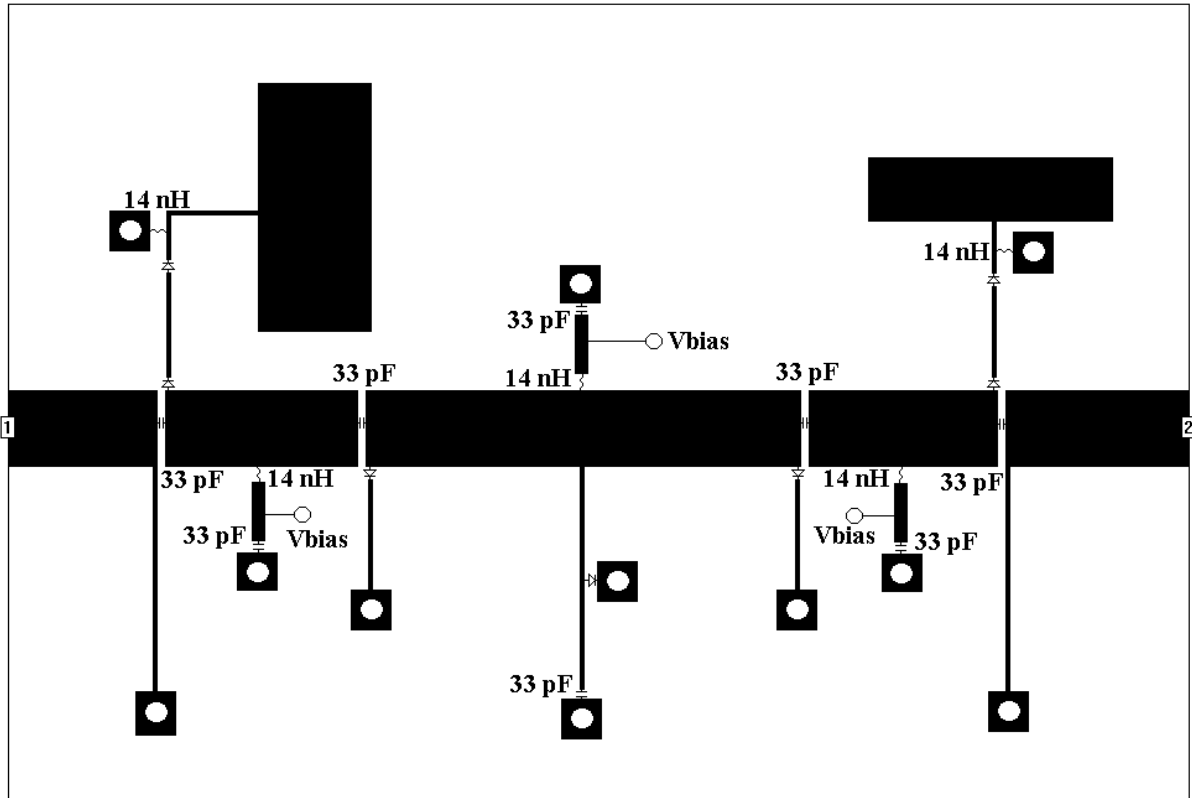


Figure 9.11: Highpass Filter design With Switchable Stepped Impedance Resonators.

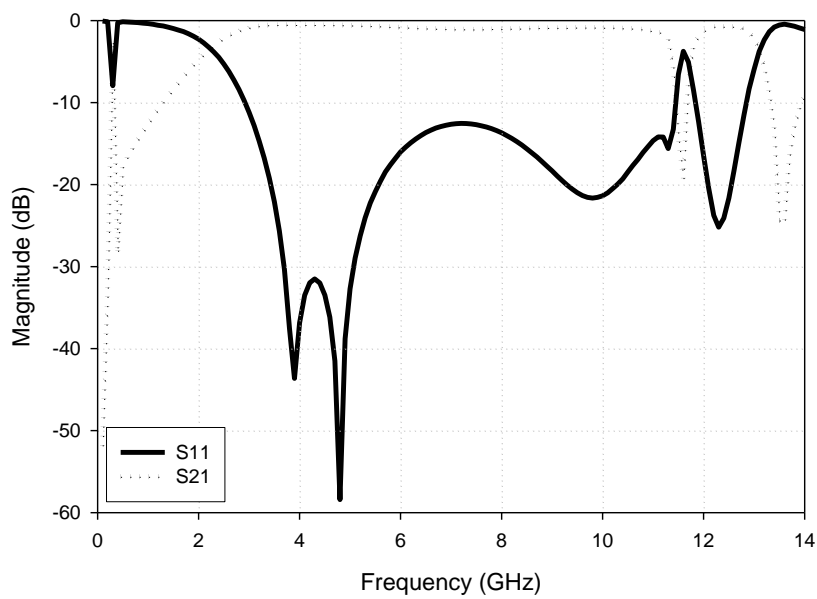


Figure 9.12: State 1 of the final design of the highpass filter.

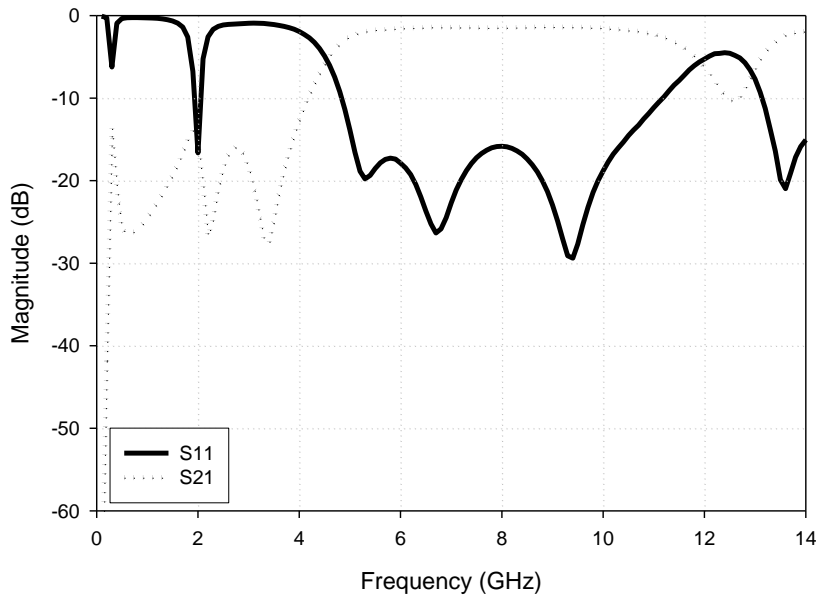


Figure 9.13: State 2 of the final design of the highpass filter.

As can be seen above, the Highpass filter can be switched a full octave from 2.3 GHz to 4.6 GHz as designed. However, two things to note about the state 2 response are (i) The extra resonance seen at 1.6 GHz; which is due to the connection of SIR's (see **Figure 9.14**) and (ii) in state 2 a small resonance appears at 12.6 GHz; this is also due to the SIR's being connected in this state, whereby the pin diodes shift down the second harmonic of the transmission zeroes created due to the impedance ratio. This means as mentioned that the maximum state allowable for the Lowpass filter cut off is dependant of the bandwidth of the Highpass filter and the position of the second transmission zero of the SIR's.

In order to show the true cause of the resonance at 1.6GHz, a few simulations were carried out in the second state without components apart from the diodes on the stubs for reconfigurability. Namely, one simulation with only the SIR's connected ideally, and a simulation also with the stubs for reconfigurability with diodes. Inspecting **Figure 9.14** it can be clearly seen that the spike at low frequencies is caused by the blocking capacitors as **Figure 9.15 and 9.16** have none. Furthermore, the resonance at 1.6 GHz is caused by the interaction of the initially designed filter and the addition of the SIR's. However, in this case the resonance is seen at 1.8 GHz, the reason for this is the addition of the diodes. The package and losses of the diode causes a shift to lower frequencies and an increase in loss.

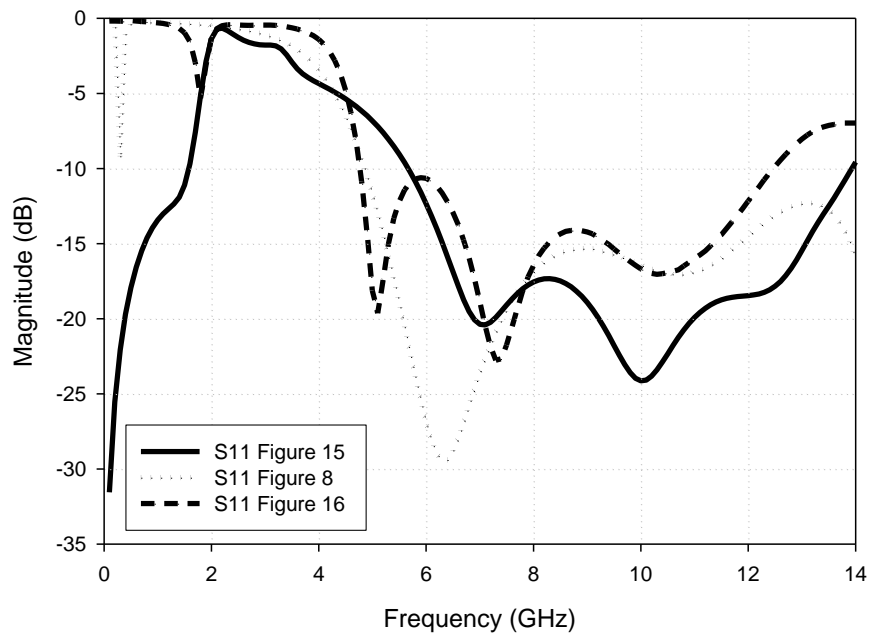


Figure 9.14: Comparison of S11 to ascertain the resonance at 1.6 GHz.

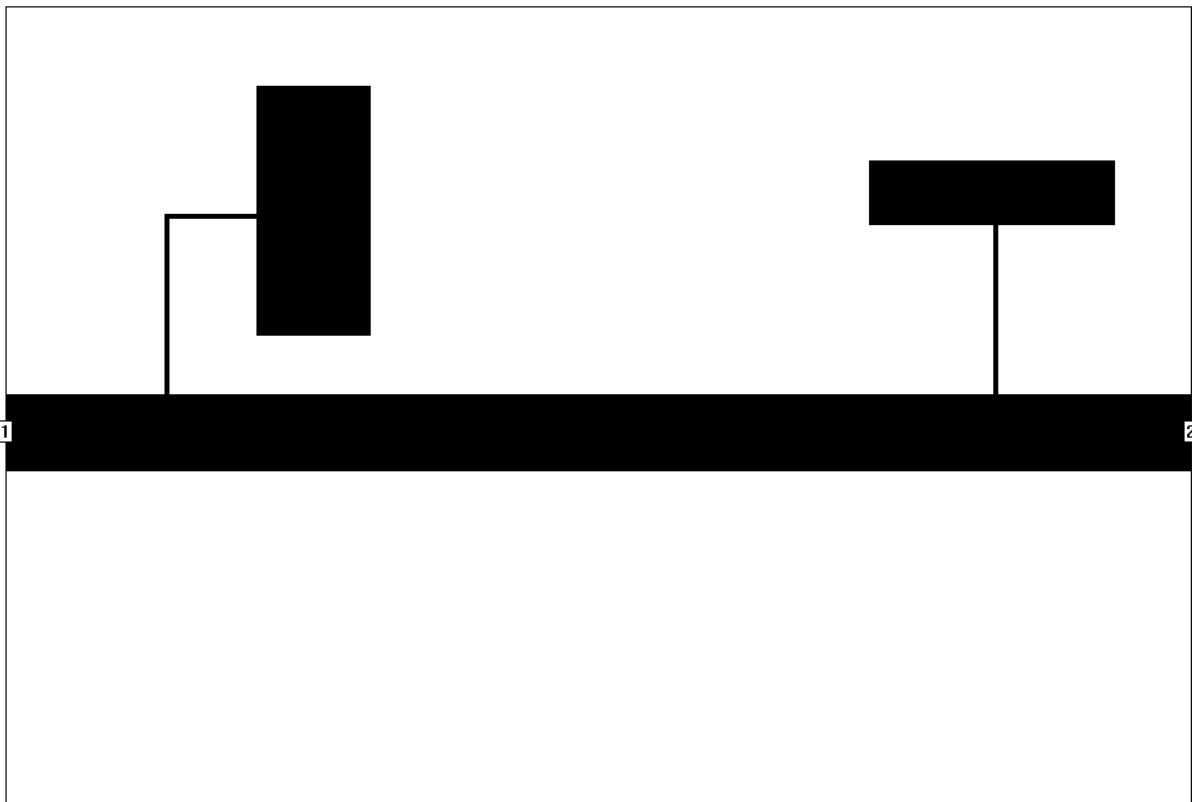


Figure 9.15: SIR's connected ideally with no stubs.

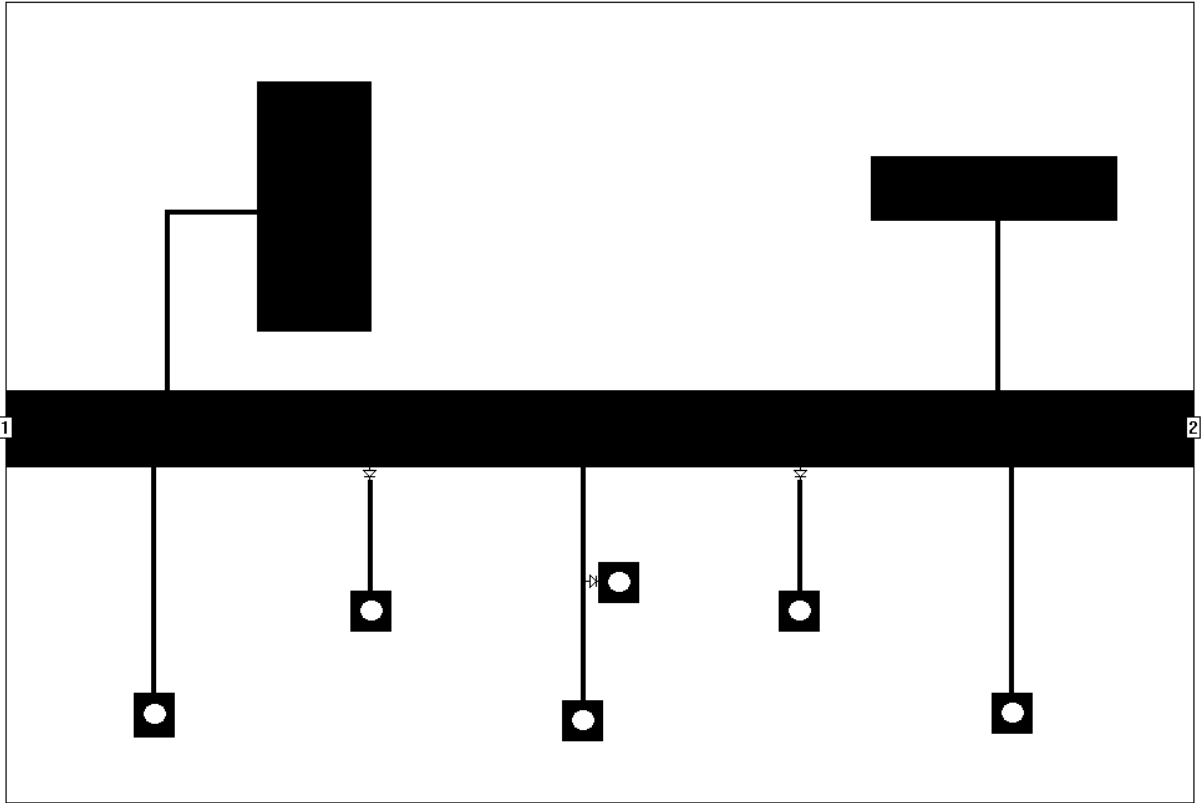


Figure 9.16: SIR's ideally connected with switchable stubs.

9.3) Reconfigurable Optimum Lowpass Filter

9.3.1) Theoretical Design

The initial design of the filter was carried out using the method detailed in Section 4.4) **Optimum Quasi Lowpass/Bandstop Filter**. If an optimum microstrip bandstop filter with three open-circuited stubs ($n = 3$) and a fractional bandwidth $FBW = 1.0$ at a midband frequency $f_0 = 5$ GHz was to be designed. Assume a passband return loss of -20 dB, which corresponds to a ripple a constant of 0.1005. From **Table 4.3**, we obtain the normalized element values $g_1 = g_3 = 0.94806$, $g_2 = 1.67311$, and $J_{1,2} = J_{2,3} = 0.56648$. The filter is designed to match 50 ohm terminations. Therefore, $Z_0 = 50$ ohms.

$$Z_A = Z_B = 50 \Omega$$

$$Z_1 = Z_3 = 52.74 \Omega$$

$$Z_2 = 29.88 \Omega$$

$$Z_{1,2} = Z_{2,3} = 88.26 \Omega$$

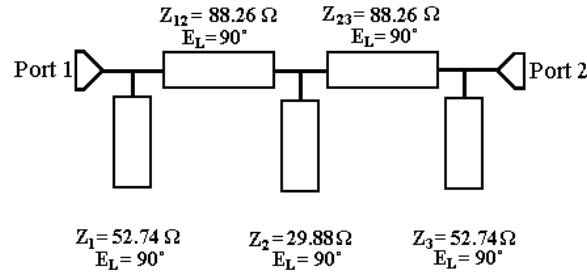


Figure 9.17: Bandstop Filter Design.

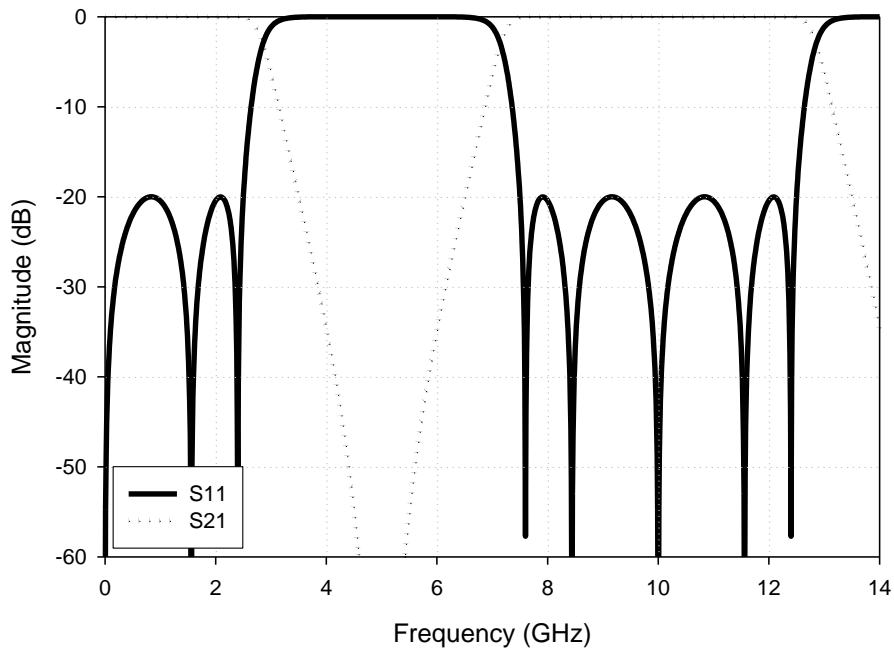


Figure 9.18: Bandstop Response.

In order to increase the performance of the filter a similar method was used to [1], whereby the impedances and the electrical lengths are altered in order to change the position of the transmission zeroes. This means the stop band can be extended and the selectivity increased.

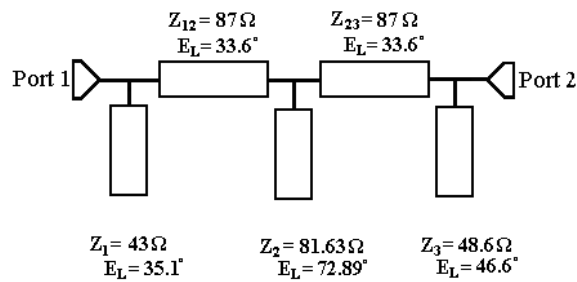


Figure 9.19: Lowpass Filter Design.

The cut off of this filter f_0 was slightly changed to 4.55 GHz in order to obtain 5 GHz cut off at -3 dB.

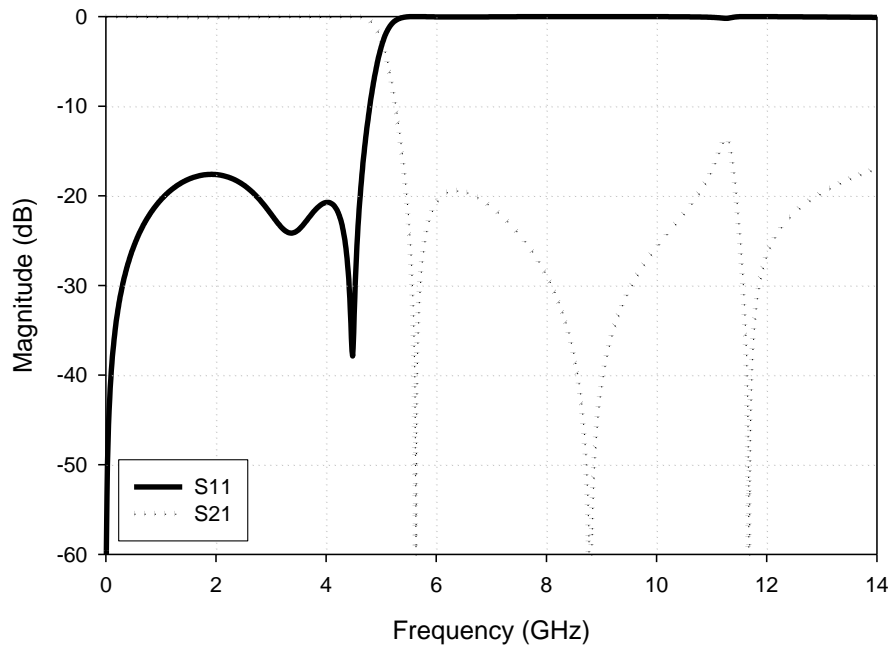


Figure 9.20: Lowpass Filter Response – State 1.

In order to make this filter reconfigurable, pin diodes need to be introduced in order to reduce the length of the stubs. The connecting lines can be neglected as when cascaded with the highpass filter which has an upper cut off of 12.6 GHz, meaning this will contribute the selectivity. With this in mind [16] was used to tune the f_0 of the stubs while keeping the connecting lines the same cut off frequency as before.

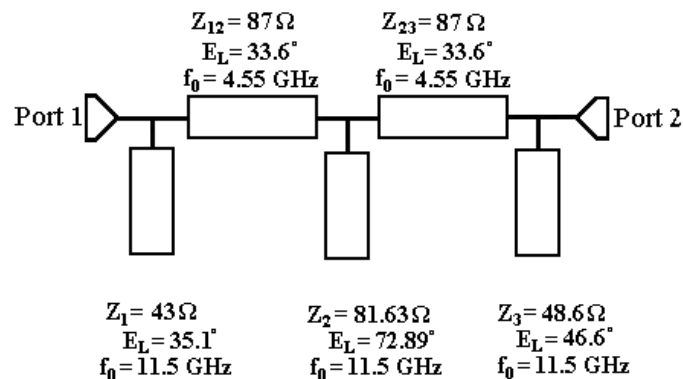


Figure 9.21: Lowpass filter parameters for state 2.

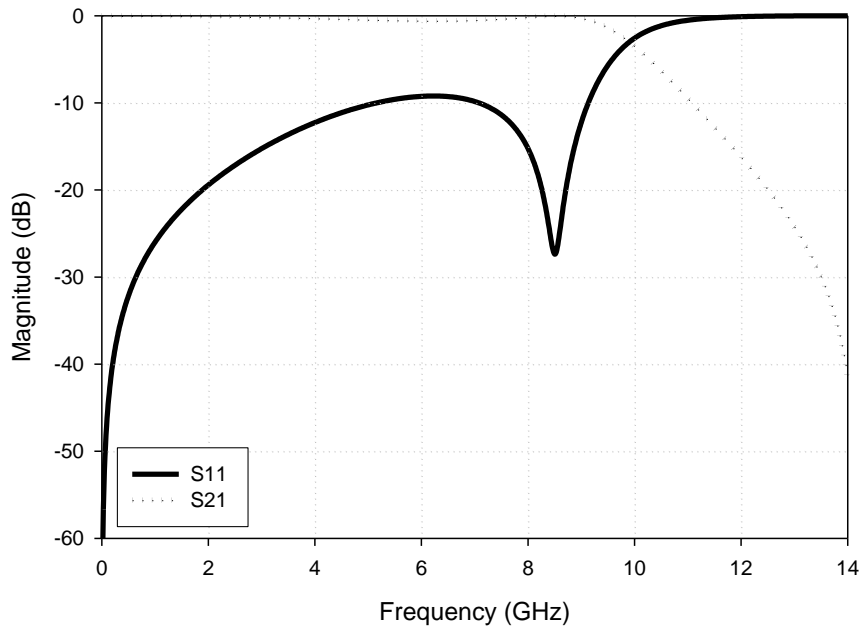


Figure 9.22: Lowpass Filter - State 2 Design.

From these parameters, the circuit can be converted to microstrip design using [16], with the same substrate parameters as the highpass filter (Thickness = 0.76 mm and $\epsilon_r = 3$).

9.3.2) EM Simulation

Figure 9.23 illustrates the lowpass filter with the bias circuitry required; the path to ground for biasing is the short circuit stub at the output of the Highpass Filter. The connecting lines are 3.7 mm in length and 0.7 mm in width. The dimensions of the stubs are as follows:

- First Stub – $w = 2.4$ mm, $l = 3.7$ (state 1) and 1.7 (state 2).
- Second Stub – $w = 0.8$ mm, $l = 8$ mm (state 1) and 3.3 mm (state 2).
- Third stub – $w = 2$ mm, $l = 4.95$ mm (state 1) and 2.3 mm (state 2).

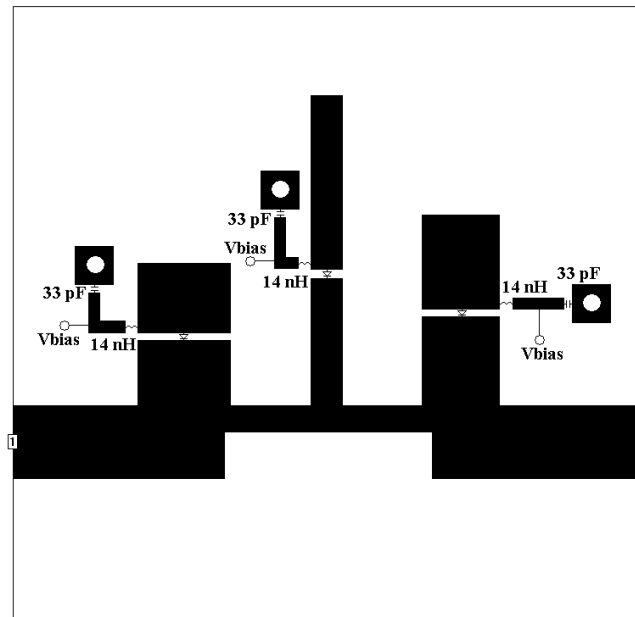


Figure 9.23: Lowpass Filter Design with Bias Circuitry.

The circuit was simulated using the full EM Simulator [17], in accordance with the design above. The responses obtained show good performance, but like the Highpass filter there were some associated problems. The bias circuit causes some problems with the response of the circuit causing an increase in losses. The electrical lengths also had to be altered slightly as the bias circuits caused some shifts on center frequency. Also of note is the small spurious response caused in state two, this can be easily suppressed with the addition of a high impedance resistor in series with the inductor of the bias circuit (see **Figure 9.26**). However, as the spike is negligible it was decided to leave the circuit as is, because the addition of a resistor will increase the losses. Furthermore, the resonance seen at very low frequencies in state one can also be ignored as it is out with the passband planned for the cascaded bandpass filter.

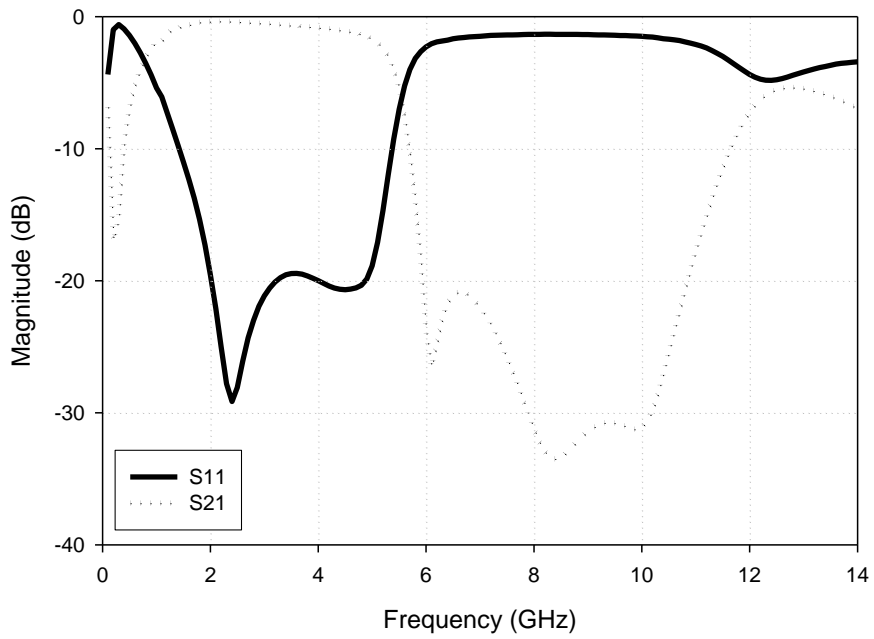


Figure 9.24: State 1 of the Lowpass Filter.

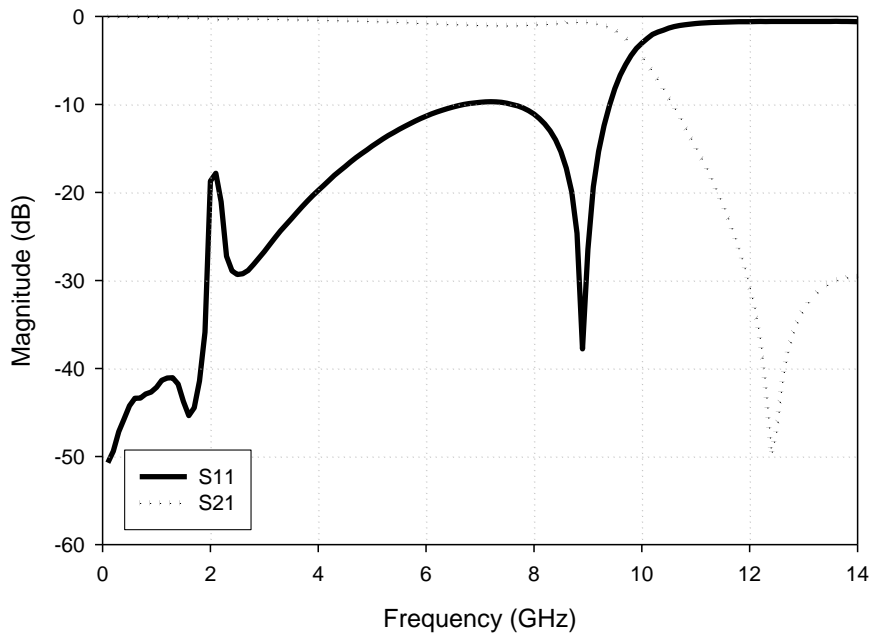


Figure 9.25: State 2 of the Lowpass Filter.

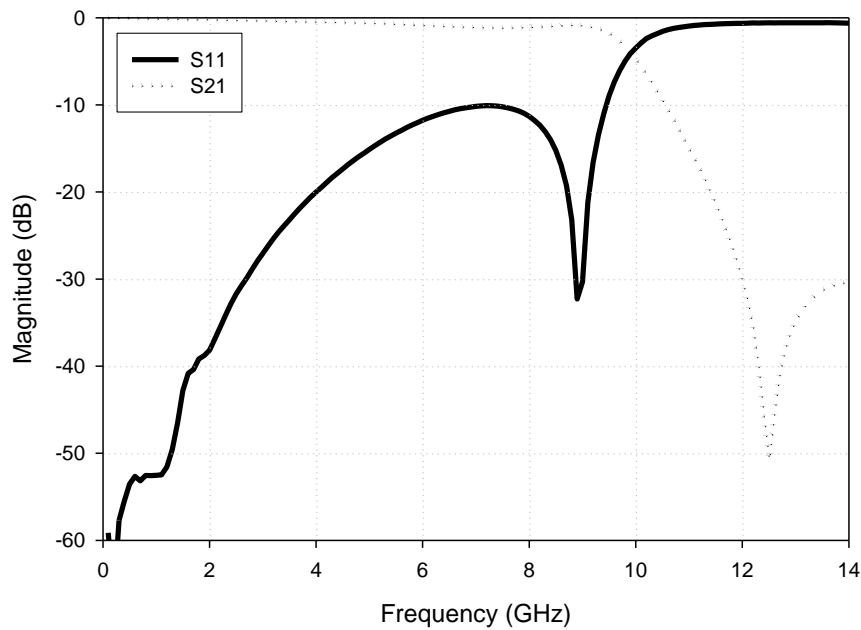


Figure 9.26: State 2 of the Lowpass Filter with a 1000 Ω Resistor in Series with the Inductors in the Bias Circuit.

9.4) Reconfigurable Bandpass Filter

The final reconfigurable bandpass filter was obtained by cascading the tunable highpass and lowpass filtering blocks described above. The resultant microstrip filter of this type is illustrated in **Figure 9.27**. With the highpass and lowpass filter having two states each means that the bandpass filter is capable of four distinct states.

- State 1: 2.3 – 5 GHz
- State 2: 2.3 – 10 GHz
- State 3: 4.6 – 10 GHz
- State 4: 4.6 – 5 GHz

The center frequency ranges from about 3.6 GHz to 7.3 GHz and a 3 dB fractional bandwidth ranging from 15.7% to 125%. The reconfigurable bandpass filter has four distinct states:

- State 1 (PINs 1 to 7 off and PINs 8 to 10 on)
- State 2 (all PINs off)

- State 3 (PINs 1 to 7 on and PINs 8 to 10 off)
- State 4 (PINs 1 to 7 on and PINs 8 to 10 off)

The final Schematic and simulated performance is summarised below in **Table 9.1**:

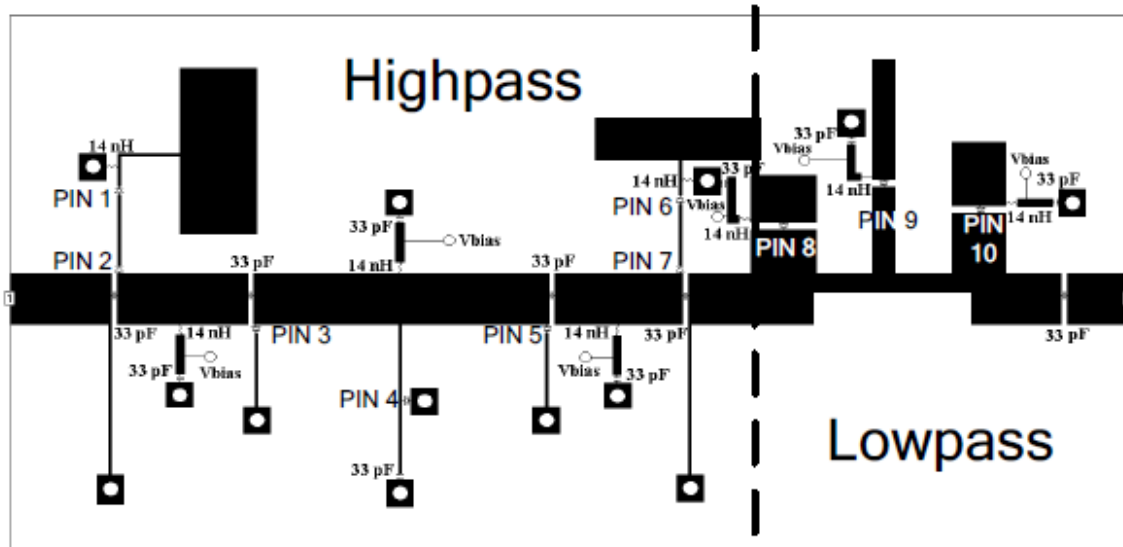


Figure 9.27: Reconfigurable Microstrip Bandpass Filter.

	State 1	State 2	State 3	State 4
<i>FBW</i> (3 dB)	88%	125%	74%	15.7%
f_0	3.6 GHz	6.15 GHz	7.3 GHz	5.1 GHz
Insertion Loss	-1.15 dB	-1.5 dB	-1.97 dB	-3.83 dB

Table 9.1: Simulated Performance.

The filter was fabricated on Rogers Duroid substrate, $\epsilon_r = 3$ and thickness = 0.76 mm as per the designed highpass and lowpass filter circuits. The bias circuitry used was the same as that of the cascaded coupled lined filters. Moreover, the path to ground for the SIR's is simply a 14 nH inductor (please see Appendix 6 and 7). The pin diodes used were MA4AGBLP912 which were modelled in all the designs using the S2P files to mimic their behaviour. The filter was then measured using a Hewlett Packard 8510B network analyser. The measured performance is contained in **Table 9.2**.

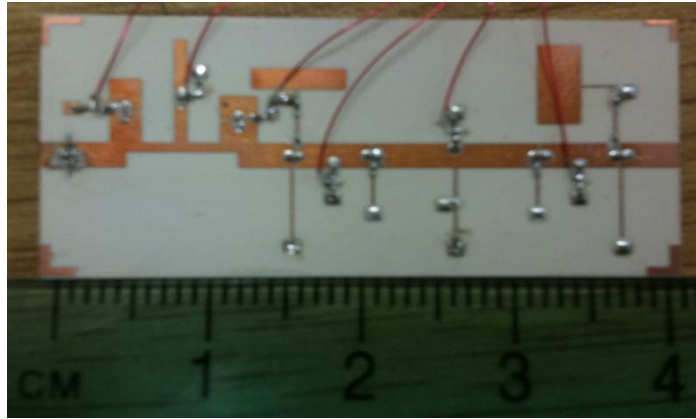
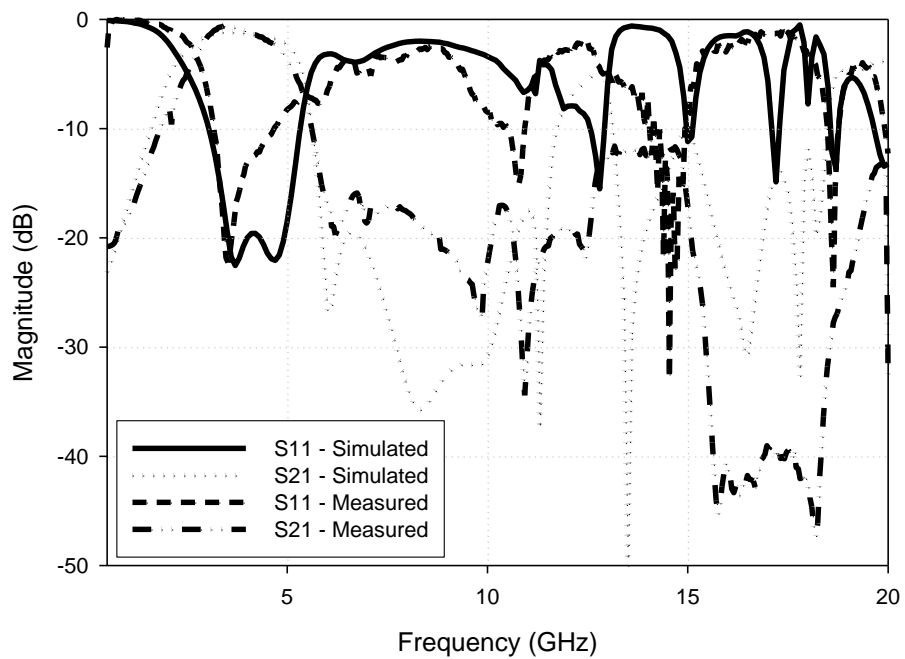


Figure 9.28: Fabricated reconfigurable microstrip bandpass filter

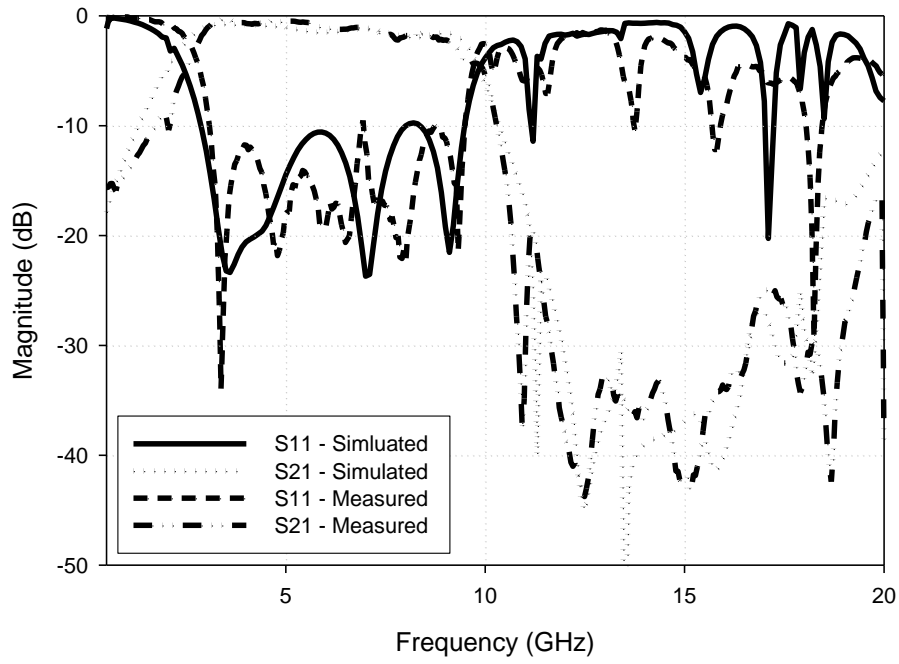
	State 1	State 2	State 3	State 4
<i>FBW</i> (3 dB)	86.9%	123.9%	74.3%	15.7%
f_o	3.7 GHz	6.2 GHz	7.5 GHz	5.2 GHz
Insertion Loss	-1.41 dB	-1.56 dB	-2.01 dB	-3.91 dB

Table 9.2: Measured Performance.

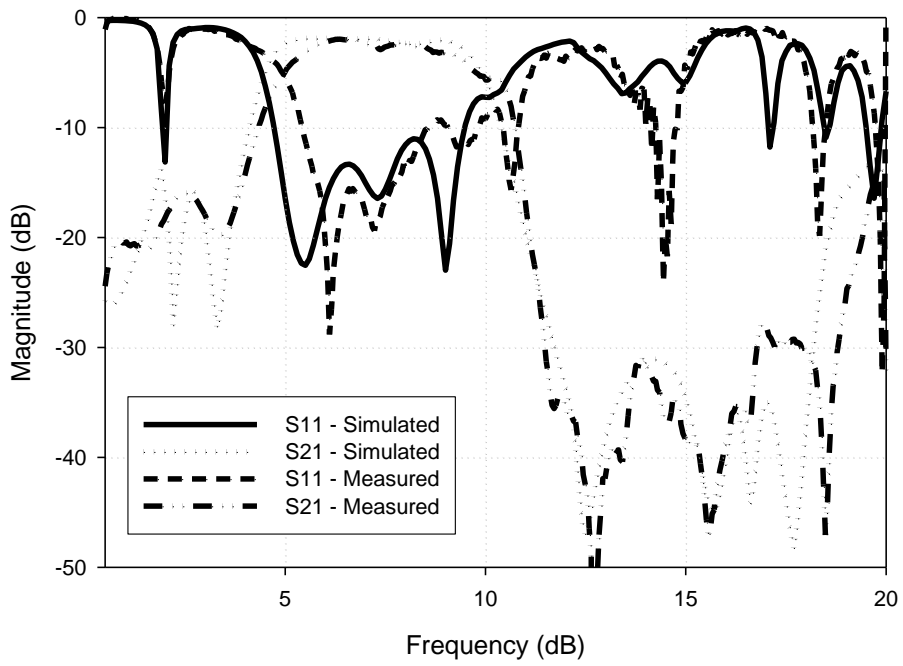
The simulated and measured results were plotted in order to show the comparison between the two:



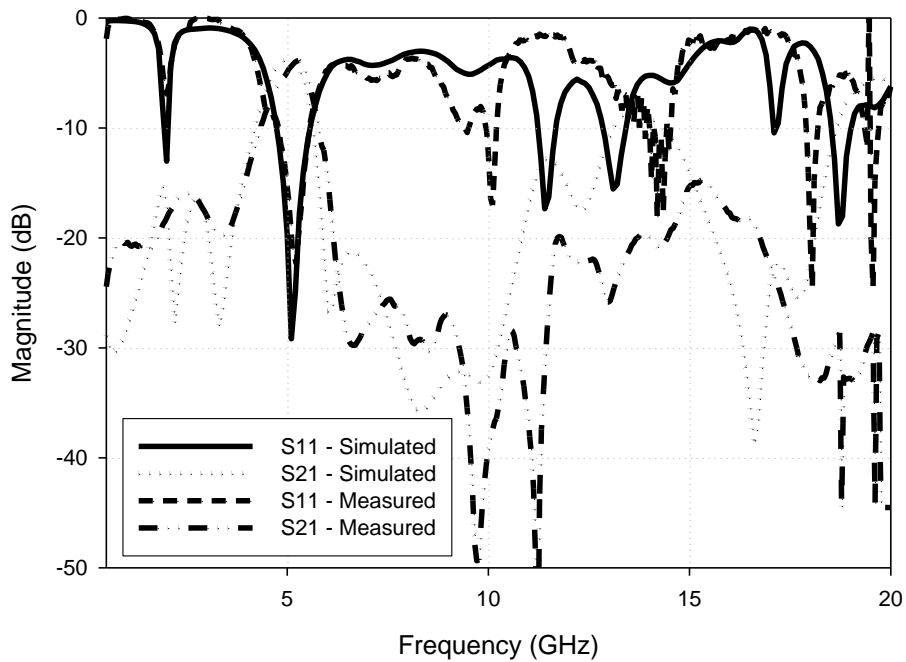
(a)



(b)



(c)



(d)

Figure 9.29: Electronically Reconfigurable Bandpass Filter Response: (a) State 1, (b) State 2, (c) State 3, (d) State 4.

On comparison, the measured responses of the fabricated filter show good agreement in general with the simulated results. There are slight changes in the fractional bandwidths and center frequencies; which is attributed to fabrication tolerances. The losses of the circuit increase in the narrowest band, as was expected [16], most of the issues were caused by the interaction between the highpass and lowpass filter. This interaction seems to be more significant when the combined passband bandwidth becomes narrower. This implies that additional care would be needed when designing a very narrowband state of this type of reconfigurable bandpass filter. The selectivity of each filter needs to be designed such that the interaction is minimal. This being one of the main drawbacks compared to the coupled line filter, where it is easier to reconfigure to lower bandwidths. The issues discussed in earlier sections when analysing the single filters are still apparent when cascaded as expected:

- The small spurious response caused in state two of the lowpass filter. **Figure 9.29 (b)**
- The resonance at 1.6 GHz caused by the interaction of the initially designed filter and the addition of the SIR's. **Figure 9.29 (c) and (d)**

- The two resonances between around 11 GHz to 14 GHz in state 1 of the highpass filter, predominantly the lower of the two. **Figure 9.29 (b)**

9.5) Non – Linearity Measurements

9.5.1) Third Intercept Point

To characterize the nonlinear behaviours of the electronically reconfigurable filter, the same set up from section **5.4.2)** was used to measure the third order intercept point or IP3 and the results are plotted against the separation of the two tones frequencies f_1 and f_2 that are symmetrical with respect to the center frequency of the passband. For this measurement, the two tones input power is 2 dBm and the dc bias current for driving pin diodes on is $I = 20$ mA. It can be seen that this four-state reconfigurable bandpass filter in general has high IP3, although the IP3 tends to be reduced when the fractional bandwidth becomes smaller and for the state that has more PIN diodes switched on.

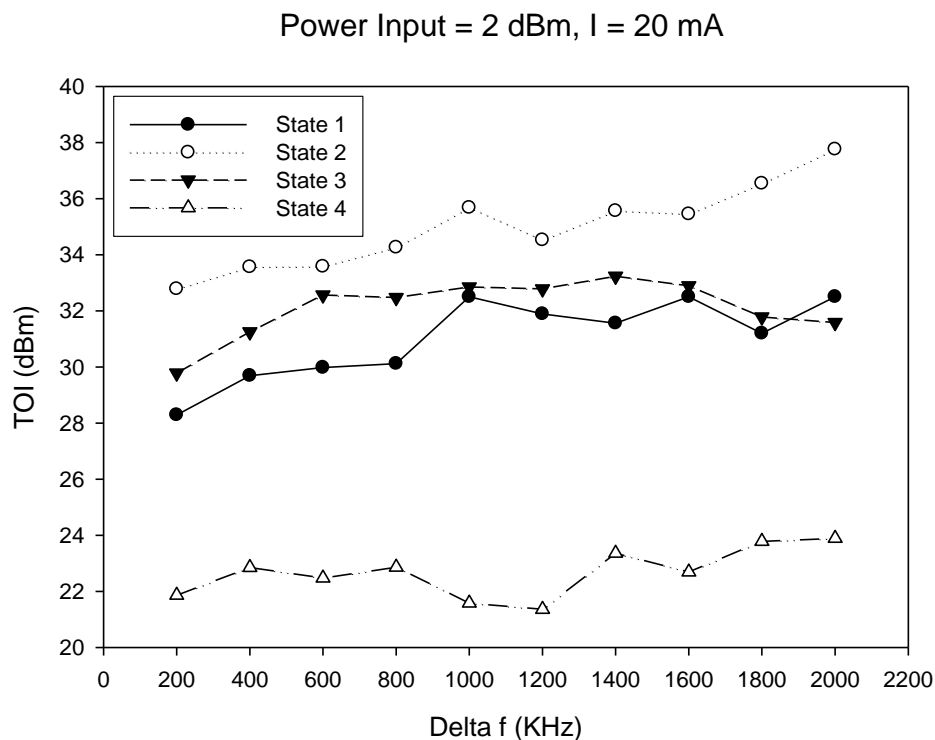


Figure 9.30: IP3 Measurements.

9.5.2) 1 dB Compression Point

The 1-dB compression measurement was also performed using the same set up from section 5.4.1) and the results are shown. Since the pin diodes used in this experiment can only handle a maximum power of 23 dBm, the input power for the 1-dB compression test varies only up to 20 dBm to avoid damaging the pin diodes. As evidence from **Figure 9.31**, the 1-dB compression point is expected to be higher than 20 dBm for all the four states.

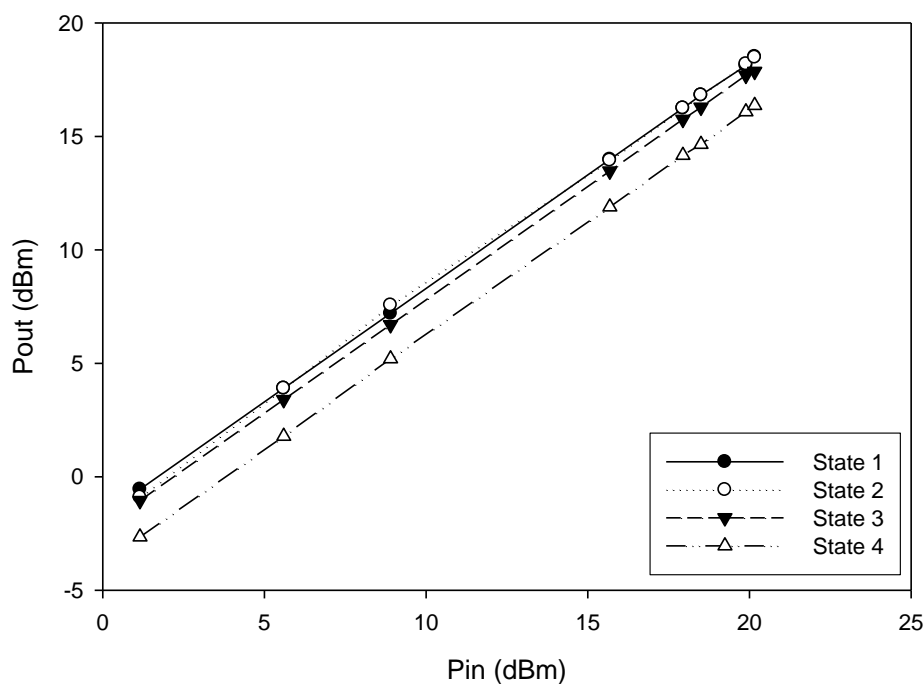


Figure 9.31: 1 dB Compression Measurement.

9.6) Highpass Filter Improved Design

One of the main issues with the bandpass filter is the out of band performance, which is caused by a number of factors; one being the stepped impedance resonators. In order to eradicate these problems, it can be shown that the highpass filter design can be improved. The reason the stepped impedance resonators were added was because of the poor selectivity in the second state due to the transmission zero at DC. The following arrangement neglects the need for the stepped impedance resonators whilst still increasing the selectivity in the second state. This is done by increasing the order of the filter in this state by switching two

shorter short circuit stubs as before, and then switching in vias to the other longer 2.3 GHz short circuit stubs to make them shorter. This meaning that in state 1 the filter has an order of five whereas in state 2 the filter has an order of nine.

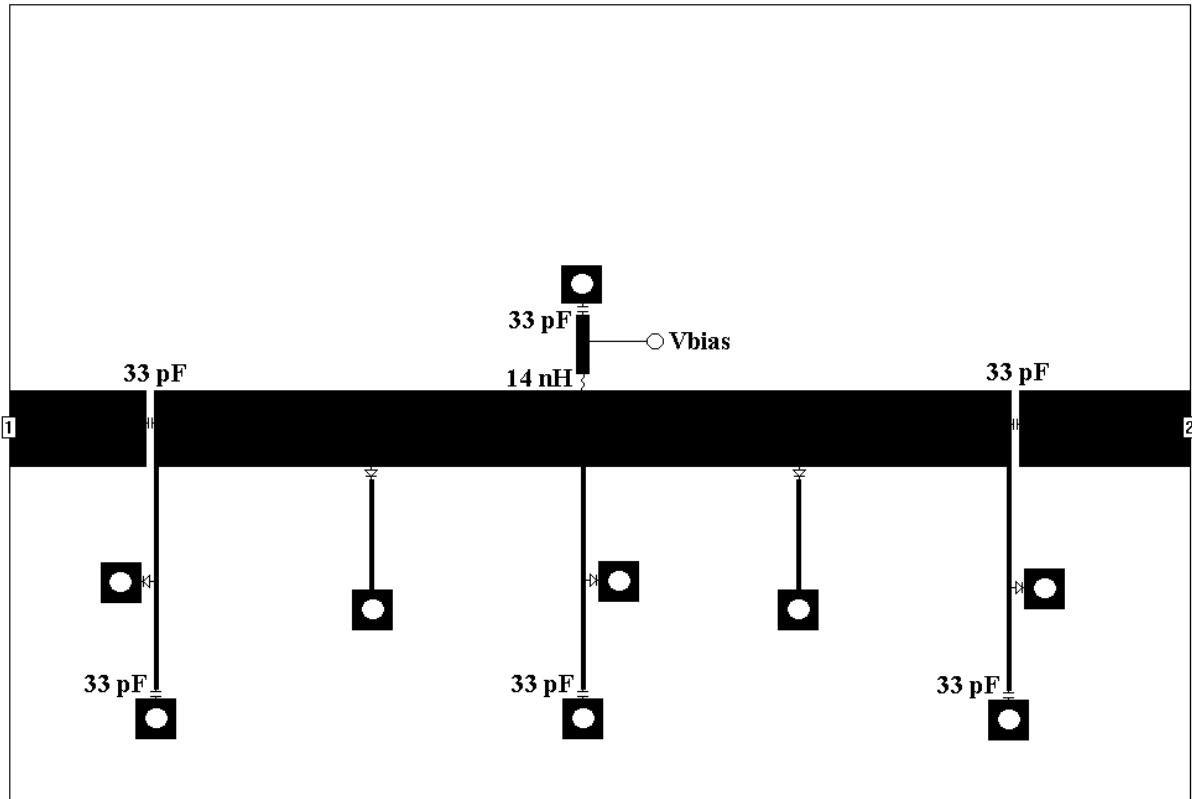


Figure 9.32: Improved Highpass Filter Design.

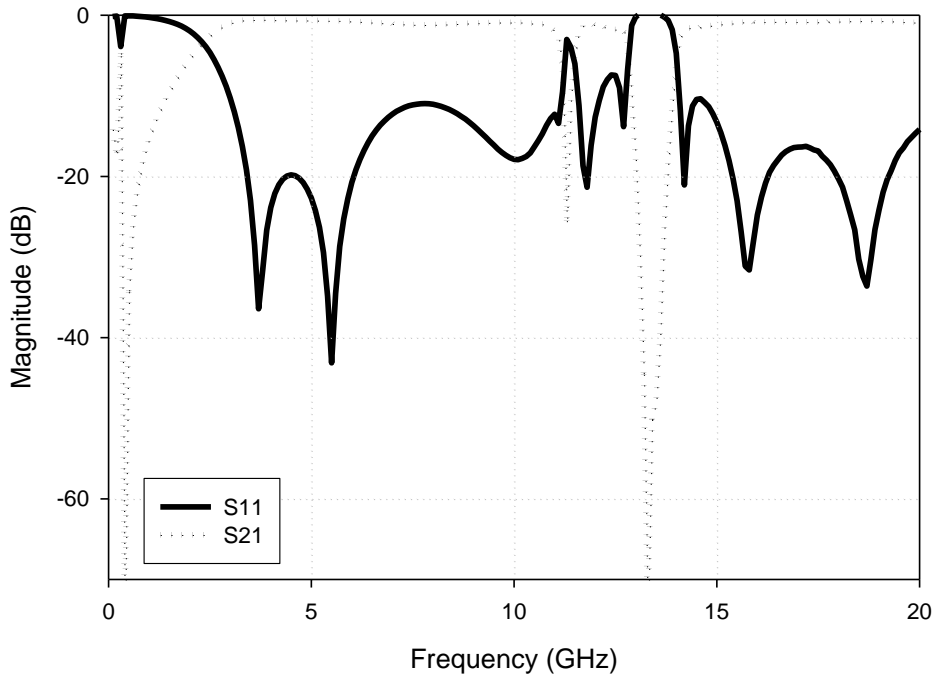


Figure 9.33: Improved Design Simulated State 1.

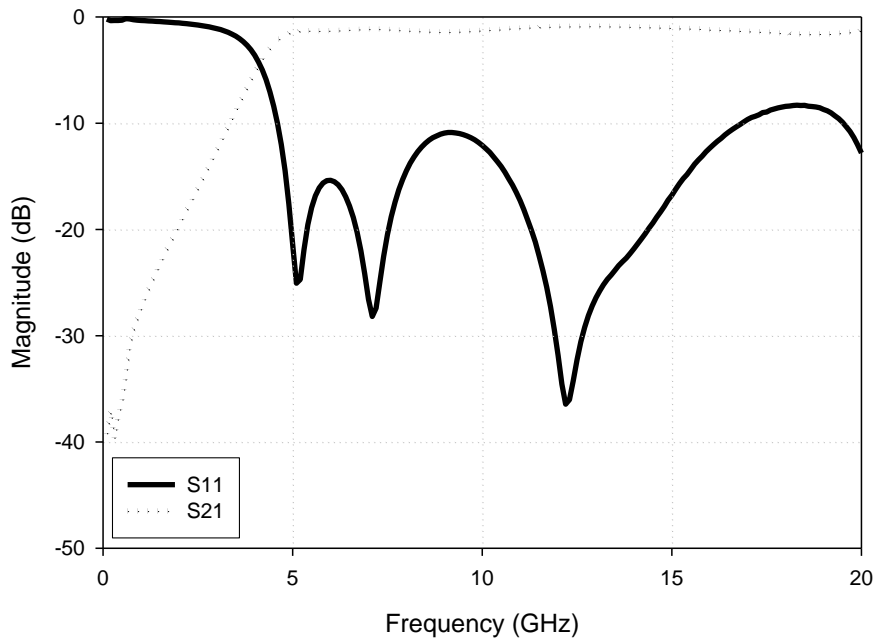


Figure 9.34: Improved Design Simulated State 2.

The filter is switched between the same two states as the previous design with SIR's, but as can be seen there is a much better out of band performance at low frequencies (resonance at

1.6 GHz) and a much wider passband, as compared with the previously designed filter from **Figure 9.11** in state 2. The losses are also better due to the reduced number of components in this design. Referring to state 1 there is still a spike at 11.3 GHz, which as discussed before is due to the isolation of the 4.6 GHz stubs; and can be eradicated by additional pin diodes (see **Figure 9.9**).

9.7) Reconfigurable Filter with New Designed Highpass Filter

It was hoped that when cascading this filter with the lowpass filter designed (as shown in **Figure 9.35**) previously will be improved upon. The highpass section as discussed can be switched between 2.3 GHz (PINs 1 to 5 off) and 4.6 GHz (PINs 1 to 5 on). The lowpass section can be switched between 5 GHz (PINs 6 to 8 on) and 10 GHz (PINs 6 to 8 off). As the results of these combinations, the reconfigurable bandpass filter has four distinct states:

- State 1 (PINs 1 to 5 off, PINs 6 to 8 on)
- State 2 (All PINs off)
- State 3 (PINs 1 to 5 on, PINs 6 to 8 off)
- State 4 (PINs 1 to 5 on, PINs 6 to 8 on)

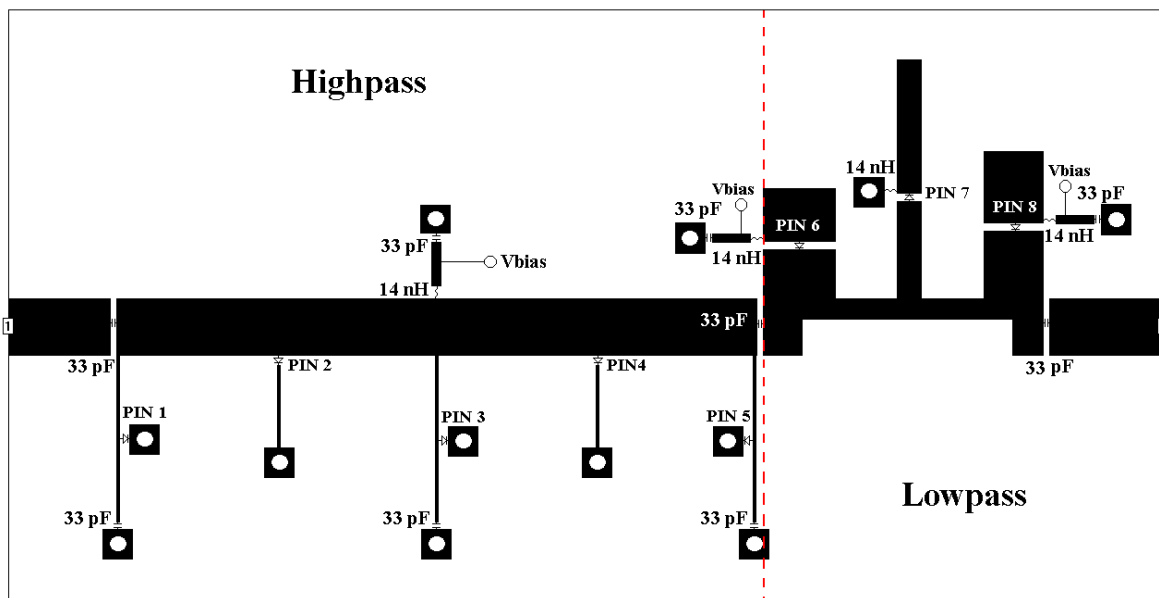


Figure 9.35: Improved Reconfigurable Filter Design.

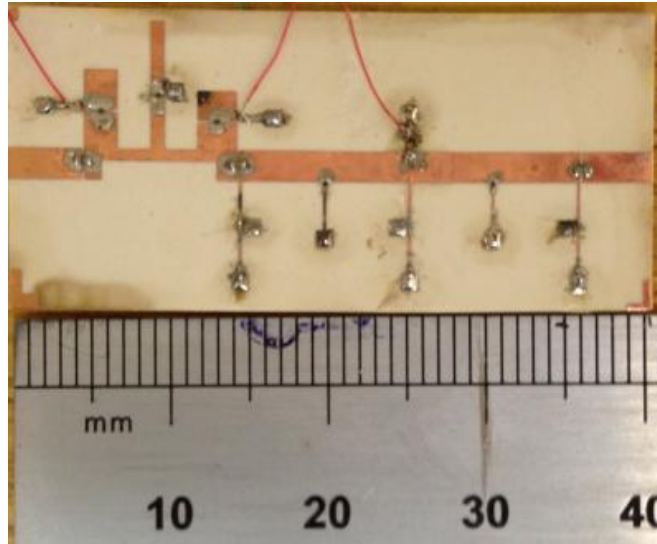
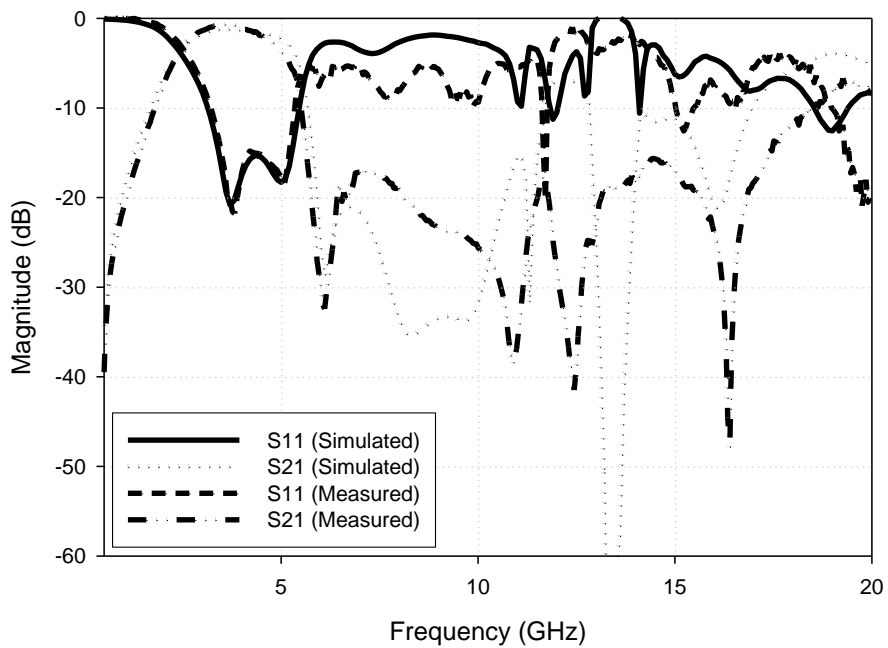
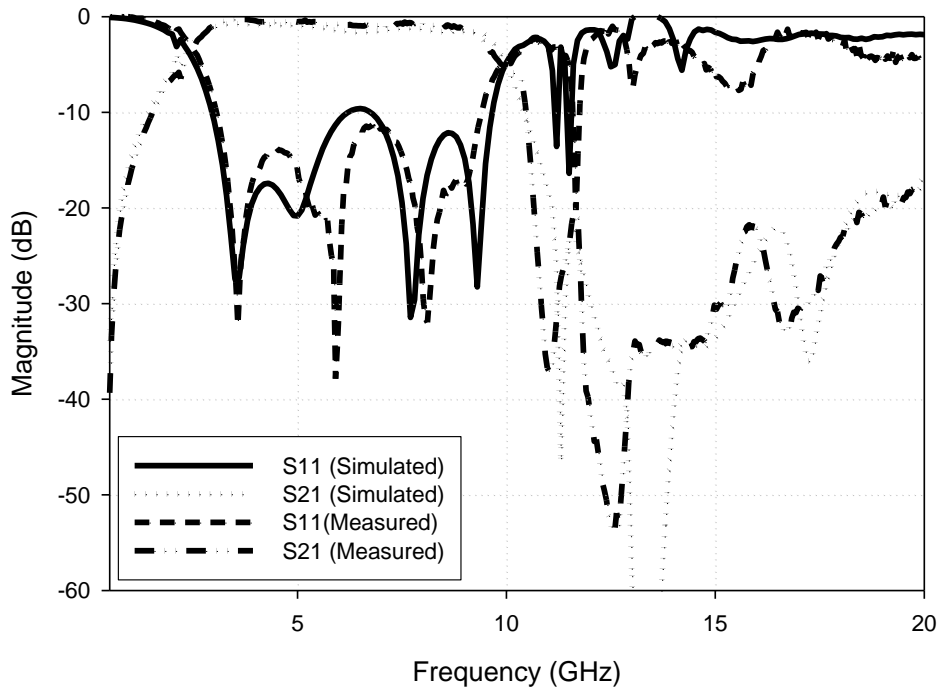


Figure 9.36: Fabrication of New Designed Filter.

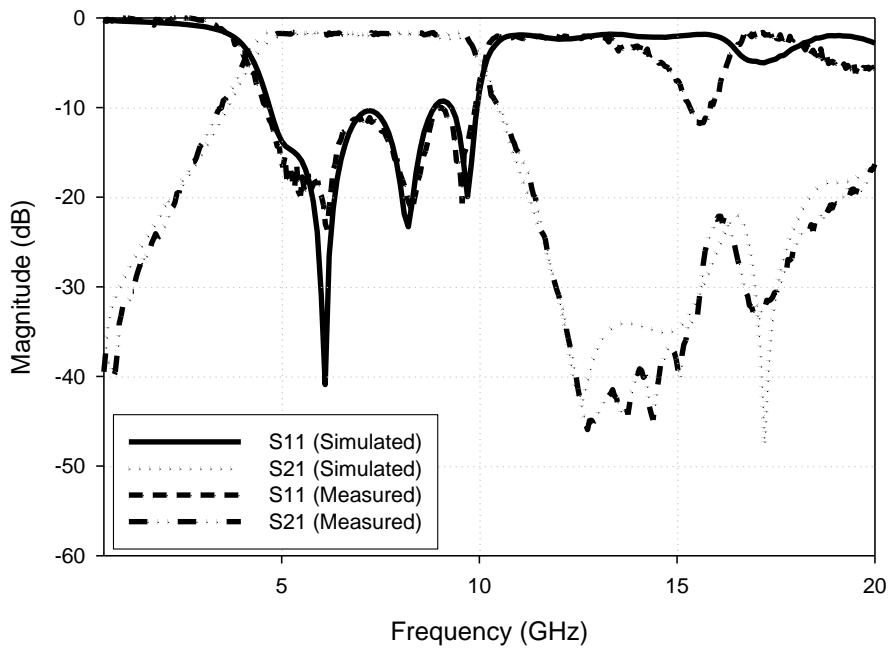
For Comparison the simulated and measured responses are plotted for comparison in each state the simulated and measured performance can be shown in **Table 9.3**:



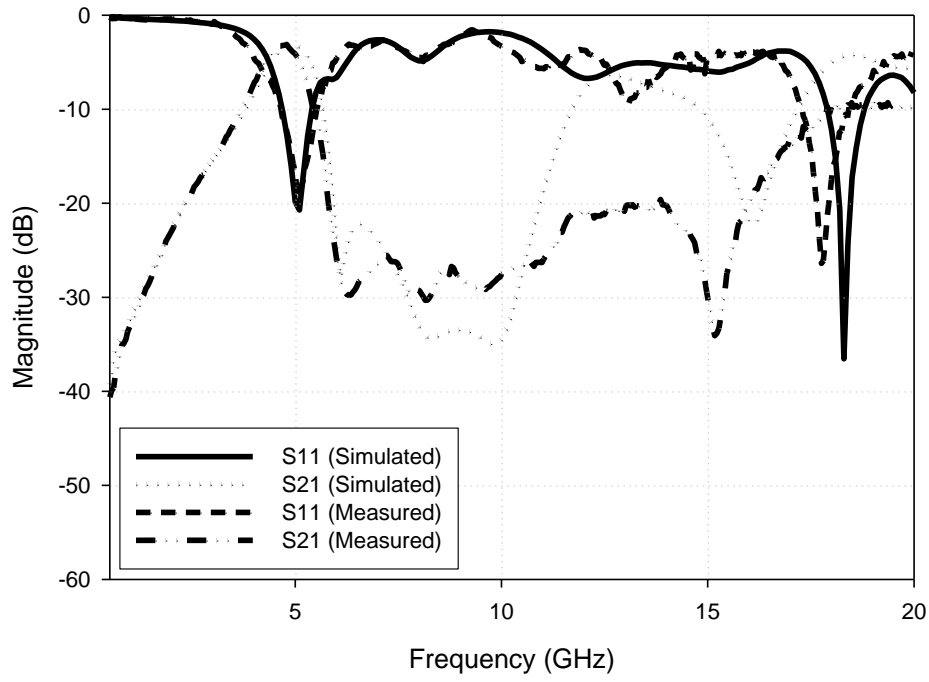
(a)



(b)



(c)



(d)
Figure 9.37: Response of Bandpass filter with newly designed Highpass Filter: (a) State 1, (b) State 2, (c) State 3 and (d) State 4

	State 1	State 2	State 3	State 4
<i>FBW</i> (3 dB)	88%	125%	74%	15.7%
f_0	3.8 GHz	6.2 GHz	7.4 GHz	5 GHz
Insertion Loss	-1.41 dB	-1.56 dB	-2.01 dB	-3.91 dB

(a)

	State 1	State 2	State 3	State 4
<i>FBW</i> (3 dB)	87.9%	123.9%	74.3%	15.7%
f_0	3.8 GHz	6.15 GHz	7.4 GHz	4.9 GHz
Insertion Loss	-1.19 dB	-1.45 dB	-1.93 dB	-3.35 dB

(b)

Table 9.3: Summary of Improved Design Performance (a) Simulated, (b) Measured

The simulated and measured results show good agreement with an improved performance in terms of loss when comparing with **Tables 9.1** and **9.2**. This is due to the reduce number of components. As expected the out of band performance has been improved, with states 3 and 4 showing the greatest improvement. This implies that the isolation of the SIR's was causing an issue as the pin diodes are obviously not perfect switches. The spike seen at 1.6 GHz before is not prevalent; also the stop band in upper frequencies show much less resonances as before with a much smoother transition. Also there is a higher rejection in the new designed filter in state 3 and 4; with the rejection being between 40 and 50 dB as compared with 30 dB. The other issues highlighted before are obviously still seen, i.e. the spike at 11.3 GHz; which as discussed before can be easily shifted up with additional diodes on the 4.6 GHz stubs.

9.8) Summary

In summary, an electronically reconfigurable microstrip bandpass filter was designed by cascading tunable optimum highpass and bandstop (or quasi-lowpass) filters. With each of the two filters having two states the bandpass filter has four states. The design was verified by EM simulation and measurement. In general, the simulated and measured results show good agreement. Many of the issue which arose occurred during the design of the separate filters. The measured reconfigurable bandpass filter shows a wide range of reconfigurability including fractional bandwidths from around 16% to 120% with center frequencies ranging from 3.7 GHz to 7 GHz. The nonlinear measurements have also shown promising results in terms of high IP3 and 1-dB compression points. In general, this filter demonstrates flexibility in the design and gives a good precursor to further develop this type of electronically reconfigurable filter. This is shown with the discussion on the improved highpass filter design, with further work needed to develop this kind of filter.

9.9) References

[1] Z.-C. Hao and J.-S. Hong, "UWB Bandpass Filter using Cascaded Miniature Highpass and Lowpass Filters with Multilayer Liquid Crystal Polymer Technology," *IEEE Trans. Microw. Theory Tech.*, vol. 58, no. 4, pp. 941 – 948, April 2010

- [2] S. Devkumar, C. K. Chakrabarty, "Using Lowpass and Highpass filters to form UWB Bandpass Filter," *Proceedings of IEEE 2008 6th National Conference on Telecommunication and Technologies and IEEE 2008 2nd Malaysia Conference on Photonics, 26th - 27th August 2008, Putrajaya, Malaysia, pp. 162 – 165*
- [3] K. C. Lee, H. T. Su and W. S. H. Wong, "Realization of a Wideband Bandpass Filter Using Cascaded Lowpass to Highpass Filter," *Proceedings of International Conference on Microwave and Millimetre Wave Technology ICMWT 2008, 21st – 24th April 2008, Nahjing, pp. 14 – 17*
- [4] Z. Tie, Q. Dexin, W. Junhui, H. Xing, "A Novel Microstrip Ultra-Wide Bandpass Filter with Highpass Filter and Lowpass Filter," *Proceedings of the 8th International Symposium on Antennas, Propagation and EM Theory ISAPE 2008, 2nd – 5th November 2008, Kunming, pp. 1354 – 1357*
- [5] C.-W. Tang, M.-G. Chen, "A Microstrip Ultra-Wideband Bandpass Filter With Cascaded Broadband Bandpass and Bandstop Filters," *IEEE Trans. Microw. Theory Tech.*, vol. 55, no. 11, pp. 2412 – 2418, November 2007
- [6] G.M. Yang, R. Jin, J. Geng, X. Huang and G. Xiao, "Ultra-wideband bandpass filter with Hybrid quasi-lumped elements and defected ground structure," *IET Microw. Propag.*, 2007, 1, (3), PP. 733 – 736
- [7] C.-L. Hsu, F.-C. Hsu, J.-T. Kuo, "Microstrip Bandpass Filters for Ultra-Wideband (UWB) Wireless Communications," *2005 IEEE MTT-S International Microwave Symposium Digest, 12th – 17th of June 2005, 4 pp.*
- [8] C. Wang, X.L. Guo, W.-X. OU-YANG, Y.-H. Zhang, Z.-S. Lai, "A Novel Tunable Low-pass Filter Based on MEMS and CPW," *The Ninth International Conference on Electronic Measurement & Instruments, ICEMI' 2009, 16th – 19th Aug 2009, pp. 687 – 690*

- [9] G. Ramzi, Z. Hassen, H. Trabelsi and H. Baudrand, "Tunable Lowpass Filters Using Folded Slots Etched in the Ground Plane," *Progress in Electromagnetics Research C*, Vol. 7, pp. 65 – 78, 2009
- [10] R. Zhang and R. R. Mansour, "Novel Tunable Lowpass Filters Using Folded Slots Etched in the Ground Plane," *Microw. Symp. Digest, 2005 IEEE MTT-S International*, 12th – 17th of June 2005, 4 pp.
- [11] J.D. Park, Y. J. Sung, S. H. Lee and Y. S. Kim, "Tunable Bandstop Filters Using Defected Ground Structure with Active Devices," *Microwave Conference Proceedings, 2005. APMC 2005. Asia-Pacific Conference Proceedings*, 4th – 7th Dec 2005, 2 pp.
- [12] S. Lee, J.-M. Kim, Y.-K. Kim and Y. Kwon, "Millimetre-Wave MEMS Tunable Lowpass Filter With Reconfigurable Series inductors and Capacitive Switches," *IEEE Microwave and Wireless Components Letters*, Vol. 15, No. 10, October 2005, pp. 691 – 693.
- [13] M. A. Sanchez-Soriano, J. Hong, "Reconfigurable Lowpass Filter Based on Signal Interference Techniques," *Microwave Symposium Digest (MTT)*, 2011, 5 – 10 June 2011, pp. 1 – 4.
- [14] A. Miller, W. Tang, J. Hong, "Reconfigurable Filter with Frequency and Bandwidth Control Using a Cascaded Highpass/Lowpass Architecture," *IEEE Microwave and wireless components letters* (being reviewed)
- [15] J.-S. Hong and M. J. Lancaster, "Microstrip Filters for RF/Microwave Applications," John Wiley & Sons, Inc., New York, 2001.
- [16] Applied Wave Research Inc, User's Manual, Version 7.5, June 2007
- [17] Sonnet Software Inc, EM User's Manual, Version 12 NY, 2009

Chapter 10: Conclusions and Future Work

10.1) Introduction

This thesis has been based on the development of Electronically Reconfigurable Wideband Microwave Filters. An overview was made of different reconfigurable filters developed in the past and it was apparent that there was a demand and need to develop reconfigurable wideband filters with bandwidth and frequency control. This formed the basis of this research.

One topology which was extensively analysed was the coupled line structure with short circuit stubs being switched on and off for reconfigurability. This concept was then developed for a cascade of coupled line sections using both single layer technology and multi-layer LCP technology, with a mathematical design method being shown. For all the filters designed and tested, IP3 and compression measurements were taken. In addition, the coupled line filter concept was then used to design a multichannel filter with simultaneous control of bandwidth and frequency.

Another topology which was studied was the cascading of a reconfigurable highpass and a reconfigurable lowpass in order to make a reconfigurable bandpass filter. Two separate designs were made, with the second showing superior performance. Again compression and IP3 point measurements were taken.

Publications were submitted for the filters analysed and designed in the main text of this thesis. [1], [2], [3], [4], [5] and [6].

10.2) Single Section Coupled line designs

There were a number of single section designs made; firstly two filters were designed with varying bandwidths one with wideband stubs and one with narrowband stubs. The filter with narrowband stubs could be reconfigured from 16.3% to 35%; the wideband stub filter could be switched from 27.8% to 37.4%. Both filters also showed good linearity performance, with

a 1 dB compression point above 20 dBm. The concept was then further developed to increase the number of states by combining these two filters. The demonstrated filter showed good agreement between measured and simulated results with reconfigurable bandwidths ranging from 13% to 33%. Furthermore, this filter also showed good linearity performance with a 1 dB compression point also above 20 dBm. All designs were documented in [1] and [2] highlighting the design steps in chapter 5.

10.3) Cascaded Coupled line Filters

Industrial applications require high selective filters, for this reason the coupled line concept was further analysed to come up with a design procedure for any number of sections. A multi-section coupled line filter was designed using the single section formulas. The filter could be tuned from a 3 dB FBW = 20% to a FBW = 50% centered at 2 GHz. It was apparent that the performance of the filter was hindered through the use of the impedance transformers. In order to improve this, a design method was developed from Matthaei design theory. There was a comparison made between the direct design equations for a coupled line filter and the new design procedure presented in this chapter. It was found that the modified design approach allows for a coupled line filter to be designed with fewer sections; this being very desirable to in the design of reconfigurable filters. The filter had a tuning range between 26% and 50% ripple fractional bandwidth (FBW) centered at 2 GHz. The reconfigurable filter exhibits insertion losses ranging from 0.57 dB for the widest passband state to 1.95 dB for the narrowest passband state. In order to obtain the even and odd mode impedances a novel manufacturing technique was needed, namely LCP technology. The non-linearity behaviour was very similar to the single section filter with an expected increased loss due to the increased number of pin diodes.

10.4) Frequency and Bandwidth Tunable Filter Using Coupled line

Concept

As mentioned the main aim of this research was to develop a filter capable of both frequency and bandwidth control. In order to do this the coupled line concept was used in its equivalent circuit form. A reason for this was due to the difficulty varying the length of the coupled lines due to the short circuits. This concept was used in order to design a multi-channel filter

that showed a wide range of reconfigurability including fractional bandwidths from around 57.9% to 89.5% with center frequencies ranging from 3.15 GHz to 4.96 GHz. This was done by introducing enough flexibility to alter the lengths of the connecting lines. This was done through setting the connecting lines to 50Ω . This approach seems to show good promise in replacing filter banks in communication and radar systems.

10.5) Cascaded Highpass – Lowpass Filter Concept

The idea behind this type of filter was to have a reconfigurable highpass filter cascaded with a reconfigurable lowpass filter. The two filters both have two states meaning that the reconfigurable bandpass filter has four states. The reconfigurable bandpass filter shows a very wide range of reconfigurability including fractional bandwidths from around 16% to 120% with center frequencies ranging from 3.7 GHz to 7 GHz. The nonlinear measurements have also shown promising results in terms of high IP3 and 1-dB compression points. It was easily seen that this approach is very flexible in the design and shows good promise in the development of reconfigurable filters.

10.6) Future Work

A lot of the sections in this thesis give rise to further work. The first area of interest would be to improve the performance of the coupled line filters by suppressing the second harmonic caused by the unequal phase velocities. There have been many methods in the past [7], and much of the future work would be to investigate these methods and come up with new and improved method. This may also relate to the frequency tunability of the coupled line filter. Although the coupled line concept was made frequency controllable the actual structure is the equivalent circuit. There may be a way to make the coupled line structure frequency tunable, related to the method to suppress the second spurious band.

Moreover, the multi-channel filter which was developed using the coupled line concept can be taken forward by increasing the number of states and hence the number of channels available. Many of the applications mentioned in this thesis would require more than one channel when reconfigurable filtering is required.

The cascaded highpass/lowpass filter also requires further work, namely to improve the out of band performance. Although there has been some work carried and documented in this thesis, it is felt that extra investigation could be carried out to increase the performance of both the highpass and lowpass filters. This would then in turn increase the performance of the bandpass filter. Moreover, other topologies for both the lowpass and highpass filters could be investigated and a comparison could be made between the cascaded highpass/lowpass filter documented in this thesis and the new designs that have been investigated.

As discussed with all the filters in this thesis a lot of the losses and performance are attributed to the fabrication and components used. An in depth investigation could be carried out on the components for potential bias circuits along with pin diodes. Also many of the filters designed above use pin diode technology, the same designs could be carried out using MEMS switches in order to make a comparison with performance. To this end it is obvious the performance of the components being developed are improving all the time and this in turn improve the performance of the reconfigurable filters. In terms of the fabrication it is felt a lot of effort needs to be made in terms of the fabrication technique for LCP for instance. A lot of the time there were many fabrications made before a working filter was produced; this meaning that the fabrication method needs to be looked at in order to make it more producible. Additionally, system integration comes in to play, for how LCP can be integrated onto a PCB for instance i.e. packaging. LCP also give rise to potential more complex reconfigurable filters.

In terms of packaging there is also an issue with temperature behaviour of the filters as they are subjected to extreme conditions in some applications. This then brings into play other factors when considering non-linearity measurements and component selection. The non-linearity behavior would alter depending on the conditions which changes the behaviors of components and makes the packaging process more complicated as more things need to be taken into account.

With all these in mind, these all could culminate into further research/PhD work with a lot of the concepts requiring a very in depth study.

10.7) References

- [1] A. Miller, J. Hong, “Wideband Bandpass Filter with Reconfigurable Bandwidth,” *IEEE Microwave and wireless components letters*, Vol. 20, No. 1, Jan 2010, pp 28 – 30.
- [2] A. Miller, J. Hong “Wideband Bandpass Filter with Multiple Reconfigurable Bandwidth States,” European Microwave Conference, Sep 2010, pp 1273 – 1276.
- [3] A. Miller, J. Hong, “Reconfigurable Cascaded Coupled Line Filter with Four Distinct Bandwidth States,” *IET Microwave Antennas and Propagation*, vol. 5 issue 4, Nov 18 2011, pp 1730 – 1737
- [4] A. Miller, J. Hong “Cascaded Coupled Line Filter with Reconfigurable Bandwidths Using LCP Multilayer Circuit Technology,” *IEEE Transactions in Microwave Theory and Technology*, Vol. 60, No. 6, June 2012, pp 1577 – 1586.
- [5] A. Miller, J. Hong, “Electronically Reconfigurable Multi-Channel Wideband Bandpass Filter With Bandwidth and Center Frequency Control,” *IET Antennas and propagation (in press)*
- [6] A. Miller, W. Tang, J. Hong, “Reconfigurable Filter with Frequency and Bandwidth Control Using a Cascaded Highpass/Lowpass Architecture,” *IEEE Microwave and wireless components letters* (being reviewed)
- [7] R. K. Mongia, I. J. Bahl, P. Bhartia, J. Hong, “RF and Microwave Coupled – Line Circuits,” Artech House, Inc. 2007

Appendix 1: Various LCP Based Circuit Constructions and Fabrication Techniques

ABSTRACT

This paper will discuss a variety of circuit constructions that have been built using LCP (Liquid Crystalline Polymer) as the circuit material. The benefits of LCP in certain circuit constructions and applications will be discussed briefly. The fabrication techniques to build LCP based circuits will be discussed in more detail. The circuit constructions to be addressed will be single sided, double sided, multilayer and rigid-flex using LCP materials. There will also be some discussion on Hybrid LCP circuits, using LCP with a combination of other circuit materials to either enhance electrical properties or make a more robust fabrication model.

INTRODUCTION

LCP materials have been available for many years, however they have not been well accepted in the traditional Printed Circuit Board (PCB) industry, due to the challenges that LCP has presented to circuit fabricators. Consequently, LCP circuits have been relegated to niche applications and manufactured by very special processes. More recently Rogers Corporation has defined LCP Circuit Fabrication guidelines that greatly enhance the reliability of a LCP circuit as well as making the circuit fabrication more robust. Furthermore the circuit fabrication process for more complex LCP circuits is now much better understood and defined.

Specifically this paper will discuss: a) LCP material overview; b) why LCP is used in current applications and the circuit constructions used; c) a detailed discussion regarding the circuit fabrication process and the particulars for multiple types of LCP circuits.

RESULTS AND DISCUSSION

(1) LCP Material Overview

There are currently several kinds of LCP circuit materials on the market. Some have glass reinforcement, some have fillers, and some are uniaxially oriented and other varying properties. The LCP circuit materials that will be discussed in this paper are a more pure LCP substrate that is biaxial oriented, non-glass reinforced and without fillers. This material is offered by Rogers Corporation as the ULTRALAM[®] 3000 product family.

To highlight some key properties of the LCP material:

- Naturally Flame retardant, with UL94VTM-0 rating possible
- Naturally Green, Halogen free material
- Adhesive-less, homogenous substrate
- Capable of very high MOT (Maximum Operating Temperature) rating

- Outstanding electrical performance across a extremely wide frequency range
- Very low outgassing
- Extremely low moisture absorption

Actually the list of key properties could be extended, as LCP substrates offer many advantages. In previous attempts to bring LCP materials to the PCB market, some LCP materials were uniaxially oriented and that gave the material very low tear initiation properties as well as tear propagation. The ULTRALAM[®] materials are biaxial oriented and the tearing issue is greatly minimized. A simple comparison of the orientation properties is given in figure 1.

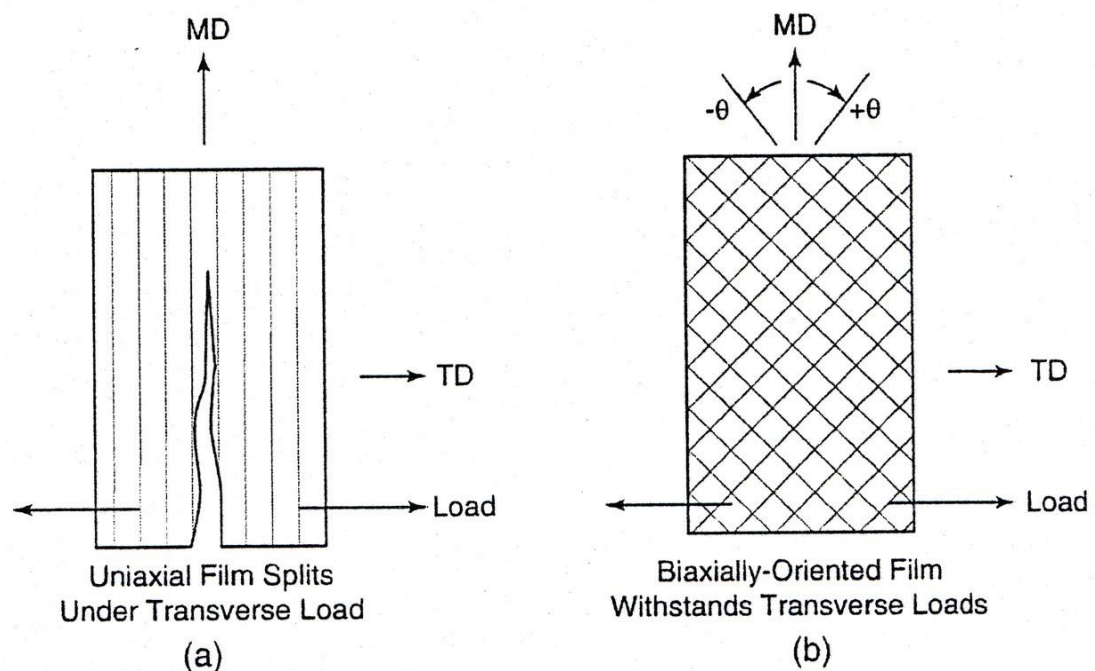


Figure 1. Comparison of uniaxially and biaxially oriented LCP film

The ULTRALAM[®] LCP material is a thermotropic thermoplastic. Its aromatic, tightly packed rod molecule structure contributes to:

- Liquid Crystal behavior
- Order retention in the melt state (good dimensional properties)
- High thermal resistance (RTI = 190°C)
- Excellent barrier properties, similar to glass
- Low dielectric loss at high frequencies
- Excellent TCdk (Thermal Coefficient of Dielectric Constant) properties, typically 24 ppm/°C
- Very high dielectric breakdown voltage ratings (>3000 V/mil)

The excellent electric properties can be seen in figures 2, 3 and 4. Figure 5 will show information regarding the very good barrier properties.

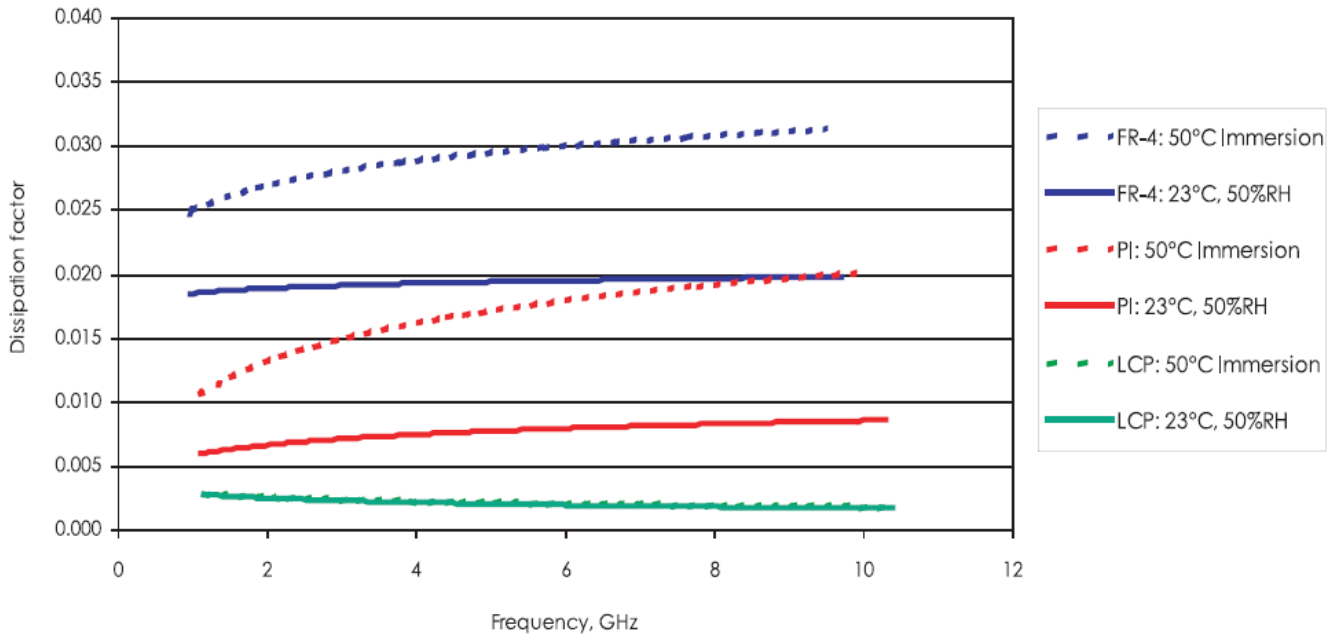


Figure 2. Dissipation Factor vs. Frequency

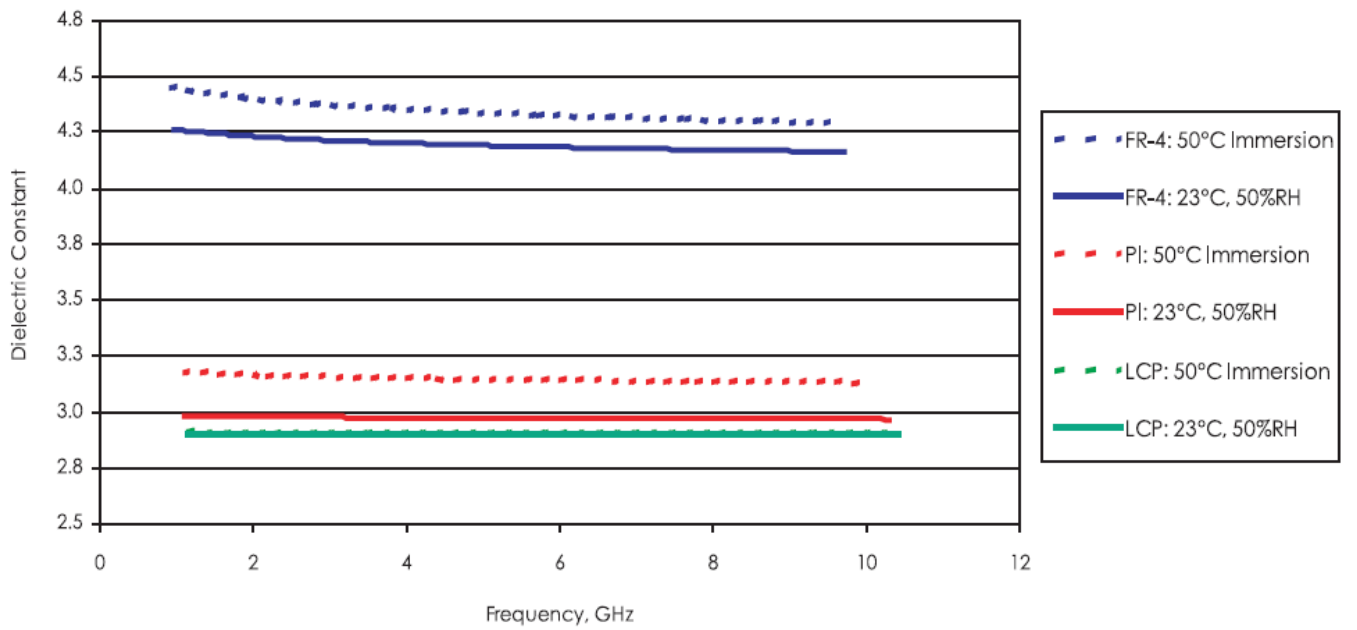


Figure 3. Dielectric Constant vs. Frequency

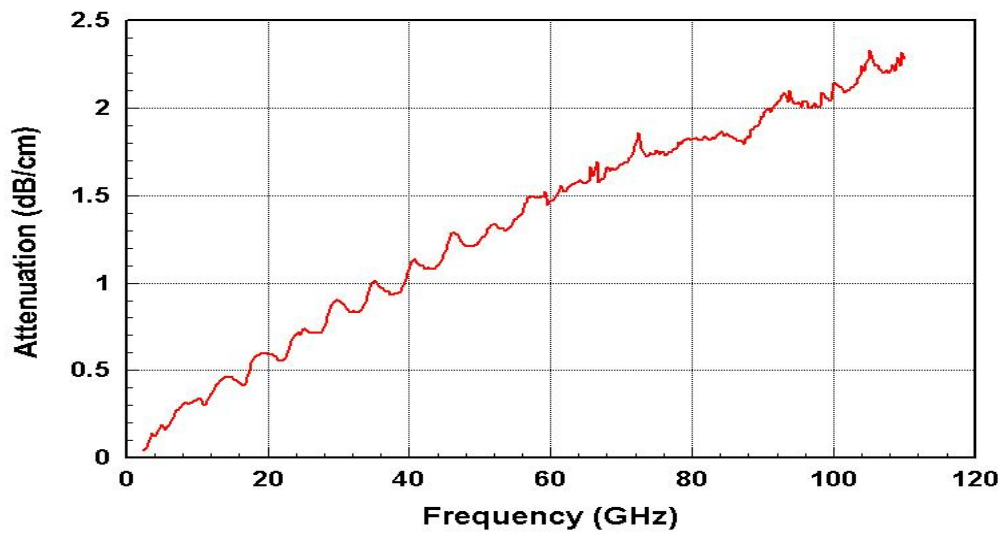


Figure 4. Attenuation vs. Frequency from [1] Georgia Institute of Technology Study using LCP on a thin Conductor Backed coplanar waveguide circuit

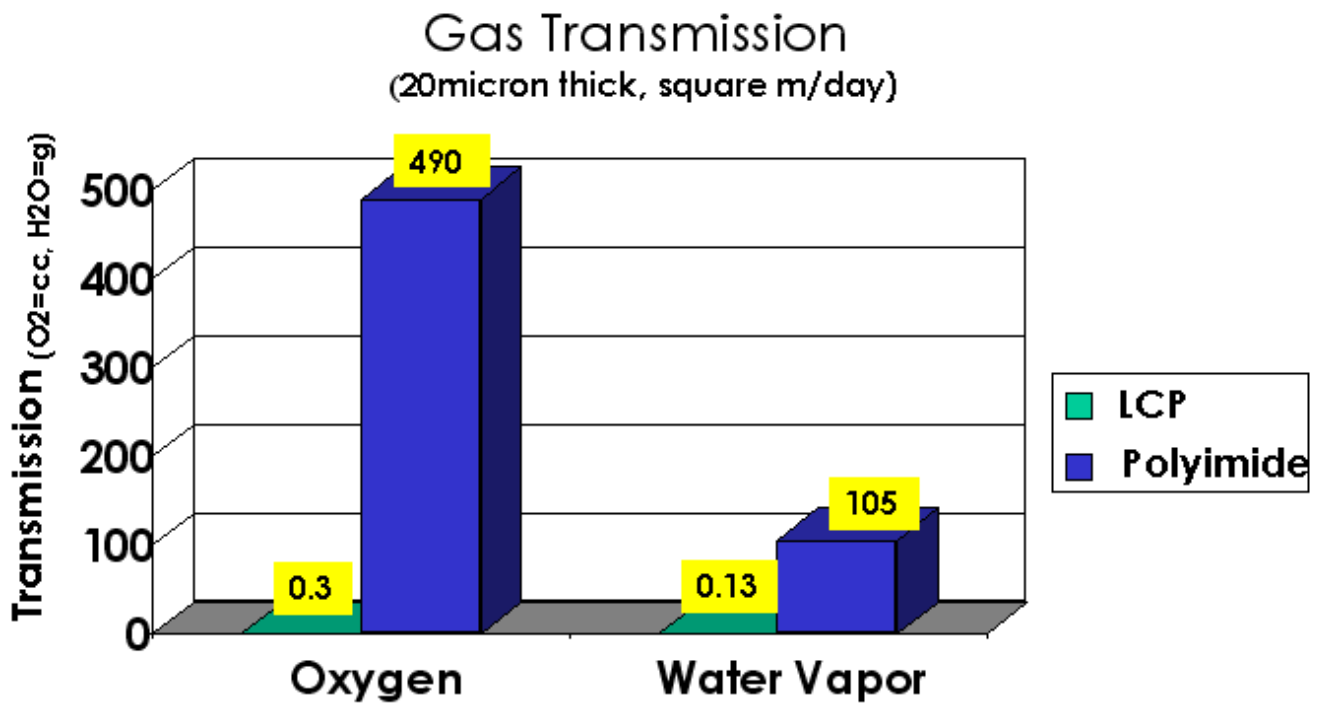


Figure 5. Gas transmission property comparisons

(2) Current LCP Circuit Applications and Constructions

There are several applications currently using LCP materials. Most of the applications are considered niche applications where some unique property of the LCP is superior to other circuit materials. Some applications are patch antennas and antennas that need to be formed. Since the LCP material is considered a flexible circuit material, then bending and forming of

the LCP circuit can be accomplished, within some limits. An example of a flexible LCP circuit is shown in figure 6.

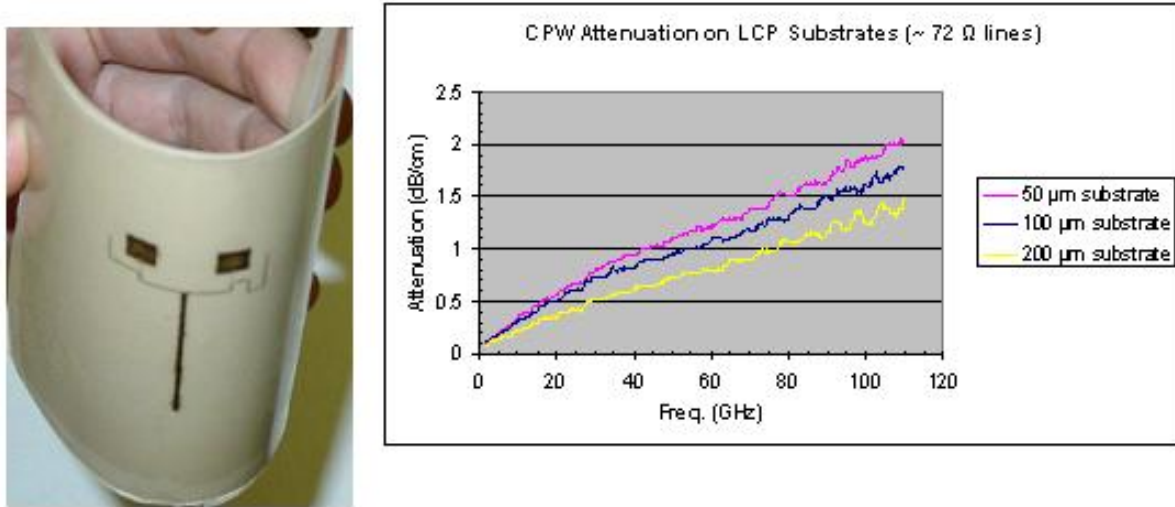


Figure 6. Flexible LCP circuit used as an antenna. Taken from [1].

Also the excellent low moisture absorption is good for antennas that may be in environments where the humidity may have large variations over time. Another application where LCP circuits have been used is in ink jet cartridge applications. The main reason LCP is used here is due to the excellent resistance that LCP offers against these chemically aggressive inks. Also, in one particular ink jet application, the fact that LCP is extremely low in outgassing was beneficial as well. Applications using double sided LCP circuits as filters / couplers have also been successful. The consistent electrical properties over wide frequency range of the LCP materials offers several advantages. There have been applications where a hermetic seal was desired and LCP performs very well due to the low gas transmission rates and low absorption rates of the material. Many different type of transmission line circuits have been used with LCP and these are typically used for thinner and sometimes flexible interconnects. Coplanar and microstrip circuits are easy to fabricate using LCP materials. Stripline or other transmission lines that are multilayer (more than 2 copper layers) are more difficult for the circuit fabrication, however they are feasible. The circuit fabrication of the multilayer LCP circuits will be discussed further and in detail. Applications using a combination of the thin LCP substrate with rigid boards has been done to use the LCP has a high speed / high density micro-via layer. An example of a 75-micron (3mil) lasered via is shown in figure 7.



Figure 7. 75 micron via in LCP circuit.

Lastly, there have been successful builds using a combination of LCP and other High Frequency rigid board material to make a very high performance rigid-flex. The High Frequency Material that was used in most cases is the Rogers RO4000[®] material series. There will be some mention of this circuit fabrication later as well.

(3) LCP Circuit Processing and Fabrication

This section will be broken up into several subsections. The first section will be the preparation, stack-up and lamination for the high temperature LCP pure package process. Next will be drilling, plated through hole preparation and routing will be discussed. Lastly a short section on general processing guidelines will be given.

(3.a) Preparation for LCP High Temperature Lamination

Please refer to table 1 for preparation of the inner layer or single sided materials for LCP lamination.

Image pre-clean	Conveyorized chem clean and microetch. Mechanical scrub not recommended.
Resist lamination and image	Standard process for flex layers
Develop	Standard aqueous or semi-aqueous developers
Etch	Ammonical or cupric chloride If leaders needed, use small pieces of tape, not one long strip
Resist Strip	Standard aqueous strippers If leaders are used - must double pass, changing tape locations, to insure complete resist removal
Microetch and acid wash (no oxide at this time)	40μ" to 60μ" – micro-roughening (persulfate microetch) to promote adhesion, followed by 4 to 5 minute soak in acetic or 10% sulfuric acid. Triple rinse in cascading DI water rinse
Bake layers and bondplies	2 to 4 hours at 250F – suspending or supporting etched layers vertically in stainless steel racks is preferred. Bondplies can be stacked but slipsheeted to allow proper venting.

Table 1. Preparation of inner layer or single sided materials for LCP High Temperature Lamination

There has been conflicting information regarding the use of alternative oxides on the laminate materials, prior to lamination. At this point, it has been found that a good microetch and a clean circuit will yield good results if the lamination cycle is done properly.

Note: The acid wash mentioned above is recommended to insure proper neutralization of the dielectric following photoresist stripping. LCP bonding films do not need to be exposed to

this wash, but should be included in the subsequent moisture bake. If the bakes are done with the circuit material lying down in an oven then clean interleaf material should be used between the layers of circuit materials being baked.

(3.b) Lamination stack-up for LCP High Temperature Lamination

In the stack-up area all materials should be kept as clean as possible and free of debris. During stack-up each circuit material, lamination material, stack-up table and equipment should be continually cleaned of debris with a tacky roller. Avoiding foreign material in the high temperature lamination is paramount.

Multiple plies of LCP bonding film should not be stacked on top of each other to increase dielectric thickness between layers. If an increase in dielectric spacing is required, alternating plies of bonding film and fully etched LCP core materials should be used to achieve the desired thickness. All LCP circuit materials should be completely free of any photoresist residue, chips, flake-off, chemical contamination and markings or inks.

In regards to the lamination book shown in figure 8, FiberFrax® press pad material has been used successfully and can be external, or internal to the caul plates as shown in the drawing. Dummy (non functional) panels should be used as shown and will need to be a material that can withstand the high temperature lamination. The skived PTFE should be 0.005” thick or thicker. Some variations of this stack-up are shown on additional figures.

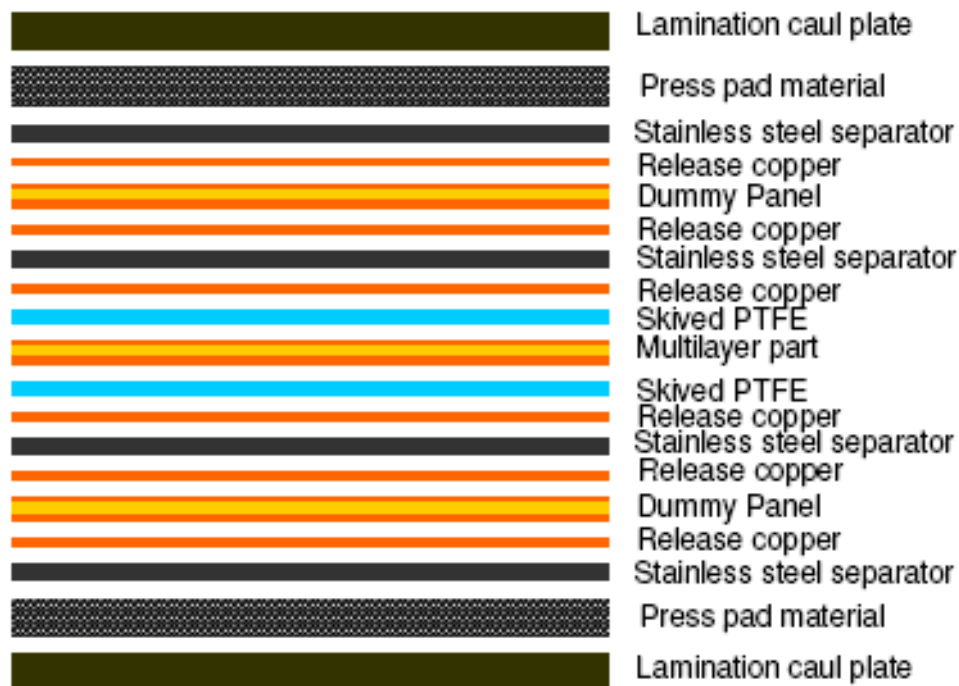


Figure 8. Lamination book stack-up for high temperature LCP lamination

The use of conformal materials in the lamination book can be very beneficial to adequately distribute pressure as well as dealing with circuit designs with low pressure areas that may be difficult to fill. These conformal materials are typically added sheets of Teflon® or Teflon® based laminates.

If dimensional stability is important then custom lamination plates should be used with as many tooling holes that can be used throughout the processing panel. Another technique that has been shown to be very effective in controlling dimensional movement involves the use of a soft, room temperature-conformable material, such as undensified RT/duroid[®] 5880 paper, against the multilayer part,

LCP material can have some outgassing at the lamination temperatures. Due to this a good venting pattern around the border is important. A recommended border pattern is a dot pattern that does not align in the z-axis. This pattern is shown in figure 10. Also dummy holes should be utilized to allow venting during lamination. The tooling holes previously mentioned to help improve material movement, can also help the venting situation during lamination. Considering the outgassing concern, an efficient vacuum assist system during lamination is critical.

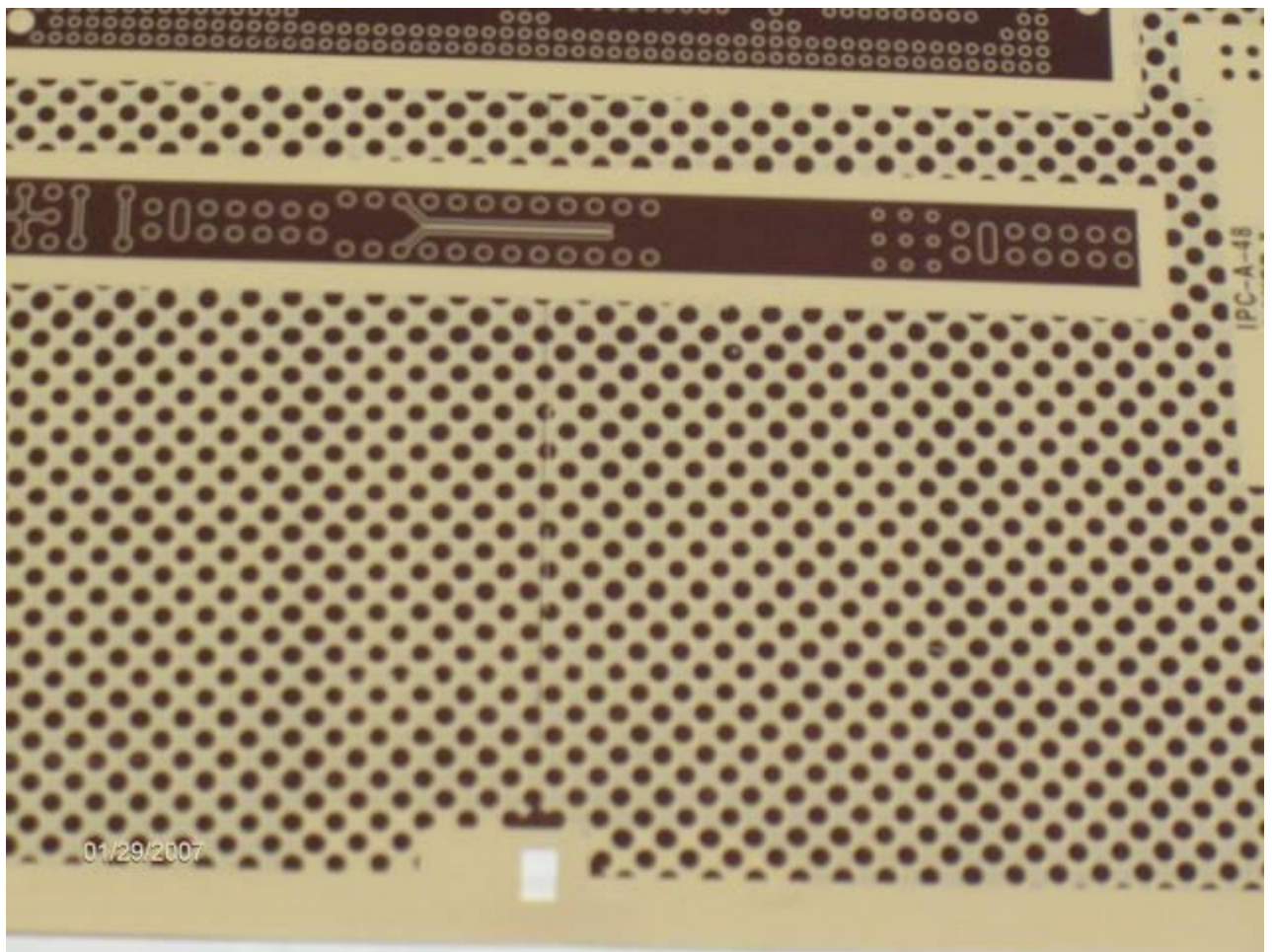


Figure 9. Good border pattern for LCP inner layers. Dots must not align in z-axis.

(3.c) LCP High Temperature Lamination

The following are the basic lamination steps: draw vacuum, close press with minimum pressure (preferable < 50 psi), platen temperature set to 260°C (500°F), book to ramp at 3° - 4°C / min. and hold 1 hour after material has reached 250°C (482°F). Next increase the platen temperature to 282°C and increase pressure to 300 psi. After product has reached 280°C maintain within 280°C (536°F) and 285°C (525°F) for 30 minutes. Cool down at -3° to 4°C /min. A representation of the lamination cycle is shown in figure 11.

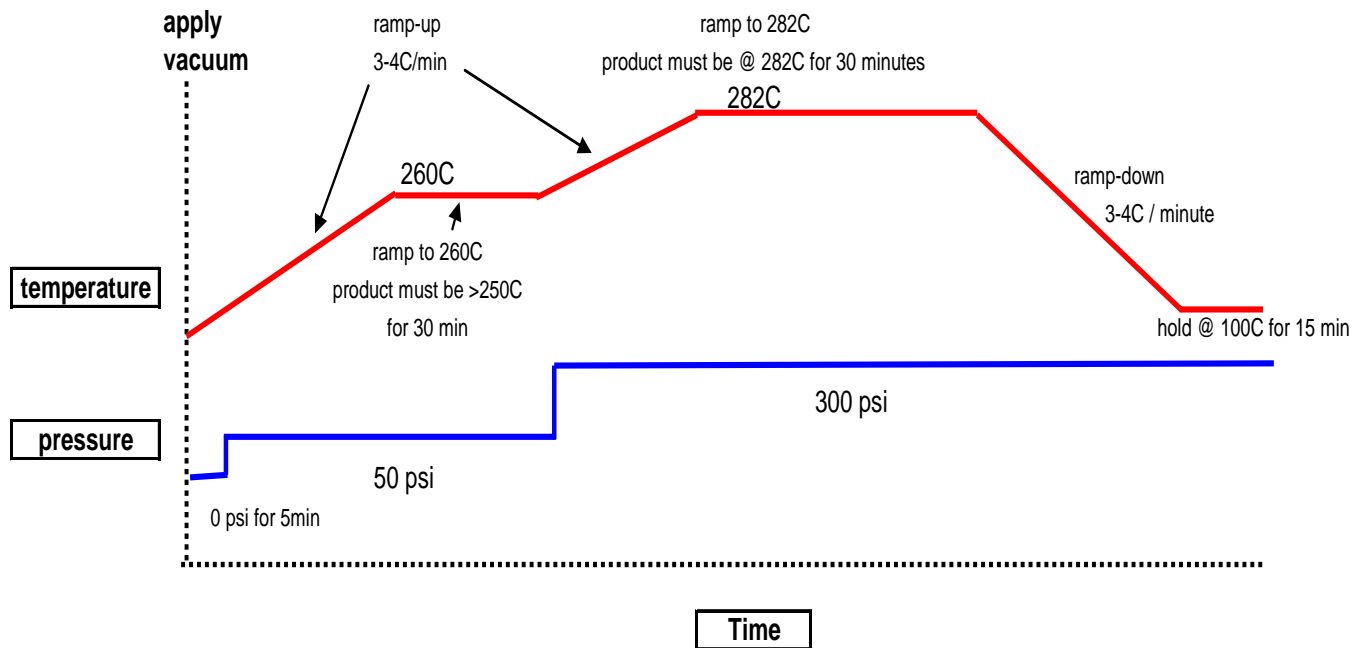


Figure 10. High Temperature LCP lamination cycle

(3.d) Drilling Through Holes in LCP Circuit Materials

The main consideration regarding drilling LCP circuit material is to minimize heating during the drill operation. LCP is a thermoplastic and the drilled hole walls can be “glazed” by melting due to overheating at the drilling operation. There are many variables to consider and this paper will give a starting point for parameters to evaluate. These parameters should be relatively successful for most circuits however some fine-tuning will probably be necessary.

- Drilling LCP Circuit Materials:
 - 0.001” to 0.002” chip load
 - 200 to 500 SFM
 - Peck drilling may be necessary for small holes or high aspect ratio’s. Maximum peck depth is 0.015”
 - For holes > 0.008”, rigid entry and exit material are needed
 - Barrier materials on small holes may cause excessive heat buildup

(3.e) Plated Through Hole Preparation for LCP Circuit Materials

The preparation of the drilled hole for plating vias can be effectively achieved by using mainly two different methods. Initially the drilled hole must be drilled clean and without smear. Then a hot caustic process or a special plasma process can be used to achieve the desired roughening and wetting needed for subsequent metalizing. The standard PCB permanganate process has no effect on the LCP circuit materials. A three-step plasma process is shown in table 2 and has been proven to be very effective for plated through hole preparation.

Segment	Gas Type, %				Chamber Vacuum, mTorr	Chamber Temperature, °C	Segment Time, min
	CF4	O2	N2	H2			
1	0	80	20	0	250	70	45
2	10	80	10	0	240	105	25
3	0	0	90	10	250	105	60

Table 2. Three step plasma process for plated through hole preparation. RF power should be 6000 watts. Information was developed in conjunction with March Plasma Systems [2].

An alternative process, which can be used, is similar to what has been used for etching LCP connector housings. Also there is a very similar process that has been used to etch polyimide films as well. The hot caustic process follows:

- 1 min. in conditioner to minimize surface tension
- DI water rinse
- 2 to 3 minutes in 30% to 35% KOH held at 90°C (194°F).
- 1 min. hot DI soak (55°C, 130°F)
- DI rinse
- Dry

(3.f) Plated through hole considerations

A low to medium electroless copper deposition should be used to avoid stresses inherent in “high” deposition rate systems. An electrolytic copper flash should follow this. Palladium-based and graphite-based direct metallization systems have also be used successfully, also followed by an electrolytic copper flash.

Standard outer layer imaging and copper plating can follow. LCP has been shown to be compatible with most common metal finishes such as HASL, ENIG and immersion silver.

(3.g) Routing LCP Circuit Materials

Due to the thermoplastic nature of the LCP materials, the routing conditions will be similar to that of other thermoplastic substrates such as PTFE materials. The general NC routing conditions are:

- Use a 2 fluted spiral-up end mill
- Rigid entry and exit materials
- Use paper interleaf between the entry / exit materials and the LCP circuit materials
- 150 SFM
- 0.001” to 0.002” lateral chip load

(3.h) General Processing notes for LCP Circuit Materials

LCP materials are generally soft and thin, so many of the standard flexible printed circuit practices should be used. Dimensional stability and scaling will be similar to flexible circuit substrates with comparable thickness. LCP materials are extremely low in moisture absorption, which means that some standard bake cycles may or may not be necessary. It is always safe to error on the side of baking. In general baking should be done prior to the high temperature lamination. After the high temperature lamination is done, the circuit should be completely dry internally and will not uptake moisture; this means that baking after circuit lamination can be eliminated, however this should be done with caution and experimentally initially. Laser ablation can be done with LCP materials and in general YAG and CO₂ have yielded good results. Typically more hits and shorter duration is necessary to minimize sidewall melt. Since the LCP materials are extremely chemically resistant most final metallization processes have been done successfully and without degradation to the material.

(4) Various LCP Circuit Constructions and Specific Processing Needs

This section will have subsections, which will detail several different types of LCP circuits. Beginning with the more simple variations and evolving to the more complex. Single sided LCP circuits will be discussed initially and then double sided and multilayer circuits. In the multilayer section there will be discussion on pure LCP multilayer circuits and hybrid multilayer circuits using a variety of circuit materials. Lastly rigid-flex constructions using LCP will be discussed.

(4.a) Single Sided LCP Circuit Constructions

Typically single sided circuits using LCP laminate can be fabricated like any other type of flexible circuit material. If the circuit needs to have the conductors covered and protected then most standard flexible soldermasks will adhere well. If a coverfilm is desired, then most standard flexible coverfilms can be used as well. LCP has extremely good electrical properties, however most flexible soldermasks and coverfilms do not and if that is a concern then a LCP film can be used as a coverfilm with some provisions.

Using LCP as coverfilm material will require the special high temperature lamination cycle discussed in section 3.a through 3.c. One item of concern is that if coverfilm openings are necessary to access the copper layer, then the flow of the LCP during lamination cannot be easily controlled and the opening size will vary greatly. If LCP coverfilm openings are necessary it is best to laminate a full sheet of LCP as the coversheet and then later use laser ablation to make the openings. And since venting is very important during the high temperature lamination, dummy holes and smaller pieces of coverfilm should be used.

Another method is to laminate the full LCP sheet and use a process that has been used in the flexible circuit industry to chemically etch through a coverfilm. Basically after the LCP coverfilm has been laminated, apply a photoresist, expose the openings desired and use the process mentioned in 3.e. for chemically etching the LCP with the KOH. Most photoresist cannot withstand the KOH for more than 2 minutes, so a higher concentration and higher temperature is used in the process to attack the LCP faster. Typically 45% KOH at 104°C (220°F) is used and the etch rate is about 25µm (1mil) of LCP per minute. Also after the DI rinsing process a microetch is used to attack any weak bonded LCP to the copper in the etched areas.

If a standard flexible coverfilm can be used, then normal processing should be done with a few exceptions. The LCP material is a very good barrier and will not allow the coverfilm adhesive to “breathe” during lamination. So it is recommended to have many dummy holes put into the coverfilm, outside of critical areas to allow more area for venting during lamination. Also the coverfilm should be cut up into smaller pieces if the part size on the panel would allow. Vacuum assist is highly recommended during lamination.

(4.b) Double Sided LCP Circuit Constructions

Most double sided applications are using plated through hole technology. If the circuit is a non-plated through hole double sided circuit, then the provisions discussed as a single sided LCP circuit apply; with the addition of the other copper layer and covering consideration.

If the circuit is a double sided plated through hole application then sections 3.d and 3.e will apply for the plated through hole process. If the application is a microstrip or grounded coplanar transmission line, these are typically not very sensitive to the cover layers. If that is the case, then a traditional flexible soldermask or coverfilm is acceptable. If the cover layer is critical for electrical performance then LCP can be used as a coverfilm as detailed in section 4.a. for single sided circuits.

(4.b) Multilayer LCP Circuit Constructions

There have been many different types of multilayers built using LCP. As a general statement, the circuit fabrication difficulty will increase as the copper layer count increases. Also some hybrid multilayers using alternatively bonding materials can greatly ease the circuit fabrication process and that will be discussed later in this report.

As previously mentioned, cleanliness is paramount in the LCP multilayer build. This is true because the high temperature lamination that is necessary for the LCP multilayer will typically cause foreign material to outgas or do something that is not desired during the high temperature lamination.

As with anything in circuit fabrication it is always best to keep the construction as simple as possible. For a three-layer LCP circuit the desired construction is shown in figure 12.

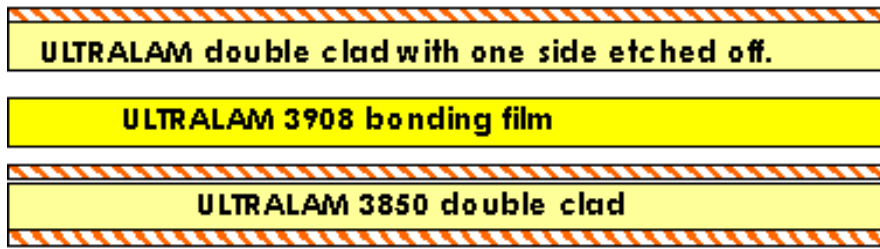


Figure 11. Recommended three layer LCP circuit construction

All of the process recommendations mentioned in sections 3.a through 3.e are mandatory to adhere to in processing any pure LCP multilayer circuit.

The next multilayer to discuss will be a 4 layer or greater circuit. There are obviously several ways to build these types of circuits regarding circuit construction. Again keeping the construction as simple as possible will yield much better fabrication results. For a typical 4 copper layer circuit, the construction shown in figure 13 is recommended.

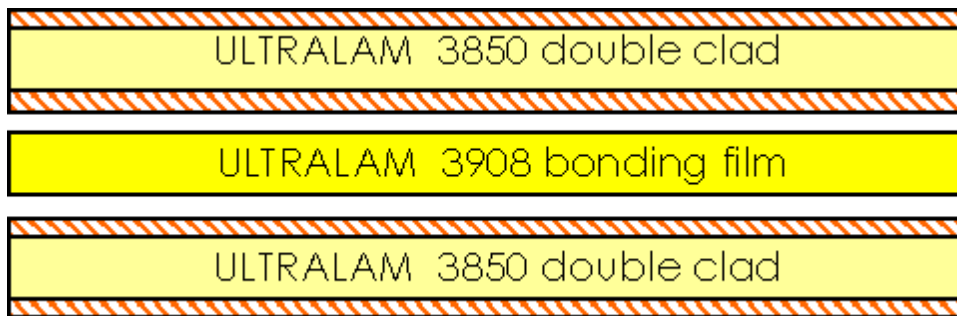


Figure 12. Typical 4 copper layer LCP circuit construction

If the thickness between the layer 2 and 3 copper layers are needed to be built up, then using multiple ply's of LCP bonding film next to each other is highly discouraged. An example of a 4 layer with additional thickness requirements between layers 2 and 3 is shown in figure 14.

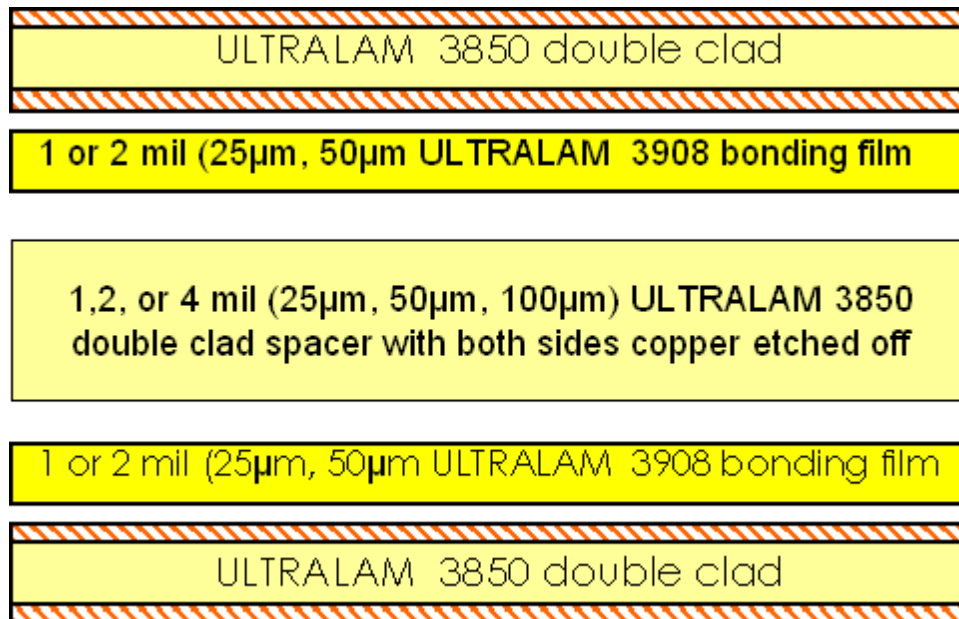


Figure 13. Example of a 4 layer LCP circuit with additional thickness requirements between copper layers 2 and 3.

(4.d) Rigid-Flex LCP Circuit Constructions

A high performance rigid-flex using LCP materials have been built at multiple sites. The rigid-flex typically uses the LCP material for the flexible portion, in combination with high frequency rigid board materials. What is known and been done to-date is the combination of the ULTRALAM[®] 3850 and Rogers RO4350[™] core materials and using the Rogers RO4450[™] prepreg. The electrical performance of this type of circuit should be far superior from traditional rigid-flex at higher frequencies. Also in applications where moisture absorption is a concern, then this type of rigid-flex will have properties that surpass any traditional rigid-flex construction.

As for the fabrication of the high performance rigid-flex, there are several considerations. The preparation prior to lamination noted in 3.a should be performed. The use of plasma to effect the LCP surface prior to lamination is not recommended at this time, due to that surface having the mirror image of the copper that was etched away to generate the circuit. This surface will provide some mechanical tooth for an improved bond. However in the future other copper types may be used with the LCP laminate which will have a much smoother surface for improved electrical performance and in that case a plasma cycle to roughen the surface may be beneficial. The specific type of RO4450[™] prepreg that should be used is the RO4450F[™] prepreg which will have improved flow properties and still maintain excellent electrical performance. The processing recommendations and the lamination cycle for the RO4000[®] materials can be found on the Rogers Corporation website. After the lamination, the drilling and plated through hole parameters should be used per the previously mentioned information in sections 3.d through 3.f in this paper. The following steps of circuit fabrication will be more traditional PCB processing, keeping in mind the issues that are dealt with any rigid-flex fabrication.

(4.e) Hybrid LCP circuits

There has been limited experience with hybrid LCP circuits thus far. In theory there are many advantages to explore this topic in further detail. The following discussion will give limited information regarding known LCP hybrids as well as hybrids with materials that should interact well.

There have been many different types of adhesive evaluated regarding general bonding to the LCP materials. By the flexible nature of the LCP materials, most of these adhesives are from the flexible circuit industry. In general the acrylic adhesives yielded relatively good results and some epoxy based adhesives were slightly better. A phenolic butyral adhesive was attempted and yielded very poor results. The epoxy adhesive of choice would be the R/flex JADE™ J version, for several reasons. This adhesive will match several properties of the LCP, such as: halogen free, lead-free capable, flame retardant and the dielectric constant is very close to the same value. The drawback would be a higher dissipation factor with the R/flex JADE™ adhesive however it does have a relatively flat relationship to frequency; within the confines of the testing that is shown in figure 15.

The use of the R/flex JADE™ J adhesive will make for a much simpler lamination cycle during the circuit fabrication. The details of the lamination cycle can be found on the Rogers Corporation website, however in general the following can yield good results: cure at 191°C (375° F) for 2 ½ hours, pressure at 300 psi, vacuum assist is mandatory, ramp rate is not critical and a 45 minute pre-bake of the adhesive prior to lamination should be done at 121°C (250°F). After the lamination, then recommendations for LCP processing which has been outlined in this report should be followed.

R/flex JADE™ Electrical Properties

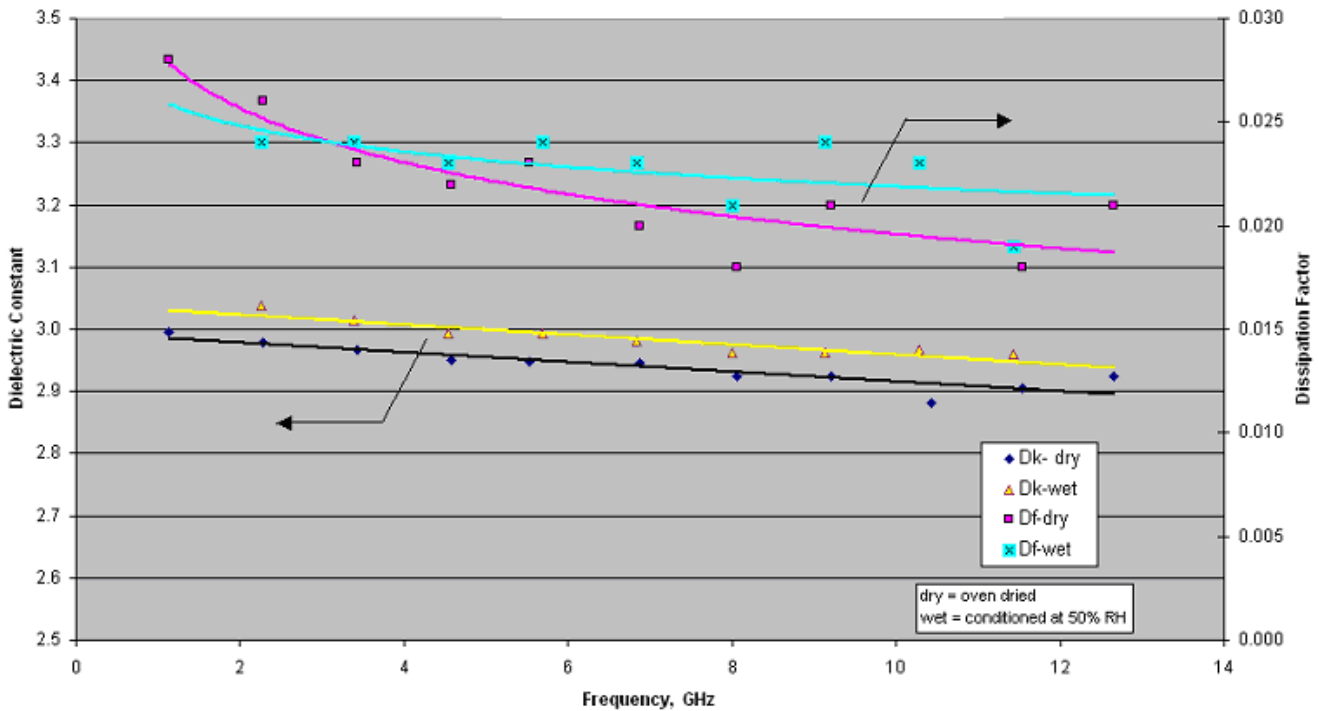


Figure 14. Electrical properties of the R/flex JADE™ J version adhesive

The use of a low temperature thermoplastic with excellent electrical properties as the bonding film could be employed. To maintain the flexible nature of the LCP, the 3001 film offered by Rogers Corporation could be used to bond LCP core materials together. This bonding film will have a much easier lamination cycle, however some constraint regarding bonding to large copper planes. The details of the lamination cycle can be found on the Rogers Corporation website and the general recommendations are: ramp to 232°C (450°F), hold for 20 minutes at 200 psi, vacuum is mandatory and ramp rate is not critical. A combination of LCP and 3001 plated through hole preparation will be needed. The recommendations mentioned in 3.d through 3.f should be done and followed by the plated through hole preparation recommended for the 3001 on the Rogers Corporation website. After which the circuit fabrication will become somewhat standard with some considerations mentioned in section 3.h for general LCP fabrication.

CONCLUSIONS

Although adoption has been slow, LCP provides too many benefits for designers to ignore – low Dk and low loss across a wide frequency range, low moisture absorption, to name a few. Due to the work of a few dedicated circuit fabricators, working in conjunction with Rogers' R & D and Technical Services, the challenges of realizing circuit designs on LCP are being met and overcome.

ACKNOWLEDGEMENTS

The authors would like to express their thanks and gratitude to Metro Circuits a Division of PJC Technologies Inc., for dedicating much time and resources to the topics of this paper.

We would also like to express our thanks to the many contributions of March Plasma Systems.

REFERENCES

[1] Thompson, Kirby, Papapolymerou, Tentzeris, “W-Band Characterization of Finite Ground Coplanar Transmission Line on Liquid Crystal (LCP) Substrates”, *IEEE Polytronic Conference 2003*.

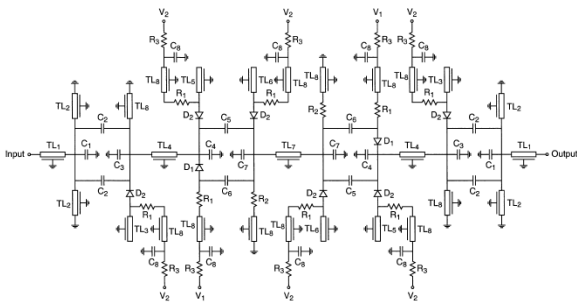
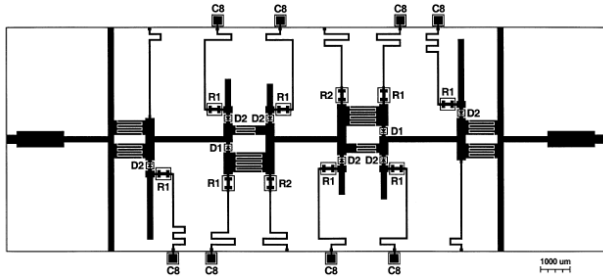
[2] Contact information for: March Plasma Systems Inc., 2470-A Bates Ave, Concord, CA 94520,
925-827-1240 or 1000 112th Circle North Suite 1200, St. Petersburg, FL 272-573-4567

Teflon is a trademark of E.I. du Pont de Nemours and Company

Fiberfrax is a trademark of Unifrax corporation

ULTRALAM, JADE & RO4000 are licensed trademarks of Rogers Corporation

Appendix 2: Literature Summary



Description:

A reconfigurable bandpass filter that can be switched between two discrete states, while keeping the passband centered at 10 GHz. The circuit employs pin diodes in order to switch fixed-value reactance elements.

Advantages:

- Is suitable for wideband and narrowband applications.
- The circuit could be easily adapted for use with MEMS.
- The filter circuit utilises only eight pin diodes.
- When filter is covered by lid there is no discernible change in pass band insertion loss for either wideband or narrowband states.

Disadvantages:

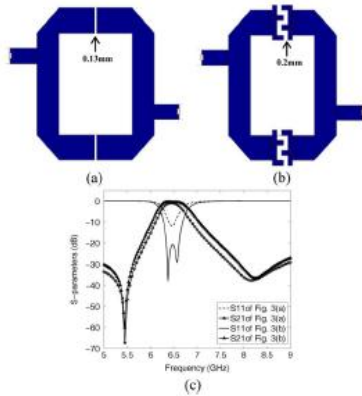
- Only bandwidth reconfigurable

Figs

1&2

Ref

[39]



Description:

Different filters with different geometries are designed and compared. A comparison of their coupling strengths are made, and are based on interdigital capacitors and etched slots. The filters designed exhibit wider bandwidths, which are easily adjustable by way of changing the geometrical parameters of interdigital capacitors and slots.

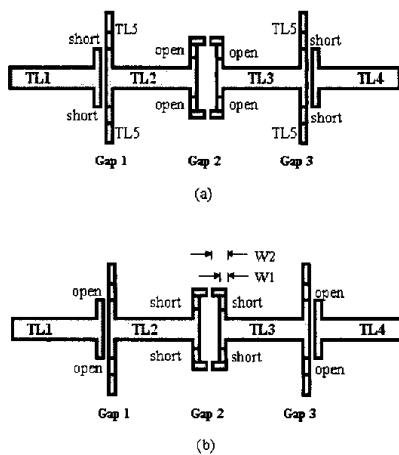
Advantages:

- Shows good response for wideband applications.
- Compact designs.

Disadvantages:

- May be difficult to implement tunable elements. However, switching circuits could be employed

Fig
5
Ref
[40]

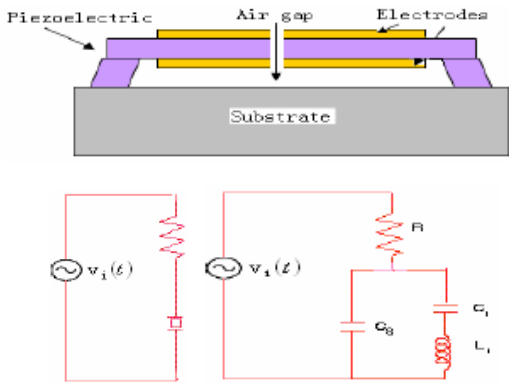


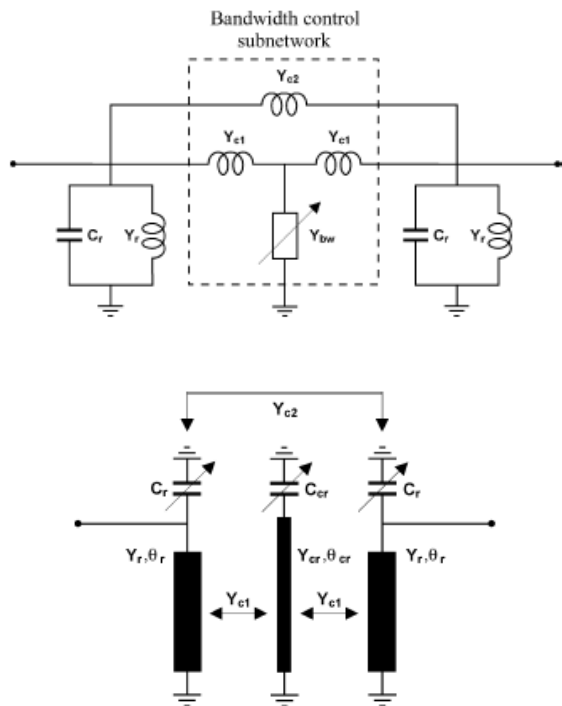
Description:

A reconfigurable bandpass filter that consists of capacitive coupled resonators, with the capability to switch between two distinct bandwidths while keeping a fixed center frequency of 5.8 GHz. The filter can be adapted between a narrowband state 4% and a wideband state 10%.

Advantages:

Fig
6
Ref
[41]

	<ul style="list-style-type: none"> • The design can be easily adapted for use with MEMS switches or pin diodes. • Reduced circuit complexity. 	
	<p>Description:</p> <p>A piezoelectric filter is designed with tunable bandwidth, through analysis of the equivalent circuit. The tunability is achieved by introducing variable capacitors and inductors in parallel with the piezoelectric resonant filter.</p> <p>Advantages:</p> <ul style="list-style-type: none"> • Compact structure. • Suitable for narrowband applications. <p>Disadvantages:</p> <ul style="list-style-type: none"> • Analysis in ANSYS has been carried out, meaning proper fabrication and measured results have not been obtained. 	<p>Figs 9 & 10</p> <p>Ref [42]</p>
	<p>Description:</p> <p>A combline filter structure is implemented, with passband width tunability being achieved by placing variable coupling reducers between filter resonators. The center frequency tunability is achieved through replacing</p>	<p>Figs 12 & 13</p> <p>Ref [27]</p>



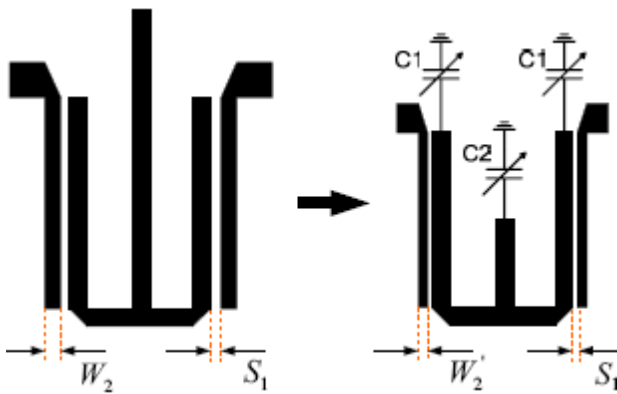
the fixed capacitances at the end of the resonators with variable ones.

Advantages:

- Allows Simultaneous control of bandwidth and center frequency.
- Compline structure has higher second passband with lower size compared to interdigital filters.
- Makes it possible to use a variety of varactors.
- Filter is compact, lossless and capable of a high tuning range.

Disadvantages:

- The use of varactors means that there has to be some sort of calibration while in use with communication applications.



Description:

A varactor-tuned hairpin bandpass filter with an attenuation pole. The center frequency and bandwidth are tuned using varactors loaded at the end of the hairpin resonator and tapped open stub.

Advantages:

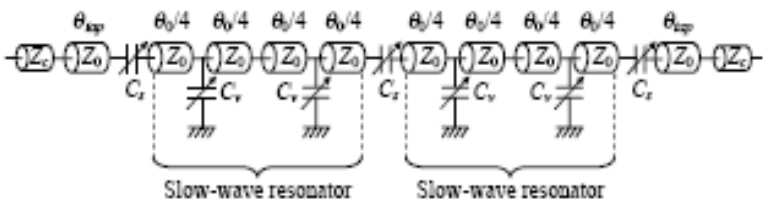
- The hairpin structure does not require short circuits like the conventional combline and

Fig 14

Refs [28] & [29]

interdigital structure.

- As a tapped open stub at the general hairpin resonator is added, the filter size can be reduced as well as the skirt characteristics become improved.
- The passband bandwidth remains nearly constant when tuning the center frequency.
- Wide tuning Range.



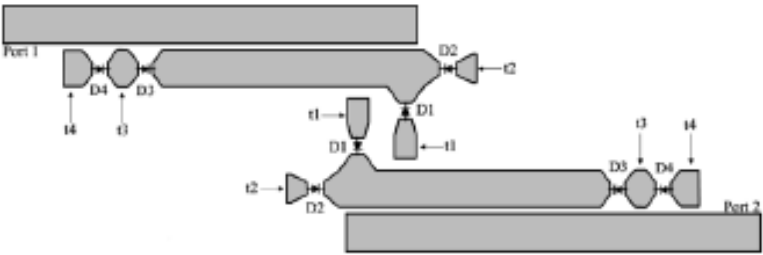
Description: Fig 15

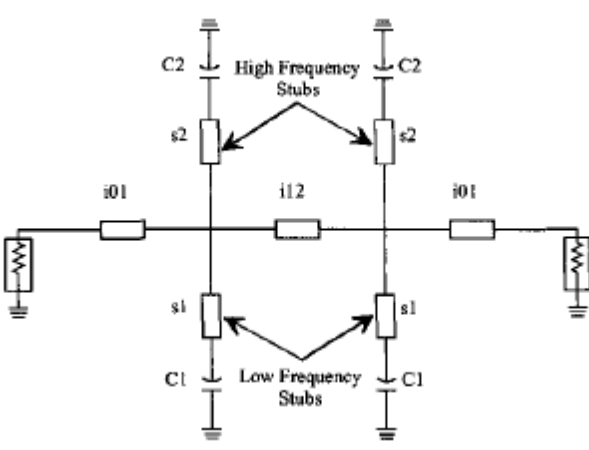
A compact hybrid tune-all bandpass filter based on coupled slow-wave resonators. Center-frequency tuning is obtained through varying shunt varactors, meaning that the loaded electrical length of the slow wave resonators is modified. Bandwidth control is obtained through tuning of the series varactors.

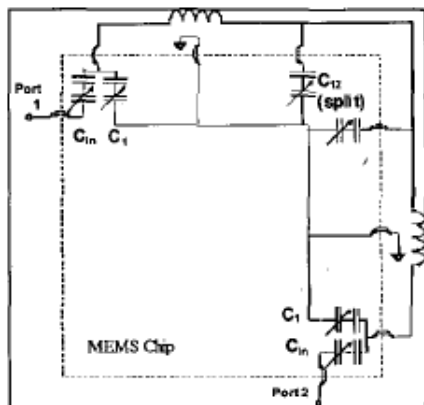
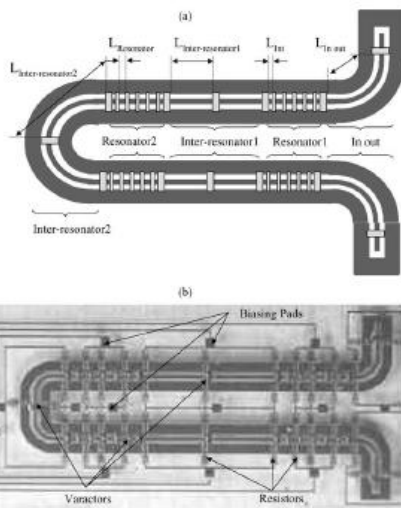
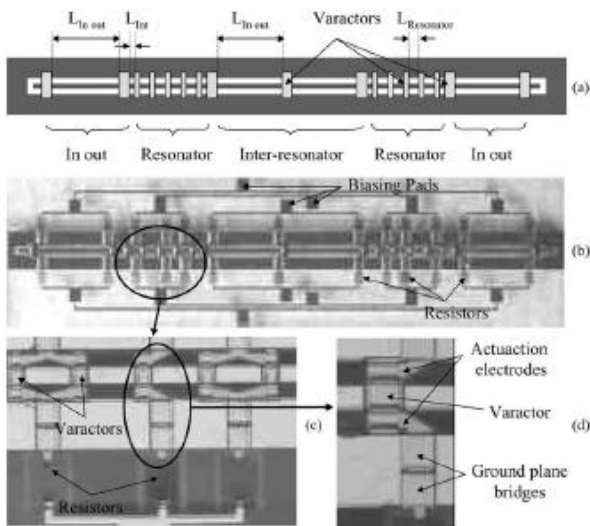
Refs [30] & [31]

Advantages:

- Wide continuous control of bandwidth and center frequency.
- The compactness of these circuits will allow designers to integrate such filter on high resistivity

	<p>substrates for higher frequency operation.</p> <p>Disadvantages:</p> <ul style="list-style-type: none"> • The insertion loss is mainly due to the series resistance of the shunt varactors. 	
	<p>Description:</p> <p>The filter is a six state re-configurable bandpass filter with tunability of center frequency and bandwidth. Pin diodes are used as witching elements which control the center frequency and bandwidth in discrete steps.</p> <p>Advantages:</p> <ul style="list-style-type: none"> • The circuit produces no significant signal distortion. • Uses switching method, meaning limiting the losses and omits the need for calibration. • The filter provides a reduced number of switches compared to previous work. • When the filter is switched between narrowband and wideband there is little or no shift in center frequency. 	<p>Fig 16</p> <p>Ref [32]</p>

	<p>Disadvantages:</p> <ul style="list-style-type: none"> Narrowband states exhibit a degree of over coupling. 	
	<p>Description:</p> <p>MEMS cantilevers are used at the ends of dual behaviour resonators. In their stable region a continuous variation of capacitance is produced by applying a bias voltage below the pull down one. By adding this variable capacitance at the ends of the resonators allows the modification of electrical length and associated transmission zero frequency.</p> <p>Advantages:</p> <ul style="list-style-type: none"> By using a DBR bandpass and MEMS variable capacities allows independent tuning of center frequency and bandwidth. MEMS cantilevers also have near zero power consumption, high isolation, low insertion loss and low noise. 	<p>Fig 20</p> <p>Ref [33]</p>



Description:

Distributed MEMS varactors on a coplanar waveguide were used to design two-pole and four-pole tune all bandpass filter. The use of MEMS bridges allowed for continuous tuning of bandwidth and center frequency. The tuning is achieved by biasing the “Resonator,” In Out” and “Inter-resonator” sections separately.

Advantages:

- The bandwidth and center frequency can be changed independently of each other.
- The filter design is very compact.

Disadvantages:

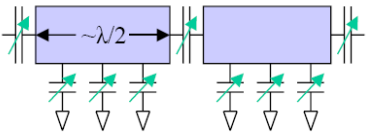
- Resistive losses have a significant impact on input/output couplings.

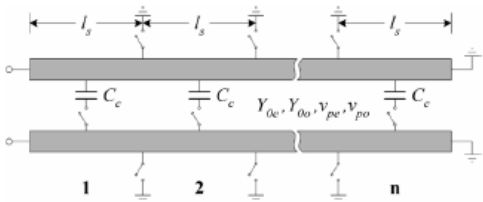
Figs
23
&
24
Ref
[34]

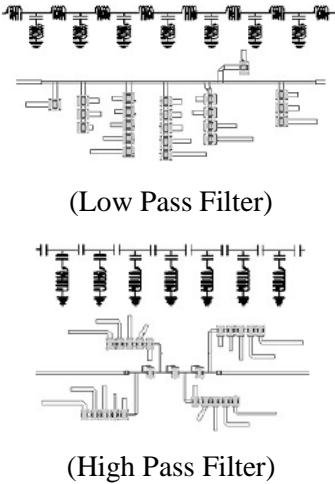
Description:

A two pole bandpass filter with independent tuning of bandwidth and center frequency. The arrangement consists of two fixed inductors and five tunable capacitor arrays. Each array consists of a four-bit set of MEMS capacitance switches, where each bit is DC separated from its neighbour by a blocking capacitor. The circuit is morphed as shown in order to compact the circuit.

Fig
29
Ref
[35]

	<p>Advantages:</p> <ul style="list-style-type: none"> • Compact design allowing easily accommodating onto a MEMS chip. • Bandwidth and center frequency is controlled independently. <p>Disadvantages:</p> <ul style="list-style-type: none"> • By morphing the circuit, two inductors are placed at right angles, thus reducing the cross coupling. 	
	<p>Description:</p> <p>A three pole tunable end-coupled filter from 6 to 10 GHz with a broad tuning range of 35%. RF MEMS capacitive switches were used as tuning elements, with coupling capacitors used to control the bandwidth independently of the center frequency.</p> <p>Advantages:</p> <ul style="list-style-type: none"> • Large tuning range. • Has potential to achieve lower losses. • Digital tuning used, provides good stability while tuning the 	<p>Fig 32</p> <p>Ref [36]</p>

	<p>bandwidth and center frequency.</p> <p>Disadvantages:</p> <ul style="list-style-type: none"> • The loss associated with switching dominates the filter loss. • When the filter is switched into the lowest two frequency states, there are additional resonances produced. 	
	<p>Description:</p> <p>A discretely tunable filter based on lumped-distributed coupled transmission lines. The topology is capable of controlling the center frequency and bandwidth.</p> <p>Advantages:</p> <ul style="list-style-type: none"> • Only a single grounding switch is in-circuit regardless of selected length, therefore, the impact of resistive switch losses on the resonator remains constant. • The filter retains a constant overlap region and coupling factor, regardless of the coupled line length. • Because the EM coupling between the transmission lines is anti-phase to the lumped 	<p>Fig 35</p> <p>Ref [37]</p>

	<p>capacitive coupling, very low couplings can be obtained regardless of coupled line spacing.</p> <p>Disadvantages:</p> <ul style="list-style-type: none"> • The tuning ranges are not uniform; at lower frequencies, there is a greater choice of both center frequency and bandwidth. • Limited only by the electrical size of the transmission lines and the placement density of the switching devices. 	
 <p>(Low Pass Filter)</p> <p>(High Pass Filter)</p>	<p>Description:</p> <p>A bandpass filter is constructed by cascading tunable low pass and high pass filters by capacitive switches. The configuration allows tunability of both center frequency and bandwidth. A direct coupled pseudo-elliptic filter topology was selected as it provided sharp skirt roll off with the fewest elements and thus lower insertion loss.</p> <p>Advantages:</p> <ul style="list-style-type: none"> • Low loss and compact size. • Center frequency and bandwidth is easily controlled across the 	<p>Figs 40 & 41 Ref [38]</p>

	<p>frequency range 6 to 15 GHz.</p> <p>Disadvantages:</p> <ul style="list-style-type: none">• Insertion loss was typically higher than anticipated and some skirt slopes were less than 40 dB per GHz.	
--	-----------------------------------------------------------------------------------------------------------------------------------------------------------------------------------------------------------------------------	--

Appendix 3: Coupled Line Filter Designs

MathCAD Program for Coupled line With No Stubs:

Impedance Values:

$Z_{oe} := 162.7$	Even Mode Impedance
$Z_{oo} := 64$	Odd Mode Impedance
$Z_o := 50$	Terminal Impedance
$Z_t := 105$	Impedance Of Impedance Transformer

Frequency Characteristics:

$\theta_o := 90\text{deg}$	Electrical Length At Center Frequency
$f_o := 2$	Center Frequency
$f := 0, 0.01 \dots 4$	Frequency Range
$\theta(f) := \frac{f}{f_o} \cdot \theta_o$	Theta At Each Frequency

ABCD Parameters of the Impedance Transformer:

$$A1(f) := \cos(\theta(f))$$
$$B1(f) := i \cdot (Z_t) \cdot \sin(\theta(f))$$
$$C1(f) := i \cdot \left(\frac{1}{Z_t} \right) \cdot \sin(\theta(f))$$
$$D1(f) := A1(f)$$

ABCD Parameters of the Coupled Line:

$$A2(f) := \cos(\theta(f)) \cdot \left[1 + \left[\frac{2 \cdot Z_{oe} \cdot Z_{oo}}{Z_{oe} \cdot (Z_{oe} - Z_{oo})} \right] \right]$$
$$B2(f) := i \cdot \left[\frac{2 \cdot Z_{oe} \cdot Z_{oo}}{(Z_{oe} - Z_{oo})} \right] \cdot \sin(\theta(f))$$
$$C2(f) := \frac{-2 \cdot i \cdot \cos(\theta(f))}{Z_{oe} \cdot \tan(\theta(f))} \cdot \left[1 + \frac{Z_{oe} \cdot Z_{oo}}{Z_{oe} \cdot (Z_{oe} - Z_{oo})} \right] + \frac{i \cdot \sin(\theta(f)) \cdot (Z_{oe} - Z_{oo})}{2 \cdot Z_{oe} \cdot Z_{oo}}$$
$$D2(f) := A2(f)$$

ABCD Parameters of Other Impedance Transformer:

$$A_3(f) := A_1(f)$$

$$B_3(f) := B_1(f)$$

$$C_3(f) := C_1(f)$$

$$D_3(f) := A_3(f)$$

Cascaded ABCD Parameters:

$$A(f) := (A_1(f) \cdot A_2(f) + B_1(f) \cdot C_2(f)) \cdot A_3(f) + (A_1(f) \cdot B_2(f) + B_1(f) \cdot D_2(f)) \cdot C_3(f)$$

$$B(f) := (A_1(f) \cdot A_2(f) + B_1(f) \cdot C_2(f)) \cdot B_3(f) + (A_1(f) \cdot B_2(f) + B_1(f) \cdot D_2(f)) \cdot D_3(f)$$

$$C(f) := (C_1(f) \cdot A_2(f) + D_1(f) \cdot C_2(f)) \cdot A_3(f) + (C_1(f) \cdot B_2(f) + D_1(f) \cdot D_2(f)) \cdot C_3(f)$$

$$D(f) := (C_1(f) \cdot A_2(f) + D_1(f) \cdot C_2(f)) \cdot B_3(f) + (C_1(f) \cdot B_2(f) + D_1(f) \cdot D_2(f)) \cdot D_3(f)$$

S-Parameters:

$$S_{11}(f) := \frac{\left[A(f) + \left(\frac{B(f)}{Z_0} \right) - (C(f) \cdot Z_0) - D(f) \right]}{\left[A(f) + \left(\frac{B(f)}{Z_0} \right) + (C(f) \cdot Z_0) + D(f) \right]}$$

$$S_{12}(f) := \frac{2 \cdot [(A(f) \cdot D(f)) - (B(f) \cdot C(f))]}{\left[A(f) + \left(\frac{B(f)}{Z_0} \right) + (C(f) \cdot Z_0) + D(f) \right]}$$

$$S_{21}(f) := \frac{2}{\left[A(f) + \left(\frac{B(f)}{Z_0} \right) + (C(f) \cdot Z_0) + D(f) \right]}$$

$$S_{22}(f) := \frac{\left[-(A(f)) + \left(\frac{B(f)}{Z_0} \right) - (C(f) \cdot Z_0) + D(f) \right]}{\left[A(f) + \left(\frac{B(f)}{Z_0} \right) + (C(f) \cdot Z_0) + D(f) \right]}$$

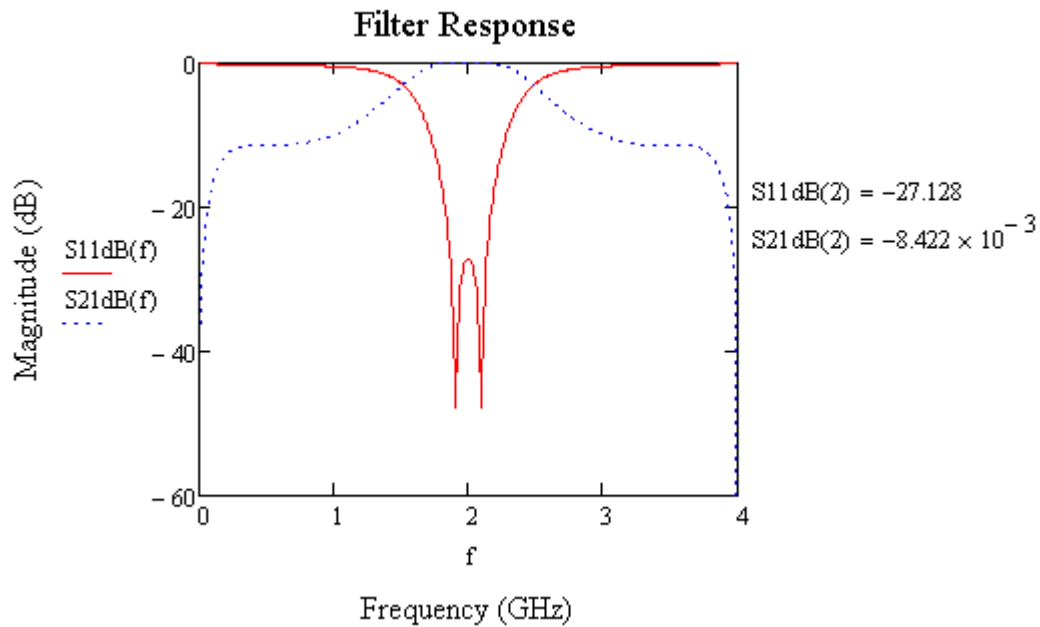
$$S_{11\text{dB}}(f) := 20 \cdot \log(|S_{11}(f)|)$$

$$S_{12\text{dB}}(f) := 20 \cdot \log(|S_{12}(f)|)$$

$$S_{21\text{dB}}(f) := 20 \cdot \log(|S_{21}(f)|)$$

$$S_{22\text{dB}}(f) := 20 \cdot \log(|S_{22}(f)|)$$

Response:



MathCAD Program for Coupled line With Wideband Stubs (151.214 Ω):

Impedance Values:

$Z_{oe} := 162.7$	Even Mode Impedance
$Z_{oo} := 64$	Odd Mode Impedance
$Z_o := 50$	Terminal Impedance
$Z_t := 105$	Impedance Of Impedance Transformer
$Z_{cs} := 151.241$	Impedance of the Stub

Frequency Characteristics:

$\theta_o := 90 \text{ deg}$	Electrical Length At Center Frequency
$f_o := 2$	Center Frequency
$f := 0, 0.01 \dots 4$	Frequency Range
$\theta(f) := \frac{f}{f_o} \cdot \theta_o$	Theta At Each Frequency

ABCD Parameters of the Impedance Transformer:

$$A1(f) := \cos(\theta(f))$$

$$B1(f) := i \cdot (Z_t) \cdot \sin(\theta(f))$$

$$C1(f) := i \cdot \left(\frac{1}{Z_t} \right) \cdot \sin(\theta(f))$$

$$D1(f) := A1(f)$$

ABCD Parameters of the Coupled Line:

$$A2(f) := \cos(\theta(f)) \cdot \left[1 + \frac{2 \cdot Z_{oe} \cdot Z_{oo}}{Z_{oe} \cdot (Z_{oe} - Z_{oo})} \right]$$

$$B2(f) := i \cdot \left[\frac{2 \cdot Z_{oe} \cdot Z_{oo}}{(Z_{oe} - Z_{oo})} \right] \cdot \sin(\theta(f))$$

$$C2(f) := \frac{-2 \cdot i \cdot \cos(\theta(f))}{Z_{oe} \cdot \tan(\theta(f))} \cdot \left[1 + \frac{Z_{oe} \cdot Z_{oo}}{Z_{oe} \cdot (Z_{oe} - Z_{oo})} \right] + \frac{i \cdot \sin(\theta(f)) \cdot (Z_{oe} - Z_{oo})}{2 \cdot Z_{oe} \cdot Z_{oo}}$$

$$D2(f) := A2(f)$$

ABCD Parameters of Other Impedance Transformer:

$$A3(f) := A1(f)$$

$$B3(f) := B1(f)$$

$$C3(f) := C1(f)$$

$$D3(f) := A3(f)$$

Cascaded ABCD Parameters:

$$A(f) := (A1(f) \cdot A2(f) + B1(f) \cdot C2(f)) \cdot A3(f) + (A1(f) \cdot B2(f) + B1(f) \cdot D2(f)) \cdot C3(f)$$

$$B(f) := (A1(f) \cdot A2(f) + B1(f) \cdot C2(f)) \cdot B3(f) + (A1(f) \cdot B2(f) + B1(f) \cdot D2(f)) \cdot D3(f)$$

$$C(f) := (C1(f) \cdot A2(f) + D1(f) \cdot C2(f)) \cdot A3(f) + (C1(f) \cdot B2(f) + D1(f) \cdot D2(f)) \cdot C3(f)$$

$$D(f) := (C1(f) \cdot A2(f) + D1(f) \cdot C2(f)) \cdot B3(f) + (C1(f) \cdot B2(f) + D1(f) \cdot D2(f)) \cdot D3(f)$$

S-Parameters:

$$S_{11}(f) := \frac{\left[A(f) + \left(\frac{B(f)}{Z_0} \right) - (C(f) \cdot Z_0) - D(f) \right]}{\left[A(f) + \left(\frac{B(f)}{Z_0} \right) + (C(f) \cdot Z_0) + D(f) \right]}$$

$$S_{12}(f) := \frac{2 \cdot [(A(f) \cdot D(f)) - (B(f) \cdot C(f))]}{\left[A(f) + \left(\frac{B(f)}{Z_0} \right) + (C(f) \cdot Z_0) + D(f) \right]}$$

$$S_{21}(f) := \frac{2}{\left[A(f) + \left(\frac{B(f)}{Z_0} \right) + (C(f) \cdot Z_0) + D(f) \right]}$$

$$S_{22}(f) := \frac{\left[-(A(f)) + \left(\frac{B(f)}{Z_0} \right) - (C(f) \cdot Z_0) + D(f) \right]}{\left[A(f) + \left(\frac{B(f)}{Z_0} \right) + (C(f) \cdot Z_0) + D(f) \right]}$$

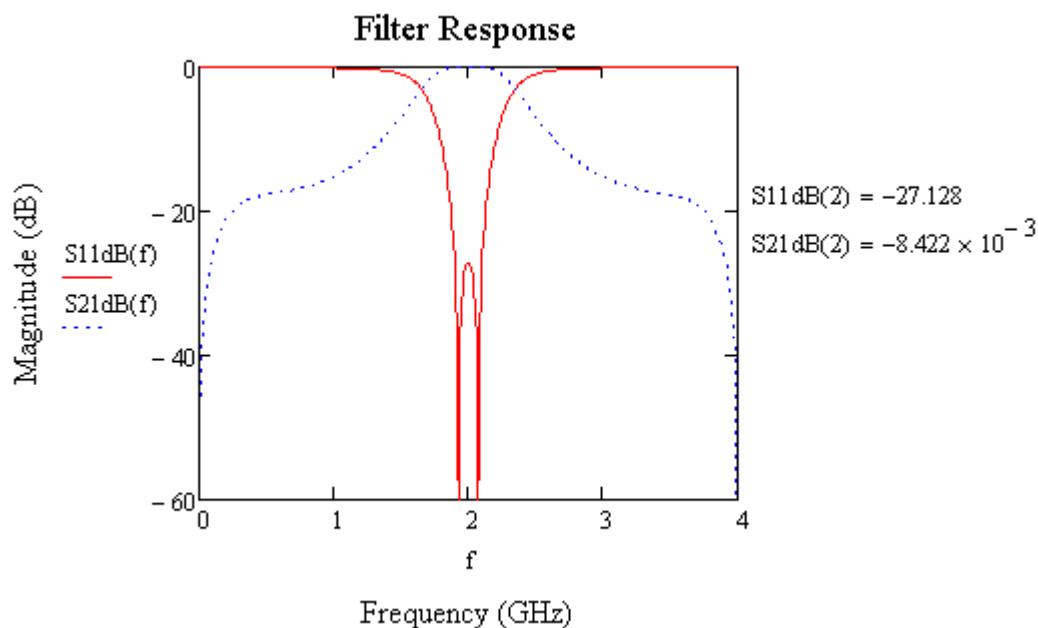
$$S_{11\text{dB}}(f) := 20 \cdot \log(|S_{11}(f)|)$$

$$S_{12\text{dB}}(f) := 20 \cdot \log(|S_{12}(f)|)$$

$$S_{21\text{dB}}(f) := 20 \cdot \log(|S_{21}(f)|)$$

$$S_{22\text{dB}}(f) := 20 \cdot \log(|S_{22}(f)|)$$

Response:



MathCAD Program for Coupled line With Narrowband Stubs (28.76 Ω):

Impedance Values:

$Z_{oe} := 162.7$	Even Mode Impedance
$Z_{oo} := 64$	Odd Mode Impedance
$Z_o := 50$	Terminal Impedance
$Z_t := 105$	Impedance Of Impedance Transformer
$Z_{cs} := 28.76$	Impedance of the Stub

Frequency Characteristics:

$\theta_o := 90 \text{ deg}$	Electrical Length At Center Frequency
$f_o := 2$	Center Frequency
$f := 0, 0.01 \dots 4$	Frequency Range
$\theta(f) := \frac{f}{f_o} \cdot \theta_o$	Theta At Each Frequency

ABCD Parameters of the Impedance Transformer:

$$A1(f) := \cos(\theta(f))$$

$$B1(f) := i \cdot (Z_t) \cdot \sin(\theta(f))$$

$$C1(f) := i \cdot \left(\frac{1}{Z_t} \right) \cdot \sin(\theta(f))$$

$$D1(f) := A1(f)$$

ABCD Parameters of the Coupled Line:

$$A2(f) := \cos(\theta(f)) \cdot \left[1 + \left[\frac{2 \cdot Z_{oe} \cdot Z_{oo}}{Z_{oe} \cdot (Z_{oe} - Z_{oo})} \right] \right]$$

$$B2(f) := i \cdot \left[\frac{2 \cdot Z_{oe} \cdot Z_{oo}}{(Z_{oe} - Z_{oo})} \right] \cdot \sin(\theta(f))$$

$$C2(f) := \frac{-2 \cdot i \cdot \cos(\theta(f))}{Z_{oe} \cdot \tan(\theta(f))} \cdot \left[1 + \frac{Z_{oe} \cdot Z_{oo}}{Z_{oe} \cdot (Z_{oe} - Z_{oo})} \right] + \frac{i \cdot \sin(\theta(f)) \cdot (Z_{oe} - Z_{oo})}{2 \cdot Z_{oe} \cdot Z_{oo}}$$

$$D2(f) := A2(f)$$

ABCD Parameters of Other Impedance Transformer:

$$A_3(f) := A_1(f)$$

$$B_3(f) := B_1(f)$$

$$C_3(f) := C_1(f)$$

$$D_3(f) := A_3(f)$$

Cascaded ABCD Parameters:

$$A(f) := (A_1(f) \cdot A_2(f) + B_1(f) \cdot C_2(f)) \cdot A_3(f) + (A_1(f) \cdot B_2(f) + B_1(f) \cdot D_2(f)) \cdot C_3(f)$$

$$B(f) := (A_1(f) \cdot A_2(f) + B_1(f) \cdot C_2(f)) \cdot B_3(f) + (A_1(f) \cdot B_2(f) + B_1(f) \cdot D_2(f)) \cdot D_3(f)$$

$$C(f) := (C_1(f) \cdot A_2(f) + D_1(f) \cdot C_2(f)) \cdot A_3(f) + (C_1(f) \cdot B_2(f) + D_1(f) \cdot D_2(f)) \cdot C_3(f)$$

$$D(f) := (C_1(f) \cdot A_2(f) + D_1(f) \cdot C_2(f)) \cdot B_3(f) + (C_1(f) \cdot B_2(f) + D_1(f) \cdot D_2(f)) \cdot D_3(f)$$

S-Parameters:

$$S_{11}(f) := \frac{\left[A(f) + \left(\frac{B(f)}{Z_0} \right) - (C(f) \cdot Z_0) - D(f) \right]}{\left[A(f) + \left(\frac{B(f)}{Z_0} \right) + (C(f) \cdot Z_0) + D(f) \right]}$$

$$S_{12}(f) := \frac{2 \cdot [(A(f) \cdot D(f)) - (B(f) \cdot C(f))]}{\left[A(f) + \left(\frac{B(f)}{Z_0} \right) + (C(f) \cdot Z_0) + D(f) \right]}$$

$$S_{21}(f) := \frac{2}{\left[A(f) + \left(\frac{B(f)}{Z_0} \right) + (C(f) \cdot Z_0) + D(f) \right]}$$

$$S_{22}(f) := \frac{\left[-(A(f)) + \left(\frac{B(f)}{Z_0} \right) - (C(f) \cdot Z_0) + D(f) \right]}{\left[A(f) + \left(\frac{B(f)}{Z_0} \right) + (C(f) \cdot Z_0) + D(f) \right]}$$

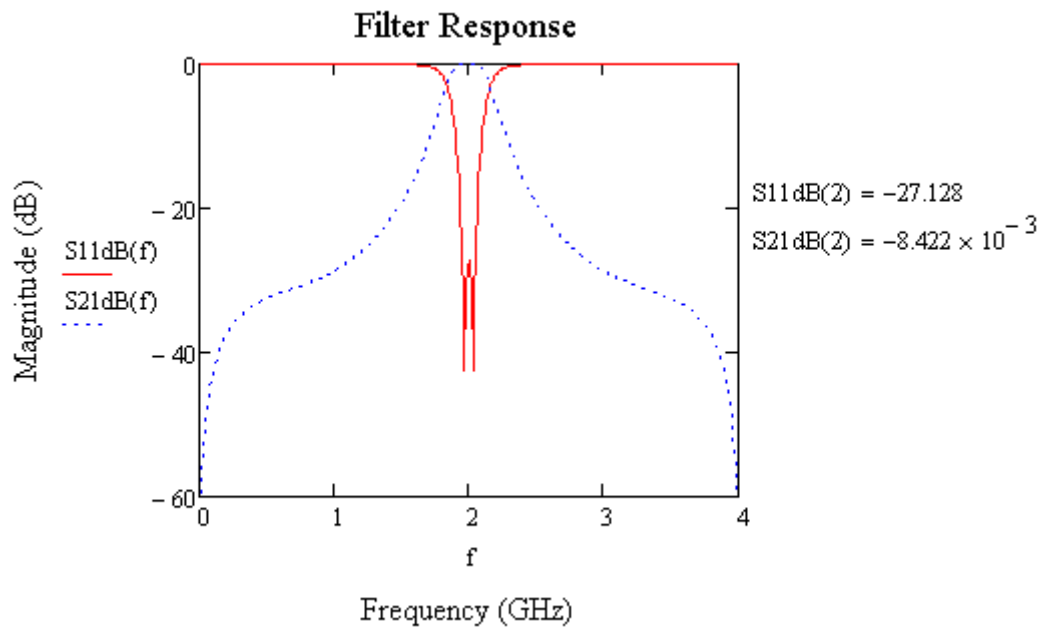
$$S_{11dB}(f) := 20 \cdot \log(|S_{11}(f)|)$$

$$S_{12dB}(f) := 20 \cdot \log(|S_{12}(f)|)$$

$$S_{21dB}(f) := 20 \cdot \log(|S_{21}(f)|)$$

$$S_{22dB}(f) := 20 \cdot \log(|S_{22}(f)|)$$

Response:



Appendix 4: Cascaded Coupled Line Filter Designs 1

Single Section Design Without Stubs Loaded:

$Z_{oe} := 200.95$ **Even Mode Impedance**
 $Z_{oo} := 66.2$ **Odd Mode Impedance**
 $Z_o := 50$ **Terminal Impedance**
 $Z_t := 100$ **Impedance Of Impedance Transformer**

$\theta_o := 90\text{deg}$ **Electrical Length At Center Frequency**

$f_o := 2$ **Center Frequency**

$f := 0, 0.01 \dots 4$ **Frequency Range**

$\theta(f) := \frac{f}{f_o} \cdot \theta_o$ **Theta At Each Frequency**

$$A1(f) := \cos(\theta(f))$$

$$B1(f) := i \cdot (Z_t) \cdot \sin(\theta(f))$$

$$C1(f) := i \cdot \left(\frac{1}{Z_t} \right) \cdot \sin(\theta(f))$$

$$D1(f) := A1(f)$$

$$A2(f) := \cos(\theta(f)) \cdot \left[1 + \left[\frac{2 \cdot Z_{oe} \cdot Z_{oo}}{Z_{oe} \cdot (Z_{oe} - Z_{oo})} \right] \right]$$

$$B2(f) := i \cdot \left[\frac{2 \cdot Z_{oe} \cdot Z_{oo}}{(Z_{oe} - Z_{oo})} \right] \cdot \sin(\theta(f))$$

$$C2(f) := \frac{-2 \cdot i \cdot \cos(\theta(f))}{Z_{oe} \cdot \tan(\theta(f))} \cdot \left[1 + \frac{Z_{oe} \cdot Z_{oo}}{Z_{oe} \cdot (Z_{oe} - Z_{oo})} \right] + \frac{i \cdot \sin(\theta(f)) \cdot (Z_{oe} - Z_{oo})}{2 \cdot Z_{oe} \cdot Z_{oo}}$$

$$D2(f) := A2(f)$$

$$\begin{aligned}A_3(f) &:= A_1(f) \\B_3(f) &:= B_1(f) \\C_3(f) &:= C_1(f) \\D_3(f) &:= A_3(f)\end{aligned}$$

$$A(f) := (A_1(f) \cdot A_2(f) + B_1(f) \cdot C_2(f)) \cdot A_3(f) + (A_1(f) \cdot B_2(f) + B_1(f) \cdot D_2(f)) \cdot C_3(f)$$

$$B(f) := (A_1(f) \cdot A_2(f) + B_1(f) \cdot C_2(f)) \cdot B_3(f) + (A_1(f) \cdot B_2(f) + B_1(f) \cdot D_2(f)) \cdot D_3(f)$$

$$C(f) := (C_1(f) \cdot A_2(f) + D_1(f) \cdot C_2(f)) \cdot A_3(f) + (C_1(f) \cdot B_2(f) + D_1(f) \cdot D_2(f)) \cdot C_3(f)$$

$$D(f) := (C_1(f) \cdot A_2(f) + D_1(f) \cdot C_2(f)) \cdot B_3(f) + (C_1(f) \cdot B_2(f) + D_1(f) \cdot D_2(f)) \cdot D_3(f)$$

$$S_{11}(f) := \frac{\left[A(f) + \left(\frac{B(f)}{Z_0} \right) - (C(f) \cdot Z_0) - D(f) \right]}{\left[A(f) + \left(\frac{B(f)}{Z_0} \right) + (C(f) \cdot Z_0) + D(f) \right]}$$

$$S_{12}(f) := \frac{2 \cdot [(A(f) \cdot D(f)) - (B(f) \cdot C(f))]}{\left[A(f) + \left(\frac{B(f)}{Z_0} \right) + (C(f) \cdot Z_0) + D(f) \right]}$$

$$S_{21}(f) := \frac{2}{\left[A(f) + \left(\frac{B(f)}{Z_0} \right) + (C(f) \cdot Z_0) + D(f) \right]}$$

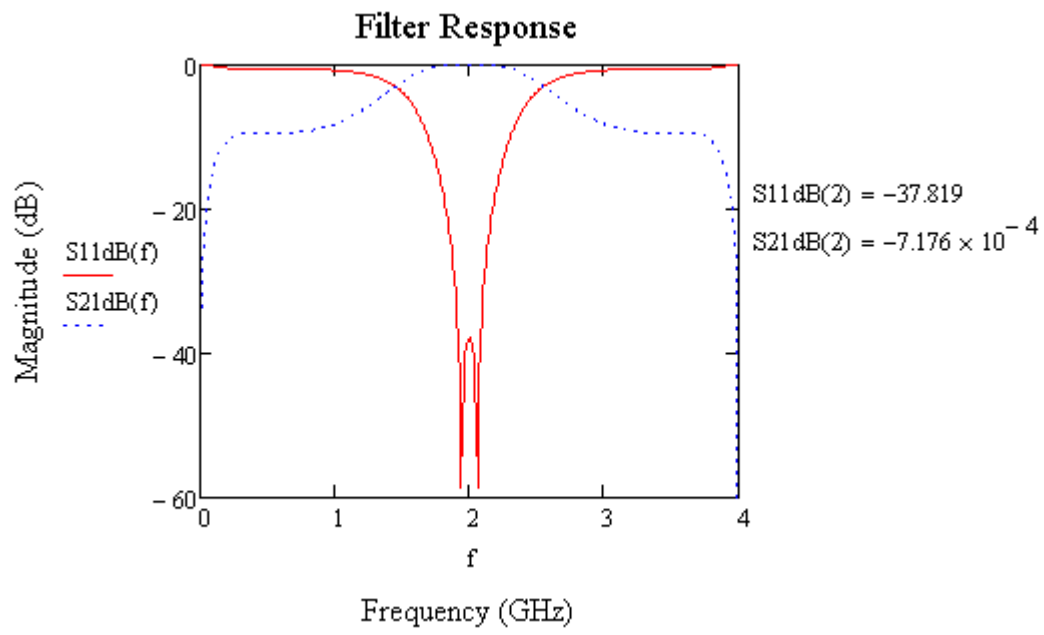
$$S_{22}(f) := \frac{\left[-(A(f)) + \left(\frac{B(f)}{Z_0} \right) - (C(f) \cdot Z_0) + D(f) \right]}{\left[A(f) + \left(\frac{B(f)}{Z_0} \right) + (C(f) \cdot Z_0) + D(f) \right]}$$

$$S_{11dB}(f) := 20 \cdot \log(|S_{11}(f)|)$$

$$S_{12dB}(f) := 20 \cdot \log(|S_{12}(f)|)$$

$$S_{21dB}(f) := 20 \cdot \log(|S_{21}(f)|)$$

$$S_{22dB}(f) := 20 \cdot \log(|S_{22}(f)|)$$



Single Section Design With Stubs Loaded:

$Z_{oe} := 200.95$	Even Mode Impedance
$Z_{oo} := 66.2$	Odd Mode Impedance
$Z_o := 50$	Terminal Impedance
$Z_t := 100$	Impedance Of Impedance Transformer
$Z_{cs} := 300$	Impedance of the Stub
$\theta_o := 90 \text{ deg}$	Electrical Length At Center Frequency
$f_o := 2$	Center Frequency
$f := 0, 0.01 .. 4$	Frequency Range
$\theta(f) := \frac{f}{f_o} \cdot \theta_o$	Theta At Each Frequency

$$A1(f) := \cos(\theta(f))$$

$$B1(f) := i \cdot (Z_t) \cdot \sin(\theta(f))$$

$$C1(f) := i \cdot \left(\frac{1}{Z_t} \right) \cdot \sin(\theta(f))$$

$$D1(f) := A1(f)$$

$$A2(f) := \cos(\theta(f)) \cdot \left[1 + \left[\frac{2 \cdot Z_{oe} \cdot Z_{oo}}{Z_{oe} \cdot (Z_{oe} - Z_{oo})} \right] \right]$$

$$B2(f) := i \cdot \left[\frac{2 \cdot Z_{oe} \cdot Z_{oo}}{(Z_{oe} - Z_{oo})} \right] \cdot \sin(\theta(f))$$

$$C2(f) := \frac{-2 \cdot i \cdot \cos(\theta(f))}{Z_{oe} \cdot \tan(\theta(f))} \cdot \left[1 + \frac{Z_{oe} \cdot Z_{oo}}{Z_{oe} \cdot (Z_{oe} - Z_{oo})} \right] + \frac{i \cdot \sin(\theta(f)) \cdot (Z_{oe} - Z_{oo})}{2 \cdot Z_{oe} \cdot Z_{oo}}$$

$$D2(f) := A2(f)$$

$$A3(f) := A1(f)$$

$$B3(f) := B1(f)$$

$$C3(f) := C1(f)$$

$$D3(f) := A3(f)$$

$$A(f) := (A1(f) \cdot A2(f) + B1(f) \cdot C2(f)) \cdot A3(f) + (A1(f) \cdot B2(f) + B1(f) \cdot D2(f)) \cdot C3(f)$$

$$B(f) := (A1(f) \cdot A2(f) + B1(f) \cdot C2(f)) \cdot B3(f) + (A1(f) \cdot B2(f) + B1(f) \cdot D2(f)) \cdot D3(f)$$

$$C(f) := (C1(f) \cdot A2(f) + D1(f) \cdot C2(f)) \cdot A3(f) + (C1(f) \cdot B2(f) + D1(f) \cdot D2(f)) \cdot C3(f)$$

$$D(f) := (C1(f) \cdot A2(f) + D1(f) \cdot C2(f)) \cdot B3(f) + (C1(f) \cdot B2(f) + D1(f) \cdot D2(f)) \cdot D3(f)$$

$$S11(f) := \frac{\left[A(f) + \left(\frac{B(f)}{Z_0} \right) - (C(f) \cdot Z_0) - D(f) \right]}{\left[A(f) + \left(\frac{B(f)}{Z_0} \right) + (C(f) \cdot Z_0) + D(f) \right]}$$

$$S12(f) := \frac{2 \cdot [(A(f) \cdot D(f)) - (B(f) \cdot C(f))]}{\left[A(f) + \left(\frac{B(f)}{Z_0} \right) + (C(f) \cdot Z_0) + D(f) \right]}$$

$$S21(f) := \frac{2}{\left[A(f) + \left(\frac{B(f)}{Z_0} \right) + (C(f) \cdot Z_0) + D(f) \right]}$$

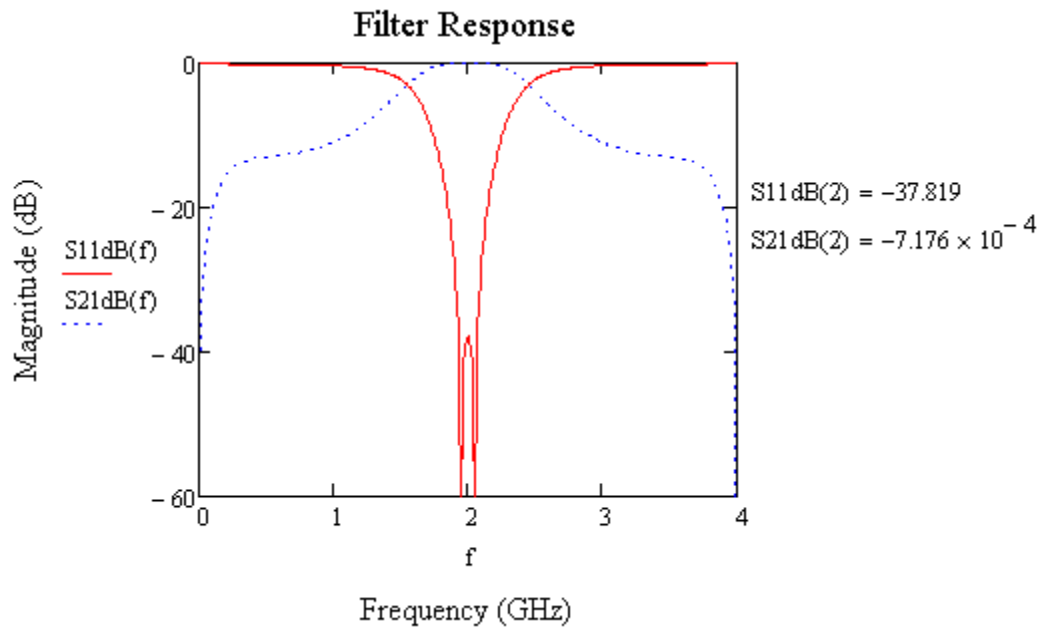
$$S22(f) := \frac{\left[-(A(f)) + \left(\frac{B(f)}{Z_0} \right) - (C(f) \cdot Z_0) + D(f) \right]}{\left[A(f) + \left(\frac{B(f)}{Z_0} \right) + (C(f) \cdot Z_0) + D(f) \right]}$$

$$S11_{dB}(f) := 20 \cdot \log(|S11(f)|)$$

$$S12_{dB}(f) := 20 \cdot \log(|S12(f)|)$$

$$S21_{dB}(f) := 20 \cdot \log(|S21(f)|)$$

$$S22_{dB}(f) := 20 \cdot \log(|S22(f)|)$$



Cascaded Coupled line filter with no Stubs Loaded:

- $Z_{oe} := 200.95$ **Even Mode Impedance**
- $Z_{oo} := 66.2$ **Odd Mode Impedance**
- $Z_o := 50$ **Terminal Impedance**
- $Z_t := 100$ **Impedance Of Impedance Transformer**
- $\theta_o := 90 \text{ deg}$ **Electrical Length At Center Frequency**
- $f_o := 2$ **Center Frequency**
- $f := 0, 0.01 \dots 4$ **Frequency Range**
- $\theta(f) := \frac{f}{f_o} \cdot \theta_o$ **Theta At Each Frequency**

$$A1(f) := \cos(\theta(f))$$

$$B1(f) := i \cdot (Z_t) \cdot \sin(\theta(f))$$

$$C1(f) := i \cdot \left(\frac{1}{Z_t} \right) \cdot \sin(\theta(f))$$

$$D1(f) := A1(f)$$

$$A2(f) := \cos(\theta(f)) \cdot \left[1 + \left[\frac{2 \cdot Z_{oe} \cdot Z_{oo}}{Z_{oe} \cdot (Z_{oe} - Z_{oo})} \right] \right]$$

$$B2(f) := i \cdot \left[\frac{2 \cdot Z_{oe} \cdot Z_{oo}}{(Z_{oe} - Z_{oo})} \right] \cdot \sin(\theta(f))$$

$$C2(f) := \frac{-2 \cdot i \cdot \cos(\theta(f))}{Z_{oe} \cdot \tan(\theta(f))} \cdot \left[1 + \frac{Z_{oe} \cdot Z_{oo}}{Z_{oe} \cdot (Z_{oe} - Z_{oo})} \right] + \frac{i \cdot \sin(\theta(f)) \cdot (Z_{oe} - Z_{oo})}{2 \cdot Z_{oe} \cdot Z_{oo}}$$

$$D2(f) := A2(f)$$

$$A3(f) := A2(f)$$

$$B3(f) := B2(f)$$

$$C3(f) := C2(f)$$

$$D3(f) := A3(f)$$

$$A4(f) := A3(f)$$

$$B4(f) := B3(f)$$

$$C4(f) := C3(f)$$

$$D4(f) := A3(f)$$

$$A5(f) := A1(f)$$

$$B5(f) := B1(f)$$

$$C5(f) := C1(f)$$

$$D5(f) := A1(f)$$

$$\underline{\underline{A}}(f) := [[(A1(f) \cdot A2(f) + B1(f) \cdot C2(f)) \cdot A3(f) + (A1(f) \cdot B2(f) + B1(f) \cdot D2(f)) \cdot C3(f)] \cdot A4(f) + [(A1(f) \cdot A2(f) + B1(f) \cdot C2(f)) \cdot B3(f) + (A1(f) \cdot B2(f) + B1(f) \cdot D2(f)) \cdot D3(f)] \cdot C4(f)] \cdot A5(f) + [[(A1(f) \cdot A2(f) + B1(f) \cdot C2(f)) \cdot B3(f) + (A1(f) \cdot B2(f) + B1(f) \cdot D2(f)) \cdot D3(f)] \cdot D4(f) + [(A1(f) \cdot A2(f) + B1(f) \cdot C2(f)) \cdot A3(f) + (A1(f) \cdot B2(f) + B1(f) \cdot D2(f)) \cdot C3(f)] \cdot B4(f)] \cdot C5(f)$$

$$B(f) := [[(A1(f) \cdot A2(f) + B1(f) \cdot C2(f)) \cdot B3(f) + (A1(f) \cdot B2(f) + B1(f) \cdot D2(f)) \cdot D3(f)] \cdot D4(f) + [(A1(f) \cdot A2(f) + B1(f) \cdot C2(f)) \cdot A3(f) + (A1(f) \cdot B2(f) + B1(f) \cdot D2(f)) \cdot C3(f)] \cdot B4(f)] \cdot D5(f) + B5(f) \cdot [[(A1(f) \cdot A2(f) + B1(f) \cdot C2(f)) \cdot A3(f) + (A1(f) \cdot B2(f) + B1(f) \cdot D2(f)) \cdot C3(f)] \cdot A4(f) + [(A1(f) \cdot A2(f) + B1(f) \cdot C2(f)) \cdot B3(f) + (A1(f) \cdot B2(f) + B1(f) \cdot D2(f)) \cdot D3(f)] \cdot C4(f)]$$

$$\underline{\underline{C}}(f) := [[(C1(f) \cdot A2(f) + D1(f) \cdot C2(f)) \cdot A3(f) + (C1(f) \cdot B2(f) + D1(f) \cdot D2(f)) \cdot C3(f)] \cdot A4(f) + [(C1(f) \cdot A2(f) + D1(f) \cdot C2(f)) \cdot B3(f) + (C1(f) \cdot B2(f) + D1(f) \cdot D2(f)) \cdot D3(f)] \cdot C4(f)] \cdot A5(f) + C5(f) \cdot [[(C1(f) \cdot A2(f) + D1(f) \cdot C2(f)) \cdot B3(f) + (C1(f) \cdot B2(f) + D1(f) \cdot D2(f)) \cdot D3(f)] \cdot D4(f) + [(C1(f) \cdot A2(f) + D1(f) \cdot C2(f)) \cdot A3(f) + (C1(f) \cdot B2(f) + D1(f) \cdot D2(f)) \cdot C3(f)] \cdot B4(f)]$$

$$D(f) := [[(C1(f) \cdot A2(f) + D1(f) \cdot C2(f)) \cdot B3(f) + (C1(f) \cdot B2(f) + D1(f) \cdot D2(f)) \cdot D3(f)] \cdot D4(f) + [(C1(f) \cdot A2(f) + D1(f) \cdot C2(f)) \cdot A3(f) + (C1(f) \cdot B2(f) + D1(f) \cdot D2(f)) \cdot C3(f)] \cdot B4(f)] \cdot D5(f) + B5(f) \cdot [[(C1(f) \cdot A2(f) + D1(f) \cdot C2(f)) \cdot A3(f) + (C1(f) \cdot B2(f) + D1(f) \cdot D2(f)) \cdot C3(f)] \cdot A4(f) + [(C1(f) \cdot A2(f) + D1(f) \cdot C2(f)) \cdot B3(f) + (C1(f) \cdot B2(f) + D1(f) \cdot D2(f)) \cdot D3(f)] \cdot C4(f)]$$

$$S_{11}(f) := \frac{\left[A(f) + \left(\frac{B(f)}{Z_0} \right) - (C(f) \cdot Z_0) - D(f) \right]}{\left[A(f) + \left(\frac{B(f)}{Z_0} \right) + (C(f) \cdot Z_0) + D(f) \right]}$$

$$S_{12}(f) := \frac{2 \cdot [(A(f) \cdot D(f)) - (B(f) \cdot C(f))]}{\left[A(f) + \left(\frac{B(f)}{Z_0} \right) + (C(f) \cdot Z_0) + D(f) \right]}$$

$$S_{21}(f) := \frac{2}{\left[A(f) + \left(\frac{B(f)}{Z_0} \right) + (C(f) \cdot Z_0) + D(f) \right]}$$

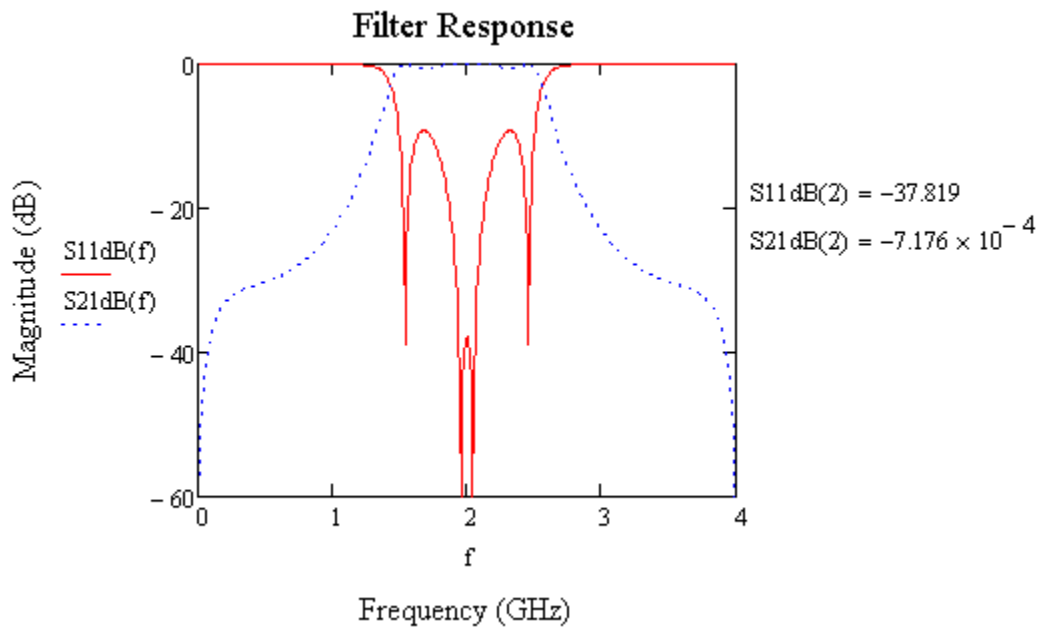
$$S_{22}(f) := \frac{\left[-(A(f)) + \left(\frac{B(f)}{Z_0} \right) - (C(f) \cdot Z_0) + D(f) \right]}{\left[A(f) + \left(\frac{B(f)}{Z_0} \right) + (C(f) \cdot Z_0) + D(f) \right]}$$

$$S_{11\text{dB}}(f) := 20 \cdot \log(|S_{11}(f)|)$$

$$S_{12\text{dB}}(f) := 20 \cdot \log(|S_{12}(f)|)$$

$$S_{21\text{dB}}(f) := 20 \cdot \log(|S_{21}(f)|)$$

$$S_{22\text{dB}}(f) := 20 \cdot \log(|S_{22}(f)|)$$



Cascaded Coupled line filter with Stubs Loaded:

$Z_{oe} := 200.95$ **Even Mode Impedance**
 $Z_{oo} := 66.2$ **Odd Mode Impedance**
 $Z_o := 50$ **Terminal Impedance**
 $Z_t := 100$ **Impedance Of Impedance Transformer**
 $Z_{cs} := 300$ **Impedance of the Stub**
 $\theta_o := 90\text{deg}$ **Electrical Length At Center Frequency**
 $f_o := 2$ **Center Frequency**
 $f := 0, 0.01 \dots 4$ **Frequency Range**
 $\theta(f) := \frac{f}{f_o} \cdot \theta_o$ **Theta At Each Frequency**

$$A1(f) := \cos(\theta(f))$$

$$B1(f) := i \cdot (Z_t) \cdot \sin(\theta(f))$$

$$C1(f) := i \cdot \left(\frac{1}{Z_t} \right) \cdot \sin(\theta(f))$$

$$D1(f) := A1(f)$$

$$A2(f) := \cos(\theta(f)) \cdot \left[1 + \left[\frac{2 \cdot Z_{oe} \cdot Z_{oo} \cdot (Z_{oe} + Z_{cs})}{Z_{oe} \cdot Z_{cs} \cdot (Z_{oe} - Z_{oo})} \right] \right]$$

$$B2(f) := i \cdot \left[\frac{2 \cdot Z_{oe} \cdot Z_{oo}}{(Z_{oe} - Z_{oo})} \right] \cdot \sin(\theta(f))$$

$$C2(f) := \frac{-2 \cdot (Z_{oe} + Z_{cs}) \cdot i \cdot \cos(\theta(f))}{Z_{oe} \cdot Z_{cs} \cdot \tan(\theta(f))} \cdot \left[1 + \frac{Z_{oe} \cdot Z_{oo} \cdot (Z_{oe} + Z_{cs})}{Z_{oe} \cdot Z_{cs} \cdot (Z_{oe} - Z_{oo})} \right] + \frac{i \cdot \sin(\theta(f)) \cdot (Z_{oe} - Z_{oo})}{2 \cdot Z_{oe} \cdot Z_{oo}}$$

$$D2(f) := A2(f)$$

$$A3(f) := A2(f)$$

$$B3(f) := B2(f)$$

$$C3(f) := C2(f)$$

$$D3(f) := A3(f)$$

$$A4(f) := A3(f)$$

$$B4(f) := B3(f)$$

$$C4(f) := C3(f)$$

$$D4(f) := A3(f)$$

$$A5(f) := A1(f)$$

$$B5(f) := B1(f)$$

$$C5(f) := C1(f)$$

$$D5(f) := A1(f)$$

$$\begin{aligned} \underline{A}(f) := & [[(A1(f) \cdot A2(f) + B1(f) \cdot C2(f)) \cdot A3(f) + (A1(f) \cdot B2(f) + B1(f) \cdot D2(f)) \cdot C3(f)] \cdot A4(f) + [(A1(f) \cdot A2(f) + B1(f) \cdot C2(f)) \cdot B3(f) + (A1(f) \cdot B2(f) + B1(f) \cdot D2(f)) \cdot D3(f)] \cdot C4(f) \cdot A5(f) + \\ & [[(A1(f) \cdot A2(f) + B1(f) \cdot C2(f)) \cdot B3(f) + (A1(f) \cdot B2(f) + B1(f) \cdot D2(f)) \cdot D3(f)] \cdot D4(f) + [(A1(f) \cdot A2(f) + B1(f) \cdot C2(f)) \cdot A3(f) + (A1(f) \cdot B2(f) + B1(f) \cdot D2(f)) \cdot C3(f)] \cdot B4(f)] \cdot C5(f) \end{aligned}$$

$$\begin{aligned} B(f) := & [[(A1(f) \cdot A2(f) + B1(f) \cdot C2(f)) \cdot B3(f) + (A1(f) \cdot B2(f) + B1(f) \cdot D2(f)) \cdot D3(f)] \cdot D4(f) + [(A1(f) \cdot A2(f) + B1(f) \cdot C2(f)) \cdot A3(f) + (A1(f) \cdot B2(f) + B1(f) \cdot D2(f)) \cdot C3(f)] \cdot B4(f)] \cdot D5(f) + \\ & B5(f) \cdot [[(A1(f) \cdot A2(f) + B1(f) \cdot C2(f)) \cdot A3(f) + (A1(f) \cdot B2(f) + B1(f) \cdot D2(f)) \cdot C3(f)] \cdot A4(f) + [(A1(f) \cdot A2(f) + B1(f) \cdot C2(f)) \cdot B3(f) + (A1(f) \cdot B2(f) + B1(f) \cdot D2(f)) \cdot D3(f)] \cdot C4(f) \end{aligned}$$

$$\begin{aligned} \underline{C}(f) := & [[(C1(f) \cdot A2(f) + D1(f) \cdot C2(f)) \cdot A3(f) + (C1(f) \cdot B2(f) + D1(f) \cdot D2(f)) \cdot C3(f)] \cdot A4(f) + [(C1(f) \cdot A2(f) + D1(f) \cdot C2(f)) \cdot B3(f) + (C1(f) \cdot B2(f) + D1(f) \cdot D2(f)) \cdot D3(f)] \cdot C4(f)] \cdot A5(f) + \\ & C5(f) \cdot [[(C1(f) \cdot A2(f) + D1(f) \cdot C2(f)) \cdot B3(f) + (C1(f) \cdot B2(f) + D1(f) \cdot D2(f)) \cdot D3(f)] \cdot D4(f) + [(C1(f) \cdot A2(f) + D1(f) \cdot C2(f)) \cdot A3(f) + (C1(f) \cdot B2(f) + D1(f) \cdot D2(f)) \cdot C3(f)] \cdot B4(f) \end{aligned}$$

$$\begin{aligned} D(f) := & [[(C1(f) \cdot A2(f) + D1(f) \cdot C2(f)) \cdot B3(f) + (C1(f) \cdot B2(f) + D1(f) \cdot D2(f)) \cdot D3(f)] \cdot D4(f) + [(C1(f) \cdot A2(f) + D1(f) \cdot C2(f)) \cdot A3(f) + (C1(f) \cdot B2(f) + D1(f) \cdot D2(f)) \cdot C3(f)] \cdot B4(f)] \cdot D5(f) + \\ & B5(f) \cdot [[(C1(f) \cdot A2(f) + D1(f) \cdot C2(f)) \cdot A3(f) + (C1(f) \cdot B2(f) + D1(f) \cdot D2(f)) \cdot C3(f)] \cdot A4(f) + [(C1(f) \cdot A2(f) + D1(f) \cdot C2(f)) \cdot B3(f) + (C1(f) \cdot B2(f) + D1(f) \cdot D2(f)) \cdot D3(f)] \cdot C4(f) \end{aligned}$$

$$S11(f) := \frac{\left[A(f) + \left(\frac{B(f)}{Z_0} \right) - (C(f) \cdot Z_0) - D(f) \right]}{\left[A(f) + \left(\frac{B(f)}{Z_0} \right) + (C(f) \cdot Z_0) + D(f) \right]}$$

$$S12(f) := \frac{2 \cdot [(A(f) \cdot D(f)) - (B(f) \cdot C(f))]}{\left[A(f) + \left(\frac{B(f)}{Z_0} \right) + (C(f) \cdot Z_0) + D(f) \right]}$$

$$S21(f) := \frac{2}{\left[A(f) + \left(\frac{B(f)}{Z_0} \right) + (C(f) \cdot Z_0) + D(f) \right]}$$

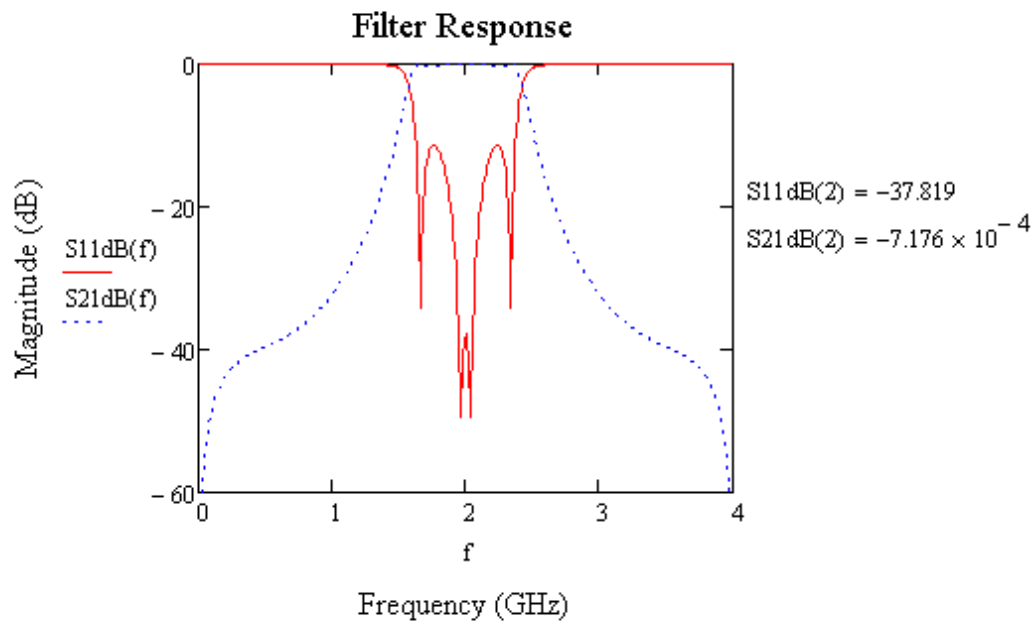
$$S22(f) := \frac{\left[-(A(f)) + \left(\frac{B(f)}{Z_0} \right) - (C(f) \cdot Z_0) + D(f) \right]}{\left[A(f) + \left(\frac{B(f)}{Z_0} \right) + (C(f) \cdot Z_0) + D(f) \right]}$$

$$S_{11\text{dB}}(f) := 20 \cdot \log(|S_{11}(f)|)$$

$$S_{12\text{dB}}(f) := 20 \cdot \log(|S_{12}(f)|)$$

$$S_{21\text{dB}}(f) := 20 \cdot \log(|S_{21}(f)|)$$

$$S_{22\text{dB}}(f) := 20 \cdot \log(|S_{22}(f)|)$$



Appendix 5: Cascaded Coupled Line Filter Designs 2

Matthaei Coupled Line Theory Filter

$$f0 := 2 \cdot 10^9$$

Set Center Frequency

$$f1 := 1.5 \cdot 10^9$$

Set Lower Cut Off

$$f2 := 2.5 \cdot 10^9$$

Set Higher Cut Off

$$FBW := \frac{f2 - f1}{f0}$$

Calculate FBW

$$FBW = 0.5$$

$$n := 5$$

Set Number of Poles

$$g_0 := 1$$

Set g values for the required Ripple Constant

$$g_1 := 0.9714$$

$$g_2 := 1.3721$$

$$g_3 := 1.8014$$

$$g_4 := 1.3721$$

$$g_5 := 0.9714$$

$$g_6 := 1$$

$$\theta1 := \frac{\pi}{2} \left(1 - \frac{FBW}{2} \right)$$

Calculate theta

$$\theta1 = 1.178$$

$$k := 0..n$$

Set range to calculate the even and odd mode impedances for the input and output sections

$$YA := 1$$

$$J_{k,k+1} := \frac{1}{\sqrt{\epsilon_k \cdot \epsilon_{k+1}}}$$

Calculate the even and odd mode impedances of the input and output sections

$$h := \frac{1}{\frac{\tan(\theta_1)}{2} + \left(\frac{J_{0,1}}{YA}\right)^2}$$

$$Y_{oo,k,k+1} := YA \cdot \left[\left(\frac{J_{k,k+1}}{YA} \cdot \sqrt{h} \right) + 1 \right]$$

$$Y_{oe,k,k+1} := (2 \cdot YA) - Y_{oo,k,k+1}$$

$$Y_{oe1,k,k+1} := Y_{oe,k,k+1} + \left[h \cdot YA \cdot \left[\frac{\tan(\theta_1)}{2} + \left(\frac{J_{k,k+1}}{YA} \right)^2 \right] \right] - YA$$

$$Y_{ool,k,k+1} := Y_{oe1,k,k+1} + Y_{oo,k,k+1} - Y_{oe,k,k+1}$$

$$Y_{oe1,0,1} = 0.322$$

$$Y_{oo0,1} = 1.678$$

$$Y_{oe0,1} = 0.322$$

$$Y_{ool0,1} = 1.678$$

$$Y_{oe1,5,6} = 0.322$$

$$Y_{oo5,6} = 1.678$$

$$Y_{oe5,6} = 0.322$$

$$Y_{ool5,6} = 1.678$$

$$Z_{oe,k,k+1} := \frac{50}{Y_{oe,k,k+1}}$$

$$Z_{oo,k,k+1} := \frac{50}{Y_{oo,k,k+1}}$$

$$Z_{oe0,1} = 155.492$$

$$Z_{oo0,1} = 29.79$$

$$Z_{oe5,6} = 155.492$$

$$Z_{ool5,6} = 29.79$$

$i := 1..n - 1$

Set range for calculating the interior section impedances

$$J_{i,i+1} := \frac{1}{\sqrt{\epsilon_i \cdot \epsilon_{i+1}}}$$

Calculate the interior impedances

$$N_{i,i+1} := \sqrt{\left(\frac{J_{i,i+1}}{2} \right)^2 + \frac{(\tan(\theta_1))^2}{4}}$$

$$Y_{oo2,i,i+1} := h \cdot YA \cdot \left(N_{i,i+1} + \frac{J_{i,i+1}}{YA} \right)$$

$$Y_{oe2,i,i+1} := h \cdot YA \cdot \left(N_{i,i+1} - \frac{J_{i,i+1}}{YA} \right)$$

$$Y_{oe2,1,2} = 0.186$$

$$Y_{oo2,1,2} = 0.961$$

$$Y_{oe2,4,5} = 0.186$$

$$Y_{oo2,4,5} = 0.961$$

$$Yoe2_{2,3} = 0.274$$

$$Yoo2_{2,3} = 0.843$$

$$Yoe2_{3,4} = 0.274$$

$$Yoo2_{3,4} = 0.843$$

$$Zoe2_{i,i+1} := \frac{50}{Yoe2_{i,i+1}}$$

$$Zoo2_{i,i+1} := \frac{50}{Yoo2_{i,i+1}}$$

$$Zoe2_{1,2} = 268.643$$

$$Zoo2_{1,2} = 52.046$$

$$Zoe2_{4,5} = 268.643$$

$$Zoo2_{4,5} = 52.046$$

$$Zoe2_{2,3} = 182.655$$

$$Zoo2_{2,3} = 59.345$$

$$Zoe2_{3,4} = 182.655$$

$$Zoo2_{3,4} = 59.345$$

Four Section Equivalent Short Circuit Stub Circuit Design:

$$f_0 := 2 \cdot 10^9 \quad \text{Set } f_0$$

$$f_1 := 1.5 \cdot 10^9 \quad \text{Set } f_1$$

$$f_2 := 2.5 \cdot 10^9 \quad \text{Set } f_2$$

$$\text{FBW} := \frac{f_2 - f_1}{f_0} \quad \text{Calculate FBW}$$

$$\text{FBW} = 0.5$$

$$n := 5 \quad \text{Set Number of Poles}$$

$$g_0 := 1 \quad \text{Choose } g \text{ Values}$$

$$g_1 := 0.9714$$

$$g_2 := 1.3721$$

$$g_3 := 1.8014$$

$$g_4 := 1.3721$$

$$g_5 := 0.9714$$

$$g_6 := 1$$

$$d := 1 \quad \text{Set } d$$

$$C_a := 2 \cdot d \cdot g_1 \quad \text{Calculate } C_a$$

$$\theta_1 := \frac{\pi}{2} \cdot \left(1 - \frac{\text{FBW}}{2} \right) \quad \text{Calculate } \theta_1$$

$$\theta_1 = 1.178$$

$$k := 1..n$$

$$Y_A := 1$$

$$Y_{I_{1,2}} := \epsilon_0 \cdot \sqrt{\frac{C_a}{\epsilon_2}} \cdot Y_A$$

Calculate Connecting Line 1,2 Impedance

$$N_{I_{1,2}} := \sqrt{\left(\frac{Y_{I_{1,2}}}{Y_A}\right)^2 + \left(\frac{\epsilon_0 \cdot \text{Catan}(\theta_1)}{2}\right)^2}$$

$$Z_{I_{1,2}} := \left(\frac{50}{Y_{I_{1,2}}}\right)$$

$$Y_{I_{1,2}} = 1.19 \quad Z_{I_{1,2}} = 42.019$$

$$Y_1 := \epsilon_0 \cdot Y_A \cdot (1 - d) \cdot \epsilon_1 \cdot \tan(\theta_1) + Y_A \cdot \left(N_{I_{1,2}} - \frac{Y_{I_{1,2}}}{Y_A}\right)$$

Calculate Stub impedance Z1

$$Z_1 := \frac{50}{Y_1}$$

$$Y_1 = 1.44 \quad Z_1 = 34.726$$

$$Y_{O_{n-1,n}} := \epsilon_0 \cdot \sqrt{\frac{C_a \cdot \epsilon_{n+1}}{\epsilon_0 \cdot \epsilon_{n-1}}} \cdot Y_A$$

Calculate Connecting Line 4,5 Impedance

$$N_{O_{n-1,n}} := \sqrt{\left(\frac{Y_{O_{n-1,n}}}{Y_A}\right)^2 + \left(\frac{\epsilon_0 \cdot \text{Catan}(\theta_1)}{2}\right)^2}$$

$$Z_{O_{4,5}} := \frac{50}{Y_{O_{4,5}}}$$

$$Y_{O_{4,5}} = 1.19 \quad Z_{O_{4,5}} = 42.019$$

$$Y_n := Y_A \cdot (\epsilon_n \cdot \epsilon_{n+1} - d \cdot \epsilon_0 \cdot \epsilon_1) \cdot \tan(\theta_1) + Y_A \cdot \left(N_{O_{n-1,n}} - \frac{Y_{O_{n-1,n}}}{Y_A}\right)$$

Calculate Stub Impedance Z5

$$Z_n := \frac{50}{Y_n}$$

$$Y_5 = 1.44 \quad Z_5 = 34.726$$

$i := 1..n - 1$

Calculate all Remaining Impedances

$$Y_{i,i+1} := YA \cdot \frac{\epsilon_0 \cdot Ca}{\sqrt{\epsilon_1 \epsilon_{i+1}}}$$

$$N_{i,i+1} := \sqrt{\left(\frac{Y_{i,i+1}}{YA}\right)^2 + \left(\frac{\epsilon_0 \cdot \text{Catan}(\theta_1)}{2}\right)^2}$$

$$y_i := YA \cdot \left[N_{i-1,i} + N_{i,i+1} - \left(\frac{Y_{i-1,i}}{YA}\right) - \left(\frac{Y_{i,i+1}}{YA}\right) \right]$$

$$z_i := \frac{50}{y_i}$$

$$Z_{i,i+1} := \frac{50}{Y_{i,i+1}}$$

$$Y_{1,2} = 1.19$$

$$Z_{1,2} = 42.019$$

All Impedances

$$y_2 = 2.619$$

$$z_2 = 19.093$$

$$Y_{2,3} = 1.236$$

$$Z_{2,3} = 40.461$$

$$y_3 = 2.83$$

$$z_3 = 17.667$$

$$Y_{3,4} = 1.236$$

$$Z_{3,4} = 40.461$$

$$y_4 = 2.619$$

$$z_4 = 19.093$$

$$Y_{4,5} = 1.19$$

$$Z_{4,5} = 42.019$$

Four Section Coupled Line Filter With no Stubs Loaded:

$Z_{oe} := 37.24$ **Even Mode Impedance**

$Z_{oo} := 13.28$ **Odd Mode Impedance**

$Z_o := 50$ **Terminal Impedance**

$\theta_o := 90\text{deg}$ **Electrical Length At Center Frequency**

$f_o := 2$ **Center Frequency**

$f := 0, 0.01 \dots 4$ **Frequency Range**

$\theta(f) := \frac{f}{f_o} \cdot \theta_o$ **Theta At Each Frequency**

$$A1(f) := \cos(\theta(f)) \cdot \left[1 + \left[\frac{2 \cdot Z_{oe} \cdot Z_{oo}}{Z_{oe} \cdot (Z_{oe} - Z_{oo})} \right] \right]$$

$$B1(f) := i \cdot \left[\frac{2 \cdot Z_{oe} \cdot Z_{oo}}{(Z_{oe} - Z_{oo})} \right] \cdot \sin(\theta(f))$$

$$C1(f) := \frac{-2 \cdot i \cdot \cos(\theta(f))}{Z_{oe} \cdot \tan(\theta(f))} \cdot \left[1 + \frac{Z_{oe} \cdot Z_{oo}}{Z_{oe} \cdot (Z_{oe} - Z_{oo})} \right] + \frac{i \cdot \sin(\theta(f)) \cdot (Z_{oe} - Z_{oo})}{2 \cdot Z_{oe} \cdot Z_{oo}}$$

$$D1(f) := A1(f)$$

$$A2(f) := A1(f)$$

$$B2(f) := B1(f)$$

$$C2(f) := C1(f)$$

$$D2(f) := A1(f)$$

$$A3(f) := A1(f)$$

$$B3(f) := B1(f)$$

$$C3(f) := C1(f)$$

$$D3(f) := A3(f)$$

$$A4(f) := A3(f)$$

$$B4(f) := B3(f)$$

$$C4(f) := C3(f)$$

$$D4(f) := A3(f)$$

$$A(f) := [(A1(f) \cdot A2(f) + B1(f) \cdot C2(f)) \cdot A3(f) + (A1(f) \cdot B2(f) + B1(f) \cdot D2(f)) \cdot C3(f)] \cdot A4(f) + [(A1(f) \cdot A2(f) + B1(f) \cdot C2(f)) \cdot B3(f) + (A1(f) \cdot B2(f) + B1(f) \cdot D2(f)) \cdot D3(f)] \cdot C4(f)$$

$$B(f) := [(A1(f) \cdot A2(f) + B1(f) \cdot C2(f)) \cdot B3(f) + (A1(f) \cdot B2(f) + B1(f) \cdot D2(f)) \cdot D3(f)] \cdot D4(f) + [(A1(f) \cdot A2(f) + B1(f) \cdot C2(f)) \cdot A3(f) + (A1(f) \cdot B2(f) + B1(f) \cdot D2(f)) \cdot C3(f)] \cdot B4(f)$$

$$C(f) := [(C1(f) \cdot A2(f) + D1(f) \cdot C2(f)) \cdot A3(f) + (C1(f) \cdot B2(f) + D1(f) \cdot D2(f)) \cdot C3(f)] \cdot A4(f) + [(C1(f) \cdot A2(f) + D1(f) \cdot C2(f)) \cdot B3(f) + (C1(f) \cdot B2(f) + D1(f) \cdot D2(f)) \cdot D3(f)] \cdot C4(f)$$

$$D(f) := [(C1(f) \cdot A2(f) + D1(f) \cdot C2(f)) \cdot B3(f) + (C1(f) \cdot B2(f) + D1(f) \cdot D2(f)) \cdot D3(f)] \cdot D4(f) + [(C1(f) \cdot A2(f) + D1(f) \cdot C2(f)) \cdot A3(f) + (C1(f) \cdot B2(f) + D1(f) \cdot D2(f)) \cdot C3(f)] \cdot B4(f)$$

$$S11(f) := \frac{\left[A(f) + \left(\frac{B(f)}{Z_0} \right) - (C(f) \cdot Z_0) - D(f) \right]}{\left[A(f) + \left(\frac{B(f)}{Z_0} \right) + (C(f) \cdot Z_0) + D(f) \right]}$$

$$S12(f) := \frac{2 \cdot [(A(f) \cdot D(f)) - (B(f) \cdot C(f))]}{\left[A(f) + \left(\frac{B(f)}{Z_0} \right) + (C(f) \cdot Z_0) + D(f) \right]}$$

$$S21(f) := \frac{2}{\left[A(f) + \left(\frac{B(f)}{Z_0} \right) + (C(f) \cdot Z_0) + D(f) \right]}$$

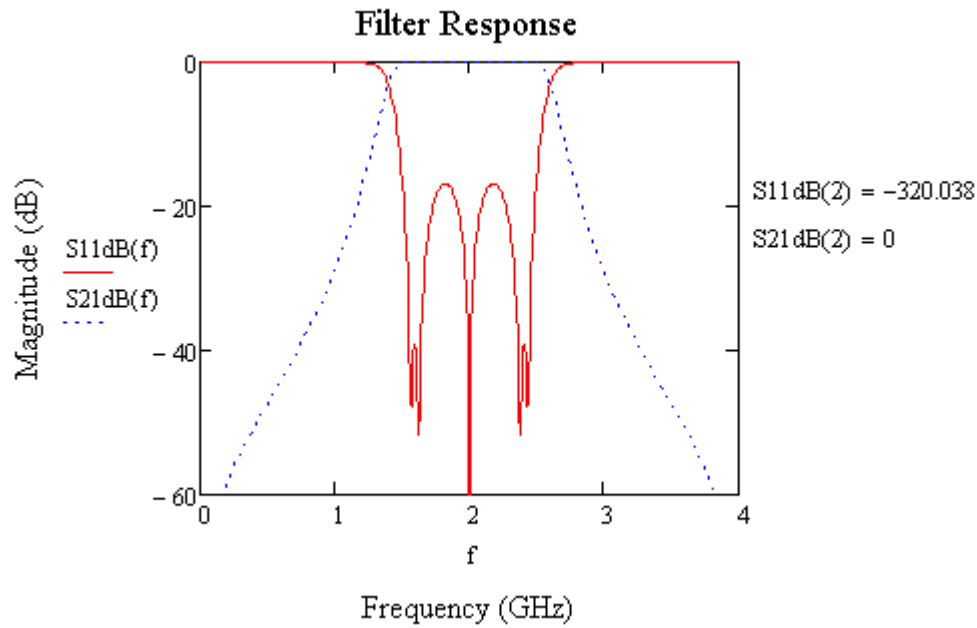
$$S22(f) := \frac{\left[-(A(f)) + \left(\frac{B(f)}{Z_0} \right) - (C(f) \cdot Z_0) + D(f) \right]}{\left[A(f) + \left(\frac{B(f)}{Z_0} \right) + (C(f) \cdot Z_0) + D(f) \right]}$$

$$S11dB(f) := 20 \cdot \log(|S11(f)|)$$

$$S12dB(f) := 20 \cdot \log(|S12(f)|)$$

$$S21dB(f) := 20 \cdot \log(|S21(f)|)$$

$$S22dB(f) := 20 \cdot \log(|S22(f)|)$$



Four Section Coupled Line Filter With Stubs Loaded:

- $Z_{oe} := 37.24$ **Even Mode Impedance**
- $Z_{oo} := 13.28$ **Odd Mode Impedance**
- $Z_o := 50$ **Terminal Impedance**
- $Z_{cs} := 100$ **Stub Impedance**
- $\theta_o := 90 \text{ deg}$ **Electrical Length At Center Frequency**
- $f_o := 2$ **Center Frequency**
- $f := 0, 0.01 \dots 4$ **Frequency Range**
- $\theta(f) := \frac{f}{f_o} \cdot \theta_o$ **Theta At Each Frequency**

$$A1(f) := \cos(\theta(f)) \cdot \left[1 + \left[\frac{2 \cdot Z_{oe} \cdot Z_{oo} \cdot (Z_{oe} + Z_{cs})}{Z_{oe} \cdot Z_{cs} \cdot (Z_{oe} - Z_{oo})} \right] \right]$$

$$B1(f) := i \cdot \left[\frac{2 \cdot Z_{oe} \cdot Z_{oo}}{(Z_{oe} - Z_{oo})} \right] \cdot \sin(\theta(f))$$

$$C1(f) := \frac{-2 \cdot (Z_{oe} + Z_{cs}) \cdot i \cdot \cos(\theta(f))}{Z_{oe} \cdot Z_{cs} \cdot \tan(\theta(f))} \cdot \left[1 + \frac{Z_{oe} \cdot Z_{oo} \cdot (Z_{oe} + Z_{cs})}{Z_{oe} \cdot Z_{cs} \cdot (Z_{oe} - Z_{oo})} \right] + \frac{i \cdot \sin(\theta(f)) \cdot (Z_{oe} - Z_{oo})}{2 \cdot Z_{oe} \cdot Z_{oo}}$$

$$D1(f) := A1(f)$$

$$A2(f) := A1(f)$$

$$B2(f) := B1(f)$$

$$C2(f) := C1(f)$$

$$D2(f) := A1(f)$$

$$A3(f) := A1(f)$$

$$B3(f) := B1(f)$$

$$C3(f) := C1(f)$$

$$D3(f) := A3(f)$$

$$A4(f) := A3(f)$$

$$B4(f) := B3(f)$$

$$C4(f) := C3(f)$$

$$D4(f) := A3(f)$$

$$A(f) := [(A1(f) \cdot A2(f) + B1(f) \cdot C2(f)) \cdot A3(f) + (A1(f) \cdot B2(f) + B1(f) \cdot D2(f)) \cdot C3(f)] \cdot A4(f) + [(A1(f) \cdot A2(f) + B1(f) \cdot C2(f)) \cdot B3(f) + (A1(f) \cdot B2(f) + B1(f) \cdot D2(f)) \cdot D3(f)] \cdot C4(f)$$

$$B(f) := [(A1(f) \cdot A2(f) + B1(f) \cdot C2(f)) \cdot B3(f) + (A1(f) \cdot B2(f) + B1(f) \cdot D2(f)) \cdot D3(f)] \cdot D4(f) + [(A1(f) \cdot A2(f) + B1(f) \cdot C2(f)) \cdot A3(f) + (A1(f) \cdot B2(f) + B1(f) \cdot D2(f)) \cdot C3(f)] \cdot B4(f)$$

$$C(f) := [(C1(f) \cdot A2(f) + D1(f) \cdot C2(f)) \cdot A3(f) + (C1(f) \cdot B2(f) + D1(f) \cdot D2(f)) \cdot C3(f)] \cdot A4(f) + [(C1(f) \cdot A2(f) + D1(f) \cdot C2(f)) \cdot B3(f) + (C1(f) \cdot B2(f) + D1(f) \cdot D2(f)) \cdot D3(f)] \cdot C4(f)$$

$$D(f) := [(C1(f) \cdot A2(f) + D1(f) \cdot C2(f)) \cdot B3(f) + (C1(f) \cdot B2(f) + D1(f) \cdot D2(f)) \cdot D3(f)] \cdot D4(f) + [(C1(f) \cdot A2(f) + D1(f) \cdot C2(f)) \cdot A3(f) + (C1(f) \cdot B2(f) + D1(f) \cdot D2(f)) \cdot C3(f)] \cdot B4(f)$$

$$S_{11}(f) := \frac{\left[A(f) + \left(\frac{B(f)}{Z_0} \right) - (C(f) \cdot Z_0) - D(f) \right]}{\left[A(f) + \left(\frac{B(f)}{Z_0} \right) + (C(f) \cdot Z_0) + D(f) \right]}$$

$$S_{12}(f) := \frac{2 \cdot [(A(f) \cdot D(f)) - (B(f) \cdot C(f))]}{\left[A(f) + \left(\frac{B(f)}{Z_0} \right) + (C(f) \cdot Z_0) + D(f) \right]}$$

$$S_{21}(f) := \frac{2}{\left[A(f) + \left(\frac{B(f)}{Z_0} \right) + (C(f) \cdot Z_0) + D(f) \right]}$$

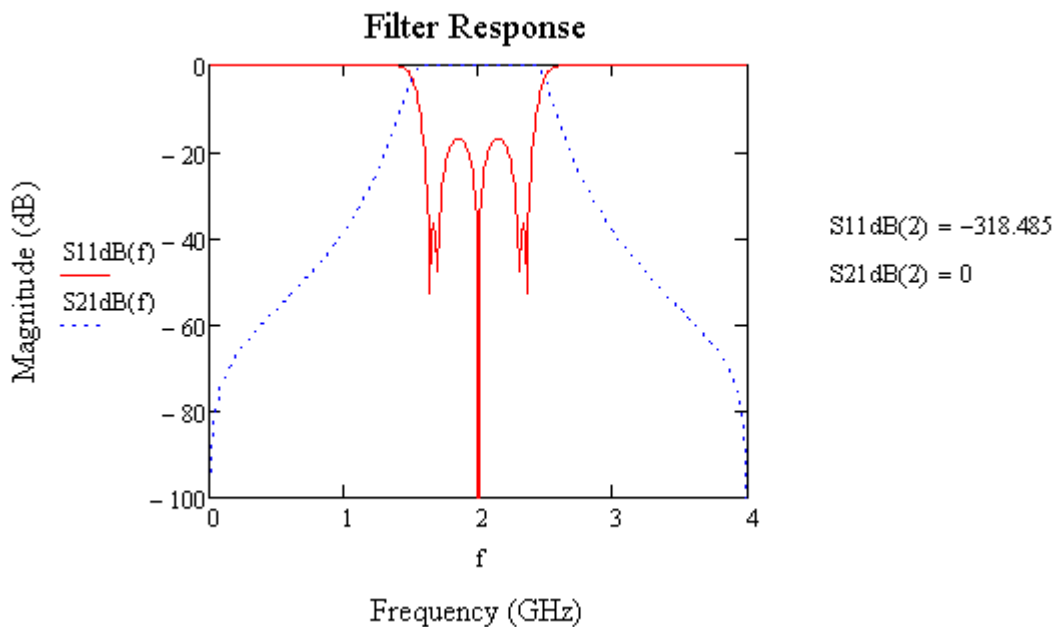
$$S_{22}(f) := \frac{\left[-(A(f)) + \left(\frac{B(f)}{Z_0} \right) - (C(f) \cdot Z_0) + D(f) \right]}{\left[A(f) + \left(\frac{B(f)}{Z_0} \right) + (C(f) \cdot Z_0) + D(f) \right]}$$

$$S_{11\text{dB}}(f) := 20 \cdot \log(|S_{11}(f)|)$$

$$S_{12\text{dB}}(f) := 20 \cdot \log(|S_{12}(f)|)$$

$$S_{21\text{dB}}(f) := 20 \cdot \log(|S_{21}(f)|)$$

$$S_{22\text{dB}}(f) := 20 \cdot \log(|S_{22}(f)|)$$



Appendix 6: Filter Designs for Chapter 8

State 1 Filter Design:

$$f_0 := 3.1 \cdot 10^9$$

Set f0

$$f_1 := 2.2 \cdot 10^9$$

Set f1

$$f_2 := 4 \cdot 10^9$$

Set f2

$$FBW := \frac{f_2 - f_1}{f_0}$$

Calculate FBW

$$FBW = 0.581$$

$$n := 3$$

Set Number of Poles

$$g_0 := 1$$

g Values

$$g_1 := 0.8516$$

$$g_2 := 1.1032$$

$$g_3 := 0.8516$$

$$g_4 := 1$$

$$d := 0.647$$

Set d

$$C_a := 2 \cdot d \cdot g_1$$

Calculate Ca

$$\theta_1 := \frac{\pi}{2} \cdot \left(1 - \frac{FBW}{2} \right)$$

Calculate Theta 1

$$\theta_1 = 1.115$$

$$k := 1..n$$

$$Y_A := 1$$

$$J_{1,2} := \epsilon_0 \cdot \sqrt{\frac{Ca}{\epsilon_2}}$$

Calculate Impedance of Stub one

$$NI_{1,2} := \sqrt{\left(\frac{J_{1,2}}{YA}\right)^2 + \left(\frac{\epsilon_0 \cdot \text{Catan}(\theta_1)}{2}\right)^2}$$

$$Y_1 := \epsilon_0 \cdot YA \cdot (1 - d) \cdot \epsilon_1 \cdot \tan(\theta_1) + YA \cdot \left(NI_{1,2} - \frac{J_{1,2}}{YA}\right)$$

$$Z_1 := \frac{50}{Y_1}$$

$$Y_1 = 1.117 \quad Z_1 = 44.766$$

$$YI_{1,2} := YA \cdot \left(\frac{J_{1,2}}{YA}\right)$$

Calculate Connecting Lines 1,2

$$YI_{1,2} = 0.999$$

$$JO_{n-1,n} := \epsilon_0 \cdot \sqrt{\frac{Ca \cdot \epsilon_{n+1}}{\epsilon_0 \cdot \epsilon_{n-1}}}$$

$$NO_{n-1,n} := \sqrt{\left(\frac{JO_{n-1,n}}{YA}\right)^2 + \left(\frac{\epsilon_0 \cdot \text{Catan}(\theta_1)}{2}\right)^2}$$

$$Y_n := YA \cdot (\epsilon_n \cdot \epsilon_{n+1} - d \cdot \epsilon_0 \cdot \epsilon_1) \cdot \tan(\theta_1) + YA \cdot \left(NO_{n-1,n} - \frac{JO_{n-1,n}}{YA}\right)$$

$$Z_n := \frac{50}{Y_n}$$

Calculate Stub Impedance Three

$$Y_3 = 1.117 \quad Z_3 = 44.766$$

$$YO_{n-1,n} := YA \cdot \left(\frac{JO_{n-1,n}}{YA}\right)$$

Calculate Connecting Lines 2,3

$$ZO_{2,3} := \frac{50}{YO_{2,3}}$$

$$YO_{2,3} = 0.999 \quad ZO_{2,3} = 50.028$$

$i := 1..n$

$$J_{i,i+1} := \frac{\epsilon_0 \cdot Ca}{\sqrt{\epsilon_i \cdot \epsilon_{i+1}}}$$

Calculate Stub Impedance 2

$$N_{i,i+1} := \sqrt{\left(\frac{J_{i,i+1}}{YA}\right)^2 + \left(\frac{\epsilon_0 \cdot \text{Catan}(\theta_1)}{2}\right)^2}$$

$$Y_i := YA \cdot \left(N_{i-1,i} + N_{i,i+1} - \frac{J_{i-1,i}}{YA} - \frac{J_{i,i+1}}{YA} \right)$$

$$Z_i := \frac{50}{Y_i}$$

$$Y_2 = 0.923$$

$$Z_2 = 54.195$$

State 2 Filter Design:

$$f_0 := 4.9 \cdot 10^9$$

Set f0

$$f_1 := 4 \cdot 10^9$$

Set f1

$$f_2 := 5.8 \cdot 10^9$$

Set f2

$$FBW := \frac{f_2 - f_1}{f_0}$$

Calculate FBW

$$FBW = 0.367$$

$$n := 3$$

Set Number of Poles

$$g_0 := 1$$

g Values

$$g_1 := 0.8516$$

$$g_2 := 1.1032$$

$$g_3 := 0.8516$$

$$g_4 := 1$$

$$d := 0.647$$

Set d

$$C_a := 2 \cdot d \cdot g_1$$

Calculate Ca

$$\theta_1 := \frac{\pi}{2} \cdot \left(1 - \frac{FBW}{2} \right)$$

Calculate Theta 1

$$\theta_1 = 1.282$$

$$k := 1..n$$

$$Y_A := 1$$

$$J_{1,2} := \epsilon_0 \cdot \sqrt{\frac{Ca}{\epsilon_2}}$$

Calculate Impedance of Stub one

$$NI_{1,2} := \sqrt{\left(\frac{J_{1,2}}{YA}\right)^2 + \left(\frac{\epsilon_0 \cdot \text{Catan}(\theta 1)}{2}\right)^2}$$

$$Y_1 := \epsilon_0 \cdot YA \cdot (1 - d) \cdot \epsilon_1 \cdot \tan(\theta 1) + YA \cdot \left(NI_{1,2} - \frac{J_{1,2}}{YA}\right)$$

$$Z_1 := \frac{50}{Y_1}$$

$$Y_1 = 2.122 \quad Z_1 = 23.565$$

$$YI_{1,2} := YA \cdot \left(\frac{J_{1,2}}{YA}\right)$$

Calculate Connecting Lines 1,2

$$YI_{1,2} = 0.999$$

$$JO_{n-1,n} := \epsilon_0 \cdot \sqrt{\frac{Ca \cdot \epsilon_{n+1}}{\epsilon_0 \cdot \epsilon_{n-1}}}$$

$$NO_{n-1,n} := \sqrt{\left(\frac{JO_{n-1,n}}{YA}\right)^2 + \left(\frac{\epsilon_0 \cdot \text{Catan}(\theta 1)}{2}\right)^2}$$

$$Y_n := YA \cdot (\epsilon_n \cdot \epsilon_{n+1} - d \cdot \epsilon_0 \cdot \epsilon_1) \cdot \tan(\theta 1) + YA \cdot \left(NO_{n-1,n} - \frac{JO_{n-1,n}}{YA}\right)$$

$$Z_n := \frac{50}{Y_n}$$

Calculate Stub Impedance Three

$$Y_3 = 2.122 \quad Z_3 = 23.565$$

$$YO_{n-1,n} := YA \cdot \left(\frac{JO_{n-1,n}}{YA}\right)$$

Calculate Connecting Lines 2,3

$$ZO_{2,3} := \frac{50}{YO_{2,3}}$$

$$YO_{2,3} = 0.999 \quad ZO_{2,3} = 50.028$$

$$i := 1..n$$

$$i = 1..n$$

$$J_{i,i+1} = \frac{\epsilon_0 \cdot Ca}{\sqrt{\epsilon_i \cdot \epsilon_{i+1}}}$$

Calculate Stub Impedance 2

$$N_{i,i+1} = \sqrt{\left(\frac{J_{i,i+1}}{YA}\right)^2 + \left(\frac{\epsilon_0 \cdot \text{Catan}(\theta l)}{2}\right)^2}$$

$$Y_i = YA \cdot \left(N_{i-1,i} + N_{i,i+1} - \frac{J_{i-1,i}}{YA} - \frac{J_{i,i+1}}{YA} \right)$$

$$Z_i = \frac{50}{Y_i}$$

$$Y_2 = 2.08$$

$$Z_2 = 24.038$$

State 3 Filter Design:

$$f_0 := 4 \cdot 10^9$$

Set f0

$$f_1 := 2.2 \cdot 10^9$$

Set f1

$$f_2 := 5.8 \cdot 10^9$$

Set f2

$$\text{FBW} := \frac{f_2 - f_1}{f_0}$$

Calculate FBW

$$\text{FBW} = 0.9$$

$$n := 3$$

Set Number of Poles

$$g_0 := 1$$

g Values

$$g_1 := 0.8516$$

$$g_2 := 1.1032$$

$$g_3 := 0.8516$$

$$g_4 := 1$$

$$d := 0.647$$

Set d

$$C_a := 2 \cdot d \cdot g_1$$

Calculate Ca

$$\theta_1 := \frac{\pi}{2} \cdot \left(1 - \frac{\text{FBW}}{2} \right)$$

Calculate Theta 1

$$\theta_1 = 0.864$$

$$k := 1..n$$

$$Y_A := 1$$

$$\Pi_{1,2} := \epsilon_0 \cdot \sqrt{\frac{Ca}{\epsilon_2}}$$

Calculate Impedance of Stub one

$$NI_{1,2} := \sqrt{\left(\frac{\Pi_{1,2}}{YA}\right)^2 + \left(\frac{\epsilon_0 \cdot Ca \tan(\theta_1)}{2}\right)^2}$$

$$Y_1 := \epsilon_0 \cdot YA \cdot (1 - d) \cdot \epsilon_1 \cdot \tan(\theta_1) + YA \cdot \left(NI_{1,2} - \frac{\Pi_{1,2}}{YA}\right)$$

$$Z_1 := \frac{50}{Y_1}$$

$$Y_1 = 0.542 \quad Z_1 = 92.234$$

$$YI_{1,2} := YA \cdot \left(\frac{\Pi_{1,2}}{YA}\right)$$

Calculate Connecting Lines 1,2

$$YI_{1,2} = 0.999$$

$$JO_{n-1,n} := \epsilon_0 \cdot \sqrt{\frac{Ca \cdot \epsilon_{n+1}}{\epsilon_0 \cdot \epsilon_{n-1}}}$$

$$NO_{n-1,n} := \sqrt{\left(\frac{JO_{n-1,n}}{YA}\right)^2 + \left(\frac{\epsilon_0 \cdot Ca \tan(\theta_1)}{2}\right)^2}$$

$$Y_n := YA \cdot (\epsilon_n \cdot \epsilon_{n+1} - d \cdot \epsilon_0 \cdot \epsilon_1) \cdot \tan(\theta_1) + YA \cdot \left(NO_{n-1,n} - \frac{JO_{n-1,n}}{YA}\right)$$

$$Z_n := \frac{50}{Y_n}$$

Calculate Stub Impedance Three

$$Y_3 = 0.542 \quad Z_3 = 92.234$$

$$YO_{n-1,n} := YA \cdot \left(\frac{JO_{n-1,n}}{YA}\right)$$

Calculate Connecting Lines 2,3

$$ZO_{2,3} := \frac{50}{YO_{2,3}}$$

$$YO_{2,3} = 0.999 \quad ZO_{2,3} = 50.028$$

$$i := 1..n$$

$i := 1..n$

$$J_{i,i+1} := \frac{\epsilon_0 \cdot Ca}{\sqrt{\epsilon_i \cdot \epsilon_{i+1}}}$$

Calculate Stub Impedance 2

$$N_{i,i+1} := \sqrt{\left(\frac{J_{i,i+1}}{YA}\right)^2 + \left(\frac{\epsilon_0 \cdot \text{Catan}(\theta l)}{2}\right)^2}$$

$$Y_i := YA \cdot \left(N_{i-1,i} + N_{i,i+1} - \frac{J_{i-1,i}}{YA} - \frac{J_{i,i+1}}{YA}\right)$$

$$Z_i := \frac{50}{Y_i}$$

$$Y_2 = 0.341$$

$$Z_2 = 146.817$$

Appendix 7: Bias Circuit Tests

As part of the filter design a suitable bias circuit and bypass network to ground needs to be considered. The following shows different arrangement for these (connected to 50 Ω) lines used in the various filters in this thesis:

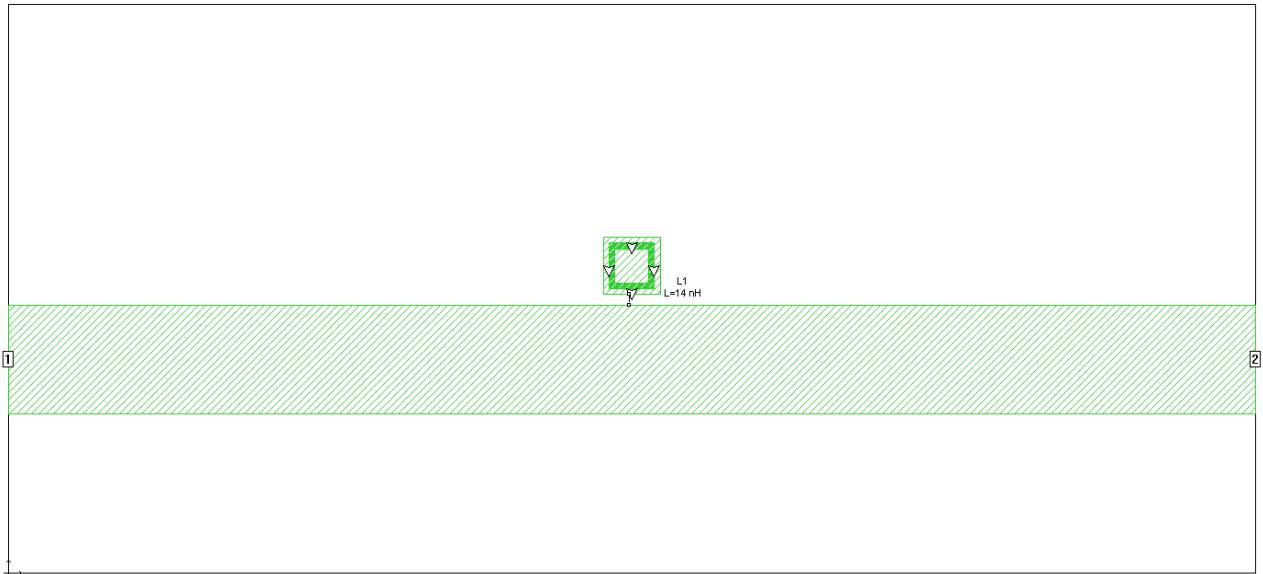


Fig1. Bypass Network to ground.

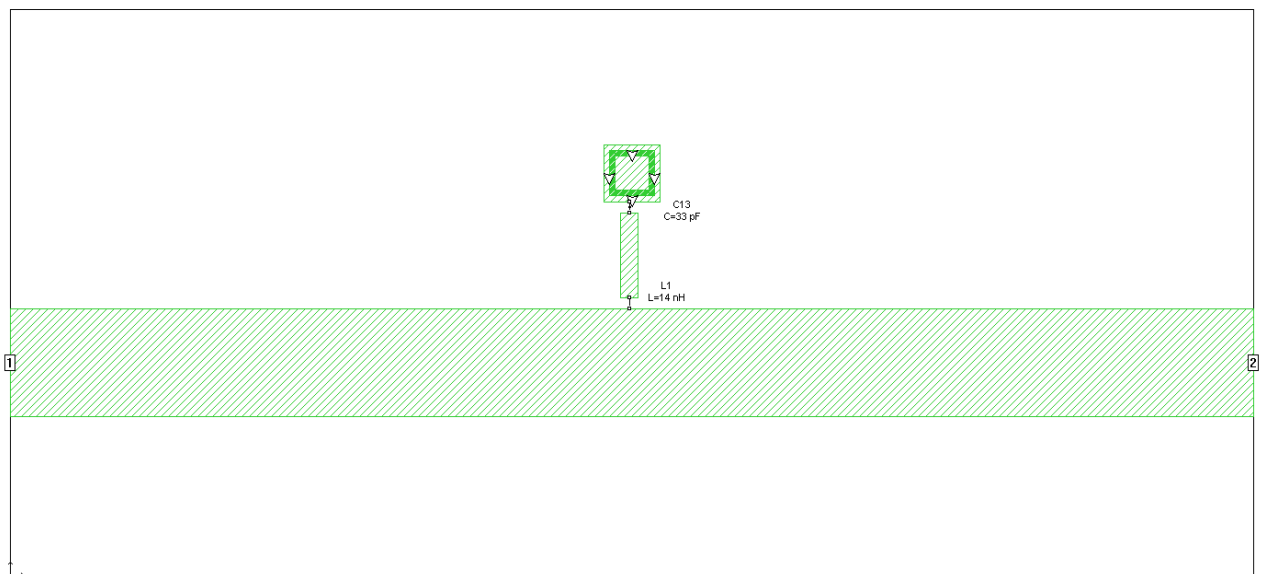


Fig 2. Bias Network used in the majority of filters designed.

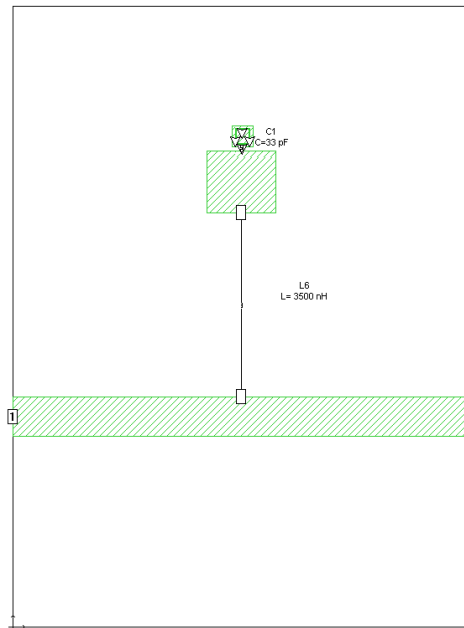


Fig 3. Bias Network used in the Multichannel Filter



Fig 4. Photograph of Bypass Network to ground



Fig 5. Photograph of Bias Network from Fig 2



Fig 6. Photograph of Bias Network from Fig 3

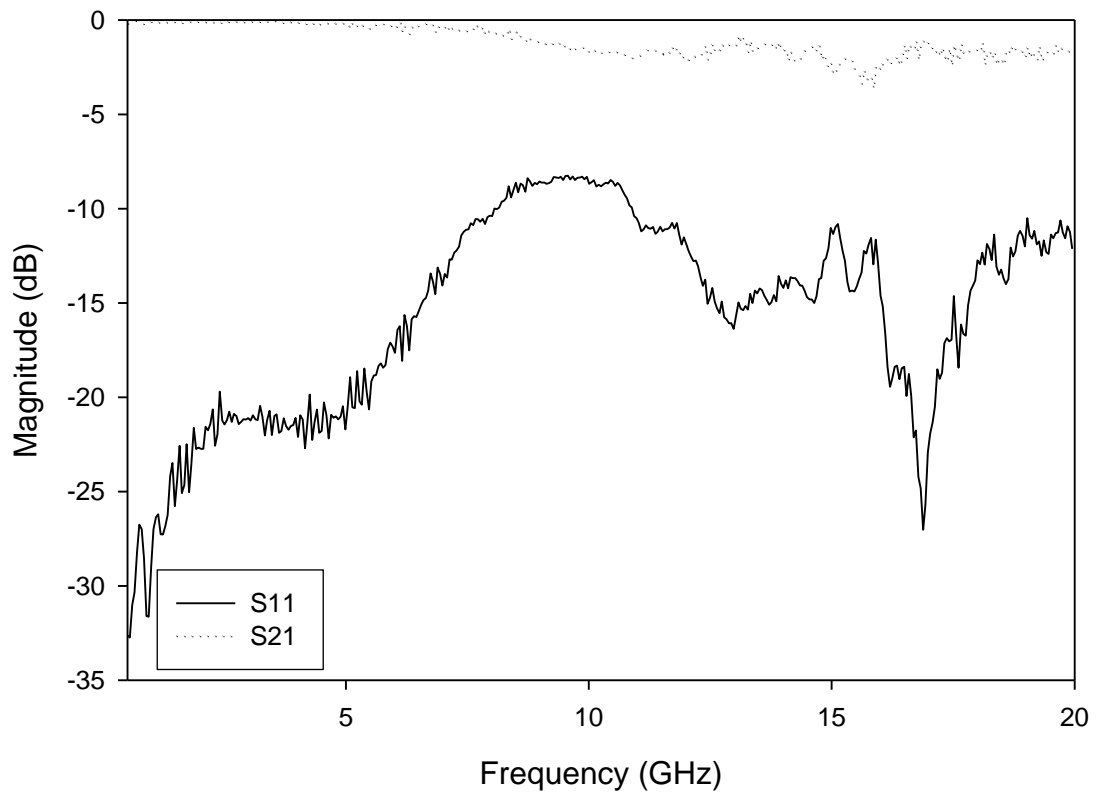


Fig 7. Measured Response of Bypass Network

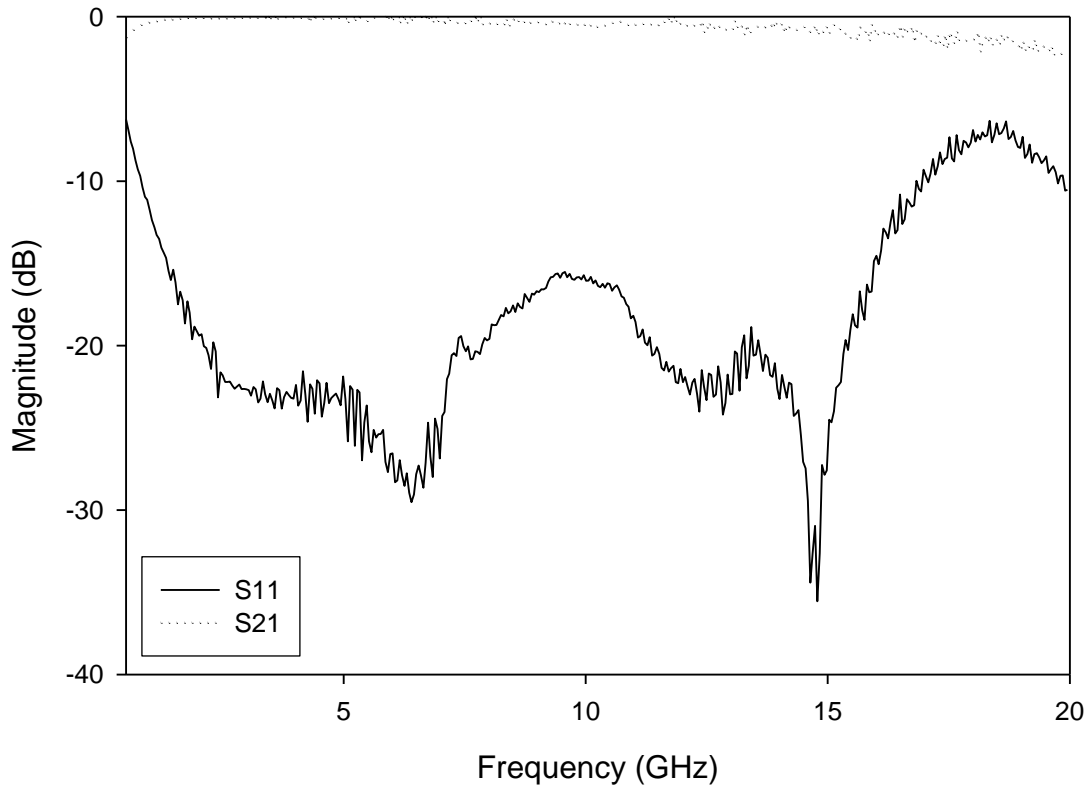


Fig 8. Measured Response of Bias Network from Fig 5

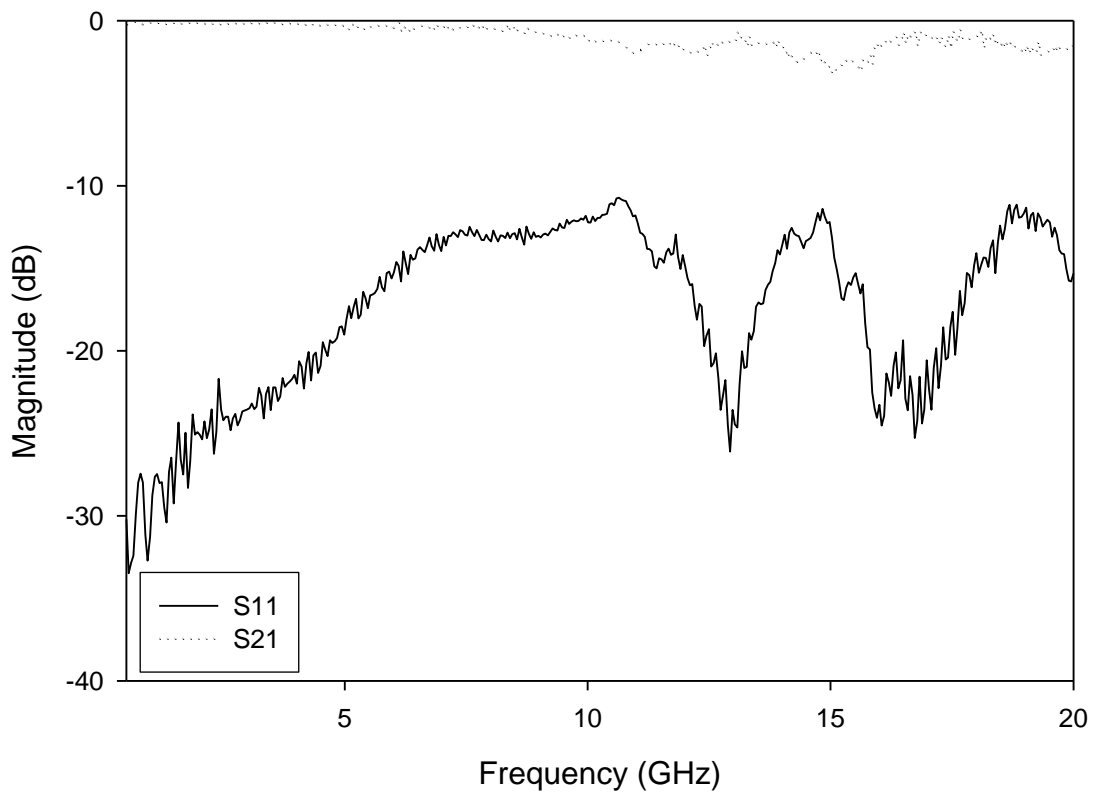


Fig 9. Measured Response of Bias Network from Fig 6

Appendix 8: Data Sheets

List of components used in this project:

Inductors:

LQW18AN18NG00 series

0201DS-14NXJL_ Series

4310LCO-352KE_

Capacitors:

ROW5L330 Series

ROW5L101 Series

Resistors:

RN73C1E20R Series

Pin Diodes:

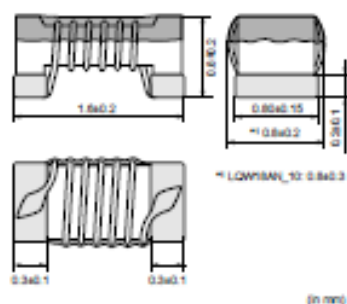
MA4ASCBP907 Series

MA4AGBLP9012 Series

Chip Inductors (Chip Coils) for High Frequency Horizontal Wire Wound

LQW18A_00 Series (0603 Size)

■ Dimension



■ Packaging

Code	Packaging	Minimum Quantity
D	180mm Paper Tape	4000
J	330mm Paper Tape	10000
B	Bulk(Bag)	500

■ Rated Value (□: packaging code)

Part Number	Inductance	Test Frequency	Rated Current	Max. of DC Resistance	Q (min.)	Test Frequency	Self Resonance Frequency (min.)
LQW18A2N2D00□	2.2nH±0.5nH	100MHz	700mA	0.049ohm	16	250MHz	6000MHz
LQW18A3N8C00□	3.6nH±0.2nH	100MHz	850mA	0.059ohm	25	250MHz	6000MHz
LQW18A3N8D00□	3.6nH±0.5nH	100MHz	850mA	0.059ohm	25	250MHz	6000MHz
LQW18A3N8C00□	3.9nH±0.2nH	100MHz	850mA	0.059ohm	35	250MHz	6000MHz
LQW18A3N8D00□	3.9nH±0.5nH	100MHz	850mA	0.059ohm	35	250MHz	6000MHz
LQW18A4N3C00□	4.3nH±0.2nH	100MHz	850mA	0.059ohm	35	250MHz	6000MHz
LQW18A4N3D00□	4.3nH±0.5nH	100MHz	850mA	0.059ohm	35	250MHz	6000MHz
LQW18A4N7D00□	4.7nH±0.5nH	100MHz	850mA	0.059ohm	35	250MHz	6000MHz
LQW18A6N8C00□	5.6nH±0.2nH	100MHz	750mA	0.082ohm	35	250MHz	6000MHz
LQW18A6N8D00□	5.6nH±0.5nH	100MHz	750mA	0.082ohm	35	250MHz	6000MHz
LQW18A8N2C00□	6.2nH±0.2nH	100MHz	750mA	0.082ohm	35	250MHz	6000MHz
LQW18A8N2D00□	6.2nH±0.5nH	100MHz	750mA	0.082ohm	35	250MHz	6000MHz
LQW18A8N8C00□	6.8nH±0.2nH	100MHz	750mA	0.082ohm	35	250MHz	6000MHz
LQW18A8N8D00□	6.8nH±0.5nH	100MHz	750mA	0.082ohm	35	250MHz	6000MHz
LQW18A7N6D00□	7.5nH±0.5nH	100MHz	750mA	0.082ohm	35	250MHz	6000MHz
LQW18A8N2D00□	8.2nH±0.5nH	100MHz	650mA	0.11ohm	35	250MHz	6000MHz
LQW18A8N7D00□	8.7nH±0.5nH	100MHz	650mA	0.11ohm	35	250MHz	6000MHz
LQW18A8N1D00□	9.1nH±0.5nH	100MHz	650mA	0.11ohm	35	250MHz	6000MHz
LQW18A8N6D00□	9.5nH±0.5nH	100MHz	650mA	0.11ohm	35	250MHz	6000MHz
LQW18A10NG00□	10nH±2%	100MHz	650mA	0.11ohm	35	250MHz	6000MHz
LQW18A10NJ00□	10nH±5%	100MHz	650mA	0.11ohm	35	250MHz	6000MHz
LQW18A11NG00□	11nH±2%	100MHz	650mA	0.11ohm	35	250MHz	6000MHz
LQW18A11NJ00□	11nH±5%	100MHz	650mA	0.11ohm	35	250MHz	6000MHz


Operating Temperature Range: -55°C to +125°C
Only for reflow soldering.

Continued on the following page.

Ⓢ This data sheet is applied for CHIP INDUCTORS (CHIP COILS) used for General Electronics equipment for your design.


▲ Note:


- This datasheet is downloaded from the website of Murata Manufacturing Co., Ltd. Therefore, its specifications are subject to change or our products in it may be discontinued without advance notice. Please check with our sales representatives or product engineers before ordering.
- This datasheet has only typical specifications because there is no space for detailed specifications. Therefore, please approve our product specifications or transact the approval sheet for product specifications before ordering.

 Continued from the preceding page.

Part Number	Inductance	Test Frequency	Rated Current	Max. of DC Resistance	Q (min.)	Test Frequency	Self Resonance Frequency (min.)
LQW18AN12NG00□	12nH±2%	100MHz	600mA	0.13ohm	35	250MHz	6000MHz
LQW18AN12NJ00□	12nH±5%	100MHz	600mA	0.13ohm	35	250MHz	6000MHz
LQW18AN13NG00□	13nH±2%	100MHz	600mA	0.13ohm	35	250MHz	6000MHz
LQW18AN13NJ00□	13nH±5%	100MHz	600mA	0.13ohm	35	250MHz	6000MHz
LQW18AN15NG00□	15nH±2%	100MHz	600mA	0.13ohm	40	250MHz	6000MHz
LQW18AN15NJ00□	15nH±5%	100MHz	600mA	0.13ohm	40	250MHz	6000MHz
LQW18AN18NG00□	18nH±2%	100MHz	550mA	0.16ohm	40	250MHz	5500MHz
LQW18AN18NJ00□	18nH±5%	100MHz	550mA	0.16ohm	40	250MHz	5500MHz
LQW18AN18NG00□	18nH±2%	100MHz	550mA	0.16ohm	40	250MHz	5500MHz
LQW18AN18NJ00□	18nH±5%	100MHz	550mA	0.16ohm	40	250MHz	5500MHz
LQW18AN20NG00□	20nH±2%	100MHz	550mA	0.16ohm	40	250MHz	4900MHz
LQW18AN20NJ00□	20nH±5%	100MHz	550mA	0.16ohm	40	250MHz	4900MHz
LQW18AN22NG00□	22nH±2%	100MHz	500mA	0.17ohm	40	250MHz	4600MHz
LQW18AN22NJ00□	22nH±5%	100MHz	500mA	0.17ohm	40	250MHz	4600MHz
LQW18AN24NG00□	24nH±2%	100MHz	500mA	0.21ohm	40	250MHz	3800MHz
LQW18AN24NJ00□	24nH±5%	100MHz	500mA	0.21ohm	40	250MHz	3800MHz
LQW18AN27NG00□	27nH±2%	100MHz	440mA	0.21ohm	40	250MHz	3700MHz
LQW18AN27NJ00□	27nH±5%	100MHz	440mA	0.21ohm	40	250MHz	3700MHz
LQW18AN30NG00□	30nH±2%	100MHz	420mA	0.23ohm	40	250MHz	3300MHz
LQW18AN30NJ00□	30nH±5%	100MHz	420mA	0.23ohm	40	250MHz	3300MHz
LQW18AN33NG00□	33nH±2%	100MHz	420mA	0.23ohm	40	250MHz	3200MHz
LQW18AN33NJ00□	33nH±5%	100MHz	420mA	0.23ohm	40	250MHz	3200MHz
LQW18AN36NG00□	36nH±2%	100MHz	400mA	0.26ohm	40	250MHz	2900MHz
LQW18AN36NJ00□	36nH±5%	100MHz	400mA	0.26ohm	40	250MHz	2900MHz
LQW18AN39NG00□	39nH±2%	100MHz	400mA	0.26ohm	40	250MHz	2800MHz
LQW18AN39NJ00□	39nH±5%	100MHz	400mA	0.26ohm	40	250MHz	2800MHz
LQW18AN43NG00□	43nH±2%	100MHz	380mA	0.29ohm	40	200MHz	2700MHz
LQW18AN43NJ00□	43nH±5%	100MHz	380mA	0.29ohm	40	200MHz	2700MHz
LQW18AN47NG00□	47nH±2%	100MHz	380mA	0.29ohm	38	200MHz	2600MHz
LQW18AN47NJ00□	47nH±5%	100MHz	380mA	0.29ohm	38	200MHz	2600MHz
LQW18AN51NG00□	51nH±2%	100MHz	370mA	0.33ohm	38	200MHz	2500MHz
LQW18AN51NJ00□	51nH±5%	100MHz	370mA	0.33ohm	38	200MHz	2500MHz
LQW18AN56NG00□	56nH±2%	100MHz	360mA	0.35ohm	38	200MHz	2400MHz
LQW18AN56NJ00□	56nH±5%	100MHz	360mA	0.35ohm	38	200MHz	2400MHz
LQW18AN62NG00□	62nH±2%	100MHz	280mA	0.51ohm	38	200MHz	2300MHz
LQW18AN62NJ00□	62nH±5%	100MHz	280mA	0.51ohm	38	200MHz	2300MHz
LQW18AN68NG00□	68nH±2%	100MHz	340mA	0.38ohm	38	200MHz	2200MHz
LQW18AN68NJ00□	68nH±5%	100MHz	340mA	0.38ohm	38	200MHz	2200MHz
LQW18AN72NG00□	72nH±2%	100MHz	270mA	0.56ohm	34	150MHz	2100MHz
LQW18AN72NJ00□	72nH±5%	100MHz	270mA	0.56ohm	34	150MHz	2100MHz
LQW18AN76NG00□	76nH±2%	100MHz	270mA	0.56ohm	34	150MHz	2050MHz


Operating Temperature Range: -55°C to +125°C
Only for reflow soldering.

Continued on the following page. 

 This data sheet is applied for CHIP INDUCTORS (CHIP COILS) used for General Electronics equipment for your design.

△ Note:


1. This datasheet is downloaded from the website of Murata Manufacturing Co., Ltd. Therefore, its specifications are subject to change or our products in it may be discontinued without advance notice. Please check with our sales representatives or product engineers before ordering.
2. This datasheet has only typical specifications because there is no space for detailed specifications. Therefore, please approve our product specifications or transact the approval sheet for product specifications before ordering.

 Continued from the preceding page.

Part Number	Inductance	Test Frequency	Rated Current	Max. of DC Resistance	Q (min.)	Test Frequency	Self Resonance Frequency (min.)
LQW18AN76NJ00□	75nH±5%	100MHz	270mA	0.56ohm	34	150MHz	2050MHz
LQW18AN82NG00□	82nH±2%	100MHz	250mA	0.60ohm	34	150MHz	2000MHz
LQW18AN82NJ00□	82nH±5%	100MHz	250mA	0.60ohm	34	150MHz	2000MHz
LQW18AN81NG00□	91nH±2%	100MHz	230mA	0.64ohm	34	150MHz	1900MHz
LQW18AN81NJ00□	91nH±5%	100MHz	230mA	0.64ohm	34	150MHz	1900MHz
LQW18ANR10G00□	100nH±2%	100MHz	220mA	0.68ohm	34	150MHz	1800MHz
LQW18ANR10J00□	100nH±5%	100MHz	220mA	0.68ohm	34	150MHz	1800MHz
LQW18ANR11G00□	110nH±2%	100MHz	200mA	1.2ohm	32	150MHz	1700MHz
LQW18ANR11J00□	110nH±5%	100MHz	200mA	1.2ohm	32	150MHz	1700MHz
LQW18ANR12G00□	120nH±2%	100MHz	180mA	1.3ohm	32	150MHz	1600MHz
LQW18ANR12J00□	120nH±5%	100MHz	180mA	1.3ohm	32	150MHz	1600MHz
LQW18ANR13G00□	130nH±2%	100MHz	170mA	1.4ohm	32	150MHz	1450MHz
LQW18ANR13J00□	130nH±5%	100MHz	170mA	1.4ohm	32	150MHz	1450MHz
LQW18ANR16G00□	150nH±2%	100MHz	160mA	1.5ohm	32	150MHz	1400MHz
LQW18ANR16J00□	150nH±5%	100MHz	160mA	1.5ohm	32	150MHz	1400MHz
LQW18ANR18G00□	160nH±2%	100MHz	150mA	2.1ohm	32	150MHz	1350MHz
LQW18ANR18J00□	160nH±5%	100MHz	150mA	2.1ohm	32	150MHz	1350MHz
LQW18ANR18G00□	180nH±2%	100MHz	140mA	2.2ohm	25	100MHz	1300MHz
LQW18ANR18J00□	180nH±5%	100MHz	140mA	2.2ohm	25	100MHz	1300MHz
LQW18ANR20G00□	200nH±2%	100MHz	120mA	2.4ohm	25	100MHz	1250MHz
LQW18ANR20J00□	200nH±5%	100MHz	120mA	2.4ohm	25	100MHz	1250MHz
LQW18ANR22G00□	220nH±2%	100MHz	120mA	2.5ohm	25	100MHz	1200MHz
LQW18ANR22J00□	220nH±5%	100MHz	120mA	2.5ohm	25	100MHz	1200MHz
LQW18ANR27G00□	270nH±2%	100MHz	110mA	3.4ohm	30	100MHz	960MHz
LQW18ANR27J00□	270nH±5%	100MHz	110mA	3.4ohm	30	100MHz	960MHz
LQW18ANR33G00□	330nH±2%	100MHz	85mA	5.5ohm	30	100MHz	800MHz
LQW18ANR33J00□	330nH±5%	100MHz	85mA	5.5ohm	30	100MHz	800MHz
LQW18ANR39G00□	390nH±2%	100MHz	80mA	6.2ohm	30	100MHz	800MHz
LQW18ANR39J00□	390nH±5%	100MHz	80mA	6.2ohm	30	100MHz	800MHz
LQW18ANR47G00□	470nH±2%	100MHz	75mA	7.0ohm	30	100MHz	700MHz
LQW18ANR47J00□	470nH±5%	100MHz	75mA	7.0ohm	30	100MHz	700MHz

Operating Temperature Range: -55°C to +125°C

Only for reflow soldering.

Continued on the following page. 

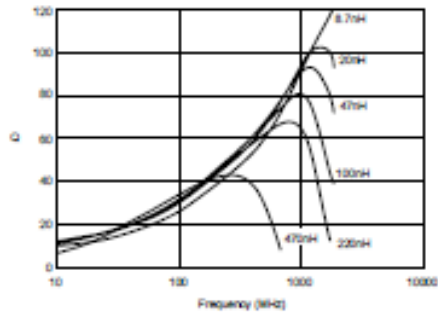
Ⓜ This data sheet is applied for CHIP INDUCTORS (CHIP COILS) used for General Electronics equipment for your design.

△ Note:

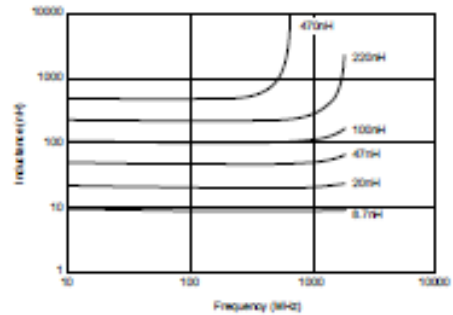
1. This datasheet is downloaded from the website of Murata Manufacturing Co., Ltd. Therefore, its specifications are subject to change or our products in it may be discontinued without advance notice. Please check with our sales representatives or product engineers before ordering.
2. This datasheet has only typical specifications because there is no space for detailed specifications. Therefore, please approve our product specifications or transact the approval sheet for product specifications before ordering.

Continued from the preceding page.

Q - Frequency Characteristics (Typ.)



Inductance - Frequency Characteristics (Typ.)



Caution/Notice

Caution (Rating)

Do not use products beyond the rated current as this may create excessive heat.

Notice

Solderability of Tin plating termination chip might be deteriorated when low temperature soldering profile where peak solder temperature is below the Tin melting point is used. Please confirm the solderability of Tin plating termination chip before use.

This data sheet is applied for CHIP INDUCTORS (CHIP COILS) used for General Electronics equipment for your design.

Note:

- This datasheet is downloaded from the website of Murata Manufacturing co., Ltd. Therefore, it's specifications are subject to change or our products in it may be discontinued without advance notice. Please check with our sales representatives or product engineers before ordering.
- This datasheet has only typical specifications because there is no space for detailed specifications. Therefore, please approve our product specifications or transact the approval sheet for product specifications before ordering.

**NEW!**

Chip Inductors - 0201DS Series (0503)

- 0201 size; world's smallest wirewound inductor
- 30 inductance values from 0.5 to 14 nH

Request free evaluation samples by contacting Coilcraft or visiting www.coilcraft.com.

Part number ¹	Inductance ² (nH)	Percent tolerance	900 MHz		1.7 GHz		SRF typ ⁴ (GHz)	DCR max ⁵ (Ohms)	I _{rms} ⁶ (mA)
			L typ	Q typ ³	L typ	Q typ ³			
0201DS-0N5XKL	0.5	10	0.50	29	0.49	43	23.5	0.020	1250
0201DS-0N6XKL	0.6	10	0.58	31	0.58	51	24.5	0.030	1000
0201DS-1N2XJL	1.2	5	1.16	42	1.16	60	17.9	0.042	870
0201DS-1N3XJL	1.3	5	1.24	38	1.24	57	17.6	0.048	820
0201DS-1N4XJL	1.4	5	1.35	27	1.34	37	17.0	0.080	630
0201DS-1N5XJL	1.5	5	1.47	28	1.47	40	17.0	0.090	600
0201DS-2N3XJL	2.3	5	2.28	45	2.28	64	16.5	0.070	670
0201DS-2N4XJL	2.4	5	2.36	35	2.36	53	13.0	0.082	620
0201DS-2N5XJL	2.5	5	2.50	31	2.49	44	12.5	0.165	440
0201DS-3N3XJL	3.3	5	3.31	42	3.32	62	12.8	0.080	630
0201DS-3N4XJL	3.4	5	3.38	42	3.42	62	12.7	0.080	630
0201DS-3N5XJL	3.5	5	3.41	44	3.45	64	12.4	0.080	630
0201DS-3N6XJL	3.6	5	3.53	40	3.57	61	12.5	0.105	550
0201DS-3N7XJL	3.7	5	3.65	39	3.66	58	10.6	0.105	550
0201DS-3N8XJL	3.8	5	3.81	38	3.81	60	10.2	0.180	420
0201DS-3N9XJL	3.9	5	3.89	35	3.89	50	11.2	0.240	360
0201DS-4N8XJL	4.8	5	4.83	34	4.83	50	11.0	0.096	570
0201DS-5N2XJL	5.2	5	5.21	36	5.21	55	10.0	0.170	430
0201DS-5N5XJL	5.5	5	5.49	35	5.49	50	9.5	0.285	330
0201DS-6N7XJL	6.7	5	6.71	40	6.72	59	6.8	0.150	460
0201DS-7N0XJL	7.0	5	6.97	39	6.97	60	6.7	0.210	390
0201DS-7N5XJL	7.5	5	7.44	36	7.46	50	6.8	0.340	300
0201DS-8N2XJL	8.2	5	8.14	37	8.22	53	6.4	0.270	340
0201DS-8N7XJL	8.7	5	8.68	38	8.74	59	6.3	0.350	300
0201DS-9N0XJL	9.0	5	9.02	42	9.04	63	6.4	0.350	300
0201DS-9N4XJL	9.4	5	9.38	36	9.39	51	6.4	0.400	280
0201DS-9N6XJL	9.6	5	9.62	38	9.64	53	6.2	0.400	280
0201DS-11NXJL	11.0	5	11.11	40	11.15	62	5.7	0.400	280
0201DS-12NXJL	12.0	5	12.15	39	12.20	56	5.6	0.360	300
0201DS-14NXJL	14.0	5	14.13	37	14.37	51	5.1	0.440	270

1. When ordering, please specify packaging code:

0201DS-14NXJLW

Packaging: W – 7" machine-ready reel, EIA-481 punched paper tape (2000 parts per full reel).

U – Less than full reel. In tape, but not machine ready. To have a leader and trailer added (\$25 charge), use code letter W instead.

- Inductance measured at 250 MHz using a Coilcraft SMD-F fixture in an Agilent/HP 4296 impedance analyzer with Coilcraft-provided correlation pieces.
- Q measured using an Agilent/HP 4291A with an Agilent/HP 16197 test fixture.
- SRF measured using an Agilent/HP 8722ES network analyzer and a test fixture with a 0.010" air gap.
- DCR measured on a micro-ohmmeter and a Coilcraft CCF858 test fixture.
- Current that causes a 15°C temperature rise from 25°C ambient. Refer to Doc 362 "Soldering Surface Mount Components" before soldering.

Core material Ceramic

Terminations RoHS compliant silver-platinum-glass frit. Other terminations available at additional cost.

Weight 0.14 – 0.23 mg

Ambient temperature –40°C to +125°C with I_{rms} current, +125°C to +140°C with derated current

Storage temperature Component: –40°C to +140°C. Packaging: –40°C to +80°C

Resistance to soldering heat Max three 40 second reflows at +260°C, parts cooled to room temperature between cycles

Temperature Coefficient of Inductance (TCL) +25 to +125 ppm/°C

Moisture Sensitivity Level (MSL) 1 (unlimited floor life at <30°C / 85% relative humidity)

Failures in Time (FIT) / Mean Time Between Failures (MTBF) One per billion hours / one billion hours, calculated per Telcordia SR-332

Packaging 2000 per 7" reel. Paper tape: 8 mm wide, 0.6 mm thick, 2 mm pocket spacing

PCB washing Only pure water or alcohol recommended

Coilcraft®

Specifications subject to change without notice.
Please check our website for latest information.

Document 699-1 Revised 01/08/09

1102 Silver Lake Road Cary, Illinois 60013 Phone 847/639-6400 Fax 847/639-1469
E-mail info@coilcraft.com Web <http://www.coilcraft.com>

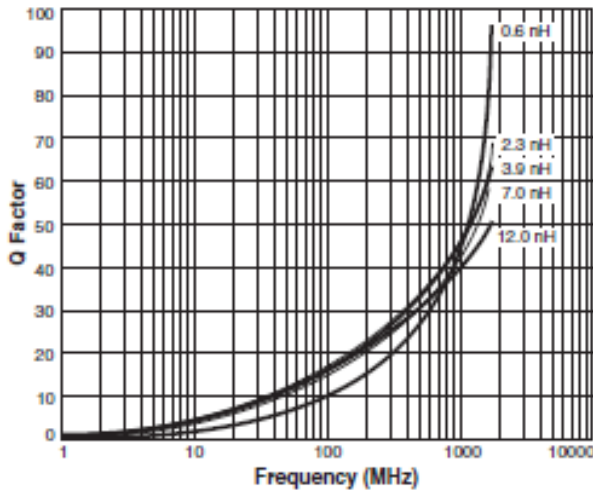
© Coilcraft, Inc. 2009

NEW!

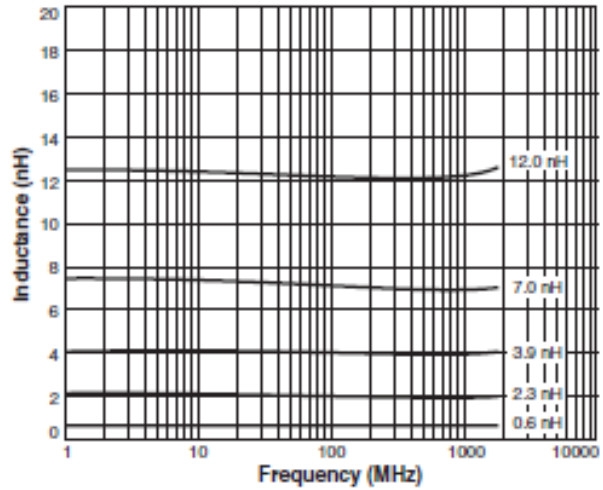


0201DS Chip Inductor Series (0503)

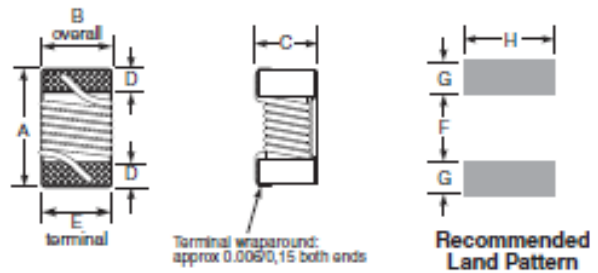
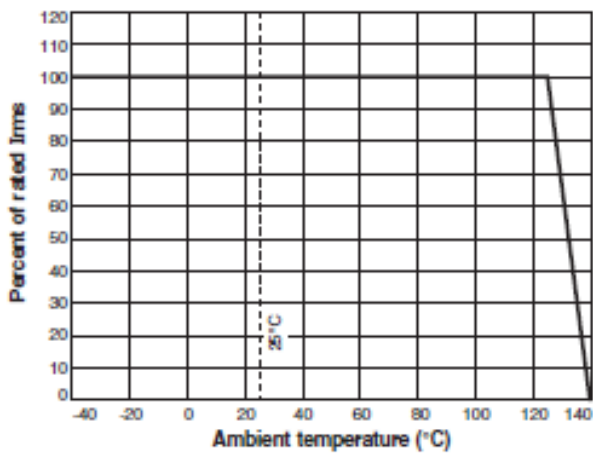
Typical Q vs Frequency



Typical L vs Frequency



Irms Derating



A max	B max	C max	D	E	F	G	H
0.023	0.018	0.0177	0.004	0.015	0.009	0.007	0.018
0.58	0.46	0.45	0.10	0.38	0.23	0.18	0.46

Coilcraft®

Specifications subject to change without notice.
Please check our website for latest information.

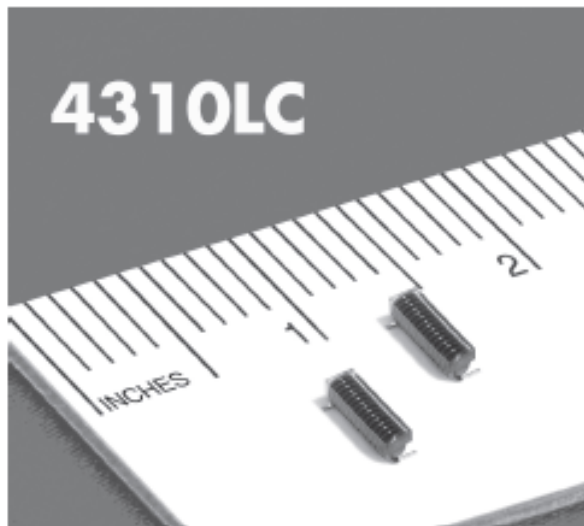
Document 699-2 Revised 01/09/09

1102 Silver Lake Road Cary, Illinois 60013 Phone 847/639-6400 Fax 847/639-1469
E-mail info@coilcraft.com Web http://www.coilcraft.com

© Coilcraft, Inc. 2009

**NEW!**

Wideband Bias Chokes – 4310LC



- High impedance over a wide range
- Low DCR and excellent current handling
- Ideal for use in high current bias tee applications

Core material Ferrite

Environmental RoHS compliant, halogen free

Terminations RoHS compliant tin-silver (96.5/3.5) over copper. Other terminations available at additional cost.

Weight 0.42 g

Ambient temperature -40°C to +85°C with Irms current, +85°C to +125°C with derated current

Storage temperature Component: -40°C to +85°C. Tape and reel packaging: -40°C to +80°C

Resistance to soldering heat Max three 40 second reflows at +260°C, parts cooled to room temperature between cycles

Moisture Sensitivity Level (MSL) 1 (unlimited floor life at <30°C / 85% relative humidity)

Failures In Time (FIT) / Mean Time Between Failures (MTBF) 38 per billion hours / 26,315,789 hours, calculated per Telcordia SR-332

Packaging 350/7" reel, 1500/13" reel; Plastic tape: 24 mm wide, 0.3 mm thick, 12 mm pocket spacing, 3.5 mm pocket depth

PCB washing Only pure water or alcohol recommended

Part number ¹	Inductance ² ±10% (µH)	SRF (typ) ³ (MHz)	DCR (max) ⁴ (mOhm)	Irms (A) ⁵	
				20°C rise	40°C rise
4310LC-132KE_	1.30	235	15.1	2.7	4.2
4310LC-352KE_	3.50	188	49.0	2.3	3.1

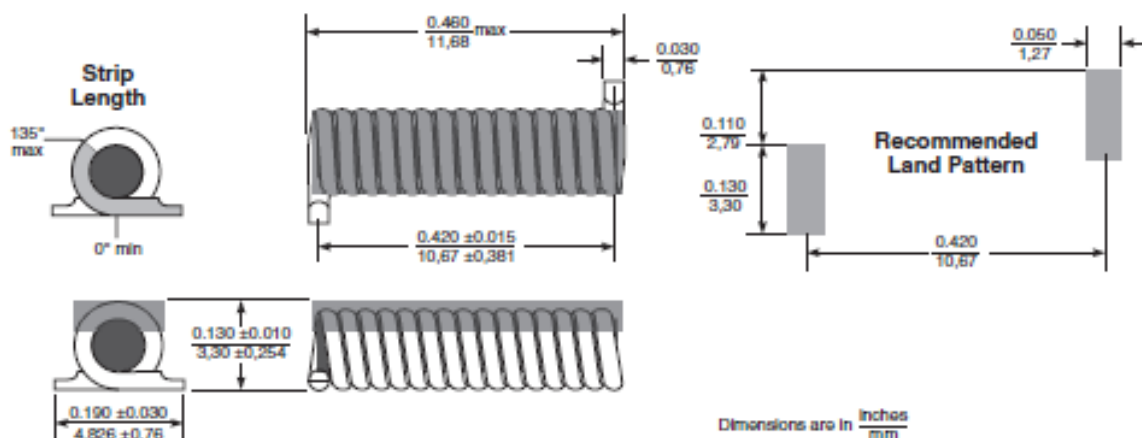
1. When ordering, please specify packaging code:

4310LC-132KEC

- Packaging:**
- C** – 7" machine-ready reel. EIA-481 embossed plastic tape (350 parts per full reel).
 - B** – Less than full reel. In tape, but not machine ready. To have a leader and trailer added (\$25 charge), use code letter C instead.
 - D** – 13" machine-ready reel. EIA-481 embossed plastic tape. Factory order only, not stocked (1500 parts per full reel).

- Inductance measured at 100 kHz, 0.1 Vrms, 0 Adc using an Agilent/HP 16193 fixture in Agilent/HP 4294A impedance analyzer.
- SRF measured using Agilent/HP 8753D network analyzer and a Coilcraft SMD-F test fixture.
- DCR measured on Keithley 580 micro-ohmmeter.
- Current that causes the specified temperature rise from 25°C ambient.
- Electrical specifications at 25°C.

Refer to Doc 362 "Soldering Surface Mount Components" before soldering.



Dimensions are in $\frac{\text{Inches}}{\text{mm}}$

Coilcraft
www.coilcraft.com

US +1-847-639-6400 sales@coilcraft.com
 UK +44-1236-730595 sales@coilcraft-europe.com
 Taiwan +886-2-2264 3646 sales@coilcraft.com.tw
 China +86-21-6218 8074 sales@coilcraft.com.cn
 Singapore +65-6484 8412 sales@coilcraft.com.sg

Document 878-1 Revised 01/03/12

© Coilcraft Inc. 2012

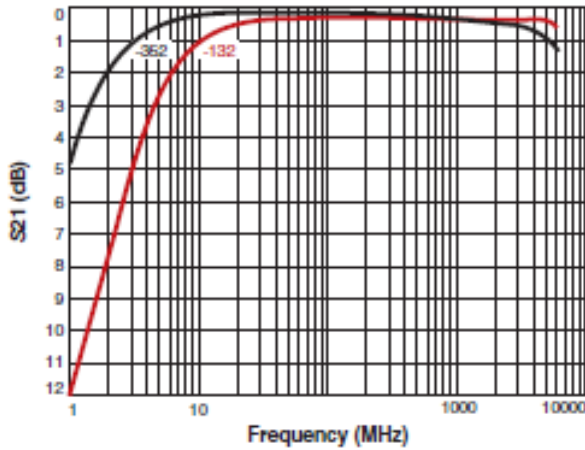
This product may not be used in medical or high risk applications without prior Coilcraft approval. Specification subject to change without notice. Please check out web site for latest information.



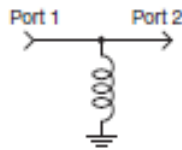
NEW!

Wideband Bias Chokes - 4310LC

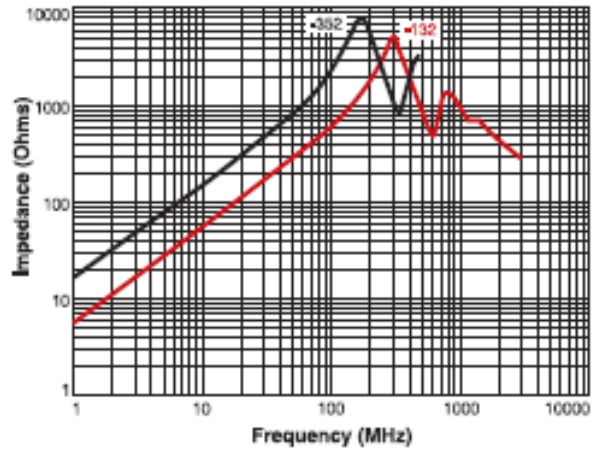
Insertion Loss (Ref: 50 Ohms)



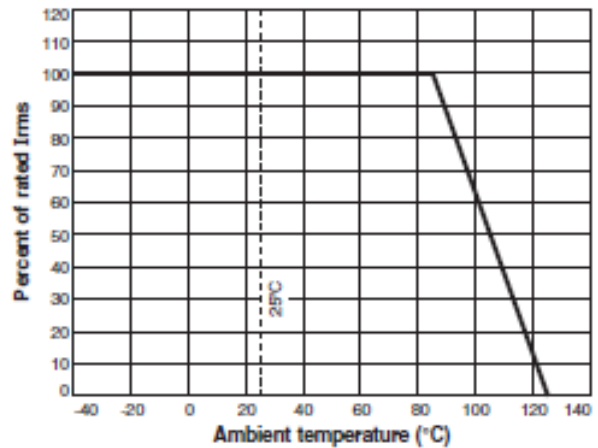
Insertion loss measured in a bias tee configuration with an Agilent/HP 8753ES network analyzer.



Impedance vs Frequency



Irms Derating



US +1-847-639-6400 sales@coilcraft.com
UK +44-1236-730595 sales@coilcraft-europe.com
Taiwan +886-2-2264 3646 sales@coilcraft.com.tw
China +86-21-6218 8074 sales@coilcraft.com.cn
Singapore + 65-6484 8412 sales@coilcraft.com.sg

Document 878-2 Revised 01/03/12

© Coilcraft Inc. 2012
 This product may not be used in medical or high risk applications without prior Coilcraft approval. Specification subject to change without notice. Please check out web site for latest information.

MULTI-LAYER HIGH-Q CAPACITORS



These lines of multilayer capacitors have been developed for High-Q and microwave applications.

- The **S-Series** (R03S, R07S, R14S, R15S) capacitors give an ultra-high Q performance, and exhibit NPO temperature characteristics.
- The **L-Series** (R05L) capacitors give mid-high Q performance, and exhibit NPO temperature characteristics.
- The **E-Series** (S42E, S48E, S58E) capacitors give excellent high-Q performance from HF to Microwave frequencies. Typical uses are high voltage, high current applications. They are offered in chip (Ni barrier or Non-Magnetic Pt-Ag) or in Non-Magnetic leaded form.
- The **W-Series** (R05W) capacitors offer a large capacitance value in an ultra-small 0201 package size. These exhibit a X7R temperature characteristic.
- RoHS compliance is standard for all unleaded parts (see termination options box).

HOW TO ORDER

252	S48	E	470	K	Y	4	E
VOLTAGE (DC) 0R3 = 6.3 V 100 = 16 V 250 = 25 V 500 = 50 V 251 = 250 V 501 = 500 V 102 = 1000 V 152 = 1500 V 202 = 2000 V 252 = 2500 V 302 = 3000 V 502 = 5000 V 722 = 7200 V	CASE SIZE R03 (01005) R05 (0201) R07 (0402) R14 (0603) R15 (0805) S42 (1111) S48 (2525) S58 (3838)	CAPACITANCE (pF) 1st two digits are significant; third digit denotes number of zeros, R = decimal. 100 = 10 pF 101 = 100 pF	DIELECTRIC S = Ultra High Q NPO L = High Q NPO E = Ultra High Q NPO, High Voltage, High Power, W = X7R	TOLERANCE A = ± 0.05 pF B = ± 0.10 pF C = ± 0.25 pF D = ± 0.50 pF F = ± 1 % G = ± 2% J = ± 5% K = ± 10% For tolerance availability, see chart.	TERMINATION Nickel Barrier Types G = Ni/Au T = Ni/Sn-Pb V = Ni / 100% Sn Non Magnetic Types *C = Non-Leaded Cu *1 = Microstrip Ribbon Leads (E-Series Only) *2 = Axial Ribbon	MARKING 3 = Cap Code & Tolerance 4 = No Marking 6 = EIA Code (Marking on 0805 and larger only)	PACKAGING S = Bulk W = Waffle Pack 01005 - 0603 Y = Paper 5" Reel T = Paper 7" Reel *R = Paper 13" Reel 0805 - 3838 Z = Embossed 5" Reel E = Embossed 7" Reel *U = Embossed 13" Reel Tape specifications conform to EIA RS481

Part Number written: **252S48E470KY4E**



*** - Not available for all MLCC - Call factory for info.

LOW ESR / HIGH-Q CAPACITOR SELECTION CHART

EIA Size Cap. Value		Miniature Size - Portable Electronics				RF Power Applications						
		01005 (R03S)	0201 (R05) NPO (R05L) X7R* (R05W)		0402 (R07S)	0603 (R14S)	0805 (R15S)	1111 (S42E)	2525** (S48E)	3838** (S58E)		
Capacitance pF	Code	Voltage										
0.1	0R1											
0.2	0R2	16 V	25 V		50 V	250 V		500V	1000V			
0.3	0R3	16 V	25 V		50 V	250 V	250 V	500V	1000V			
0.4	0R4	16 V	25 V		50 V	250 V	250 V	500V	1000V			
0.5	0R5	16 V	25 V		50 V	250 V	250 V	500V	1000V			
0.6	0R6	16 V	25 V		50 V	250 V	250 V	500V	1000V			
0.7	0R7	16 V	25 V		50 V	250 V	250 V	500V	1000V			
0.8	0R8	16 V	25 V		50 V	250 V	250 V	500V	1000V			
0.9	0R9	16 V	25 V		50 V	250 V	250 V	500V	1000V			
1.0	1R0	16 V	25 V		50 V	250 V	250 V	500V	1000V	2500V	3600V	7200V
1.1	1R1	16 V	25 V		50 V	250 V	250 V	500V	1000V			
1.2	1R2	16 V	25 V	A	50 V	250 V	250 V	500V	1000V	2500V	3600V	7200V
1.3	1R3	16 V	25 V	B	50 V	250 V	250 V	500V	1000V			
1.4	1R4	16 V	25 V	C	50 V	250 V	250 V	500V	1000V			
1.5	1R5	16 V	25 V	D	50 V	250 V	250 V	500V	1000V	2500V	3600V	7200V
1.6	1R6	16 V	25 V		50 V	250 V	250 V	500V	1000V			
1.7	1R7	16 V	25 V		50 V	250 V	250 V	500V	1000V			
1.8	1R8	16 V	25 V		50 V	250 V	250 V	500V	1000V	2500V	3600V	7200V
1.9	1R9	16 V	25 V		50 V	250 V	250 V	500V	1000V			
2.0	2R0	16 V	25 V		50 V	250 V	250 V	500V	1000V			
2.1	2R1	16 V	25 V		50 V	250 V	250 V	500V	1000V			
2.2	2R2	16 V	25 V		50 V	250 V	250 V	500V	1000V	2500V	3600V	7200V
2.4	2R4	16 V	25 V		50 V	250 V	250 V	500V	1000V			
2.7	2R7	16 V	25 V		50 V	250 V	250 V	500V	1000V	2500V	3600V	7200V
3.0	3R0	16 V	25 V		50 V	250 V	250 V	500V	1000V			
3.3	3R3	16 V	25 V		50 V	250 V	250 V	500V	1000V	2500V	3600V	7200V
3.6	3R6	16 V	25 V		50 V	250 V	250 V	500V	1000V			
3.9	3R9	16 V	25 V		50 V	250 V	250 V	500V	1000V	2500V	3600V	7200V
4.3	4R3	16 V	25 V		50 V	250 V	250 V	500V	1000V			
4.7	4R7	16 V	25 V		50 V	250 V	250 V	500V	1000V	2500V	3600V	7200V
5.1	5R1	16 V	25 V	B	50 V	250 V	250 V	500V	1000V			
5.6	5R6	16 V	25 V	C	50 V	250 V	250 V	500V	1000V	2500V	3600V	7200V
6.2	6R2	16 V	25 V	D	50 V	250 V	250 V	500V	1000V			
6.8	6R8	16 V	25 V		50 V	250 V	250 V	500V	1000V	2500V	3600V	7200V
7.5	7R5	16 V	25 V		50 V	250 V	250 V	500V	1000V			
8.2	8R2	16 V	25 V		50 V	250 V	250 V	500V	1000V			
9.1	9R1	16 V	25 V		50 V	250 V	250 V	500V	1000V			
10	100	16 V	25 V		50 V	250 V	250 V	500V	1000V	2500V	3600V	7200V
11	110	16 V	25 V		50 V	250 V	250 V					
12	120	16 V	25 V	F	50 V	250 V	250 V	500V	1000V	2500V	3600V	7200V
13	130	16 V	25 V	G	50 V	250 V	250 V	500V	1000V			
15	150	16 V	25 V	H	50 V	250 V	250 V	500V	1000V	2500V	3600V	7200V
16	160	16 V	25 V	I	50 V	250 V	250 V	500V	1000V			
18	180		25 V	J	50 V	250 V	250 V	500V	1000V	2500V	3600V	7200V
20	200		25 V	K	50 V	250 V	250 V	500V	1000V			
22	220		25 V		50 V	250 V	250 V	500V	1000V	2500V	3600V	7200V
24	240		25 V		50 V	250 V	250 V	500V	1000V			
27	270		25 V		50 V	250 V	250 V	500V	1000V	2500V	3600V	7200V
30	300		25 V		25 V	250 V	250 V	500V	1000V			
33	330		25 V		25 V	250 V	250 V	500V	1000V	2500V	3600V	7200V

* The R05W parts, which are X7R, can only be provided with "K" tolerance.
Consult factory for Non-Standard values.

LOW ESR / HIGH-Q CAPACITOR SELECTION CHART

EIA Size Cap. Value		Miniature Size - Portable Electronics				RF Power Applications						
		01005 (R03S)	0201 (R05) NPO (R05L) X7R* (R05W)		0402 (R07S)	0603 (R14S)	0805 (R15S)	1111 (S42E)		2525** (S48E)	3838** (S58E)	
Capacitance pF	Code	Voltage										
36	360		25 V			250 V	250 V	500V	1000V			
39	390		25 V			250 V	250 V	500V	1000V	2500V	3600V	7200V
43	430		25 V			250 V	250 V	500V	1000V			
47	470		25 V			250 V	250 V	500V	1000V	2500V	3600V	7200V
51	510		25 V			250 V	250 V	500V	1000V			
56	560		25 V			250 V	250 V	500V	1000V	2500V	3600V	7200V
62	620		25 V			250 V	250 V	500V	1000V			
68	680		25 V			250 V	250 V	500V	1000V	2500V	3600V	7200V
75	750		25 V			250 V	250 V	500V	1000V			
82	820	F	25 V			250 V	250 V	500V	1000V	2500V	3600V	7200V
91	910		25 V			250 V	250 V	500V	1000V			
100	101	G	25 V			250 V	250 V	500V	1000V	2500V	3600V	7200V
110	111			16 V		250 V	250 V	300V				
120	121	J				250 V	250 V	300V		2500V	3600V	5000V
130	131					250 V	250 V	300V				
150	151	K				250 V	250 V	300V		2500V	3600V	5000V
160	161					250 V	250 V	300V				
180	181					250 V	250 V	300V		2500V	3600V	5000V
200	201					250 V	250 V	300V				
220	221			16 V		250 V	250 V	200V		2500V	3600V	
240	241					250 V		200V				
270	271					250 V		200V		2500V	3600V	
300	301					250 V		200V				
330	331					250 V		200V		1500V	3600V	
360	361					250 V		200V				
390	391					250 V		200V		1500V	3600V	
430	431					250 V		200V				
470	471			16 V				200V		1500V	2500V	
510	511							100V				
560	561							100V		1000V	2500V	
620	621							100V				
680	681			16 V				50V		1000V	2500V	
750	751							50V				
820	821			16 V				50V		1000V	1000V	
910	911	G						50V				
1000	102	J						50V		1000V	1000V	
1200	122									1000V	1000V	
1500	152									500V	1000V	
1800	182	K								500V	1000V	
2200	222									300V	1000V	
2700	272			10 V						300V	500V	
3300	332										500V	
3900	392										500V	
4700	472			10 V							500V	
5100	512										500V	
10000	103			6.3 V								

* The R05W parts, which are X7R, can only be provided with "K" tolerance.
Consult factory for Non-Standard values.

DIELECTRIC CHARACTERISTICS**NPO****X7R**

TEMPERATURE COEFFICIENT:	0 ± 30ppm /°C, -55 to 125°C	± 15%, -55 to 125°C
QUALITY FACTOR / DF:	Q > 1,000 @ 1 MHz, Typical 10,000	16VDC DF ≤ 3.5% @ 1 KHz, 25°C 10VDC DF ≤ 5.0% @ 1 KHz, 25°C
INSULATION RESISTANCE:	> 10 GΩ @ 25°C, WVDC; 125°C IR is 10% of 25°C rating	> 500 ΩF* or 10 GΩ* @ 25°C, WVDC; 125°C IR is 10% of 25°C rating * whichever is less
DIELECTRIC STRENGTH:	2.5 X WVDC Min., 25°C, 50 mA max	2.5 X WVDC Min., 25°C, 50 mA max
TEST PARAMETERS:	1MHz ±50kHz, 1.0±0.2 VRMS, 25°C	1KHz ±50Hz, 1.0±0.2 VRMS, 25°C
AVAILABLE CAPACITANCE:	Size 01005: 0.2 - 10 pF Size 0201: 0.2 - 100 pF Size 0402: 0.2 - 33 pF Size 0603: 0.2 - 430 pF Size 0805: 0.3 - 220 pF Size 1111: 0.2 - 1000 pF Size 2525: 1.0 - 2700 pF Size 3838: 1.0 - 5100 pF	100 - 10,000 pF

MECHANICAL & ENVIRONMENTAL CHARACTERISTICS

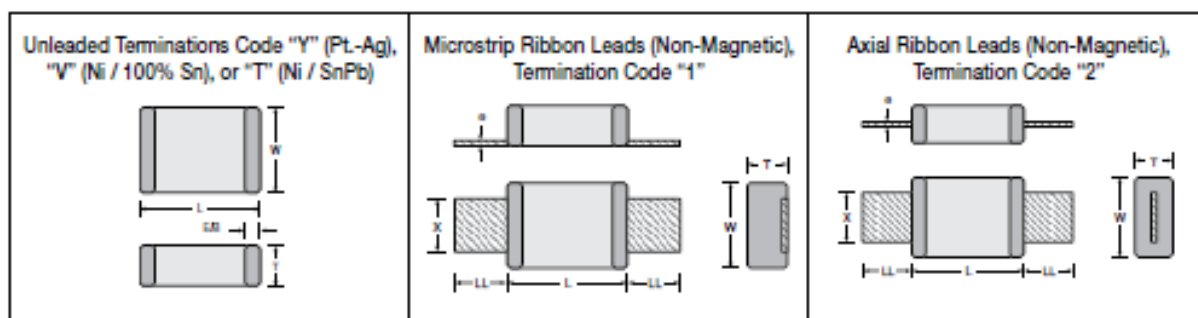
	SPECIFICATION	TEST PARAMETERS
SOLDERABILITY:	Solder coverage ≥ 90% of metalized areas No termination degradation	Preheat chip to 120°-150°C for 60 sec., dip terminals in rosin flux then dip in Sn62 solder @ 240°±5°C for 5±1 sec
RESISTANCE TO SOLDERING HEAT:	No mechanical damage Capacitance change: ±2.5% or 0.25pF Q>500 I.R. >10 G Ohms Breakdown voltage: 2.5 x WVDC	Preheat device to 80°-100°C for 60 sec. followed by 150°-180°C for 60 sec. Dip in 260°±5°C solder for 10±1 sec. Measure after 24±2 hour cooling period
TERMINAL ADHESION:	Termination should not pull off. Ceramic should remain undamaged.	Linear pull force* exerted on axial leads soldered to each terminal. *0402 ≥ 2.0lbs, 0603 ≥ 2.0lbs (min.)
PCB DEFLECTION:	No mechanical damage. Capacitance change: 2% or 0.5pF Max	Glass epoxy PCB: 0.5 mm deflection
LIFE TEST:	No mechanical damage Capacitance change: ±3.0% or 0.3 pF Q>500 I.R. >1 G Ohms Breakdown voltage: 2.5 x WVDC	Applied voltage: 200% rated voltage, 50 mA max. Temperature: 125°±3°C Test time: 1000+48-0 hours
THERMAL CYCLE:	No mechanical damage. Capacitance change: ±2.5% or 0.25pF Q>2000 I.R. >10 G Ohms Breakdown voltage: 2.5 x WVDC	5 cycles of: 30±3 minutes @ -55°±0/-3°C, 2-3 min. @ 25°C, 30±3 min. @ +125°±3/-0°C, 2-3 min. @ 25°C Measure after 24±2 hour cooling period
HUMIDITY, STEADY STATE:	No mechanical damage. Capacitance change: ±5.0% or 0.50pF max. Q>300 I.R. ≥ 1 G-Ohm Breakdown voltage: 2.5 x WVDC	Relative humidity: 90-95% Temperature: 40°±2°C Test time: 500 +12/-0 Hours Measure after 24±2 hour cooling period
HUMIDITY, LOW VOLTAGE:	No mechanical damage. Capacitance change: ±5.0% or 0.50pF max. Q>300 I.R. = 1 G-Ohm min. Breakdown voltage: 2.5 x WVDC	Applied voltage: 1.5 VDC, 50 mA max. Relative humidity: 85±2% Temperature: 40°±2°C Test time: 240 +12/-0 Hours Measure after 24±2 hour cooling period
VIBRATION:	No mechanical damage. Capacitance change: ±2.5% or 0.25pF Q>1000 I.R. ≥ 10 G-Ohm Breakdown voltage: 2.5 x WVDC	Cycle performed for 2 hours in each of three perpendicular directions Frequency range 10Hz to 55 Hz to 10 Hz traversed in 1 minute. Harmonic motion amplitude: 1.5mm



MECHANICAL CHARACTERISTICS

Size	Units	Length	Width	Thickness	End Band
01005 (0402)	In mm	.016 ±.001 (0.40 ±0.03)	.008 ±.001 (0.20 ±0.03)	.008 ±.001 (0.20 ±0.03)	.006 Max. (0.15 Max.)
0201 (0603)	In mm	.024 ±.001 (0.60 ±0.03)	.012 ±.001 (0.30 ±0.03)	.012 ±.001 (0.30 ±0.03)	.008 Max. (0.20 Max.)
0402 (1005)	In mm	.040 ±.004 (1.02 ±0.1)	.020 ±.004 (0.51 ±0.1)	.020 ±.004 (0.51 ±0.1)	.010 ±.006 (0.25 ±.15)
0603 (1608)	In mm	.062 ±.006 (1.57 ±0.15)	.032 ±.006 (0.81 ±0.15)	.030 +.005/- .003 (0.76 +.13-.08)	.014 ±.006 (0.35 ±.15)
0805 (2012)	In mm	.080 ±.008 (2.03 ±0.20)	.050 ±.008 (1.27 ±0.20)	.040 ±.006 (1.02 ±.15)	.020 ±.010 (0.50 ±.25)

E-SERIES LEAD STYLE SELECTION



Lead	Size	Units	L	Tol	W	Tol	T	E/B
Y, V, T	S42E	In	0.110	+0.020 -0.010	0.110	±.020	0.102 Max.	0.015 Typ.
		mm	2.79	+0.51 -0.25	2.79	±.051	2.59 Max.	0.38 Typ.
	S48E	In	0.230	+0.025 -0.010	0.250	±.015	0.150 Max.	0.025 Typ.
		mm	5.84	+0.63 -0.25	6.35	±.038	3.81 Max.	0.63 Typ.
	S58E	In	0.380	+0.015 -0.010	0.380	±.010	0.170 Max.	0.025 Typ.
		mm	9.65	+0.38 -0.25	9.65	±.025	4.32 Max.	0.63 Typ.

For all E-Series Models:

OPERATING TEMP. :

-55 to +125°C

INSULATION RESISTANCE:

>1000 ΩF or >10 GΩ,
whichever is less @ 25°C WVDC

TEMPERATURE COEFFICIENT:

0 ± 30ppm /°C, -55 to 125°C

DISSIPATION FACTOR (TYP):

< 0.05% @ 1 MHz

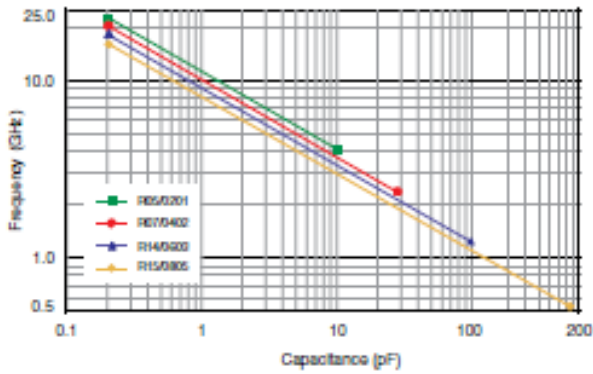
Lead	Size	Units	L	Tol	W	Tol	T (max)	E/B (typ)	LL (min)	X	Tol	e	Tol
1	S42E	In	0.135	±.015	0.110	±.020	0.120	0.015	0.25	0.093	±.0005	0.004	±.0001
		mm	3.43	±.038	2.79	±.051	3.05	0.38	6.35	2.36	±.013	0.102	±.0025
	S48E	In	0.245	±.025	0.250	±.015	0.160	0.025	0.50	0.240	±.0005	0.004	±.0001
		mm	6.22	±.064	6.35	±.038	3.81	0.63	12.7	6.10	±.013	0.102	±.0025
	S58E	In	0.38	+0.035 / - 0.010	0.38	±.010	0.170	0.04 MAX.	0.750	0.35	±.0010	0.010	±.0005
		mm	9.65	+0.89 / -0.25	9.65	±.025	4.32	1.02 MAX.	19.05	8.89	±.025	0.25	±.013
2	S42E	In	0.135	±.015	0.110	±.020	0.102	0.015	0.25	0.093	±.0005	0.004	±.0001
		mm	3.43	±.038	2.79	±.051	2.59	0.38	6.35	2.36	±.013	0.102	±.0025
	S48E	In	0.245	±.025	0.250	±.015	0.160	0.025	0.50	0.240	±.0005	0.004	±.0001
		mm	6.22	±.064	6.35	±.038	3.81	0.63	12.7	6.10	±.013	0.102	±.0025
	S58E	In	0.38	+0.035 / - 0.010	0.38	±.010	0.170	0.04 MAX.	0.750	0.35	±.0010	0.010	±.0005
		mm	9.65	+0.89 / -0.25	9.65	±.025	4.32	1.02 MAX.	19.05	8.89	±.025	0.25	±.013



www.johansontechnology.com

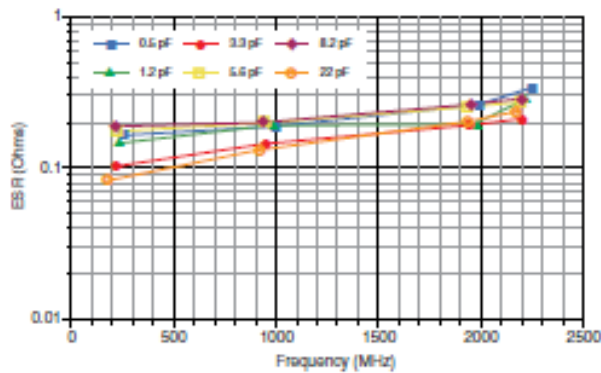
SERIES RESONANCE CHART

Typical Series Resonant Frequency (Series Mounted)

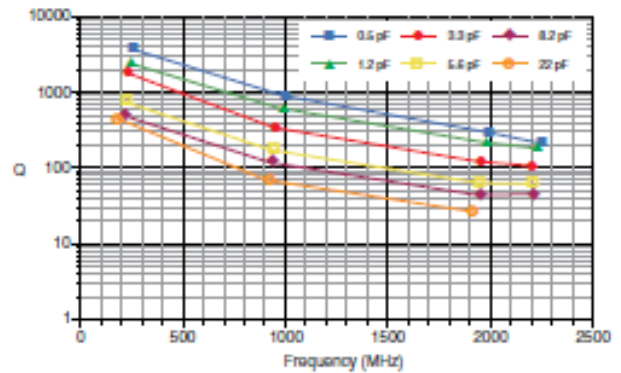


RF CHARACTERISTICS - L-SERIES

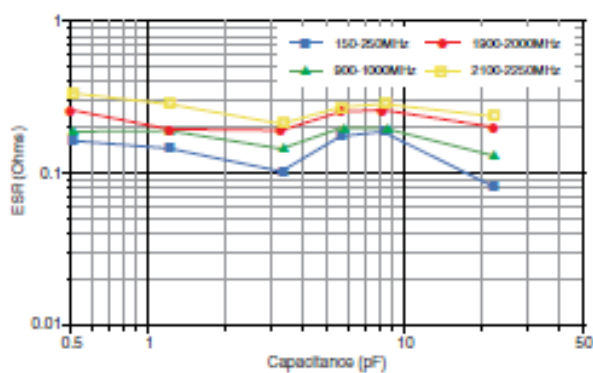
ESR vs Frequency: 0201/R05L



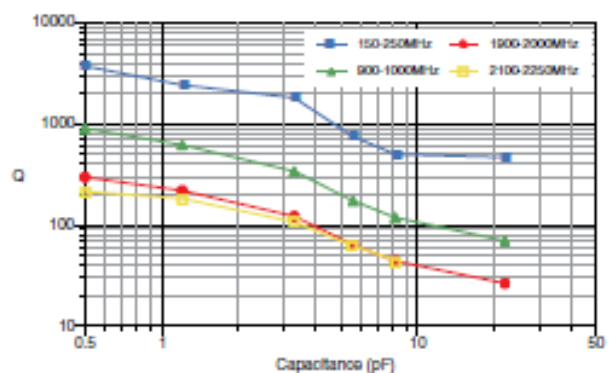
Q vs Frequency: 0201/R05L



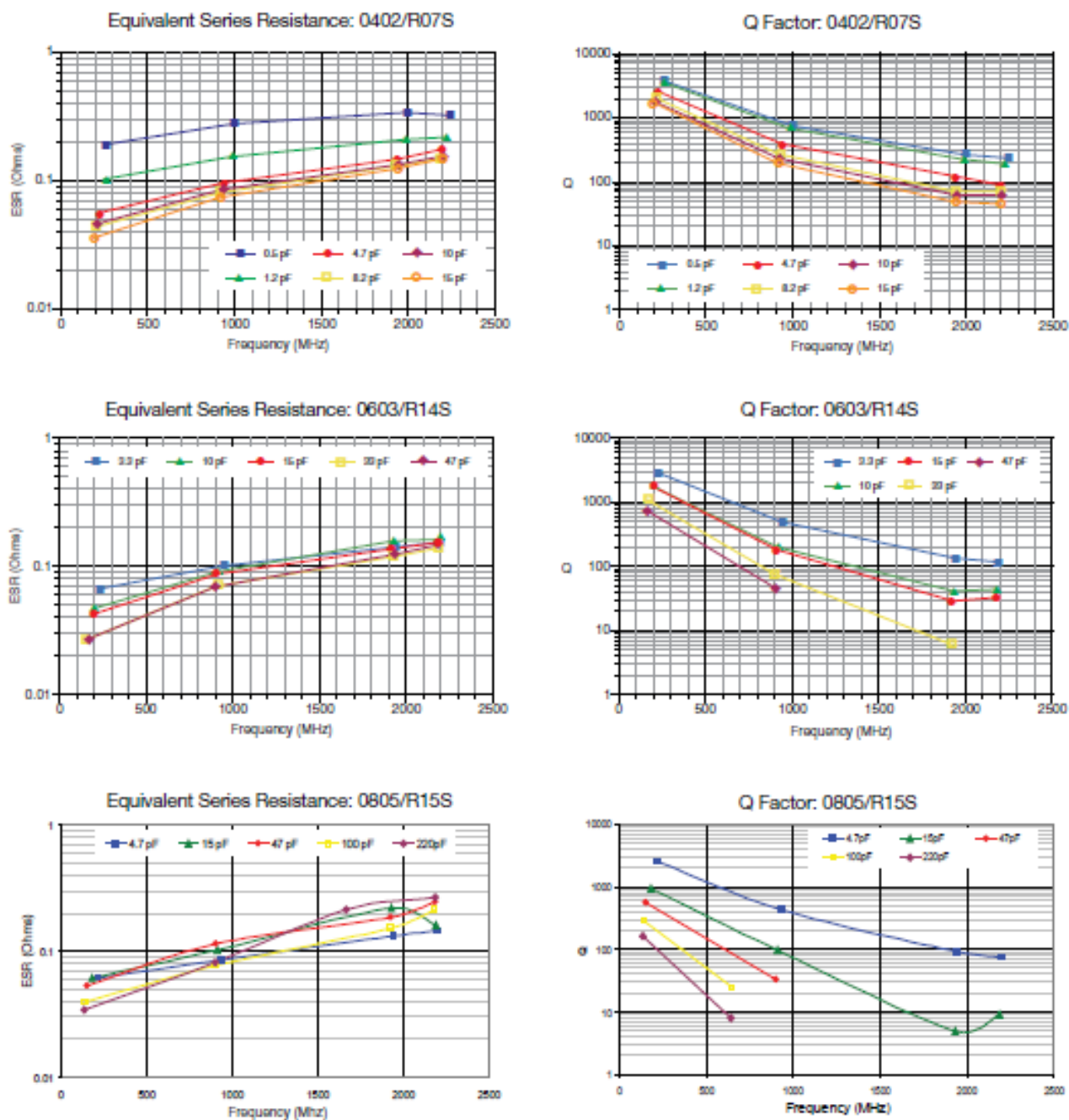
ESR vs Capacitance: 0201/R05L



Q vs Capacitance: 0201/R05L

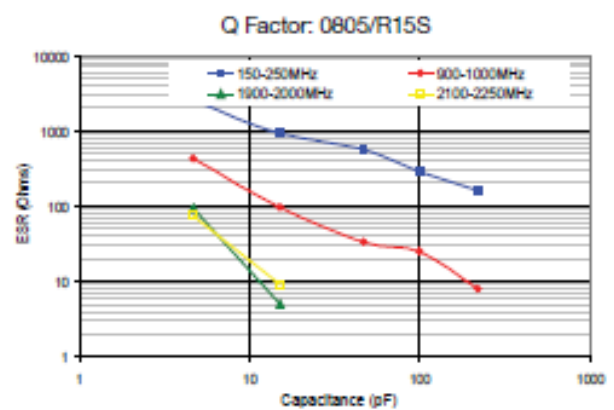
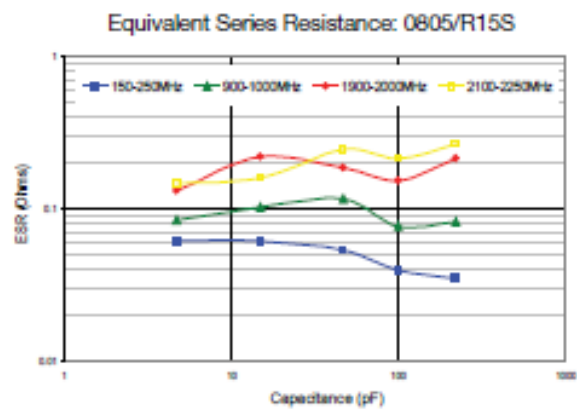
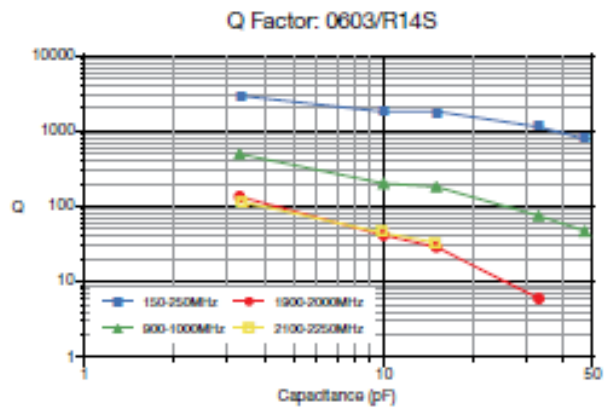
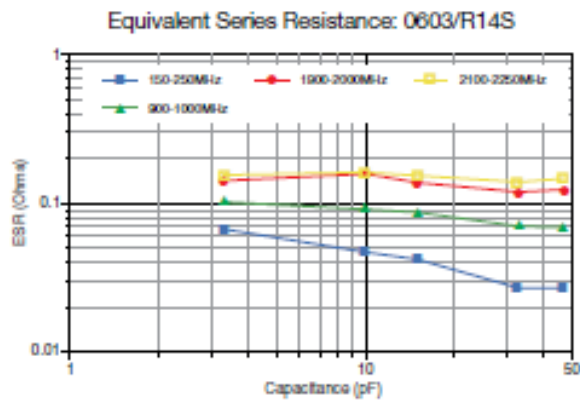
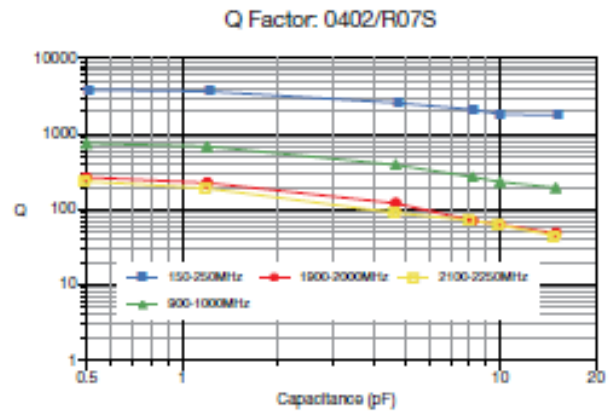
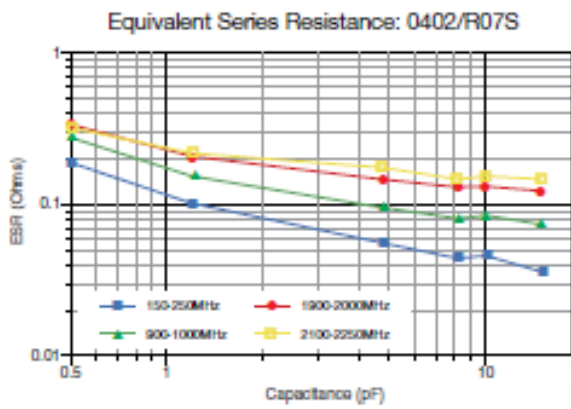


S-SERIES RF CHARACTERISTICS VERSUS FREQUENCY



Measurements performed on a Boonton 34A Resonant Coaxial Line and represent typical capacitor performance.

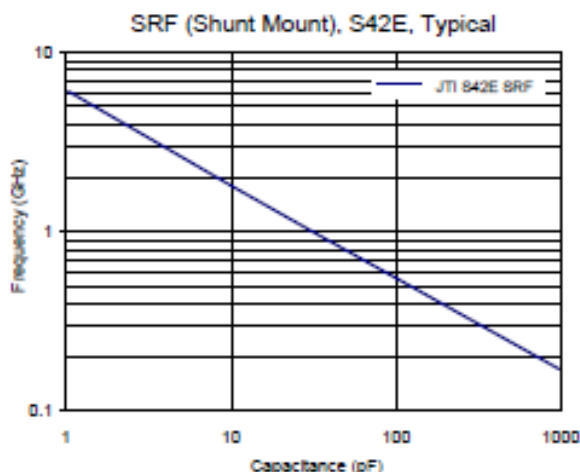
S-SERIES RF CHARACTERISTICS VERSUS CAPACITANCE



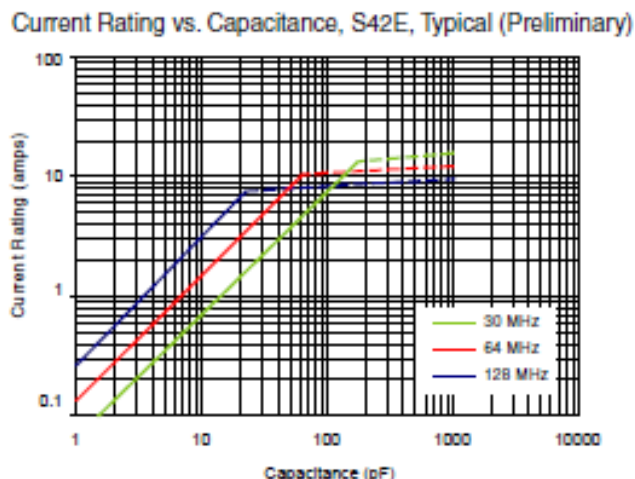
Measurements performed on a Boonton 34A Resonant Coaxial Line and represent typical capacitor performance.



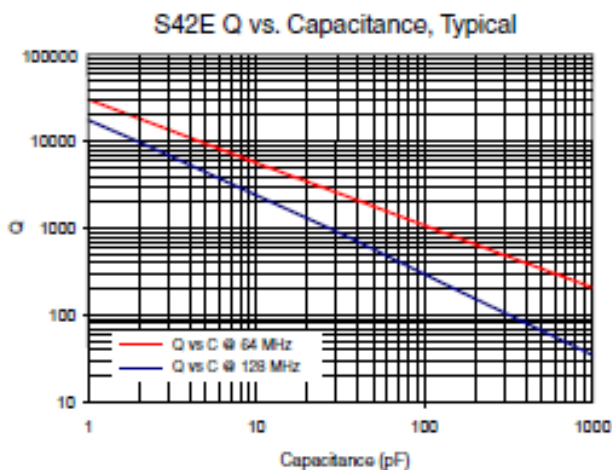
JTI S42E GRAPHICAL DATA



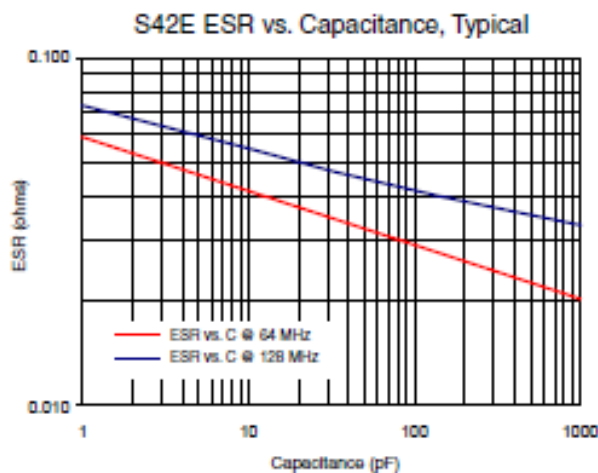
As measured on a 8720C VNA, using a Shunt-Through fixture, and using the S11 magnitude dip to determine the SRF



Solid traces show voltage limited current (Vrms)
Dotted traces show power dissipation limited current (Based on 3 Watts Power Dissipation, and 125 degrees C case temp.)



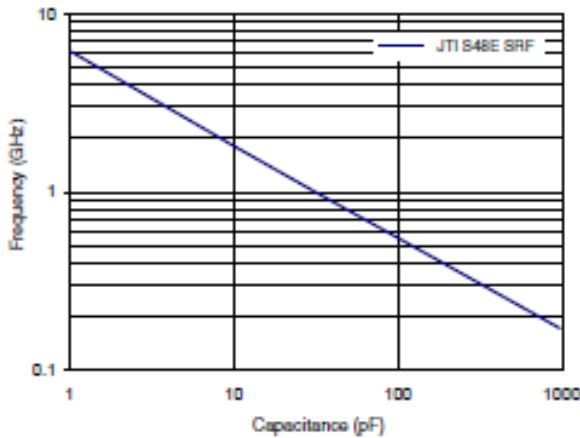
As measured on a 4287A LCR meter, using a 16092A fixture



As measured on a 4287A LCR meter, using a 16092A fixture

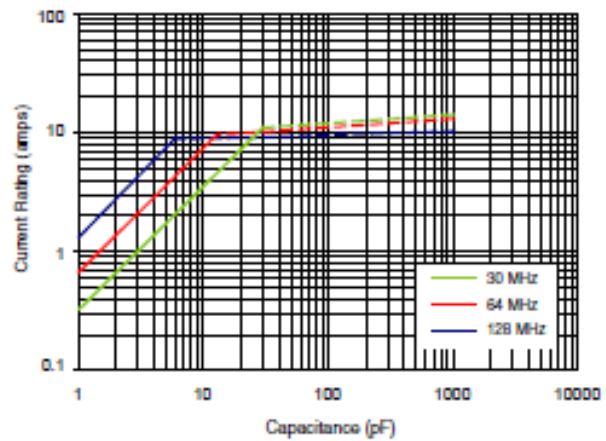


SRF (Shunt Mount), S48E, Typical (Preliminary)



As measured on a 8720C VNA, using a Shunt-Through fixture, and using the S11 magnitude dip to determine the SRF

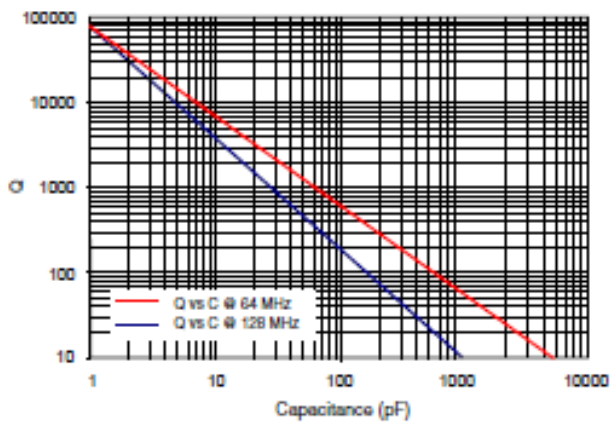
Current Rating vs. Capacitance, S48E, Typical (Preliminary)



Solid traces show voltage limited current (Vrms)

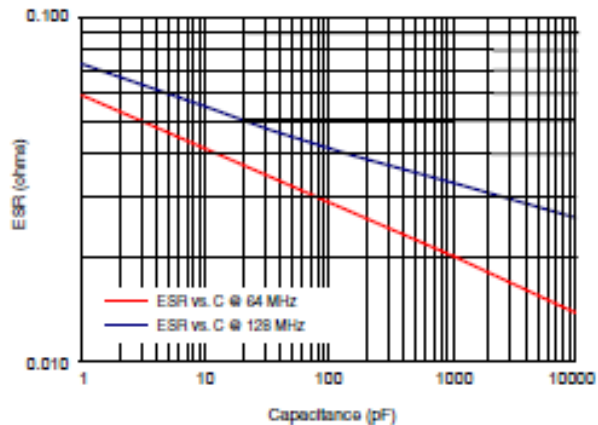
Dotted traces show power dissipation limited current (Based on 4 Watts Power Dissipation, and 125 degrees C case temp.)

S48E Q vs. Capacitance, Typical (Preliminary)



As measured on a 4287A LCR meter, using a 16092A fixture

S48E ESR vs. Capacitance, Typical (Preliminary)



As measured on a 4287A LCR meter, using a 16092A fixture

Type RN73 Series

Type RN73 Series



The RN73 series is a high stability precision chip resistor range offering various power dissipations relating to chip size, TCR's down to 5ppm/°C and resistance tolerances to 0.01%. The resistor is produced with three sputtered layers giving optimum performance. Values are restricted to the E96 and E24 value grids. The RN73 has accurate and uniform physical dimensions to facilitate placement.

Key Features

- High Precision - TCR 5ppm/°C and 10ppm/°C
- Tolerance down to 0.01%
- Thin Film (Nichrome)
- Choice of Packages
- Stable High Frequency Performance
- Temperature Range -55°C to +125°C

Characteristics - Electrical

	0402			0603			0805			1206		
Rated Power (@ 70°C (W):	0.063			0.063			0.1			0.125		
Resistance Range (Ohms) Min:	50R	49R9	25R	4R7	25R	4R7	25R	4R7	25R	4R7	25R	
Max:	15K	15K	100K	332K	200K	500K	30K	500K	1M0	50K		
Tolerance (%):	0.01	0.05	0.1	0.01	0.05	0.1	0.01	0.05	0.1	0.01	0.05	
Code Letter:	L	A	B	L	A	B	L	A	B	L	A	
Selection Series:	E24 / E96			E24 / E96			E24 / E96			E24 / E96		
Temperature Coefficient (ppm/°C):	10ppm			10ppm			10ppm			5ppm		
Code Letter:	C			C			C			A		
Limiting Element Voltage (V):	25			50			100			150		
Maximum Overload Voltage (V):	50			100			200			300		
Operating Temp. Range (°C):	-55 to +125			-55 to +125			-55 to +125			-55 to +125		
Climatic Category:	55/125/55			55/125/55			55/125/55			55/125/55		
Insulation Resistance Dry Min (Mohms):	10000			10000			10000			10000		
Stability (%):	0.5			0.5			0.5			0.5		

Characteristics - Environmental

Test Item	Specification		Test Method
	ToL ±0.05%	ToL >0.05%	
Temperature Coefficient of Resistance	As Spec		MIL-STD-202F Method 304 +25/-55/+25/+125/+25°C
Short Time Overload	ΔR±0.05%	ΔR±0.5%	JIS-C-5202-5.5 RCWV*2.5 or Max. Overloading Voltage for 5 seconds
	ΔR±0.5% for high power rating		
Dielectric Withstand Voltage	By type		MIL-STD-202F Method 301 Apply Max Overload Voltage for 1 minute
Insulation Resistance	>1000M Ω		MIL-STD-202F Method 302 Apply 100V _{DC} for 1 minute
Thermal Shock	ΔR±0.05%	ΔR±0.25%	MIL-STD-202F Method 107G -55°C-150°C, 100 cycles
Load Life	ΔR±0.05%	ΔR±0.2%	MIL-STD-202F Method 108A RCWV, 70°C, 1.5 hours ON, 0.5 hours OFF, total 1000-1048 hours
	>7% Ω ΔR±0.5%		
	ΔR±0.5% for high power rating		
Humidity (Steady State)	ΔR±0.05%	ΔR±0.3%	MIL-STD-202F Method 103B 40°C, 90-95%RH, RCWV 1.5 hours ON, 0.5 hours OFF, total 1000-1048 hours
	ΔR±0.5% for high power rating		
Resistance to Dry Heat	ΔR±0.05%	ΔR±0.2%	JIS-C-5202-7.2 96 hours @ +155°C without load
Low Temperature Operation	ΔR±0.05%	ΔR±0.2%	JIS-C-5202-7.1 1 hours, -65°C, followed by 45minutes of RCWV
	ΔR±0.5% for high power rating		
Bending Strength	ΔR±0.05%	ΔR±0.2%	JIS-C-5202-6.1.4 Bending Amplitude 3mm for 10 seconds
Solderability	95% min coverage		MIL-STD-202F Method 208H 235°C±5°C, 2±0.5 (sec)
Resistance to Soldering Heat	ΔR±0.05%	ΔR±0.2%	MIL-STD-202F Method 210E 260±5°C, 10±1 seconds

*Storage Temperature -25±3°C; Humidity <80%RH

Type RN73 Series

Marking Codes - Case Sizes 0805 to 2512

IEC 4 Digit Marking

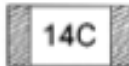
Resistance	100Ω	2.2KΩ	10KΩ	49.9KΩ	100KΩ
Marking Code	1000	2201	1002	4992	1003

Case Sizes 0603

E24 3 Digit Marking - Example: 101=100ff 102=1Kff

E24	10	11	12	13	15	16	18	20	22	24	27	30
	33	36	39	43	47	51	56	62	68	75	82	91

E96 3 Digit Marking - Examples: 14C=13K7ff, 13C=13K3ff, 68B=4K99ff, 68X=49.9ff

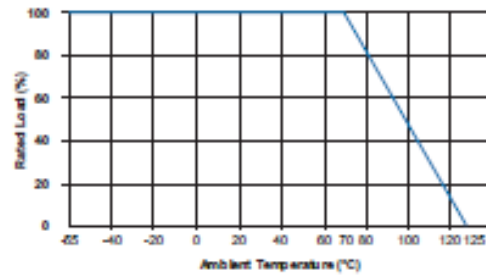


0603 E96 Marking Code Table

Code	E96	Code	E96	Code	E96	Code	E96				
01	100	25	178	49	316	73	562				
02	102	26	182	50	324	74	576				
03	105	27	187	51	332	75	590				
04	107	28	191	52	340	76	604				
05	110	29	196	53	348	77	619				
06	113	30	200	54	357	78	634				
07	115	31	205	55	365	79	649				
08	118	32	210	56	374	80	665				
09	121	33	215	57	383	81	681				
10	124	34	221	58	392	82	698				
11	127	35	226	59	402	83	715				
12	130	36	232	60	412	84	732				
13	133	37	237	61	422	85	750				
14	137	38	243	62	432	86	768				
15	140	39	249	63	442	87	787				
16	143	40	255	64	453	88	806				
17	147	41	261	65	464	89	825				
18	150	42	267	66	475	90	845				
19	154	43	274	67	487	91	866				
20	158	44	280	68	499	92	887				
21	162	45	287	69	511	93	909				
22	165	46	294	70	523	94	931				
23	169	47	301	71	536	95	953				
24	174	48	309	72	549	96	976				
Code	A	B	C	D	E	F	G	H	X	Y	Z
Multiplier	10 ⁰	10 ¹	10 ²	10 ³	10 ⁴	10 ⁵	10 ⁶	10 ⁷	10 ⁻¹	10 ⁻²	10 ⁻³

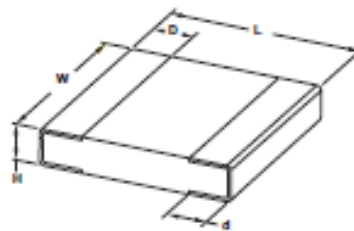
Type RN73 Series

Power Derating Curve



For temperatures in excess of 70°C the load shall be derated in accordance with this curve.

Dimensions



Type	L ±0.2	W ±0.2	D	d ± ^{+0.1} / _{-0.1}	H ± 0.1
RN73 1E	1.0	0.5	0.2	0.2	0.35
RN73 1J	1.6	0.8	0.3 ± 0.2	0.3	0.4
RN73 2A	2.0	1.25	0.4 ± 0.2	0.3	0.5
RN73 2B	3.2	1.6	0.5 ± 0.3	0.4	0.6

Packaging

Type	E24 Pack Qty	E96 Pack Qty
RN73 1E	1000 / 5000 / 10000	250* / 1000 / 5000 / 10000
RN73 1J	1000 / 5000	250* / 1000 / 5000
RN73 2A	1000 / 5000	250* / 1000 / 5000
RN73 2B	5000	1000 / 5000

*250 piece packs are supplied in vacuum sealed bags of cut tape length

How to Order

RN73	C	2A	100K	B	TDF
Common Part	Temp. Coefficient	Chip Size	Resistance Value	Tolerance	Pack Quantity
RN73 - High Precision Resistors (RoHS Compliant)	A - ±5ppm/°C *C - ±10ppm/°C	1E - 0402 *1J - 0803 *2A - 0805 2B - 1206	100 ohms (100 ohms) 100R 1K ohms (1000 ohms) *K0 100K ohms (10000 ohms) 100K	A ±0.05% *B ±0.1% L ±0.01% *Preferred Stock Item	T0 - Cut Tape Lengths (1E, 1J, 2A only) TDF - 1000 (1E, 1J, 2A only) TD - 5000
RN73 - High Precision Resistors (Non RoHS Compliant)	*Preferred Stock Item	*Preferred Stock Item			

MA4AGSBP907



AlGaAs Solder Bump
Flip-Chip PIN Diode

RoHS Compliant

M/A-COM Products
Rev. 5

Features

- ◆ Solderable Bump Die Attach
- ◆ Low Series Resistance
- ◆ Ultra Low Capacitance
- ◆ Millimeter Wave Switching & Cutoff Frequency
- ◆ 2 Nanosecond Switching Speed
- ◆ Can be Driven by a Buffered TTL
- ◆ Silicon Nitride Passivation
- ◆ Polyimide Scratch Protection
- ◆ RoHS Compliant

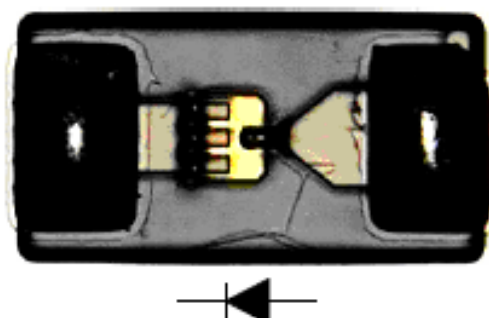
Description

M/A-COM's MA4AGSBP907 is an aluminum gallium arsenide flip-chip PIN diode with solder bumps. These devices are fabricated on OMCVD epitaxial wafers using a process designed for high device uniformity and extremely low parasitics. The diodes exhibit an extremely low RC product, 0.1ps and 2nS switching characteristics. The useable frequency range is 100MHz to 40GHz. They are fully passivated with silicon nitride and have an additional layer of a polymer for scratch protection. The protective coating prevents damage to the junction and the anode airbridge during handling and circuit attachment.

Applications

The 25fF capacitance of the MA4AGSBP907 allows usage through millimeter frequencies for RF switches and switched phase shifter applications. This diode is designed for use in pulsed or CW applications, where single digit nanosecond switching speed is required. The low capacitance of the MA4AGSBP907 makes it ideal for use in microwave multi-throw switch assemblies, where the series capacitance of each "off" port adversely loads the input and affects VSWR.

Mounting Side with Solder Bumps



Absolute Maximum Ratings @ T_{AMB} = 25°C (unless otherwise specified)

Parameter	Absolute Maximum
Reverse Voltage	-50V
Operating Temperature	-55°C to +125°C
Storage Temperature	-55°C to +150°C
Junction Temperature	+175°C
Dissipated Power (RF & DC)	50mW
C.W. Incident Power	+23 dBm
Mounting Temperature	+280°C for 10 seconds

Ordering Information

Part Number	Packaging
MA4AGSBP907	Die in Carrier

ADVANCED: Data Sheets contain information regarding a product M/A-COM is considering for development. Performance is based on target specifications, simulated results, and/or prototype measurements. Commitment to develop is not guaranteed.

PRELIMINARY: Data Sheets contain information regarding a product M/A-COM has under development. Performance is based on engineering tests. Specifications are typical. Mechanical outline has been fixed. Engineering samples and/or test data may be available. Commitment to produce in volume is not guaranteed.

• North America Tel: 800.366.2266 / Fax: 978.366.2266
• Europe Tel: 44.1908.574.200 / Fax: 44.1908.574.300
• Asia/Pacific Tel: 81.44.844.8296 / Fax: 81.44.844.8298
Visit www.macom.com for additional data sheets and product information.

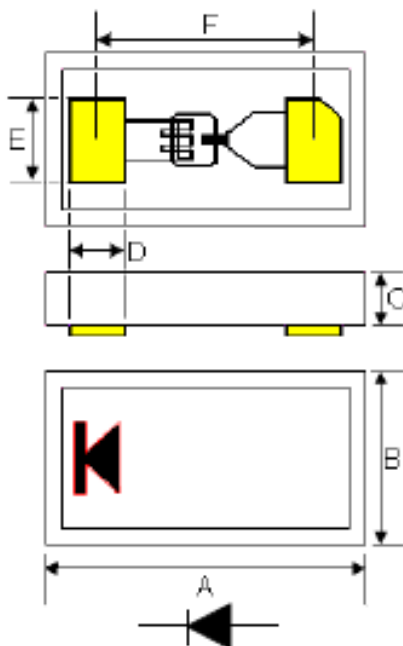
M/A-COM/Inc. and its affiliates reserve the right to make changes to the product(s) or information contained herein without notice.

Electrical Specifications at $T_{AMB} = 25^{\circ}C$

Parameters and Test Conditions	Symbol	Units	1MHz & DC Specs.		10GHz Reference Data
			Typ.	Max.	Typ.
Total Capacitance at -10V	C_t	pF	0.025	0.030	0.025 ¹
Series Resistance at +10mA	R_s	Ω	5.2	7.0	4.2 ²
Forward Voltage at +10mA	V_F	Volts	1.33	1.45	—
Reverse Breakdown Voltage at $10\mu A^3$	V_B	Volts	45	50	—
Switching Speed 10 to 90% RF Voltage ⁴ 90 to 10% RF Voltage ⁴	T_{RISE} T_{FALL}	nS	—	—	2

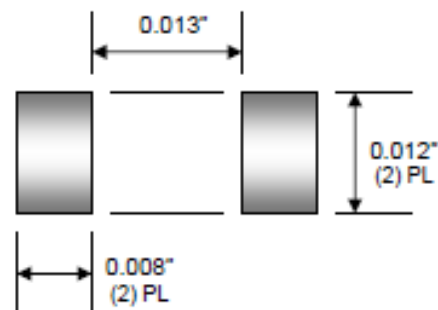
Notes:

1. Capacitance is determined by measuring single series diode isolation in a 50 Ω line at 10GHz.
2. Forward series resistance is determined by measuring single series diode insertion loss in a 50 Ω line at 10GHz.
3. Reverse current will not exceed 10 μA at the maximum voltage rating.
4. Switching speed is measured between 10% to 90% or 90% to 10% RF voltage for a single series mounted diode. Driver delay is not included.



DIM	INCHES		MM	
	MIN.	MAX.	MIN.	MAX.
A	0.026	0.027	0.6604	0.6858
B	0.0135	0.0145	0.3429	0.3683
C	0.0065	0.0075	0.1651	0.1905
D	0.0043	0.0053	0.1092	0.1346
E	0.0068	0.0073	0.1727	0.1854
F	0.0182	0.0192	0.4623	0.4877

Circuit Pad Layout



Note:

1. Yellow areas indicate solder bumps.

ADVANCED: Data Sheets contain information regarding a product M/A-COM is considering for development. Performance is based on target specifications, simulated results, and/or prototype measurements. Commitment to develop is not guaranteed.

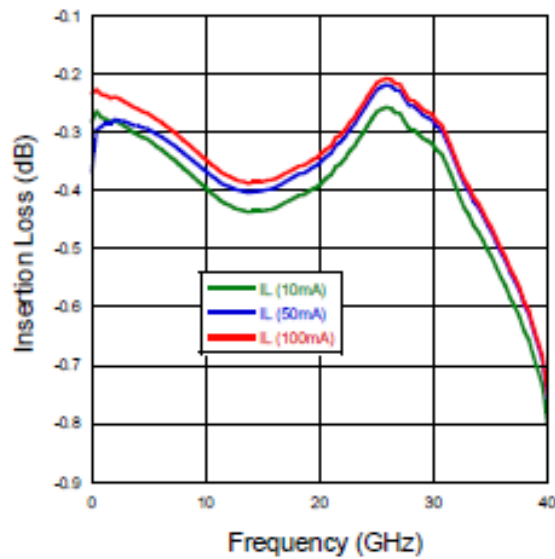
PRELIMINARY: Data Sheets contain information regarding a product M/A-COM has under development. Performance is based on engineering tests. Specifications are typical. Mechanical outline has been fixed. Engineering samples and/or test data may be available. Commitment to produce in volume is not guaranteed.

• North America Tel: 800.366.2266 / Fax: 978.366.2266
 • Europe Tel: 44.1908.574.200 / Fax: 44.1908.574.300
 • Asia/Pacific Tel: 81.44.844.8296 / Fax: 81.44.844.8298
 Visit www.macom.com for additional data sheets and product information.

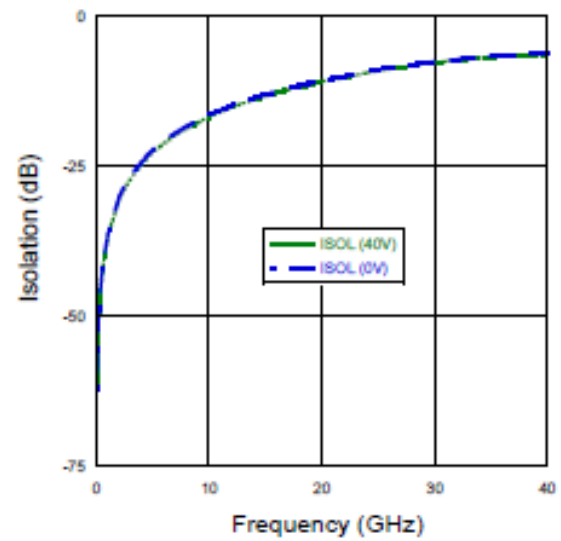
M/A-COM/Inc. and its affiliates reserve the right to make changes to the product(s) or information contained herein without notice.

Electrical Specifications @ $T_{AMB} = 25^{\circ}C$ (unless otherwise noted)

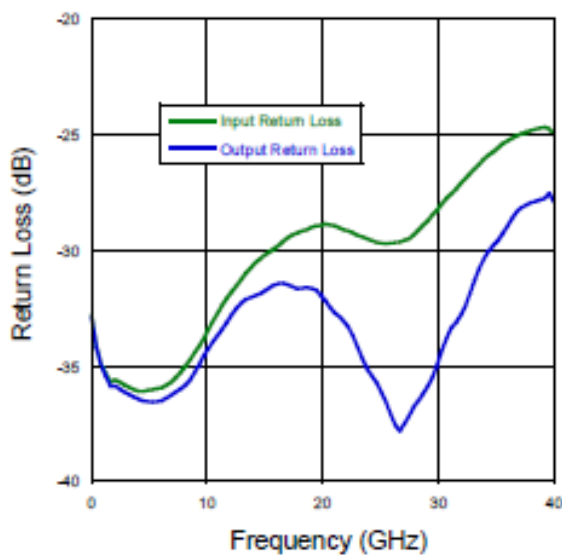
Insertion Loss



Isolation



Return Loss



ADVANCED: Data Sheets contain information regarding a product M/A-COM is considering for development. Performance is based on target specifications, simulated results, and/or prototype measurements. Commitment to develop is not guaranteed.

PRELIMINARY: Data Sheets contain information regarding a product M/A-COM has under development. Performance is based on engineering tests. Specifications are typical. Mechanical outline has been fixed. Engineering samples and/or test data may be available. Commitment to produce in volume is not guaranteed.

• North America Tel: 800.366.2266 / Fax: 978.366.2266
 • Europe Tel: 44.1908.574.200 / Fax: 44.1908.574.300
 • Asia/Pacific Tel: 81.44.844.8296 / Fax: 81.44.844.8298
 Visit www.macom.com for additional data sheets and product information.

M/A-COM/Inc. and its affiliates reserve the right to make changes to the product(s) or information contained herein without notice.

Device Installation Guidelines

The following guidelines should be observed to avoid damaging the AlGaAs flip-chips.

Cleanliness

These devices should be handled in a clean environment.

Static Sensitivity

Aluminum gallium arsenide PIN diodes are ESD sensitive and can be damaged by static electricity. Proper ESD techniques should be used when handling these devices. These devices are rated Class 0, (0-199V) per HBM MIL-STD-883, method 3015.7 [C = 100pF±10%, R = 1.5kW±1%]. Even though tested die pass 50V ESD, they must be handled in a static-free environment.

General Handling

These devices have a polymer layer which provides scratch protection for the junction area and the anode air bridge. Die can be handled with plastic tweezers or picked and placed automatically with a #27 tip vacuum pencil.

Assembly Requirements using Tin / Lead Solder

The flip chip diode employs a 6µm thick, Sn/Pb, 63/37 solderable interface as part of the 50µm high solder bump. These chips are designed to be soldered onto hard or soft substrates with the junction side down. They should be mounted onto silkscreened circuits using 63/37 Sn/Pb solder paste. A typical profile for a Sn/Pb 63/37 soldering process is provided in on the M/A-COM website at this address: <http://www.macom.com/Application%20Notes/pdf/M538.pdf>.

ADVANCED: Data Sheets contain information regarding a product M/A-COM is considering for development. Performance is based on target specifications, simulated results, and/or prototype measurements. Commitment to develop is not guaranteed.
PRELIMINARY: Data Sheets contain information regarding a product M/A-COM has under development. Performance is based on engineering tests. Specifications are typical. Mechanical outline has been fixed. Engineering samples and/or test data may be available. Commitment to produce in volume is not guaranteed.

• **North America** Tel: 800.366.2266 / Fax: 978.366.2266
• **Europe** Tel: 44.1908.574.200 / Fax: 44.1908.574.300
• **Asia/Pacific** Tel: 81.44.844.8296 / Fax: 81.44.844.8298
Visit www.macom.com for additional data sheets and product information.

M/A-COM/Inc. and its affiliates reserve the right to make changes to the product(s) or information contained herein without notice.

Features

- ◆ Low Series Resistance
- ◆ Low Capacitance
- ◆ Millimeter Wave Switching & Cutoff Frequency
- ◆ 5 Nanosecond Switching Speed
- ◆ Can be Driven by a Buffered +5V TTL
- ◆ Silicon Nitride Passivation
- ◆ Polyimide Scratch Protection
- ◆ RoHS Compliant

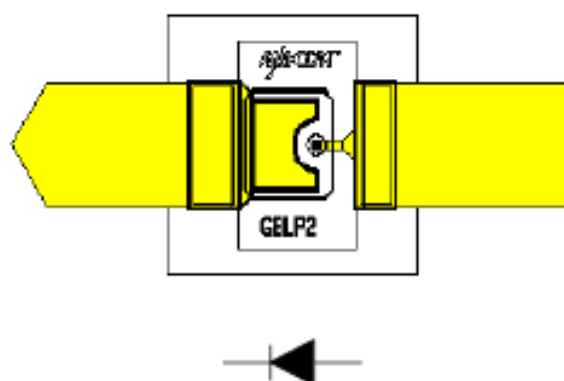
Description

M/A-COM's MA4AGBLP912 is an Aluminum-Gallium-Arsenide anode enhanced, beam lead PIN diode. AlGaAs anodes, which utilize M/A-COM's patent pending hetero-junction technology, produce less diode "On" resistance than conventional GaAs devices. These devices are fabricated on a OMCVD epitaxial wafer using a process designed for high device uniformity and extremely low parasitics. The diodes exhibit low series resistance, 4Ω, low capacitance, 28fF, and an extremely fast switching speed of 5nS. They are fully passivated with silicon nitride and have an additional layer of a polymer for scratch protection. The protective coating prevents damage to the junction and the anode air bridges during handling and assembly.

Applications

The ultra low capacitance of the MA4AGBLP912 device makes it ideally suited for use through W-band. The low RC product and low profile of the beamlead PIN diode allows for use in microwave and millimeter wave switch designs, where low insertion loss and high isolation are required. The operating bias conditions of +10mA for the low loss state, and 0v, for the isolation state permits the use of a simple +5V TTL gate driver. These AlGaAs, beamlead diodes, can be used in switching arrays on radar systems, high speed ECM circuits, optical switching networks, instrumentation, and other wideband multi-throw switch assemblies.

MA4AGBLP912



Absolute Maximum Ratings @ T_{AMB} = 25°C (unless otherwise specified)

Parameter	Absolute Maximum
Reverse Voltage	-50V
Operating Temperature	-65°C to +125°C
Storage Temperature	-65°C to +150°C
Junction Temperature	+175°C
Forward DC Current	40mA
C.W. Incident Power	+23dBm
Mounting Temperature	+235°C for 10 seconds

ADVANCED: Data Sheets contain information regarding a product M/A-COM is considering for development. Performance is based on target specifications, simulated results, and/or prototype measurements. Commitment to develop is not guaranteed.

PRELIMINARY: Data Sheets contain information regarding a product M/A-COM has under development. Performance is based on engineering tests. Specifications are typical. Mechanical outline has been fixed. Engineering samples and/or test data may be available. Commitment to produce in volume is not guaranteed.

• North America Tel: 800.366.2266 / Fax: 978.366.2266
 • Europe Tel: 44.1908.574.200 / Fax: 44.1908.574.300
 • Asia/Pacific Tel: 81.44.844.8296 / Fax: 81.44.844.8298
 Visit www.macom.com for additional data sheets and product information.

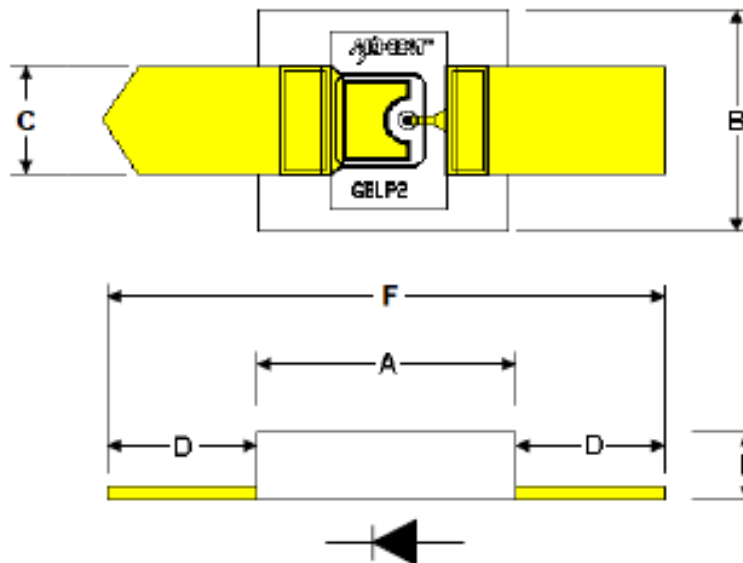
M/A-COM/Inc. and its affiliates reserve the right to make changes to the product(s) or information contained herein without notice.

Electrical Specifications at T_{AMB} = 25°C

Test Conditions	Parameters	Units	Min	Typical	Max.
Total Capacitance @ -5V/10 GHz ¹	Ct	fF	-	26	30
Forward Resistance @ +20mA/10 GHz ²	Rs	Ohms	-	4	4.9
Forward Voltage at +10mA	Vf	Volts	1.2	1.36	1.5
Leakage Current at -40 V	Ir	nA	-	50	300
Minority Carrier Lifetime	TL	nS	-	5	10

Notes:

1. Capacitance is determined by measuring the isolation of a single series diode in a 50Ω line at 10GHz.
2. Forward series resistance is determined by measuring the insertion loss of a single series diode in a 50Ω line at 10GHz.



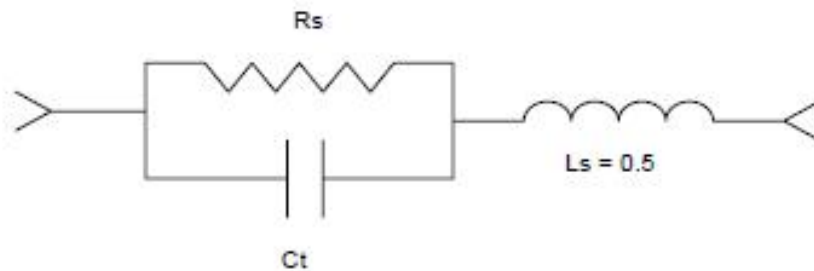
DIM	INCHES		MM	
	MIN.	MAX.	MIN.	MAX.
A	0.009	0.013	0.2286	0.3302
B	0.0049	0.0089	0.1245	0.2261
C	0.0037	0.0057	0.0940	0.1448
D	0.0049	0.0089	0.1245	0.2261
E	0.002	0.006	0.0508	0.1524
F	0.0218	0.0278	0.5537	0.70612

ADVANCED: Data Sheets contain information regarding a product M/A-COM is considering for development. Performance is based on target specifications, simulated results, and/or prototype measurements. Commitment to develop is not guaranteed.

PRELIMINARY: Data Sheets contain information regarding a product M/A-COM has under development. Performance is based on engineering tests. Specifications are typical. Mechanical outline has been fixed. Engineering samples and/or test data may be available. Commitment to produce in volume is not guaranteed.

• North America Tel: 800.366.2266 / Fax: 978.366.2266
 • Europe Tel: 44.1908.574.200 / Fax: 44.1908.574.300
 • Asia/Pacific Tel: 81.44.844.8296 / Fax: 81.44.844.8298
 Visit www.macom.com for additional data sheets and product information.

M/A-COM/Inc. and its affiliates reserve the right to make changes to the product(s) or information contained herein without notice.

Diode Model

MA4AGBLP912 SPICE Model

$I_s = 1.0E-14$ A
 $V_i = 0.0$ V
 $\mu_{e-} = 8600$ cm²/V-sec
 $W_i = 3.0$ μ m
 $R_r = 10$ K Ohms
 $C_{jmin} = 0.020$ pF
 $\tau = 10$ nsec
 $R_s(I) = R_c + R_j(I) = 0.10$ Ohm + $R_j(I)$
 $C_{j0} = 0.022$ pF
 $V_j = 1.35$ V
 $M = 0.5$
 $F_c = 0.5$
 $I_{max} = 0.04$ A
 $K_f = 0.0$
 $A_f = 1.0$
 $wBv = 50$ V
 $wPmax = 100$ mW
 $Ffe = 1.0$

ADVANCED: Data Sheets contain information regarding a product M/A-COM is considering for development. Performance is based on target specifications, simulated results, and/or prototype measurements. Commitment to develop is not guaranteed.

PRELIMINARY: Data Sheets contain information regarding a product M/A-COM has under development. Performance is based on engineering tests. Specifications are typical. Mechanical outline has been fixed. Engineering samples and/or test data may be available. Commitment to produce in volume is not guaranteed.

• North America Tel: 800.366.2266 / Fax: 978.366.2266
 • Europe Tel: 44.1908.574.200 / Fax: 44.1908.574.300
 • Asia/Pacific Tel: 81.44.844.8296 / Fax: 81.44.844.8298
 Visit www.macom.com for additional data sheets and product information.

M/A-COM/Inc. and its affiliates reserve the right to make changes to the product(s) or information contained herein without notice.

Handling and Assembly Procedures

The following precautions should be observed to avoid damaging these devices.

Cleanliness

These devices should be handled in a clean environment.

Static Sensitivity

Aluminum Gallium Arsenide PIN diodes are Class 1 ESD sensitive and can be damaged by static electricity. Proper ESD techniques should be used when handling these devices.

General Handling

These devices have a polymer layer which provides scratch protection for the junction area and the anode air bridge. Beam lead devices must, however, be handled with extreme care since the leads may easily be distorted or broken by the normal pressures exerted when handled with tweezers. A vacuum pencil with a #27 tip is recommended for picking and placing.

Attachment

These devices were designed to be inserted onto hard or soft substrates. Recommended methods of attachment include thermo-compression bonding, parallel-gap welding and electrically conductive silver epoxy.

See Application Note M541 page 8, [Bonding and Handling and Procedures for Chip Diode Devices](#) for more detailed assembly instructions.

Ordering Information

Part Number	Packaging
MA4AGBLP912	Gel Pak

ADVANCED: Data Sheets contain information regarding a product M/A-COM is considering for development. Performance is based on target specifications, simulated results, and/or prototype measurements. Commitment to develop is not guaranteed.

PRELIMINARY: Data Sheets contain information regarding a product M/A-COM has under development. Performance is based on engineering tests. Specifications are typical. Mechanical outline has been fixed. Engineering samples and/or test data may be available. Commitment to produce in volume is not guaranteed.

• **North America** Tel: 800.366.2266 / Fax: 978.366.2266
 • **Europe** Tel: 44.1908.574.200 / Fax: 44.1908.574.300
 • **Asia/Pacific** Tel: 81.44.844.8296 / Fax: 81.44.844.8298
 Visit www.macom.com for additional data sheets and product information.

M/A-COM/Inc. and its affiliates reserve the right to make changes to the product(s) or information contained herein without notice.